Author:
Owen, John Shaw

Title:
A power spectral approach to the analysis of the dynamic response of cable stayed bridges to spatially varying excitation.

A Power Spectral Approach to the Analysis of the Dynamic Response of Cable Stayed Bridges to Spatially Varying Excitation

By

John Shaw Owen

A thesis submitted to the University of Bristol in accordance with the requirements of the degree of Doctor of Philosophy in the faculty of Engineering. The work was performed in the Department of Civil Engineering between September 1989 and June 1993 and the thesis submitted in March 1994.

Abstract

The response of cable stayed bridges to spatially varying loads is introduced by considering their response to seismic excitation. After reviewing different methods of representing the ground motion and calculating the response, a power spectral method was chosen as this enabled efficient calculation of the response whilst allowing the random nature of the loading to be taken into account. This approach is developed in detail and validated by comparison with a Monte Carlo simulation of the response of a simple footbridge to asynchronous seismic excitation. This comparison showed clearly the effects of asynchronous excitation and also that it is essential to take into account the random nature of the loading. Finally, the method was used in a study of the response of a cable stayed bridge to asynchronous seismic excitation, the results of which showed that the ground wave velocity influenced both the size and location of the maximum response. By using an evolutionary spectral approach account was also taken of the non stationary nature of seismic excitation which was found to have a significant effect on the bridge response.

To validate the approach further, testing had to be carried out on either a real or model structure. The analysis technique considers the dynamic response to spatially varying random loads, properties which are shared by wind and traffic excitation. The thesis describes a project which was set up to monitor the dynamic response of Kessock Bridge in Scotland to wind excitation over a period of several months. The instrumentation and monitoring strategy are described in full together with comparisons between finite element modelling and a modal survey of the bridge. A large amount of data was collected during the monitoring period and only limited processing is presented in this thesis. Although this has not been sufficient to validate the theoretical approach, it does demonstrate the possible influence of spatial variations in the wind on the dynamic response of the bridge.

Dedication

"Of making many books there is no end, and much study wearies the body.

Now all has been heard; here is the conclusion of the matter:

Fear God and keep his commandments,

for this is the whole duty of man.

For God will bring every deed into judgement,

including every hidden thing,

whether it is good or evil."

Ecclesiastes 12 vv 12-14

Acknowledgements

I would like to acknowledge the help and support of all the members of the Department of Civil Engineering at the University of Bristol. I especially want to thank,

Dr. Tony Blakeborough for his guidance and supervision

Professor David Blockley for providing constructive criticism, encouragement and ideas,

Mr Andy Vann for his invaluable help and computing expertise monitoring Kessock Bridge

Dr. John Davis for suffering my driving through the lanes of Scotland,

Dr. Wendy Daniell for her encouragement whilst writing up,

and Dave Ward, Ken Jones, Roy Sampson and John Bool for their technical support.

I would also like to acknowledge the good will and assistance given us by the staff of Highland Regional Council in Inverness, and especially Mr. Jeff Hanson, Mr. Freddie Bartlett and Mr. Ernie Walker.

Throughout the time it has taken me to produce this thesis there have been many ups and downs. I owe an enormous debt of gratitude to those people who showed me love and encouragement during the times when the end seemed far away. Special thanks go to John and Maya Bimson, without whom this thesis would not have been written, and my parents, who were always just a phone call away.

Finally I am indebted to Professor Steve Brown in the Department of Civil Engineering at the University of Nottingham, for his permission to complete this thesis in Nottingham.

Declaration

I declare that, unless otherwise cited in the text, the work contained in this thesis is my own original work. The monitoring of Kessock Bridge was performed in close collaboration with Mr. Andy Vann and who developed the IMCES system used to collect the data.

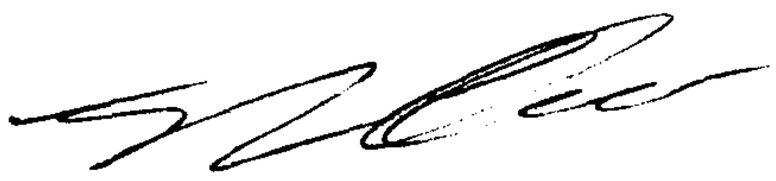

John S. Owen

Table of Contents

Chapter Three

The Power Spectral Analysis of the Response of Extended Structures to Spatially Varying Seismic Excitation

Chapter Four

Validation of the Power Spectral Analysis of the Response to Asynchronous Seismic Excitation

Chapter Five

Analysis of The Response of A Cable Stayed Bridge To Asynchronous Seismic Excitation

Chapter Six

The Response of Cable Stayed Bridges to Wind Excitation: An Introduction and Review

Chapter Seven

The Response of Cable Stayed Bridges to Wind Excitation: The Prototype Testing of Kessock Bridge

Chapter Eight

The Response of Cable Stayed Bridges to Wind Excitation: Results of Prototype Testing

Chapter Nine

Conclusions and Suggestions for Further Study

References

By Author ref.1

List of Tables

List of Figures

Chapter Five

Chapter Six

Chapter Seven

Chapter Eight

List of Plates

Chapter Seven

Notation

a	Acceleration
$(a + bj)$	General complex number
$(c + dj)$	General complex number
A	Area
$A_{i,j}$	Response in degree of freedom i to unit displacement in ground degree of freedom j
A_{xk}	Response at x to unit displacement at support k
$A(t,\omega)$	Window function for evolutionary spectrum
A_0	Amplitude of exponential envelope function
b	Half width of bridge deck
b	Length of element of thin walled section
B	Typical length dimension
b_1	Parameter for exponential envelope function
b_2	Parameter for exponential envelope function
c	Damping of single degree of freedom system
c	Ground wave velocity
c_{med}	Wave velocity in medium
c_{axis}	Relative wave velocity along bridge axis
C_D	Drag coefficient
C_L	Lift coefficient
C_M	Moment coefficient
C_P	Pressure coefficient
d_i	Number of ground degrees of freedom in direction i
D	Typical length dimension
D	Anemometer distance constant
$D_{xy}(n)$	Davenport's spatial cross-correlation spectrum
E	Elastic modulus
E_c	Elastic modulus of cable material
E_{eq}	Equivalent elastic modulus of cable
$E[\ .\ ]$	Expectation of the quantity in square brackets
f	Reduced frequency

F_D	Aerodynamic drag force
F_L	Aerodynamic lift force
F_x	Cumulative distribution function of random variable X
G	Shear modulus
G_0	Amplitude of Kanai-Tajimi spectrum
$G_{aa}(\omega\ )$	Single sided ground power spectral density function
$G_{filt}(\omega\ )$	Clough Penzien filter function
$G_{pp}(\omega\ )$	Single sided power spectral density function of excitation $p(t)$
$G_{vv}(\omega\ )$	Single sided power spectral density function of global response $v(t)$
$G_{xx}(\omega\ )$	Single sided power spectral density function of random process X(t)
$G_{xy}(\omega\ )$	Single sided cross spectral density function betwenn random processes X(t) and Y(t)
$G_{yy}(\omega\ )$	Power spectral density function of modal response
$h(t)$	Impulse response function
$h(t)_r$	Impulse response function mode r
H	Horizontal projected length of inclined cable stay
$H(\kappa\ )$	Wavenumber response function
$H(\omega\ )$	Frequency response function
$H(\omega\ )_r$	Frequency response function in mode r
I	Second moment of area
j	Square root of -1
J	Torsional constant
J_{eq}	Equivalent torsional constant including warping
$\lvert J_r(n)\rvert^2$	Joint mode acceptance
k	Stiffness of single degree of freedom system
K	Reduced frequency
K_r	Stiffness in rth generalised coordinate
l	Length of beam
l_k	Distance to support k
L	Ground length
L_h	Aerodynamic lift force
$L(\beta\ ,t)$	Reliability function
$L_u^x\ L_u^y\ L_u^z$	Integral length scales

m	Mass of single degree of freedom system
M_α	Aerodynamic moment
$M(t,\omega\ )$	Evolutionary frequency response function
n	Frequency
nm	Number of modes
N_s	Frequency of vortex shedding
p	Force or load function
p	Air pressure
p_0	Air pressure in far upstream flow
P_r	Force in rth generalised coordinate
p_x	Probability density function of random variable X
P_x	Cumulative probability density function of random variable X
$r_x(s)$	Influence line of response at x to unit load at s
$R_x(\kappa\ )$	Wavenumber response function at x
$R_{xx}(\tau\ )$	Auto-correlation function of stationary random process X(t)
$R_{xy}(\tau\ )$	Cross-correlation function of stationary random processes X(t) and Y(t)
s	Ground position coordinate
s	Spatial variable
$S_{aa}(\omega\ )$	Ground power spectral density function
$S_{pp}(\omega\ )$	Power spectral density function of excitation $p(t)$
$S_{vv}(\omega\ )$	Power spectral density function of global response $v(t)$
$S_{xx}(\omega\ )$	Power spectral density function of random process X(t)
$S_{xy}(\omega\ )$	Cross spectral density function betwenn random processes X(t) and Y(t)
$S_{yy}(\omega\ )$	Power spectral density function of modal response
t	Time variable
t	Thickness of element of open section
T	Period of periodic time function
T	Duration of finite random process
T	Cable tension
u	Instantaneous wind speed
u_*	Friction velocity
U	Uniform wind speed

$\overline{U}$	Mean wind speed
ν	Mean zero crossing rate of random process
ν_e	Reduced mean zero crossing rate of random process
$\nu(\beta\ ,t)$	Mean barrier level crossing rate
$v_G(s,t)$	Ground displacement
v_g	Rigid body displacement of single degree of freedom system
v_d	Dynamic displacement of single degree of freedom system
v_k	Response in kth global degree of freedom
v_{kr}	Response in kth global degree of freedom corresponding to response in mode r
V_r	Response in rth generalised coordinate
$V_x(\kappa\ )$	Wavenumber response at point x in the structure
w	Cable weight per unit length
x	Space variable
x	Coordinate of position within structure
X	Random variable
z	Height
α	Dispersion of Gumbel distribution
α	Angle of attack
α	Bending deflection
β	Barrier level
δ	Spectral dispersion parameter
δ	Dirac delta function
$\phi_r(x)$	r^{th} mode shape vector
ϕ	Phase angle
γ	Euler's constant
γ^2_{xy}	Coherence function
Γ	Warping constant
$\varphi_{xx}(t_1,t_2)$	Auto-correlation function of the random process X(t)
$\varphi_{xy}(t_1,t_2)$	Cross-correlation function of the random processes X(t) and Y(t)
Φ	Twist of section
κ	Wavenumber
κ_n	n^{th} cumulant function of a random process

$\kappa_{xx}(t_1,t_2)$	Auto-covariance function of random process X(t)
λ_n	n^{th} spectral moment
μ_x	Mean value of random variable X
$\mu_x(t)$	Mean value of random process X(t)
$\mu_r(x)$	rth generalised coordinate
ρ_{ij}	Cross corelation coefficient
δ	Strouhal number
σ_x^2	Variance of random process X(t)
$\theta(t)$	General oscillatory function
$\theta(\omega)$	Phase spectrum between two processes
τ	Time variable
τ	Time separation
ω	Circular frequency
ω	Sample value
ω_d	Damped natural circular natural frequency
ω_f	Natural frequency of Clough and Penzien filter
ω_g	Ground natural frequency for Kanai Tajimi filter
ω_r	Circular natural frequency of mode r
Ω_k	k^{th} characteristic frequency of a random process
Ω	Sample space
ξ	Space separation parameter
ξ_f	Damping factor for Clough and Penzien filter
ξ_g	Ground damping factor for Kanai Tajimi filter
ξ_r	Modal damping in mode r

Vectors and Matrices

[A]	General matrix
[B]	General matrix
[C(ω)]	Damping matrix
$[\mathbf{C}(\omega)]_r$	Modal damping matrix
$[\mathbf{H}(\omega)]_r$	Modal frequency response matrix

$[\mathbf{I}]$	Identity matrix
$[\mathbf{K}(\omega)]$	Stiffness matrix
$[\mathbf{K}(\omega)]_r$	Modal stiffness matrix
$[\mathbf{M}(\omega)]$	Mass matrix
$[\mathbf{M}(\omega)]_r$	Modal mass matrix
$\{\mathbf{N}(\kappa)\}$	Pseudo static ground influence vector, wavenumber domain
$\{\mathbf{p}\}$	Force vector in global coordinates
$\{\mathbf{r}(s)\}$	Ground influence vector, space domain
$\{\mathbf{R}(\kappa)\}$	Ground influence vector, wavenumber domain
$\{\mathbf{R}\}$	Earthquake participation vector
$[\mathbf{T_e}]$	Element stress recovery matrix
$\{\mathbf{v}\}$	Displacement vector in global coordinates
$\{\mathbf{v_d}\}$	Dynamic component of displacement vector in global coordinates
$\{\mathbf{v_s}\}$	Pseudo static component of displacement vector in global coordinates
$\{\mathbf{v_g}\}$	Rigid body displacement vector in global coordinates
$\{\mathbf{y}\}$	Displacement vector in modal coordinates
$\{\mathbf{y_d}\}$	Dynamic component of displacement vector in modal coordinates
$\{\mathbf{y_s}\}$	Pseudo static component of displacement vector in modal coordinates
$\{\mathbf{Y}\}$	Displacement vector in modal coordinates, frequency domain
$\{\mathbf{Y_d}\}$	Dynamic component of displacement vector in modal coordinates, frequency domain
$\{\mathbf{Y_s}\}$	Pseudo static component of displacement, modal coordinates, frequency domain
$[\Phi]$	Matrix of mode shape vectors
$[\Gamma]$	Matrix of modal forces
$\{\kappa\}$	Space time separation vector
$[\lambda_c]_r$	Modal spectral moment matrix of dynamic/pseudo static cross terms
$[\lambda_d]_r$	Modal spectral moment matrix of dynamic response
$[\lambda_s]_r$	Modal spectral moment matrix of pseudo static response
$\{\xi\}$	Space time separation vector

Chapter One

Introduction

1.0 The Dynamic Loading Of Cable-Stayed Bridges

Since earliest times, bridging rivers or ravines has presented mankind with major engineering problems. However, the passage of time has seen great technological strides as new materials were found and perfected, construction techniques developed, and new methods of analysis gave a greater insight into structural behaviour. These advances have resulted in longer and longer spans being achieved; what was a record 100 years ago is commonplace today. Over the past 250 years five different types of long span bridges have evolved; the arch, the girder, the cantilever truss, the suspension bridge and the cable-stayed bridge. The last of these, the cable-stayed bridge, is the most recent to gain widespread acceptance, and is now regarded by many as the first choice approach for medium to long span bridges. Since the construction of the first modern cable-stayed bridge, the Stromsund Bridge, in Sweden in 1955, cable-stayed bridges have been built in most parts of the World, including Europe, North and South America, Asia and the Far East. However, cable-stayed bridges still present a challenge to designers because they are complex three dimensional structures which are subject to several forms of non linearity. Therefore, because of their popularity, their novelty and their complex behaviour, cable-stayed bridges have become an important subject of research.

Long span bridges undergo several types of loading which can be steady state, such as their self weight, or vary with time, such as traffic, wind, earthquake, and the effects of temperature. If the loads vary rapidly with time, as with earthquake, wind and traffic, then a dynamic analysis of the

bridge is advisable to design against them. Now, as mentioned in the previous paragraph, bridges in general, and cable-stayed bridges in particular, are being built with longer and longer spans. This gives rise to extra complications because the dynamic excitation can vary along the length of the bridge. For example gusts in the wind will affect different parts of the bridge at different times, and traffic will be non uniformly distributed along the span. This spatial variation of the dynamic load has two effects on the bridge. Firstly, different distributions of load can preferentially excite particular modes of vibration. Secondly, relative movement between different parts of the bridge, caused by the spatial variation in the time varying loads, will cause the bridge to deform. These deformations are termed pseudo-static displacements since they vary with time but occur due to the stiffness of the bridge rather than its inertia. These two effects can lead to both attenuation and amplification of the dynamic response depending on the structural properties and the distribution of the loading.

In order to calculate the dynamic response of a structure it is necessary to have a representation of the dynamic loading. This could take the form of a power spectrum or a time history record. However, when the types of dynamic load mentioned above are examined, they are found to be random, or pseudo-random processes, and this has certain implications when calculating the response of a structure. If a deterministic method is used, such as the time history approach where the equations of motion are integrated numerically, then the results for two statistically identical events might be quite different. The calculations would then need to be repeated many times using different time histories to obtain an acceptable estimate of the bridge response. However if a stochastic method is adopted the statistics of the response to a random excitation can be obtained from a single set of calculations.

1.1 Objectives Of The Research

To summarise the previous section many medium to long span bridging problems are now being solved, and will be solved in the future, using cable-stayed bridges. Long span bridges are also subjected to random time varying loads which vary spatially across the structure. With these points in mind the aim of the research presented in this thesis was to determine the importance of the spatially varying dynamic loads on cable-stayed bridges, focusing in particular on seismic and wind excitation. To this end two objectives have been pursued. The first was to develop a stochastic approach to the analysis of the response of a structure to spatially varying seismic excitation and to use this to investigate the response of a typical cable stayed bridge to travelling seismic waves. The second was to measure the response of a prototype bridge to wind excitation and to use the results to assess the importance of spatial variations in wind loading. The results could then also be used to validate the analytical approach developed on the computer.

1.2 Overview Of Thesis

The work presented in this thesis can be conveniently subdivided into two areas, covering each of the objectives outlined above.

The analysis of the response to spatially varying seismic excitation is presented in chapters two to five. Chapter two outlines the concept of spatially varying seismic excitation, and reviews previous work on the analysis of suspension and cable stayed bridges, and the representation of seismic excitation. It is concluded from this review that a power spectral approach is most favourable, and this is developed in chapter three where the theoretical background is considered and the major assumptions outlined. Chapter four then presents the analysis of a simple portal frame which was

used to validate the approach; the statistics of the response to asynchronous excitation were calculated using the power spectral approach developed in chapter three and were compared with the results from a set of time history analyses. Finally, chapter five describes the results obtained from using the method to analyse the response of a typical cable stayed bridge to travelling earthquake excitation. These results were then used to determine the key factors that influence the response to travelling seismic excitation and to assess the importance of assuming stationarity in the power spectral analysis.

The second area of the work, the response of Kessock bridge to wind excitation, is contained in chapters six, seven and eight. Chapter six introduces the concept of wind loading and discusses its significance for long span bridges. It then reviews previous work on modelling the response of bridges to wind excitation and on prototype testing. Chapter seven describes the monitoring program on Kessock bridge, outlining the aims of the exercise and the experimental methods used. It presents the detailed finite element modelling of the bridge, and compares predictions of the dynamic properties with the findings of a modal survey. Finally chapter eight presents the results of the prototype testing and discusses their implications on the relevance of the spatial variation of wind loading to cable-stayed bridges.

Chapter nine concludes the thesis by presenting an appraisal of the work together with final conclusions and suggests areas for further study.

Chapter Two

The Response Of Cable Stayed Bridges To Seismic Excitation: A Review

2.0 Introduction

It was mentioned in chapter one that cable stayed bridges are subject to several forms of dynamic loading, one of which is seismic excitation and this will form the subject of the first part of this thesis. Hence, the ideas followed for the response to seismic excitation underlie all the subsequent research including the work on the response to wind excitation. Therefore, before proceeding to outline the method developed in this thesis to analyse the response of cable-stayed bridges to spatially varying seismic excitation, it is necessary to look at the work which has been carried out by other researchers in the field. What methods have they used, and why? How do their results influence the aims of this research? What are the major omissions from the published work? What can be learned from the response of other extended structures to travelling or spatially varying loads? The answers to these and other similar questions directed the research presented in this thesis, and will show the reader why particular approaches were adopted.

The purpose of this chapter is to review the literature relevant to the response of cable-stayed bridges to spatially varying seismic excitation, and in doing so answer some of the questions that were posed above. It will start by considering the representation of seismic loading, looking briefly at the history of earthquake engineering and outlining the principal methods of modelling seismic excitation and comparing the approaches that have been adopted down the years. It will then move on to consider the effect of spatially varying seismic loads, how they can be modelled

and their effect on structures. Here it will present an overview of the methods published for the analysis of the response to spatially varying excitation. Finally, it will consider the static and dynamic analysis of long span bridges, both suspension and cable stayed bridges, and present their response to travelling seismic excitation. The conclusions from this chapter will then set the direction for the subsequent studies.

At this point it must be noted that there is a vast literature on these subjects and the author is fully aware that it is only possible to scratch the surface in the limited space available here. For example, a bibliography on cable-stayed bridges [Narayanan *et al.* 1987] supplies a total of 850 references, many of which would merit inclusion here. There is a similar number of references available on the representation of earthquake loading, and again on the methods of analysing the response to earthquakes. Therefore, this review does not claim to be exhaustive, but aims to present a sound overview of relevant topics which will both help the understanding of, and explain the direction of, subsequent chapters.

2.1 Earthquake Representation

There are several causes of seismic excitation; underground explosions, volcanic activity, subsidence of mine workings, impounding of large dams or movements along faults in the Earth's crust. The last is of course the major cause of damaging earthquakes and consequently much work has been done to model the source of these events and describe the ground motions which result. The study of earthquakes, including both the source events and the propagation of the wave front, is a subject in its own right, the science of seismology, and is only of passing interest here. Of more importance for the work in this thesis, and for the practising engineer, is a reliable representation of the loads that these ground motions will impose upon a structure.

However, finding such a reliable representation is complicated by three factors. Firstly, there is a paucity of earthquake data available, although this is being reduced year by year as more earthquakes are recorded. Secondly, even if sufficient past earthquakes had been recorded, earthquakes of the future will not necessarily bear any relation to those of the past. Thirdly, because earthquake motions represent random or pseudo-random processes, two earthquakes with similar energy and frequency content can have very different effects on a particular structure. There have been many attempts to overcome these problems and Vanmarcke [Vanmarcke 1976] divides them into three major classes; response spectra, artificial time histories and power density spectra.

2.1.1 Response Spectra

One approach to overcome the difficulties outlined in the previous section is to define the earthquake in terms of the peak response it causes in a single degree of freedom system. Since this will be a function of both the system damping and the natural frequency, the model produced must also be a function of these factors. The result is known as the response spectrum and was introduced in the 1930's and 1940's [Benioff 1934, Biot 1941]. The approach was developed as a design tool by Housner who combined the response spectra for several earthquake records into a design response spectrum by drawing an envelope function around the major peaks. This allowed the influence of different earthquakes to be considered in a more robust manner than simply averaging the spectra. The response spectrum approach is especially suited to design applications as it allows a simple modal type of analysis to be used. The response in a given mode is assumed to be a single degree of freedom system, and the peak response in this mode can then be obtained directly form the design response spectrum. The response of the different modes is then combined to give the total response of the structure. The simplicity of this approach accounts for

the popularity of the response spectrum method in design codes. However, a further advantage arises because the response spectrum of a single degree of freedom system represents an harmonic oscillator. The peak acceleration, velocity and displacement response can then be read directly off the same graph (figure 2.1).

2.1.2 Generation of Artificial Earthquake Time Histories

Another approach to overcome the lack of earthquake time histories is to create artificial records and calculate the structural response directly from these using numerical methods. This approach has been greatly helped by the advance in computing technology which has enabled both the creation of records and the subsequent calculation of structural response to be performed more quickly. However, the necessary calculations are still time consuming, especially when they have to be repeated to overcome the problems associated with the random nature of the response. It is convenient to consider this approach under two sub headings, generation from stochastic models and generation from seismological models, although this division is somewhat arbitrary since many seismological models have a stochastic basis and vice versa.

2.1.2.1 Stochastic Models

As with the response spectra discussed above, G. W. Housner is much cited in the literature as being a pioneer in developing the synthesis of artificial earthquake time histories. He suggested the phenomenological model in which the seismic waves are considered to be generated by irregular slippages and then subjected to many random reflections and refractions. This model justifies the assumption that the earthquake time history can be treated as a random process and the likely nature of an earthquake described by a probabilistic model. Such a probabilistic model

can then be used to generate many realisations of the process. The simplest approach of this kind was to model the excitation using white noise [Bycroft 1960]. Bycroft used an analogue computer to generate band limited white noise records of thirty seconds duration, and then compared these with actual earthquake records by calculating response spectra. He obtained reasonable agreement between the sets of data and was satisfied with the white noise model. White noise is in fact a stationary shot noise, and can be considered as the superposition of a series of delta function processes; it therefore fits in with the original Housner paradigm. However, Rosenblueth [Rosenblueth & Bustamente 1962] proposed a more detailed model giving a definite wave shape to the pulses. The response spectra obtained from this type of excitation again showed good agreement both with those obtained from other synthetic earthquakes and from actual earthquake records.

There are two major drawbacks with the random pulse models described above, and especially the white noise model. Firstly, white noise has a uniform frequency content which does not accurately represent the frequency content of recorded data. Secondly, real earthquakes are non stationary events, they have a finite length and their statistics change during this period. To overcome the first problem more advanced models were developed that calculated the time history from a power spectrum obtained from recorded data; this was equivalent to filtering the white noise representation. One of the most widely used models is the Kanai-Tajimi filter which was proposed by Tajimi [Tajimi 1960] and made use of the results of investigations into the frequency content of recorded earthquake records [Kanai 1957, Kanai 1961]. However, it needs to be noted that the Kanai-Tajimi model includes a finite acceleration response at zero frequency which is clearly wrong as it corresponds to an infinite ground displacement. Therefore, the filter is often modified to remove the low frequency components [Clough & Penzien 1975].

The problem of non stationarity was addressed by further modulating the filtered white noise in the time domain using a window function. Much of the work which has been done to improve the modelling of non stationarity in synthetic earthquakes has been based on the theory of evolutionary spectra presented by Priestly [Priestly 1965 & 1967] in which the power density spectrum is modulated using a deterministic time domain function. The early work of Bycroft and others using simply white noise implicitly assumed a rectangular or box car window to give the required duration. Simple improvements to this were made by using trapezoidal windows but a more realistic exponential window function was proposed by Shinozuka [Shinozuka & Sato 1967] for synthesising ground motion using the Kanai-Tajimi filter. Amin [Amin & Ang 1968] pursued a similar approach, and used the time histories obtained to investigate structural reliability. Their results indicated both the presence and importance of non stationarity in earthquake records, and the need to consider the full earthquake record, not just the period of maximum ground acceleration. They identified three phases of the ground motion; starting, strong and final; and used these to define an appropriate time window. They also compared filtering the white noise using first and second order filters, and found that a second order filter (such as the Kanai-Tajimi model mentioned above) was essential to represent the earthquake adequately.

The approaches discussed in the previous paragraph improved the original filtered white noise models, however the time variation was restricted to the amplitude of the signals. In contrast, both observations of actual earthquakes and seismological models indicated that there were variations in the frequency content, as well as amplitude, with time. Hence, the next step was to introduce a time variation of the frequency content of the earthquake. Saragoni [Saragoni & Hart 1974] suggested dividing the time domain into three contiguous time regions and defining a

unique power density spectrum for each of them. This approach was successful in simulating artificial earthquake motions which possess a time variation both in amplitude and frequency, although, as later researchers were to point out, the resulting seismograms contained discontinuities at the junction of time regions. A further refinement of the Kanai-Tajimi model was presented by Lin [Lin & Yong 1987] in which the results from an evolutionary Kanai-Tajimi model incorporating both non stationary amplitude and frequency were compared with more complicated models assuming an elastic or Maxwellian material model. The seismograms generated from the evolutionary Kanai-Tajimi model bore a closer resemblance to records from the Mexico 1985 earthquake than those generated from the more complicated models. A further study using the records of the 1985 Mexico earthquake [Grigoriu et al 1988] again emphasised the importance of taking account of the variation in frequency content with time. The results showed that ignoring the frequency variation could lead to a significant underestimate of structural response. A more rigorous instantaneous power spectrum interpretation was used by Yeh [Yeh & Wen 1990] to simulate ground motions for the study of the behaviour of non linear structural response. Random vibration and Monte Carlo approaches were used and both lead to realistic results.

Another problem that remains with the time modulated models, including those that allow the frequency to vary, is an error in the low frequency response which occurs because the envelope function itself has a low frequency component. Safak [Safak & Boore 1988] discussed the implications of this and found that significant errors could arise in structures that had natural periods longer than the source duration of the earthquake. Comparisons were made between uniformly modulated filtered white noise and filtered shot noise; these two models differ in the order in which the filtering and modulation are applied. The results indicated that the filtered

shot noise avoids the systematic low frequency errors associated with the filtered uniform white noise models.

A more detailed review of the engineering modelling of ground motion was presented to the 9th World Conference on Earthquake Engineering by Masanobu Shinozuka [Shinozuka 1988] and this gives a fuller reference list for the work discussed in this section.

2.1.2.2 Seismological Models

The methods described above have essentially been an engineering solution to the problem of modelling earthquake excitation. As Shinozuka points out [Shinozuka 1988] there is an essential difference between the models created and used by engineers and those created by seismologists. Yet many of the engineering methods have a seismological basis to them, be it the original paradigm proposed by Housner or the more detailed models used by some other researchers [Lin & Yong 1987]. In more recent times the models of earthquake excitation have become considerably more complicated, as explained by Shinozuka, and a review of the development of the latest approaches is given in a state of the art report by Aki [Aki 1988]. It is not relevant here to discuss in great detail the advances in these models, but only necessary to note their existence.

2.1.3 Power Density Spectra

The third approach to modelling the earthquake ground motion is to represent it by its power density spectrum. This approach is very closely related to the stochastic models outlined in §2.1.2.1, however rather than use the stochastic models of the random process to generate artificial time histories, the power density spectra of the processes are used directly. The power density spectra of the structural response are then found via a frequency domain analysis, and

random vibration theory used to calculate the response statistics. There is therefore a clear link with the stochastic models discussed above, many of which used power density spectra to define the ground motion, for example the Kanai-Tajimi spectrum. In the field of aseismic structural design an important statistic is the expected time for a given response to exceed a certain barrier level, the first passage problem. This can be used to assess the reliability of a structure, and estimate the probability that a structure will fail during a design earthquake. The development of this theory is outside the remit of this chapter, and will not be reviewed here. However it should be noted that the first passage problem has been considered both for stationary [Vanmarcke 1975, Der Kiureghian 1980] and non stationary [Corotis *et al* 1972] random processes. Again, as with the time history methods, it is essential to take account of both the evolutionary nature of the problems and also the random nature of the excitation.

Many authors have applied these theories to the solution of problems of earthquake loading on structures. However, these random vibration approaches rely on calculating the spectral moments of the response which are found by integrating its power density spectrum. Therefore, these methods rely on evaluating a set of integrals, many of which are far from simple, and not many of which can be solved analytically. Langley [Langley 1986] derived equations for the spectral moments of the structural response in terms of the Hilbert transform of the response process. These were then integrated numerically to obtain estimates of the survival probability of a structure subjected to a uniformly modulated Kanai-Tajimi earthquake excitation. The results obtained compared well with results for the same structure published by other authors. Borino [Borino *et al* 1988] derived similar expressions for the non stationary spectral moments of a structure subject to earthquake excitation. Here, a complex evolutionary spectral matrix was defined which again contained the Hilbert transform of the response process. This paper

identified the need for this complex matrix, and the Hilbert transform, arose because the envelope process was considered in evaluating the first passage problem. As in the paper by Langley, the integral expressions for the spectral moments were evaluated by numerical means.

However, not all authors recognise the need for such detailed analysis. Zembaty [Zembaty 1988] produced realistic solutions to the first passage problem when investigating the influence of strong motion duration on the response of a single degree of freedom system by applying more basic expressions originally suggested by Yang [Yang 1972]. The same approach was used by Quek [Quek *et al* 1990]. In this paper they used a seismological model for the earthquake power density spectrum and considered modulation by both an exponential and boxcar type of window. The structural response to the evolutionary ground model was found and closed form solutions for the modulating function of the response obtained for each ground window type. The results were used in a reliability analysis, and the predictions of peak response used to obtain the response spectrum by calculating the expected peak response of a single degree of freedom system for various frequencies. A final, and important, conclusion to come out of this paper was that using a stationary approximation to the ground motion resulted in a conservative approximation to the true response.

Finally, it needs to be noted that the power spectral approach can be applied to many other areas of structural dynamics, such as wind excitation. To [To 1982] presented closed form expressions for the evolutionary spectral and cross spectral densities of the response of a structure to non stationary random excitation modelled as an evolutionary process. He then applied these equations to both a single degree of freedom system and a ship board antenna system which was modelled as a MDOF system. This study was complemented in a subsequent paper which

presented the time dependent variance and covariance of the response [To 1984] of the same antenna system to non stationary random excitation.

2.1.4 Concluding Remarks On Ground Motion Representation

The above outline of ground motion representation methods suggests that the main aspects that need to be considered in the modelling of earthquake ground motions are their random nature and their lack of stationarity. We must now compare the three methods that have been described and decide which of them is the most appropriate for use in this thesis. The first method described, the response spectrum, is essentially a design tool and therefore incorporates a simplification both of the ground motion and the response calculation technique. Although it might be argued that work ought to concentrate on approaches that are suitable for design as these are likely to be most relevant to practising engineers, it is thought that over simplification of the problem is inappropriate for the work in this thesis. Furthermore, as will be discussed below, there is a growing body of belief that random vibration methods have a significant contribution to make in design. It is also thought that a detailed seismological model of the ground motion would be too complex for this study and therefore a stochastic representation, either in the time or frequency domain would be preferred.

An important factor that must be considered in making the decision between these two alternatives will be the calculation procedures associated with each method. The time history approach requires the integration of the equations of motion or the evaluation of the Duhammel integral; both procedures can be computationally expensive. Moreover, since the ground motion is random, this expense will be amplified by the need to carry out repeated calculations to find the response statistics. However, the Duhammel integral is a convolution, and by the convolution

theorem a convolution in the time domain is equivalent to a multiplication in the frequency domain. Hence, if a frequency domain representation is used the calculation procedure is greatly simplified, and the need to repeat the calculations is removed since the random vibration approach allows the statistics of the response to be found directly. Therefore, it is far more efficient to use the power density spectrum to represent the earthquake ground motion. However, the frequency domain approach has a major drawback, it assumes that the problem is linear. This of course will not be the case with many structures, especially if ultimate load conditions are being analysed. In contrast analysis in the time domain allows a full non linear model to be used.

In the light of the foregoing discussion it is decided to implement a model which uses the power density spectrum to represent the ground motion, and to use random vibration analysis in the frequency domain to calculate the statistics of the response. This approach has some applications in design, several authors now recommend the power spectral approach in preference to the response spectrum for design [Christian 1989]. However, the problem of non linearity will have to be overcome, though it will be seen later that this is not a major problem for cable stayed bridges.

2.2 Spatially Varying Seismic Loads

Having looked at the various approaches to modelling earthquakes in general it is now necessary to focus more sharply on the aspect of spatial variations in seismic excitation. To do this, the main factors that give rise to the spatial variations will be outlined, and then some of the models that have been developed in recent years will be discussed. Finally, the way that these models have been applied in the analysis of the response of simple structures to spatially varying seismic

excitation will be reviewed, and conclusions drawn that can be applied to the subsequent work in this thesis.

2.2.1 Causes of Spatial Variations in Seismic Loading

There are three major causes of ground motion variability, and these have been summarised as follows [Der Kiureghian & Neuenhofer 1992]:

a. difference in the arrival times of seismic waves, the "wave passage" effect

b. loss of coherence due to reflection and refraction, the "incoherence" effect

c. differences in local soil conditions, the "local" effect.

The wave passage effect arises because the energy released in a seismic event radiates from the source in the form of waves; body, shear and pressure waves through the Earth's crust, and Rayleigh and Love waves along its surface. These waves move with a finite velocity, and therefore they take a finite length of time to pass between two given points on the Earth's surface. Hence, the excitation felt at these points at any given time will be different. Consequently, for a structure which has widely spaced supports, such as a long span bridge, the excitation at each point of support will be different. Since this difference in excitation is caused by a time delay this phenomenon is known as asynchronous excitation.

However, the wave propagation model on its own is too simple to describe the spatial variations in the ground motion fully. In reality, the Earth's crust is not a uniform homogeneous medium and stress waves passing through it are subject to many and varied reflections and refractions due to these changes in geology. Topographic changes, such as valleys and ravines, influence the passage of surface waves which undergo defraction as well as reflection and refraction. The

situation is further complicated by the distributed nature of the source for real earthquakes where slippage occurs over a large area of a fault. The ground motion at a point on the Earth's surface is the superposition of many waves arriving from many sources via many different routes and so there is a rapid loss of coherence with only a small change in spatial position. It is interesting to note the similarity here with the non stationary nature of the frequency content of an earthquake discussed above; the two problems are closely related.

The final source of spatial variability in the seismic excitation is due to local variations in the soil conditions. These soil conditions greatly influence the size of the excitation experienced at a given location since different soil conditions can lead to both amplification and attenuation of the underlying ground motion. For example, the magnitude of ground motion may vary between different locations across the floor of a valley if the depth of alluvial deposits varies. Both the local and incoherence effects give rise to apparently independent excitations at the supports of extended structures and the resulting phenomenon is often termed multi support excitation.

2.2.2 Models of Spatially Varying Seismic Excitation

Early models of spatially varying ground motion for use in aseismic design were often rules of thumb based on intuitive ideas of wave propagation. Christian [Christian 1976] compared the results from five of these rule of thumb approaches with the recorded data from three historical earthquakes and found that all but one were conservative. However, these rules of thumb are by necessity over simplifications of the real situation; a more detailed analysis was presented by O'Rourke [O'Rourke *et al* 1982] who proposed a method for calculating the apparent propagation velocity of seismic waves. His approach accounted for several important factors including the predominant direction of excitation, the type of wave and the overall propagation direction. The

method was then applied to data from the 1971 San Fernando Earthquake and the 1979 Imperial Valley earthquake, and produced shear wave velocities for the latter event which compared well with those calculated from epicentral distances and travel times.

The major drawback with all the early models of spatially varying ground motion was the lack of sufficient raw data to validate them. The two studies discussed above had to make use of data collected from seismographs that had not been installed with the express purpose of measuring spatial variations in the seismic loading. Therefore, the locations of the instruments were determined by other factors, some were positioned in the basements of buildings others in the "free field", and no attempt was made to ensure that the local geology was similar. As a result, only crude comparisons could be drawn between the recorded events and only wave propagation effects were considered. Bearing these points in mind, perhaps the most important step taken to obtain models of the spatial variations in seismic loading was the installation of the SMART 1 array. The SMART 1 strong motion array at Lotung in Taiwan consists of a central instrument station, with 12 stations arranged at equal intervals around each of three concentric rings [Bolt *et al.* 1982]. The results from this array have been used by various authors, not only to model the wave propagation effect but also to propose spatial coherence models.

Loh [Loh *et al.* 1982] used the results of data collected from the array to perform analyses of the response of multiply supported structures to spatially varying ground motion. A particularly interesting set of results was obtained for a single degree of freedom system with two points of support. The ratios of the response of this system to spatially varying ground motion compared to the response to uniform excitation was to produce a "response spectrum" type model of the excitation. In a later study [Loh & Yeh 1988] the results from the SMART 1 array were used to propose a space time stochastic model of the ground motion taking account of source

characteristics as well as the wave passage and incoherency effects. An underlying assumption in this analysis was that the ground excitation could be considered as a multi dimensional space time random field. Calculations of spatial correlation functions, frequency wavenumber analysis and coherence analysis were each used to process the data and the results of the different methods compared. Significantly the results from the frequency wavenumber analysis showed that for a given frequency the ground motion is concentrated around a single wavenumber indicating that the spatial variation is dominated by the wave passage effect. The different types of seismic wave were identified and treated separately; for each type the propagation direction and velocity were identified, the latter being estimated from arrival times. For the following discussion it is interesting to note from these results the high velocity values and large spread of velocity estimates.

Harichandran [Harichandran & Vanmarcke 1986] also suggested a two dimensional random field representation on the basis of SMART 1 results, but chose to describe the event in terms of coherence (incoherence effect) and phase (propagation effect) spectra. Their investigation of lag times showed, as with the work of Loh, that the waves tend to propagate as line fronts and therefore the predominant effect was wave propagation. Again large velocities were calculated and the authors concluded that propagation occurred principally through the bedrock, the ground motion itself being caused by shear waves propagating almost vertically through the overlying soil. The results indicated that a simple correlation structure that assumed that the time and space domains were independent was inadequate, as was a representation combining deterministic propagating waves with stochastic noise. The ground motion model proposed made use of a completely random field superposed on a deterministic wave propagation model.

Zerva [Zerva 1992a] presented analysis which compared the response of extended structures to two spatial variability models. The first, based on SMART 1 data, was that of Harichandran and Vanmarcke cited above, the second, based on wave propagation through a random media, was proposed by Luco and Wong [Luco & Wong 1986]. The Clough-Penzien Spectrum was used to define the frequency content of the motion, and wave propagation effects were ignored. The results for both buried and above surface lifelines showed large discrepancies between the different models, especially for buried structures. In this case the response to the Harichandran model was much greater. The response for above ground structures was more comparable, but in this case the Luco model produced the greater response. As wave propagation was ignored, the differences were caused by different rates of coherence loss and therefore the results must be interpreted with care. For a buried structure, the relative displacements are most important, and so the model which gives the greatest loss of coherence over the given length will produce the largest response. For above ground structures, the direction of shaking, the structural mode shapes and the frequency of the excitation all influence whether it is coherent or incoherent base excitations that will produce the greatest response. It is therefore very unwise to draw conclusions from a single model.

2.2.3 Structural Response to Spatially Varying Seismic Excitation

The analysis of the response of structures to spatially varying seismic excitation is well known and the basic theory in which the matrix equations of motion are partitioned into ground and response degrees of freedom is presented in standard text books [Clough & Penzien 1975]. The aim of this section is to consider how different solution schemes have been applied to these equations, and more especially how the different ground motion models have been used. The results of the different studies will not generally be discussed in detail. As mentioned above these

will be specific to particular structures and ground motion models, and so only the general results will be commented on. It should also be noted that the response of suspension and cable-stayed bridges to spatially varying seismic excitation will be discussed separately later.

Clearly, until the advent of the more realistic space time models of ground motion obtained from field data taken from the SMART 1 array, only limited analyses could be performed. However, some important factors were noted. Werner [Werner *et al.* 1979] considered the response of a single span bridge mounted on a half space to travelling SH waves. Although the ground excitation was treated as band limited white noise, and only the wave propagation effect was considered, the results clearly showed the importance of the wave propagation direction. Altinisik [Altinisik & Severn 1981] used a time history approach to calculate the response to both multi support and asynchronous excitation. The method used was validated using an impulse type loading on simple structures (a beam and portal frame) and was then applied to finite element models of rock fill and arch dams using recorded time histories from the Port Hueneme and San Fernando earthquakes. A similar approach was subsequently used by Dumanoglu [Dumanoglu & Severn 1984] to predict the response of dams to purely asynchronous excitation. Here the responses of one and three bay portal frames were found for a range of propagation velocities, and then the same velocities were considered for embankment and gravity dams. The advantage of performing the analysis using time history records is that a complete solution accounting for the pseudo static as well as the dynamic response can be obtained directly. However, the last two references cited used a recorded time history from a real earthquake and therefore tell us only a limited amount about the behaviour of the structures themselves.

The availability of better space time models of the ground motion has now allowed more comprehensive studies to be carried out. In particular the stochastic models of ground motion

discussed previously have allowed several authors to apply the theories of random vibration to this problem, thus avoiding results that are specific to a given event. Both Monte Carlo simulations, using time histories generated from the stochastic models, and power spectral methods have been used effectively. The former has the advantage of allowing a complete solution to be obtained, including non linear effects, although it is computationally expensive. The latter is more efficient, although care has to be taken when combining the different components of the response. The total response is a combination of the response to excitation at different feet including dynamic with pseudo static components, and all relevant cross correlations have to be considered.

Zerva [Zerva *et al* 1988] applied random vibration theory to look at the response both of buried pipes and bridges modelled as simply supported beams using the power spectral approach. The spatial variations in the ground motion were found to be significant for pipelines but not for the bridges considered. However, a further study looking at bridge modelled as multi span beams [Zerva 1990] showed a significant effect in contrast to the earlier paper. In this study, an analytical approach to finding the power density spectrum of the beam response was derived and this spectrum used to obtain the response statistics. Most importantly she was able to conclude:

> *"Thus, fully correlated motions may produce higher or lower response than the one induced by partially correlated motions, depending on the dynamic characteristics of the structures, the position along the beams where the response is evaluated, the different quantities that are evaluated (bending moments or shear forces), the relative location of the natural frequencies of the beams with respect to the dominant frequencies of the ground motion as well as the degree of partial correlation between the support motions."*

The relevance of these conclusions to this study will be seen later in this thesis.

The conclusion that spatial variations in the seismic excitation do influence the response of beam like structures is supported by the work of Harichandran. He has shown that spatial variations in the ground motion can have significant effects on both simply supported [Harichandran & Wang 1988] and two span indeterminate beams [Harichandran & Wang 1990]. In these papers a power spectral random vibration model was used to describe the ground motion taking account of both wave propagation and incoherency effects. These papers showed the important rôle that interaction of the structural properties with spatial variations in the loading plays in determining the response. The latter paper, on the two span indeterminate beam, showed the importance of the cross correlations between the dynamic and pseudo static response, and also that complicated structures can adequately be treated using the finite element method. The finite element method represents a continuous structure as a multi degree of freedom system (MDOF) and in a subsequent paper Harichandran presented closed form solutions for an MDOF system subject to propagating seismic excitation [Harichandran 1992]. Finally at this point it is important to mention a paper by Perotti [Perotti 1990] in which the results of a random analysis of a viaduct were presented. This combined many of the features that have been commented on in previous sections as representing the strengths of the random vibration approach, to produce a reliability analysis of the response to spatially varying seismic excitation.

There has also been significant work done recently in developing response spectrum methods for the analysis of the response to spatially varying ground motion, mainly motivated by the use of response spectra in codes of practice and their consequent popularity with practising engineers. Rutenberg [Rutenberg & Heidebrecht 1988] produced a response spectrum method that modelled the wave passage effect in a deterministic manner. Although the authors believed their approach would produce conservative estimates for the response, the underlying assumptions and

neglecting of incoherence effects makes the method unattractive. The most promising work in this area has been done by authors who have tried to develop a response spectrum model out of the random vibration approach. Two key papers that discuss this work have been presented by Berrah [Berrah & Kausel 1992] and Der Kiureghian [Der Kiureghian & Neuenhofer 1990]. The former presents a method that uses power density spectra obtained from the ground spatial variability model to modify the values of the design response spectrum. An assumption that the excitation can be treated as a broad band process, effectively white noise, enabled the authors to simplify the equations resulting in an analytical expression for the response spectrum. This takes account of both the structural properties and the spatial variations in the load. This paper however fails to take account of the wave passage and local effects, and also neglects the pseudo static response and its cross correlation with the dynamic response. The second paper presents a full description of the power spectral method, including all the necessary cross correlations, for an analysis of the problem. It then suggests an iterative procedure for obtaining a power density spectrum from the design response spectrum thus enabling a power spectral analysis to be performed from a response spectrum description of the loading. This paper also investigates several of the different phenomena that influence the response of a structure to spatially varying loads.

To this point the discussion of the random vibration approach has concentrated almost entirely on the power spectral density method. However, as has been pointed out in §2.1.4 there are certain disadvantages in relying on this approach. These disadvantages are not present in the time history approach, although this is a computationally far more expensive method. Therefore, comment ought to be made regarding the use of the stochastic models of spatially varying ground motion to generate sets of artificial time histories. These sets not only avoid the problems

of using only specific time histories, but also allow non linear problems to be dealt with. Shinozuka [Shinozuka 1987] describes the generation of samples of a multi variate multi dimensional random field which could be applied to the generation of artificial earthquake ground motions. This approach is indeed taken up by Zerva [Zerva 1992b] who generates sets of earthquake records from a wavenumber frequency power density spectrum.

2.2.4 Concluding Remarks on Spatially Varying Seismic Excitation

In section 2.1.4 it was decided to adopt a power spectral random vibration approach to the analysis in this thesis. The literature discussed in the preceding sections has shown that this approach can be applied to the analysis of the response to spatially varying seismic loading. However, most authors have performed such an analysis in the frequency space domain making use of spatial correlation functions to define the input at each foot. This effectively only goes half way to a full power spectral analysis. The next step forward is perhaps to follow Zerva [Zerva 1992b] who used a two dimensional frequency wavenumber power density spectrum to calculate sample functions of a two dimensional random field. Independently the author thought it interesting and possibly beneficial to extend the spectral analysis approach to make use of a spectral representation of the ground motion in both the space and time domains. This is the method that will be followed in the rest of this thesis.

2.3 Bridge Analysis

Having discussed the different methods of describing the earthquake ground motion it is now necessary to review the methods of modelling cable stayed bridges. The rapid advances made recently in both computer technology and computer modelling techniques has revolutionised the

analysis of structures. However, reliance on black box computer techniques can lead to important structural concepts being ignored or misunderstood. Therefore, this section will start by considering some of the earlier analysis techniques before reviewing the more detailed finite element modelling that can now be performed. There are three factors that complicate the analysis of cable stayed bridges:

i. Their three dimensional nature: It would be convenient if these structures could be treated as planar systems, but to model the torsional behaviour, which is essential when considering the dynamic properties, it is necessary to consider a three dimensional analysis.

ii. The large degree of redundancy: In most cases, cable stayed bridges are highly redundant and the analysis must ensure compatibility between the tower deck and cables.

iii. Their non linear behaviour: Cable stayed bridges can exhibit considerable geometric non linearity; the deck girders are usually very flexible and so large displacements have to be considered and the cables impart large compression forces into both the towers and the deck. Since these members are also carrying large bending moments, the beam column effect can be important. Finally, sagging introduces a further non linearity in the stiffness of the cables.

There are many text books which address these problems in more detail than can be done here. Of these amongst the most thorough are those by Troitsky [Troitsky 1988], Podolny [Podolny & Scalzi 1976] and Walther [Walther *et al.* 1988].

2.3.1 Static Analysis Of Cable Stayed Bridges

Examples of cable stayed bridges date back to at least the 18th century, and perhaps the earliest example of their analysis is given by Navier [Billington & Nazmy 1990]. However, due to the complexities described above full analyses of these structures was not possible and hence they were not widely adopted as solutions to bridging problems. In more recent years their increased popularity has been matched by an increasing understanding of their behaviour as structures. The analysis of a cable stayed bridge is effectively that of a continuous beam on a series of elastic (cable) and rigid (pier) supports. The deflection of the elastic supports (cables) is related to the tower deflections, thus presenting the compatibility condition discussed above. This compatibility condition is evident in the analysis presented by B. S. Smith. He suggested a flexibility approach to the problem for bridges with both one [Smith 1968a] and two [Smith 1968b] planes of cables. The stiffness approach, which is the method used in most structural finite element analyses, was used by Lazar [Lazar 1972] and Tang [Tang 1971] who both treated bridges as plane frame problems. These analyses neglected the three dimensional nature of the problem and would have to be improved on to be of practical use. This was achieved by Baron [Baron & Lien 1973] who presented an analysis of a three dimensional model, making use of symmetry to make the reductions in problem size which were essential at that time.

As mentioned in the introduction to this section, other approaches to the analysis which use global approximations rather than the discretisation of the finite element approach have much to teach us about the structural behaviour. Hegab [Hegab 1986] proposed an energy method in which the deflected shape of the deck was described as a Fourier series. The cable forces and Fourier amplitudes were then found iteratively, and finally compatibility applied at the tower bases. However, this approach was only convergent for rigid towers and Aboul-Ella [Aboul-Ella

1988] subsequently improved the method to take into account both the flexibility of the towers and soil structure interaction. His results compared well with a finite element analysis, which also showed that non linear effects were not important; a conclusion which will be discussed further below. A different global approach to the analysis of cable stayed bridge was suggested by Lazar [Lazar *et al.* 1972] who developed a method of optimising either the bending moments or deflections of the deck girder. This was achieved by applying the principles of the load balancing method, used in the design of prestressed concrete, to calculate the required post tensioning force in the stay cables.

Finally mention must be made of some of the more recent finite element models that have been used to analyse cable stayed bridges. Finite element packages are now very powerful, and are routinely capable of taking account of geometric and material non linearities. Furthermore, they allow a detailed model to be analysed efficiently on a desk top PC. Nazmy [Nazmy & Abdel-Ghaffar 1990a] presented a full non linear analysis of a cable stayed bridge taking into account all the sources of non linearity discussed earlier. The results of the analysis showed that the geometric non linearities are very important, especially for the more modern bridges which are being designed with ever increasing spans. The bridge model showed significant hardening and the authors concluded that a full non linear analysis of the dead load condition must be performed at the very least, even if it is a precursor to a linear dynamic or live load analysis. This result is a contrast to that mentioned above and other literature is unclear about the real significance of the non linearities. Some authors side with Nazmy and recommend full non linear or combined non linear / linear analyses, whereas others are prepared to argue that a purely linear model produces adequate results. One of the areas of non linearity mentioned earlier was the cable sag and Kanok-Nukulchai [Kanok-Nukulchai *et al.* 1992] presented three methods of modelling this. The

first and most popular with other authors is the equivalent modulus approach. Here, the cable is modelled as a strut with a modified modulus of elasticity which is defined in terms of the cable geometry and the load. The other methods suggested by Kanok-Nukulchai were to represent the cables either as a series of links or as a curved finite element.

2.3.2 The Dynamic Analysis of Long Span Bridges

In this section both the dynamic behaviour of cable stayed and suspension bridge will be considered. Although there are major differences between the behaviour of these two types of bridge, the author believes that the large amount of work performed on suspension bridges provides a useful resource for planning the analysis of cable stayed bridges.

2.3.2.1 The Dynamic Analysis of Cable-Stayed Bridges

As will be apparent from the foregoing discussion of the static analysis of cable stayed bridges, the growth of computing power and computational techniques such as the finite element method have revolutionised the analysis procedure. Nowhere is this process more apparent than in the dynamic analysis of complex structures and almost all dynamic analyses of cable stayed bridges have been performed using finite element discretisation techniques. In this case the crux of the problem is to ensure an accurate representation of the structure in the finite element model, including the full torsional behaviour of the deck and the system non linearities. Fleming has presented non linear analyses for both the static [Fleming 1979] and dynamic [Fleming & Egesli 1980] response of these bridges. For the dynamic problem he presented an analysis of a simple two dimensional model that included the cable non linearity by using the equivalent modulus of elasticity approach described above. The response of the model to the El Centro earthquake was

then used to compare various combinations of linear and non linear analyses. It was concluded that an initial non linear static analysis was essential, but that subsequently a linear dynamic analysis would be adequate, a conclusion in broad agreement with the static study by Nazmy cited above. However, the literature is not in full agreement on this issue and other studies have shown that a fully linear analysis may be adequate. Wilson [Wilson & Gravelle 1991] came to this conclusion, although it must be pointed out here that the aim of his analysis was not to calculate the response of a bridge to a given earthquake but to predict the dynamic properties for comparison with the results of field investigations. Rajaraman [Rajaraman et al. 1980] attempted to quantify the non linear behaviour suggesting that non linearities could produce deviations of up to 20 % from the linear results.

A further and fuller discussion of the effect of non linearity on the response of these structures to earthquake loading has been presented by Nazmy [Nazmy & Abdel-Ghaffar 1990b, 1990c, 1992] and Abdel-Ghaffar [Abdel-Ghaffar & Nazmy 1991]. These papers present the theory and application of work which was carried out at the University of Princeton in the 1980's. The authors again conclude that at least a non linear dead load analysis is required and performed a full non linear analysis for a series of given earthquake records using direct time integration by Wilson's Θ method. This showed that non linearities could be important especially for longer spans where displacements are much larger. However, this analysis procedure is computationally intensive so they also used a transformation to a modal system of coordinates, a procedure first suggested for non linear analysis by Morris [Morris 1977]. This step is acceptable provided the degree of non linearity is small, otherwise the mode shapes would have to be recalculated at each time step. These reports also present some detailed results on the response of cable stayed bridges to spatially varying seismic excitation. They show quite clearly that both the asynchronous and

coherence effects play an important part in determining the maximum response and its likely location within the structure. However, as with the work described earlier, the use of specific earthquake time histories limits the generality of the results.

Other work which has also considered the response of cable stayed bridges to asynchronous seismic excitation includes the work of Garevski [Garevski *et al.* 1988, Garevski 1990]. He compared finite element prediction of the modal properties of a scale model of the Jindo Bridge with results obtained from testing on the six axis shaking table at the University of Bristol [Garevski *et al.* 1991]. His analysis of the response to asynchronous seismic excitation showed that the travelling wave effect was significant, especially for the tower response. Another aspect of his research considered the damping of cable stayed bridges and in particular the contribution of the cables to the overall structural damping. The dynamic behaviour of the cables and their influence on the bridge behaviour has been investigated in detail by Abdel-Ghaffar [Abdel-Ghaffar & Khalifa 1991]. Each cable was modelled by a whole series of elements allowing the detailed cable behaviour to be predicted as well as previously unobserved deck / tower / cable interactions. These interactions and the complicated modes which cannot be predicted by the simple cable models used by other researchers were found to have a strong influence on the response to earthquake loading.

2.3.2.2 The Dynamic Analysis of Suspension Bridges

The aim of this section is to give passing reference to some of the work which has been done in the allied field of suspension bridge analysis, and mention will be made almost exclusively to the work of Abdel-Ghaffar and his collaborators. This is because the work that he has done covers all the major aspects of relevance to this study, starting with the formulation of the equations of

motion for a suspension bridge and their solution in finite element form [Abdel-Ghaffar 1978a, 1979, 1980 & 1982]. In these papers he derives the equations of motion for vertical, lateral and torsional modes of vibration from first principles and then uses a finite element approach to predict natural frequencies and mode shapes. In collaboration with Rubin he extends this work to look at the free vibrations of these structures taking into account their non linearity [Abdel-Ghaffar & Rubin 1983a, 1983b]. These two researchers also looked at the response of suspension bridges to travelling seismic excitation [Abdel-Ghaffar & Rubin 1982, 1983c, 1983d, 1984] work which was continued with Stringfellow [Abdel-Ghaffar & Stringfellow 1984a, 1984b]. An important point to note about this work is that a random vibration approach was used successfully for part of the analysis. Dumanoglu has also published similar work on the response of suspension bridges to travelling seismic excitation [Dumanoglu & Severn 1987], and also on a stochastic approach to calculating their response [Dumanoglu & Severn 1990]. However, these two aspects of the work had not been combined into a single stochastic analysis of the asynchronous loading problem.

2.3.3 Summary of Bridge Analysis

The foregoing sections have shown that there have been many approaches used to the analysis of long span bridges and that there are still some areas which need further investigation, such as the cable behaviour, and areas over which there is much disagreement, such as the relevance of non linearities in the system. However, the aim at this point is to select and justify a modelling technique that can be used for the job in hand, that is developing the power spectral approach to the analysis of spatially varying seismic excitation. Therefore, the analysis must be performed in the frequency domain and so the most suitable way forward is to use a linear finite element model. I believe that this is an acceptable simplification given the conflicting evidence of other

researchers and providing the limits on the applicability of the results are clearly stated and understood. I also believe that a simplified model of the bridge is acceptable for the development purposes and I propose to use a two dimensional planar representation. Again, this is justifiable, provided the model is only used for the development of the analysis procedures and that these can readily be extended to three dimensions when necessary.

2.4 Summary and Conclusions

The review of the literature presented in this chapter has shown the importance of randomness in earthquake ground motions and its consequent impact on the modelling of ground motion and the analysis of the aseismic response of structures. It has also shown that spatial variations occur in the seismic loading both due to the wave passage effect and the loss of coherence, and that these variations can be described in a stochastic manner. The spatial variation of seismic loading has been shown by various authors to be an important consideration in aseismic design and is therefore an important subject for study. The most efficient way of estimating the response of a system to these types of loads is with a power spectral analysis using the theories of random vibration. However, the cost of this efficiency is that the method is inappropriate for non linear systems. Fortunately, it is acceptable to treat cable stayed bridges as linear systems, at least for the dynamic part of the analysis.

As a result of this review I propose to develop an approach that uses a two dimensional power spectrum to describe the spatially varying seismic excitation, and to develop a power spectral analysis procedure to calculate the response statistics of a cable stayed bridge to such excitation.

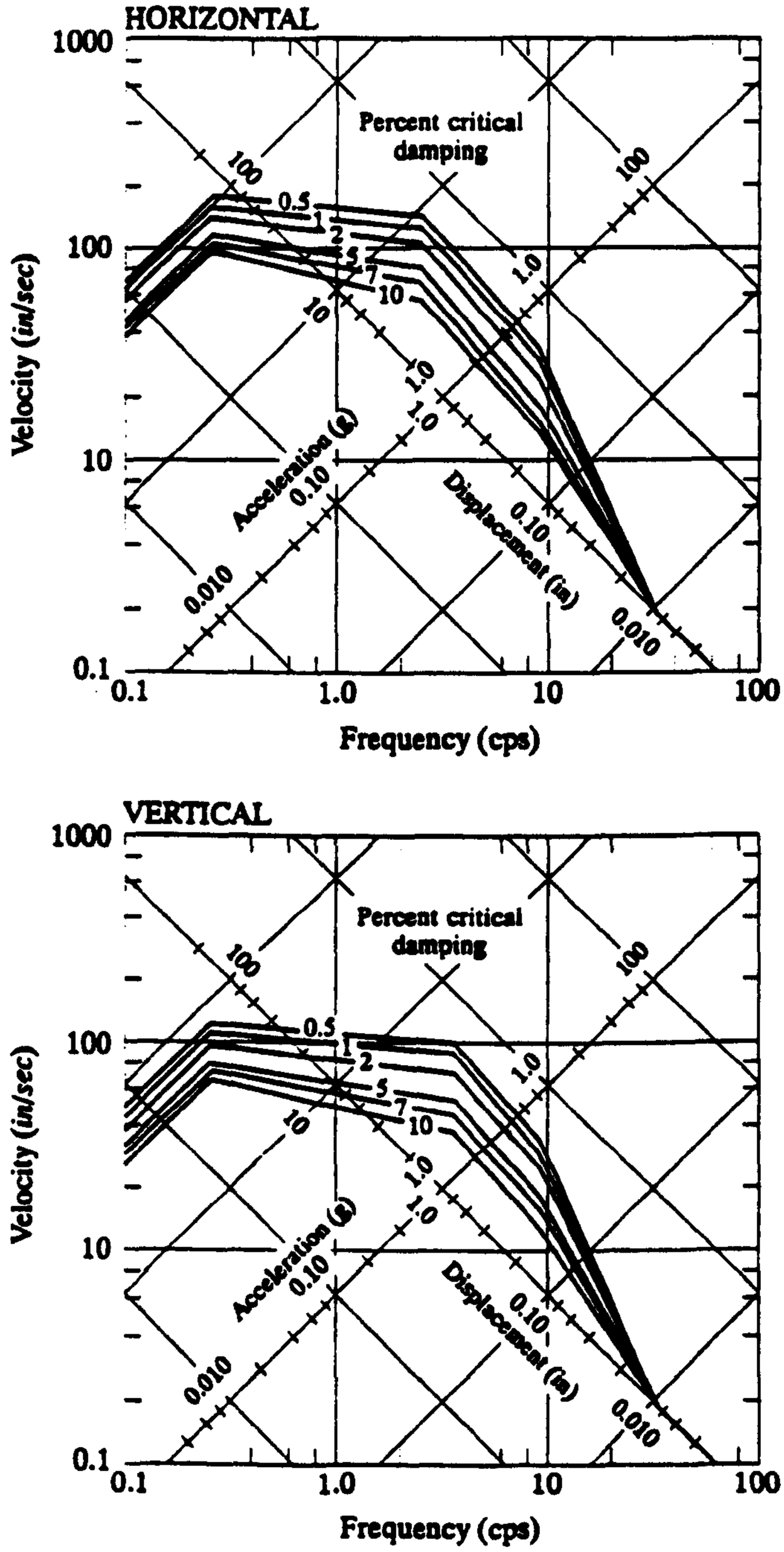

Figure 2.1 : Design Response Spectra (After Clough & Penzien 1975)

Chapter Three

The Power Spectral Analysis Of The Response Of Extended Structures To Spatially Varying Seismic Excitation

3.0 Introduction

In the previous chapter various approaches to dealing with the problem of seismic loading of cable-stayed bridges were discussed. It was concluded that because of the pseudo-random nature of seismic excitation, a statistical approach based upon calculating the power spectrum of the structural response should be used. To achieve this it is necessary to be able to represent the ground excitation, and its spatial variation, in the form of a power density spectrum. This can then be used in a frequency domain analysis to calculate the response using the structural properties.

The aim of this chapter is to present the background to this approach both by considering standard methods of power spectral analysis, and by discussing the modifications necessary to apply it in this situation. Firstly, the background to stochastic analysis will be discussed and the concept of the random field introduced as a means of describing the spatially varying seismic load. Then the analysis of the seismic loading of long span bridges will be presented, and the equations of motion derived as functions of both space and time. Next, methods of representing spatially varying seismic loads as random fields will be discussed. Finally, simplifications will be outlined to facilitate the implementation of these ideas in a computer programme.

3.1 The Stochastic Approach

In many branches of science and engineering the behaviour of a physical system is described by equations written in terms of variables or parameters. These variables and parameters represent the properties of the system, such as mass, displacement etc. However, it is rare for these quantities to be known exactly for a given physical system, and this introduces an element of uncertainty into predictions made using these equations. This uncertainty is especially prevalent in engineering design, where neither the system properties nor the applied loads are known precisely. Furthermore, the models used in design to predict the structural behaviour rely on assumptions which introduce yet more uncertainty into the answer. The level of available knowledge and consequent uncertainty involved in modelling the seismic loading of a long-span bridge is illustrated in table 3.1. One approach to deal with these uncertainties is to use the ideas of probability and statistics to predict the likely properties and behaviour of the system. In order to follow this approach further it is therefore necessary to be able to describe the system, its response and the applied loads in a probabilistic way.

3.1.1 Random Variables

The first step in developing a stochastic model for a given system is to find a method of describing the random quantities. Consider a simple experiment with an uncertain result, such as tossing a coin. There are two possible outcomes, heads and tails, which form the *sample space*. The outcome of this experiment can be described by a *random variable*, X, which maps the sample space onto a *range space*, say 1 and 0:

$$\begin{aligned} X(Heads) &= 1 \\ X(Tails) &= 0 \end{aligned} \quad \text{.....(3.1)}$$

More formally a random variable is defined as follows:

A random variable $X(\omega), \omega \in \Omega$, *is a function defined on a sample space* Ω , *such that for every real number x there exists a probability* $P[\omega: X(\omega) \leq x]$ [Lin 1967].

The experiment of tossing a coin is somewhat trivial but the same ideas can be applied to more general engineering problems, for example the displacement of the mass in a single degree of freedom system (figure 3.1). Here the mass can take up a range of positions which form the sample space. If each position is then described by measuring its distance from a datum, say the equilibrium position, then a random variable is introduced which maps the position of the mass onto the range space of all possible displacement values. A random variable is defined or described in terms of a probability function if it is discrete, i.e. if the range space is finite or countably infinite, or a probability density function if it is continuous. The random variable therefore provides the means of modelling the uncertainty in the state of the system being considered.

3.1.2 Random Processes

Random variables can be used to describe uncertain parameters, such as the displacement of the single degree of system considered above. However, in structural dynamics, the response of a system also varies with time, and for each point in time there will be a corresponding random variable. This series of random variables forms a random process dependent on the parameter time. More formally a random process is defined as:

A random process is a parametered family of random variables with the parameter (or parameters) belonging to an indexed set (or sets) [Lin 1967].

Just as a random variable is defined by its probability or probability density function, a random process is also described by its probability structure. A continuous random process will then be

defined by joint probability density functions of the range space of the random variables and the parameter:

$$p_{\{x\}}(x_1,t_1)$$
$$p_{\{x\}}(x_1,t_1;x_2,t_2) \qquad \text{.....(3.2)}$$
$$p_{\{x\}}(x_1,t_1;x_2,t_2;\ldots;x_n,t_n)$$

It is usual to describe a random variable by statistical measures such as its mean or standard deviation. Similar statistical parameters are also used to define random processes and most useful of these are the moment and cumulant functions. The moment functions are defined as follows:

$$E[X(t_1)] = \int_{-\infty}^{\infty} x\, p_{\{x\}}(x_1,t_1)dx$$
$$E[X(t_1)X(t_2)] = \int_{-\infty}^{\infty}\int_{-\infty}^{\infty} x_1 x_2 p_{\{x\}}(x_1,t_1;x_2,t_2)dx_1dx_2 \qquad \text{.....(3.3)}$$
$$E[X(t_1)X(t_2)..X(t_n)] = \int_{-\infty}^{\infty}\int_{-\infty}^{\infty}\ldots\int_{-\infty}^{\infty} x_1 x_2 ..x_n p_{\{x\}}(x_1,t_1;x_2,t_2;..;x_n,t_n)dx_1dx_2\ldots dx_n$$

Although all the moment functions are needed to describe a random process fully, in most physical situations it is sufficient to use just the first two and these are then given special names, the mean and the auto correlation functions:

$$E[X(t)] = \mu_x(t)$$
$$E[X(t_1),X(t_2)] = \varphi_{xx}(t_1,t_2) \qquad \text{.....(3.4)}$$

The cumulant functions are defined by the following expressions:

$$\kappa_1[X(t_1)] = E[X(t_1)]$$
$$\kappa_2[X(t_1)X(t_2)] = E[\{X(t_1)-\mu_x(t_1)\}\{X(t_2)-\mu_x(t_2)\}] \qquad \text{.....(3.5)}$$
$$\kappa_n[X(t_1)X(t_2)..X(t_n)] = E[\{X(t_1)-\mu_x(t_1)\}\{X(t_2)-\mu_x(t_2)\}..\{X(t_n)-\mu_x(t_n)\}]$$

As with the second moment function, the second cumulant function is also given a special name, the auto-covariance function, and is related to the auto-correlation function by:

$$\kappa_{xx}(t_1,t_2)=\kappa_2\left[X(t_1)X(t_2)\right]=\varphi_{xx}(t_1,t_2)-\mu_x(t_1)\mu_x(t_2) \quad \text{.....(3.6)}$$

3.1.3 Homogeneous Random Processes

As mentioned above, each of the statistics describing a random process are defined in terms of the parameter, t. Now, if these statistics remain constant with a change in parametric origin then the process is described as strongly homogeneous, and several simplifications can be made. For a time parametered process this means that the statistics remain constant for all time; hence the term stationary is used to describe homogeneous time parametered processes. In practice this condition is not often met, and even when it is, it is difficult to prove. However, if the first and second order statistics are parameter invariant, then this is sufficient to make the more important simplifications. In this case the process is described as weakly homogeneous or weakly stationary.

3.1.3.1 Power Density Spectra

Perhaps the most important simplification which can be made for an homogeneous or weakly homogeneous process is that the auto-correlation function can be expressed as a function of the parametric separation of the random variables:

$$\varphi_{xx}(t_1,t_2)=\varphi_{xx}(t_1,t_1+\tau)=R_{xx}(\tau) \quad \text{.....(3.7)}$$

The Wiener-Khintchine theorem states that for a weakly stationary random process the auto-correlation function is related to a new quantity, the power spectral density function, by the Fourier transform pair:

$$S_{xx}(\omega) = \frac{1}{2\pi}\int_{-\infty}^{\infty} R_{xx}(\tau)e^{-j\omega\tau}d\tau$$
$$R_{xx}(\tau) = \int_{-\infty}^{\infty} S_{xx}(\omega)e^{j\omega\tau}d\tau \qquad \text{.....(3.8)}$$

The power spectral density function, or power spectrum, represents the distribution of power in a random process across the frequency domain and is a very powerful tool for analysing random processes; for a dynamic problem it allows the analysis to be performed in the frequency domain which is computationally more efficient than the time domain, and it allows the statistics of the response to be predicted using spectral moments.

Two further points need to be noted. Firstly, there are expressions analogous to equations 3.3 and 3.5 which describe the correlation structure between two different random processes and these lead to expressions for the cross correlation function:

$$\varphi_{xy}(t_1,t_2) = E[X(t_1)]E[Y(t_2)] = R_{xy}(t_2 - t_1) = R_{xy}(\tau) \qquad \text{.....(3.9)}$$

and the cross spectral density function:

$$S_{xy}(\omega) = \frac{1}{2\pi}\int_{-\infty}^{\infty} R_{xy}(\tau)e^{-j\omega\tau}d\tau$$
$$R_{xy}(\tau) = \int_{-\infty}^{\infty} S_{xy}(\omega)e^{j\omega\tau}d\tau \qquad \text{.....(3.10)}$$

Secondly, it is often useful to calculate the power spectral density function of a random process from its Fourier transform:

$$S_{xx}(\omega) = E[X(\omega)X^*(\omega)] \quad \text{.....(3.11)}$$

although for a stationary process this should more correctly be expressed in terms of the finite Fourier transform [Bendat & Piersol 1971, Lin 1967]:

$$S_{xx}(\omega) = \lim_{T \to \infty} \frac{1}{T} E[X(\omega,T)X^*(\omega,T)] \quad \text{.....(3.12)}$$

This is because infinite range Fourier transforms do not exist for stationary data which are theoretically infinite, and therefore not absolutely integrable, in the time domain.

3.1.3.2 Spectral Moments

It is possible to draw an analogy between the probability density functions used to describe a continuous random process and the power spectral density function. It is then possible to calculate moments for the power spectrum which are analogous to the moment functions defined in equation 3.3. These are the spectral moments, and the *n*th spectral moment is defined by:

$$\lambda_n = \int_{-\infty}^{\infty} \omega^n S_{xx}(\omega) d\omega \quad \text{.....(3.13)}$$

There are several parameters defined in terms of the spectral moments which describe the frequency distribution of a random process. Firstly, the *k*th characteristic frequency of a process is defined by:

$$\Omega_k = \left(\frac{\lambda_k}{\lambda_0}\right)^{\frac{1}{k}} \quad \text{.....(3.14)}$$

The first of these, Ω_1, represents the mean frequency of the process, and the second, Ω_2, is the root mean square frequency and is closely related to the mean zero crossing rate:

$$\nu = \frac{1}{\pi}\left[\frac{\lambda_2}{\lambda_0}\right]^{\frac{1}{2}} \quad \text{.....(3.15)}$$

which represents the frequency at which most of the energy in the spectrum is concentrated. If the process is assumed to be Gaussian then two further parameters can be derived. The first of these is the mean square value of the process, and corresponds to the auto-correlation function for τ=0:

$$\sigma_x^2 = \lambda_0 = \int_{-\infty}^{\infty} S_{xx}(\omega)d\omega = R_{xx}(\tau = 0) \quad \text{.....(3.16)}$$

The second is the dispersion parameter which corresponds to the standard deviation of the frequency and therefore offers a measure of the bandwidth of the process:

$$\delta = \left[1 - \frac{\lambda_1^2}{\lambda_0 . \lambda_2}\right]^{\frac{1}{2}} \quad \text{.....(3.17)}$$

These parameters have been illustrated in figure 3.2.

3.1.3.3 Prediction of Peak Response Statistics

The importance of the spectral parameters discussed above is that they can be used to predict the peak values of a random process. The Poisson distribution:

$$p_x(x) = \frac{(\lambda t)^x e^{-\lambda t}}{x!} \quad \text{.....(3.18)}$$

describes the probability of an event occurring at least x times within an interval t, where λ is the mean rate of occurrence of the event. If it is assumed that the probability of a random process exceeding a barrier level follows a Poisson distribution, then the cumulative probability function of the

process exceeding that level in the interval $(0,t)$ is described by the exponential distribution [Benjamin & Cornell 1970]:

$$P_T(t) = 1 - e^{-\lambda t} \qquad (3.19)$$

This is a specific example of the more general Gumbel distribution for which the mean and standard deviation of the peak response are given by:

$$\mu_{peak} = u + \frac{\gamma}{\alpha}$$
$$\sigma_{peak} = \frac{\pi}{\alpha\sqrt{6}} \qquad (3.20)$$

where u is the mode of the distribution, α is a measure of the dispersion and $\gamma = 0.5772$ is Euler's constant [Benjamin & Cornell 1970]. Davenport [Davenport 1964] applied this asymptotic approach to predict the peak wind gusts in a given period τ:

$$\mu_{peak} = \left\{(2\ln\nu\tau)^{\frac{1}{2}} + \frac{\gamma}{(2\ln\nu\tau)^{\frac{1}{2}}}\right\}\sigma_x$$
$$\sigma_{peak} = \left\{\frac{1}{\sqrt{6}}\frac{\pi}{(2\ln\nu\tau)^{\frac{1}{2}}}\right\}\sigma_x \qquad (3.21)$$

where ν is the mean zero crossing rate defined in § 3.1.3.2. However, an underlying assumption in the Poisson model of barrier crossings is that the events are independent and for a narrow band process this is not valid. To overcome this Der Kiureghian [Der Kiureghian 1980] proposed a reduced mean zero crossing rate, ν_e, given empirically by:

$$\nu_e = \begin{cases} (1.63\delta^{0.45} - 0.38)\nu & \delta < 0.69 \\ \nu & \delta \geq 0.69 \end{cases} \qquad (3.22)$$

which he used to modify equations 3.21:

$$\mu_{peak} = \left\{ (2\ln \nu_e \tau)^{\frac{1}{2}} + \frac{\gamma}{(2\ln \nu_e \tau)^{\frac{1}{2}}} \right\} \sigma_x$$

$$\sigma_{peak} = \left\{ \frac{1.2}{(2\ln \nu_e \tau)^{\frac{1}{2}}} + \frac{5.4}{13 + (2\ln \nu_e \tau)^{\frac{1}{2}}} \right\} \sigma_x \quad \text{.....(3.23)}$$

It now needs to be noted that these equations are not restricted to predicting peak wind gusts, but were developed by Der Kiureghian for general stationary Gaussian random processes including models of earthquake excitation. They have been shown to agree reasonably well with simulation results and will be used in the majority of the analyses presented in this thesis. However, these equations are not suitable for use in the analysis of the response to non stationary excitation which is presented in chapter five. In this case a more complicated model of barrier crossing will be used based on the assumptions that the barrier crossing can be represented by a two stage Markov process [Corotis *et al.* 1972, Vanmarcke 1975]. Vanmarcke suggested the following expression for the cumulative probability distribution of the maximum value x_τ of the response x in the period τ :

$$P_{x_\tau}(x) = \left[1 - \exp\left(\frac{-x^2}{2\lambda_0} \right) \right] \exp\left[-\nu\tau \frac{1 - \exp\left(-\sqrt{\frac{\pi}{2\lambda_0}} x\delta^{1.2} \right)}{\exp\left(\frac{x^2}{2\lambda_0} \right) - 1} \right] \quad \text{.....(3.24)}$$

Der Kiureghian cites Cook [Cook 1964] as evidence that this expression agrees well with simulation results.

3.1.4 Random Fields

In the discussion so far it has been shown that random processes can be used to deal with the uncertainties that are present in modelling the dynamic response of engineering systems. Both the system response and the applied loads can be random in nature, and both can be modelled using random processes. However, the preceding sections have considered only random processes which depend upon a single parameter, say time. Now, if this method is to be applied to the problem of spatially varying dynamic loads, it is necessary to extend the definitions to random variables which are dependent upon two or more parameters. This has been shown to be possible [Shinozuka 1987, Vanmarcke 1981 & 1984] and such processes are referred to as random fields. For an homogeneous random field the definition of the auto-correlation function given by equation 3.7 becomes a function of a separation vector:

$$R_{xx}(\{\xi\}) = E\left[X(\{s\}_1)X(\{s\}_2)\right] \quad : \quad \{\xi\} = \{s\}_1 - \underline{\{s\}}_2 \qquad \text{.....(3.25)}$$

Similarly the Wiener-Khintchine relationship of equation 3.8 becomes:

$$\begin{aligned} S_{xx}(\{\kappa\}) &= \frac{1}{(2\pi)^2}\int_{-\infty}^{\infty} R_{xx}(\{\xi\})e^{-j\{\kappa\}.\{\xi\}}d\{\xi\} \\ R_{xx}(\{\xi\}) &= \int_{-\infty}^{\infty} S_{xx}(\{\kappa\})e^{j\{\kappa\}.\{\xi\}}d\{\kappa\} \end{aligned} \qquad \text{.....(3.26)}$$

It can, however, be noted that for the case of seismic excitation of long span bridges only a single space variable needs to be considered as the structure is approximately line like. The vectors in equations 3.25 and 3.26 will then be two dimensional and contain the time and space separation on the one hand, and the wavenumber and frequency on the other. The evaluation of the response statistics can now be simplified by noting that the terms can be expanded as follows:

$$\{\xi\}=\begin{Bmatrix}\xi\\ \tau\end{Bmatrix} \quad : \quad \{\kappa\}=\begin{Bmatrix}\kappa\\ \omega\end{Bmatrix} \quad \Rightarrow \quad \{\kappa\}.\{\xi\}=\xi\kappa+\tau\omega \qquad \text{.....(3.27)}$$

and the relationships in 3.26 become:

$$\begin{aligned} S_{xx}(\{\kappa\}) &= S_{xx}(\kappa,\omega)=\frac{1}{(2\pi)^2}\int_{-\infty}^{\infty}\int_{-\infty}^{\infty}R_{xx}(\xi,\tau)e^{-j\kappa\xi}e^{-j\omega\tau}d\xi d\tau \\ R_{xx}(\{\xi\}) &= R_{xx}(\xi,\tau)=\int_{-\infty}^{\infty}\int_{-\infty}^{\infty}S_{xx}(\kappa,\omega)e^{j\kappa\xi}e^{j\omega\tau}d\kappa d\omega \end{aligned} \qquad \text{.....(3.28)}$$

3.1.5 Evolutionary Spectra

The aim of the preceding sections has been to show how the power spectral density function of a random process can be used to calculate the statistics of a random process or field. This theory can be applied to the analysis of various engineering phenomena which can be described as random processes, such as the response of a structure to dynamic excitation. This has advantages both in computational efficiency and in producing the statistics of the response. However, this approach relies on an underlying assumption of stationarity, and is invalid if this assumption is not met. Unfortunately, many of the processes encountered in the real world, including civil engineering, are not stationary. Most importantly for the work in hand seismic excitation is non-stationary because of its short duration. Therefore, in order to apply some of the advantages of the power spectral approach to non-stationary processes, various attempts have been made to modify the approach by avoiding this assumption. One of the more popular is attributable to Priestly [Priestly 1965, 1967] who developed an approach using what he termed evolutionary power spectra. In a standard power density spectrum the ordinates represent the squared amplitudes of a family of oscillatory functions $\theta(\omega)$ which are chosen to be complex exponential functions. The time domain version of the process is then obtained by summing all the contributions from each of the functions:

$$X(t) = \int_{-\infty}^{\infty} S_{xx}(\omega)\theta(\omega)d\omega = \int_{-\infty}^{\infty} S_{xx}(\omega)e^{-j\omega t}d\omega \quad \text{.....(3.29)}$$

In the evolutionary spectral approach the family of oscillatory functions are defined as amplitude modulated complex exponential functions:

$$\theta(\omega,t) = A(\omega,t)e^{j\omega t} \quad \text{.....(3.30)}$$

where $A(\omega,t)$ is a deterministic function of both time and frequency that defines an envelope for the process. The evolutionary spectral density is then given by the following expression:

$$S_{xx}(\omega,t) = \left|A(\omega,t)\right|^2 S_{xx}(\omega) \quad \text{.....(3.31)}$$

This approach will not be considered in more detail here, it has been included to demonstrate that there are methods of dealing with non stationary processes. The application of evolutionary spectra to the response of a cable stayed bridge will be outlined in chapter five where the results of stationary and non stationary analyses are compared.

3.2 Analysis of Response to Seismic Excitation

Having selected an approach to dealing with the uncertainties in the problem being tackled it is now necessary to develop the equations of motion of the system in a way which allows these methods to be used. The standard approach to dealing with the problem of spatially varying ground excitation, either multi-support or asynchronous, is to partition the equations of motion into ground and response degrees of freedom [Clough & Penzien 1975]. However, to develop a power spectrum analysis it is necessary to specify the general ground excitation as a function of both time and space. In the following sections the method will be derived by first considering the dynamic response of a structure.

Then the solution for a structure subject to a spatially varying static loading will be developed. Finally these two results will be combined to give the required equations of motion for the response of a structure to spatially varying dynamic excitation.

3.2.1 Response of Structures to Synchronous Seismic Excitation

Consider first a single degree of freedom system subject to seismic excitation (figure 3.3). The displacements can be divided into two parts, a dynamic component, v_d, caused by the inertia forces and a component, v_g, corresponding to the displacement of the ground. This latter component shall be referred to as the rigid body displacement. Using Newton's laws the equation of motion can be written as:

$$m(\ddot{v}_g + \ddot{v}_d) + c(\dot{v}_g + \dot{v}_d) + k(v_g + v_d) = p \quad \text{.....(3.32)}$$

though in the case of seismic excitation it is usual to consider the forcing function, p, to be zero. Equation 3.32 must contain the static solution:

$$kv_g = 0 \quad \text{.....(3.33)}$$

and therefore the stiffness term in the equation of motion depends only on the dynamic displacement. If the damping is assumed to occur because of internal displacements of the structure, then a similar simplification applies to the velocity term in 3.32 because there are no internal displacements for rigid body motion. The equation of motion then reduces to the expected form:

$$m\ddot{v}_d + c\dot{v}_d + kv_d = -m\ddot{v}_g \quad \text{.....(3.34)}$$

Equation 3.32 can be applied to a multi-degree of freedom system subject to synchronous seismic loading (figure 3.4) by replacing the scalar terms by matrices and vectors:

$$[\mathbf{M}]\{\ddot{\mathbf{v}}_d + \ddot{\mathbf{v}}_g\} + [\mathbf{C}]\{\dot{\mathbf{v}}_d + \dot{\mathbf{v}}_g\} + [\mathbf{K}]\{\mathbf{v}_d + \mathbf{v}_g\} = \{\mathbf{p}\} \quad \text{.....(3.35)}$$

As with the single degree of freedom example the forcing function is generally taken to be zero, and equation 3.35 must contain the static solution. The equation of motion then simplifies to give:

$$[\mathbf{M}]\{\ddot{\mathbf{v}}_d\} + [\mathbf{C}]\{\dot{\mathbf{v}}_d\} + [\mathbf{K}]\{\mathbf{v}_d\} = -[\mathbf{M}]\{\ddot{\mathbf{v}}_g\} \quad \text{.....(3.36)}$$

However, the elements of the vector $\{\ddot{\mathbf{v}}_g\}$ do not depend only on the magnitude of the ground acceleration, but also upon its direction. For example if the ground acceleration is purely horizontal then the elements of $\{\ddot{\mathbf{v}}_g\}$ which correspond to vertical degrees of freedom on the structure will be zero. This is accounted for in the equation of motion by introducing an earthquake participation vector which relates the ground excitation to the response degrees of freedom:

$$\{\ddot{\mathbf{v}}_g\} = \{\mathbf{R}\}\ddot{v}_G(t) \quad \text{.....(3.37)}$$

Equation 3.36 then becomes:

$$[\mathbf{M}]\{\ddot{\mathbf{v}}_d\} + [\mathbf{C}]\{\dot{\mathbf{v}}_d\} + [\mathbf{K}]\{\mathbf{v}_d\} = -[\mathbf{M}]\{\mathbf{R}\}\ddot{v}_G(t) \quad \text{.....(3.38)}$$

However, the matrices in equations 3.38 contain off-diagonal terms representing coupling between the different response degrees of freedom. This makes the solution of the equations complicated and inefficient to solve and it would be clearly advantageous if they could be simplified. The first step in this simplification is to transform the problem from global response co-ordinates to a set of

generalised co-ordinates which will decouple the equations of motion. The mode shapes of the structure are a suitable set of generalised co-ordinates and are given by the eigenvectors of the characteristic equation:

$$[\mathbf{M}]\{\ddot{\mathbf{v}}_d\}+[\mathbf{K}]\{\mathbf{v}_d\}=\underline{\mathbf{0}} \quad \text{.....(3.39)}$$

Usually only the first few eigenvectors are required to achieve sufficient accuracy in the solution. The response in modal co-ordinates can then be found from the response in global co-ordinates by:

$$\{\mathbf{v}\}=[\Phi]\{\mathbf{y}\} \quad \text{.....(3.40)}$$

where $[\Phi]$ is a matrix of mode shape column vectors. Assuming that the mode shapes are mass normalised:

$$[\Phi][\mathbf{M}][\Phi]^T=[\mathbf{M}]_r=[\mathbf{I}] \quad \text{.....(3.41)}$$

equation 3.38 can then be recast in the following modal form:

$$[\mathbf{M}]_r\{\ddot{\mathbf{y}}_d\}+[\mathbf{C}]_r\{\dot{\mathbf{y}}_d\}+[\mathbf{K}]_r\{\mathbf{y}_d\}=-[\Phi]^T[\mathbf{M}]\{\mathbf{R}\}\ddot{v}_G(t) \quad \text{.....(3.42)}.$$

where both sides of the equation have been pre multiplied by the transpose of the mode shape matrix. This latter operation produces the modal stiffness matrix $[\mathbf{K}]_r$ which is diagonal and has elements given by $1/\omega_r^2$. This analysis also assumes that the damping matrix is decoupled by the transformation to modal coordinates giving a diagonal modal damping matrix $[\mathbf{C}]_r$ which has elements $2\omega_r\xi_r$. The effect of the transformation to modal co-ordinates is therefore to decouple the equations of motion as required, and simplify the problem to a series of single degree of freedom

systems. Equation 3.42 could now be solved quite simply by direct integration. However, the problem can be simplified further by transforming to the frequency domain; this is of course essential to develop the power spectral approach. The frequency response function can be found by assuming that the response is harmonic:

$$\{\ddot{\mathbf{y}}\} = -\omega^2\{\mathbf{y}\} \quad \text{.....(3.43)}$$

and rewriting equation 3.42 as:

$$\left[-[\mathbf{M}]_r\omega^2 + [\mathbf{C}]_r j\omega + [\mathbf{K}]_r\right]\{\mathbf{y}_d(t)\} = -[\mathbf{\Phi}]^T[\mathbf{M}]\{\mathbf{R}\}\ddot{v}_G(t) \quad \text{.....(3.44)}$$

This can then transformed to the frequency domain using a Fourier transform:

$$\begin{aligned}\left[-[\mathbf{M}]_r\omega^2 + [\mathbf{C}]_r j\omega + [\mathbf{K}]_r\right]\{\mathbf{Y}_d(\omega)\} &= -[\mathbf{\Phi}]^T[\mathbf{M}]\{\mathbf{R}\}\ddot{v}_G(\omega) \\ \Rightarrow \{\mathbf{Y}_d(\omega)\} &= -[\mathbf{H}(\omega)]_r[\mathbf{\Phi}]^T[\mathbf{M}]\{\mathbf{R}\}\ddot{v}_G(\omega)\end{aligned} \quad \text{.....(3.45)}$$

where the frequency response matrix of the structure is defined by:

$$[\mathbf{H}(\omega)]_r = \left[-[\mathbf{M}]_r\omega^2 + [\mathbf{C}]_r j\omega + [\mathbf{K}]_r\right]^{-1} \quad \text{.....(3.46)}$$

All that remains now is to form the power density spectrum which can be found using equation 3.11:

$$\left[\mathbf{S}_{yy,d}(\omega)\right] = E\left[\{\mathbf{Y}_d(\omega)\}\{\mathbf{Y}_d(\omega)\}^{*T}\right] \quad \text{.....(3.47)}$$

where, because the response is given in terms of a vector, the power spectral representation is a matrix. The diagonal terms of this matrix are the modal power spectra, and the off-diagonal terms the cross spectral density functions between the modes.

3.2.2 Response of Structures to Spatially Varying Static Loads

Having reviewed the derivation of an expression for the power spectrum of the time domain response it is now necessary to find the corresponding result for the response to loads in the space domain. One approach to dealing with spatially varying loads is to describe them using generalised co-ordinates. This approach has been summarised by Davenport [Davenport 1961a] and he illustrated it by applying it to the case of a simply supported beam with a spatially varying load (figure 3.5). The load acting along the beam can be described in terms of the generalised co-ordinate system as follows:

$$p(x) = \sum_{r=1}^{\infty} P_r \mu_r(x) \qquad (3.48)$$

If the generalised co-ordinates are orthogonal, that is:

$$\int_0^l \mu_r(x)\mu_s(x)dx = \begin{cases} 0 & r \neq s \\ N_r & r = s \end{cases} \qquad (3.49)$$

then equation 3.48 is a Fourier series. The coefficients, P_r, can then be found by multiplying both sides of equation 3.48 by μ_r and integrating over the length of the beam:

$$P_r = \frac{1}{N_r}\int_0^l p(x)\mu_r(x)dx \qquad (3.50)$$

A similar expression can be used to describe the response of the beam:

$$v(x) = \sum_{r=1}^{\infty} V_r \mu_r(x) \qquad \text{where} \qquad V_r = \frac{1}{N_r}\int_0^l v(x)\mu_r(x)dx \quad \text{.....(3.51)}$$

It now remains to relate the loads to the beam response. If the loading is a force distribution, and the response displacements, then the two are linked by the stiffness of the beam. The stiffness in the generalised co-ordinate system is given by:

$$K_{rs} = \frac{1}{N_r}\int_0^l EI(x)\left(\frac{d^2\mu_r}{dx^2}\right)\left(\frac{d^2\mu_s}{dx^2}\right)dx \quad \text{.....(3.52)}$$

The stiffness defined in 3.52 will couple the response in the different generalised co-ordinates unless the second derivatives of these co-ordinates are also orthogonal. Davenport chose the mode shapes of the beam as his set of generalised co-ordinates and these are defined by sine functions:

$$\mu_r = \sin\left(r\frac{\pi x}{l}\right) \qquad \Rightarrow \qquad N_r = \frac{l}{2} \quad \text{.....(3.53)}$$

In this case the second derivatives are orthogonal, and the stiffness terms in equation 3.52 will not couple the response in the different modes. The stiffness relationship in the generalised co-ordinate system is then given by:

$$P_r = K_r V_r \quad \text{.....(3.54)}$$

The preceding analysis has assumed that the structure, i.e. the beam, and the load are fully coincident which made it possible to use the mode shapes of the structure as the generalised co-ordinate system. However, this assumption is not valid for a structure subject to spatially varying seismic excitation as the excitation is defined on a domain which extends beyond the limits of the structure. Furthermore there may be many points on a structure which are not in direct contact with the ground. However, if

the load is now considered to be defined over an extended domain of length L, and complex exponential functions are used to represent the sinusoidal generalised co-ordinates, then equation 3.50 can be written as:

$$P_r = \frac{1}{L}\int_{-\frac{L}{2}}^{\frac{L}{2}} p(x)e^{-j\kappa_r x}dx \qquad \text{where} \qquad \kappa_r = \frac{r\pi}{L} \quad \text{.....(3.55)}$$

Taking the limit of LP_r as L tends to infinity will then yield a continuous rather than discrete spectrum:

$$P(\kappa) = \int_{-\infty}^{\infty} p(s)e^{-j\kappa s}ds \quad \text{.....(3.56)}$$

where κ now represents the phase change per unit length and is termed the wavenumber. Equation 3.56 is the Fourier transform between the space and wavenumber domains and there is a corresponding inverse transform:

$$p(s) = \frac{1}{2\pi}\int_{-\infty}^{\infty} P(\kappa)e^{j\kappa s}d\kappa \quad \text{.....(3.57)}$$

which represents the limit of the summation in equation 3.48 as L tends to infinity.

So, transformation to the wavenumber domain gives a means of representing any spatially varying load in terms of a generalised co-ordinate system. It now remains to relate this description of the load to some response parameter on a structure which is not necessarily coincident with the load. To do this it is useful to think in terms of influence lines which describe the variation of a given effect with the position of a unit load. An influence line could therefore be constructed which relates the response, say bending moment or displacement, at a point x in the structure due to a unit load, say

force or ground acceleration, at a position s on a line within the infinite ground domain (figure 3.6). The total response at x on the structure is then given by summing the effects of all the applied loads:

$$v_x = \int_{-\infty}^{\infty} v_x(s)ds = \int_{-\infty}^{\infty} r_x(s)p(s)ds \quad \text{.....(3.58)}$$

If the influence line, $r_x(s)$, is now described in terms of the generalised co-ordinate system, i.e. transformed to the wavenumber domain, then the response will be given by a corresponding summation of the response in each wavenumber:

$$v_x = \int_{-\infty}^{\infty} V_x(\kappa)d\kappa = \int_{-\infty}^{\infty} R_x(\kappa)P(\kappa)d\kappa \quad \text{.....(3.59)}$$

where $V_x(\kappa\ )$ represents the wavenumber response and $R_x(\kappa\ )$ the wavenumber response function at x on the structure. Here it has been assumed that the response is uncoupled in the wavenumber domain, i.e. the excitation in one wavenumber does not produce response at a different wavenumber. The result in equation 3.59 is in fact just an application of Parseval's theorem for Fourier transforms:

$$\int_{-\infty}^{\infty} r_x(s)p(s)ds = \int_{-\infty}^{\infty} R_x(\kappa)P(\kappa)d\kappa \quad \text{.....(3.60)}$$

3.2.2.1 Response of Portal Frame

It is useful now to illustrate the work of §3.2.2 by looking at the response of a simple structure to a spatially varying static ground excitation. This will clarify the meaning of the wavenumber response and wavenumber response function, and show how a wavenumber power spectrum can be developed. The example structure will be the portal frame shown in figure 3.7. The ground displacements in this figure can be expressed in terms of wavenumber by the space domain Fourier transform described

above. To do this however it is necessary to define an arbitrary origin at which the phase relationship of the different generalised co-ordinates, $e^{-j\kappa s}$, can be defined (figure 3.8).

For the portal frame, or indeed for a structure such as a bridge, the structure is only excited for values of s that correspond to points of support. Therefore, the influence line for the response to ground excitation is a series of delta functions at the supports:

$$r_x(s) = A_{x1}\delta(s-l_1) + A_{x2}\delta(s-l_2) \quad \text{.....(3.61)}$$

The wavenumber domain version of this is then given by:

$$R(\kappa) = \int_{-\infty}^{\infty} \{A_{x1}\delta(s-l_1) + A_{x2}\delta(s-l_2)\} e^{-j\kappa s} ds = A_{x1}e^{-j\kappa l_1} + A_{x2}e^{-j\kappa l_2} \quad \text{.....(3.62)}$$

It is important to note again that an arbitrary origin has to be used to define the problem. Figure 3.9 shows the response of a point on the portal frame to a series of sinusoidal ground displacements of unit magnitude, and illustrates the meaning of the wavenumber response function.

To proceed with the probabilistic approach it is now necessary to develop a power spectral description of the response. This is defined in terms of the wavenumber domain response as:

$$S_{vv}(\kappa) = E\left[V(\kappa)V^*(\kappa)\right] \quad \text{.....(3.63)}$$

Substituting equation 3.59 and 3.62 into 3.63 produces:

$$S_{xx}(\kappa) = E\left[\left(R_x(\kappa)P(\kappa)\right)\left(R_x(\kappa)P(\kappa)\right)^*\right] = E\left[R_x(\kappa)R_x^*(\kappa)P(\kappa)P^*(\kappa)\right]$$
$$= \left\{A_{x1}e^{-j\kappa l_1} + A_{x2}e^{-j\kappa l_2}\right\}\left\{A_{x1}e^{-j\kappa l_1} + A_{x2}e^{-j\kappa l_2}\right\}^* S_{pp}(\kappa) \quad \text{.....(3.64)}$$
$$= \left({A_{x1}}^2 + {A_{x2}}^2 + 2A_{x1}A_{x2}\,\mathrm{Re}\left\{e^{-j\kappa(l_2-l_1)}\right\}\right)S_{pp}(\kappa)$$

which shows that the power spectrum is a function of the separation of the two supports and hence the phase difference between them. This is an important result as it means that the power spectrum is independent of the origin chosen to define the generalised co-ordinates.

3.2.3 Response of Structures to Spatially Varying Seismic Excitation

Having considered the response of structures to dynamic and spatially varying static loads, these results can now be combined for the case of structures subject to spatially varying seismic loading. Firstly, in recasting the equations of motion, equation 3.35, it must be noted that both asynchronous and multi-support seismic excitation introduce a third type of displacement caused by differential movement of the supports. These displacements of the structure vary with time, but, since they are caused by the stiffness of the structure rather than its inertia, they will be referred to as pseudo-static displacements $\{\mathbf{v}_s\}$. Consider for example a simple portal frame (figure 3.10); when the displacements at the feet are equal and in phase there is no pseudo-static displacement of the frame, i.e. $\{\mathbf{v}_s\}$ is zero. However if the displacements are exactly 180° out of phase then there will be no rigid body displacement, $\{\mathbf{v}_g\} = \mathbf{0}$, but there will be a pseudo-static displacement as shown. Finally for a case where the phase difference between the supports is between 0 and 180° there will be a combination of both pseudo-static and ground displacements. It is therefore possible to write down the equation of motion by replacing $\{\mathbf{v}_g\}$ with $\{\mathbf{v}_g + \mathbf{v}_s\}$ in equation 3.35:

$$[\mathbf{M}]\{\ddot{\mathbf{v}}_d + \ddot{\mathbf{v}}_g + \ddot{\mathbf{v}}_s\} + [\mathbf{C}]\{\dot{\mathbf{v}}_d + \dot{\mathbf{v}}_g + \dot{\mathbf{v}}_s\} + [\mathbf{K}]\{\mathbf{v}_d + \mathbf{v}_g + \mathbf{v}_s\} = \{\mathbf{p}\} \quad \text{.....(3.65)}$$

Making the same assumptions as before; that the forcing function is zero, and the damping is due to the internal movements of the structure; equation 3.65 then reduces to:

$$[\mathbf{M}]\{\ddot{\mathbf{v}}_d\}+[\mathbf{C}]\{\dot{\mathbf{v}}_d\}+[\mathbf{K}]\{\mathbf{v}_d\}=-[\mathbf{M}]\{\ddot{\mathbf{v}}_g+\ddot{\mathbf{v}}_s\} \quad \text{.....(3.66)}$$

It is useful at this juncture to compare equation 3.66 with equations 3.34 and 3.36. For the synchronous examples, 3.34 and 3.36, the dynamic response is governed by the rigid body accelerations. However with spatially varying excitation, equation 3.66, the dynamic response of the structure depends not only on the rigid body accelerations but also on the pseudo-static accelerations. Hence spatial variations in seismic loading not only give rise to pseudo-static response, but also modify the dynamic behaviour.

As with the MDOF system subject to synchronous excitation, the terms in the acceleration vector on the right hand side of 3.66 can be defined in terms of an earthquake participation vector. However, it will now be a function of the space domain defining the ground excitation:

$$\{\ddot{\mathbf{v}}_g+\ddot{\mathbf{v}}_s\}=\{\mathbf{r}(s)\}\ddot{v}_G(s,t) \quad \text{.....(3.67)}$$

The elements of the participation vector represent the ground influence lines for the corresponding response degrees of freedom; the vector will therefore be termed the ground influence vector. As discussed in §3.2.2.1, for a structure such as a bridge this will be a series of delta functions corresponding to each of the ground degrees of freedom. The ground influence vector will then be given by:

$$\{\mathbf{r}(s)\} = \begin{Bmatrix} \sum_{i=1}^{n} A_{1,i}\delta(s-l_i) \\ \sum_{i=1}^{n} A_{2,i}\delta(s-l_i) \\ \vdots \\ \sum_{i=1}^{n} A_{m,i}\delta(s-l_i) \end{Bmatrix} \quad \text{.....(3.68)}$$

where n is the number of ground degrees of freedom and m is the number of structural degrees of freedom. The coefficients $A_{i,j}$ represent the response in structural degree of freedom i due to a unit displacement in ground degree of freedom j. Therefore, by summing over all ground degrees of freedom the components of seismic excitation in different directions are automatically accounted for in $\{\mathbf{r}(s)\}$.

As with the dynamic response, the equations of motion now need to be transformed to the modal system of co-ordinates. Equation 3.66 then becomes:

$$[\mathbf{M}]_r\{\ddot{\mathbf{y}}_d(s,t)\}+[\mathbf{C}]_r\{\dot{\mathbf{y}}_d(s,t)\}+[\mathbf{K}]_r\{\mathbf{y}_d(s,t)\} = -[\mathbf{\Phi}]^T[\mathbf{M}]\{\mathbf{r}(s)\}\ddot{v}_G(s,t) \quad \text{.....(3.69)}$$

where the ground influence vector has been included. Finally the equations are transformed to the wavenumber frequency domain using a double Fourier transform:

$$\{\mathbf{Y}_d(\kappa,\omega)\} = -[\mathbf{H}(\omega)]_r[\mathbf{\Phi}]^T[\mathbf{M}]\{\mathbf{R}(\kappa)\}\ddot{v}_G(\kappa,\omega) \quad \text{.....(3.70)}$$

3.2.4 The Pseudo-Static Response

Equation 3.70 gives an expression for the dynamic response of the structure, but as mentioned in §3.2.3 spatial variations in the seismic loading will give rise to a further set of displacements known

as the pseudo-static response. These can be found by considering the superposition of the response to loads in each of the ground degrees of freedom and is given by:

$$\left\{\ddot{\mathbf{v}}_g + \ddot{\mathbf{v}}_s\right\} = \{\mathbf{r}(s)\}\ddot{v}_G(s,t)$$
$$\Rightarrow \left\{\ddot{\mathbf{v}}_s\right\} = \{\mathbf{r}(s)\}\ddot{v}_G(s,t) - \left\{\ddot{\mathbf{v}}_g\right\} \quad \text{.....(3.71)}$$

Assuming an harmonic response, the expression in 3.71 can be modified to give the pseudo-static displacements:

$$\{\mathbf{v}_s\} = \frac{1}{\omega^2}\left(\{\mathbf{r}(s)\}\ddot{v}_G(s,t) - \left\{\ddot{\mathbf{v}}_g\right\}\right) \quad \text{.....(3.72)}$$

As with the dynamic response the calculations are best performed by transforming to a modal system of co-ordinates and then to the frequency wavenumber domain. Equations 3.40 and 3.41 allow equation 3.72 to be written as:

$$\{\mathbf{y}_s(s,t)\} = -\frac{1}{\omega^2}[\Phi]^T[\mathbf{M}]\left(\{\mathbf{r}(s)\}\ddot{v}_G(s,t) - \left\{\ddot{\mathbf{v}}_g\right\}\right) \quad \text{.....(3.73)}$$

the two dimensional Fourier transform of which is:

$$\{\mathbf{Y}_s(\kappa,\omega)\} = -\frac{1}{\omega^2}[\Phi]^T[\mathbf{M}]\left(\{\mathbf{R}(\kappa)\}\ddot{v}_G(\kappa,\omega) - \left\{\ddot{\mathbf{v}}_g\right\}\right) \quad \text{.....(3.74)}$$

The rigid body response appears as a term on the right hand side of both equations 3.73 and 3.74, and therefore in order to proceed further it is necessary to find an expression for this. Consider again the portal frame in figure 3.10. For the general case, the seismic loading can be assumed to consist of two parts, an in phase component and a component which is 180° out of phase. These components give rise to the ground and pseudo-static displacements of the structure respectively. Hence the rigid body

displacements of the structure can be found by considering the base acceleration which is common to each of the supports, that is the spatial mean ground acceleration:

$$\{\mathbf{v}_g\} = \{\mathbf{r}(s)\}\overline{v_G(s,t)} \quad \text{.....(3.75)}$$

Again it needs to be noted that the direction of the ground shaking is important and a different mean will need to be calculated for each direction of the ground degrees of freedom. Finally equation 3.74 can be simplified using 3.75:

$$\begin{aligned}\{\mathbf{Y}_s(\kappa,\omega)\} &= -\frac{1}{\omega^2}[\Phi]^T[\mathbf{M}]\{\mathbf{R}(\kappa)\}\left(\ddot{v}_G(\kappa,\omega) - \overline{\ddot{v}_G(\kappa,\omega)}\right) \\ &= -\frac{1}{\omega^2}[\Phi]^T[\mathbf{M}]\{\mathbf{N}(\kappa)\}\ddot{v}_G(\kappa,\omega)\end{aligned} \quad \text{.....(3.76)}$$

where it has been noted that the spatial mean ground acceleration is a function of the ground acceleration.

3.2.3.2 Power Spectral Density Function of the Response

In the last two sections equations have been presented which give the dynamic (equation. 3.70) and pseudo-static (equation. 3.76) response in the frequency domain in terms of the ground acceleration. All that is required now is to combine these two components and find an expression for the overall power spectrum of the response. The power spectral representation of the response is given by:

$$\left[\mathbf{S}_{yy}(\kappa,\omega)\right] = E\left[\{\mathbf{Y}(\kappa,\omega)\}\{\mathbf{Y}(\kappa,\omega)\}^{*T}\right] \quad \text{.....(3.77)}$$

so noting that:

$$\{\mathbf{Y}(\kappa,\omega)\} = \{\mathbf{Y}_d(\kappa,\omega)\} + \{\mathbf{Y}_s(\kappa,\omega)\} \quad \text{.....(3.78)}$$

and using the identities:

$$\begin{aligned} &\left((a+bj)+(c+dj)\right)^* = (a+bj)^* + (c+dj)^* \\ &[\mathbf{A}+\mathbf{B}]^T = [\mathbf{A}]^T + [\mathbf{B}]^T \end{aligned} \quad \text{.....(3.79)}$$

equation 3.77 can be expanded to give the cross spectral density matrix in terms of the dynamic and pseudo-static components:

$$\begin{aligned} \left[\mathbf{S}_{yy}(\kappa,\omega)\right] = &\{\mathbf{Y}_d(\kappa,\omega)\}\{\mathbf{Y}_d(\kappa,\omega)\}^{*T} + \{\mathbf{Y}_d(\kappa,\omega)\}\{\mathbf{Y}_s(\kappa,\omega)\}^{*T} \\ &+\{\mathbf{Y}_s(\kappa,\omega)\}\{\mathbf{Y}_d(\kappa,\omega)\}^{*T} + \{\mathbf{Y}_s(\kappa,\omega)\}\{\mathbf{Y}_s(\kappa,\omega)\}^{*T} \end{aligned} \quad \text{.....(3.80)}$$

Here the first term represents the dynamic contribution and the last the contribution of the pseudo-static behaviour. The two central terms represent the interaction of the dynamic and pseudo-static components and shall be referred to as the cross terms. Finally the terms on the right hand side of equation 3.80 can be expanded using equations 3.70 and 3.76, and the identities:

$$\begin{aligned} &[\mathbf{A}.\mathbf{B}]^T = [\mathbf{B}]^T[\mathbf{A}]^T \\ &\left((a+bj)(c+dj)\right)^* = (a+bj)^*(c+dj)^* \end{aligned} \quad \text{.....(3.81)}$$

to give the following expressions:

$$\begin{aligned} \{\mathbf{Y}_d(\kappa,\omega)\}\{\mathbf{Y}_d(\kappa,\omega)\}^{*T} = &[\mathbf{H}(\omega)]_r[\Phi]^T[\mathbf{M}]\{\mathbf{R}(\kappa)\} \\ &\{\mathbf{R}(\kappa)\}^{*T}[\mathbf{M}]^T[\Phi][\mathbf{H}(\omega)]_r^{*T} S_{aa}(\kappa,\omega) \end{aligned} \quad \text{.....(3.82)}$$

$$\{\mathbf{Y}_d(\kappa,\omega)\}\{\mathbf{Y}_s(\kappa,\omega)\}^{*T} = \frac{1}{\omega^2}[\mathbf{H}(\omega)]_r[\Phi]^T[\mathbf{M}]\{\mathbf{R}(\kappa)\}\{\mathbf{N}(\kappa)\}^{*T}[\mathbf{M}]^T[\Phi]S_{aa}(\kappa,\omega) \quad \text{.....(3.83)}$$

$$\{\mathbf{Y}_s(\kappa,\omega)\}\{\mathbf{Y}_d(\kappa,\omega)\}^{*T} = \frac{1}{\omega^2}[\mathbf{\Phi}]^T[\mathbf{M}]\{\mathbf{N}(\kappa)\}\{\mathbf{R}(\kappa)\}^{*T}[\mathbf{M}]^T[\mathbf{\Phi}][\mathbf{H}(\omega)]_r^{*T} S_{aa}(\kappa,\omega) \quad \text{.....(3.84)}$$

$$\{\mathbf{Y}_s(\kappa,\omega)\}\{\mathbf{Y}_s(\kappa,\omega)\}^{*T} = \frac{1}{\omega^4}[\mathbf{\Phi}]^T[\mathbf{M}]\{\mathbf{N}(\kappa)\}\{\mathbf{N}(\kappa)\}^{*T}[\mathbf{M}]^T[\mathbf{\Phi}] S_{aa}(\kappa,\omega) \quad \text{.....(3.85)}$$

where $S_{aa}(\kappa,\omega)$ is the ground power spectrum.

3.3 Representation of the Loading

Having obtained a set of equations relating the power spectrum of the response to the power spectrum of the ground acceleration it is now necessary to obtain an appropriate representation of the ground acceleration. To fit in with the theory outlined above this will take the form of a two dimensional frequency wavenumber power spectrum. There are several commonly used models for the frequency power spectrum of earthquake excitation, and so what is required is a method of extending these to include the wavenumber power spectrum. The similarity between two random processes $X(t)$ and $Y(t)$ can be expressed in terms of the coherence function:

$$\gamma_{xy}^2(\omega) = \frac{\left|S_{xy}(\omega)\right|^2}{S_{xx}(\omega)S_{yy}(\omega)} \leq 1 \quad \text{.....(3.86)}$$

which varies from 1 for perfectly correlated processes to zero for totally uncorrelated processes. Equation 3.86 can therefore be used to compare the ground excitation at different points, and for an homogeneous process will be a function of the spatial separation between the points. The expression in 3.86 represents the squared modulus of a complex function defined by:

$$\gamma_{xy}(\omega) = \frac{S_{xy}(\omega)}{\left(S_{xx}(\omega)S_{yy}(\omega)\right)^{\frac{1}{2}}} = \left|\gamma(\omega)\right| e^{i\theta(\omega)} \quad \text{.....(3.87)}$$

where, $|\gamma(\omega)|$, is a magnitude between 0 and 1, and, $\theta\ (\omega)$, is the phase relationship between the processes. If the spatial variation of the ground motion is defined using these two functions, then an estimate of the cross spectral density can be made from equation 3.87:

$$S_{xy}(\omega) = \gamma_{xy}(\omega)\left(S_{xx}(\omega)S_{yy}(\omega)\right)^{\frac{1}{2}} \quad \text{.....(3.88)}$$

It can now be noted that for an homogeneous process the frequency domain power spectra are the same at each point and 3.88 then simplifies further to:

$$S_{xx}(\xi,\omega) = \gamma(\xi,\omega)S_{xx}(\omega) \quad \text{.....(3.89)}$$

Finally the Fourier transformation from the space to the wavenumber domain yields the required frequency wavenumber power density spectrum:

$$S_{xx}(\kappa,\omega) = S_{xx}(\omega)\int_{-\infty}^{\infty}\gamma(\xi,\omega)e^{-i\xi\kappa}d\xi \quad \text{.....(3.90)}$$

As mentioned in chapter two the causes of spatial variation in seismic loading can be considered in two parts, that due to wave propagation and that due to loss of coherence. These two effects are described by the two components $\theta(\xi,\omega)$ and $|\gamma(\xi,\omega)|$, respectively, and shall now be considered in turn.

3.3.1 Power Spectrum for Asynchronous Ground Motion

In the case of asynchronous seismic loading the finite propagation velocity of the seismic waves gives rise to a phase difference between the points of support. The frequency wavenumber power spectrum

can then be found by combining equations 3.87 and 3.90. Noting that the magnitude $|\gamma(\xi,\omega)|$ equals one and that the phase relationship is:

$$\theta(\xi,\omega) = \frac{\omega\xi}{c} \qquad (3.91)$$

the power spectrum is given by:

$$S_{xx}(\kappa,\omega) = S_{xx}(\omega)\int_{-\infty}^{\infty} e^{j\left(\frac{\omega\xi}{c}\right)} e^{-j\xi\kappa} d\kappa = S_{xx}(\omega)\,\delta\left(\kappa-\frac{\omega}{c}\right) \qquad (3.92)$$

This equation shows that the frequency wavenumber power spectral density of the ground excitation is only defined for combinations of frequency and ground wave velocity that satisfy:

$$\kappa = \frac{\omega}{c} \qquad (3.93)$$

Assuming that c is constant with frequency, this results in a power spectrum which projects onto a straight line in the frequency wavenumber plane, at an angle $\frac{1}{c}$ to the frequency axis (figure 3.11). The value of the ground wave velocity is therefore very important and is influenced by many factors, such as the geology and topology of the location. However, most of these factors will cause a variation in the coherence between the waves at different points along the length of the bridge, and so will not be taken into account in the purely asynchronous model being considered here. Assuming that the waves travel with a uniform velocity through an homogeneous medium, the important factors determining the velocity of the wave along the bridge axis are the propagation velocity of the seismic waves in the chosen medium and the location of the epicentre. This latter point is important as the velocity along the length of the bridge deck depends upon the direction of propagation of the wave front (figure 3.12). The velocity along the length of the bridge is then given by:

$$c_{axis} = \frac{c_{med}}{\sin\theta} \quad \text{.....(3.94)}$$

3.3.2 Power Spectrum for Spatial Varying Excitation With Loss of Coherence

In order to develop the model for the more complicated case where there is a loss of coherence with spatial distribution it is necessary to have a model for the spatial coherence function. Several models have been proposed following processing of data from field measurements; one of these is to assume that the coherence decays exponentially with space [Der Kiureghian & Neuenhofer 1992]:

$$\gamma_{xx}(\omega,\xi) = \exp\left[-\left(\frac{\alpha\omega\xi}{c_s}\right)^2\right]\exp\left(j\frac{\omega\xi^L}{c}\right) \quad \text{.....(3.95)}$$

where α is a decay constant. The required power spectral density function is then given by the Fourier transform of 3.95. Assuming that $\xi = \xi^L$, both terms in 3.95 will be functions of ξ and the result of the transformation will be a convolution in the wavenumber domain:

$$\begin{aligned} S_{xx}(\kappa,\omega) &= \int_{-\infty}^{\infty} \exp\left[-\left(\frac{\alpha\omega\xi}{c_s}\right)^2\right] e^{-j\kappa\xi} d\xi \otimes \int_{-\infty}^{\infty} \exp\left(j\frac{\omega\xi}{c}\right) e^{-j\kappa\xi} d\xi \\ &= \frac{1}{a\omega/c_s\sqrt{2}} \exp\left[-\left(\frac{\xi c_s}{2\alpha\omega}\right)^2\right] \otimes \delta\left(\xi + \frac{\omega}{c}\right) \end{aligned} \quad \text{.....(3.96)}$$

3.4 Implementation of Background Theory

Having developed the background to the approach it is now necessary to adapt the method so that it can be efficiently be implemented in a computer program. This will involve simplifying the procedures and combining the modal results to yield the statistics of the global response.

3.4.1 Single and Double Sided Spectra

The development of the approach so far has made use of Fourier analysis to transform to the frequency wavenumber domain, and spectral moments to calculate the statistics of the modal response. However, both Fourier transforms and spectral moments are defined over the entire frequency wavenumber domain, and include negative as well as positive frequencies (and wavenumbers). Consequently to calculate the statistics of the response the power spectra are integrated over the range $\pm\infty$, a process which involves a large amount of computation. However, the amount of calculation necessary can be reduced by using the properties of power spectra to introduce the concept of a single sided spectrum. For a random process defined by $f(t)$, with frequency domain function $F(\omega)$, the power spectrum is defined by:

$$S_{ff}(\omega) = E\left[|F(\omega)|^2\right] \quad : \quad \omega \in [-\infty, \infty] \qquad (3.97)$$

Two observations can be made about the function; it is real, and it is even. Because it is an even function, integrating the power spectrum over the range $\pm\infty$ is the same as twice the integral of the same function over the range 0 to ∞. Therefore the power spectral expressions can be replaced with single sided spectra defined by:

$$G_{ff}(\omega) = 2E\left[|F(\omega)|^2\right] \quad : \quad \omega \in [0, \infty] \qquad (3.98)$$

which simplifies the calculation of the spectral moments by reducing the domain of the integration:

$$\lambda_n = \int_{-\infty}^{\infty} \omega^n S_{xx}(\omega) d\omega = \int_0^{\infty} \omega^n G_{xx}(\omega) d\omega \qquad (3.99)$$

To apply this to the preceding work, it should be noted that equations 3.82 to 3.85 result in cross spectral density matrices. The diagonal elements of these matrices are the power spectra of the modal response and are even, real valued functions as in 3.97. The off diagonal elements are the cross spectral density functions of the different modes; these retain information about the phase relationship between the modes and so, unlike the power spectra, have a real and imaginary part. Therefore, on first inspection it would seem that evaluation of the spectral moments for the cross spectral terms cannot be simplified and will involve integration of both real and imaginary parts over the entire frequency and wavenumber domains. However, if it can be shown that the imaginary parts of each of the products in 3.82 to 3.85 are odd functions, then they need not be evaluated as they will vanish when the spectral moments are calculated. Furthermore, if the real parts can be shown to be even functions then it will be possible to use single sided spectra.

3.4.1.1 The Dynamic Response

The cross spectral density matrix for the dynamic response is given by equation 3.82, and this shows that the response in the wavenumber domain is given by the product:

$$\{\mathbf{R}(\kappa)\}\{\mathbf{R}(\kappa)\}^{*T} \quad \text{.....(3.100)}$$

The ground influence vector is defined as a summation of delta functions in the space domain (equation 3.68), which when transformed to the wavenumber domain become a summation of complex exponential functions:

$$\{R(\kappa)\} = \begin{Bmatrix} \sum_{i=1}^{n} A_{1,i} e^{j\kappa l_i} \\ \sum_{i=1}^{n} A_{2,i} e^{j\kappa l_i} \\ \vdots \\ \sum_{i=1}^{n} A_{m,i} e^{j\kappa l_i} \end{Bmatrix} \quad \text{.....(3.101)}$$

The elements in the matrix formed by the product in 3.100 are therefore products of these complex exponentials and are analogous to the result given in equation 3.64:

$$a_{kl} = \sum_{i=1}^{n} \sum_{j=1}^{n} A_{ki} A_{lj} \ \mathrm{Re}\left\{ e^{-j\kappa(l_j - l_i)} \right\} \quad \text{.....(3.102)}$$

where a_{kl} is the element in row k and column l and is both real and even.

Now consider the response in the frequency domain, which is given by the triple product:

$$[\mathbf{H}(\omega)]_r [\mathbf{A}]_r [\mathbf{H}(\omega)]_r^{*T} \quad \text{.....(3.103)}$$

where $[\mathbf{A}]_r$ is a matrix which represents the response in the wavenumber domain:

$$[\mathbf{A}]_r = [\Phi]^T [\mathbf{M}] \{\mathbf{R}(\kappa)\} \{\mathbf{R}(\kappa)\}^{*T} [\mathbf{M}]^T [\Phi] \quad \text{.....(3.104)}$$

The real part of the dynamic response function is defined by:

$$\mathrm{Re}(H(\omega)_r) = \frac{\omega_r^2 - \omega^2}{\left(\omega_r^2 - \omega^2\right)^2 + \left(2\omega\omega_r\zeta_r\right)^2} \quad \text{.....(3.105)}$$

which is an even function (figure 3.13) and the imaginary part by:

$$\mathrm{Im}(H(\omega)_r) = \frac{-2\omega\omega_r\zeta_r}{\left(\omega_r^2 - \omega^2\right)^2 + \left(2\omega\omega_r\zeta_r\right)^2} \quad \text{.....(3.106)}$$

which is odd (figure 3.14). Therefore, the real part of the product in 3.103 consists of products of even functions with even functions and of odd functions with odd functions and is an even function. Similarly the imaginary part is an odd function and vanishes when integrated of the range $\pm\infty$. It can now be concluded that the moments of the cross spectral density matrix can be calculated from single sided spectra, and that only the real parts of the cross spectra need to be considered.

3.4.1.2 Pseudo-Static Response

From equation 3.85 the pseudo-static response in the wavenumber domain is given by:

$$\{\mathbf{N}(\kappa)\}\{\mathbf{N}(\kappa)\}^{*T} \quad \text{.....(3.107)}$$

Now the modified ground influence vector is defined in terms of the ground influence vector $\{\mathbf{R}(\kappa)\}$ and the mean ground acceleration:

$$\{\mathbf{N}(\kappa)\} = \left\{ \begin{array}{l} \sum_{i=1}^{n} A_{1,i}\left[e^{-j\kappa l_i} - \frac{1}{d_i}\sum_{j=1}^{d_i} e^{-j\kappa l_j} \right] \\ \sum_{i=1}^{n} A_{2,i}\left[e^{-j\kappa l_i} - \frac{1}{d_i}\sum_{j=1}^{d_i} e^{-j\kappa l_j} \right] \\ \vdots \\ \sum_{i=1}^{n} A_{m,i}\left[e^{-j\kappa l_i} - \frac{1}{d_i}\sum_{j=1}^{d_i} e^{-j\kappa l_j} \right] \end{array} \right\} \quad \text{.....(3.108)}$$

where d_i is the total number of ground degrees of freedom with the same orientation as degree of freedom i. Therefore the terms in 3.85 are products of complex exponentials similar to those discussed for the dynamic response; consequently the spectral moments can be calculated from the

real parts of single sided spectra. The pseudo-static response in the frequency domain is given by the term $\frac{1}{\omega^4}$ which is clearly a real, even function.

3.4.1.3 The Cross Terms

Equations 3.83 and 3.84 contribute extra terms to the overall cross-spectral density matrix that represent the interaction of the pseudo-static and dynamic responses. Considering first the wavenumber domain it can be noted by following the same logic as in the previous two sections that the products:

$$\{\mathbf{R}(\kappa)\}\{\mathbf{N}(\kappa)\}^{*T} \quad \text{and} \quad \{\mathbf{N}(\kappa)\}\{\mathbf{R}(\kappa)\}^{*T} \qquad \text{.....(3.109)}$$

have even real parts and odd imaginary parts. Therefore, the imaginary part vanishes when the spectral moments are calculated and a single sided spectrum can be used. For the frequency domain component $[\mathbf{H}(\omega)]_r$ is a diagonal matrix and so:

$$\frac{1}{\omega^2}[\mathbf{H}(\omega)]_r[\Phi]^T[\mathbf{M}]\{\mathbf{R}(\kappa)\}\{\mathbf{N}(\kappa)\}^{*T}[\mathbf{M}]^T[\Phi] \qquad \text{.....(3.110)}$$

$$= \frac{1}{\omega^2}\left[[\Phi]^T[\mathbf{M}]\{\mathbf{R}(\kappa)\}\{\mathbf{N}(\kappa)\}^{*T}[\mathbf{M}]^T[\Phi]\right]^T[\mathbf{H}(\omega)]_r$$

Now, because the imaginary part of the wavenumber response can be neglected when calculating the moments, the following simplification can be made:

$$\mathrm{Re}\left(\left[[\Phi]^T[\mathbf{M}]\{\mathbf{R}(\kappa)\}\{\mathbf{N}(\kappa)\}^{*T}[\mathbf{M}]^T[\Phi]\right]^T\right)$$

$$= \mathrm{Re}\left(\left[[\Phi]^T[\mathbf{M}]\{\mathbf{R}(\kappa)\}\{\mathbf{N}(\kappa)\}^{*T}[\mathbf{M}]^T[\Phi]\right]^{*T}\right) \qquad \text{.....(3.111)}$$

$$= \mathrm{Re}\left([\Phi]^T[\mathbf{M}]\{\mathbf{N}(\kappa)\}\{\mathbf{R}(\kappa)\}^{*T}[\mathbf{M}]^T[\Phi]\right)$$

This allows 3.110 to be rewritten as:

$$\frac{1}{\omega^2}[\mathbf{H}(\omega)]_r \mathrm{Re}\left([\Phi]^T[\mathbf{M}]\{\mathbf{R}(\kappa)\}\{\mathbf{N}(\kappa)\}^{*T}[\mathbf{M}]^T[\Phi]\right) = \frac{1}{\omega^2}\mathrm{Re}\left([\Phi]^T[\mathbf{M}]\{\mathbf{N}(\kappa)\}\{\mathbf{R}(\kappa)\}^{*T}[\mathbf{M}]^T[\Phi]\right)[\mathbf{H}(\omega)]_r \quad \text{.....(3.112)}$$

It was noted from 3.106 that the imaginary part of the dynamic frequency response function is odd and so the imaginary part of 3.112 vanishes when integrated over the range $\pm\infty$. Therefore equations 3.83 and 3.84 can be combined to give:

$$\mathrm{Re}\left(\{\mathbf{Y}_d(\kappa,\omega)\}\{\mathbf{Y}_s(\kappa,\omega)\}^{*T} + \{\mathbf{Y}_d(\kappa,\omega)\}\{\mathbf{Y}_s(\kappa,\omega)\}^{*T}\right) = \mathrm{Re}\left(\frac{2}{\omega^2}[\Phi]^T[\mathbf{M}]\{\mathbf{N}(\kappa)\}\{\mathbf{R}(\kappa)\}^{*T}[\mathbf{M}]^T[\Phi][\mathbf{H}(\omega)]_r\right) \quad \text{.....(3.113)}$$

where it has been noted that because $[\mathbf{H}(\omega)]_r$ is diagonal:

$$[\mathbf{H}(\omega)]_r + [\mathbf{H}(\omega)]_r^{*T} = 2\mathrm{Re}\left([\mathbf{H}(\omega)]_r\right) \quad \text{.....(3.114)}$$

3.4.1.4 Summary of Simplifications

The three preceding sections have shown that the spectral moments can be calculated by considering only the real part of the cross spectral density matrix. Furthermore, because the real part of each element in this matrix is an even function, the calculations can be performed using a single sided spectrum; this leads to a fourfold increase in efficiency for a two dimensional random field. The spectral moments are then given by:

$$[\lambda_d]_r = \int_0^\infty \int_0^\infty \mathrm{Re}\left([H(\omega)]_r[\Phi]^T[\mathbf{M}]\{\mathbf{R}(\kappa)\}\{\mathbf{R}(\kappa)\}^{*T}[\mathbf{M}]^T[\Phi][H(\omega)]_r^{*T}\right)S_{aa}(\omega,\kappa)d\omega d\kappa \text{ . (3.115)}$$

$$[\lambda_c]_r = \int_0^\infty \int_0^\infty \mathrm{Re}\left(\frac{2}{\omega^2} [\Phi]^T [\mathbf{M}] \{\mathbf{N}(\kappa)\} \{\mathbf{R}(\kappa)\}^{*T} [\mathbf{M}]^T [\Phi] [H(\omega)]_r \right) S_{aa}(\kappa, \omega) d\omega d\kappa \quad \text{..... (3.116)}$$

$$[\lambda_s]_r = \int_0^\infty \int_0^\infty \mathrm{Re}\left(\frac{1}{\omega^4} [\Phi]^T [\mathbf{M}] \{\mathbf{N}(\kappa)\} \{\mathbf{N}(\kappa)\}^{*T} [\mathbf{M}]^T [\Phi] \right) S_{aa}(\kappa, \omega) d\omega d\kappa \quad \text{..... (3.117)}$$

Finally it needs to be noted that to use these simplifications the model of the ground power density spectrum also needs to be an even function.

3.4.2 Recombination of Modal Results

Once the results have been calculated in modal co-ordinates it is necessary to transform them back to the global co-ordinate system in order to obtain useful answers. One method of combining modal results is the complete quadratic combination (CQC) [Wilson et al. 1982] which is defined by:

$$\nu_k = \left(\sum_{r=1}^{nm} \sum_{s=1}^{nm} \nu_{kr} \rho_{rs} \nu_{ks} \right)^{\frac{1}{2}} \quad \text{..... (3.118)}$$

where:

$$\rho_{rs} = \frac{\kappa_{rs}}{\sigma_r \sigma_s} = \frac{\lambda_{0,rs}}{\sigma_r \sigma_s} \quad \text{..... (3.119)}$$

is the modal cross correlation coefficient. Consider now the RMS displacements of the structure which are defined by:

$$\sigma(\nu_{kr}) = \sigma_r \phi_{kr} \quad \text{..... (3.120)}$$

and hence 3.117 becomes:

$$\sigma(\nu_k)=\left(\sum_{r=1}^{nm}\sum_{s=1}^{nm}\frac{\sigma_r\phi_{kr}\lambda_{0,rs}\sigma_s\phi_{ks}}{\sigma_r\sigma_s}\right)^{\frac{1}{2}}=\left(\sum_{r=1}^{nm}\sum_{s=1}^{nm}\phi_{kr}\lambda_{0,rs}\phi_{ks}\right)^{\frac{1}{2}} \quad \text{.....(3.121)}$$

This indicates that the zeroth spectral moments of the response in global co-ordinates can be obtained by using a simple transformation of the spectral moment matrix:

$$[\lambda_0]=[\sigma^2] \quad \text{.....(3.122)}$$

where

$$[\sigma]=[\Phi]^T[\lambda_0]_r[\Phi] \quad \text{.....(3.123)}$$

The diagonal elements of $[\lambda_0]$ are the zeroth spectral moments of the displacements in each of the global degrees of freedom. A similar transformation can be shown to apply for the higher spectral moments, which are also needed to calculate the statistics of the response. The *n*th spectral moment is defined by equation 3.13 as:

$$\lambda_n=\int_{-\infty}^{\infty}\omega^n S_{xx}(\omega)d\omega \quad \text{.....(3.13)}$$

If a new function $S^n(\omega)$ is now defined as follows:

$$S^n(\omega)=S_{xx}(\omega)\omega^n \quad \text{.....(3.124)}$$

then it can be seen that the zeroth moment of $S^n(\omega)$ equals the *n*th moment of $S_{xx}(\omega)$:

$$\lambda_0\left(S^n(\omega)\right)=\lambda_n\left(S_{xx}(\omega)\right) \quad \text{.....(3.125)}$$

Therefore 3.119 can be used to obtain a cross correlation coefficient for the higher spectral moments, and the transformation in 3.118 applied for all spectral moments:

$$\left[\sqrt{\lambda_n}\right]=[\Phi]^T[\lambda_n]_r[\Phi] \quad \text{.....(3.126)}$$

3.4.2.1 Calculation of Internal Forces

The displacements, though helpful in characterising the behaviour of a structure, are not the most useful measure of the response for its design. It would be more useful to be able to predict the bending moments and internal forces in a structure as these can be used to determine the size of structural members. Therefore, the theory discussed so far needs to be adapted to consider these internal forces and produce results in terms of them. If, as has been assumed so far, the structure is linear elastic, then the internal forces will be linear functions of the structural displacements, and can be obtained from the stress recovery matrices. Noting that the transformation from modal to global co-ordinates is also a linear combination of the results an equation analogous to 3.126 can be written down for the calculation of the spectral moments of the internal forces:

$$\left[\sqrt{\lambda_{f,n}}\right]=[\mathbf{T}_e]^T[\lambda_n][\mathbf{T}_e] \quad \text{.....(3.127)}$$

However, if equation 3.127 is used then all the global cross correlation terms have to be calculated to correctly predict the internal forces. This represents extra computation which should be avoided if possible. An alternative approach is to consider the internal forces which correspond to the modal deflections of the structure, the modal forces, and use these in place of the mode shape matrices in equation 3.126:

$$\left[\sqrt{\lambda_{f,n}}\right] = [\Gamma]^T [\lambda_n]_r [\Gamma] \quad \text{.....(3.128)}$$

This is equivalent to expanding the expression in 3.126:

$$\left[\sqrt{\lambda_{f,n}}\right] = [T_e]^T [\Phi]^T [\lambda_n]_r [\Phi][T_e] \quad \text{.....(3.128)}$$

and replacing the product $[T_e]^T [\Phi]^T$ with a matrix of modal forces $[\Gamma]^T$ which relates the internal forces for selected degrees of freedom to the modal response.

3.5 Conclusions

The theoretical work reviewed and outlined in this chapter has shown that it is possible to analyse the response of extended structures to spatially varying seismic loads using a power spectral approach. In designing a long span bridge account needs to be taken of the uncertainties that exist both in the structural system itself and in the description of the loading. One method for dealing with these uncertainties is to use probability theory and to consider both the excitation and the structural response as random processes. Power spectral analysis can then be used to predict the statistics of the system response.

To predict the response of an extended structure to asynchronous or multi support seismic excitation, the spatial distribution of the loading can be described in terms of a wavenumber power density spectrum. The structural response can then be found in terms of a two dimensional cross spectral density matrix in the wavenumber frequency domain.

It is now necessary to implement the method outlined in this chapter and to validate the approach by comparing the results with the results of other methods. This task will now be outlined in chapter four.

	Actual Event	Detailed Analysis	Design Analysis
Structure	Behaviour of structure governed by material and geometrical properties which are influenced by structural flaws, localised residual stresses, temperature etc.	Material and geometric properties have to be estimated from measured data. Complex mathematical models of structural behaviour can be used, but lack of detailed knowledge of material and geometric flaws limits applicability of the analysis	Material and geometric properties obtained from standard tables. Greatly simplified models of structural behaviour used.
Interaction of earthquake and structure.	Response will depend on size, mode shapes, damping, natural frequencies of structure, and on the frequency content, source, and propagation velocity of the seismic wave.	Investigations of local geology and topography can be used to help define the input to a detailed analysis that takes account of soil structure interaction and the spatial variations in the loading.	Design analyses disregard the effects of spatial variations in the loading, and use approximate models of soil structure interaction.
Earthquake	A given earthquake is described by the location(s) and mechanisms of fault slippage, energy released, duration and frequency content.	Recordings of previous events, and general seismic activity, can be used to predict likely properties and locations of future events.	Recordings of previous events are used to generate design response spectra.

Table 3.1 : Applicable Knowledge in Design and Analysis of Seismic Response of Long Span Bridges

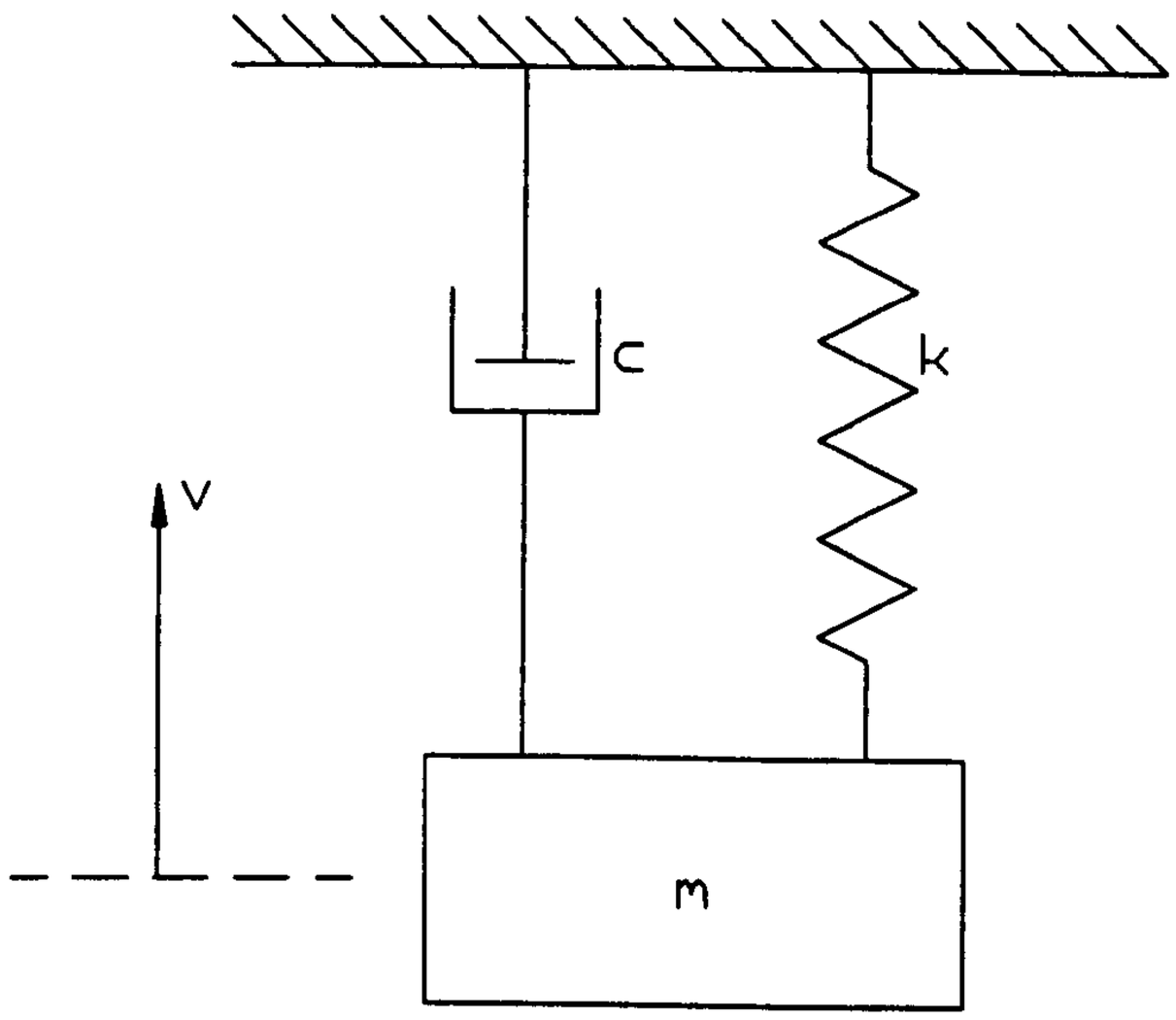

Figure 3.1 -:- Single Degree Of Freedom System

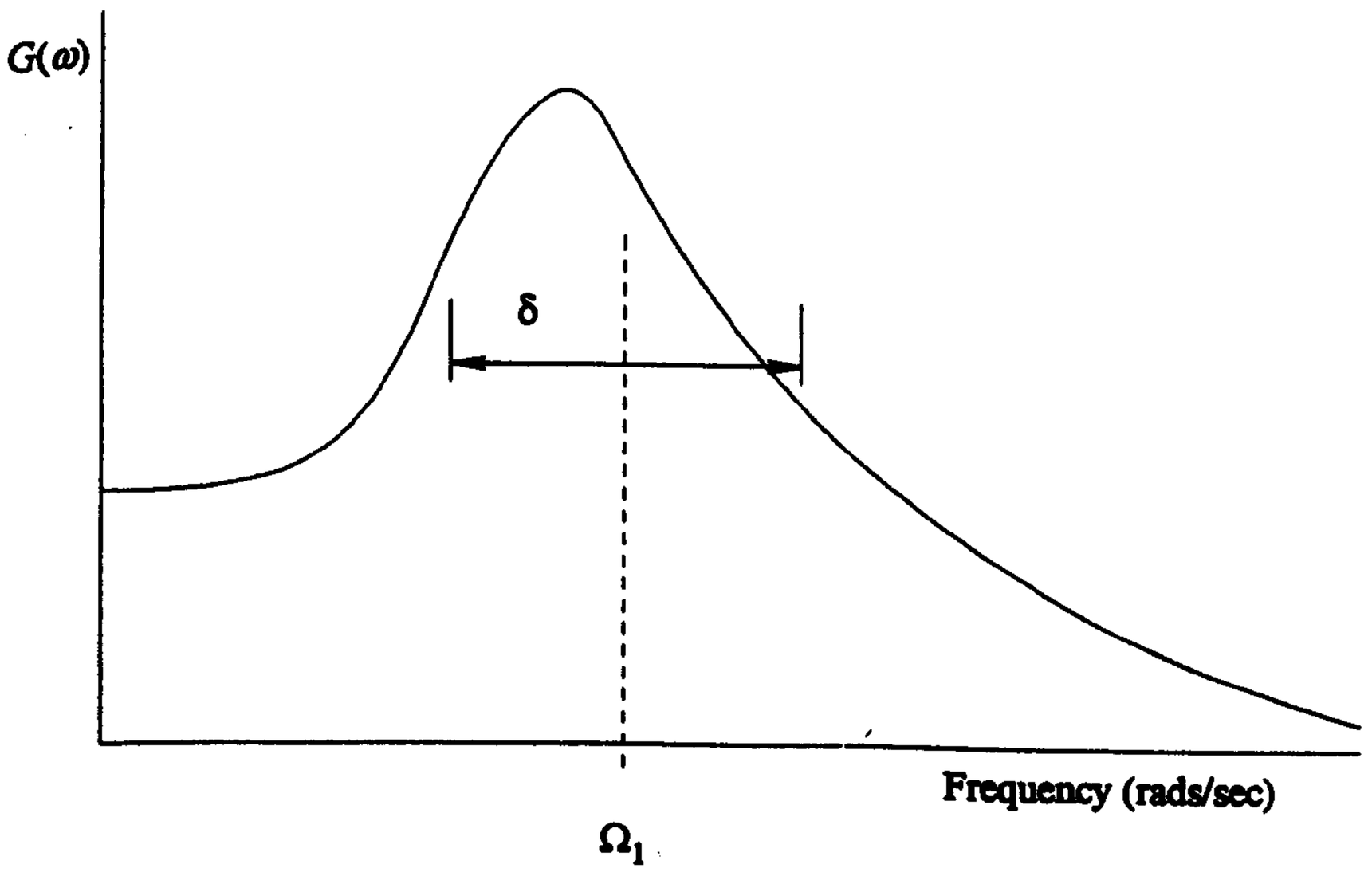

Figure 3.2 -:- Spectral Parameters (After Vanmarcke 1975)

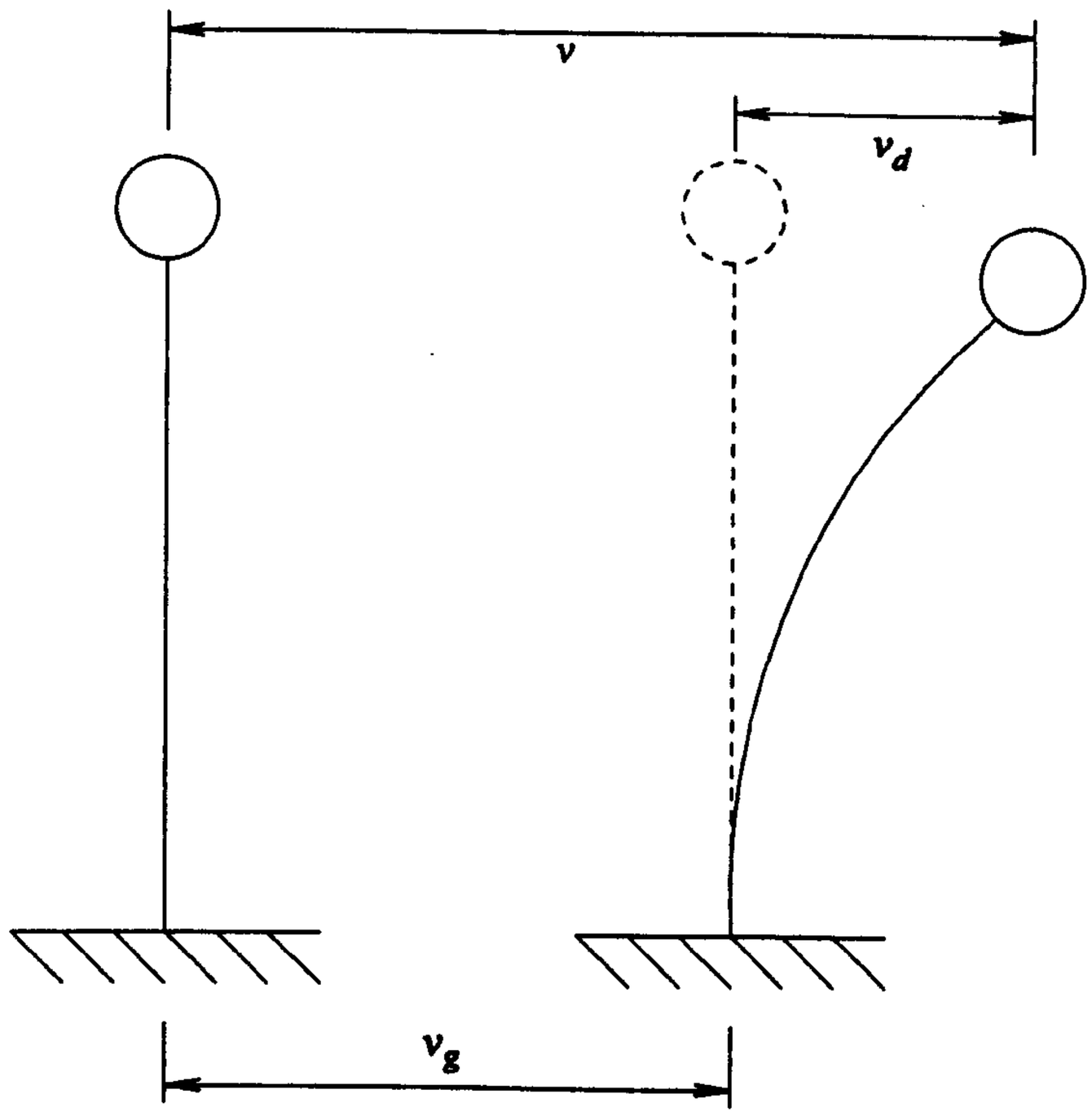

Figure 3.3 -:- Response Of SDOF System To Seismic Excitation

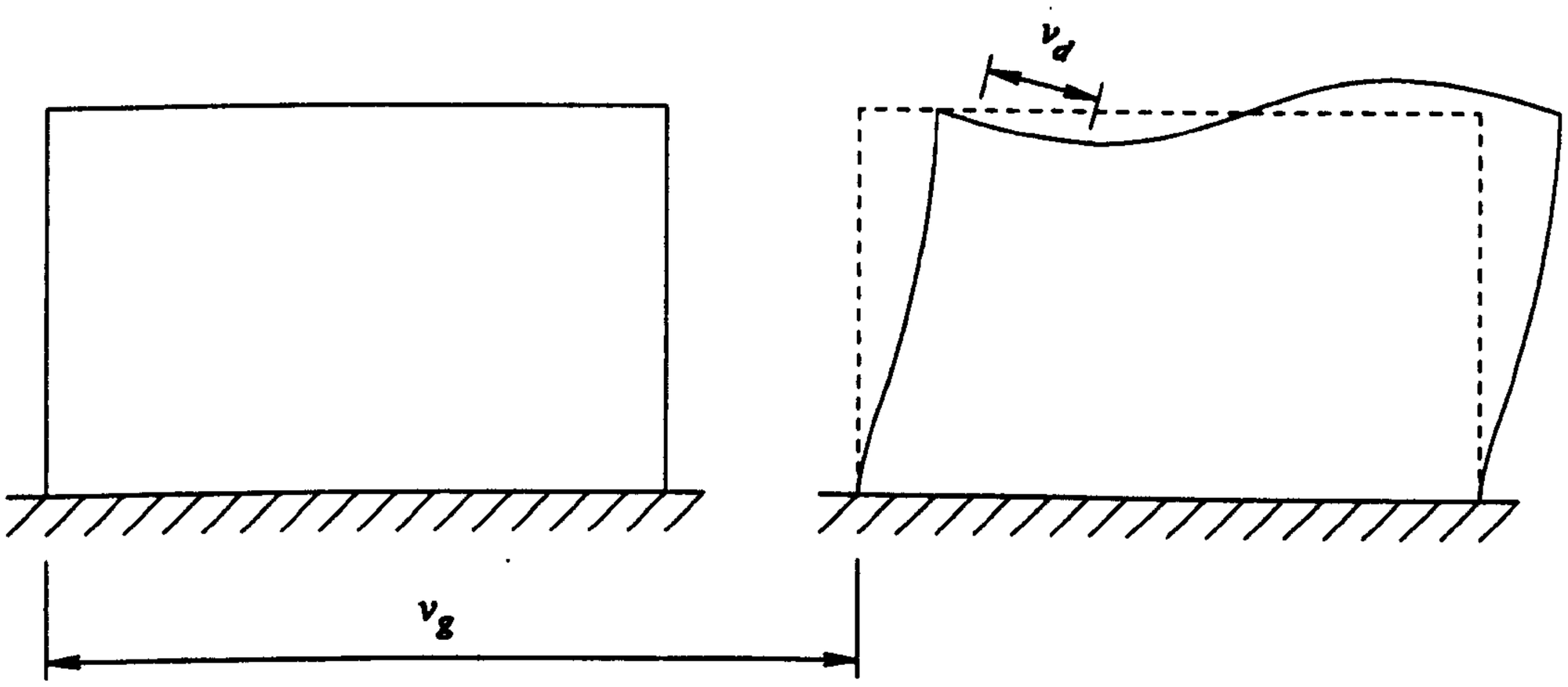

Figure 3.4 -:- Response Of MDOF System To Synchronous Seismic Excitation

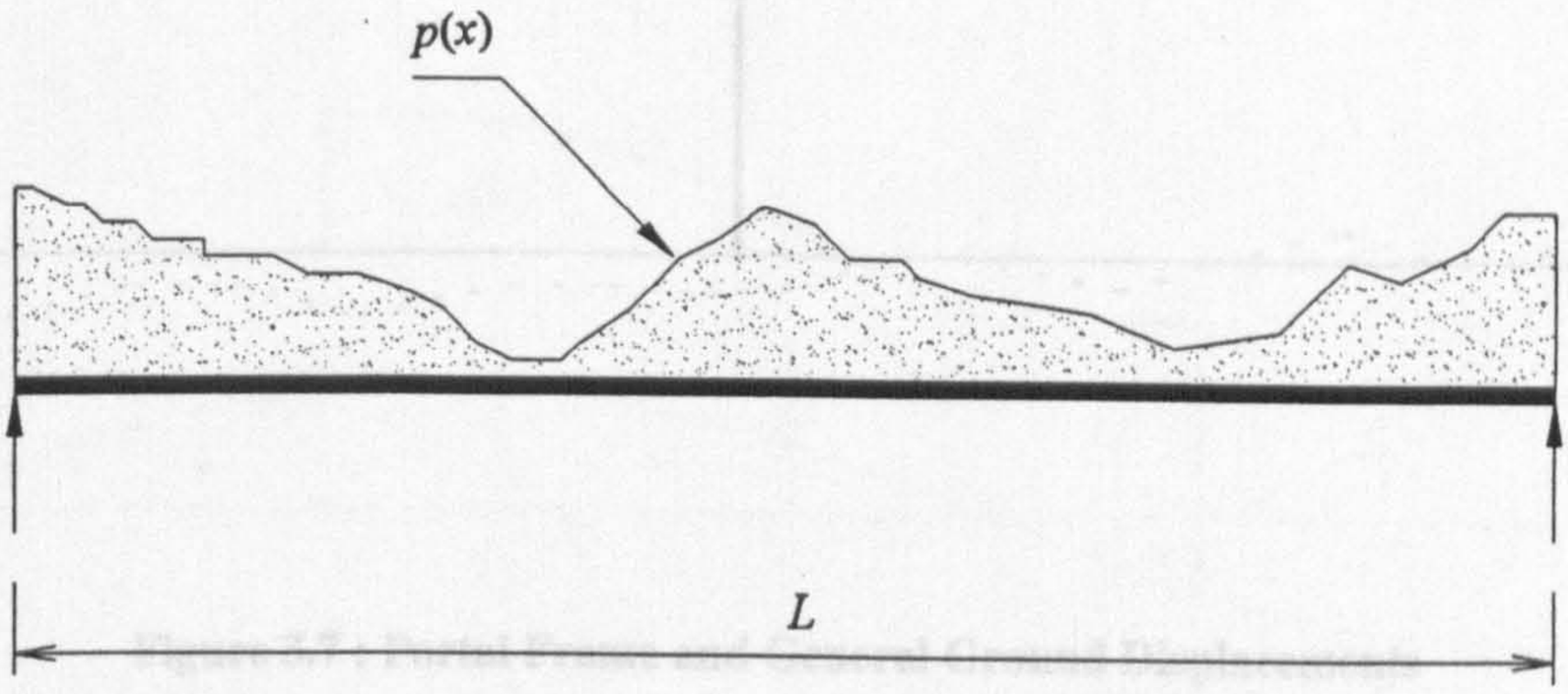

Figure 3.5 -:- Simply Supported Beam Subject To Spatially varying Load

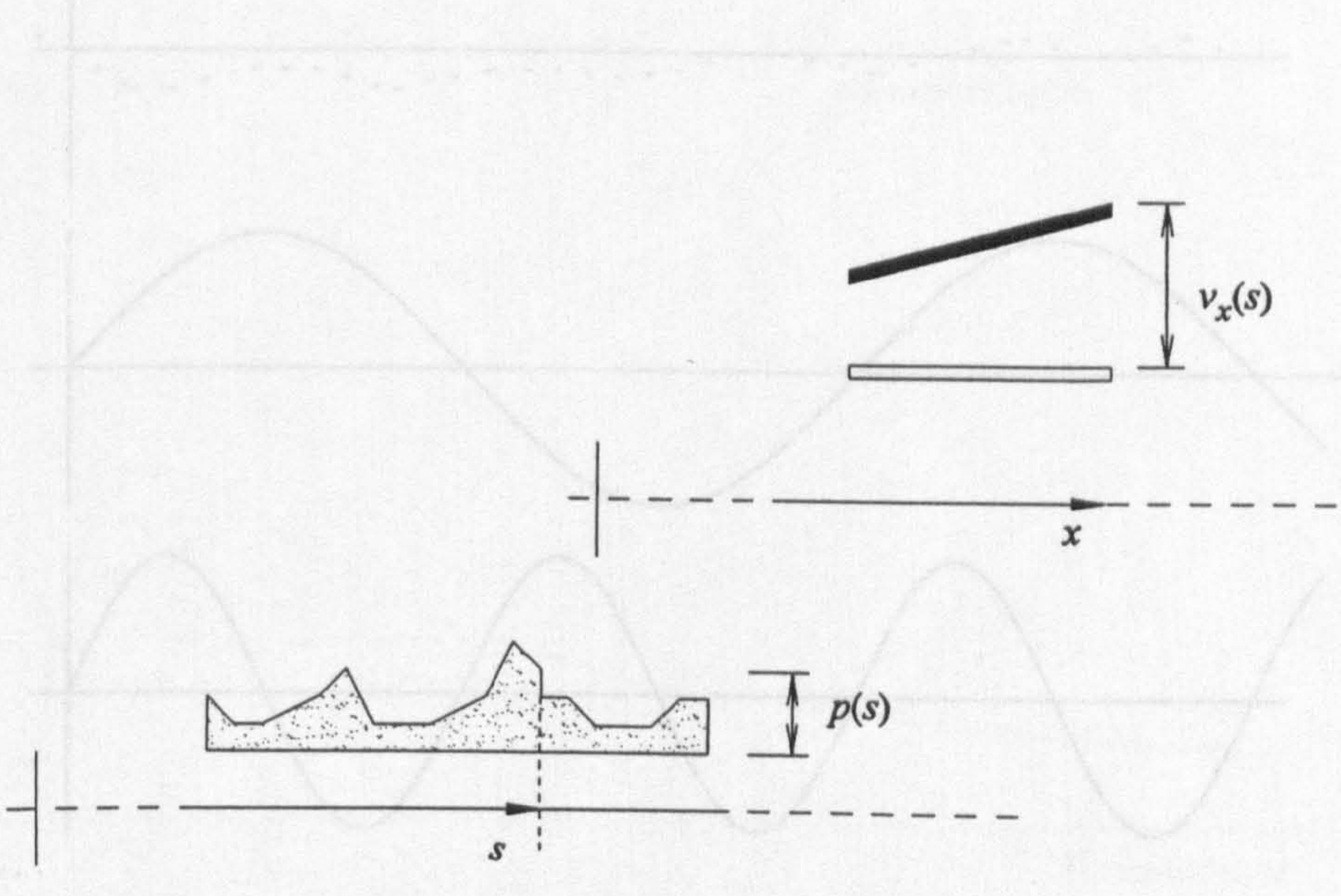

Figure 3.6 -:- Derivation Of Ground Influence Line For Response At *x* To Load At *s*

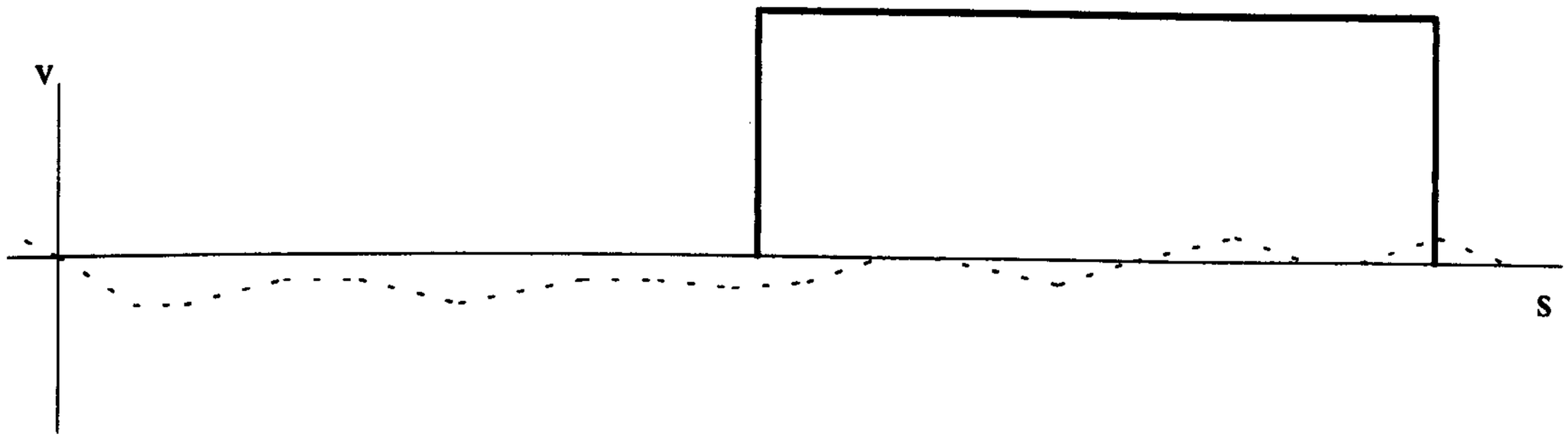

Figure 3.7 : Portal Frame and General Ground Displacements

Arbritrary Origin Fixes Phase Of Generalised Coordinates

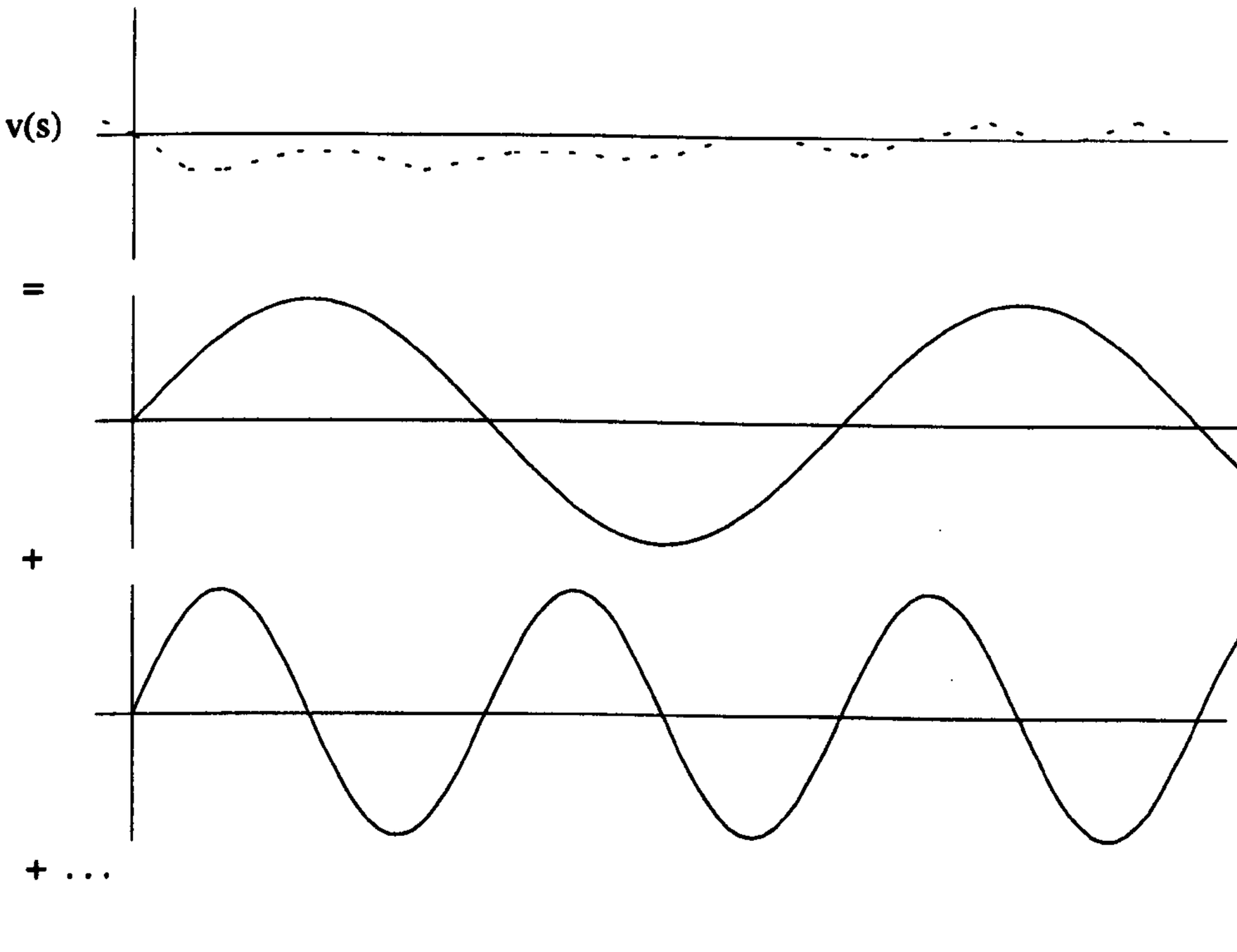

Figure 3.8 : Ground Displacements in Terms of Generalised Coordinates With Arbritrary Origin

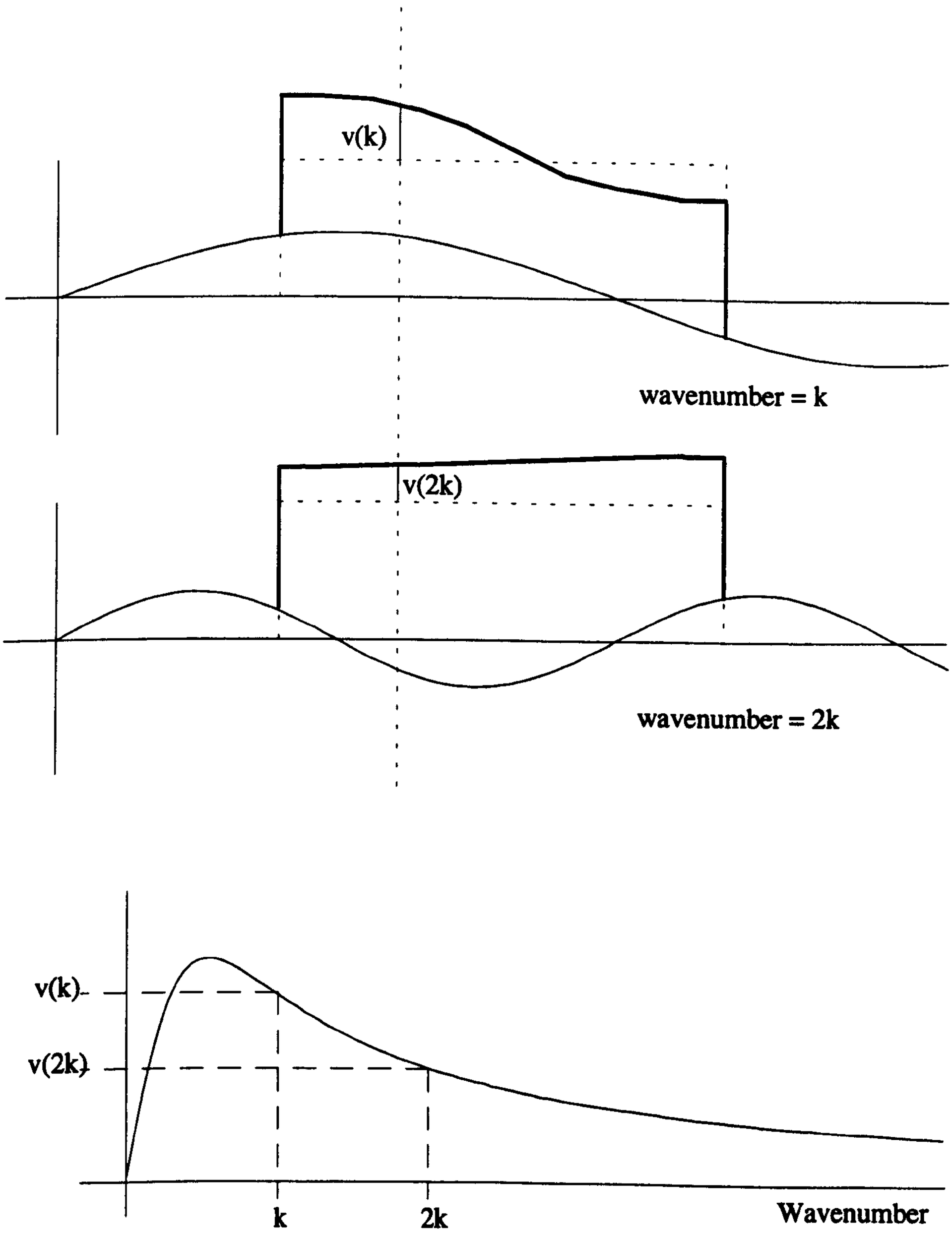

Figure 3.9 : Illustration of Wavenumber Response at a Point in a Portal Frame

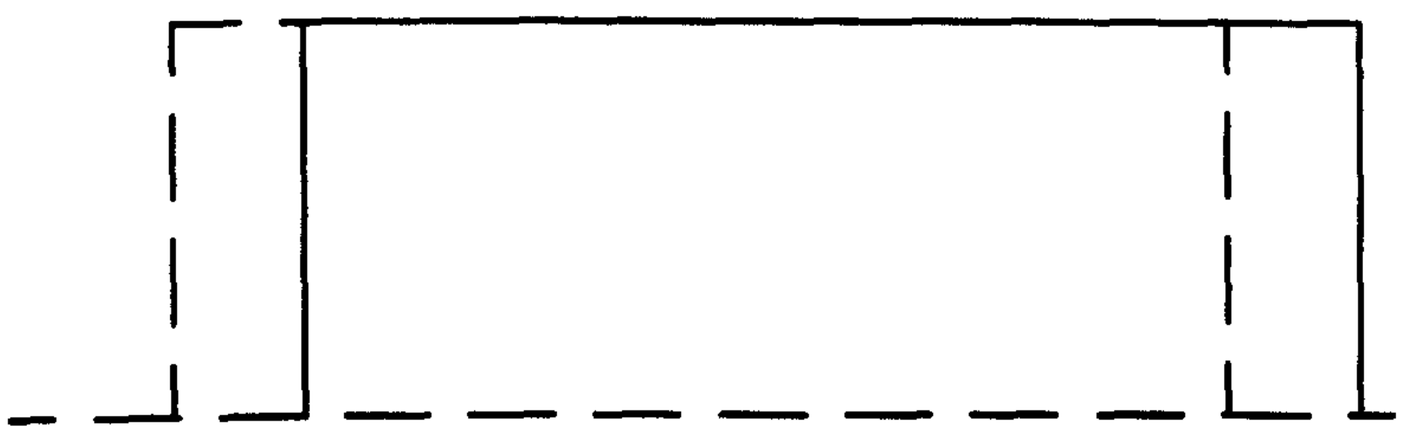

Ground Motion in Phase

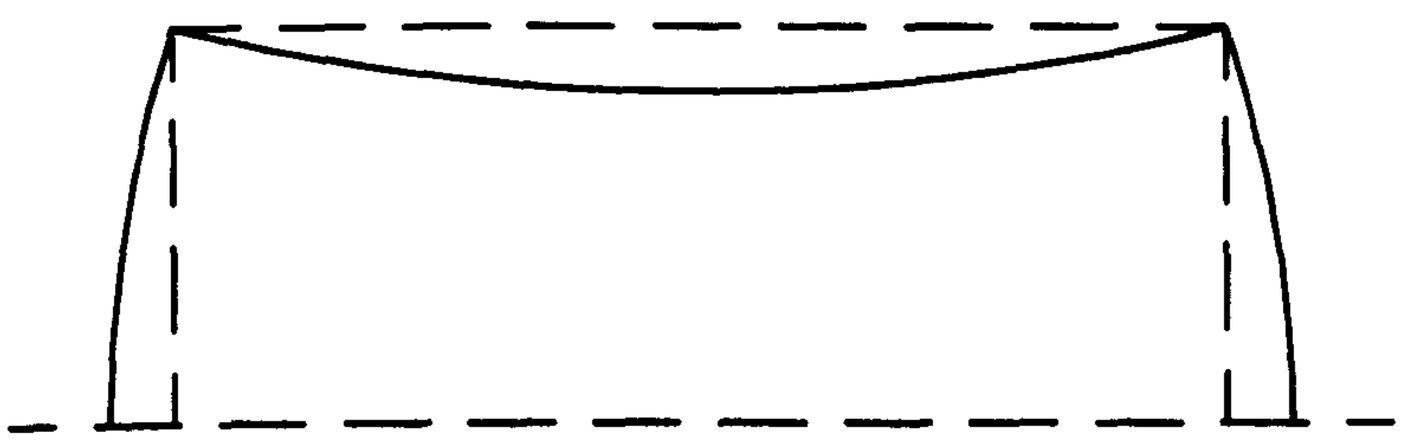

Ground Motion out of Phase

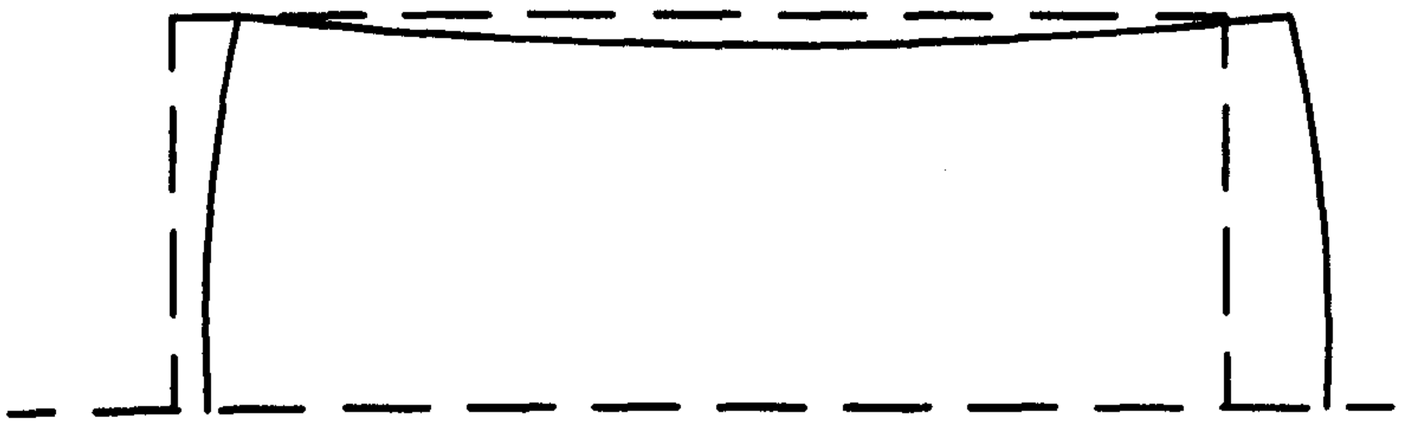

General Ground Motion

Figure 3.10 : Response of Portal Frame to Asynchronous Horizontal Seismic Input

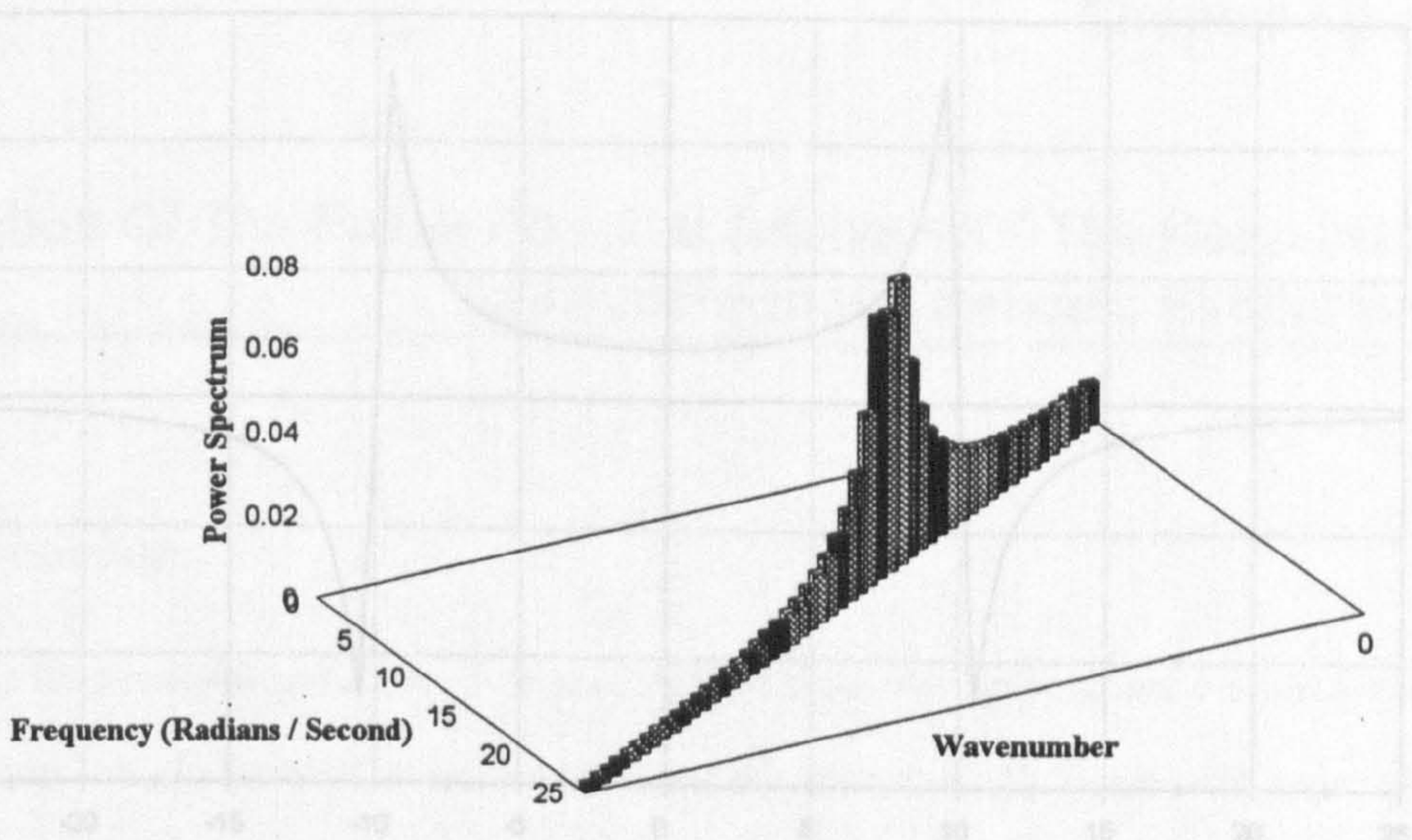

Figure 3.11 -:- Two Dimensional Ground Power Density Spectrum

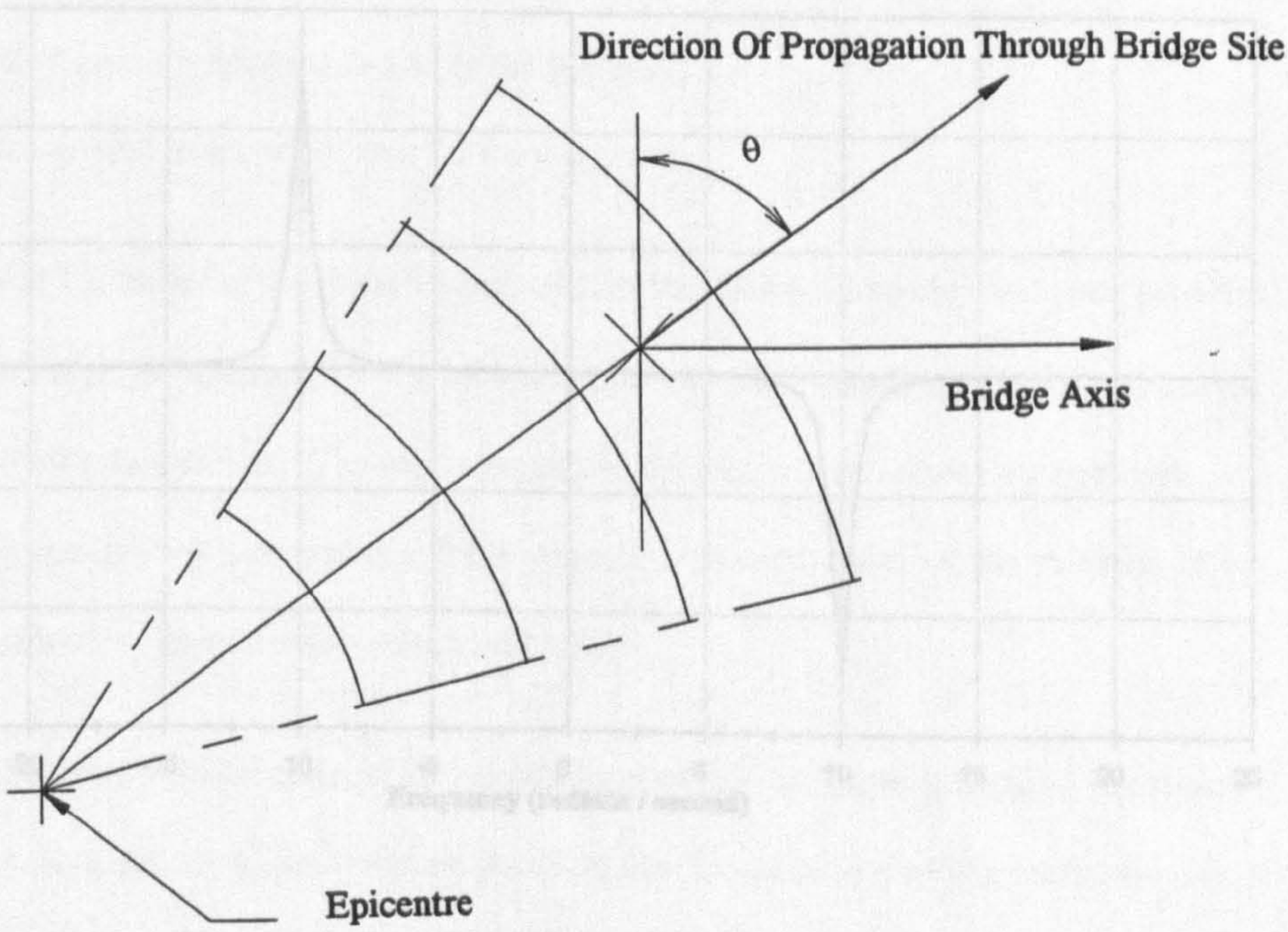

Figure 3.12 -:- Influence Of Epicentral Location On Relative Propagation Velocity

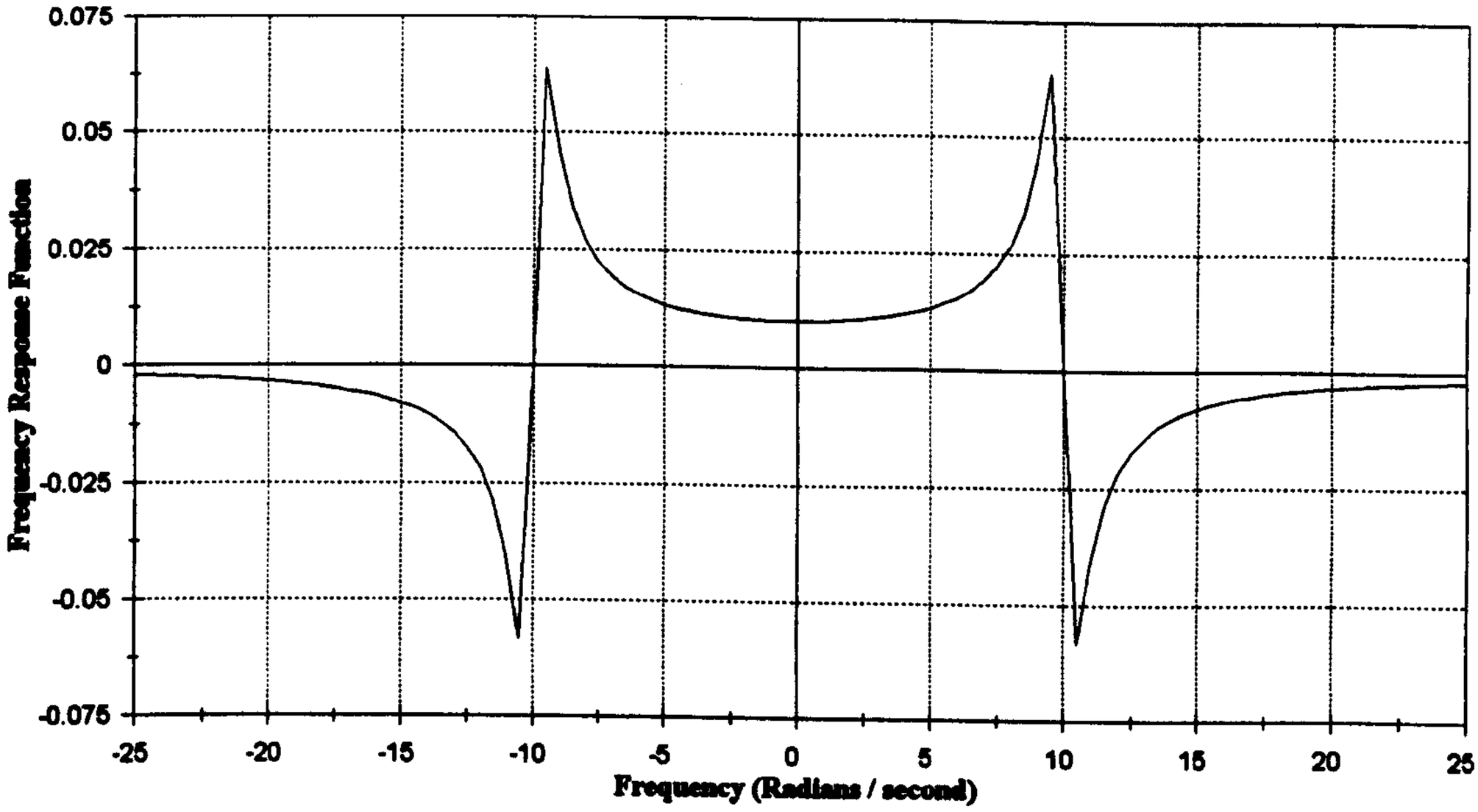

Figure 3.13 -:- Real Part Of SDOF Frequency Response Function

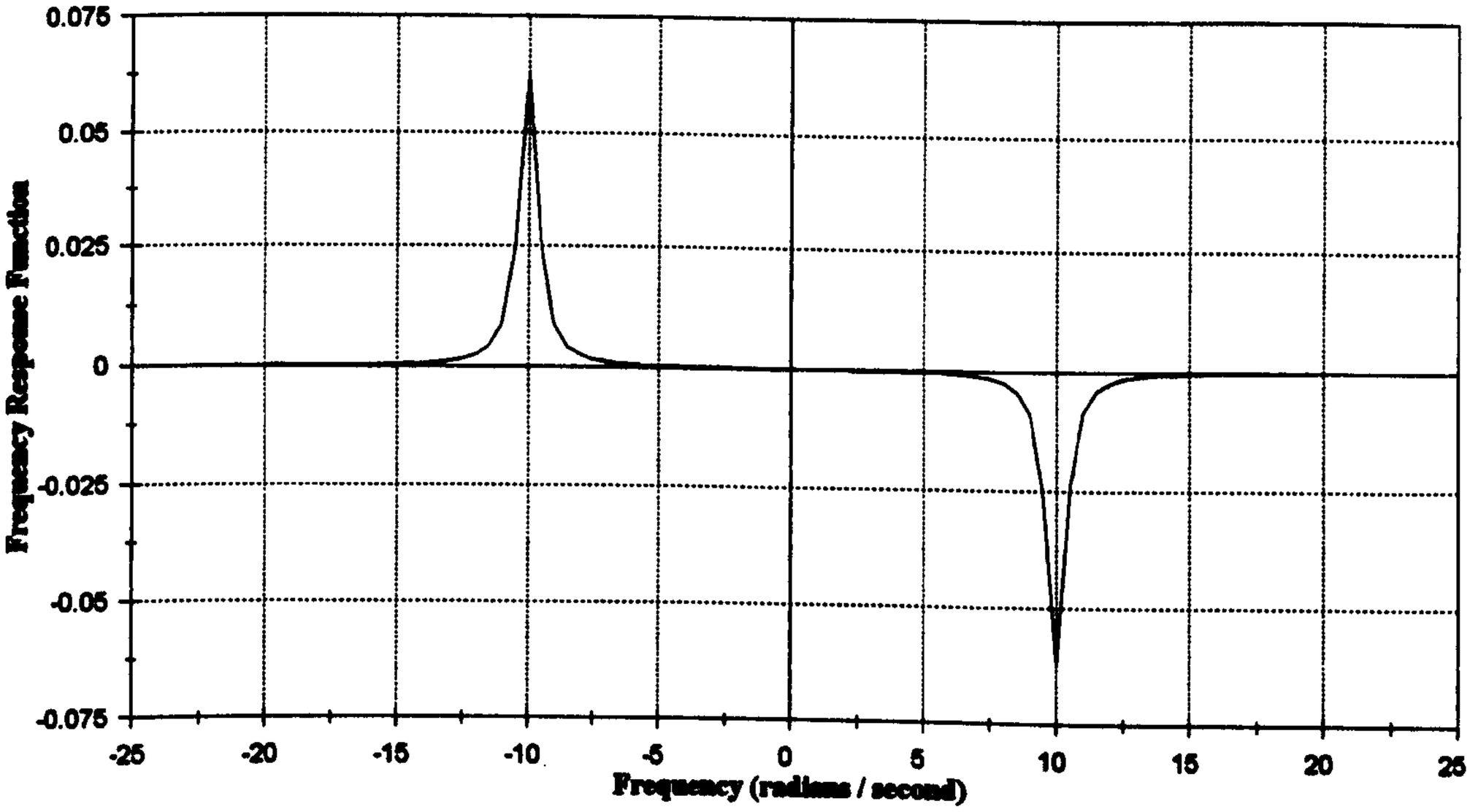

Figure 3.14 -:- Imaginary Part Of SDOF Frequency Response Function

Chapter Four

Validation Of The Power Spectral Analysis Of The Response To Asynchronous Seismic Excitation

4.0 Introduction

In chapter three the power spectral approach to structural dynamics was reviewed and a method was proposed applying it to the problem of multi-support seismic excitation. To pursue this approach further it is necessary to implement the procedures from chapter three in a computer program. Chapter three showed that this will require:

i. a model of the ground motion,

ii. the mode shapes of the structure,

iii. the frequency response matrix of the structure, and

iv. the ground influence vectors for the structure

With the exception of the model of the ground input, each of the above can be obtained from standard finite element analyses of the structure; an eigensolution provides the dynamic properties and a static analysis the ground influence vectors. The implementation program will therefore be a specialist post processor using the results from a commercial finite element package to calculate the statistics of the response to multi-support or asynchronous seismic excitation.

Verification and validation are vital parts in the development of any computer program. Verification is a demonstration that the code faithfully implements the intended algorithm, validation is a demonstration that the coded algorithm produces bona fide results. Verification of the code is

achieved by a rigorous checking of the code as it is written, subroutine by subroutine, and by comparing intermediate results at different stages of execution. Validation of the code and algorithm is a more complicated procedure which requires comparing the results from the program either with results from other analyses or from physical models. For the power spectral approach considered in this thesis two factors have to be validated, the modelling of the spatially varying load and the calculation of the response statistics. These can be achieved by comparing the results with the results from a standard time history analysis of the problem, repeated many times for statistically similar earthquakes. This represents a Monte Carlo simulation of the problem.

To help in validation it is useful to consider simple problems for which the results can be interpreted easily. The simplest type of spatially varying ground motion is asynchronous loading which is caused purely by the relative time delay as the ground wave passes along the length of the structure. Similarly, possibly the simplest structure that can experience asynchronous motion is a portal frame. This chapter, therefore outlines the analysis of a simple portal frame using both the power spectral and time history methods. The results of the two analyses are then compared to validate the power spectral approach. Finally, conclusions from the analysis of this simple structure are drawn regarding the efficacy of the power spectral approach, the importance of asynchronous loading, and the validity of the proposed method.

4.1 Program STASY

The program STASY (STochastic ASYnchronous) was written to incorporate the ideas presented in chapter three into a single piece of code which could be use to calculate the response of a given structure to asynchronous seismic loading. The program uses structural details - mass matrix, ground influence vectors, mode shapes and natural frequencies - obtained from a finite element analysis to

form the frequency wavenumber response matrix of the structure in the modal system of co-ordinates. This is then combined with the power density spectrum of the ground excitation before being integrated to yield the zeroth, first and second spectral moments of the response in modal co-ordinates. These are then transformed back into the global system of co-ordinates and finally used to calculate the statistics of the response. The structure of the program is shown in flow chart form in figure 4.1.

4.1.1 Input Power Density Spectrum

The model used by the program to create a power density spectrum to represent the ground excitation is the filtered white noise approach using the Kanai-Tajimi filter [Kanai 1957, Tajimi 1960]. This model for the power density spectrum was chosen as it is simple to program, and has been widely used in other studies. The Kanai-Tajimi filter is defined by:

$$G_{aa}(\omega) = G_0 \frac{1+\left(\frac{2\xi_g\omega}{\omega_g}\right)^2}{\left(1-\left(\frac{\omega}{\omega_g}\right)^2\right)^2+\left(\frac{2\xi_g\omega}{\omega_g}\right)^2} \qquad \text{.....(4.1)}$$

for a single sided power spectrum (figure 4.2). However, the Kanai-Tajimi spectrum creates a problem when dealing with the pseudo-static part of the response. The expressions for the spectral moments derived in chapter three include terms in $\frac{1}{\omega^2}$ and $\frac{1}{\omega^4}$. As the expression in 4.1 equals 1 for zero frequency, the resulting response will therefore tend to infinity for low frequencies. This is unrealistic. To remove this problem it is necessary to apply a second filter which removes the low frequency components from the expression in equation 4.1. Clough and Penzien [Clough & Penzien 1975] recommended multiplying the Kanai-Tajimi filter by the following expression:

$$G_{filt}(\omega) = \frac{\left(\frac{\omega}{\omega_f}\right)^4}{\left(1-\left(\frac{\omega}{\omega_f}\right)^2\right)^2 + \left(\frac{2\xi_f\omega}{\omega_f}\right)^2} \quad \text{.....(4.2)}$$

which has the effect shown in figure 4.3. Finally, §3.3.1 has shown that for the case of asynchronous excitation the wavenumber component of the power density spectrum is simply a delta function, hence the frequency wavenumber spectrum is just a transformed version of 4.2.

4.1.2 Integration Schemes

The spectral moments derived in chapter three are all integral expressions (equations 3.115-117) and these have to be evaluated by the program using numerical techniques. However, this introduces several possible sources of error. Firstly, each of the integrals is defined over the range 0 to ∞ which is not possible to do numerically. Secondly, the choice of points at which the integrand is evaluated has to be made in a systematic manner, and therefore the scheme programmed may not be the optimum case for the integral in question. Finally, any numerical integration scheme is an approximation and there will therefore be some numerical errors in the results.

It was decided to implement a four point Gauss scheme in program STASY which uses a third order polynomial to interpolate the integrand. This approach required the domain to be divided into a series of intervals which depended on the domain of the integration being performed. The integrand for the wavenumber domain is a delta function as discussed above, and because of this integration of the wavenumber domain can be included in the integration of the frequency domain as follows. A typical element of the matrices described in equations 3.115-117 can be expressed as the following integral of a product:

$$\lambda_{rs} = \int_0^\infty \int_0^\infty A(\omega)B(\kappa)G_{aa}(\kappa,\omega)d\kappa d\omega \quad \text{.....4.3}$$

Now, since the wavenumber power density spectrum of the ground excitation is described by a delta function, equation 4.3 simplifies to:

$$\lambda_{rs} = \int_0^\infty A(\omega)B\left(\frac{\omega}{c}\right)G_{aa}(\omega)d\omega \quad \text{.....4.4}$$

The evaluation of the integration in the frequency domain is more complicated and two cases have to be considered; integration of single mode response (the diagonal elements of the cross spectral response matrix) and the integration of mixed mode response (the off diagonal terms). For response in a single mode, there is just a single peak in the frequency response function and the frequency domain is divided up into 12 intervals based on the natural frequency (figure 4.4) giving a total of 48 integration points. This division of the domain was used by Button *et al* in the program STOCAL [Button *et al* 1981], and it ensures that the integration points are concentrated around the natural frequency of the mode being considered. For the mixed mode case there are two peaks present and the division of the domain has to take account of this; Button *et al*. were followed again and the domain divided up as shown in figure 4.5. In this scheme, two sets of points are defined centred around each of the natural frequencies involved. The points defined by the lower mode are then used to integrate the response up to a frequency mid way between the two modes. Above this frequency the points defined by the higher mode are used.

Finally a comment needs to be made about the integration of the pseudo-static response. Although this does not contain any peaks, it varies as $\frac{1}{\omega^4}$ and so the choice for the first integration point is very important. The integration points for the dynamic response vary from mode to mode because they are defined in terms of the natural frequencies. Therefore, if the same points were used to integrate the

modal pseudo-static response errors will occur in the higher modes as there are fewer points in the more important lower frequency range. Therefore, for the pseudo-static response all modes were integrated using the points defined for the integration of the first dynamic mode.

4.2 Validation Of Program STASY

As mentioned in the introduction the program and theory were validated by comparing the predicted statistics of the response of a portal frame with statistics calculated from the response to 99 simulated ground acceleration records. STASY was used to predict the peak and RMS values of the displacements and bending moments at two points on the transom, and at the top of the left hand stanchion to both vertical and horizontal excitation. These were then compared with the peak and RMS values from the time history analysis. The portal frame used in the analyses was based loosely on a steel footbridge with a span of 50 m (figure 4.6) and has the section and material properties given in figures 4.7 and 4.8. The first three vibration modes were used in both the time history and power spectral analyses. These were found using the SOLVIA finite element package [SOLVIA Engineering 1989] and are shown together with the natural frequencies in figures 4.9, 4.10 and 4.11. For the subsequent dynamic analyses modal damping factor of 2 percent was assumed for each mode.

4.2.1 Time History Analysis

There were three stages to the time history analysis procedure. Firstly, a set of 99 different earthquake time histories had to be generated which had identical power spectra. Secondly, the response of the structure had to be found to each of these records. Finally, the statistics of the response had to be calculated from the results of these analyses so that they could be compared with the results from the power spectral analyses.

4.2.1.1 Generation Of Earthquake Time Histories

The earthquake time histories were generated using the program EQSIM [Taylor 1989], which implements an algorithm developed by Gasparini and Vanmarcke [Gasparini & Vanmarcke 1976]. The power density spectrum required was defined in the input to the program and this was then used to form the Fourier amplitude spectrum of the simulated acceleration time history. An inverse Fourier transform was then used to generate the simulated time history from this spectrum using a set of randomly generated phase angles. To obtain different time histories from the same power spectrum, different seeds were used to generate the random phase angles.

The magnitude of the required motion was defined by giving a peak value of the acceleration as part of the input to the program. Unfortunately this produced records which contained single spikes that were significantly larger than the rest of the record. Consequently, the records were not stationary and the structural behaviour was dominated by an impulse response to these spikes. Therefore, records were generated which were twice as long as desired and these were processed further to remove those portions which contained the large peaks (figure 4.12). A further correction had to be applied to ensure that the excitation did not arise suddenly since this could have an effect similar to an impulse loading. To avoid this the first 2.5 seconds of each simulated time history were tapered linearly so that the excitation arose gradually.

There were two important factors governing the choice for the duration of the records. Firstly, EQSIM can only generate time histories containing 2^n points, where the maximum value of n is 12. Considering the problems discussed in the previous paragraph this limits the length of records to 2048 points. Secondly, the length of the excitation had to be significantly greater than the period of the structure for the response to be considered stationary; the literature suggests a duration that is at least ten times the period of the first mode. This would mean that for the portal frame considered here the

duration of the excitation must be at least 7 seconds. In the event the integration time step was chosen to be 0.00625 seconds, which lead to a total record length of 12.8 seconds for the excitation. The input power density spectrum was based on the Clough-Penzien spectrum with

$$\omega_g = 5.\pi \quad : \quad \xi_g = 0.6$$
$$\omega_f = 2.0 \quad : \quad \xi_f = 1.0$$

which is illustrated in figure 4.3. A typical acceleration time history record obtained by following the procedures outlined above is shown in figure 4.13.

4.2.1.2 Time History Analysis Method

The SOLVIA finite element package was used both to create the model and to perform the dynamic analysis. To simplify and speed up the process a mode superposition approach was employed which used the trapezoidal rule to integrate the time histories. Two problems had to be overcome in performing the time domain analysis. Firstly, an approach for modelling travelling ground excitation had to be developed. Secondly, SOLVIA does not allow accelerations to be defined at specific degrees of freedom and so a method of relating the acceleration time histories either to applied forces or displacements had to be found.

The first problem was overcome by calculating the response of the frame to excitation at each foot in turn and combining the results using linear superposition. When these results were combined a delay equivalent to the time taken for the wave to travel the length of the frame was introduced between the response records so that the net response to a travelling input could be found. This approach had the advantage that all wave speeds could be modelled using only a single set of analyses.

There are several solutions to the second problem. The acceleration time history could be integrated twice in the time domain to give a displacement time history which could then be used to define the movement of each foot. However, this would introduce further problems since integrating an acceleration record often gives rise to unwanted large deflections because of errors in the low frequency components. An alternative approach is to use the relationship:

$$f = ma \quad \text{.....(4.5)}$$

to relate the acceleration time history to a force acting in one of the ground degrees of freedom. By attaching one of the feet in turn to a single degree of freedom system (figure 4.14) the acceleration record could be scaled to define the force acting on the mass using equation 4.5. This would then produce a base acceleration equal to the original record. In doing this two criteria had to be met. Firstly, the natural frequency of the base system had to be very much less than both the frequency of the frame and the frequency of the excitation. This was to ensure that the base system did not influence the dynamic properties of the frame, and that the response of the base was controlled by its inertia (figure 4.15). Secondly, the stiffness of the base had to be much greater than the contribution made by the stiffness of the frame so that the frame did not influence the response of the base system. The properties of the base system were chosen to be:

Mass	2×10^7 kg
Stiffness	2×10^6 N m^{-1}
Modal Damping	200 %
Natural Frequency	0.05 Hz.

To demonstrate that this superposition method accurately calculated the response of the structure, an analysis was carried out for the frame subject to synchronous loading using both superposition and the standard approach of defining a global acceleration field. The response at node 10 on the frame for both cases is shown in figure 4.16 and it is clear that there is close agreement between the two sets of results which have a correlation coefficient of 1.000.

It needs now to be noted that it was not necessary to calculate the pseudo-static part of the response explicitly in the approach outlined here because it included the independent motion of each foot of the frame. Results calculated from the superposition method therefore contained all three components mentioned in §3.2.3, that is the dynamic, pseudo-static and rigid body terms. However, because the rigid body terms were removed from the results calculated using the program STASY, they also have to be removed from the time history results to allow valid comparisons to be made. This was done at the superposition stage by removing the mean ground offset.

4.2.2 The STASY Analysis

The input to the STASY analysis of the frame was obtained from the same finite element model used in the time history analysis. A critical part of the analysis was to ensure that the power spectrum used to define the ground excitation for the analysis corresponded to the input used in the time history analyses. To achieve this the power spectrum of each of the input records was calculated and the average found. A least squares method was then used to fit the Clough and Penzien ground spectrum model to the mean power spectrum (figure 4.17). It is important here to consider the processes involved in this as assumptions underlying the method may be a source of error in matching the spectra. To calculate the spectrum of a time history of finite length the assumption that the signal is periodic has to be made. Because of this, it is often necessary to weight the terms in the record to

reduce the influence of the ends and so avoid problems caused by discontinuities between first and last values. This is termed windowing, and the choice of window function influences the spectrum produced. In this case the FAMOS signal processing package [IMC Meßsysteme GmbH 1992] was used to perform the analysis and this offered a choice of five windows; rectangular (no window), Hamming, Hanning, Blackman, and Blackman-Harris. The choice between these was made by comparing the mean square value of the records with integral of the power spectrum:

$$\sigma_x^2 = \int_0^\infty G_{xx}(\omega)\,d\omega \qquad \text{.....4.6}$$

Using this method the Rectangular window gave the best agreement, probably because of the tapering of the records mentioned above § 4.2.1.1, but even this over estimated the RMS response. Therefore, the mean power spectrum was calculated using the rectangular window, and then scaled further to match the mean RMS values of the time history records.

4.3 Results

The response to the time history records were saved for three points on the frame (figure 4.6), horizontal displacements at node 5 and vertical displacements at nodes 10 and 15, together with bending moments at all three points. 41 different wave velocities were considered which corresponded to time delays ranging from 0 seconds (infinite speed) to 0.5 seconds (100 m s^{-1}). The absolute peak and root mean square of each response were found for every combination of wave speed and ground excitation record, and these values were then used to obtain upper and lower bounds and the mean of the response. The mean values were found for both the peak and RMS values of the displacement, and the bounds for the peak displacements.

To identify any variations in the response caused by the asynchronous excitation these results had to be plotted against some measure of the asynchronicity of the excitation. There were two possible quantities which could be used for this, the ground wave velocity, c, and the time delay, Δt, between supports a distance L apart. These quantities are related by the following expression:

$$\Delta t = \frac{L}{c} \qquad \text{.....4.7}$$

which indicates that use of velocity as the abscissa will show trends for higher velocities more clearly but will obscure details for lower velocities. Conversely use of time delay will show clearly the trends for lower velocities and obscure those in the higher velocity range. For the results being discussed here it was decided to use the time delay between points of support as the abscissa because the significant behaviour occurred for lower values of ground wave velocity.

4.3.1 Applicability Of Extreme Value Analysis

Before considering the results in detail, it is worth considering the applicability of the extreme value analysis used to predict the peak response, does the peak response obtained from the time history analysis follow the expected distribution? The assumed cumulative probability density function of the normalised peak response [Davenport 1964, Der Kiureghian 1980] is given by:

$$P_{x,\max}(x) = \exp\left[-\nu_e \tau \exp\left(\frac{-x^2}{2}\right)\right] \qquad \text{.....(4.8)}$$

Comparing this with the results of a typical set of time history analyses (figure 4.18), shows that the results do approximately follow this distribution. It should be noted that value of ν_e may be different for each of the points in figure 4.18, and so a least squares approach was used to fit equation 4.8 to the data points. Considering the distribution of the peaks, a comparison of the calculated and predicted

distributions is given in figure 4.19. The χ^2 goodness of fit test provides a suitable means of quantifying the agreement between two histograms [Benjamin & Cornell 1970]. The total normalised square error between the two histograms in 4.19 is 16.16 which is less than $\chi^2_{0.05,14} = 23.68$ indicating that the distribution used is valid at the 5 % significance level.

4.3.2 Displacement Response

For horizontal excitation the peak and RMS results are shown in figures 4.20 and 4.21 (node 5), 4.22 and 4.23 (node 10) and 4.24 and 4.25 (node 15). The corresponding results for vertical excitation are shown in figures 4.26 and 4.27 (node 5), 4.28 and 4.29 (node 10) and 4.30 and 4.31 (node 15).

The predicted values for both the RMS and peak displacements should agree with the mean values calculated from the acceleration time histories. However, the level of agreement is variable with some records matching very well whilst others show quite large disparity; agreement was best at node 15 and worst at node 5. Nevertheless, all the predicted results lie within the upper and lower bounds of the time history calculations and the trends in both sets of data are the same. There are several possible explanations for the lack of agreement in some of the data. Firstly, all the comparisons assume that the power spectrum used in the spectral analysis truly represents the time history records used in the time history analyses. Any errors in the estimate of the input power density spectrum, either in its magnitude or frequency content, could introduce differences between the predicted and calculated values. Secondly, the predictions were made assuming that both the excitation and response were stationary. Clearly this was not so, since the acceleration time histories had a finite length and this again could have introduced an element of error in the predictions. This is the more likely cause of the differences between the data sets because errors in the estimate of the ground power

density spectrum would be likely to cause a consistent disparity between the calculated and predicted results. This was not observed

Considering now the spread of the results, the first comment that can be made is that the predictions tend to over estimate the spread of the results. The predicted 99 percentile limits show the range within which 99 out of every 100 events should fall (lower limit is the 0.5 percentile, upper limit is the 99.5 percentile). The upper limit is generally above the upper bound to the time history results, and in some cases exceeds it by a considerable amount, though this is usually when the mean level is also greater than the time history results. On the other hand, the lower limit is generally much closer to the lower bound. This difference occurs because the distribution of peak response is skewed and so the prediction of an upper limit is more sensitive to parameter changes; i.e. the difference between the 0.5 and 1 percentiles is less than the difference between the 99 and 99.5 percentiles. This result could have important consequences for design where a reliable estimate of the upper limits to the distribution of peak response is needed.

As mentioned above, the general trends of response with time delay are correctly predicted by the power spectral method; each of the predictions agrees closely with the time history results for the values of time delay that lead to peaks and troughs in the response. The only differences that occur are several additional small waves in some of the predicted peak curves, most notably those for node 5. These appear to be caused contributions from different modes and so the variation of modal response will now be considered in more detail.

4.3.3 The Variation Of The Modal Response

To discuss the results further it is useful to consider the trends in the response of the different modes and to correlate these with the trends in the global data. For a given frequency of excitation the phase angle of the excitation between the two feet is given by:

$$\phi = \frac{360.L.f}{c} = \frac{18000.f}{c} \quad \text{.....4.9}$$

and using this expression values of wave speed corresponding to in phase and out of phase excitation can be calculated for each natural frequency (table 1). Looking at the mode shapes (figures 4.9 - 4.11) it can be seen that mode 1, the first bending mode of the transom, is symmetrical and that modes 2, the sway mode, and 3, the second bending mode of the transom, are anti-symmetrical. It would therefore be expected that for horizontal excitation the maximum response in mode 1 will be occur when the inputs are 180° out of phase, and in modes 2 and 3 when the excitation is in phase. Conversely there will be a minimum response in mode 1 for excitation that is in phase and in modes 2 and 3 when the excitation is 180° out of phase. For vertical excitation the opposite will be true. The results from STASY support this hypothesis as can be seen from the variations in the zeroth modal moments (figures 4.32 and 4.33). These show the mean square response in each mode. The nodal results presented earlier can now be interpreted further by considering the contributions of the different modes. Moreover, some of the differences between the predicted and calculated response can be explained.

Looking again at the peak response at node 5, it can be seen that each of the anomalous blips corresponds to a time delay where there is either a peak or trough in the response of mode 3. Therefore, it would seem that STASY predicted that mode 3 has a greater influence on the displacement at node 5 than the SOLVIA results demonstrate. This could be either because STASY

predicts a greater response in mode 3, or because STASY predicts a greater interaction between the second mode, which dominates the response at node 5, and the third mode. STASY uses the complete quadratic combination method to recombine the modal spectral moments and this takes account of interaction between the modes using the cross spectral terms. The cross spectral moments for the second and third modes are greater than those for the first and second or first and third modes (figure 4.34 and 4.35). This is probably because modes two and three have similar anti-symmetric shapes.

4.3.4 Bending Moment Response

In §3.4.2.1 a method was proposed for calculating the statistics of the bending moments from the modal spectral moments which were calculated in finding the spectral moments of the global response. To validate this part of the procedure the bending moments at the three nodes being considered were found for each of the time histories and the upper and lower bounds together with mean values found as with the displacements. Unlike displacements, which are nodal properties, internal stresses and forces within a finite element model have to be evaluated as element properties. Consequently they cannot be expressed directly in terms of the global degrees of freedom and it is therefore not possible to use mode shapes to transform between the modal and global coordinate systems. Instead the forces arising in an individual element due to displacements in each mode shape have to be used and these combined, including the modal cross correlations, to give the total moments and forces acting on each element. The resultant internal forces at a given node can then be found by superposition of the effects of the elements connected to that node. However, since the portal frame was a simple structure with no node connected to more than two elements, the bending moments at a particular node could be found from the end moments of just one of the elements connected to it (the moments on the second element must equal these to satisfy equilibrium).

The bending moments for horizontal excitation are shown in figures 4.36 and 4.37 (node 5), 4.38 and 4.39 (node 10) and 4.40 and 4.41 (node 15) and for vertical excitation in figures 4.42 and 4.43 (node 5), 4.44 and 4.45 (node 10) and 4.46 and 4.47 (node 15). As with the results for the displacement analysis, these figures show marked variations in the agreement between the predicted and the time history results. The results from node 15 show close agreement for both horizontal and vertical excitation whereas the results for nodes 5 and 10 show reasonable agreement for horizontal excitation, but very poor agreement for vertical excitation.

Considering first of all those that agree well, these are the response at node 15 for both horizontal and vertical excitation and the response at node 10 for horizontal excitation. All of these are characterised by being dominated by a single mode, mode 2 for node 10 and mode 1 for node 15. Both of the results for node 15 include unexpected erratic behaviour in the predicted peak response curves that otherwise agree exceptionally well with the time history results. This erratic behaviour does not occur in any other predictions, which are generally smooth curves, including the RMS results. It is therefore something peculiar to node 15 and is probably due to truncation errors which arise when calculating the statistics of the peak response because the bending moments in both modes 2 and 3 are very close to zero.

As with the displacement results it is useful to consider the modal response to help interpret the results. The distribution of bending moments along the transom of the portal frame for each of the modes is shown in figure 4.48, 4.49 and 4.50 and these show that for node 15 the bending moments arise purely from the first mode. This is, of course, only to be expected as both modes two and three have points of contra-flexure at mid span and is apparent from the trends in figures 4.40, 4.41, 4.46 and 4.47. Conversely, mode 1 makes only a small contribution to the bending moments at node 10, which are instead dominated by modes 2 and 3. This is reflected in the trends in the response to

horizontal excitation presented in figures 4.38 and 4.39. However, the response to vertical excitation does not show such similar trends and this could be one of the reasons for the disparity between the predictions and the time history results. The time history results show a large trough at 3.5 seconds delay which would imply a much more dominant contribution from the first mode. Finally, figures 4.48 - 4.50 show that the response at node 5 will have major contributions from each of the first three modes. This is clearly apparent in the response to horizontal excitation (figures 4.36 and 4.37) where the trends are not dominated by any one mode in particular.

4.4 Conclusions

The aim of this chapter has been to validate the power spectral approach described in chapter three by considering the asynchronous seismic excitation of a portal frame. More specifically it was hoped to validate both the modelling of the spatially varying loads and the calculation of the response statistics. The difficulty in comparing the time history results with predictions using power spectra, which arises when an estimate has to be made of the power spectra of the input, has already been outlined. However, the work that has been presented does make it possible to draw some conclusions both on the efficacy of that power spectral method and on the importance of asynchronous loading for a portal frame.

4.4.1 The Efficacy Of The Power Spectral Approach

The implementation of the power spectral method for spatially varying seismic excitation was effective in predicting the variation of the response of a portal frame with ground wave speed. This would therefore indicate that the proposed method for describing the frequency wavenumber power density spectrum for asynchronous seismic excitation is valid. However, there were some

discrepancies between the results of the time history analyses and the predictions made from the program STASY, and these have some bearing on the validity of the procedures for predicting the response statistics. Several comments need to be made. Firstly, the power spectral method assumed that the response to the excitation was stationary; but because the excitation was of finite duration this assumption was not valid. It is not possible to estimate the influence of this on the results but it can be seen that this effect will be more serious for structures like long-span bridges which have a much lower fundamental frequency. This in turn is a good reason for introducing the evolutionary spectra approach discussed briefly in §3.1.5 when applying the approach to a cable-stayed bridge. Secondly, once set up the performance of a power spectral analysis is far quicker than even a single time history analysis. This, together with the very wide range of results obtained for time histories with nominally the same power spectra, makes the power spectral approach a very attractive and speedy tool for investigating the dynamic behaviour of a structure.

4.4.2 The Influence Of Asynchronous Seismic Excitation On A Portal Frame

The results of both the time history analyses and the power spectral method have shown that the response of a portal frame can vary widely with the speed of propagation of the seismic loading. The results have shown that the displacements or bending moments at a given point can vary by an order of magnitude depending on the ground wave velocity. Furthermore, the location at which the maximum bending moment will occur can also vary with ground wave velocity. It can therefore be concluded that asynchronous seismic excitation can have serious implications even for a relatively short structure such as a portal frame.

Table One : Ground Wave Velocities For Minimum And Maximum Modal Excitation

Mode	Frequency	Wave Speed			Time Delay		
		180°	360°	540°	180°	360°	540°
1	1.427 Hz	143 m s^{-1}	71.5 m s^{-1}	47.7 m s^{-1}	0.350 s	0.700 s	1.048 s
2	2.308 Hz	231 m s^{-1}	116 m s^{-1}	77 m s^{-1}	0.216 s	0.432 s	0.649 s
3	4.357 Hz	436 m s^{-1}	218 m s^{-1}	145.3 m s^{-1}	0.115 s	0.230 s	0.344 s

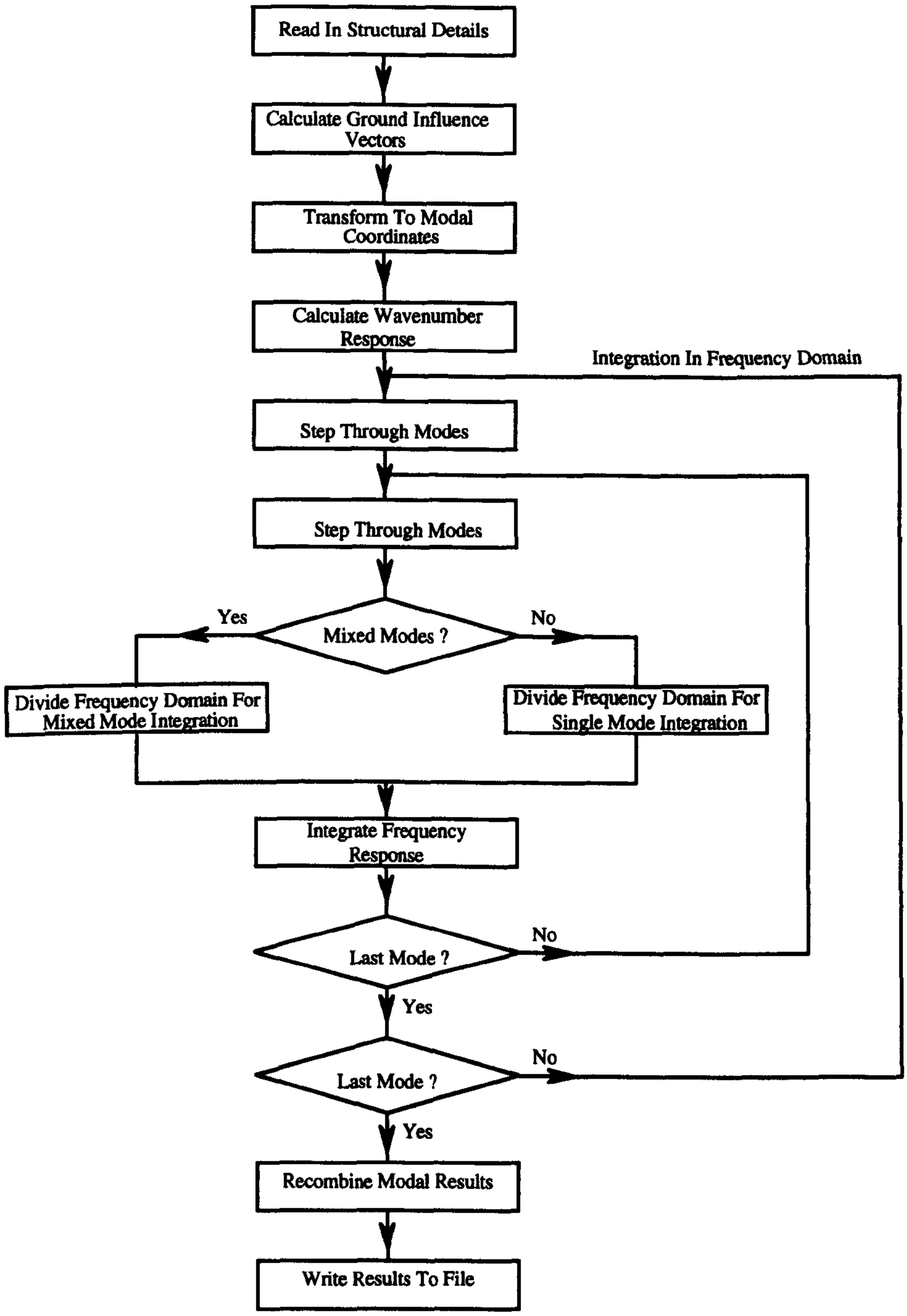

Figure 4.1 : Flow Chart for Program STASY

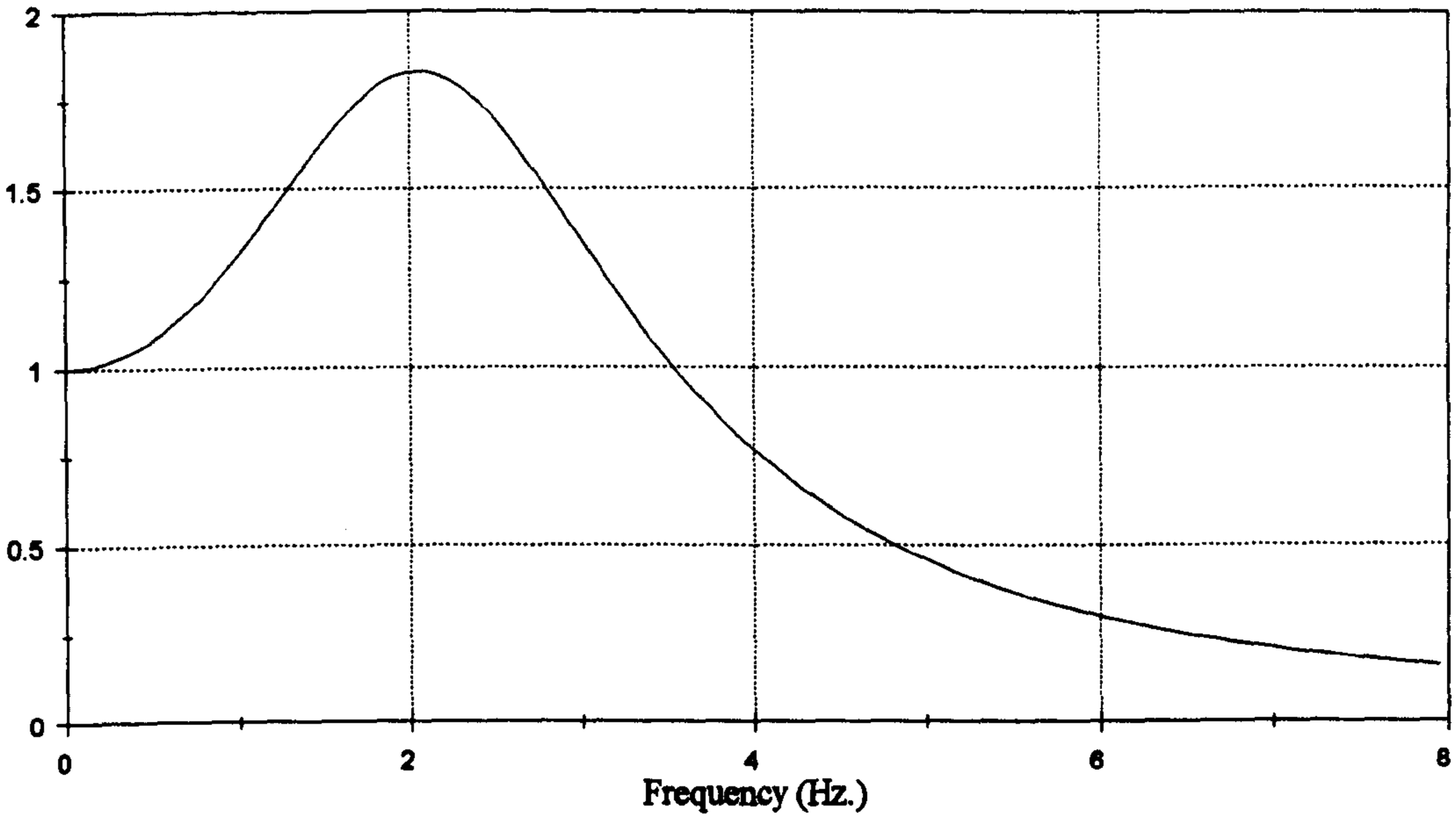

Figure 4.2 -:- Kanai-Tajimi Power Density Spectrum

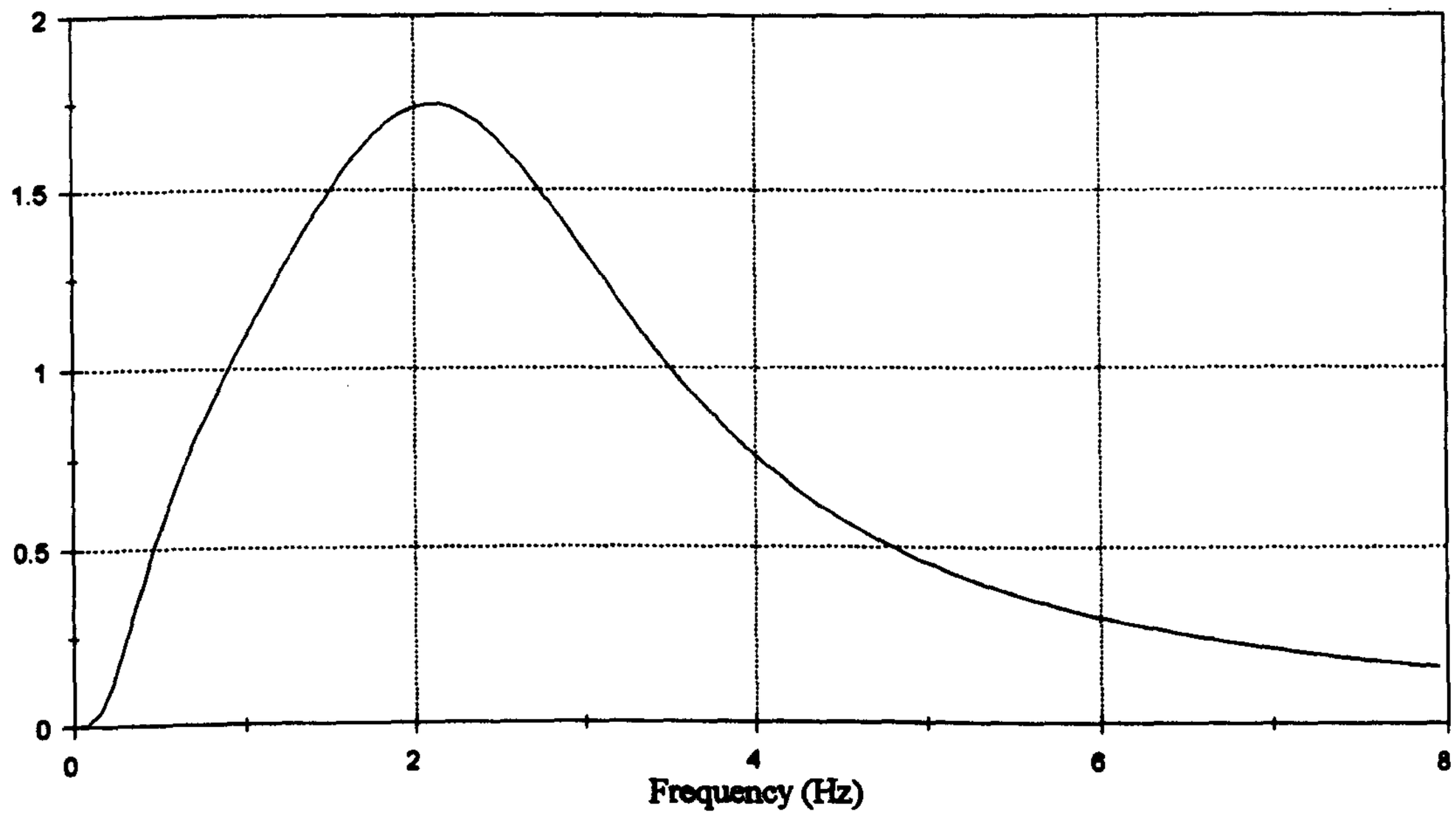

Figure 4.3 -:- Clough-Penzien Power Density Spectrum

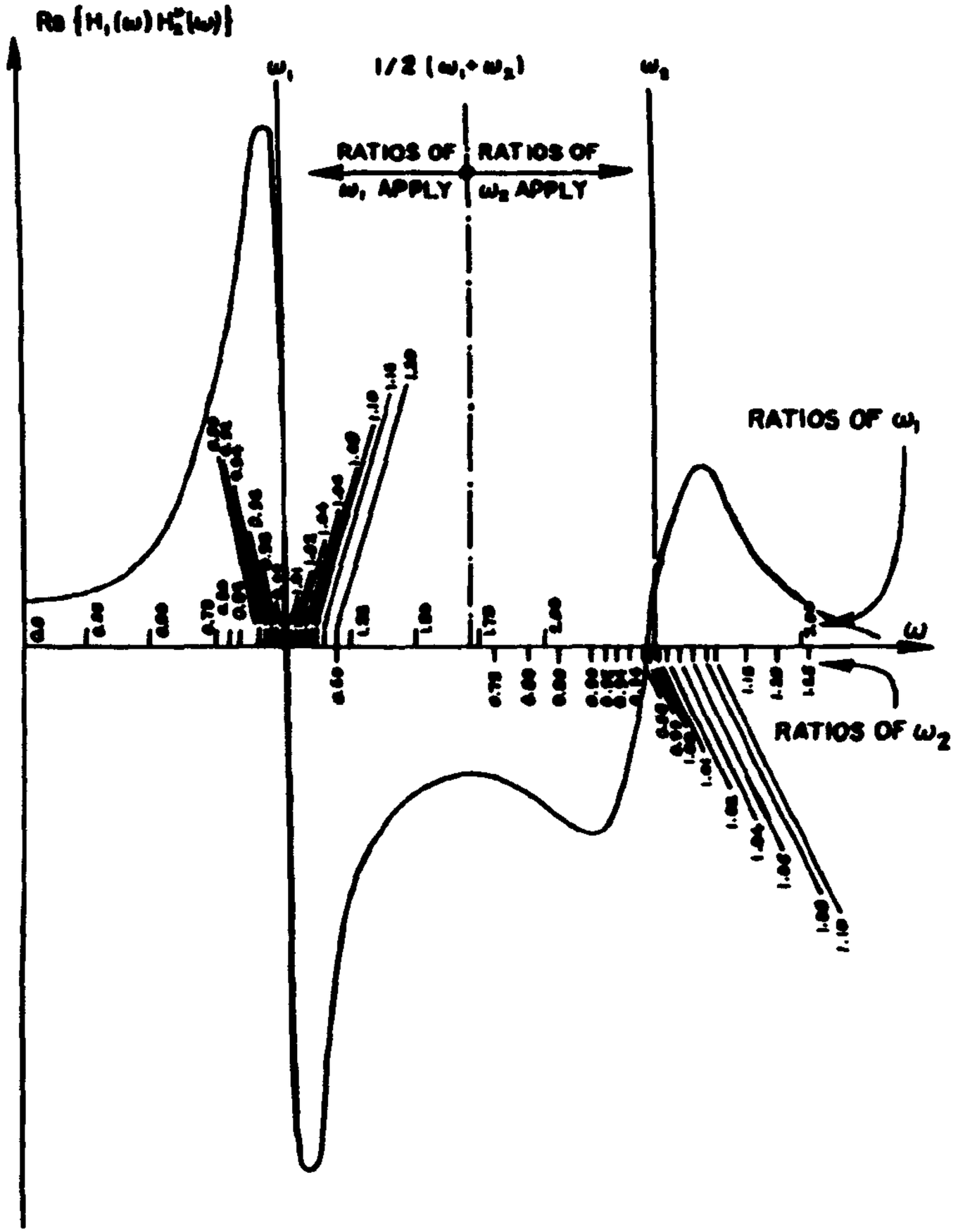

Figure 4.5 : Mixed Mode Integration Scheme

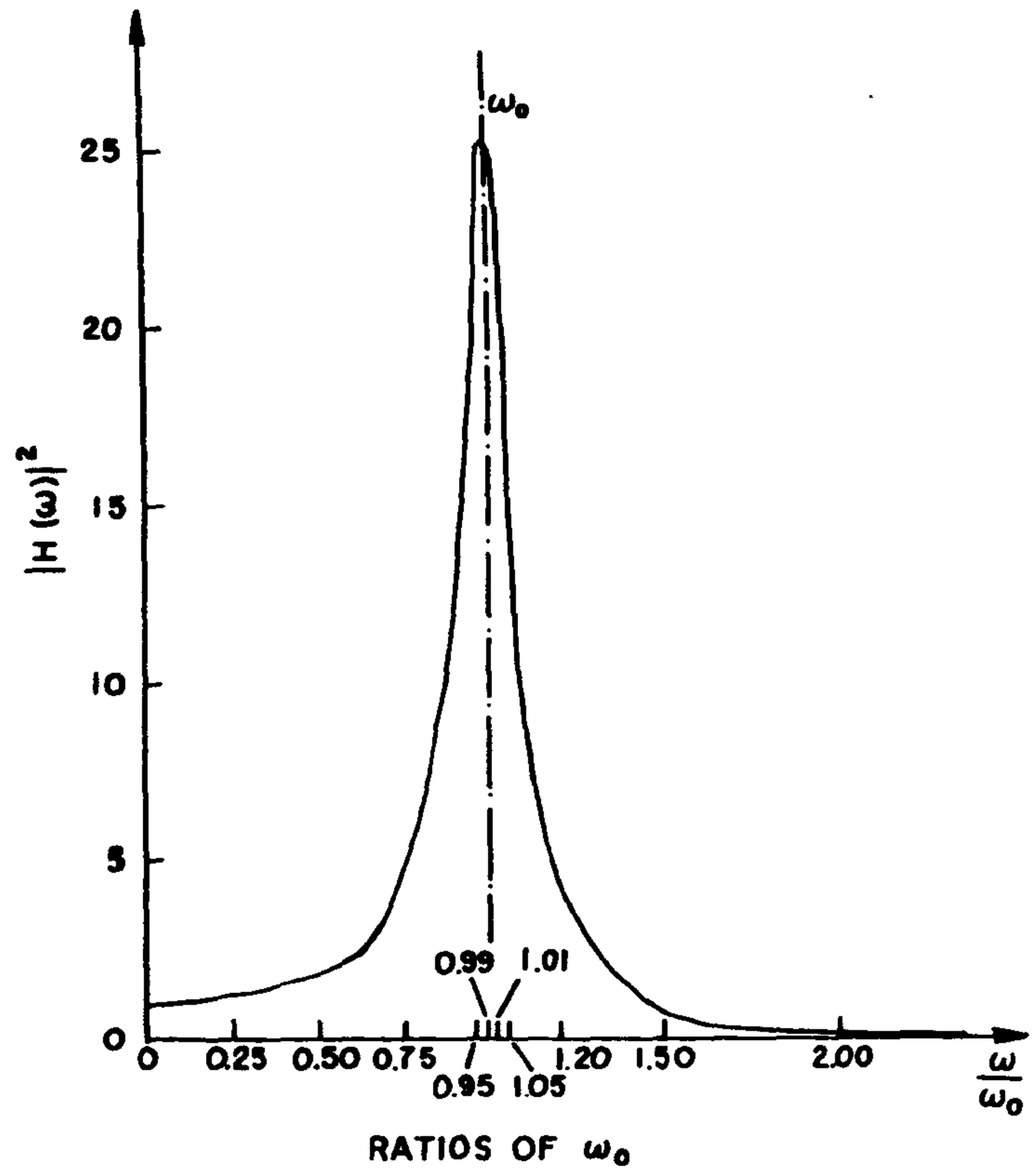

Figure 4.4 : Single Mode Integration Scheme

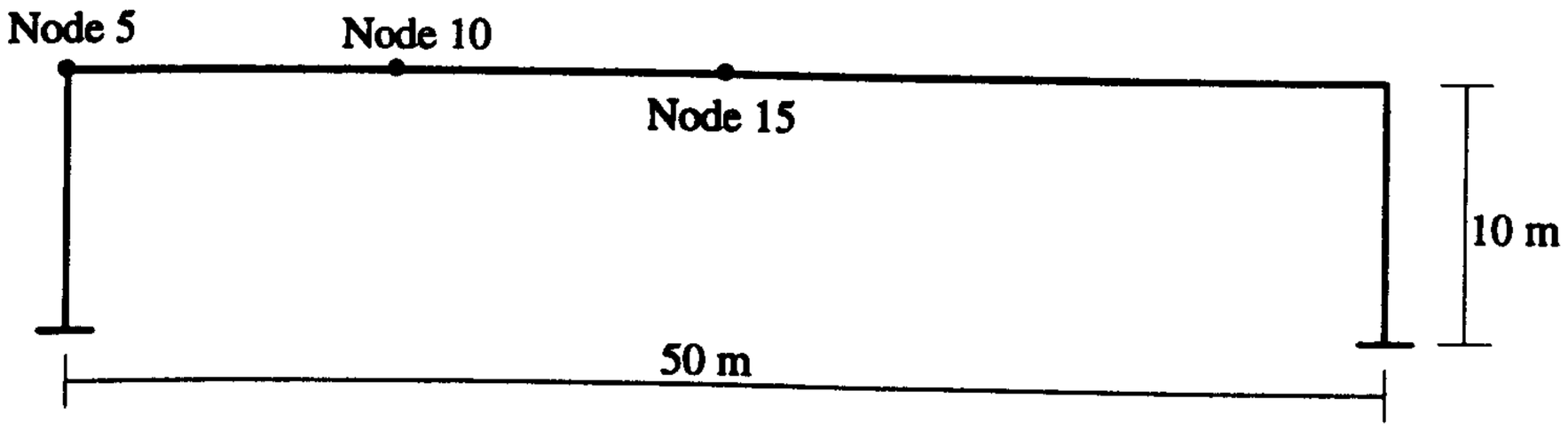

Figure 4.6 : General Arrangement of Portal Frame Example

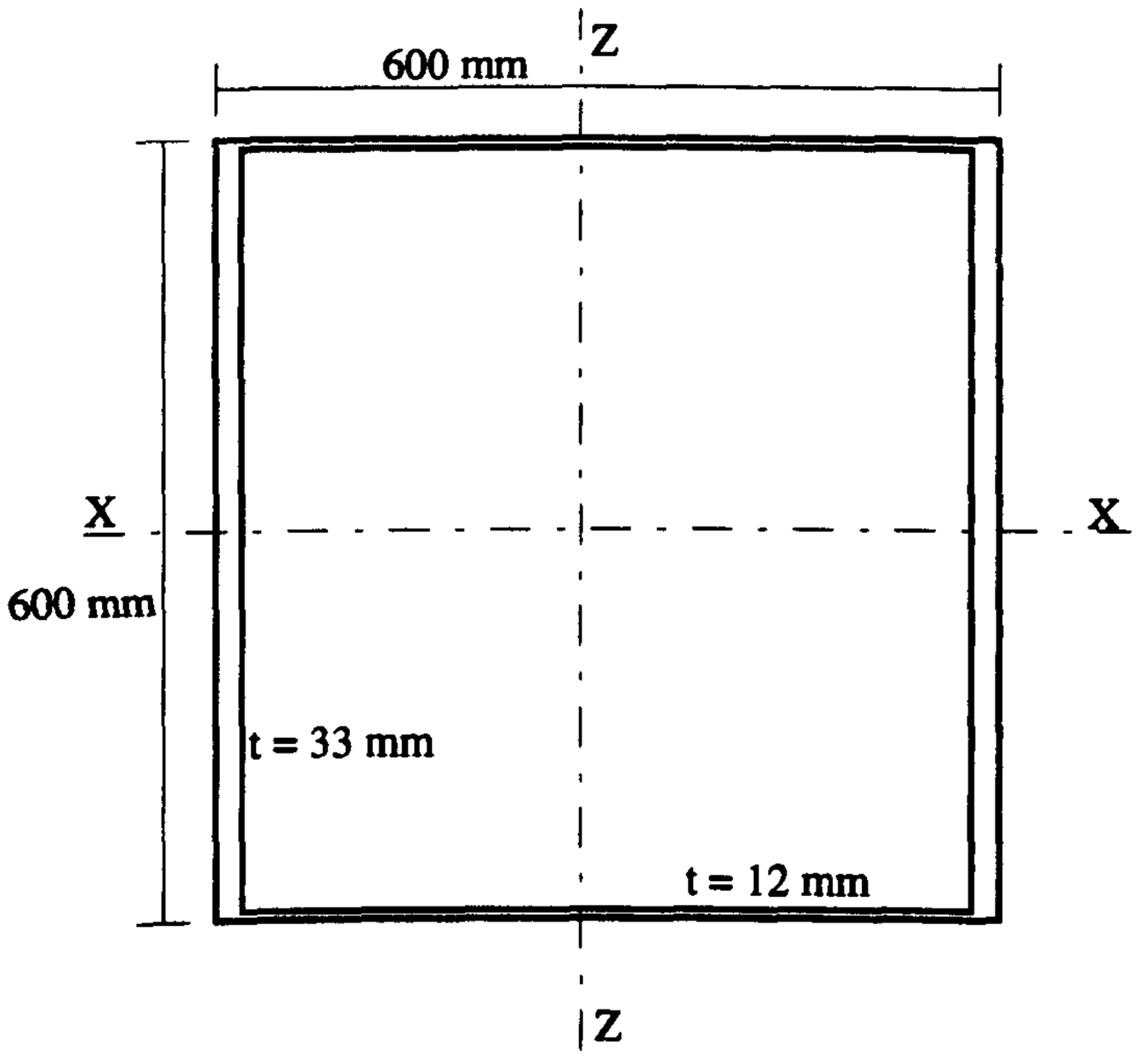

Section Properties

Area = 0.0524 m^2

Ixx = 0.00230 m^4

Iyy = 0.00349 m^4

Material Properties

E = 200 GN m^{-2}

υ = 0.3

ρ = 7850 kg m^{-3}

Figure 4.7 : Section and Material Properties of Portal Stanchion

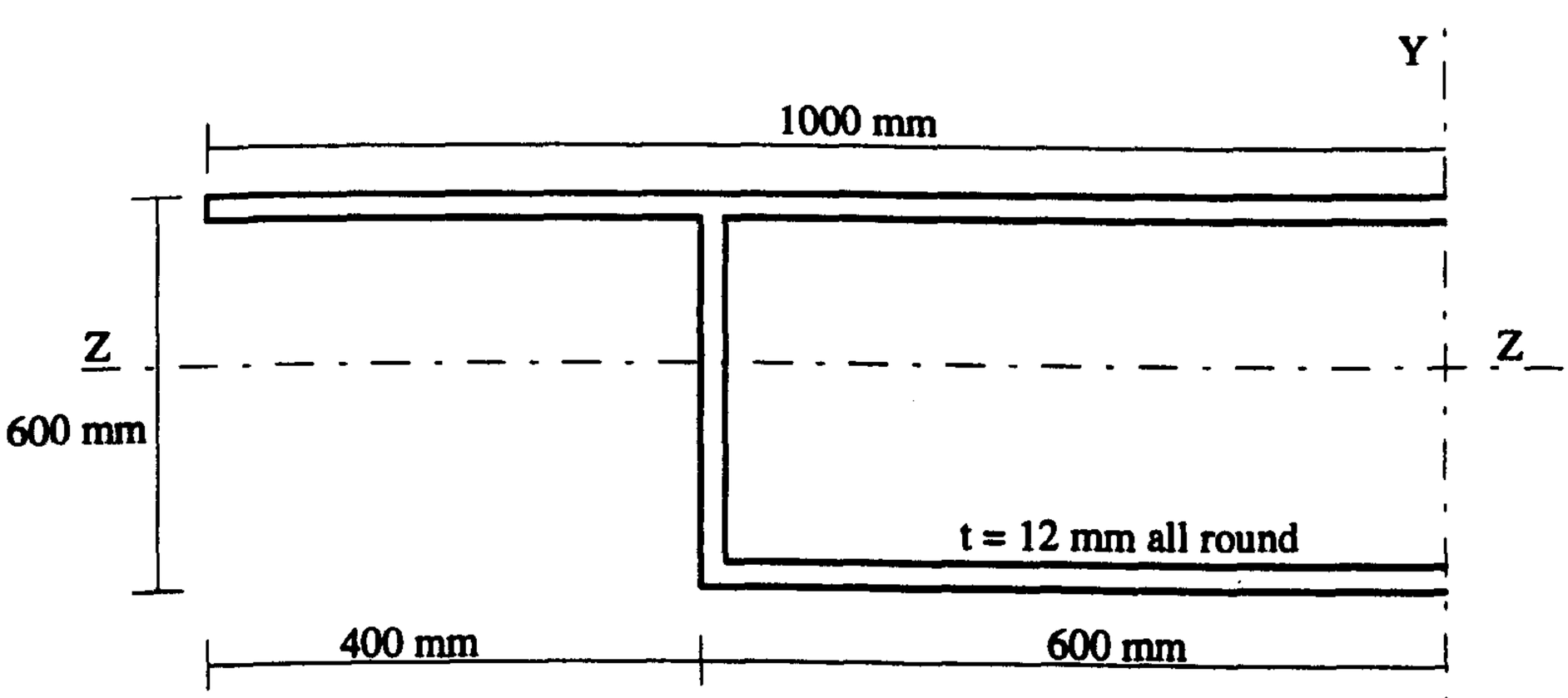

Section Properties

Area = 0.0522 m^2 Izz = 0.0035 m^4 Iyy = 0.0145 m^4

Material Properties

E = 200 GN m^{-2} υ = 0.3 ρ = 7850 kg m^{-3}

Figure 4.8 : Section and Material Properties of Portal Transom

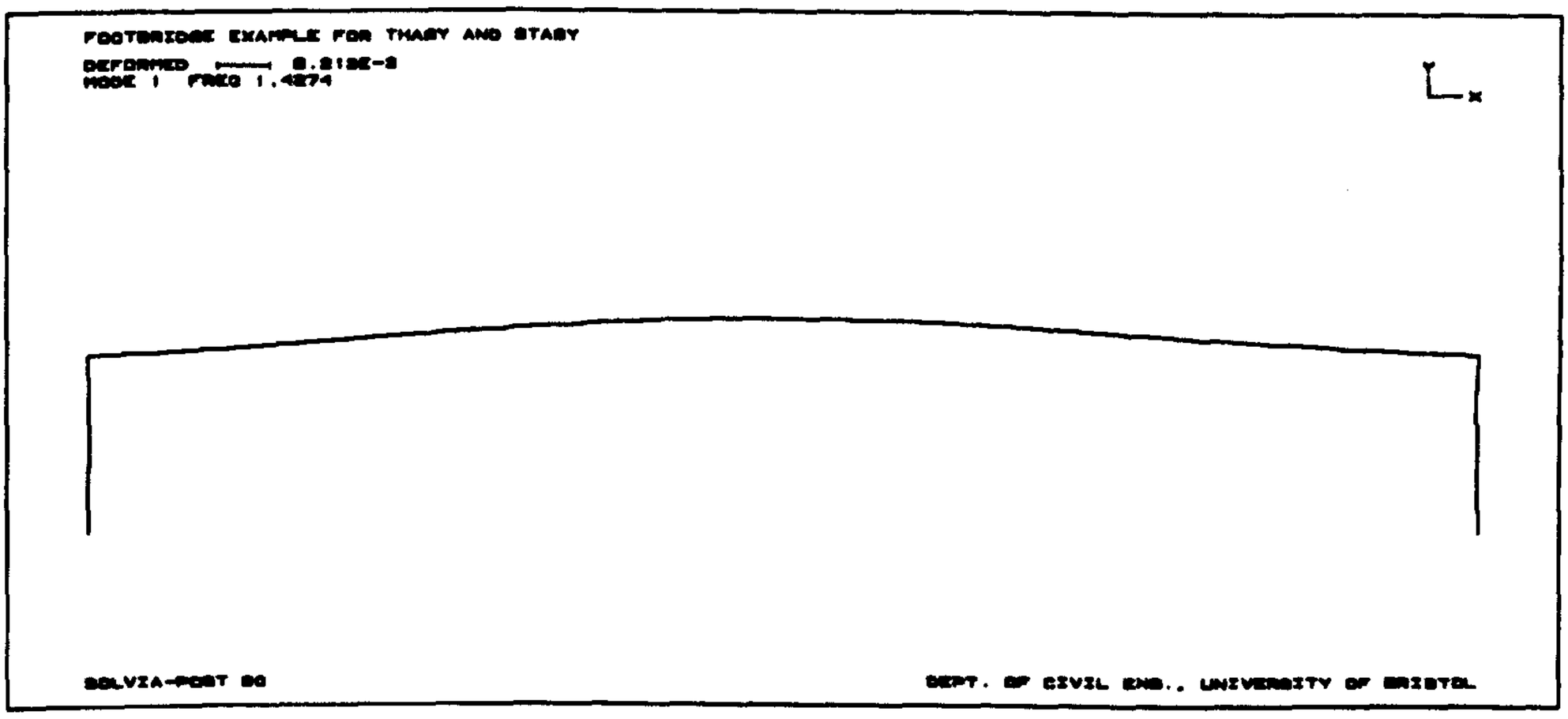

Figure 4.9 -:- Portal Frame Mode One

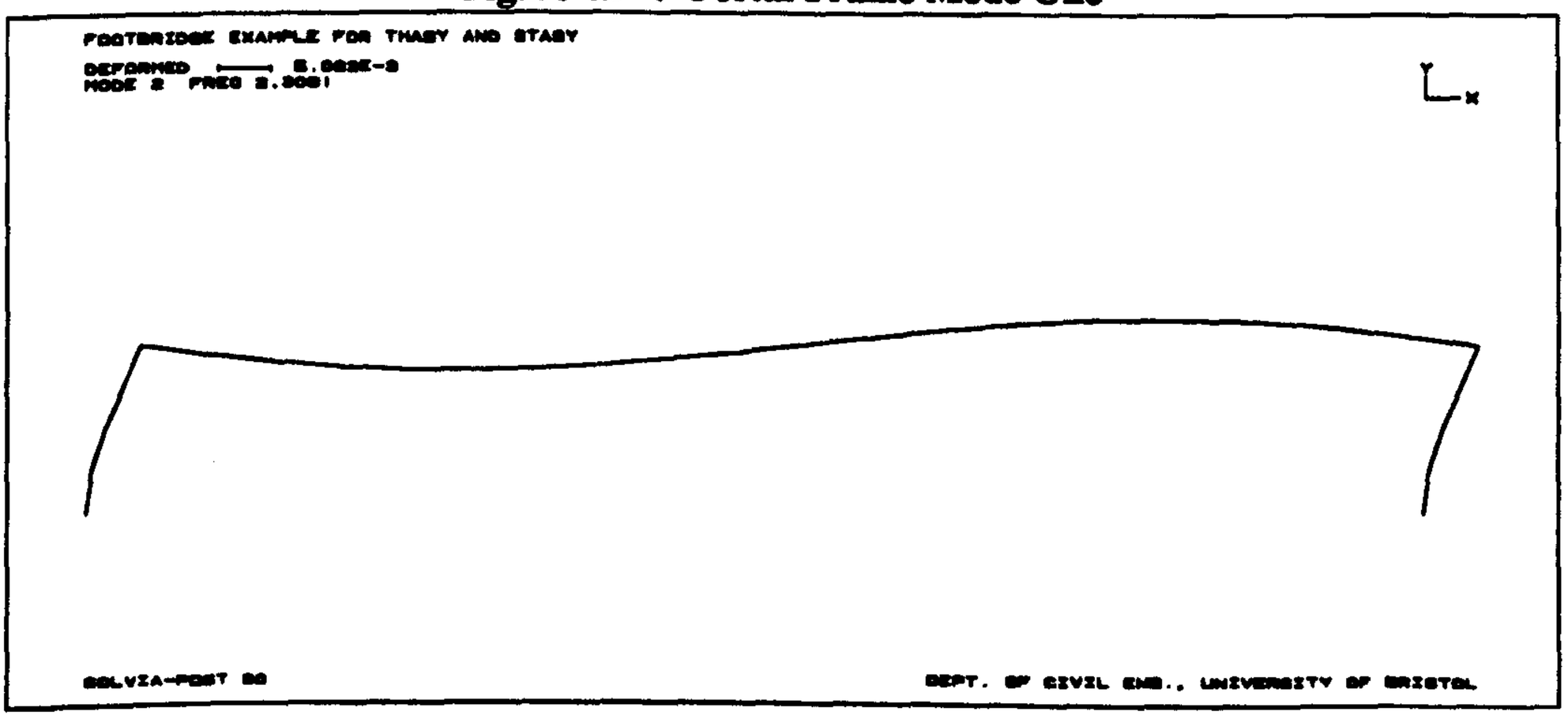

Figure 4.10 -:- Portal Frame Mode Two

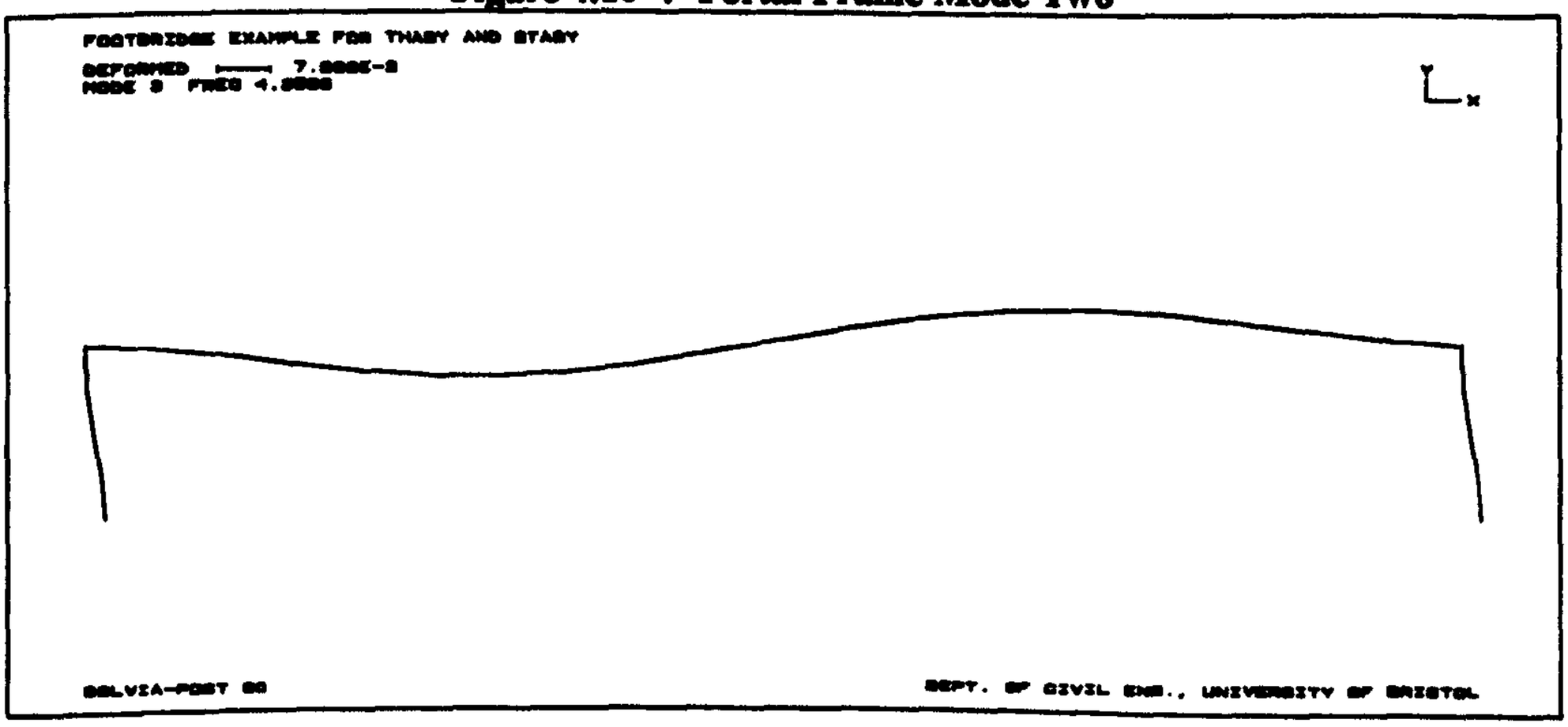

Figure 4.11 -:- Portal Frame Mode Three

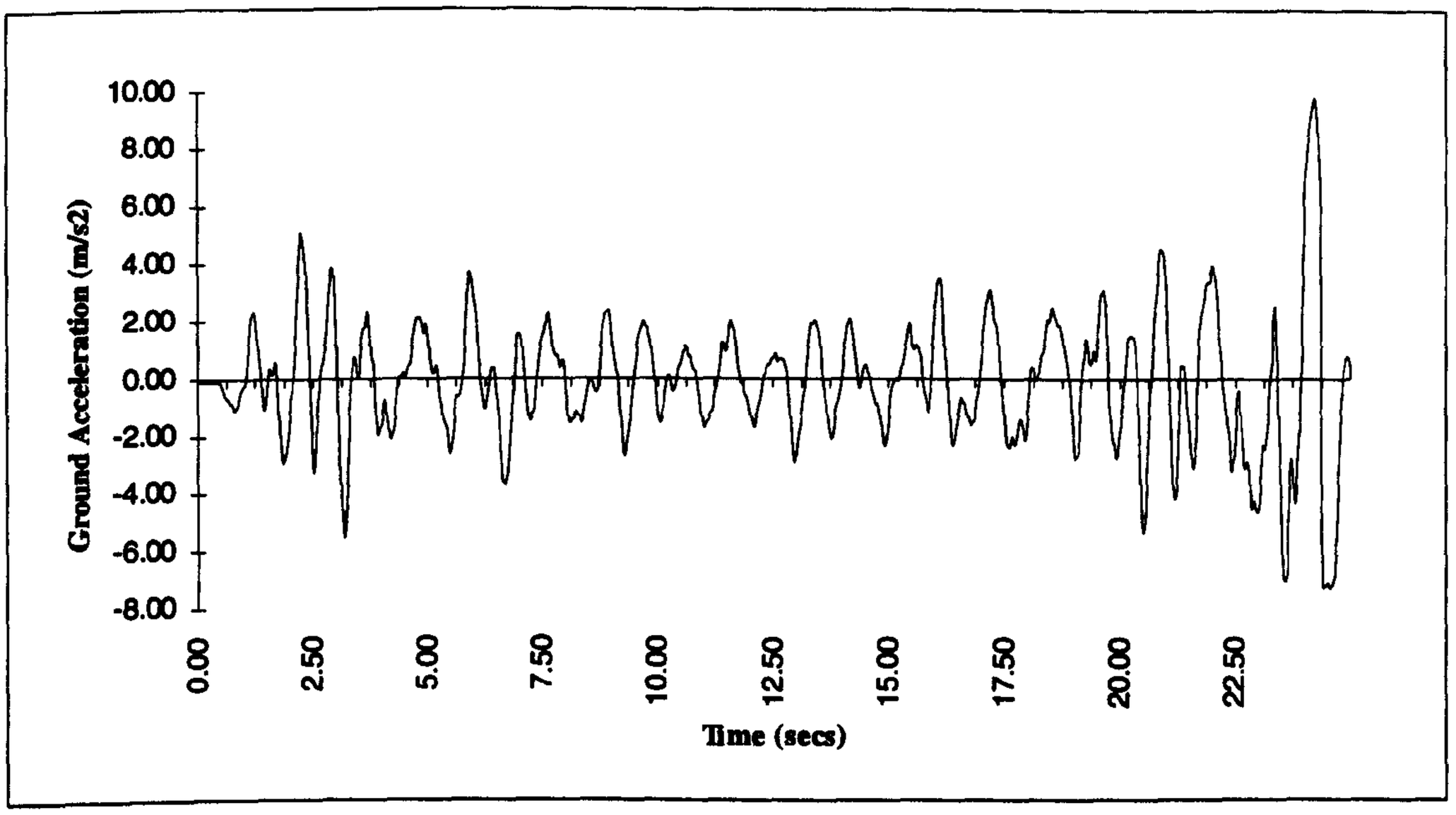

Figure 4.12 : Typical Raw Ground Motion Time History

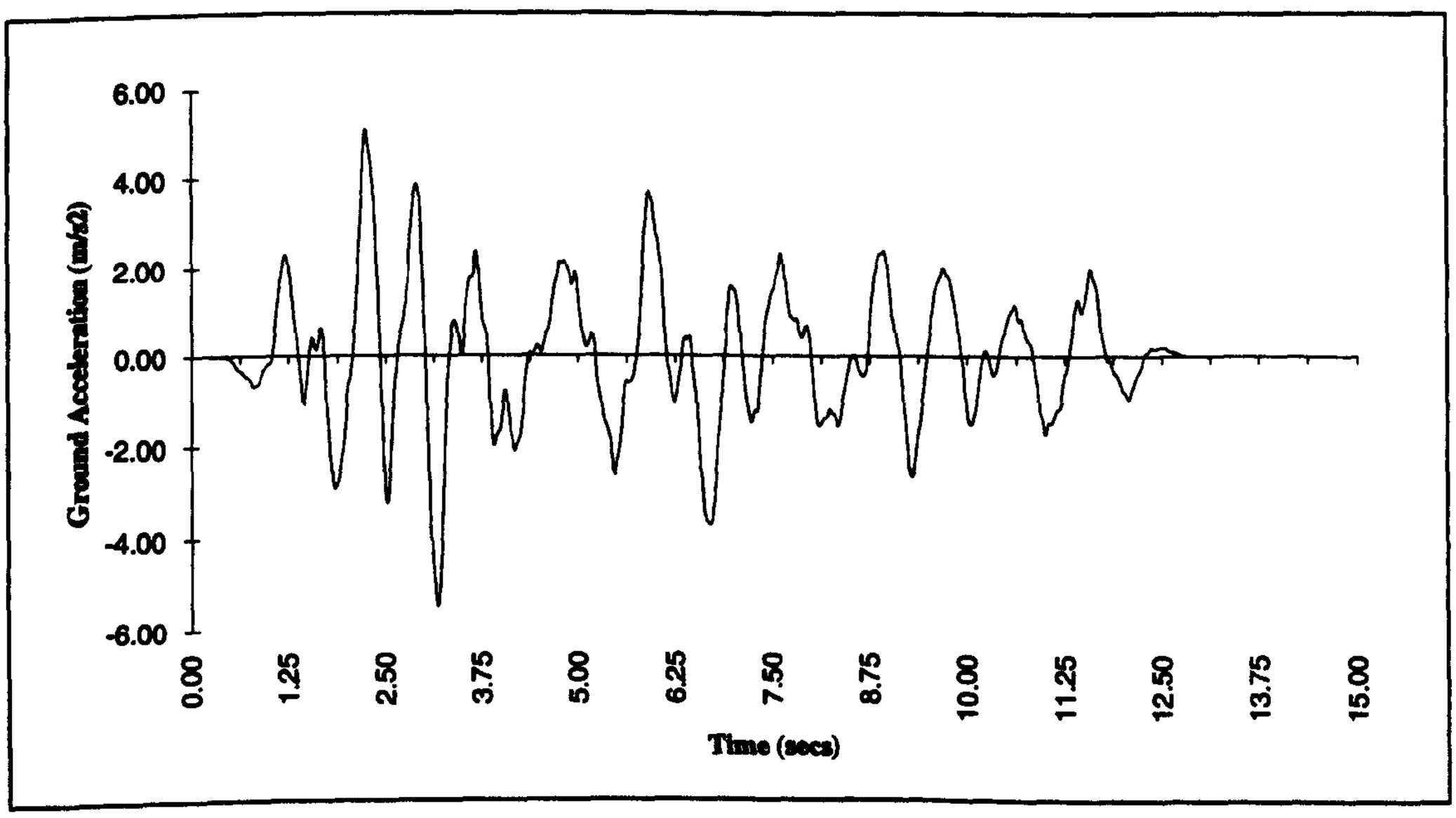

Figure 4.13 : Typical Ground Motion Time History Used In Analysis

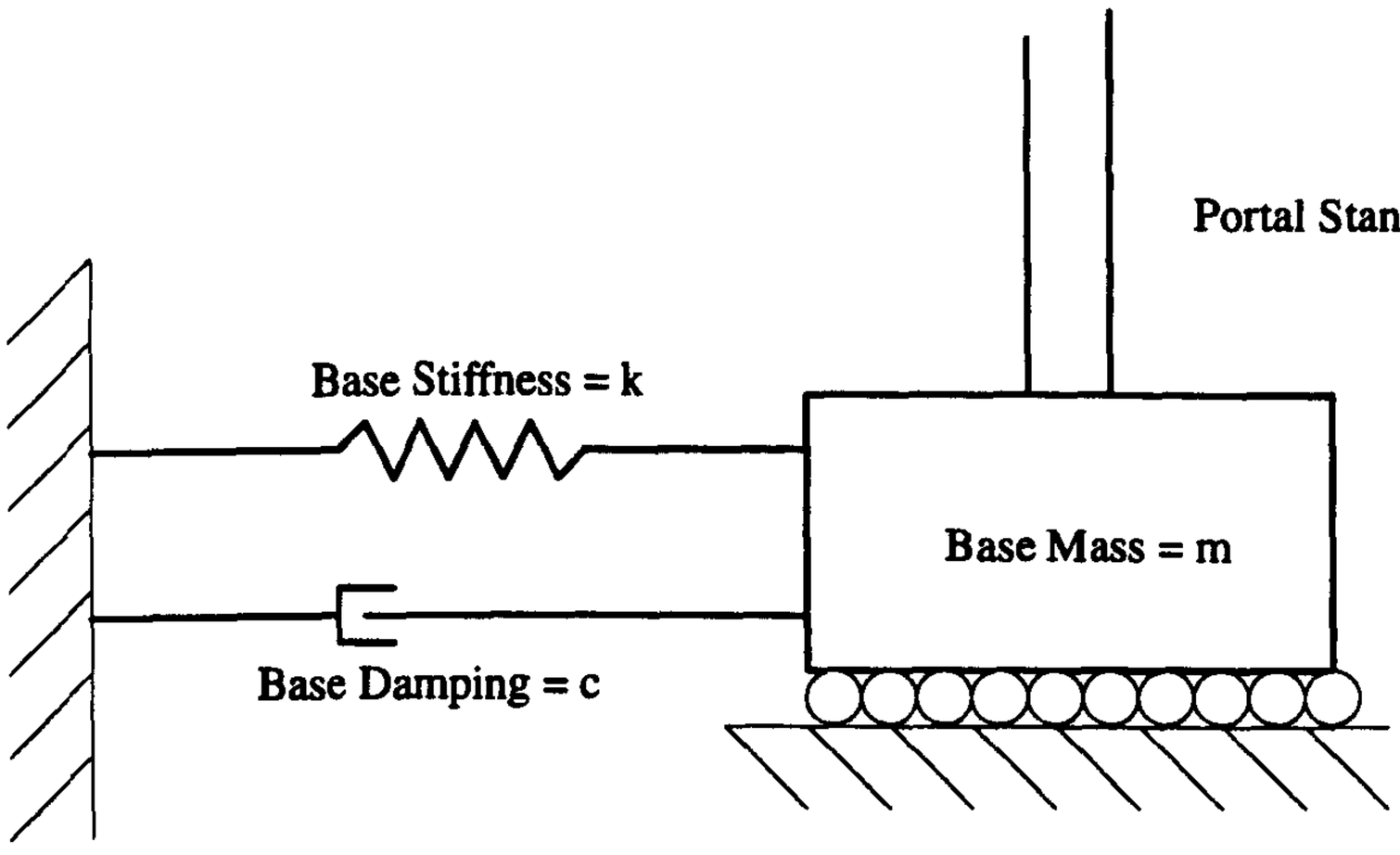

Figure 4.14 : Single Degree of Freedom System Used at Portal Base

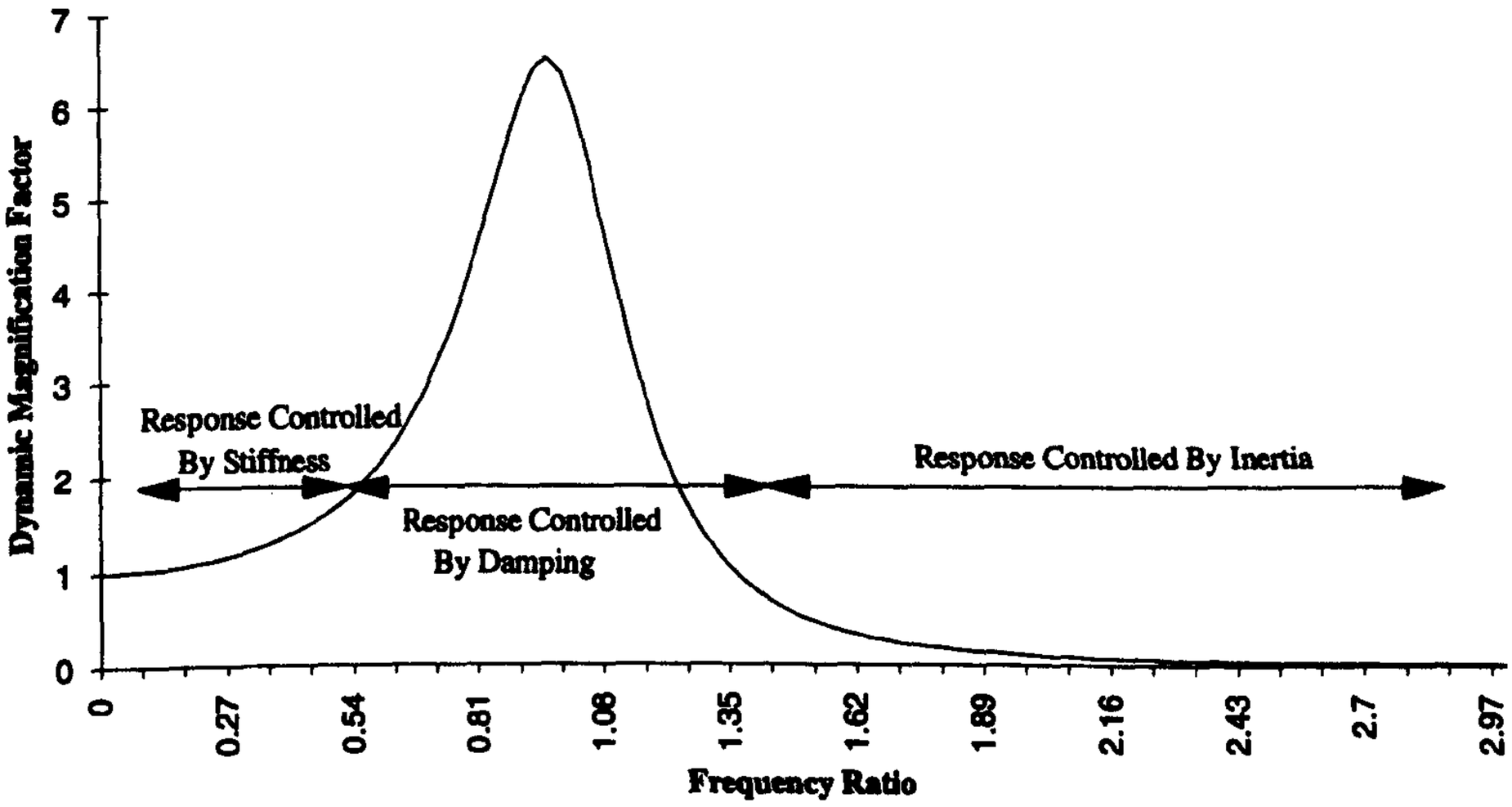

Figure 4.15 : Frequency Domain Response of Single Degree of Freedom System

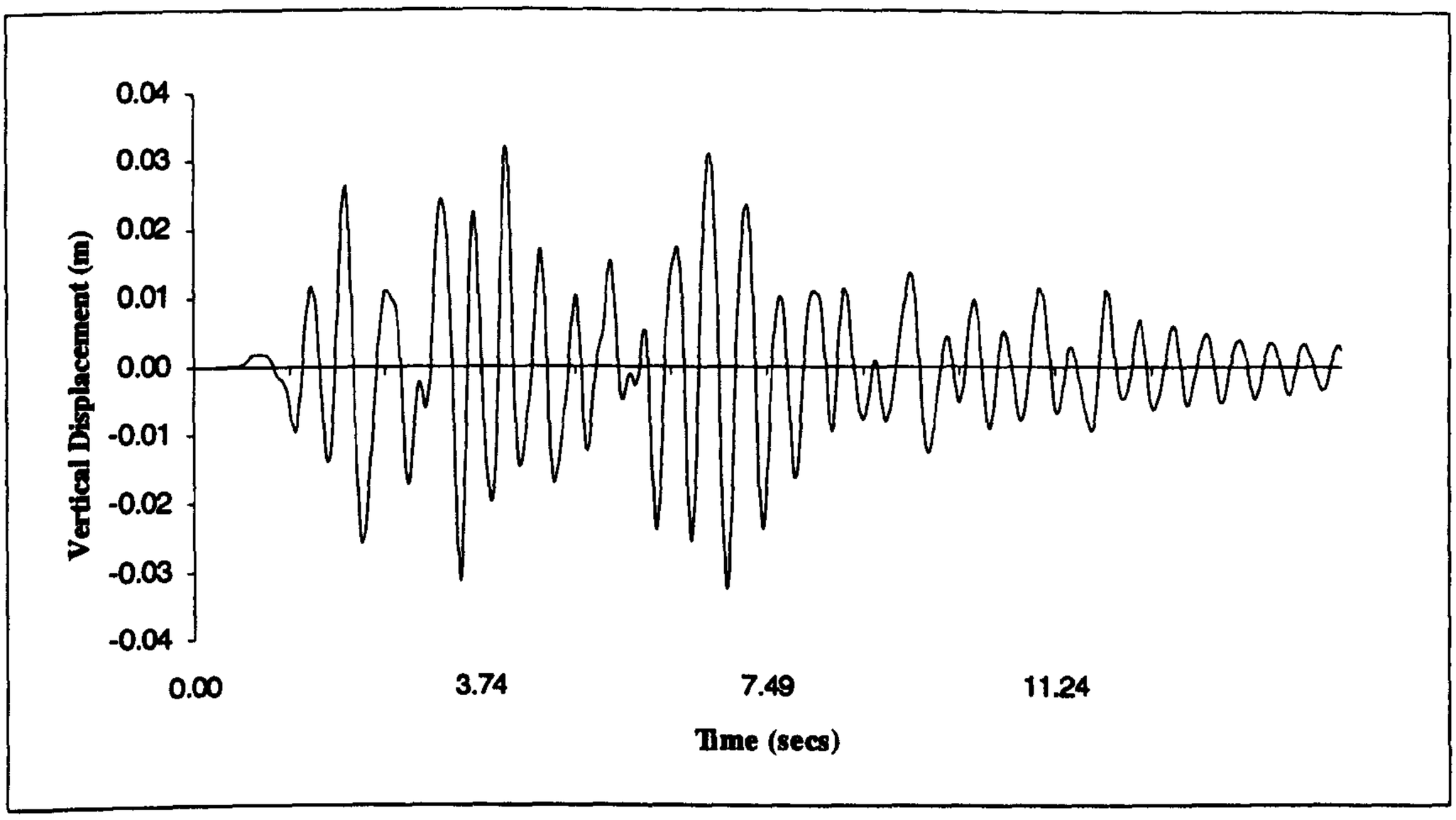

4.16a. Displacement at Node 10 Found From Uniform Acceleration

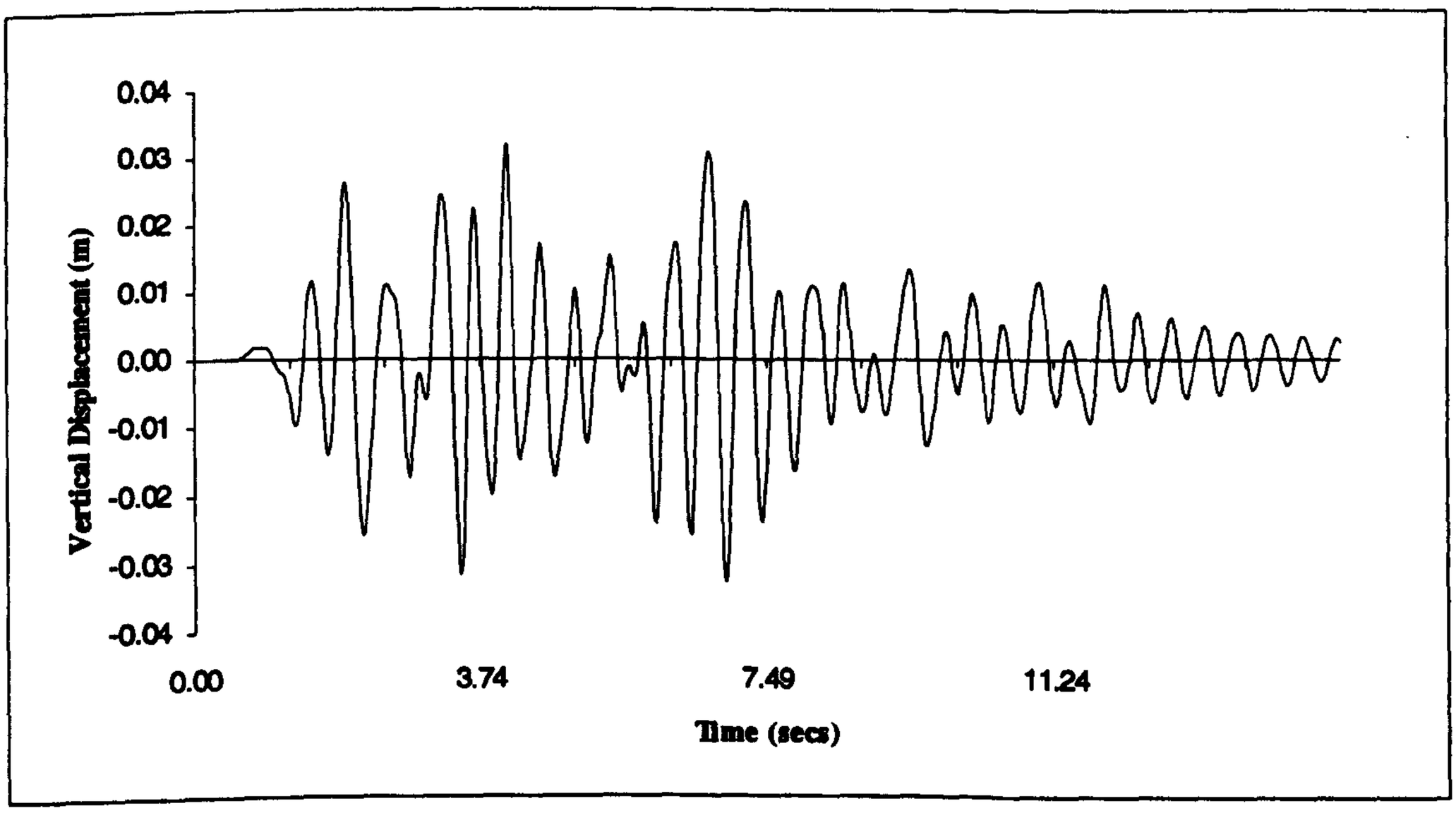

4.16b. Displacement at Node 10 Found By Superposition

Figure 4.16 : Validation of Superposition Approach for Synchronous Excitation

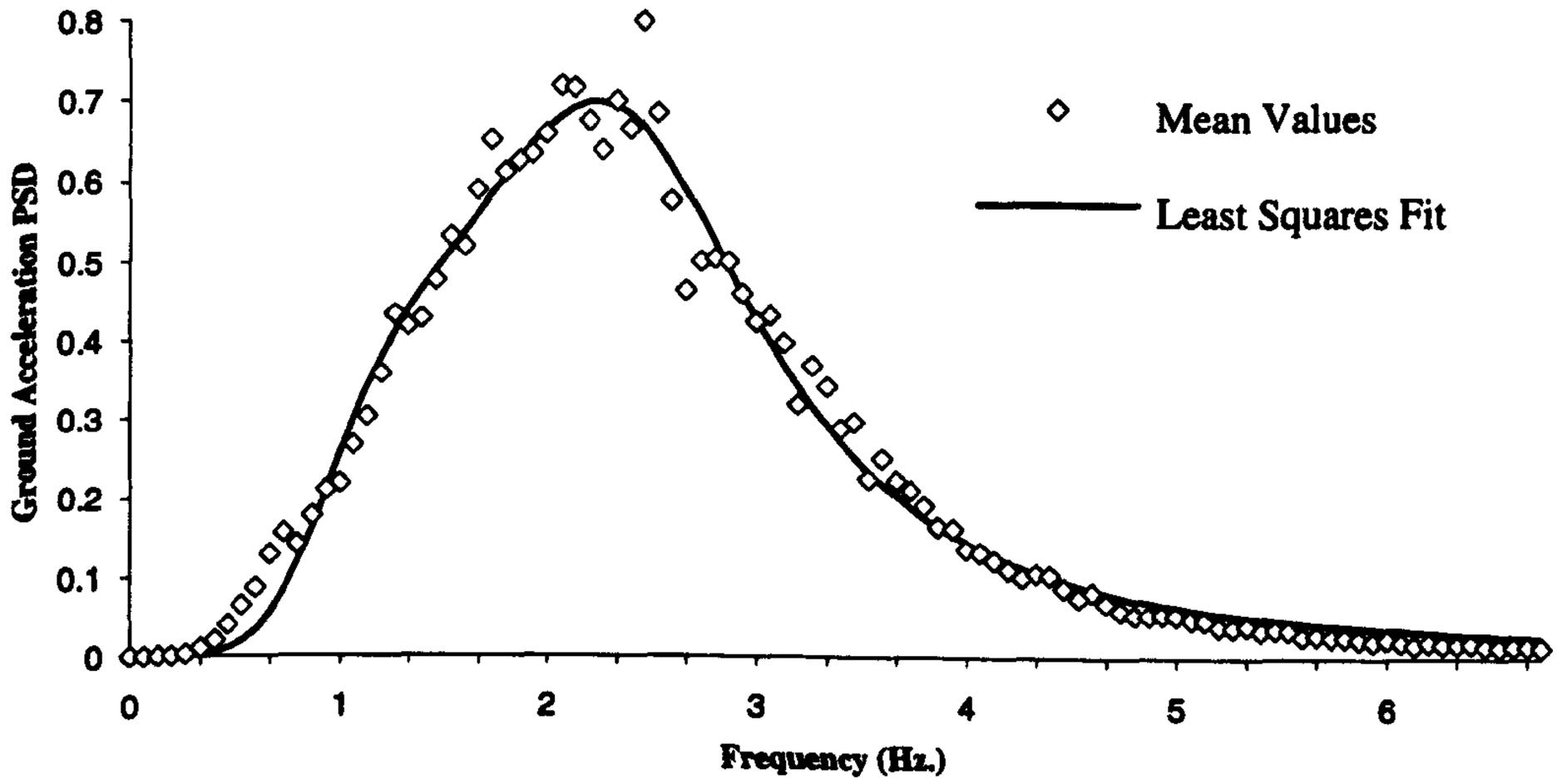

Figure 4.17 : Least Squares Fit to Mean Power Density of Time History Records

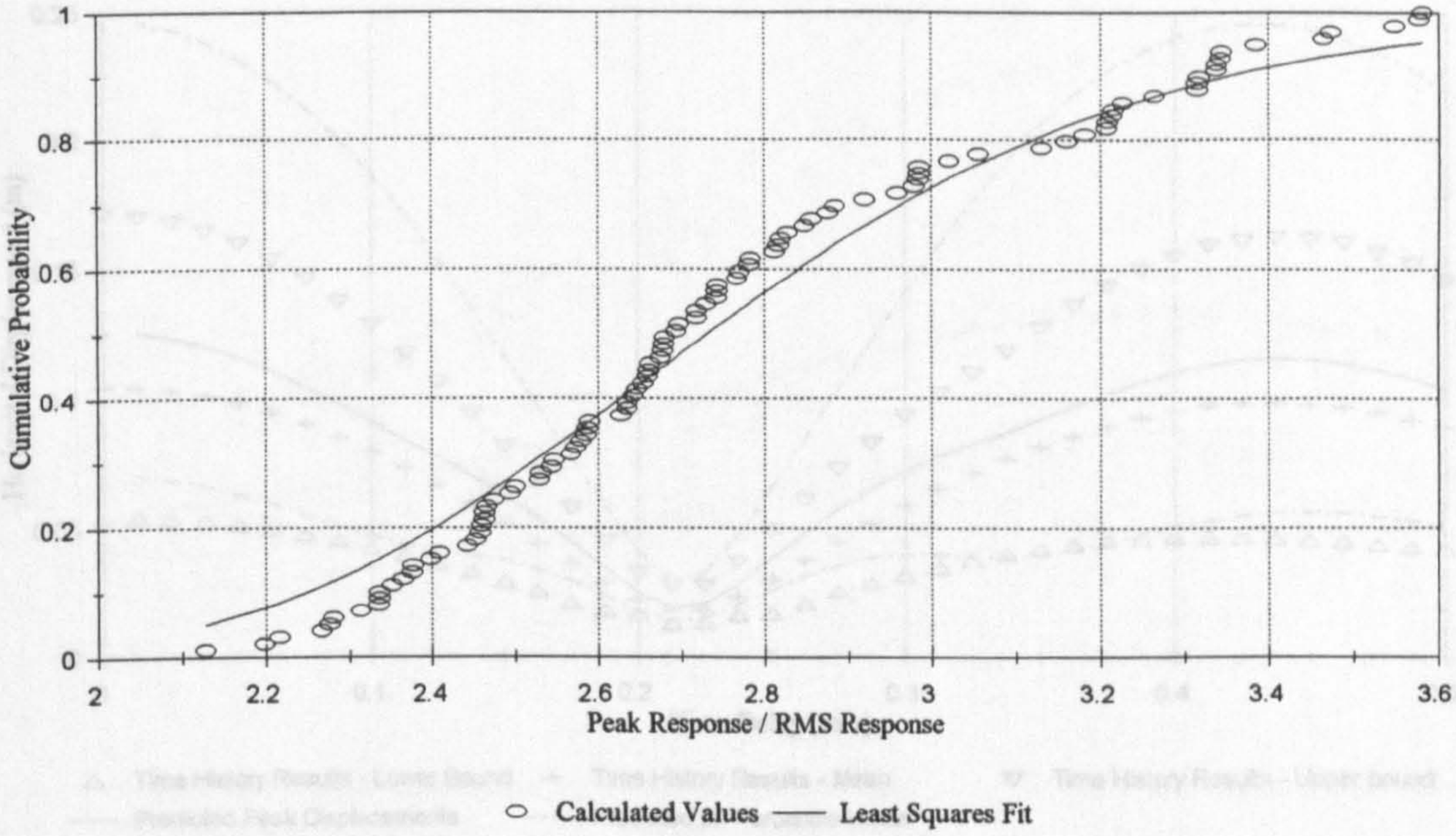

Figure 4.18 -:- Cumulative Probability Function For Typical Set Of Time History Results

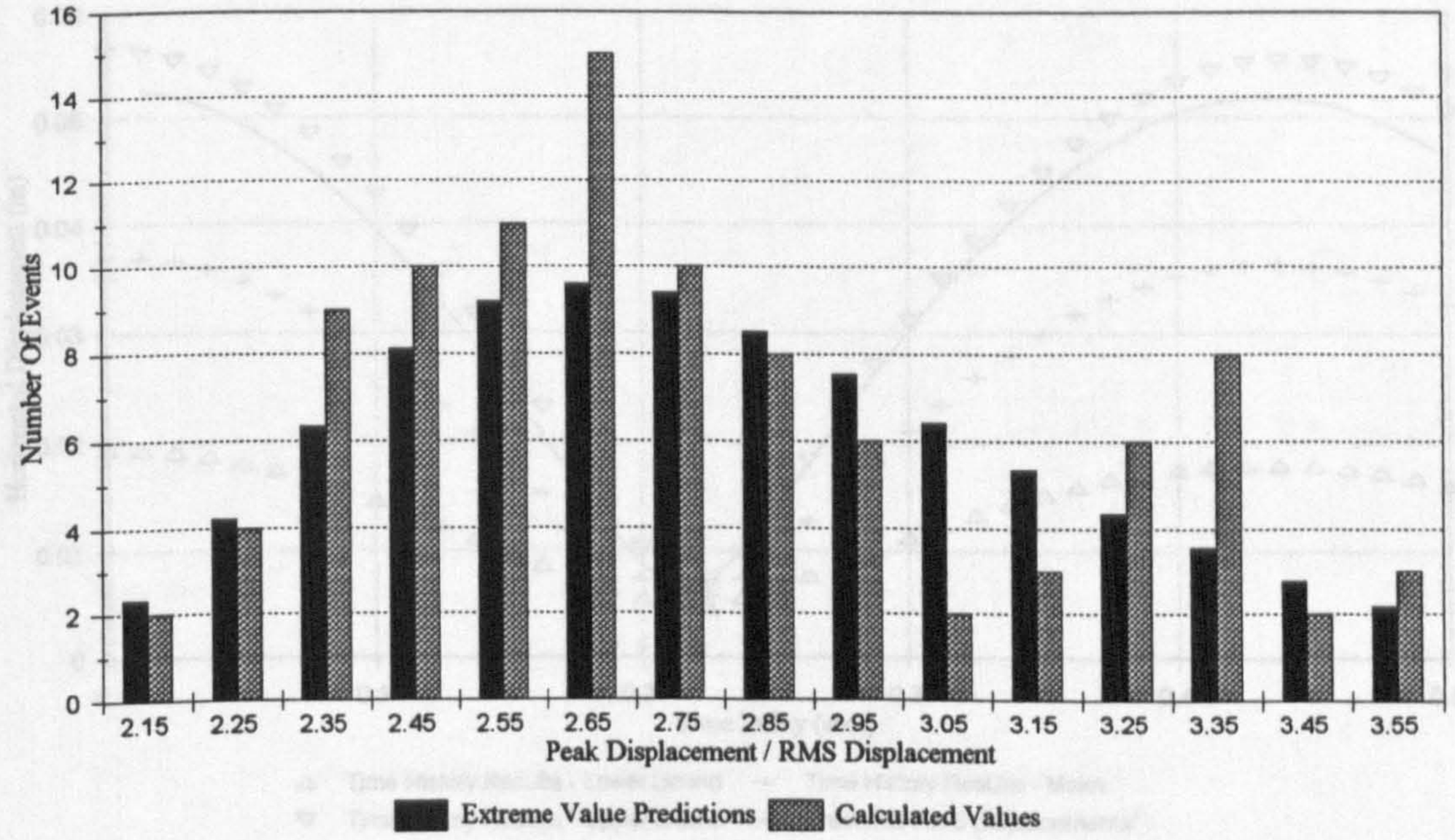

Figure 4.19 -:- Distribution Of Peak Time History Results And Extreme Value Predictions

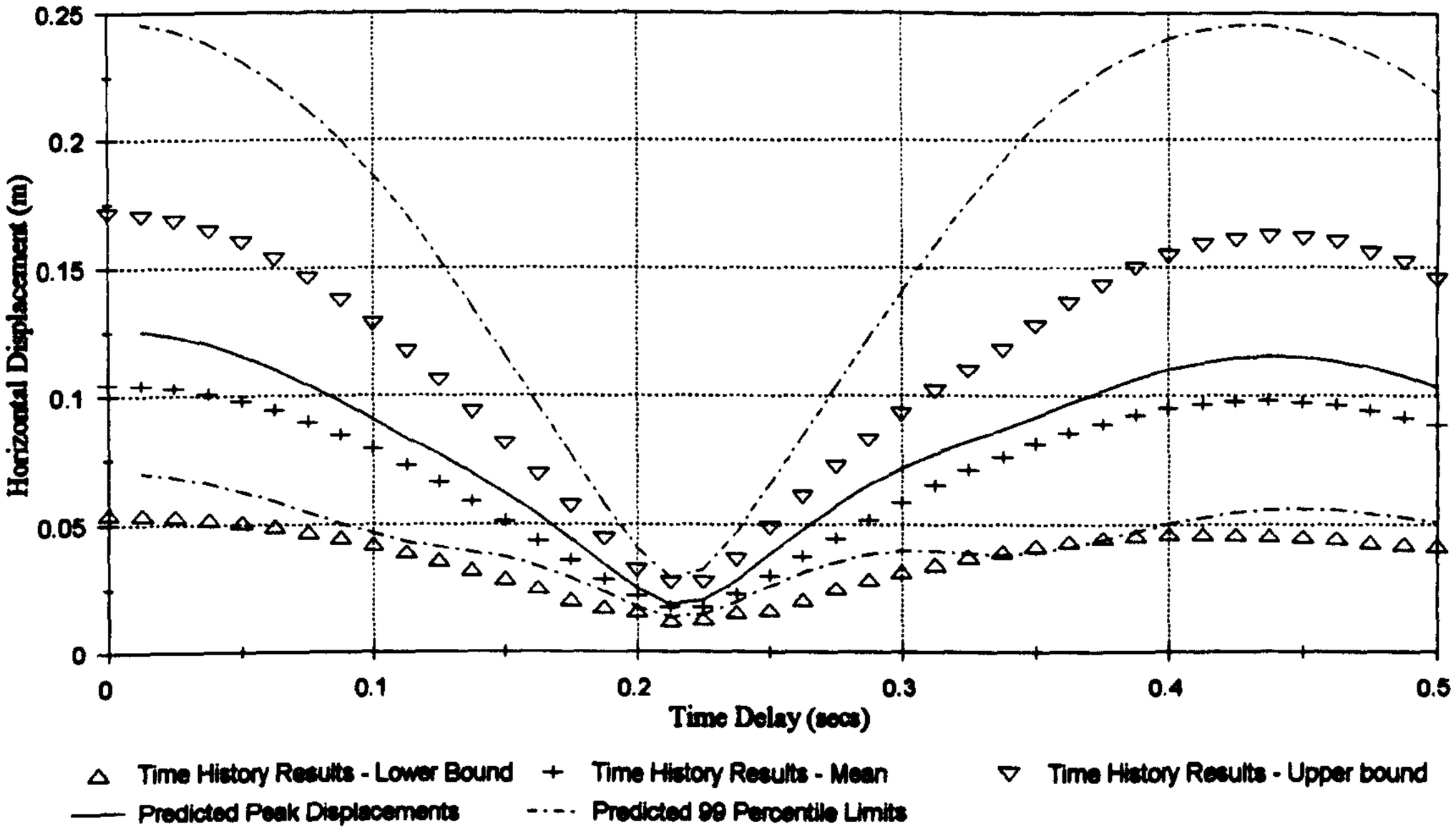

Figure 4.20 -:- Peak Displacements At Node 5, Horizontal Excitation

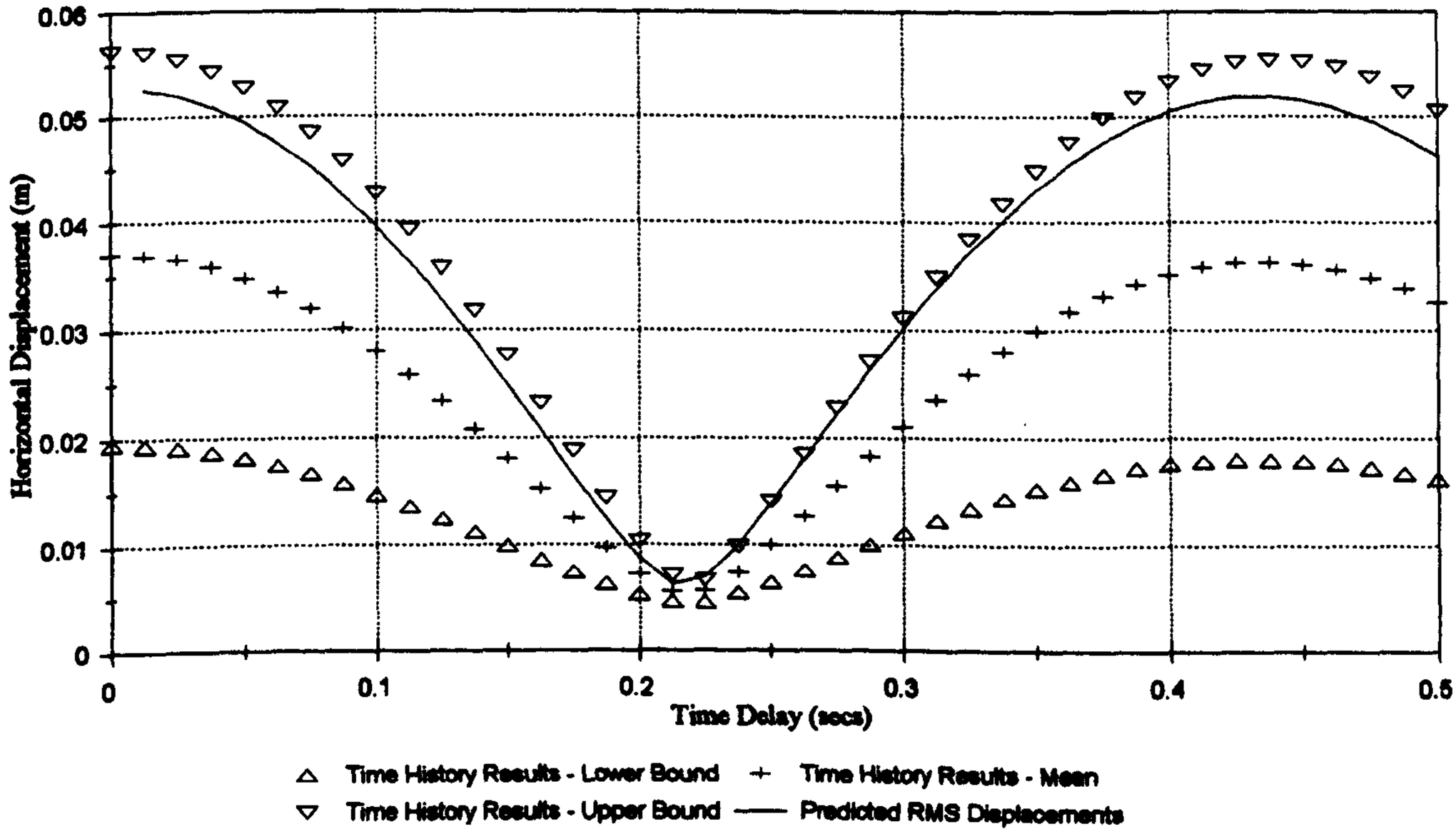

Figure 4.21 -:- RMS Displacements At Node 5, Horizontal Excitation

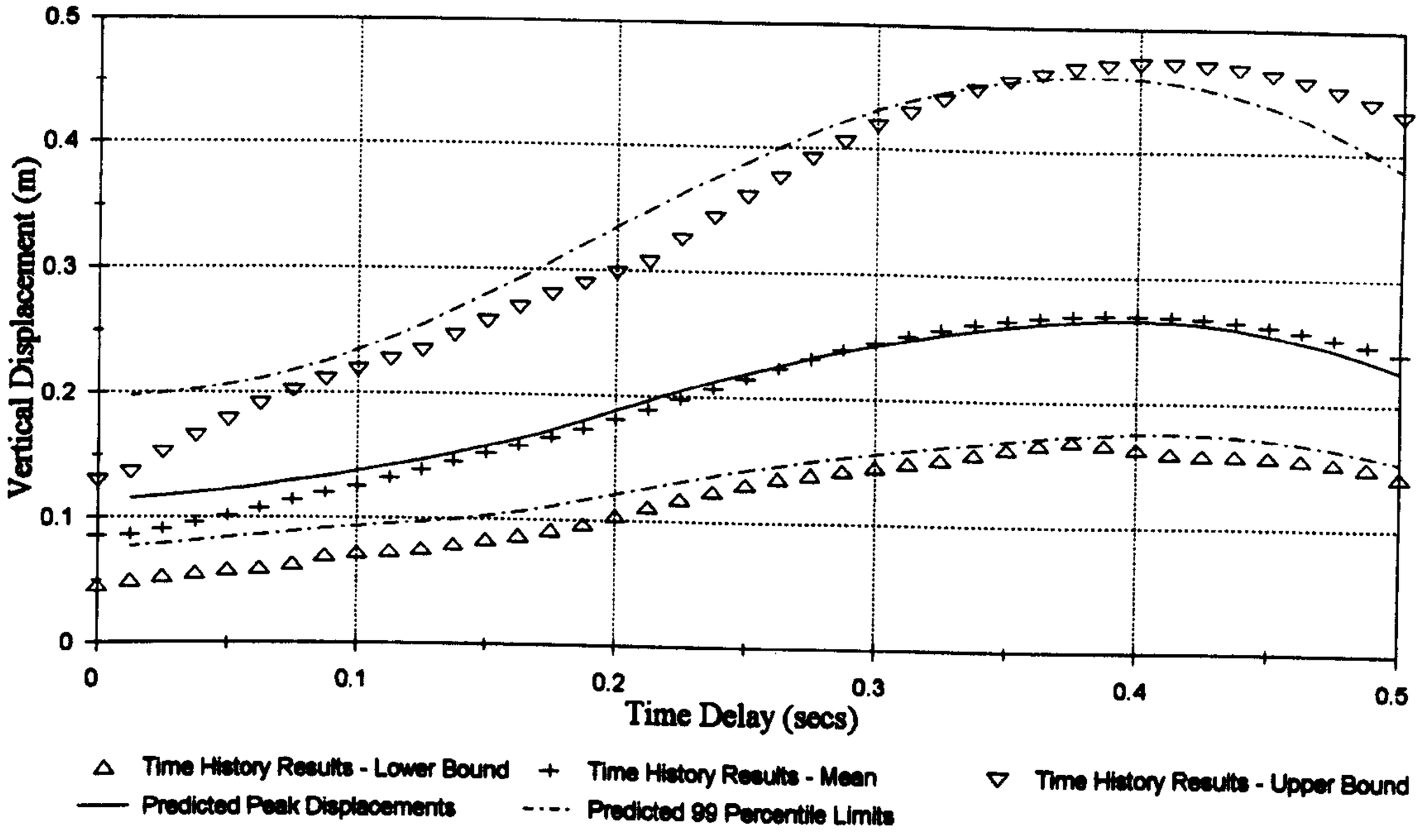

Figure 4.22 -:- Peak Displacements At Node 10, Horizontal Excitation

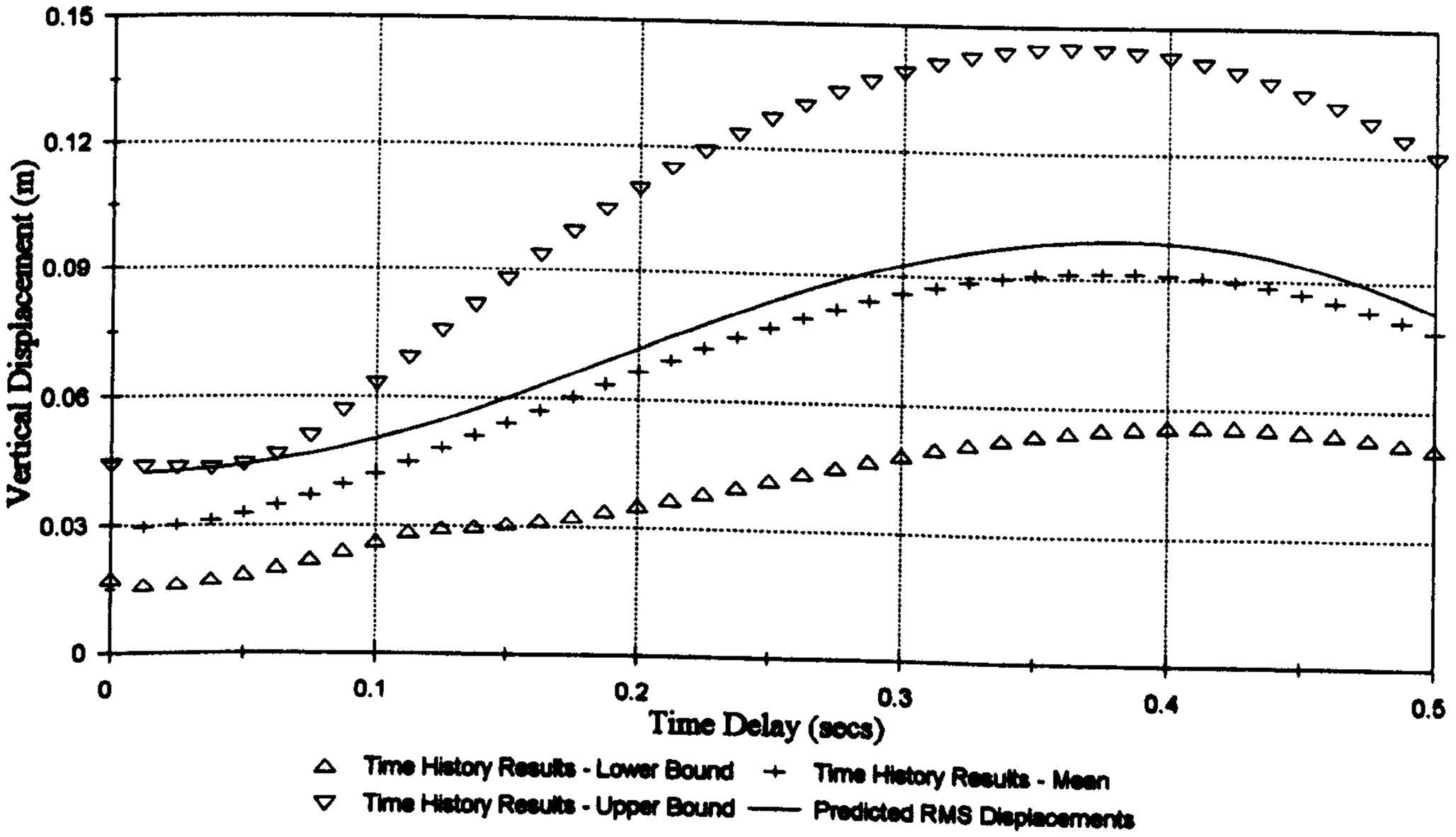

Figure 4.23 -:- RMS Displacements At Node 10, Horizontal Excitation

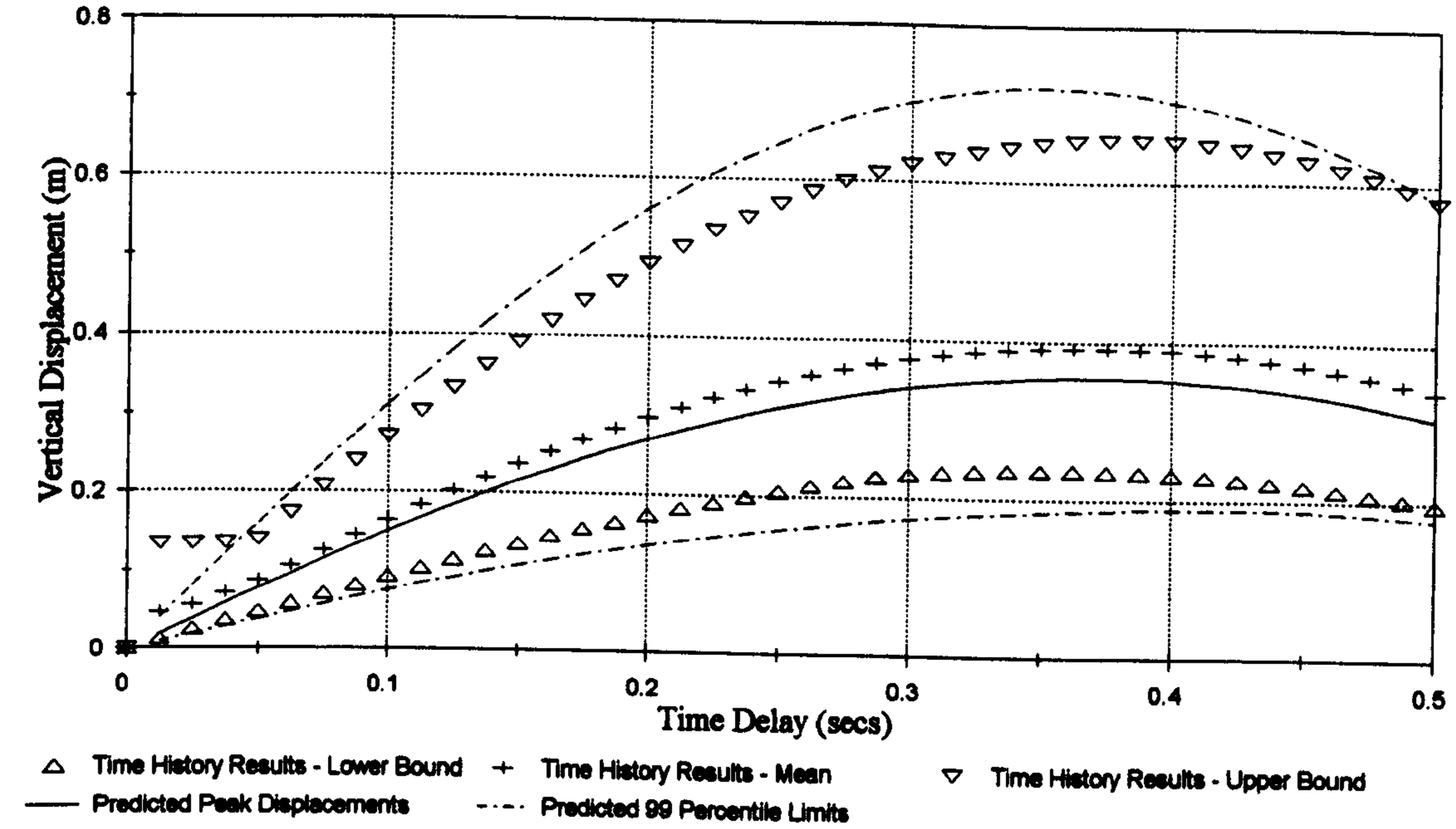

Figure 4.24 -:- Peak Displacements At Node 15, Horizontal Excitation

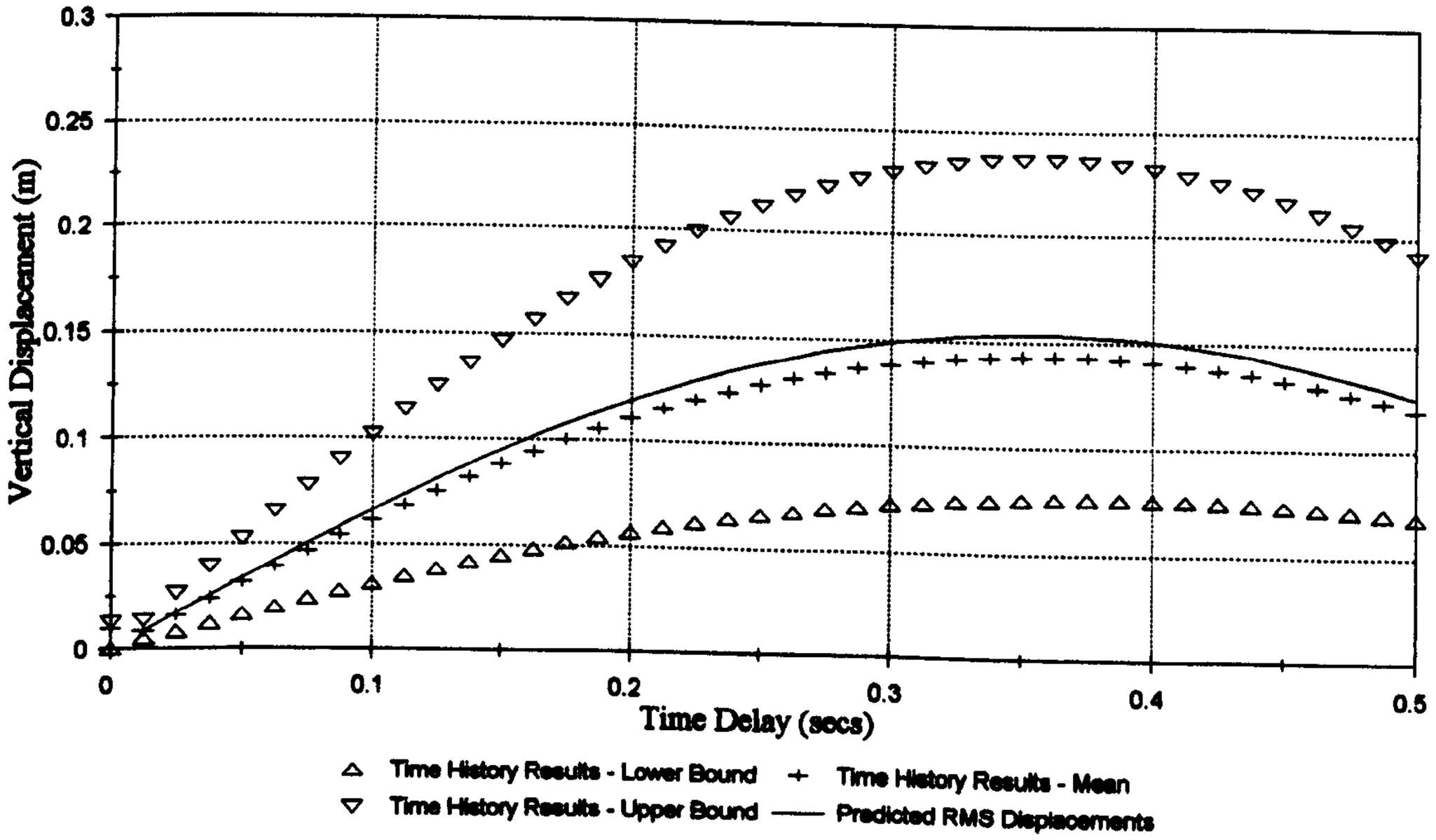

Figure 4.25 -:- RMS Displacements At Node 15, Horizontal Excitation

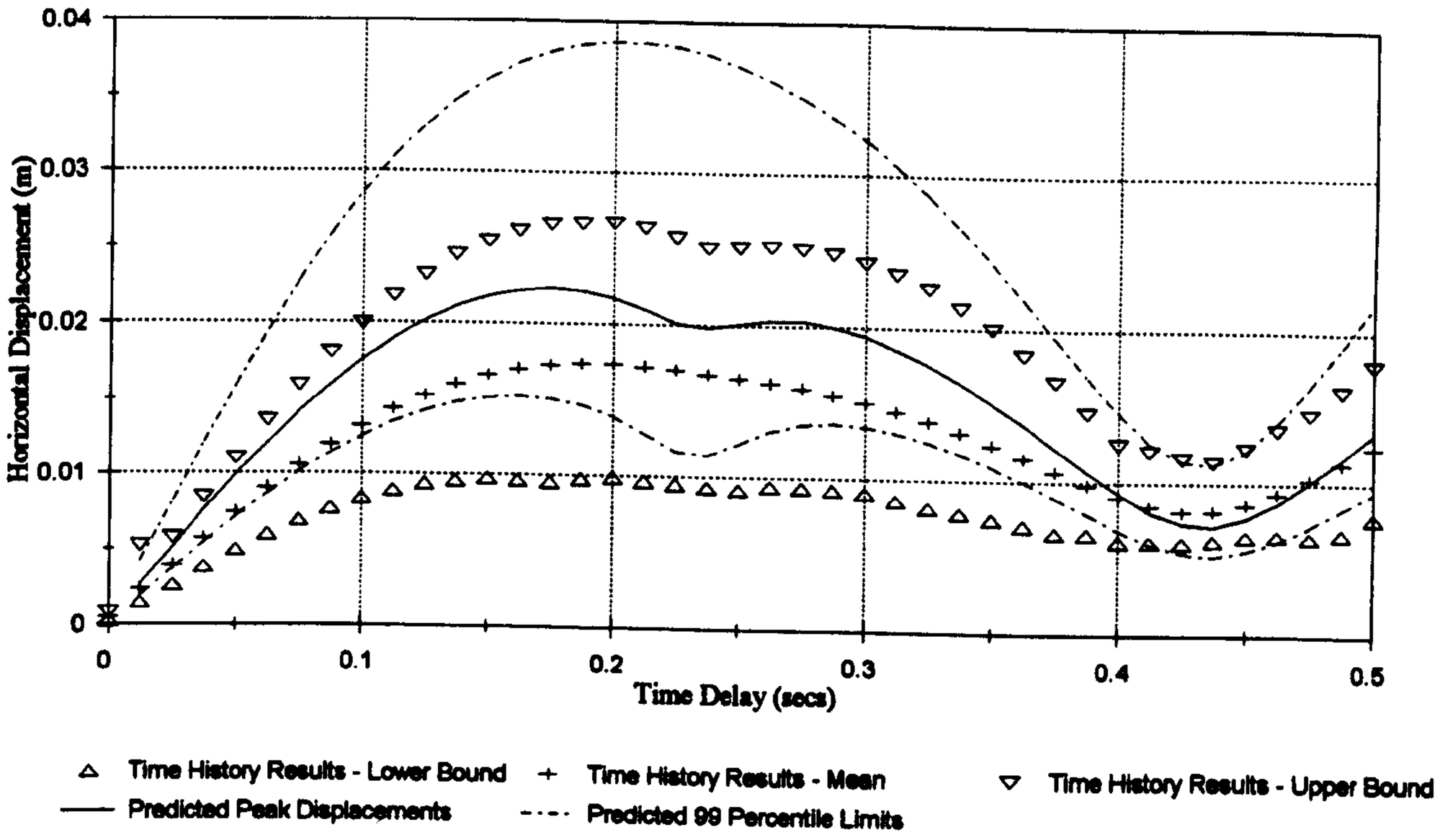

Figure 4.26 -:- Peak Displacements At Node 5, Vertical Excitation

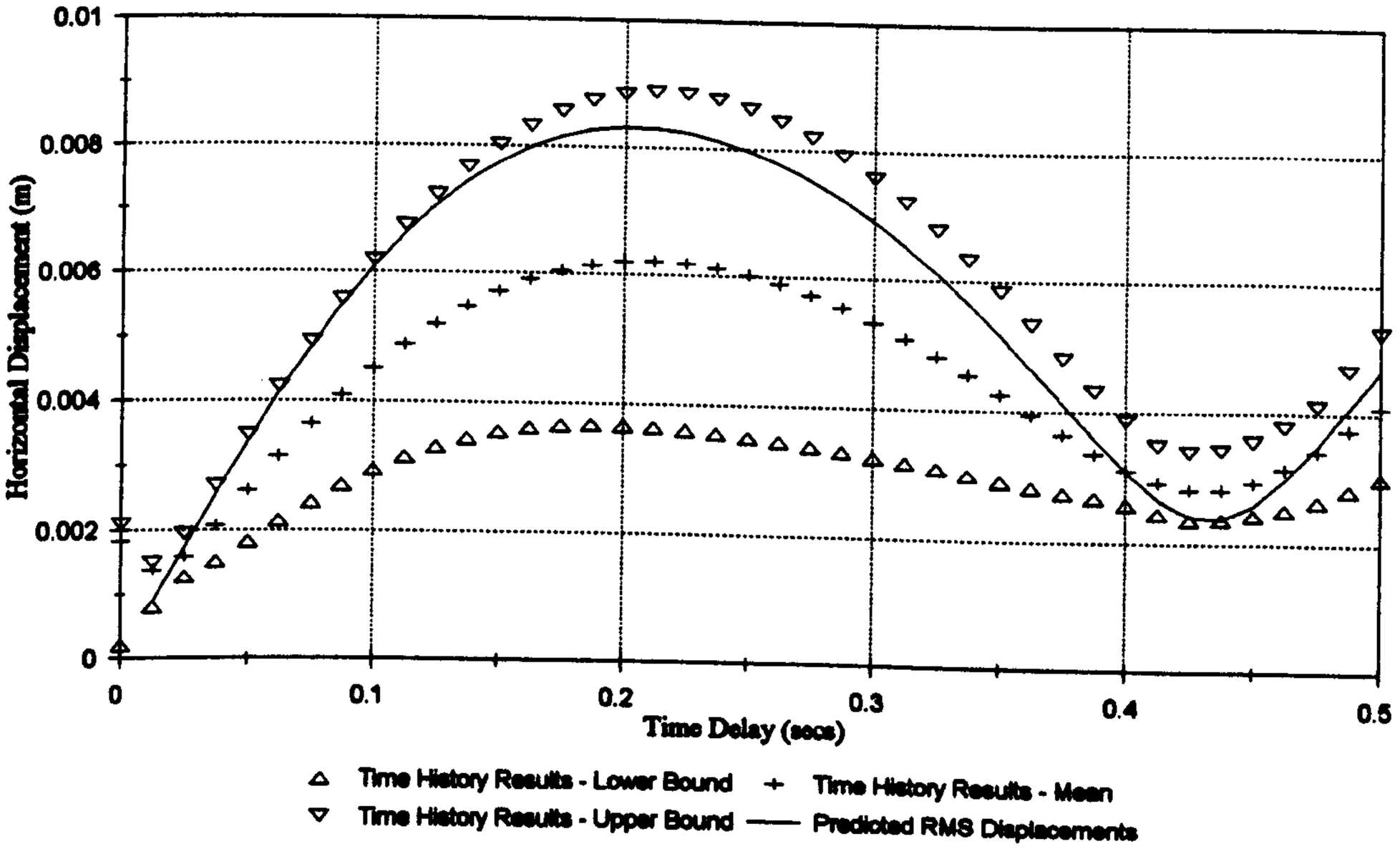

Figure 4.27 -:- RMS Displacements At Node 5, Vertical Excitation

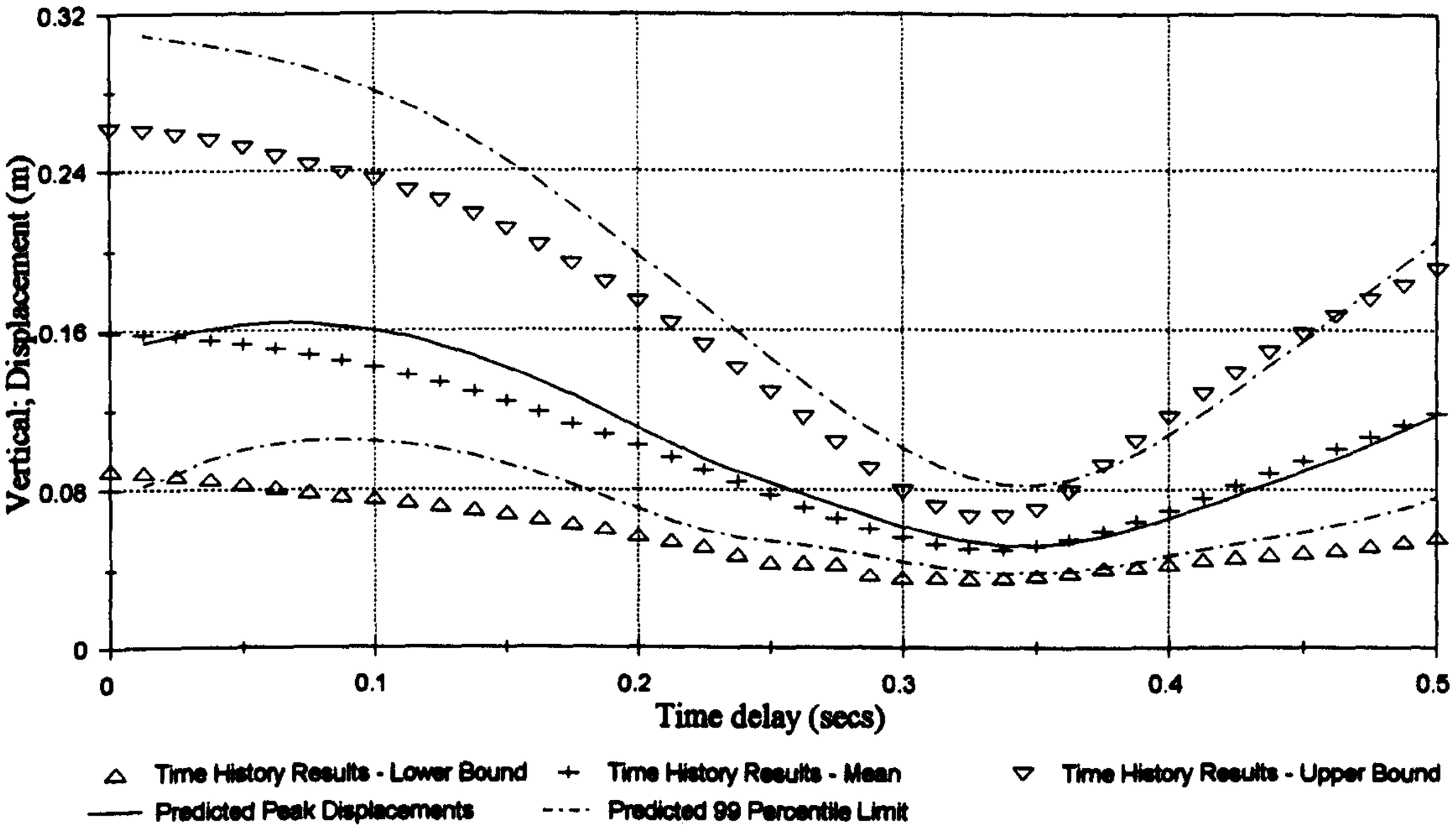

Figure 4.28 -:- Peak Displacements At Node 10, Vertical Excitation

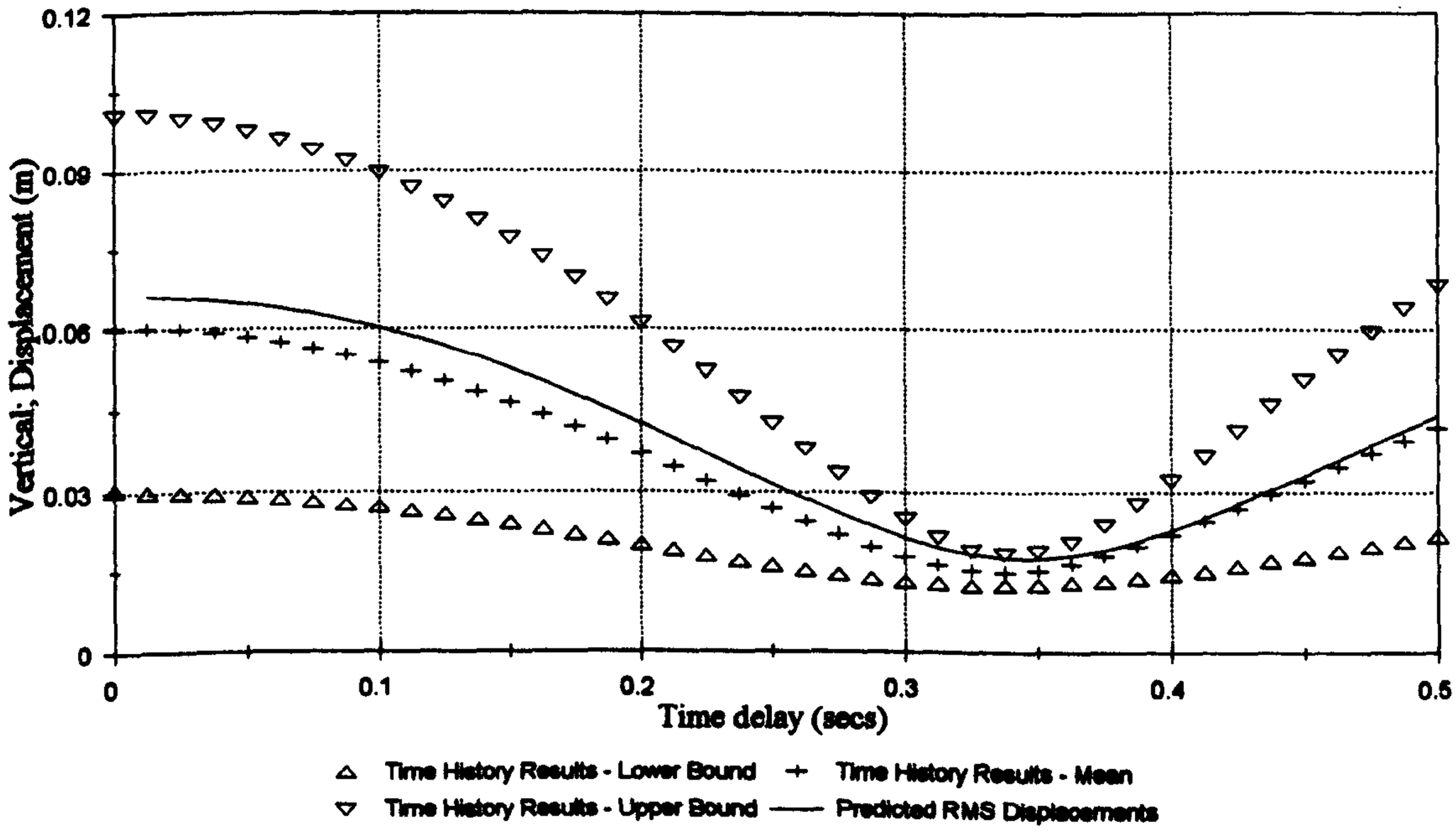

Figure 4.29 -:- RMS Displacements At Node 10, Vertical Excitation

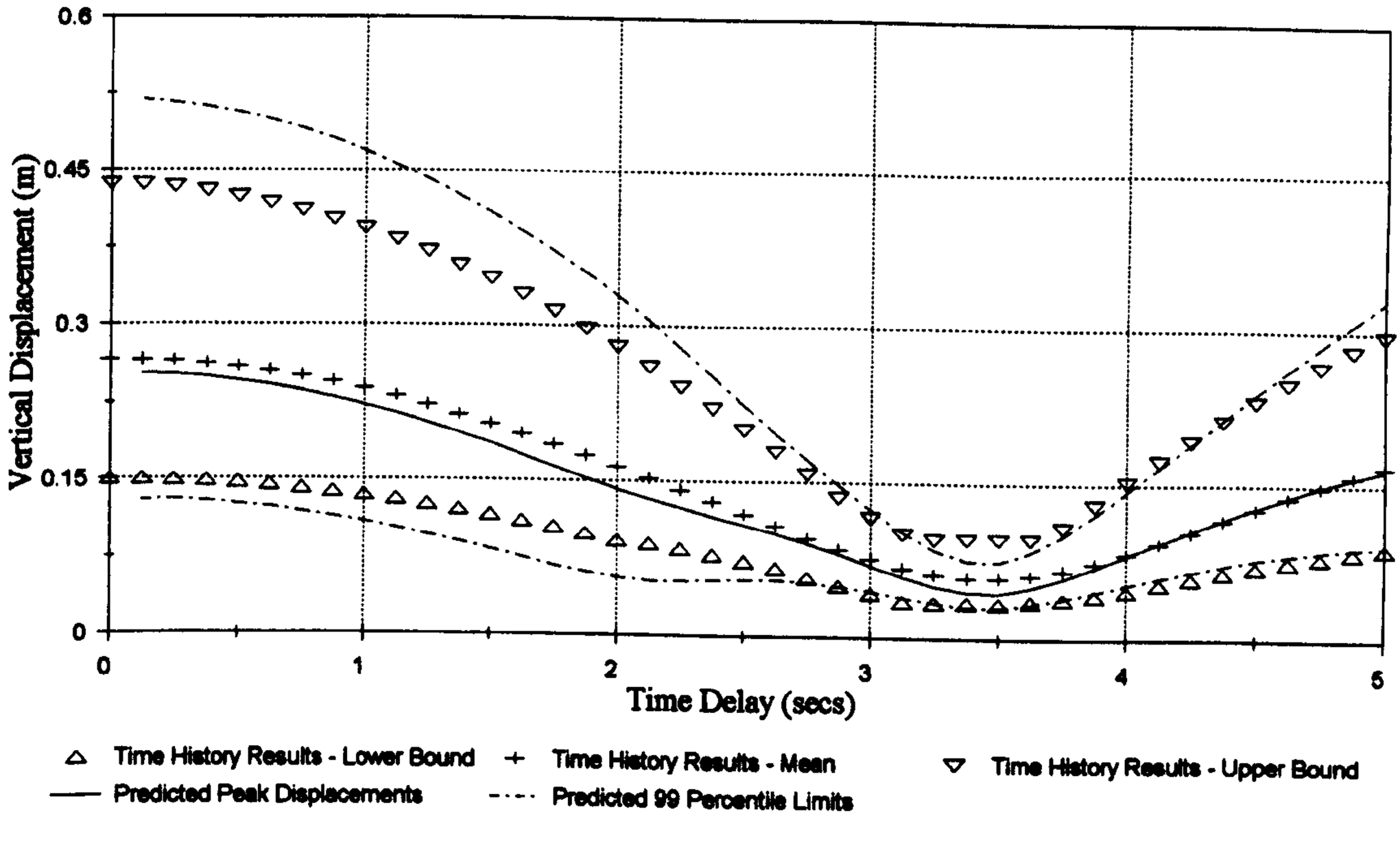

Figure 4.30 -:- Peak Displacements At Node 15, Vertical Excitation

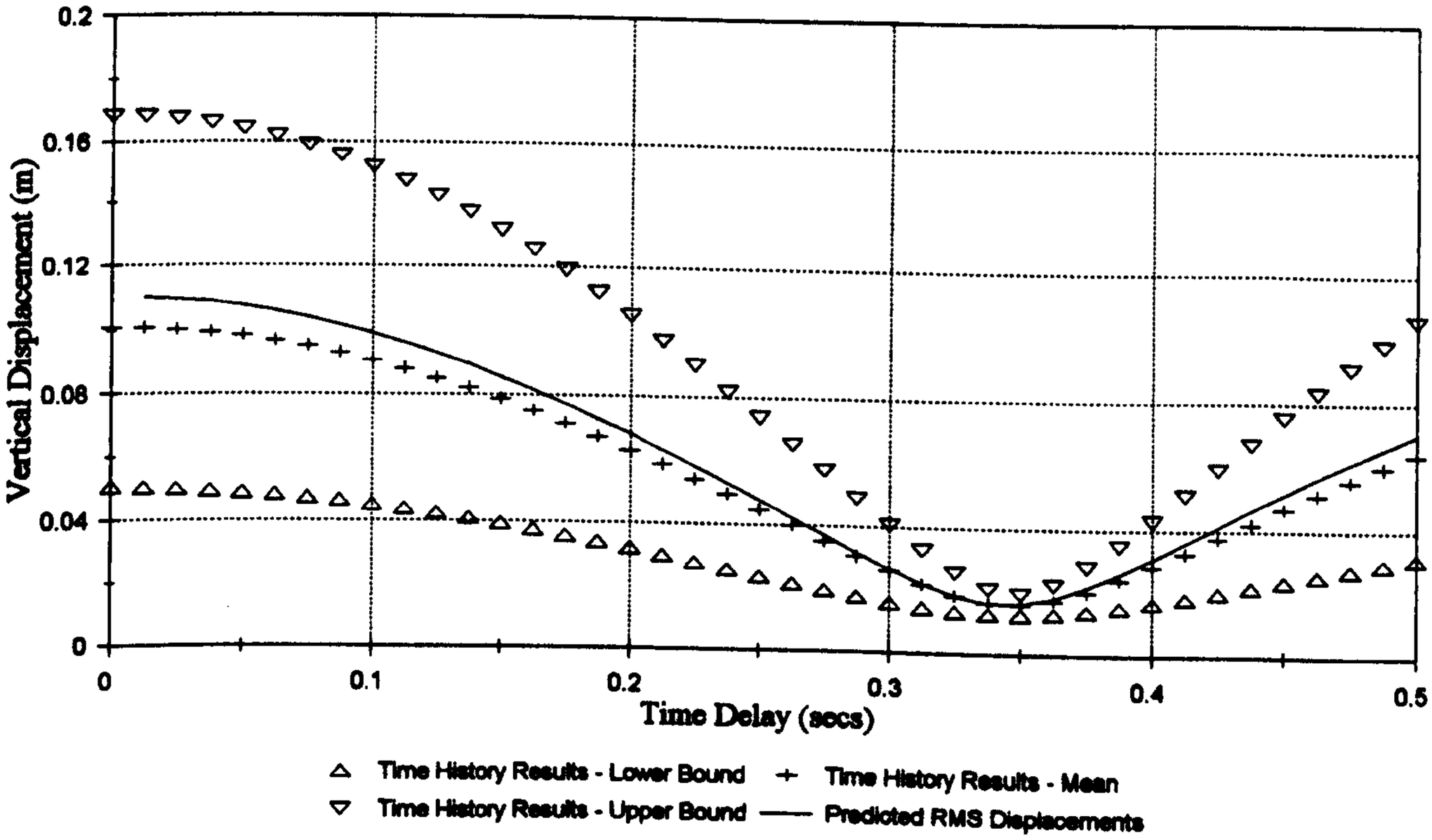

Figure 4.31 -:- RMS Displacements At Node 15, Vertical Excitation

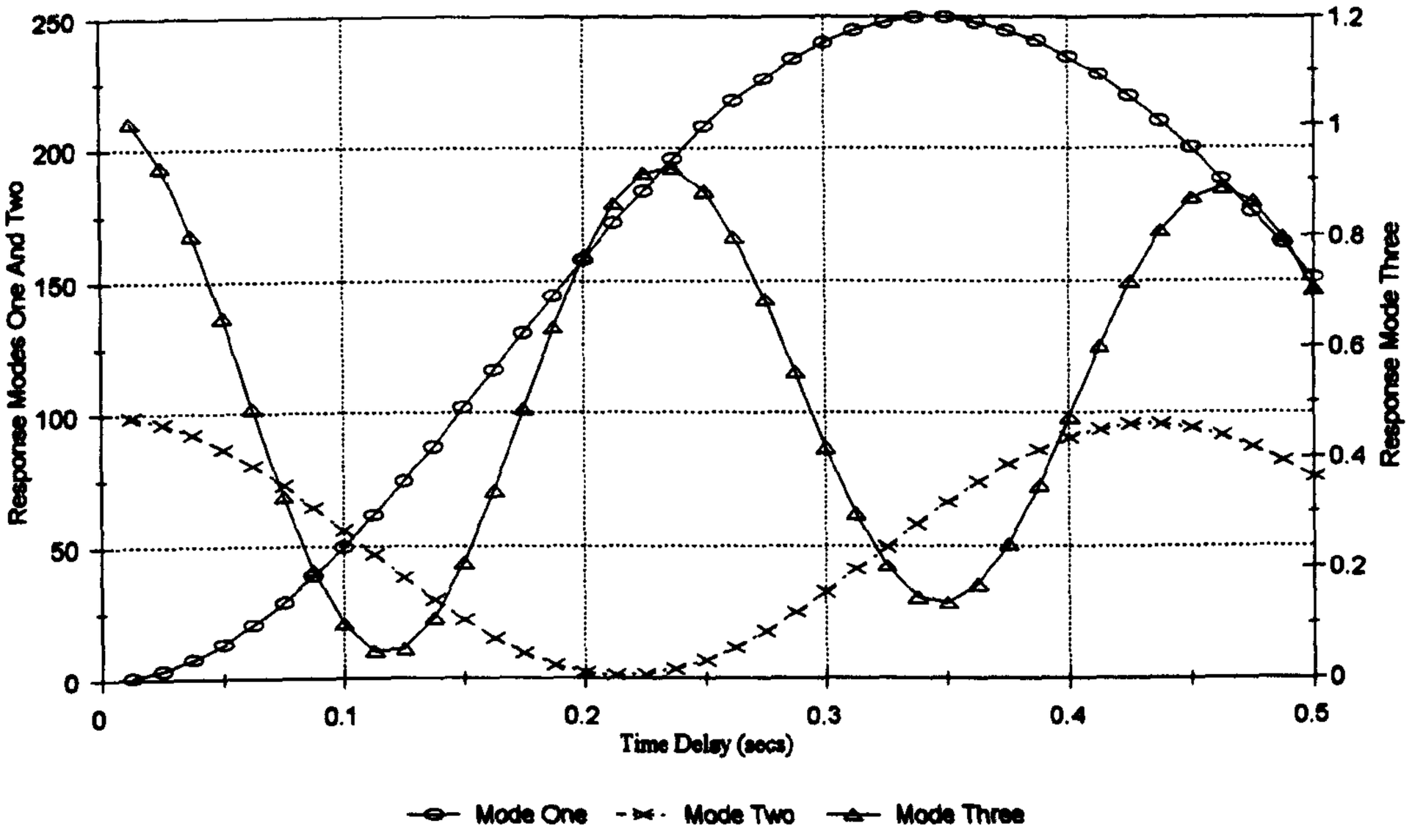

Figure 4.32 -:- Modal Zeroth Moments, Horizontal Excitation

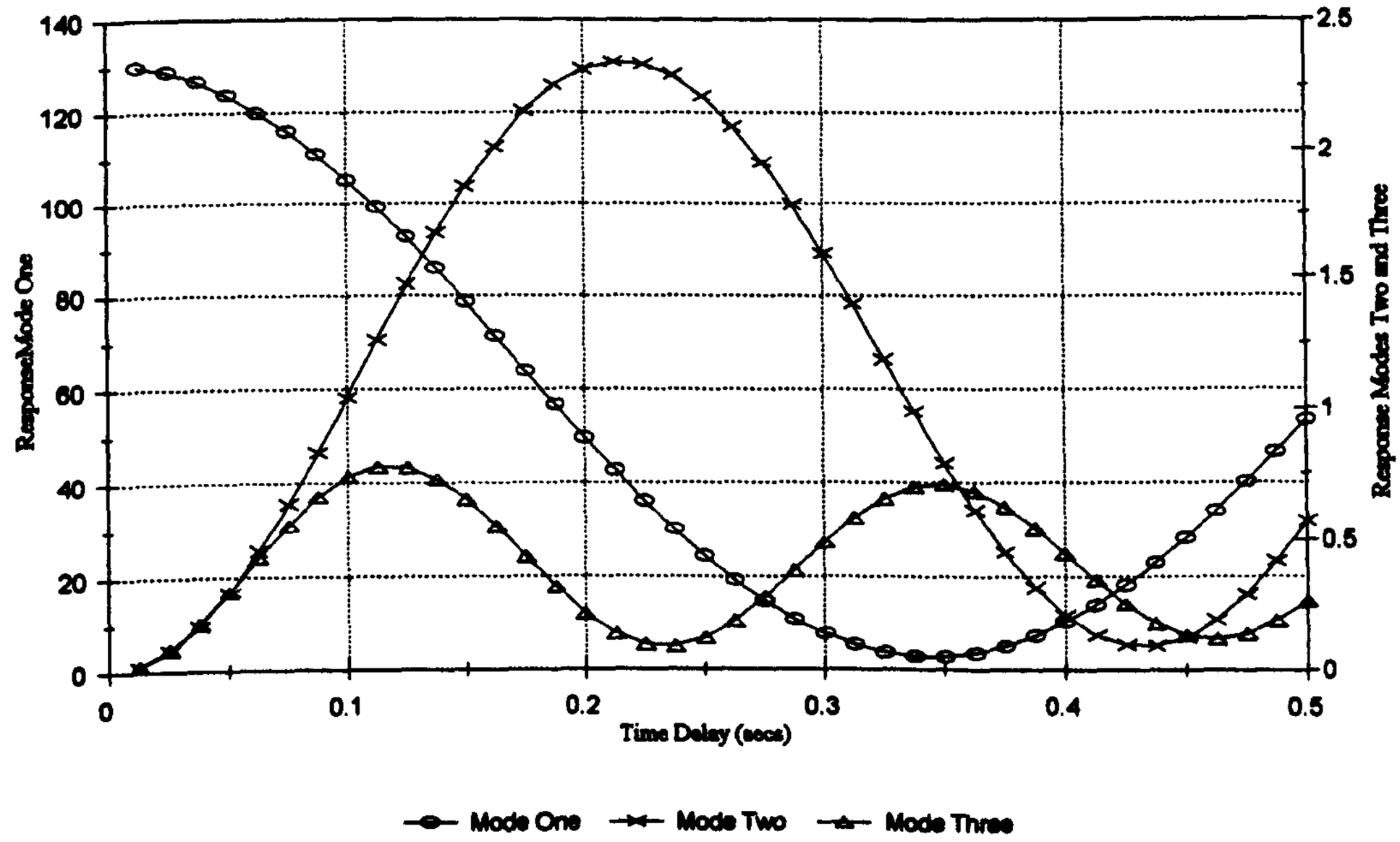

Figure 4.33 -:- Modal Zeroth Moments, Vertical Excitation

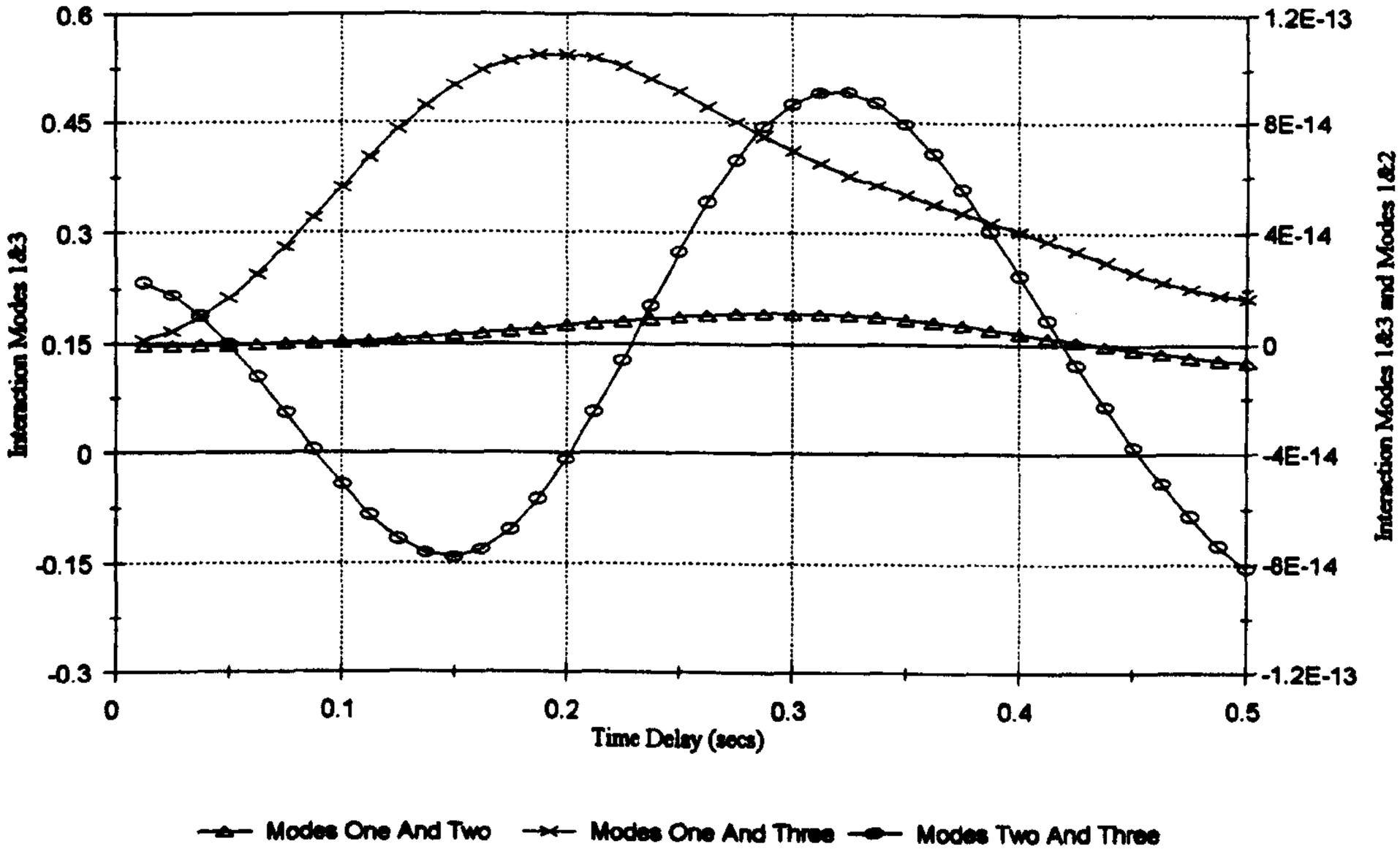

Figure 4.34 -:- Zeroth Modal Cross Spectral Moments, Horizontal Excitation

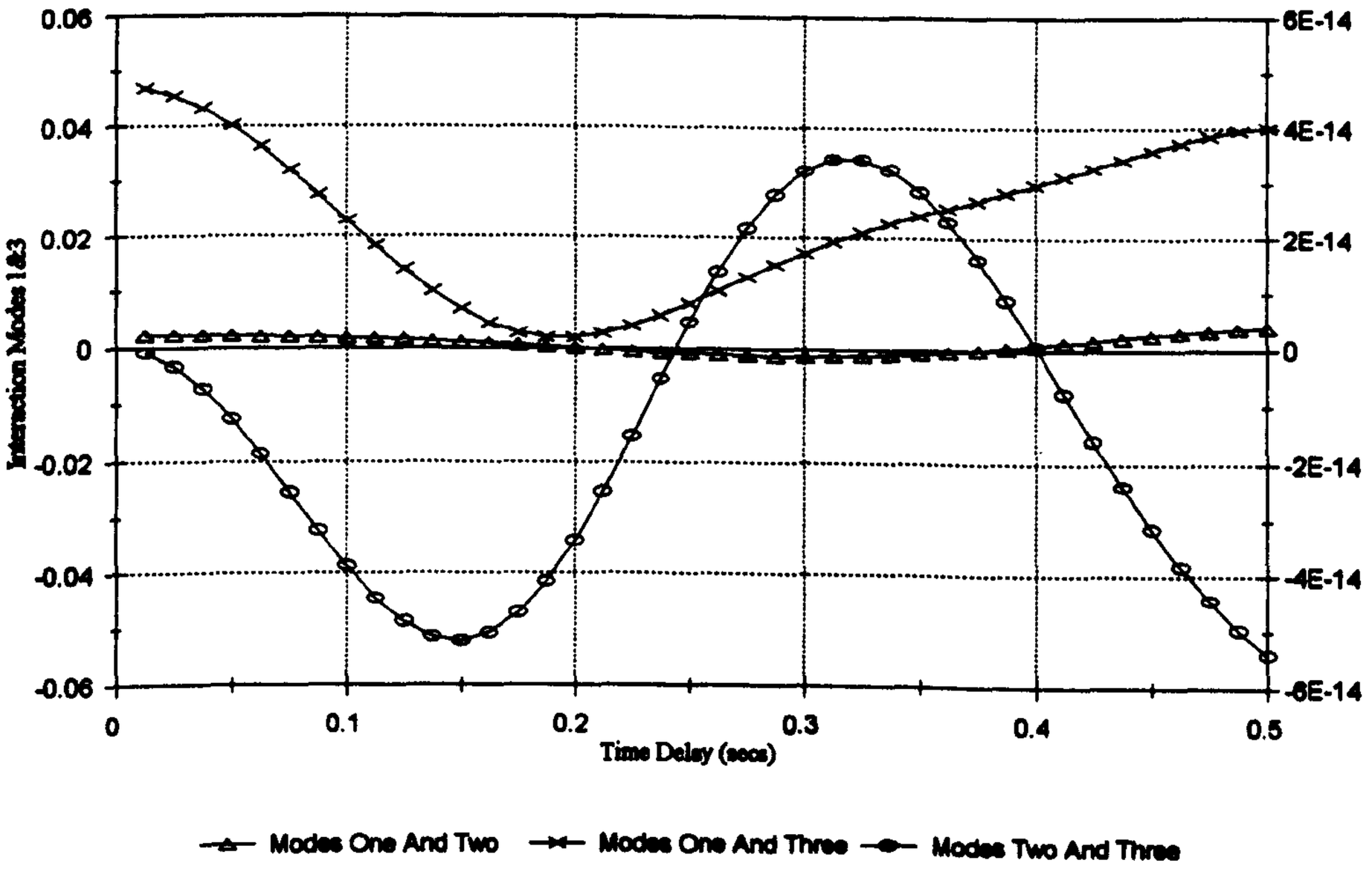

Figure 4.35 -:- Zeroth Modal Cross Spectral Moments, Vertical Excitation

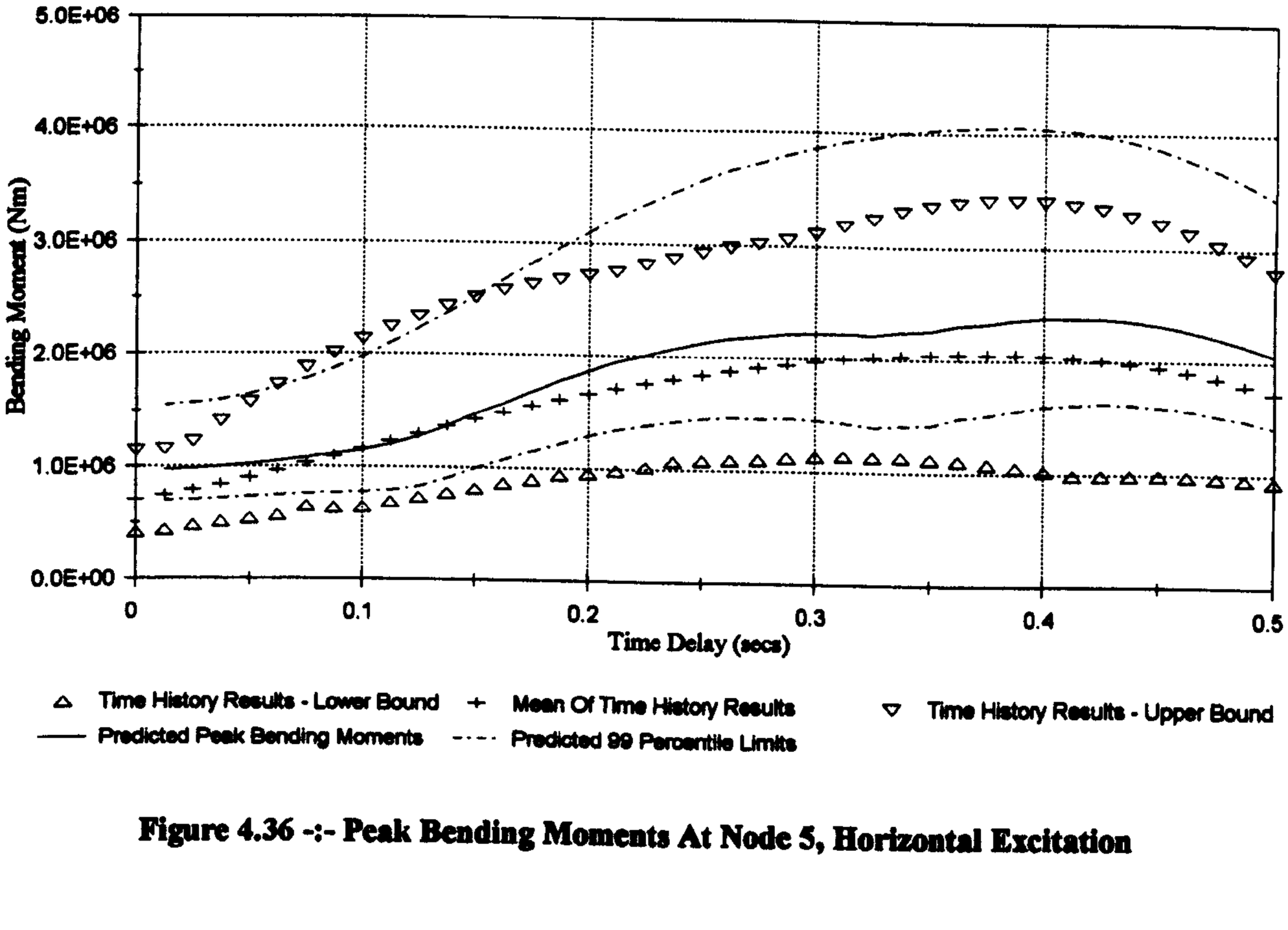

Figure 4.36 -:- Peak Bending Moments At Node 5, Horizontal Excitation

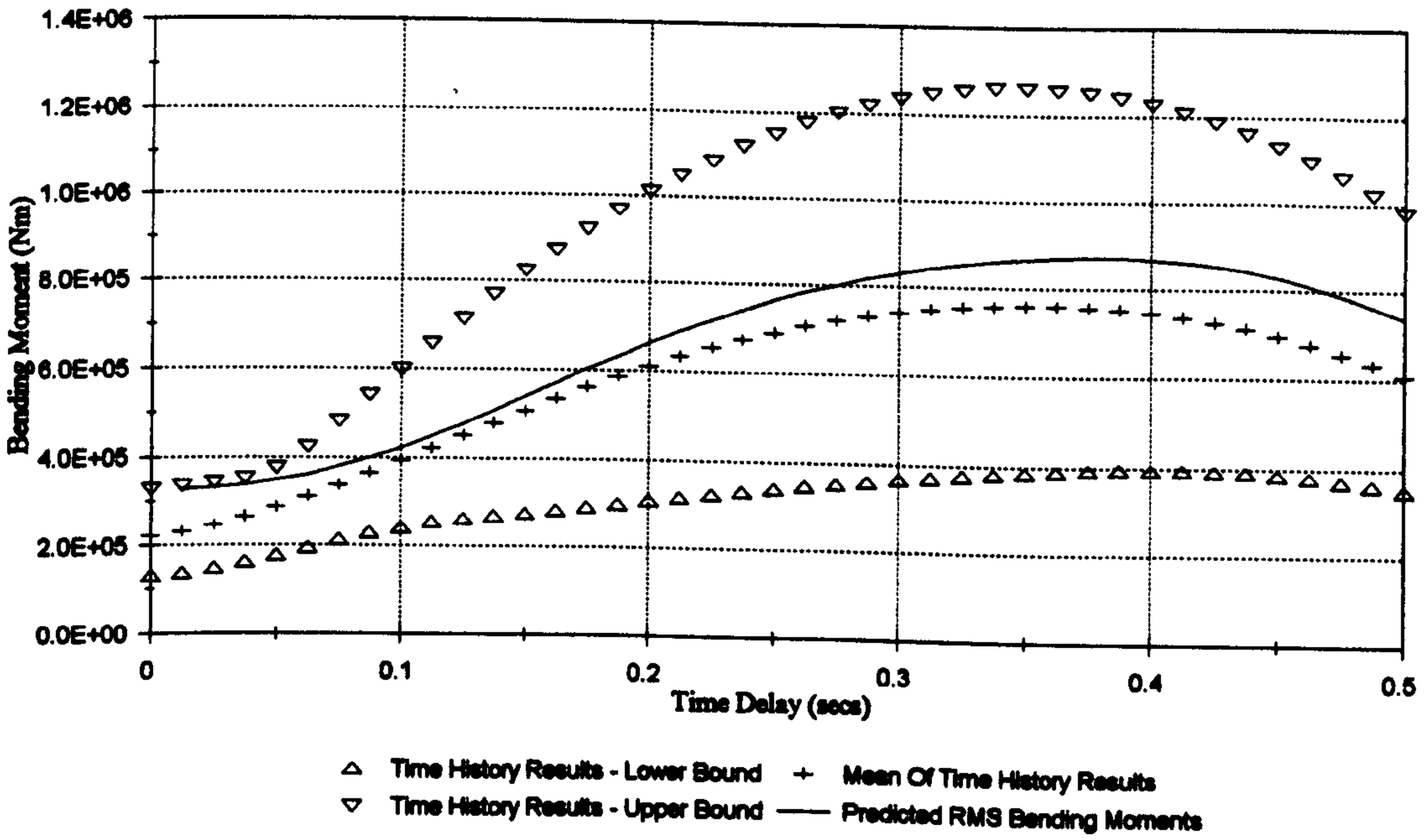

Figure 4.37 -:- RMS Bending Moments At Node 5, Horizontal Excitation

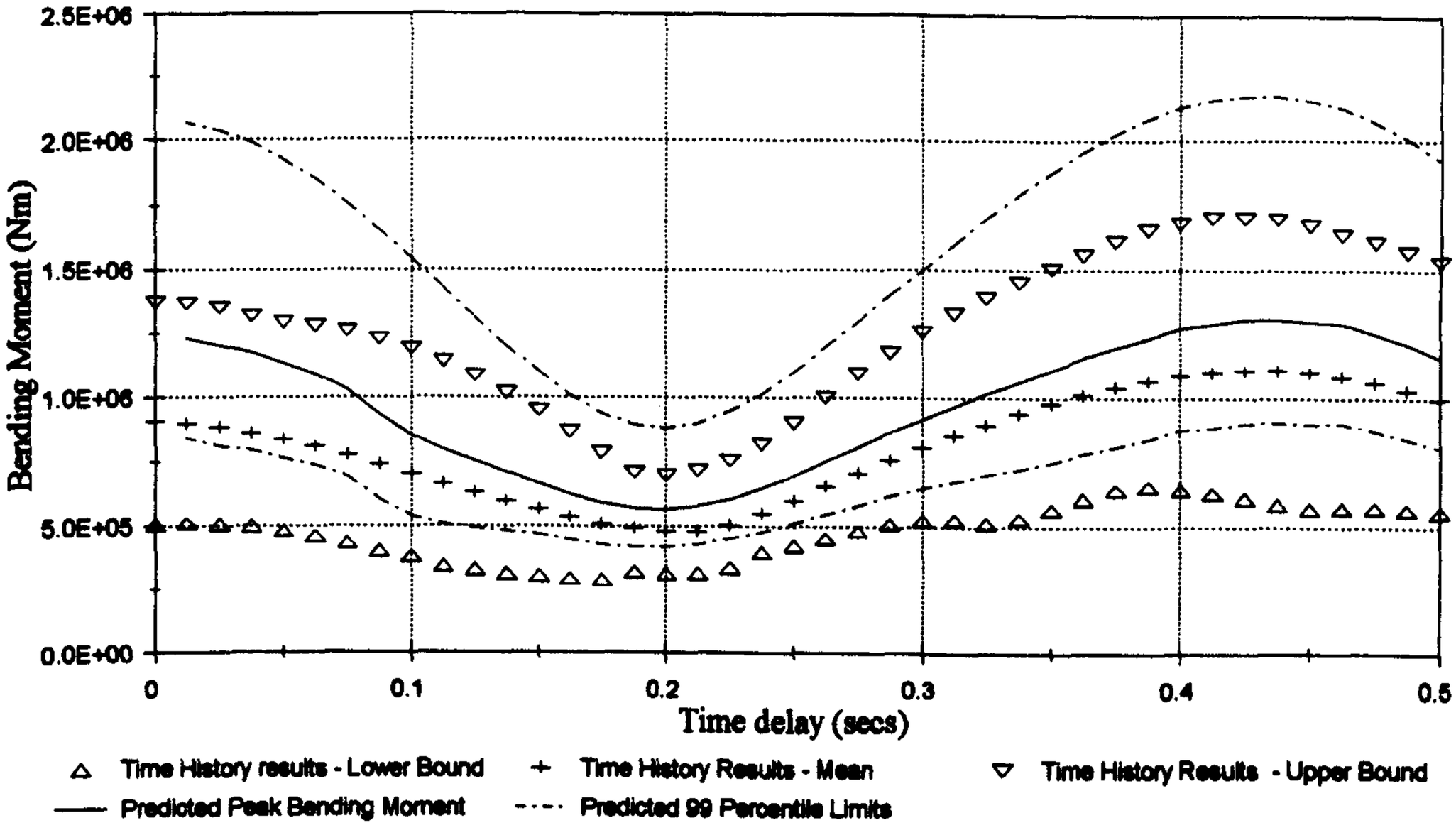

Figure 4.38 -:- Peak Bending Moments At Node 10, Horizontal Excitation

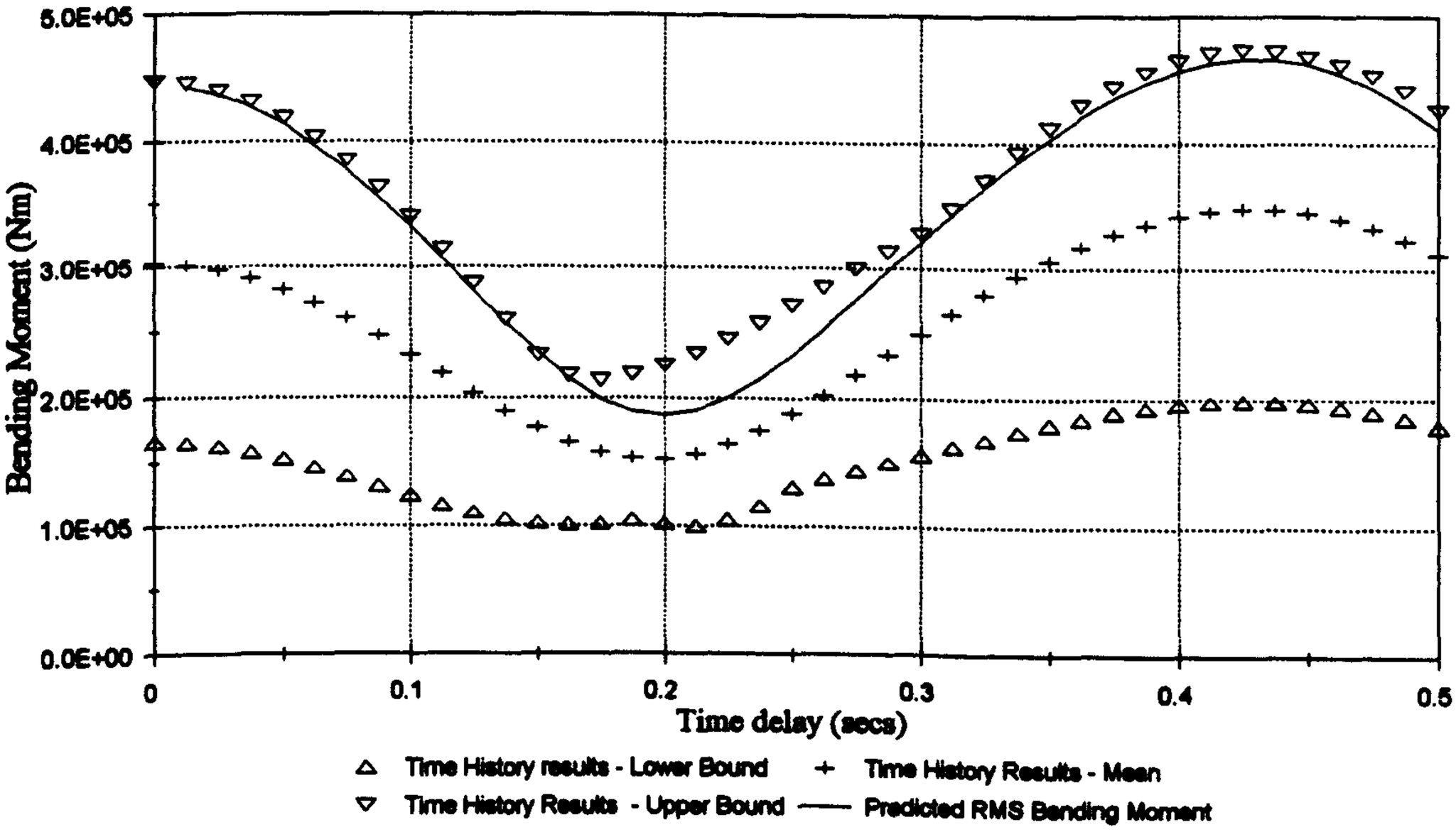

Figure 4.39 -:- RMS Bending Moments At Node 10, Horizontal Excitation

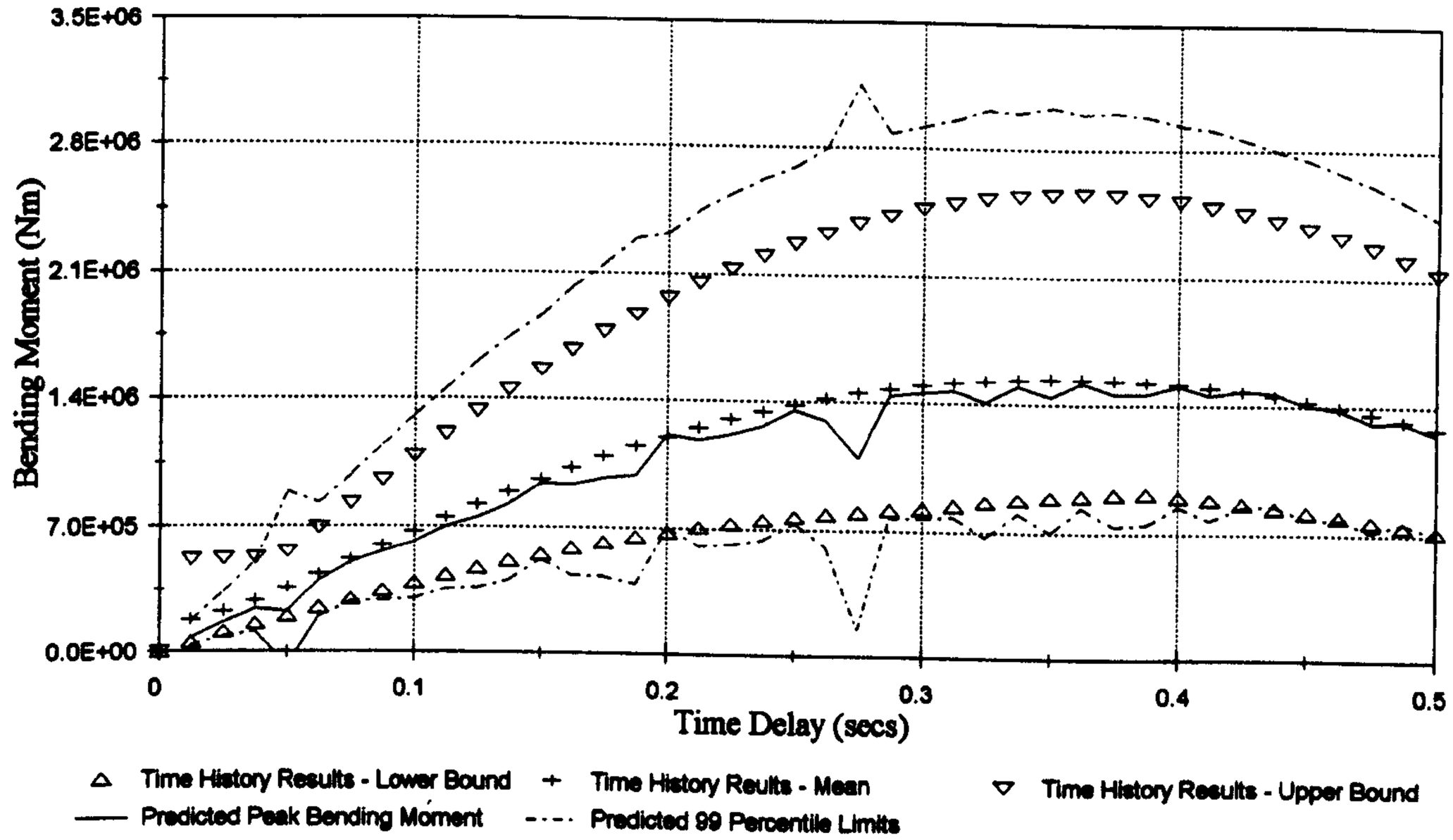

Figure 4.40 -:- Peak Bending Moments At Node 15, Horizontal Excitation

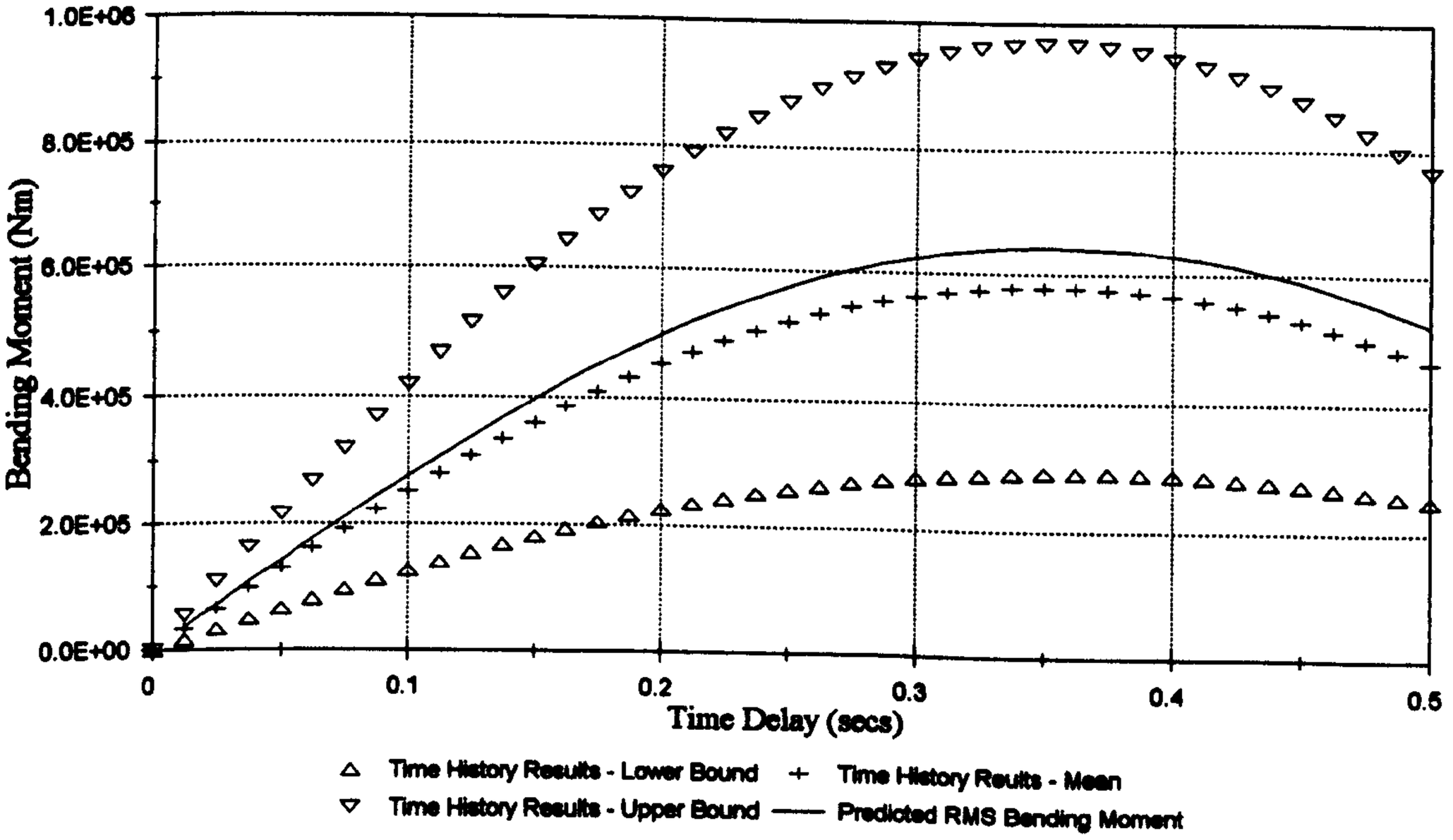

Figure 4.41 -:- RMS Bending Moments At Node 15, Horizontal Excitation

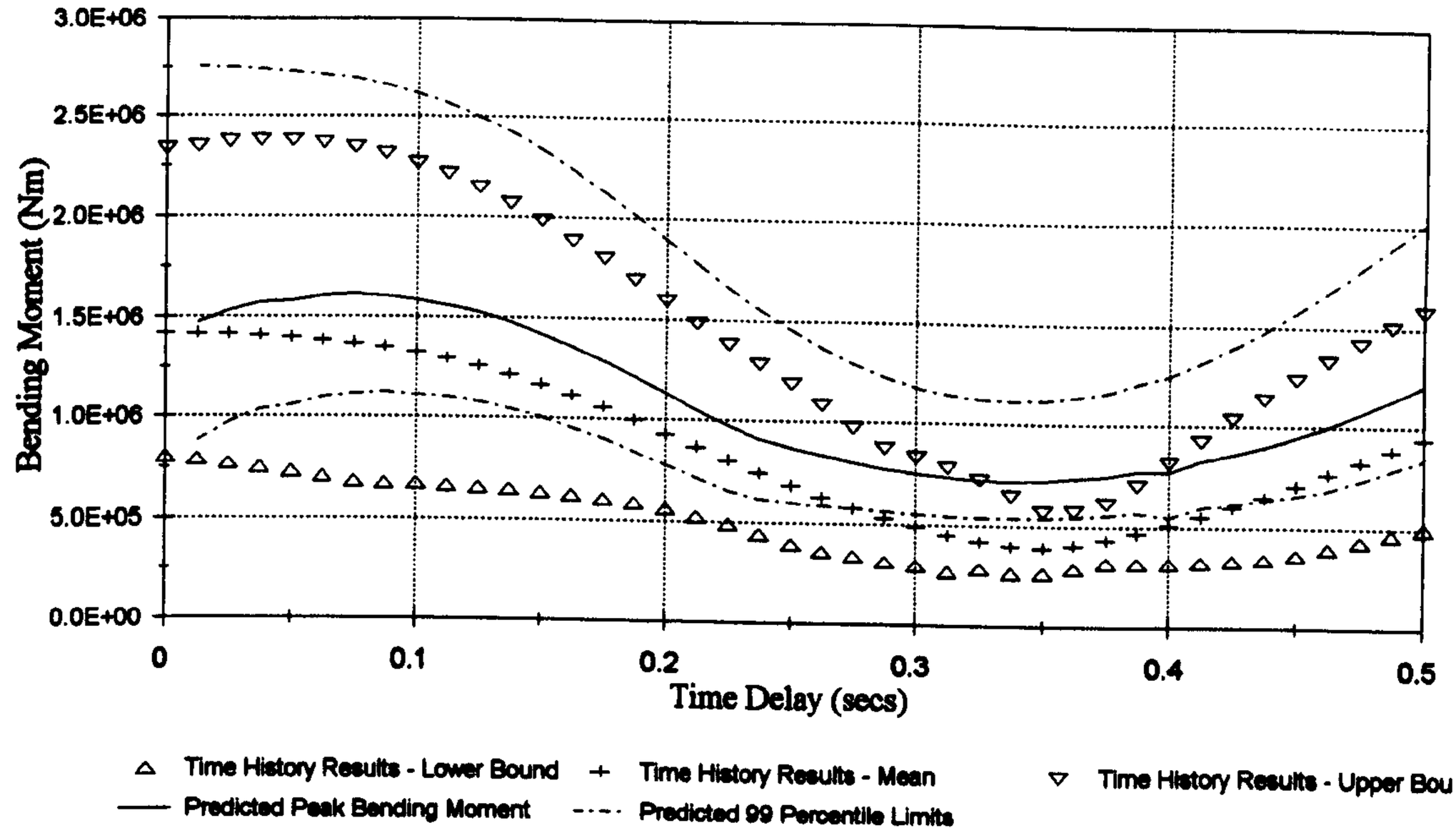

Figure 4.42 -:- Peak Bending Moments At Node 5, Vertical Excitation

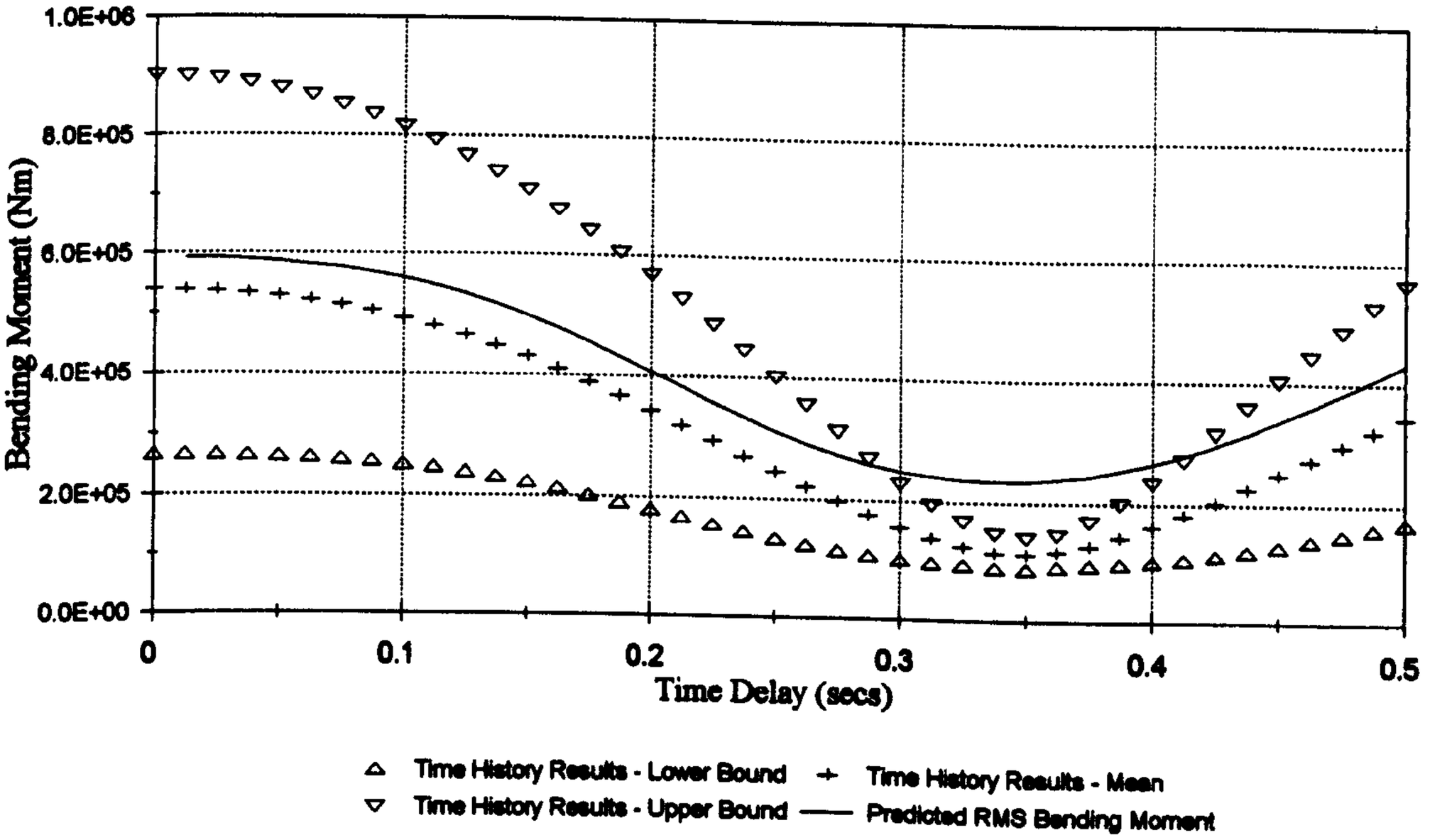

Figure 4.43 -:- RMS Bending Moments At Node 5, Vertical Excitation

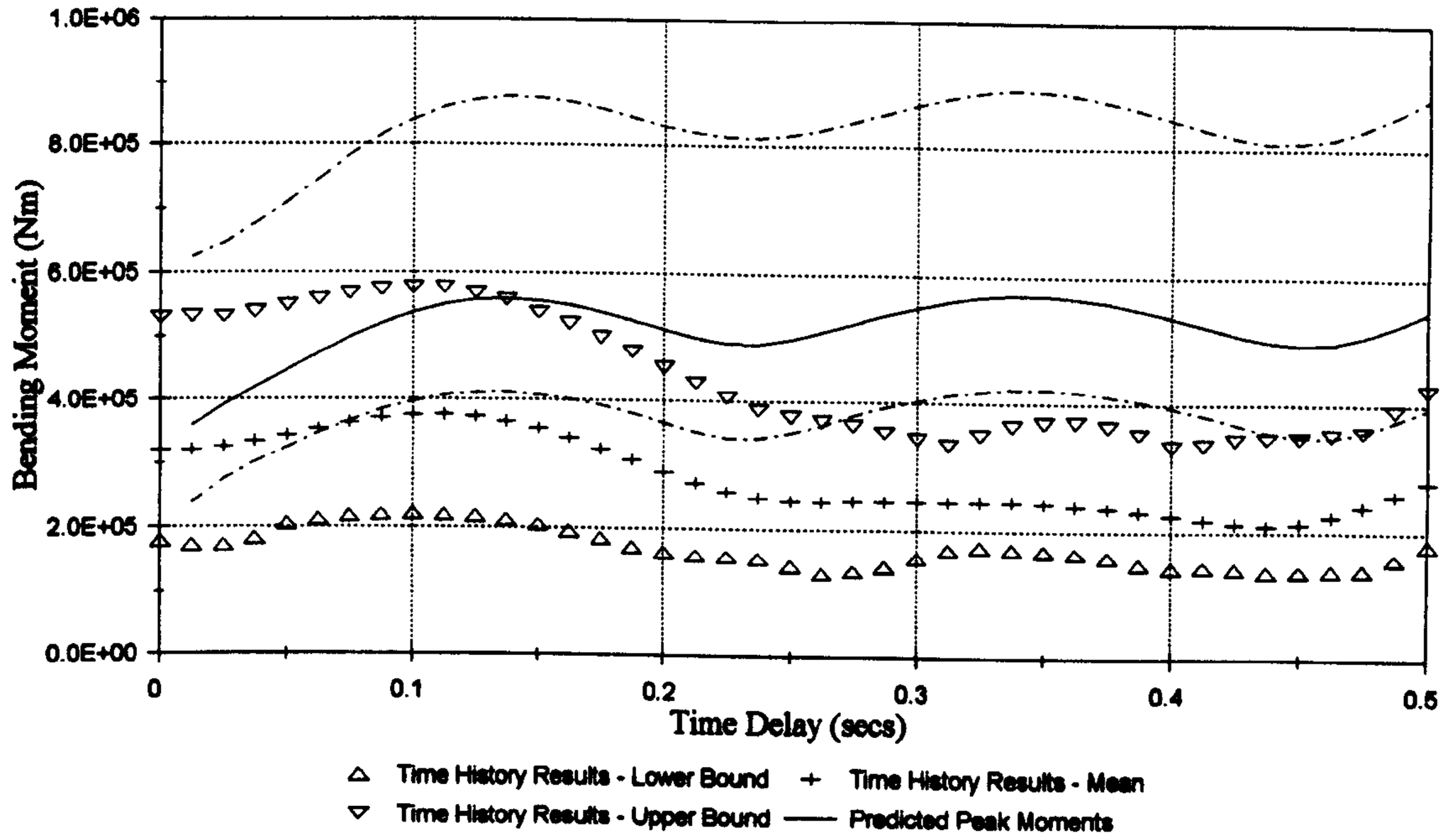

Figure 4.44 -:- Peak Bending Moments At Node 10, Vertical Excitation

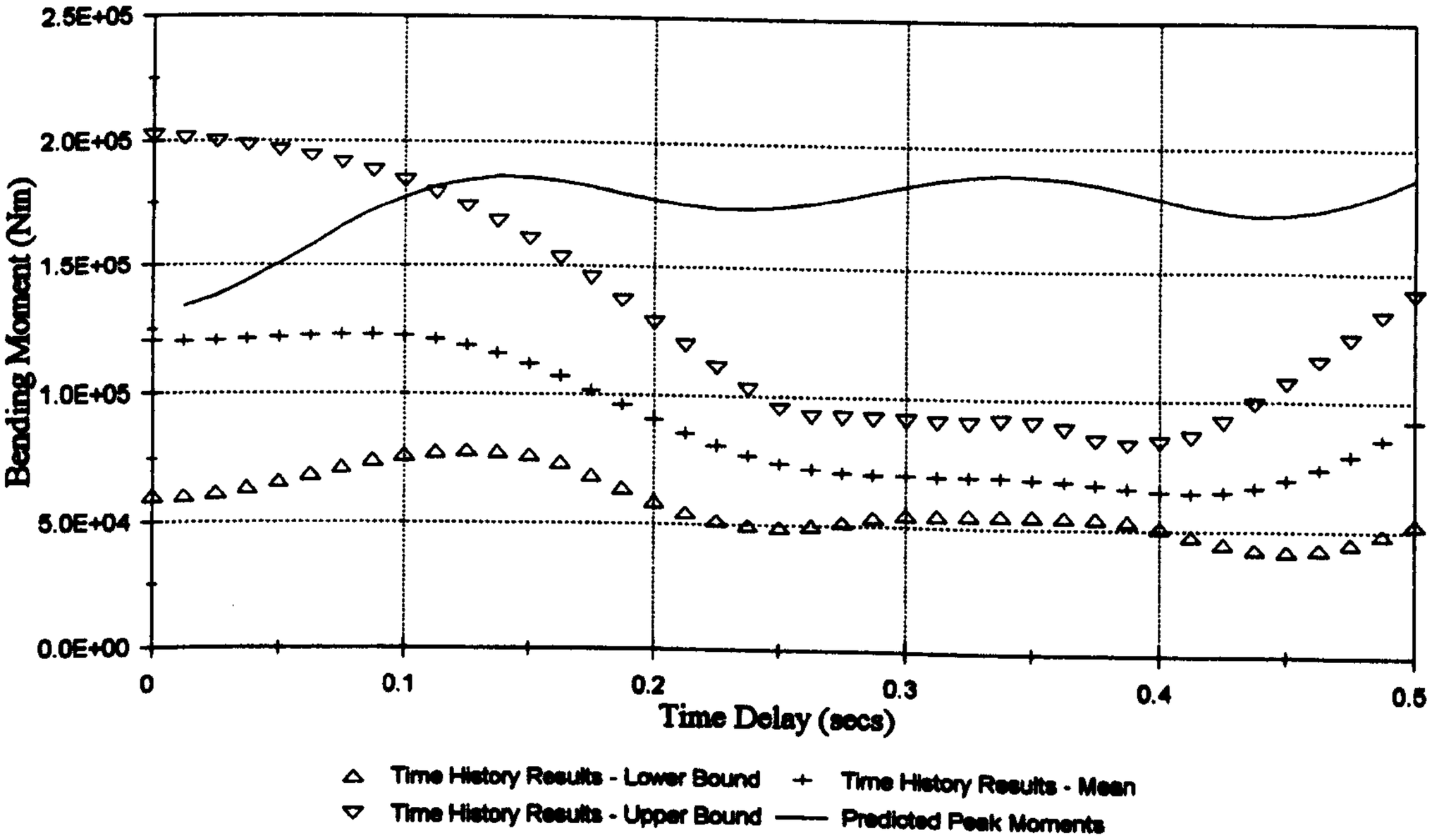

Figure 4.45 -:- RMS Bending Moments At Node 10, Vertical Excitation

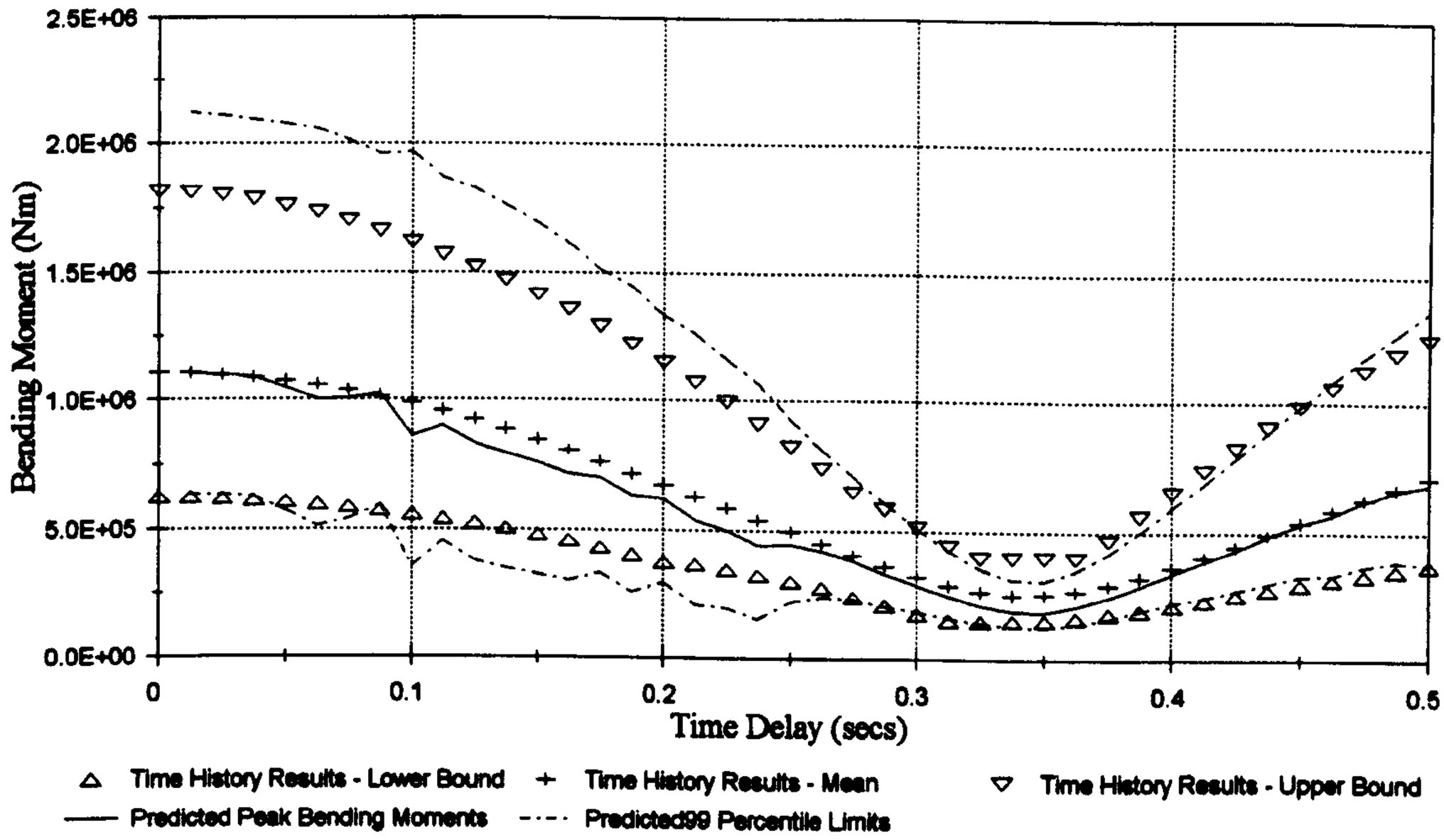

Figure 4.46 -:- Peak Bending Moments At Node 15, Vertical Excitation

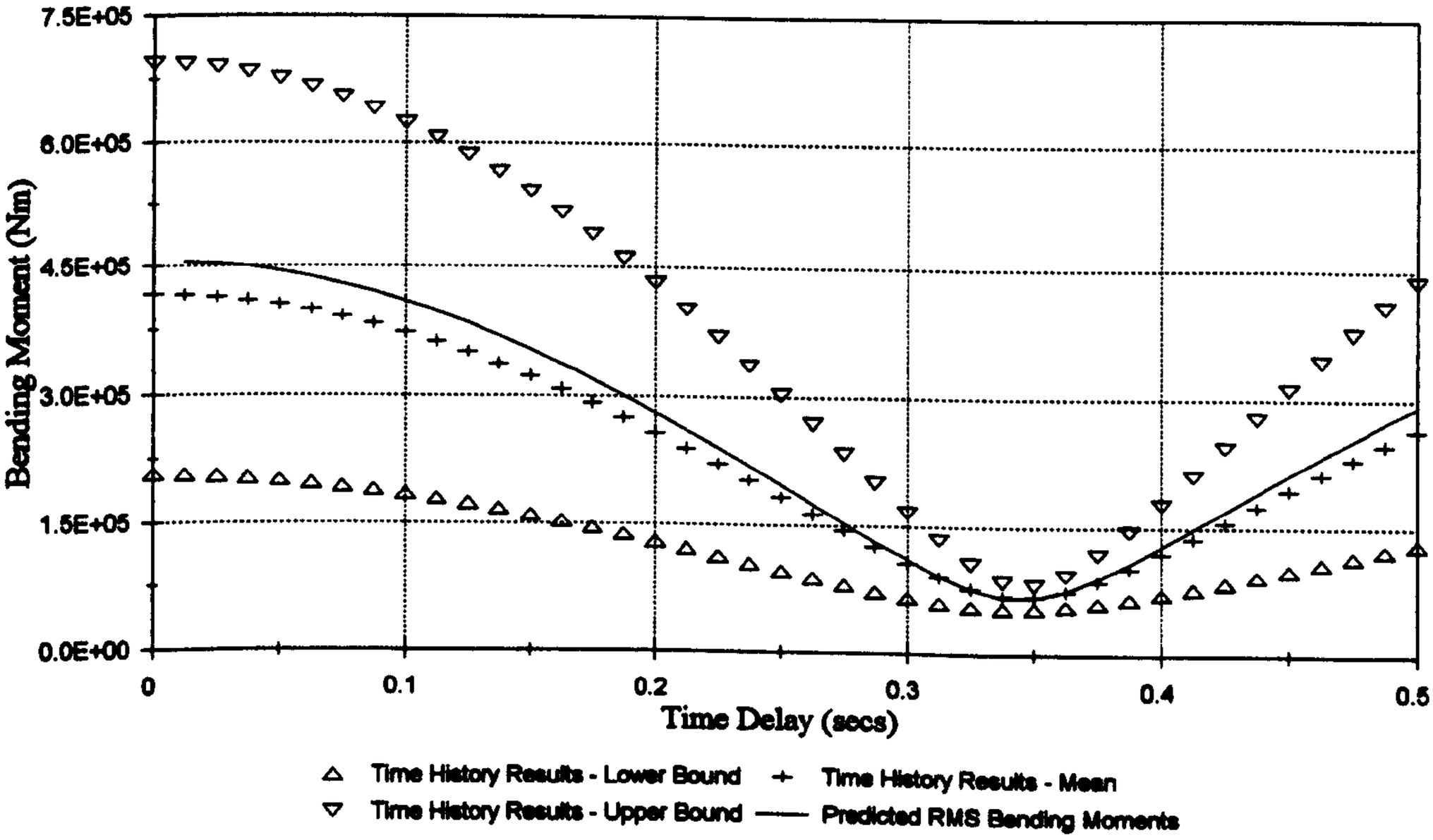

Figure 4.47 -:- RMS Bending Moments At Node 15, Vertical Excitation

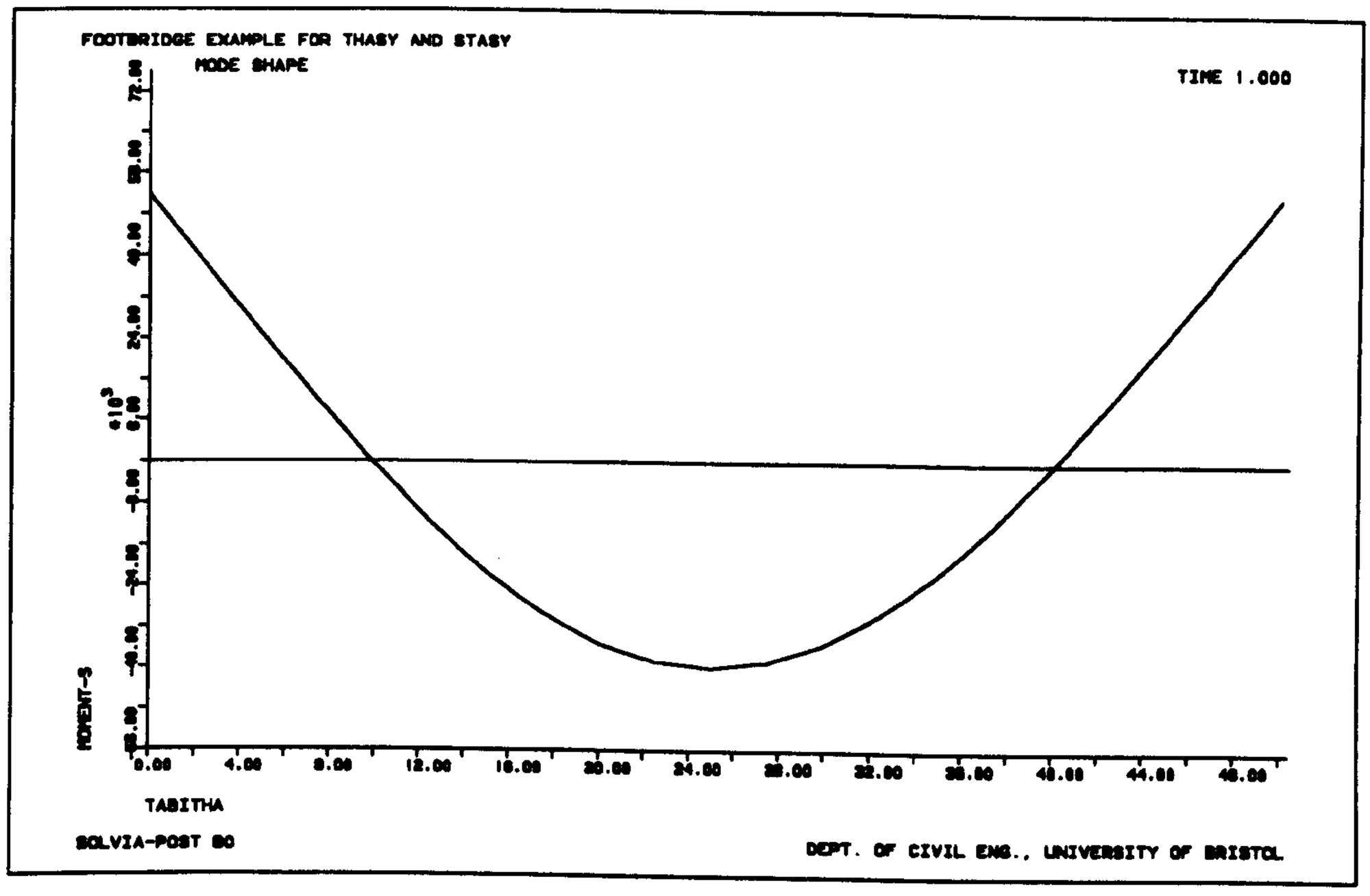

Figure 4.48 -:- Bending Moment Distribution In Transom For Mode One

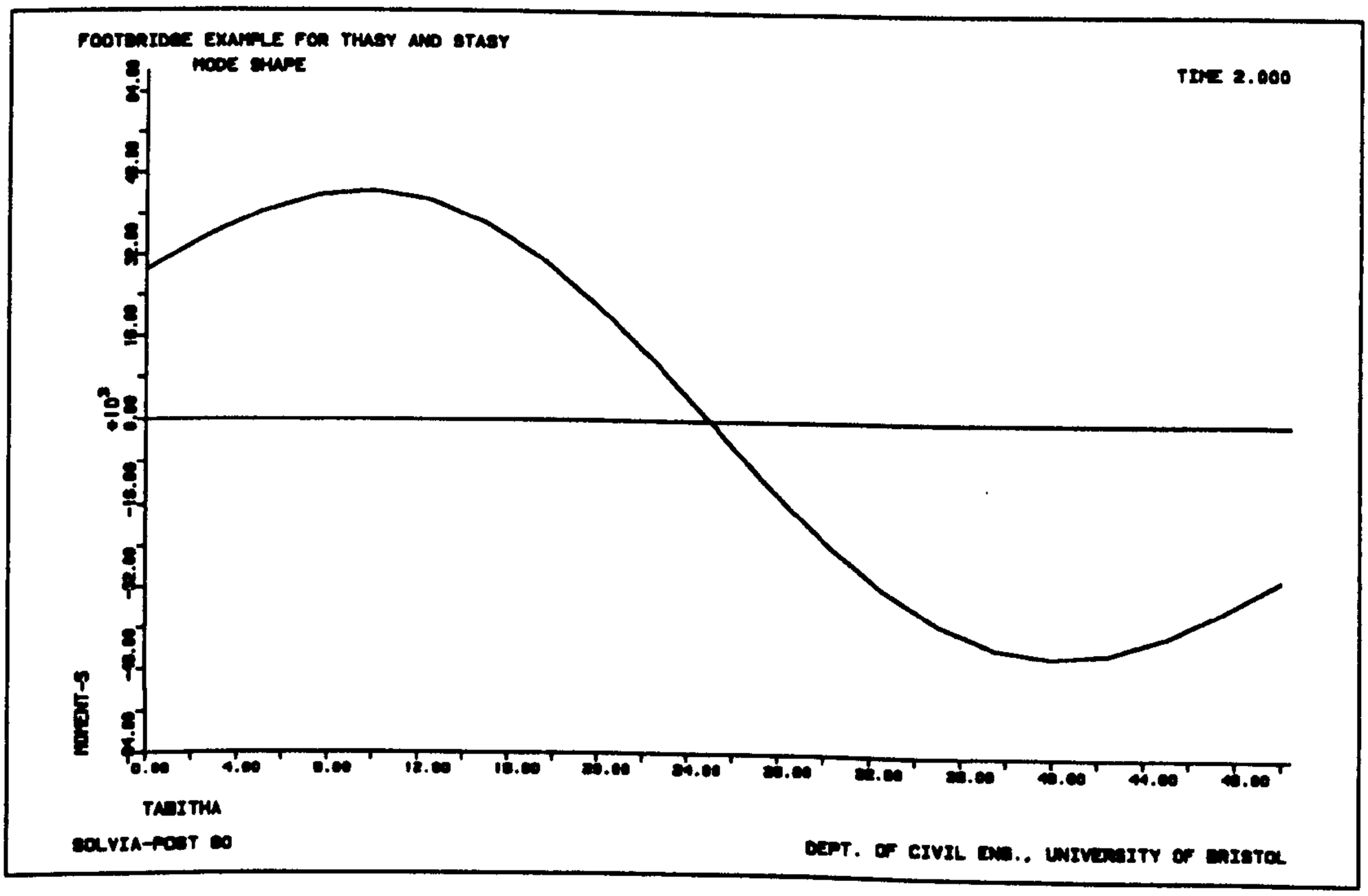

Figure 4.49 -:- Bending Moment Distribution In Transom For Mode Two

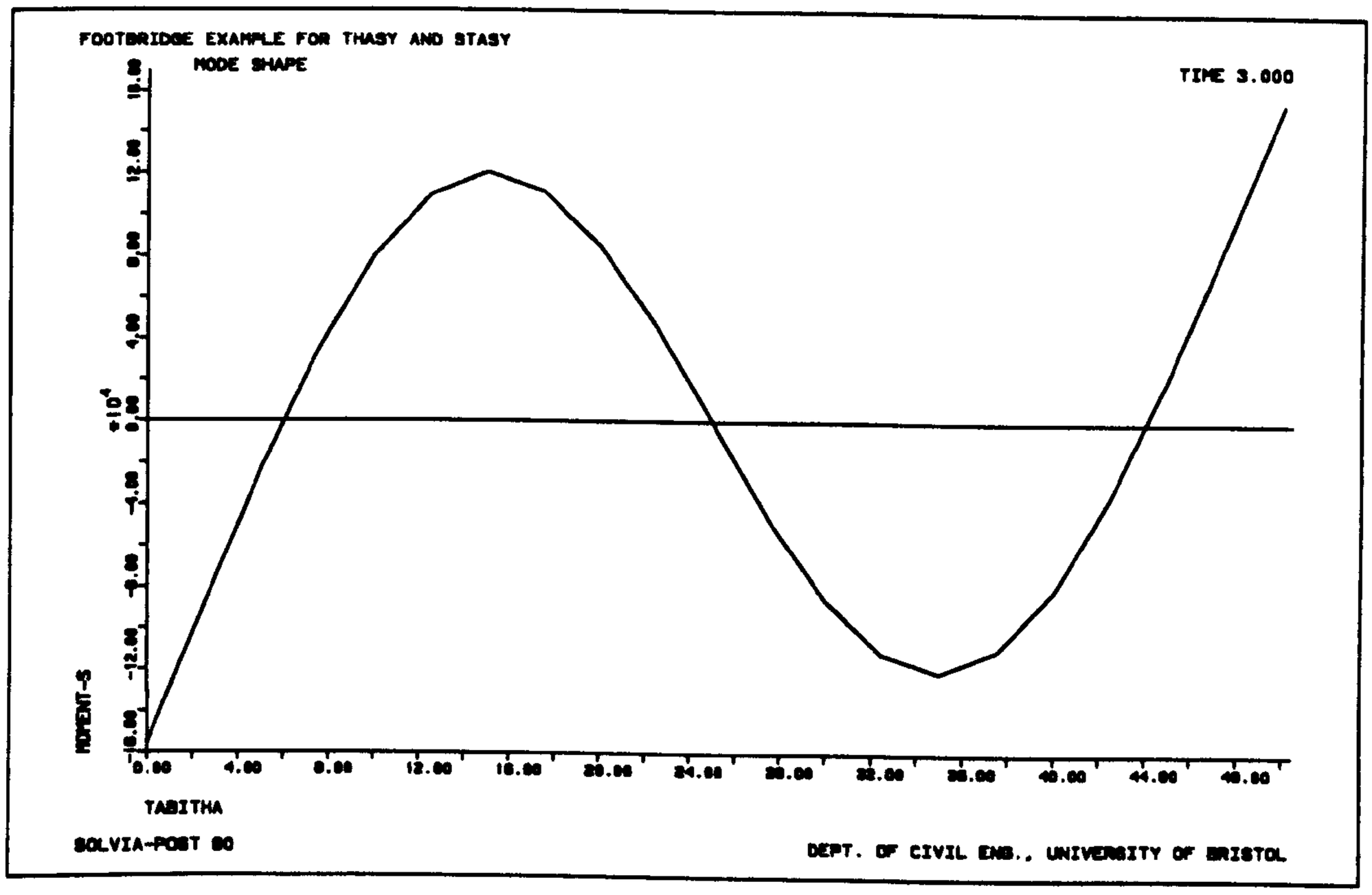

Figure 4.50 -:- Bending Moment Distribution In Transom Mode Three

Chapter 5

Analysis Of The Response Of A Cable Stayed Bridge To Asynchronous Seismic Excitation

5.0 Introduction

In chapter four, the power spectral approach developed in chapter three was shown to be a useful and powerful tool for investigating the response of a simple structure to asynchronous seismic excitation. Program STASY predicted statistics for the response of a portal frame which were in broad agreement with the results of a set of time history analyses, but which were considerably quicker to produce. The aim of this thesis is to examine the response of cable stayed bridges to spatially varying dynamic loads, therefore it is now necessary to apply the method to the analysis of a cable stayed bridge.

Despite the generally good agreement, there were marked discrepancies between the results of the time history analyses and the predictions made by the program STASY for some of the cases considered in chapter four. Several explanations for these have already been discussed, and one of them was the non stationary nature of the loading used in the time history analyses. Now, because the natural frequencies of a cable stayed bridge are likely to be much lower than the frequencies of the frame considered in chapter four, the effects of non stationarity will be more important. Therefore, it may be necessary to take account of the non stationary nature of the excitation when predicting the response of the bridge.

This chapter will present the analysis of a cable stayed bridge to asynchronous seismic excitation using the power spectral approach developed in chapter three. Two sets of analysis will be performed,

one assuming that the excitation is stationary and the other using an evolutionary power spectral model of non stationary ground excitation. Each analysis will consider the effects of horizontal and vertical excitation, and also predict the response to a general excitation which includes both horizontal and vertical components. Finally, the results of the stationary and non-stationary analyses will be compared to assess the importance of stationarity.

5.1 Definition Of The Problem

The method developed in chapter three requires the results of a finite element analysis of the example structure, and a power density spectrum representation of the ground motion. Furthermore, for the non stationary analysis, it is necessary to define evolutionary versions of the ground power density and the structural frequency response function. The example problem will now be outlined and these aspects considered in more detail.

5.1.1 The Example Cable Stayed Bridge

The model chosen for the example analysis was based on the Kessock Bridge (figure 5.1) in Scotland. A detailed three dimensional finite element model of Kessock Bridge is presented in chapter seven where the full scale testing of the bridge is described. However, for the asynchronous seismic analysis considered here, a two dimensional model was used (figure 5.2) which included the following simplifications:

a. Only the cable supported spans were modelled

b. A uniform deck section was used throughout the bridge.

c. A uniform section was used for the pylons

d. Identical properties were used for each of the cables

As with the portal frame in chapter four, the model was created using SOLVIA [Solvia Engineering AB 1989]. Elastic beam elements were used to represent both the bridge deck and pylons and the cables were represented by truss elements. The section and material properties used in the model are given in table 5.1.

One further change was introduced in developing the model for the asynchronous analysis. On the real bridge the bases of the pylons are integral with the edge beams of the deck so that the deck and pylon bases move together in both horizontal and vertical directions. The bridge bearings then allow longitudinal movement of the structure at all points of support except at the base of the southern pylons (figure 5.3), which means that the bridge will only be subject to synchronous horizontal excitation. It is more typical for cable stayed bridges to have the pylons fully restrained at their bases thus allowing only the deck to move longitudinally. Changing the restraint conditions at the base of the pylons to this arrangement (figure 5.4) leads to two ground degrees of freedom in the horizontal direction and hence gives rise to the possibility of asynchronous seismic excitation.

The asynchronous analysis was performed using the first eight vibration modes and these were found from the SOLVIA model together with the natural frequencies. The results of the eigensolution are shown in figures 5.5 a-h.

5.1.2 Ground Excitation Model

As with the analysis of the portal frame in chapter four the Clough and Penzien modified Kanai-Tajimi model was used to describe the power density spectrum of the stationary ground excitation. The following factors were used to define the two filter functions (equations 4.1 and 4.2) [Perotti 1990]:

$$\omega_g = 15.46 \qquad \xi_g = 0.623$$
$$\omega_f = 1.636 \qquad \xi_f = 0.619$$

producing a spectrum which is typical of firm soil conditions [Ruiz & Penzien 1969]. The magnitude of the spectrum, G_0, was taken as 0.15 which corresponds to a root mean square acceleration of approximately 2.7 m s^{-2}.

To make use of the evolutionary power spectral approach it is also necessary to choose a modulating function to define the non stationary nature of the ground excitation. Several different envelope functions have been used such as the box car and trapezoidal functions [Hou 1968]. However, these are crude approximations to the envelope of real ground excitation and a more realistic representation is given by the exponential envelope [Shinozuka & Sato 1967]:

$$A(t,\omega) = A(t) = A_0(e^{-b_1 t} - e^{-b_2 t}) \qquad \text{with} \qquad b_2 > b_1 \qquad \text{.....(5.1)}$$

In this the variation is assumed to be independent of frequency. The values of the constants A_0, b_1 and b_2 which define the shape of this exponential window have to be selected to match records from historical earthquakes and various methods have been proposed for doing this [Quek *et al* 1990]. However, again for simplicity, the following values were used for the constants following the example of Perotti [Perotti 1990]:

$$A_0 = 9.4967 \qquad b_1 = 0.1079 \qquad b_2 = 0.1438$$

These produce the window shown in figure 5.6 which has a maximum (unit) value at t=8 seconds and decays to a value of 0.1 at t=40 seconds.

Finally the orientation of the ground motion for the case of general excitation is defined by giving the component of the excitation in each of the ground degree of freedom directions. For the general excitation considered here the ratio of horizontal to vertical excitation was assumed to be 1:0.7 based on the proposals in Eurocode 8 [Eurocode Nº. 8 1988]. This gave values of 0.819 and 0.573 for the horizontal and vertical components respectively.

5.1.3 Application Of Evolutionary Power Density Spectra To Non Stationary Excitation

The concept of evolutionary power density spectra was briefly discussed in chapter three as a means of applying power spectral methods to the analysis of non stationary random processes. It is now necessary to develop this approach to deal with the response of a system to non-stationary asynchronous excitation.

5.1.3.1 Response To Non Stationary Excitation

A non stationary random process $X(t)$, can be described in terms of a generalised Fourier integral as follows [Priestly 1966]:

$$X(t) = \int_{-\infty}^{\infty} A(t,\omega) e^{-j\omega t} dZ(\omega) \qquad \text{.....(5.2)}$$

where $A(t,\omega\ )$ is a deterministic function which modulates a stationary random process $X_s(t)$ defined by:

$$X_s(t) = \int_{-\infty}^{\infty} e^{-j\omega t} dZ(\omega) \quad \text{.....(5.3)}$$

In both 5.2 and 5.3 the terms $dZ(\omega)$ form an orthogonal random process, i.e. the values of $dZ(\omega)$ at different values of ω are uncorrelated, and are related to the power spectrum, $S_{xx}(\omega)$, of the stationary random process $X_s(t)$:

$$E\left[dZ(\omega_i)dZ^*(\omega_j)\right] = \begin{cases} 0 & i \neq j \\ S_{xx}(\omega)d\omega & i = j \end{cases} \quad \text{.....(5.4)}$$

Combining equations 5.2 and 5.4 then gives the following expression for the evolutionary power density spectrum of a non stationary process [Priestly 1966]:

$$S_{xx}(t,\omega) = |A(t,\omega)|^2 \frac{dF(\omega)}{d\omega} = |A(t,\omega)|^2 S_{xx}(\omega) \quad \text{where} \quad dF(\omega) = \overline{|dZ(\omega)|^2} \quad \text{.....(5.5)}$$

The application of evolutionary spectra to the analysis of the response of structures to non stationary excitation is well documented [Perotti 1990, Quek *et al.* 1990, To 1982, To 1984] and the approach of Quek for single degree of freedom systems shall be followed here. The response of a single degree of freedom system to an excitation $p(\tau)$ is given by the convolution:

$$v(t) = \int_0^t p(\tau)h(t-\tau)d\tau \quad \text{.....(5.6)}$$

If $p(\tau)$ is a non stationary random excitation that can be described by equation 5.2 then 5.6 becomes:

$$v(t) = \int_0^t \int_{-\infty}^{\infty} A(t,\omega)e^{-j\omega t} dZ(\omega)\, h(t-\tau)d\tau \quad \text{.....(5.7)}$$

Changing the order of integration and performing some simple algebraic manipulation reduces 5.7 to:

$$v(t) = \int_{-\infty}^{\infty} \left[\int_0^t A(t,\omega) h(t-\tau) e^{j\omega(t-\tau)} d\tau \right] e^{-j\omega t} dZ(\omega) = \int_{-\infty}^{\infty} M(t,\omega)\, e^{-j\omega t} dZ(\omega) \quad \text{.....(5.8)}$$

This is of the same form as 5.2 but with a new modulating function M(t,ω) defined by:

$$M(t,\omega) = \int_0^t A(t,\omega) h(t-\tau) e^{j\omega(t-\tau)} d\tau \quad \text{.....(5.9)}$$

which represents the response of the system to a modulated sinusoidal excitation. The evolutionary power density spectrum of the response of a single degree of freedom system to non-stationary excitation is therefore given by:

$$S_{vv}(t,\omega) = \left| M(t,\omega) \right|^2 S_{pp}(\omega) \quad \text{.....(5.10)}$$

For a multi degree of freedom system a modal approach is used in which each mode can be considered to be a single degree of freedom system. Hence, the time dependent frequency response function in mode *r* is given by:

$$M_r(t) = \int_0^t A(t,\omega) h_r(t-\tau) e^{j\omega(t-\tau)} d\tau$$

where .....(5.11)

$$h_r(t) = \frac{e^{-\xi_r \omega_r}}{\omega_d} \qquad \text{and} \qquad \omega_d = \omega_r \sqrt{1-\xi_r^2}$$

The evolutionary power spectrum of the response is then given by:

$$S_{rs}(t,\omega) = M_r(t,\omega) M_s^*(t,\omega) S_{rs}(\omega) \quad \text{.....(5.12)}$$

Which is directly analogous to the stationary case discussed in chapter three. Finally the exponential envelope function given in 5.1 can be introduced:

$$M_r(t) = \int_0^t A_0 (e^{-b_1 t} - e^{-b_2 t}) h_r(t-\tau) e^{j\omega(t-\tau)} d\tau \quad \text{.....(5.13)}$$

The evaluation of 5.13 in closed form is available from the literature [To 1980, Quek *et al.* 1990] and is given by Quek *et al.* as:

$$\mathrm{Re}(M_r(t,\omega)) = \frac{A_0}{2\omega_d} \sum_{j=1}^{2} \sum_{i=1}^{2} \frac{(-1)^i}{(b_i - \xi_r \omega_r)^2 + \omega_j^2}$$
$$\left\{ e^{-\omega_r t} \left[(b_i - \xi_r \omega_r) \sin \omega_j t - \omega_j \cos \omega_j t \right] + \omega_j e^{-b_i t} \right\} \quad \text{.....(5.14a)}$$

$$\mathrm{Im}(M_r(t,\omega)) = \frac{A_0}{2\omega_d} \sum_{j=1}^{2} \sum_{i=1}^{2} \frac{(-1)^{i+j-1}}{(b_i - \xi_r \omega_r)^2 + \omega_j^2}$$
$$\left\{ e^{-\omega_r t} \left[(b_i - \xi_r \omega_r) \cos \omega_j t - \omega_j \sin \omega_j t \right] - (b_i - \xi_r \omega_r) e^{-b_i t} \right\} \quad \text{.....(5.14b)}$$

where

$\omega_1 = \omega_r + \omega$ and $\omega_2 = \omega_r - \omega$

The expressions in 5.14 a and b for the time dependent frequency response function were simplified by assuming that the damped natural frequency ω_d is equal to the modal natural frequency ω_r. This assumption is justified as long as the structure is lightly damped which is the case for the cable stayed bridge.

5.1.3.2 Statistics Of The Response To Non Stationary Excitation

The final step in the non stationary analysis is to calculate the statistics of the response from its evolutionary power density spectrum. However, the spectral parameters, spectral moments, dispersion parameter and mean zero crossing rate, discussed in chapter three are now all functions of time and therefore it is not possible to use the simplified formula (equation 3.23) applied to the stationary case.

Instead it is necessary to calculate the statistics of the peak response numerically from expressions which have been developed for first passage problems [Corotis *et al.* 1972, Vanmarcke 1975]. The reliability function describes the probability that the maximum level of the response does not exceed a barrier level, β, within the interval $(0,t)$ and therefore represents the cumulative probability distribution of the peak response. An estimate of the reliability function [Perotti 1990] is given by:

$$L(\beta,t) = \exp\left\{-\int_0^t \nu(\beta,\tau)d\tau\right\} \quad \text{.....(5.15)}$$

where $\nu(\beta,t)$ is the reduced up and down crossing rate of the barrier β. The mean value of the peak response is defined in terms of its probability distribution by:

$$\mu_x = \int_{-\infty}^{\infty} xp(x)dx \quad \text{.....(5.16)}$$

The probability distribution is in turn related to the cumulative probability distribution by:

$$P(x) = \int_{-\infty}^{x} p(x)dx \quad \text{.....(5.17)}$$

and so the mean peak response can be related to the reliability function as follows [Quek *et al.* 1990]:

$$\mu_{peak}(t) = \int_0^{\infty} \beta dP(\beta) = \int_0^{\infty}[1-P(\beta)]d\beta = \int_0^{\infty}[1-L(\beta,t)]d\beta \quad \text{.....(5.18)}$$

Finally the barrier crossing rate can be found from the spectral parameters as follows:

$$\nu(\beta,t) = \nu^+(0,t)\frac{1-\exp\left(\frac{-\delta(t)\beta}{\sigma(t)}\right)}{\exp\left[\frac{1}{2}\left(\frac{\beta}{\sigma(t)}\right)^2\right]-1} \quad \text{.....(5.19)}$$

where

$$\nu^{+}(0,t) = \frac{1}{2\pi}\left[\frac{\lambda_2(t)}{\lambda_0(t)}\right]^{\frac{1}{2}} \qquad \text{.....(5.20)}$$

is the expected rate of zero up crossing and:

$$\delta(t) = \left\{2\pi\left[1 - \frac{\lambda_1^2(t)}{\lambda_0(t)\lambda_2(t)}\right]\right\}^{\frac{1}{2}} \qquad \text{.....(5.21)}$$

is the spectral shape parameter.

The preceding theory shows that it is necessary to evaluate two sets of integrals to predict the mean peak response to non stationary excitation (5.15 and 5.18). These have to be found by a numerical procedure and a four point Gauss scheme was chosen for each integration to ensure that a reasonable accuracy was achieved. However, this numerical integration was costly in respect to time and so only a single ground wave velocity was considered for the non stationary analyses, namely 540 m s^{-1} which corresponds to a time delay over the length of the bridge of 1 second.

5.2 Results

There are two aims in presenting the results from the stationary analyses:

a. to show the variations in selected response parameters with degree of asynchronicity,

b. to illustrate changes in the bridge behaviour for selected ground wave velocities.

Several quantities could be used to typify the response of the bridge, such as bending moments or displacements. However, it was found that the trends in the displacement response generally followed those for bending moments. Therefore, since bending moments are more useful during the design

process, it was decided to present only the bending moment results in the following sections; displacements are only presented where they contrast with the bending moment behaviour.

To meet the first aim three points were selected to monitor the response, the mid point of the first side span (node 15 in figure 5.2), the left hand quarter point in the main span (node 28) and the mid point of the main span (node 35). The variation of asynchronicity was measured using the delay in the seismic excitation travelling the full length of the bridge i.e. the time taken to travel 544 m. To meet the second aim the response, displacement and bending moment, was noted at each of the nodes along the deck for selected time delays.

5.2.1 Modal Response To Stationary Excitation

Before considering the response in the global degrees of freedom it is useful to examine how the response in each mode varies with the degree of asynchronicity. The response of a structure to asynchronous seismic excitation is greatly influenced by the relationship between ground wave speed, distance between supports and natural frequencies, its mode shapes and the direction of the excitation. Each mode will have "resonant wave speeds" which give rise to peaks and troughs in the modal response. Therefore, the response of the different modes provide a means of interpreting the global results and can be found by plotting the modal zeroth spectral moments (mean square response) against time delay. The modal response is given in figures 5.7 a-h (response to vertical excitation), 5.8 a-h (response to horizontal excitation) and 5.9 a-h (response to combined horizontal and vertical excitation).

The variation of the mean square response for vertical excitation shows a clear correlation with the phase shift between points of support for both the first two modes. Response in the first mode is dominated by a peak which occurs when the phase change is 540° between supports B and D or C and

E (320 m, time delay = 4.43 seconds). For the second mode the maximum response occurs when the excitations at supports B and D or supports C and E are in phase (time delays of 1.59, 3.18 and 4.77 seconds) and there are corresponding minima in the response when these excitations are out of phase (time delays of 2.38 and 4.97 seconds). The peak at a time delay of 3.18 seconds dominates the other two since this delay also corresponds to a 540° phase shift across the main span. In contrast to this the correlations between the phase shift and response for the higher modes are much less clear. This is because the six points of support define nine different lengths, and each combination of length and ground wave velocity produces a different phase relationship for a particular mode. Many of these combinations have little influence on the first two modes which are dominated by the response in the main span, but do affect the higher modes which have much larger contributions from the side spans. Hence the variation of the higher mode response with asynchronicity is more complicated.

In contrast to vertical excitation, horizontal excitation produces a regular trend in the response of each mode. This is because there are only two ground degrees of freedom for the horizontal excitation and hence only one length over which the excitation change occurs, namely 240 m. These differences between the horizontal and vertical excitation have a clear influence on the global response as will be noted later.

When the horizontal and vertical excitation are combined the modal response is dominated by the response to the vertical component even though this may be less than the horizontal excitation. This is predictable since the mean square response to vertical excitation is an order of magnitude greater than the response to horizontal excitation. The influence of the direction of the excitation on the modal response is illustrated in figures 5.10 (mode one) and 5.11 (mode two), where the modal response has been plotted against the angle between the resultant direction of excitation and the vertical for two values of ground wave velocity. These figures indicate clearly the dominant effect that

the vertical excitation has on the response in both the first two modes; a factor which could be very important considering the more complicated nature of the response to asynchronous vertical excitation.

5.2.2 Response To Stationary Vertical Excitation

For vertical excitation the bending moments at the centre of the side span are dominated by the pseudo static component of the response (figures 5.12 and 5.13). These figures also show that the pseudo static component has a greater influence on the RMS response than on the mean peak response. This is because the mean peak values are predicted using the spectral moments of the response which differ between the dynamic and pseudo static components. Finally, it can be seen that no single mode dominates the dynamic response in the side span.

The pseudo static response has less influence on the bending moment at the quarter point than in the side span even at slower ground wave speeds (figure 5.14). Instead, the total response is dominated by the dynamic component of the bending moment response which follows the trend of the second mode with a peak response at a delay of 3.2 seconds. In contrast, the dynamic displacement at the quarter point follows the trend of the first mode (figure 5.15). This indicates that the bending moments in the second mode are greater than those in the first mode even though the displacements are less which is because higher modes represent systems with a higher stiffness.

At mid span the influence of the pseudo static component of the response on the bending moments is minimal; the bending moment is dominated by the dynamic response (figure 5.16) which follows the trend of the first mode. This is exactly what would be expected for mid span and the only evidence of a contribution from other modes is slight undulations in the predicted peak response (figure 5.17).

Considering now the variations in the response along the length of the bridge, the results show that the position of the maximum dynamic bending moment changes position with ground wave speed (figures 5.18 and 5.19). This is because different ground wave speeds preferentially excite different modes which have their peak response at different locations. However, this trend is not reflected in the dynamic displacements which are clearly dominated by the first mode (figure 5.20) and are only influenced by the second mode for one of the time delays illustrated. The pseudo static displacements are symmetrical, and have maximum values at positions which are offset from mid span (figure 5.21). This contrasts with the pseudo static bending moments which have an unsymmetrical distribution along the bridge deck (figure 5.22 and 5.23). This unsymmetrical response can only arise from a lack of symmetry in the structure and must therefore be due to the unsymmetrical longitudinal boundary conditions at the pylon bases (figure 5.4). Finally, the influence of this non symmetrical pseudo static behaviour is to introduce a lack of symmetry into the total response (figures 5.24 and 5.25).

5.2.3 Response To Stationary Horizontal Excitation

The response of the bridge to horizontal excitation shows several key differences from the response to vertical excitation. The bending moments in the side span (figures 5.26 and 5.27) show that the influence of the pseudo static response is less than for vertical excitation and this is probably due to there being fewer ground degrees of freedom. However, as with the vertical excitation the influence is more noticeable in the RMS response than in the predicted peak response. There is no clearly identifiable modal trend and the peaks that do occur (at time delays of 2.0 and 4.5 seconds) are likely to be caused by the interaction of more than one mode. The reduced influence of the pseudo static component on the overall response is also apparent at the quarter point. Here, as with the response to vertical excitation, the bending moment response is dominated by the second mode (figure 5.28) and the displacements are dominated by the first mode (figure 5.29). The response at mid span is

completely dominated by the first mode dynamic response (figures 5.30 and 5.31) which is similar to the behaviour described above for the vertical excitation.

Considering the variations in the response along the length of the bridge, the results for the dynamic excitation again show that the position of the maximum bending moment changes with ground wave speed (figures 5.32 and 5.33). The reasons for this were discussed above. In contrast to the response to vertical excitation, the pseudo static displacements have an unsymmetrical distribution along the bridge deck (figure 5.34) as well as the bending moments (figure 5.35). However, this unsymmetrical behaviour is less pronounced than for vertical excitation, and the total response is almost perfectly symmetrical (figures 5.36 and 5.37).

5.2.4 Response To General Stationary Excitation

As might be expected from the modal response discussed earlier, the response of the bridge when the ratio of the horizontal to vertical excitation is 1:0.7 is dominated by the response to vertical excitation. The bending moments in the side span (figure 5.38), bending moments and displacements at the quarter point (figures 5.39 and 5.40), and the bending moments at mid span (figure 5.41) all follow the trends of the response to vertical excitation. The level of the response is less than that to vertical excitation but is significantly larger than the response to horizontal excitation. However, there is an important difference in the variation of the pseudo static displacements along the deck (figure 5.42) which is significantly less symmetrical than either of the individual cases. This is reflected in the distribution of the total displacements (figure 5.43). The distribution of bending moments is symmetrical for the dynamic case (figure 5.44) but the pseudo static response once again introduces an unsymmetrical response (figure 5.45) which again has an influence on the total bending moment response (figures 5.46 and 5.47).

5.2.5 Results Of Non Stationary Analysis

The results of the analyses of the response of the bridge to non stationary excitation are presented in figures 5.48 to 5.65. These figures show the RMS and predicted peak values of the bending moments at nodes 15 28 and 35 to vertical, horizontal and general seismic excitations. There are several comments which are worth making on these figures.

Firstly, in all of them the results of the stationary analyses are greater than those of the non stationary analyses which agrees with the results obtained by other researchers [Quek *et al.* 1990, Perotti 1990]. This shows that the stationary assumption produces a conservative estimate of the response and therefore has important consequences for the aseismic design of these structures. Conservative assumptions in design will lead to solutions which are inherently safe, but which fail to make the most efficient use of available materials. Therefore, when making the choice as to whether or not to use the non stationary approach both the consequent safety and cost implications have to be considered.

Secondly, there is closer agreement between stationary and non stationary predictions of RMS response than between predictions of peak response. This could be the result of having to use different methods to predict the mean value of the peak response for the station and non-stationary analyses. However, it also needs to be mentioned that the full 40 second duration of the shaking was assumed in the stationary calculations and perhaps a modified value may be more suitable. Such a value could be selected either by considering the energy content of the excitation or by using just a portion of the excitation.

Thirdly, in each of the graphs for the RMS response, the maximum non stationary pseudo static response matches the RMS response predicted by the stationary analyses. These maxima occur after eight seconds which corresponds to the peak in the envelop function (figure 5.6). These effects are to

be expected since the pseudo static response is directly related to the ground excitation and is independent of inertia of the structure. In contrast the maximum value in the dynamic response occurs significantly after the peak in the ground excitation. However, for the peak response, the maximum pseudo static response occurs later than eight seconds and this could indicate that the method of calculating the mean peak response is not applicable to the pseudo static component. As mentioned in § 5.2.2 the peak predictions are calculated using the spectral moments and this approach may not be suitable for the pseudo static response.

5.2.6 General Comments On the Influence Of Asynchronous Excitation

It is clear from the preceding sections that asynchronous excitation caused by the finite velocity of seismic waves has a dramatic influence on the response of a cable stayed bridge. There are four principal effects which can be identified:

a. The magnitude of the peak response varies with ground wave velocity.

b. The position of the peak response along the deck varies with ground wave velocity.

c. Asynchronous excitation accentuates any unsymmetrical elements in the response.

d. All these effects are influenced by the direction of the ground shaking.

These effects are important since they will influence the choice of section properties during the design of the bridge and so it can be concluded that some account of wave propagation effects ought to be taken into account during the aseismic design of long span structures. However, two further factors have to be considered. Firstly, the largest effects occur for time delays which are greater than 1 second. For the bridge modelled here this corresponds to wave speeds of less than 544 m s^{-1}, and these are unlikely to be experienced in reality. Clearly, though, for bridges with longer spans these effects at longer time delays will be more important. Secondly, only the response to earthquake

excitation has been considered. To understand the relevance of this to the structure as built it is necessary to compare this with the response to other load cases and figure 5.66 shows the bending moments in the bridge deck under its own self weight. This indicates that even for a delay of only 1.0 second the bending moments induced by the asynchronous excitation are significantly greater than the static bending moments. This has to be qualified, of course, by stating that this is in response to a hypothetical earthquake with an RMS acceleration of approximately 2.7 m s^{-2} which was chosen on a purely arbitrary basis.

To sum up, the results of this evolutionary spectral analysis have demonstrated that it is possible to apply the power spectral approach developed in chapter three to problems with non stationary excitation. They have also shown that the assumption that the response is stationary produces conservative results and therefore it may be advantageous to use the non stationary approach for structures such as a cable stayed bridge which have low natural frequencies.

5.3 The Efficacy Of The Power Spectral Approach

Having used the method proposed in chapter three to find the response of both a portal frame (chapter four) and cable stayed bridge to asynchronous excitation it is now important to use the results of these analyses to assess whether this approach is appropriate for use in aseismic design. There are several methods of analysing the response of a structure to seismic excitation and each of them has advantages and disadvantages as outlined in chapter two. These methods also use different models to represent the earthquake excitation. Therefore, in assessing the usefulness of the power spectral approach outlined in chapter three it is necessary to compare both the analytical approach used and the representation of the ground motion with these other methods.

5.3.1 Discussion Of Analytical Approach

There are three main analytical approaches which have been used in aseismic analysis; direct integration in the time domain with a time history record to represent the ground excitation; frequency domain analysis using a response spectrum input; and random vibration analysis using a ground power spectrum. The first of these has been used by several researchers to investigate the problem of spatially varying seismic excitation of long span bridges [Dumanoglu & Severn 1987, Garevski 1990, Abdel-Ghaffar & Stringfellow 1984 a & b] and has several clear advantages over the other methods. Most importantly, analysis in the time domain allows non linearities to be modelled and automatically accounts for the non stationarity of the excitation. However, such an approach is computationally time consuming and ignores the random nature of the loading.

These disadvantages make the alternative spectral methods very appealing since they allow swift computation of results and can be used to predict peak response statistics thus accounting for the random nature of the loading. Again, the response spectrum approach has been popular [Der Kiureghian & Neuenhofer 1992, Berrah & Kausel 1991] and the results emphasise some of its advantages. Der Kiureghian and Neuenhofer suggest two reasons why the response spectrum approach is preferable to the power spectral approach. Firstly, response spectra are widely used to specify earthquake loading in design codes and are therefore the preferred means of analysis in aseismic design. Secondly, they point out that response spectra can automatically take account of the non stationary nature of the excitation. However, they also admit that the power spectral approach has possibly greater potential due to its statistical basis and there are other authors who advocate the power spectral approach in place of the response spectrum [Christian 1989]. Its statistical basis enables the power spectral approach to predict the peak response [Abdel-Ghaffar & Rubin 1982] and calculate reliability functions for bridges subject to spatially varying seismic excitation [Perotti 1990].

The main disadvantage with the spectral approaches is that they assume that the system considered is linear elastic. This is an acceptable assumption if the aim of the analysis is to investigate the behaviour of the bridge to a non damaging earthquake. However, if the analysis is to be used for design several problems arise with the linear assumption. Firstly, in design it is necessary to consider the ultimate load, and in this case the structure will exhibit highly non linear behaviour. Secondly, when designing in materials such as steel it is usual to make the most efficient use of a chosen section by allowing plastic hinges to form. Thirdly, a popular approach to aseismic design is to provide a structure with sacrificial members which undergo plastic deformation during a damaging earthquake and so absorb energy, protecting the rest of the structure from damage. Methods are available of applying spectral methods to non linear systems, but they are not well documented in the engineering literature; this is obviously an area for further research. A further drawback of the power spectral approach when applied to aseismic analysis is the non stationary nature of the excitation which has been shown to be a problem for structures with long periods [Dumanoglu & Severn 1990]. However, both the results presented earlier and the literature [Perotti 1990, Quek *et al.* 1990, To 1982, To 1984] show that the evolutionary spectral approach provides an adequate solution to this problem.

5.3.2 Discussion Of The Ground Motion Representation

The representation of the spatial variations in the loading plays a major rôle in the analysis of the response to spatially varying seismic excitation. For the time history analysis either real earthquake records can be used or different records can be synthesised for each of the supports from a probabilistic model of the ground motion. In the spectral methods described above, most authors choose to describe the spatial variation of the excitation in terms of cross correlation functions between the supports. The power spectral approach outlined in chapter three differs from this by describing the spatial variation in terms of a two dimensional random field, an approach which has

been suggested before [Vanmarcke 1984], but to the best of the author's knowledge it has not been pursued to date. It is now important to consider the validity of this approach; two questions need to be answered:

a. Does the method produce correct results?

b. Is it better or worse than the existing methods?

In answer to the first question, the results presented in chapter four would suggest that the method does produce results which are acceptably accurate. Comparing the method with the existing cross correlation approach, it must first of all be stated that both approaches fully model the cross correlations both between the different points of support and the different components of the response. In calculating the results the existing method is significantly more efficient since it only requires making n^2 summations where n is the number of ground degrees of freedom. In contrast the power spectral model not only performs these summations to form the wavenumber response function, but also requires an integration over the wavenumber domain to yield the spectral moments. However, if repeated calculations have to be made then the power spectral approach becomes relatively more efficient as the summations only have to be performed once to form the modal wavenumber response functions. This point becomes more important as the number of ground degrees of freedom increases, such as for a multi span viaduct, and will be most significant when the interaction of the structure and the excitation is continuous in the space domain. This will occur, for example, in the seismic excitation of a dam [Altinisik & Severn 1982, Dumanoglu & Severn 1984] or buried pipeline [O'Rourke & Castro 1980, O'Rourke & El Hmadi 1988]. Obviously, for bridges a spatially continuous seismic loading such as this cannot occur because the supports are at discrete points in the space domain. However, a similar condition does arise for wind excitation [Davenport 1962] and traffic

[Bryja & Šniady 1991] and in these cases the cross correlation functions have to be integrated across the length of the deck.

A final comment ought now to be made regarding the type of seismic excitation discussed in this chapter, where the examples have been limited to the simple case of asynchronous excitation. As mentioned in chapter two, loss of coherence is likely to represent the most important cause of spatial variations in the loading. It is important, therefore, that the power spectral approach should be able to deal with this type of excitation as well as the asynchronous problem; § 3.3.2 showed that the method could be applied to more general multi support problems.

5.4 Conclusions

1. Asynchronous seismic excitation has important consequences for the response of a cable stayed bridge and needs to be taken into account during design.

2. Assuming that the excitation is stationary produces a conservative solution to the problem which has important cost and safety implications for aseismic design.

3. The method of evolutionary power density spectra provides a suitable method for modelling the non stationary excitation and response.

4. The power spectral approach described in this thesis provides a workable method for calculating the response to asynchronous excitation, but it would be more suited to problems where the interaction of the excitation and structure is continuous in the space domain.

Table 5.1

Material And Section Properties For 2-D Finite Element Model Of kessock Bridge

Deck

Density	7800 kg m^{-3}
Elastic modulus	2.11 x 10^{11}
Poisson's Ratio	0.3
Second Moment Of Area	1.2 m^4
Area	0.72 m^2

Pylons

Density	7800 kg m^{-3}
Elastic modulus	2.11 x 10^{11}
Poisson's Ratio	0.3
Second Moment Of Area	0.28 m^4
Area	0.4 m^2

Cables

Density	8360 kg m^{-3}
Elastic modulus	1.497 x 10^{11}
Area	0.72 m^2
Pre-strain	3.1 x 10^{-3}

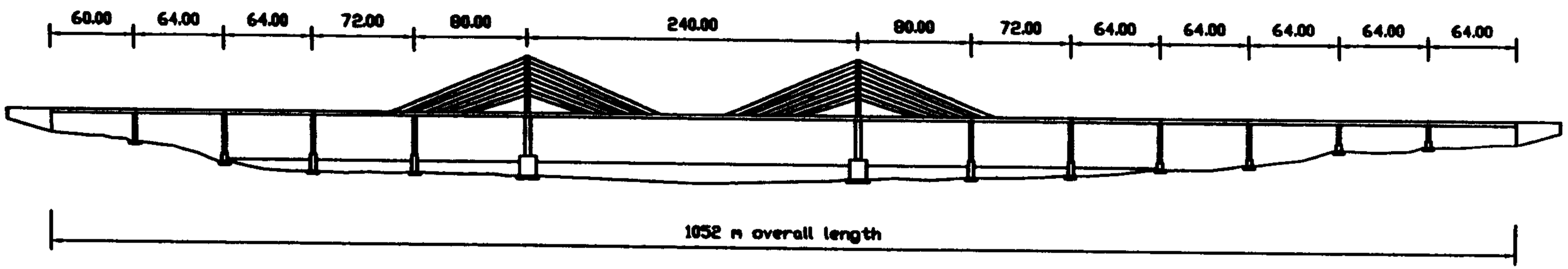

Figure 5.1 : General Arrangement of Kessock Bridge

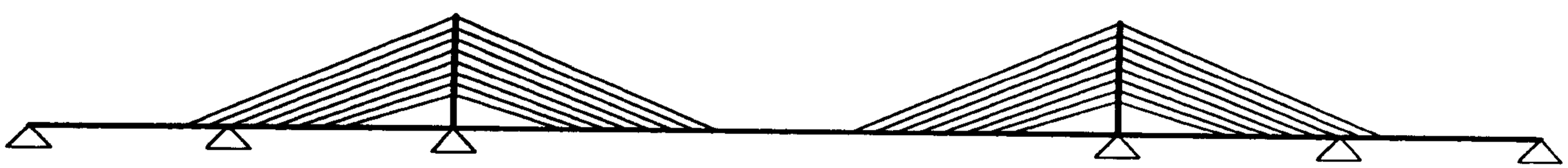

Figure 5.2 : Two Dimensional Model of Kessock Bridge

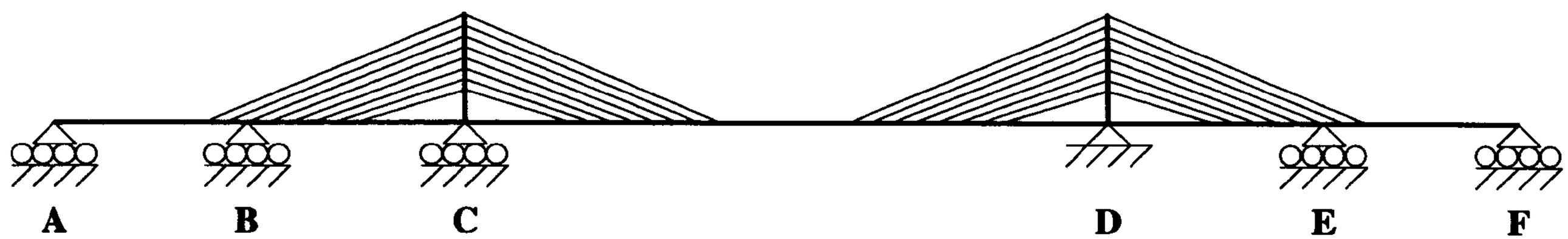

Figure 5.3 : Boundary Conditions on Kessock Bridge

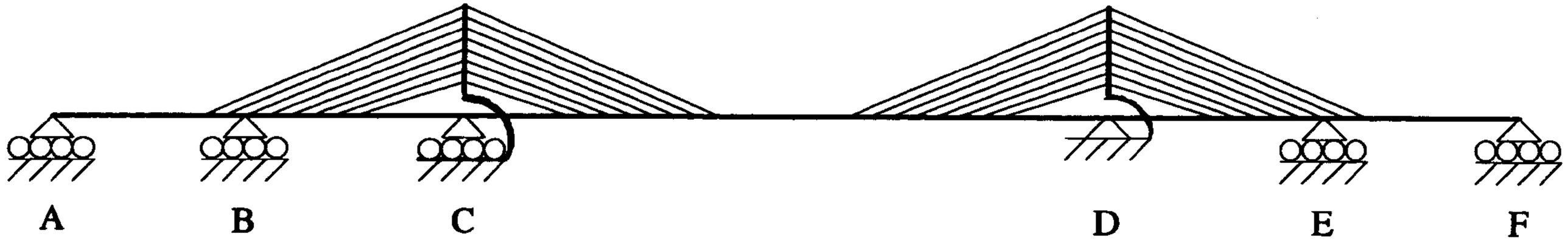

Figure 5.4 : Modified Boundary Conditions on Two Dimensional Model

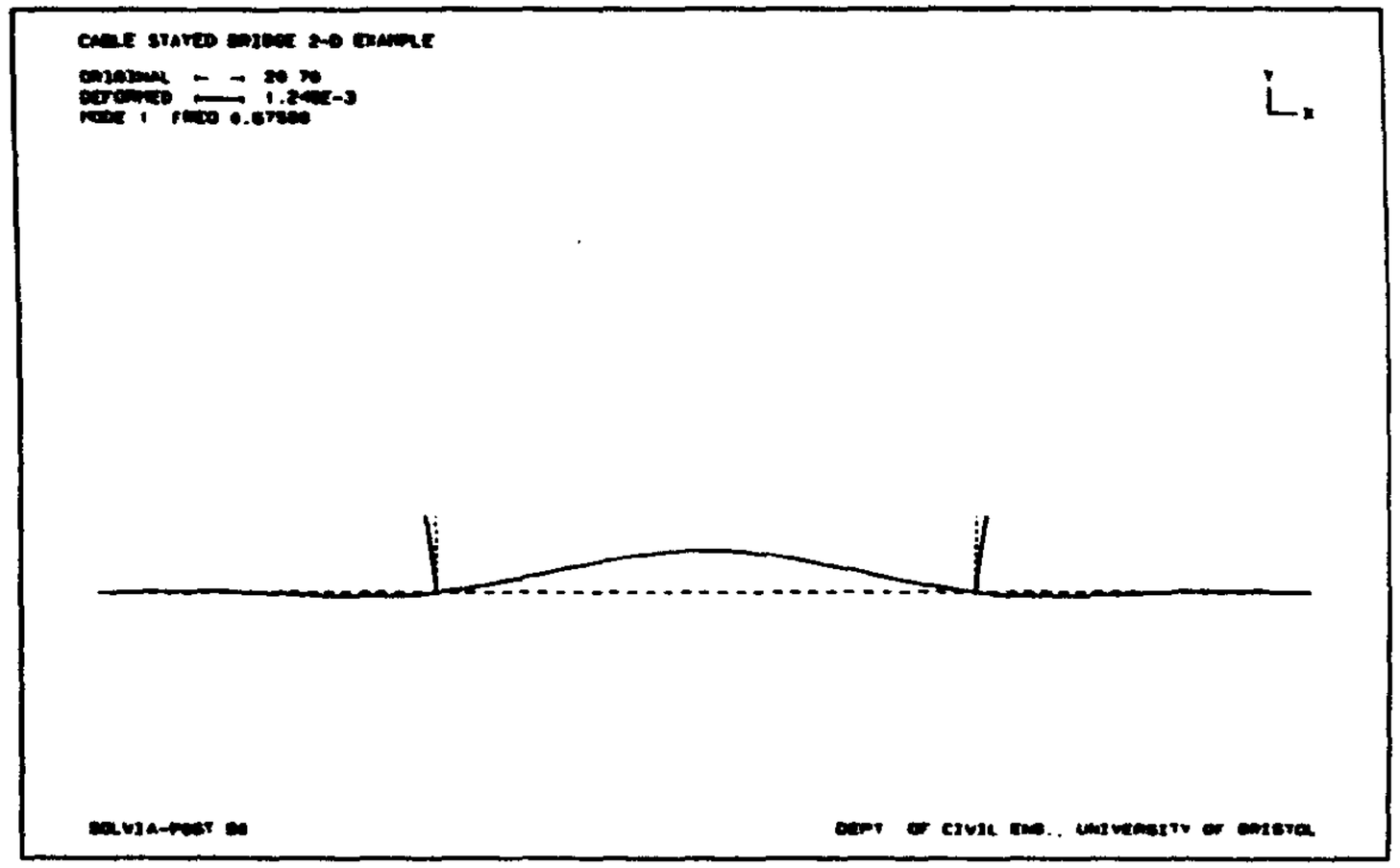

Figure 5.5a -:- Cable Stayed Bridge Mode One, 0.576 Hz.

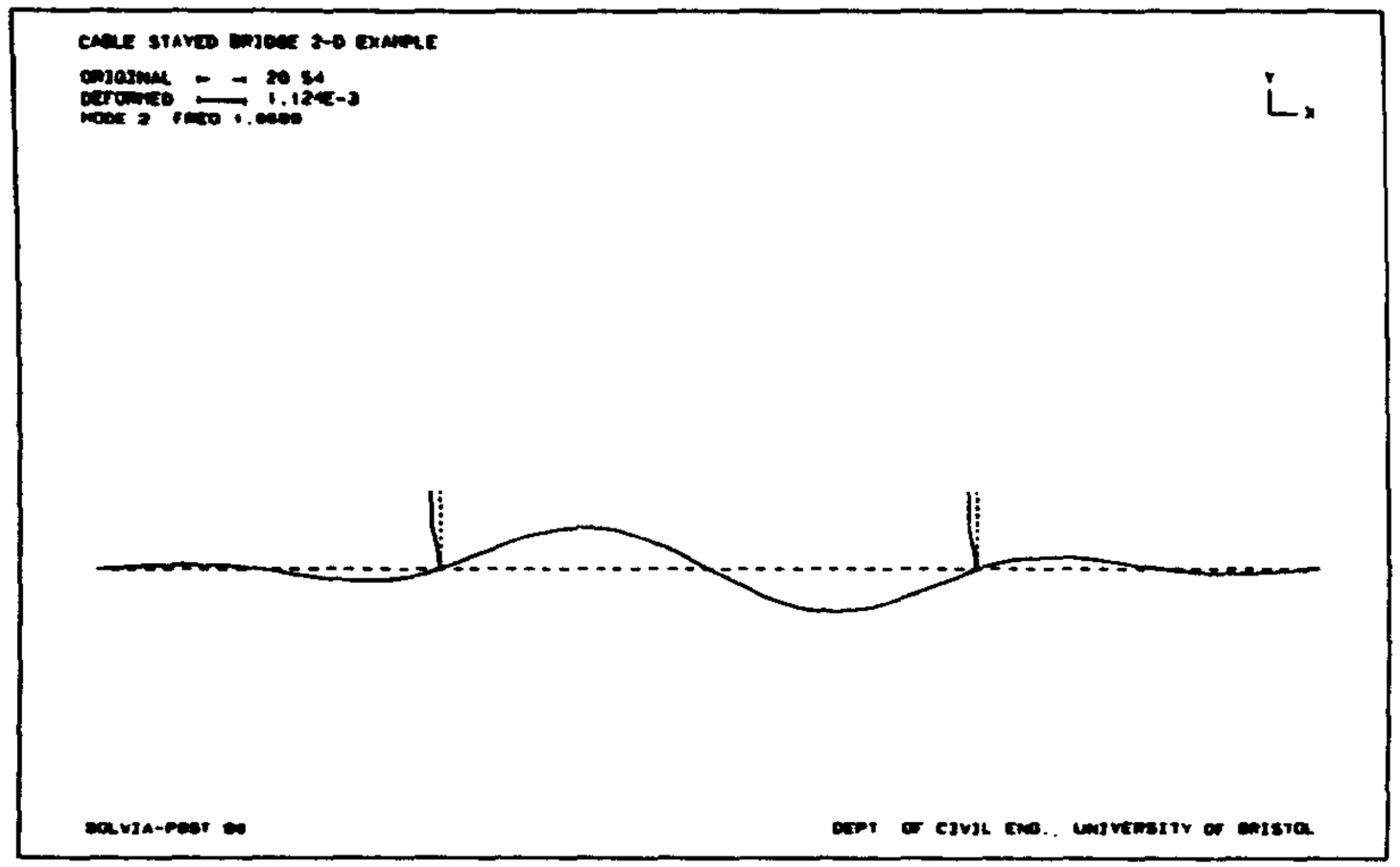

Figure 5.5b -:- Cable Stayed Bridge Mode Two, 1.069 Hz.

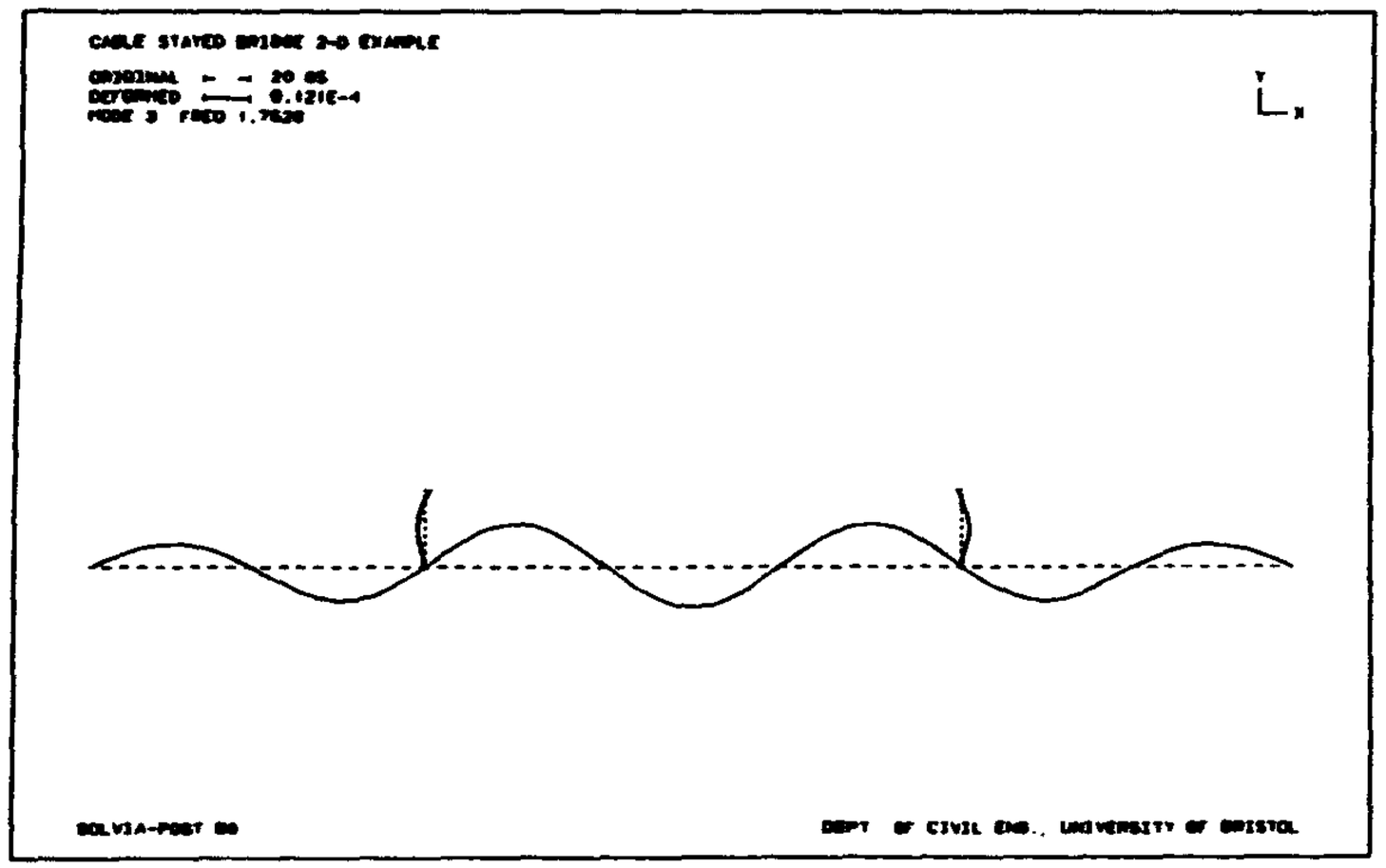

Figure 5.5c -:- Cable Stayed Bridge Mode Three, 1.753 Hz.

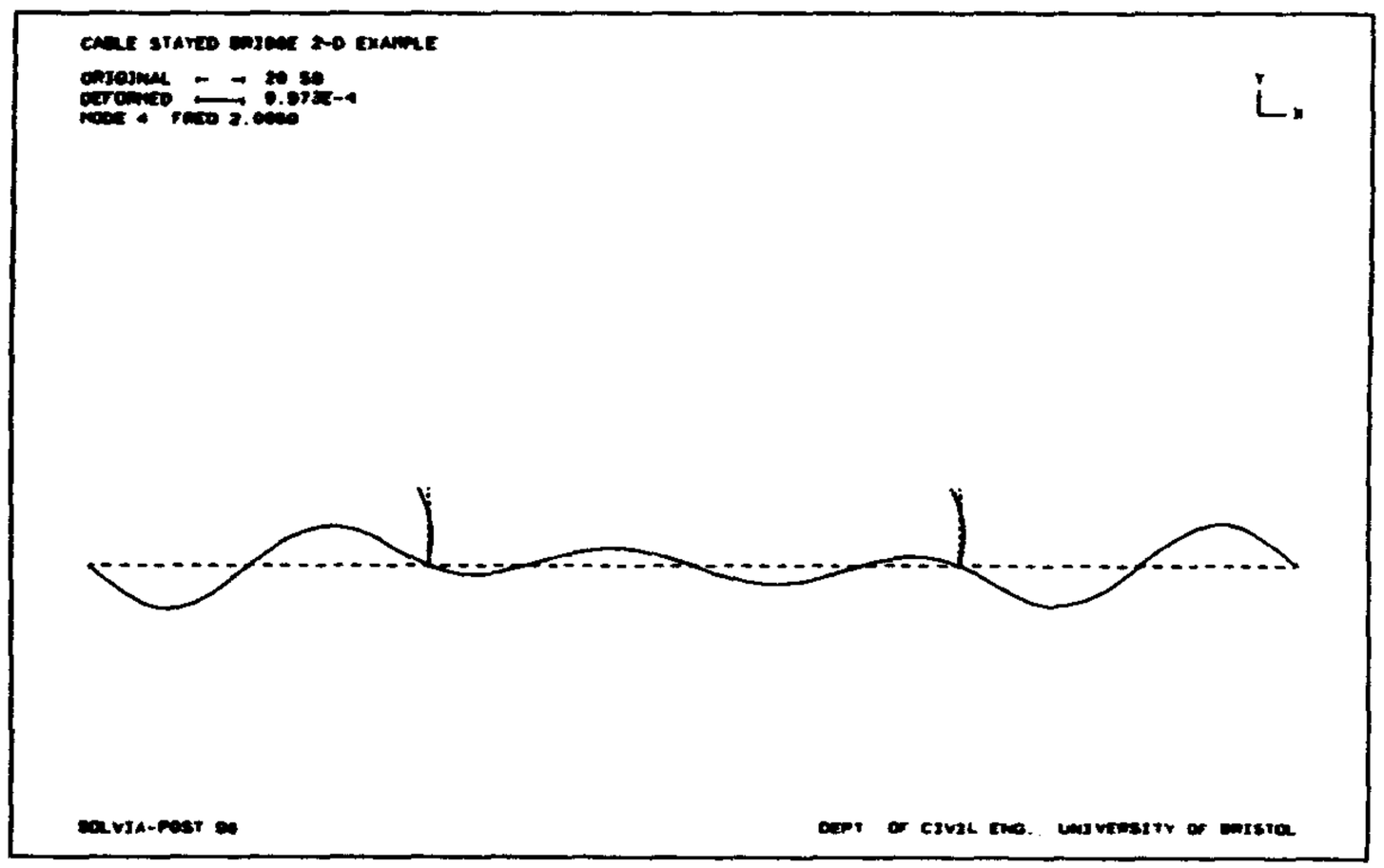

Figure 5.5d -:- Cable Stayed Bridge Mode Four, 2.096 Hz.

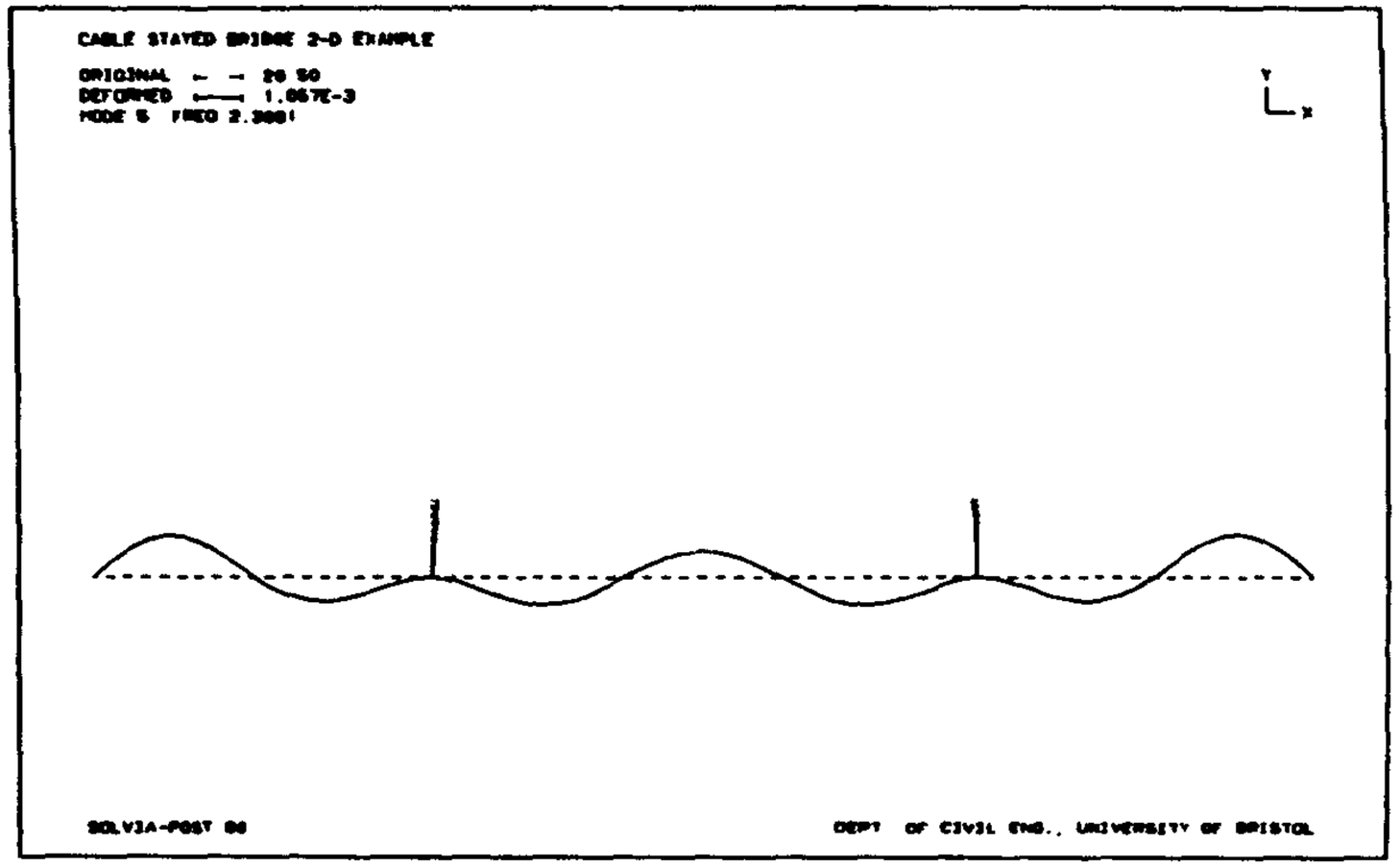

Figure 5.5e -:- Cable Stayed Bridge Mode Five, 2.308 Hz.

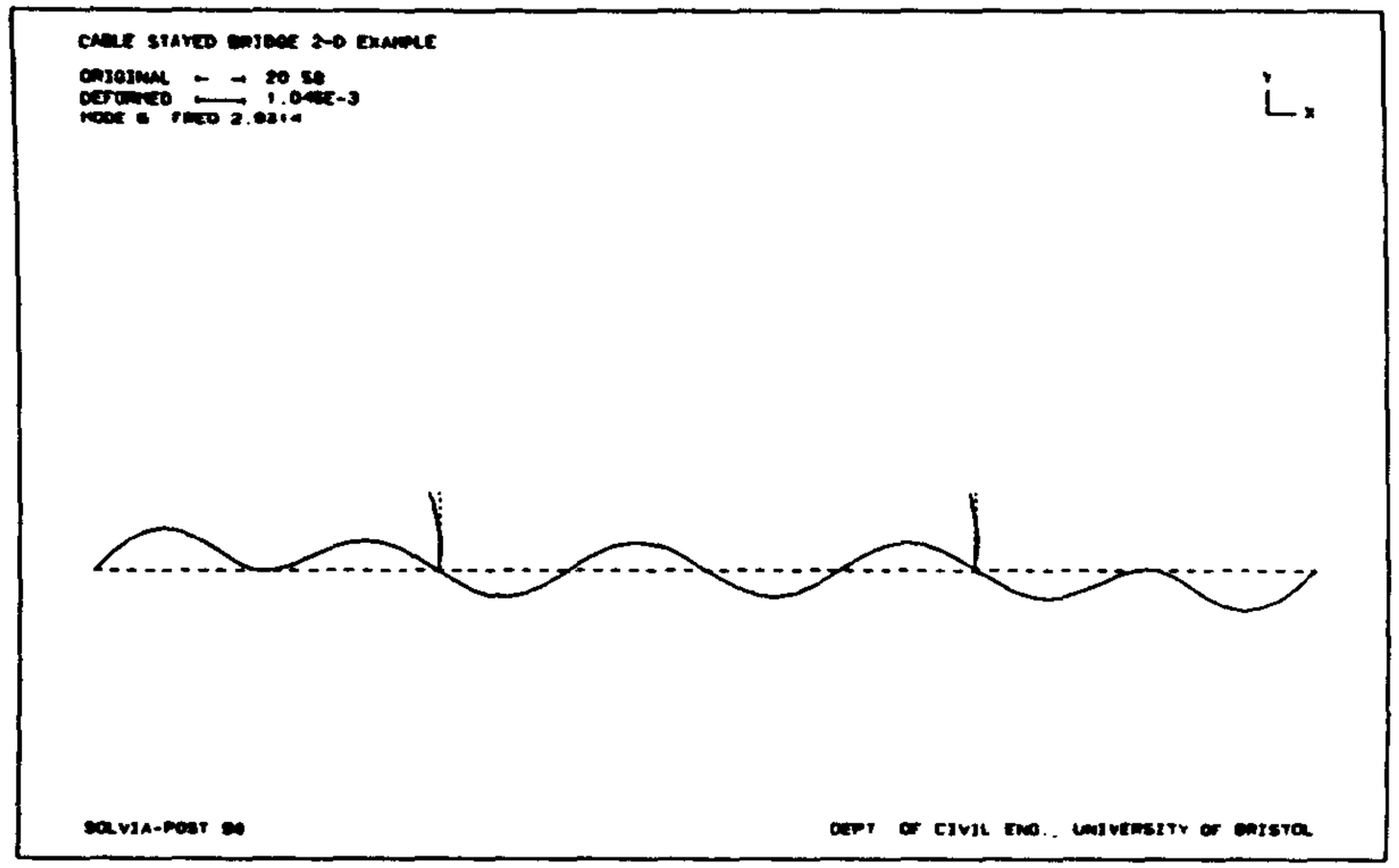

Figure 5.5f -:- Cable Stayed Bridge Mode Seven, 2.931 Hz.

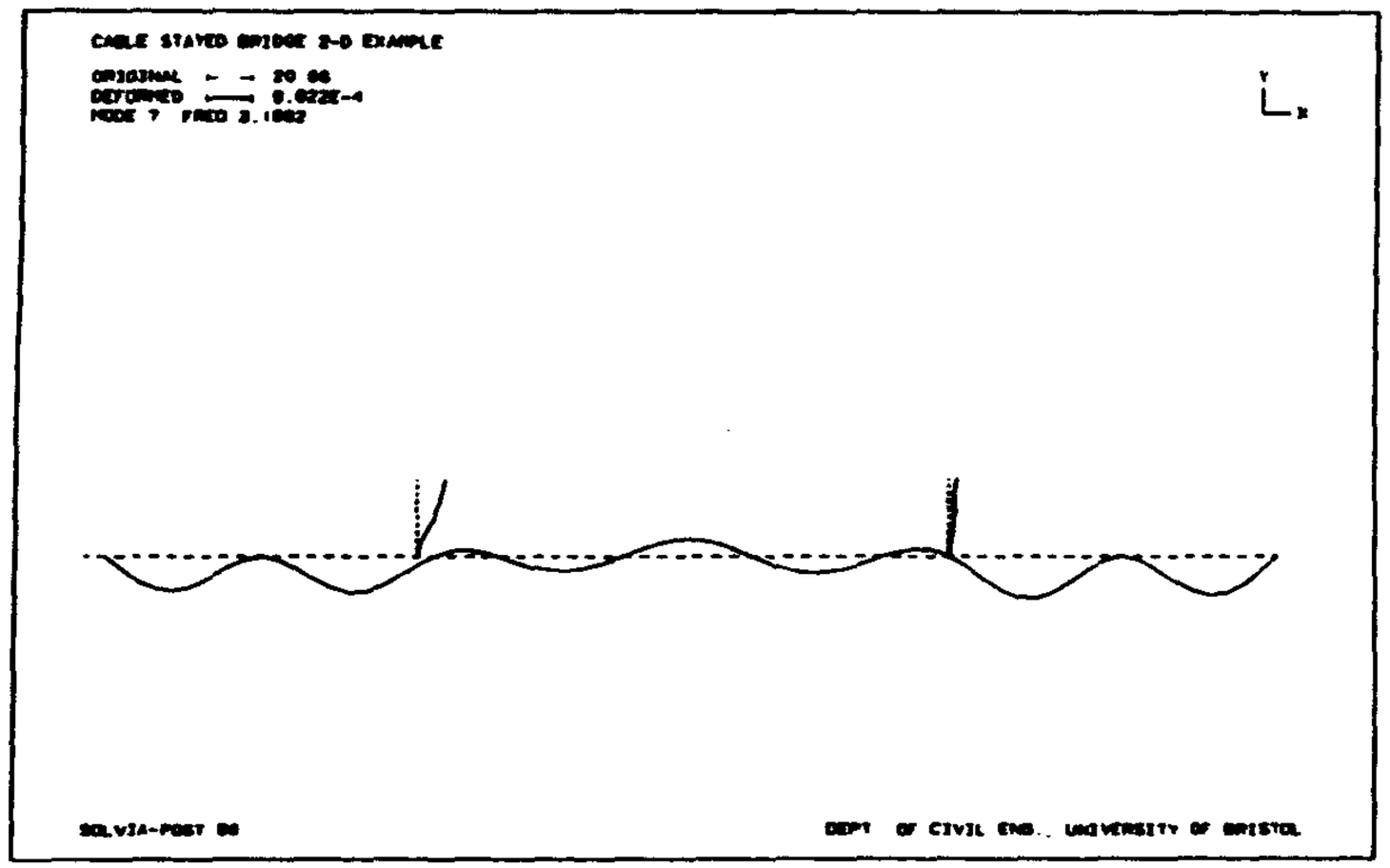

Figure 5.5g -:- Cable Stayed Bridge Mode Eight, 3.188 Hz.

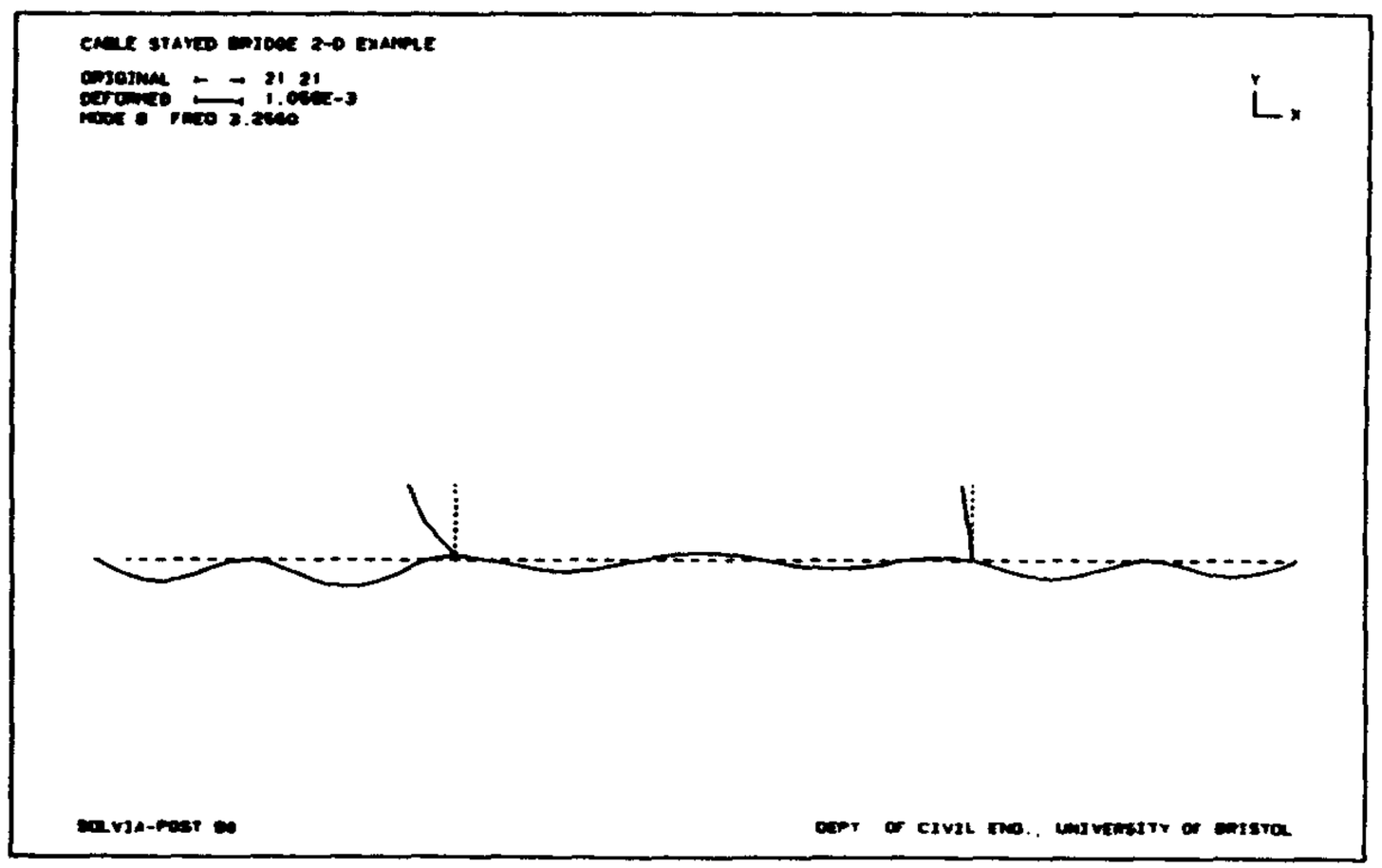

Figure 5.5h -:- Cable Stayed Bridge Mode Nine, 3.256 Hz.

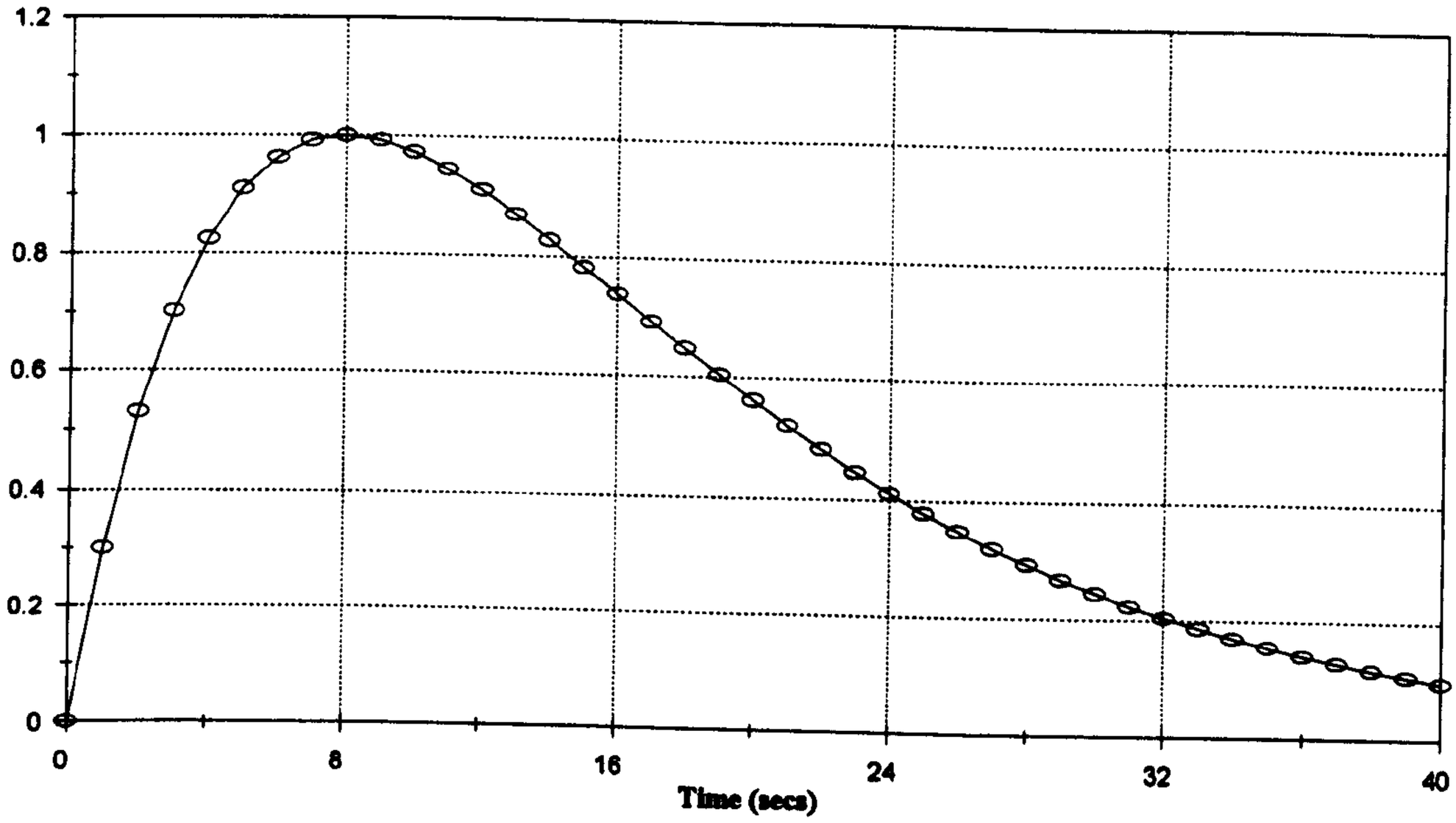

Figure 5.6 -:- Exponential Window For Non Stationary Excitation

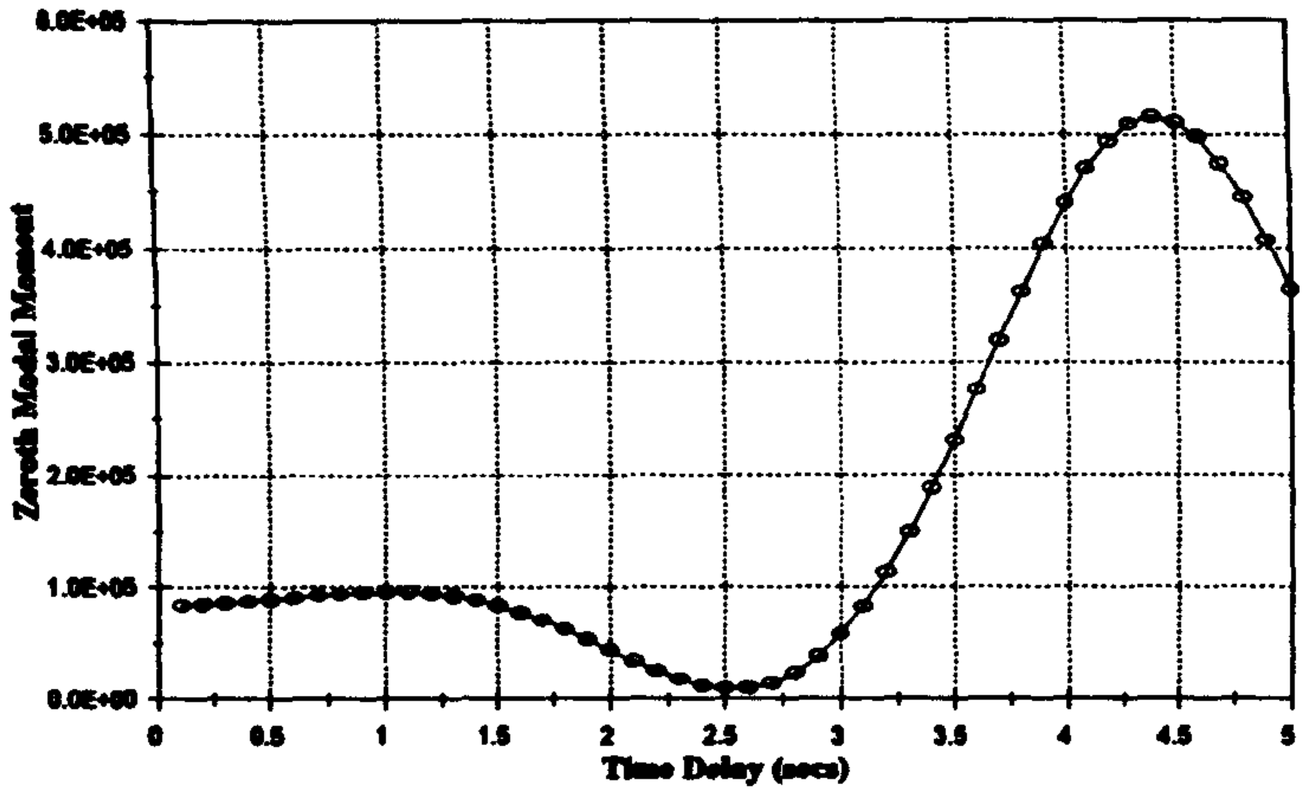

Figure 5.7a -:- Mean Square Response Mode One
Vertical Excitation

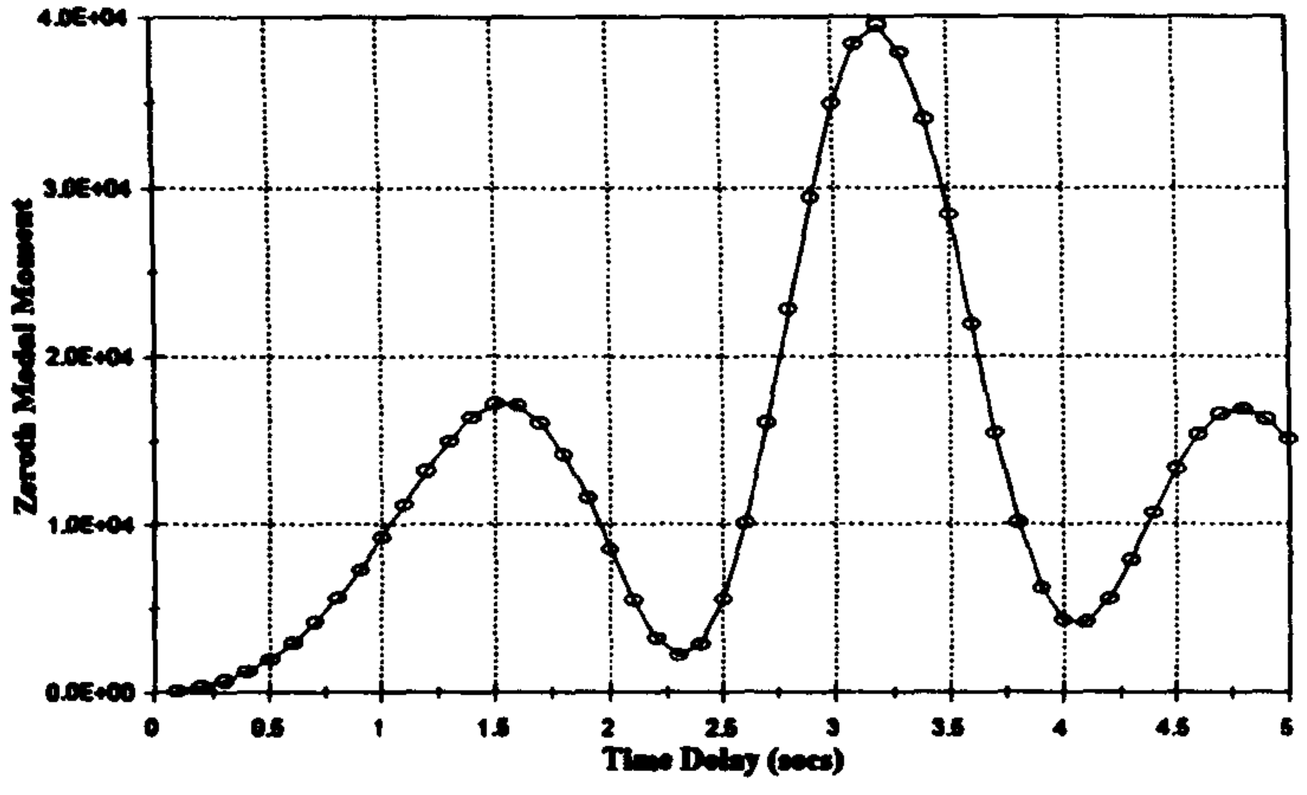

Figure 5.7b -:- Mean Square Response Mode Two
Vertical Excitation

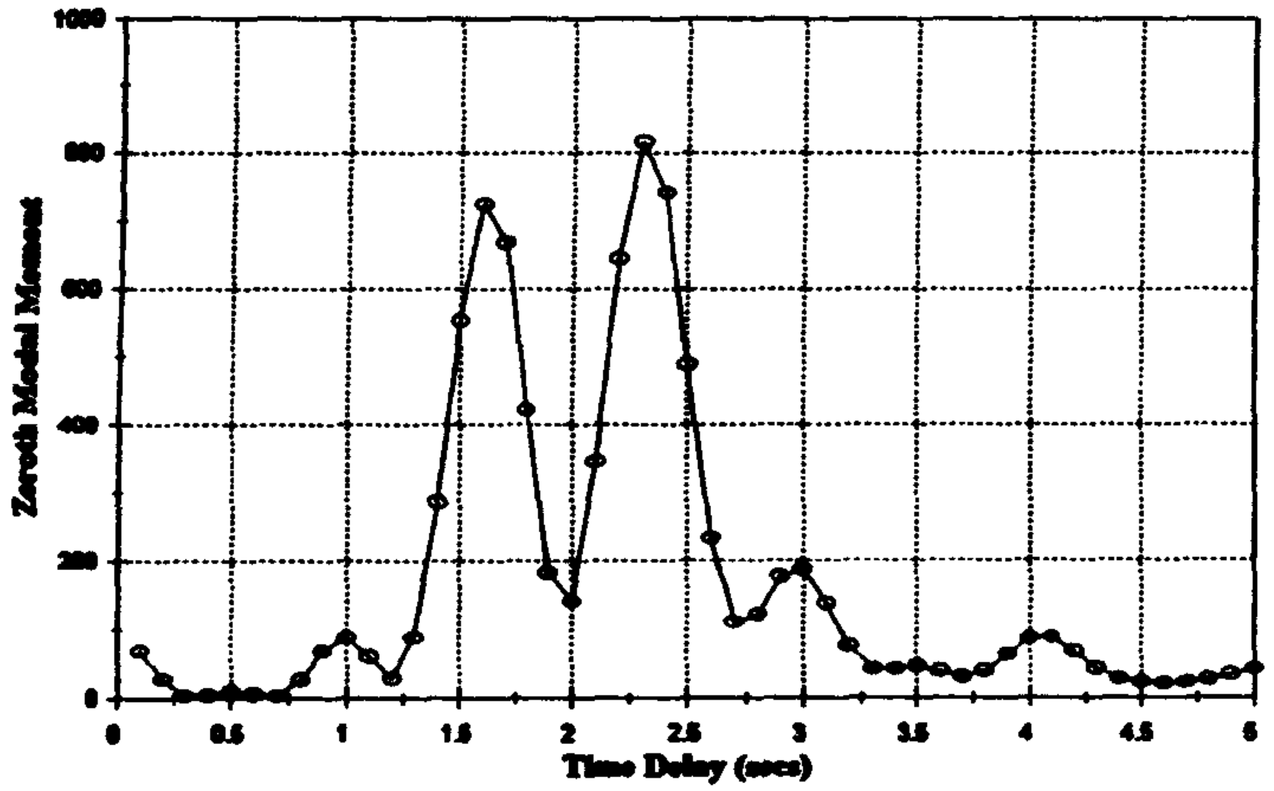

Figure 5.7c -:- Mean Square Response Mode Three
Vertical Excitation

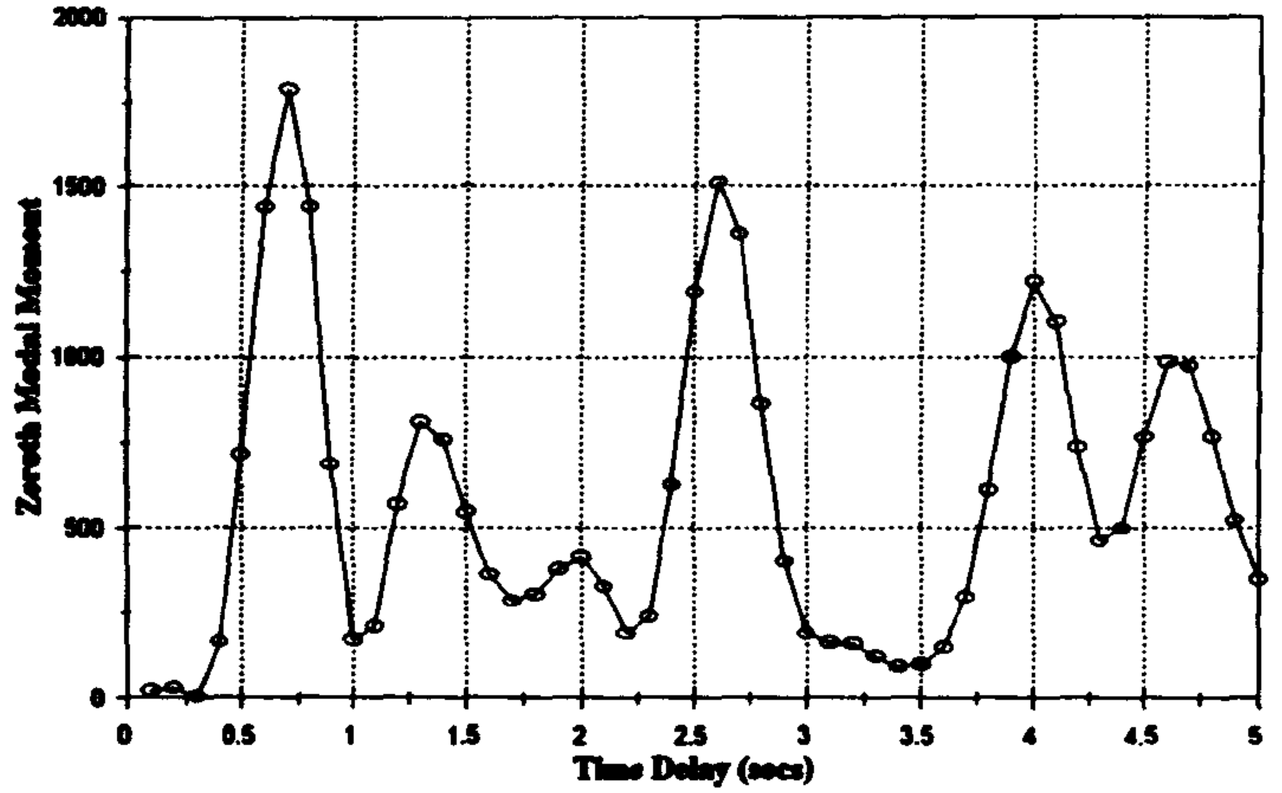

Figure 5.7d -:- Mean Square Response Mode Four
Vertical Excitation

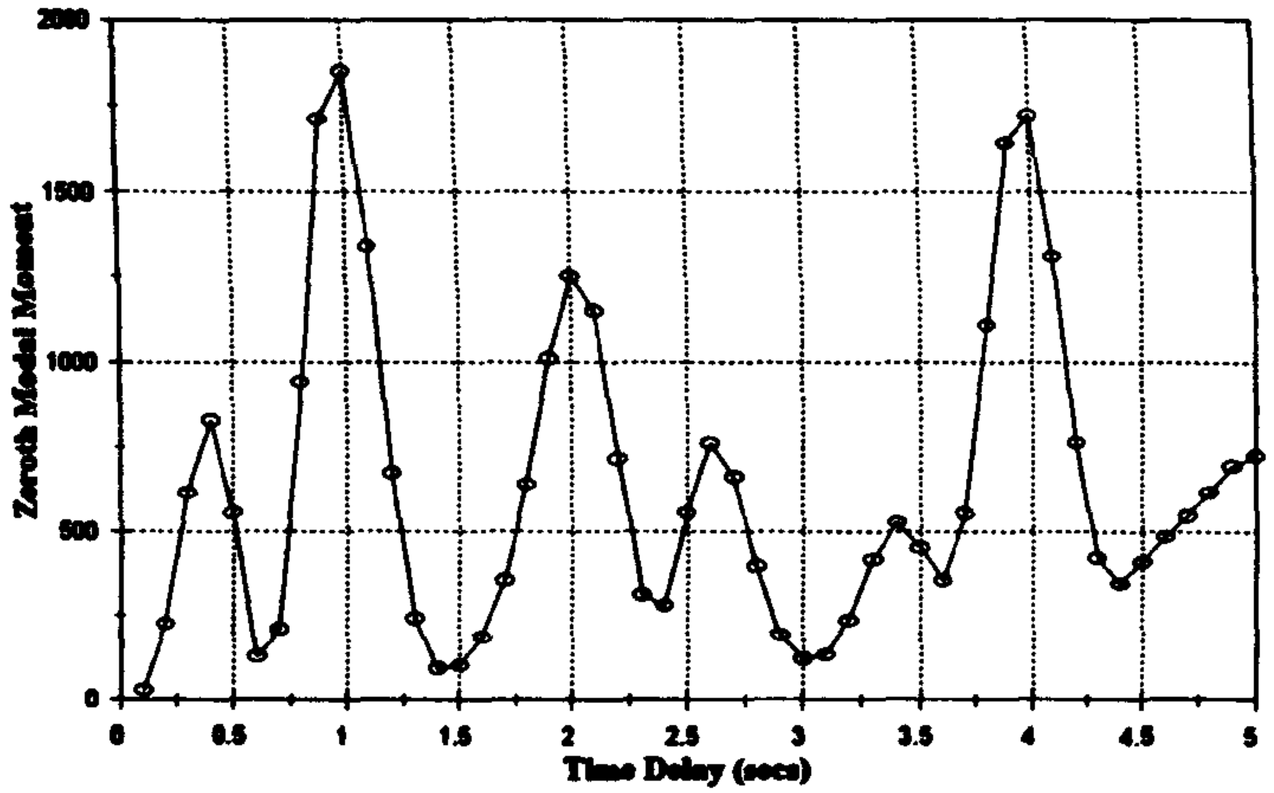

Figure 5.7e -:- Mean Square Response Mode Five Vertical Excitation

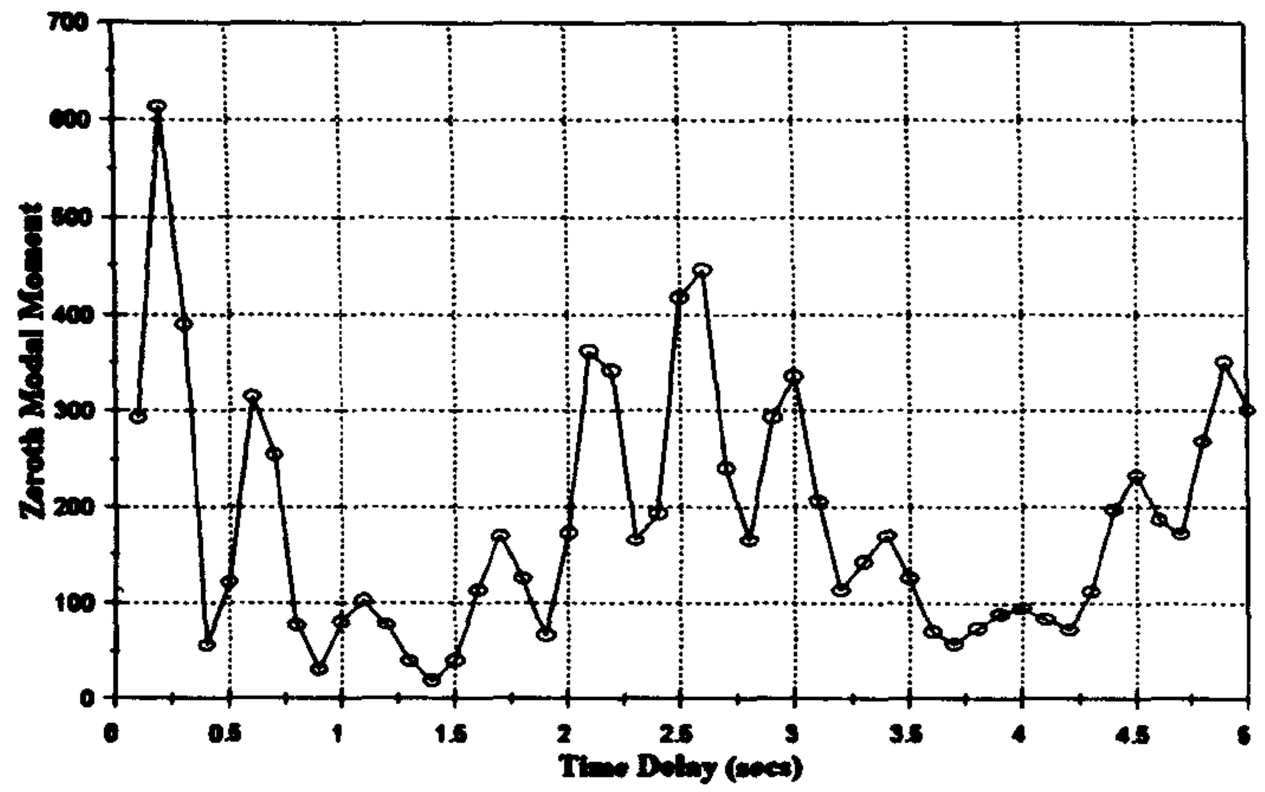

Figure 5.7f -:- Mean Square Response Mode Six Vertical Excitation

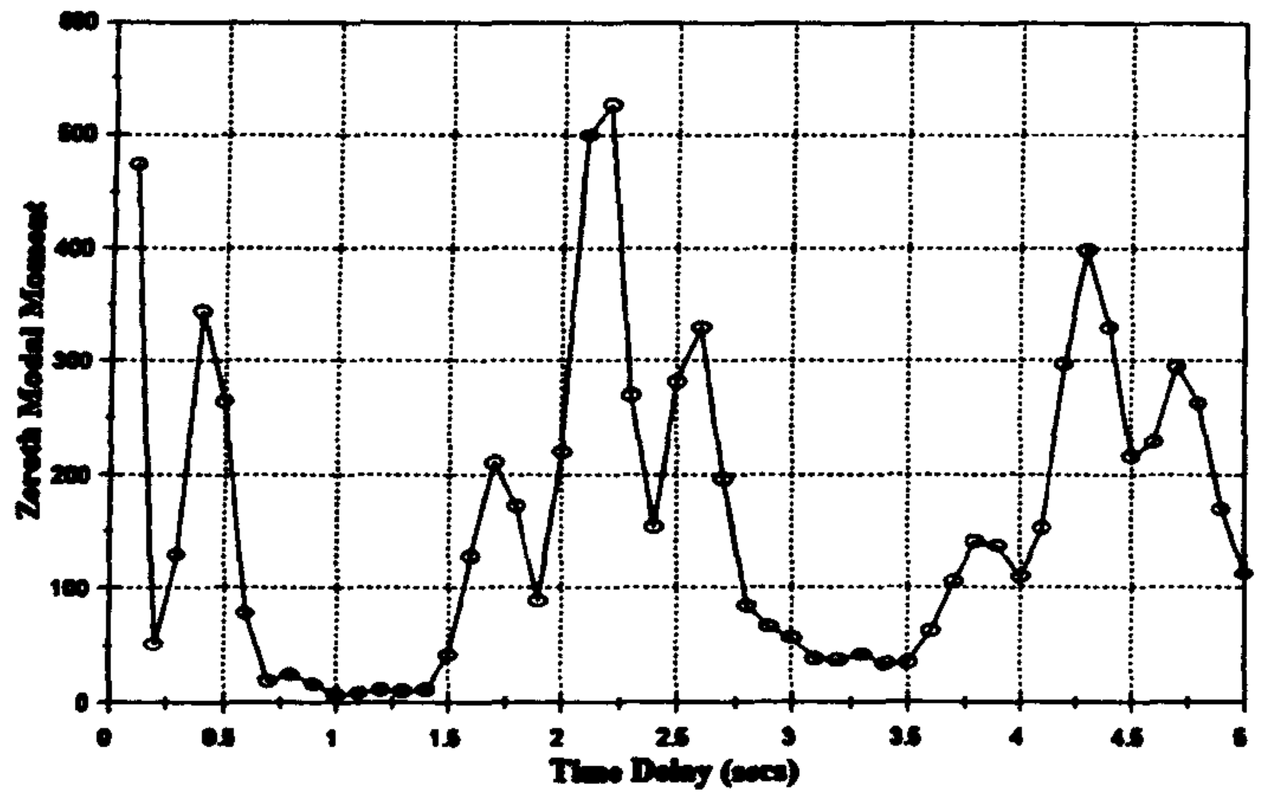

Figure 5.7g -:- Mean Square Response Mode Seven Vertical Excitation

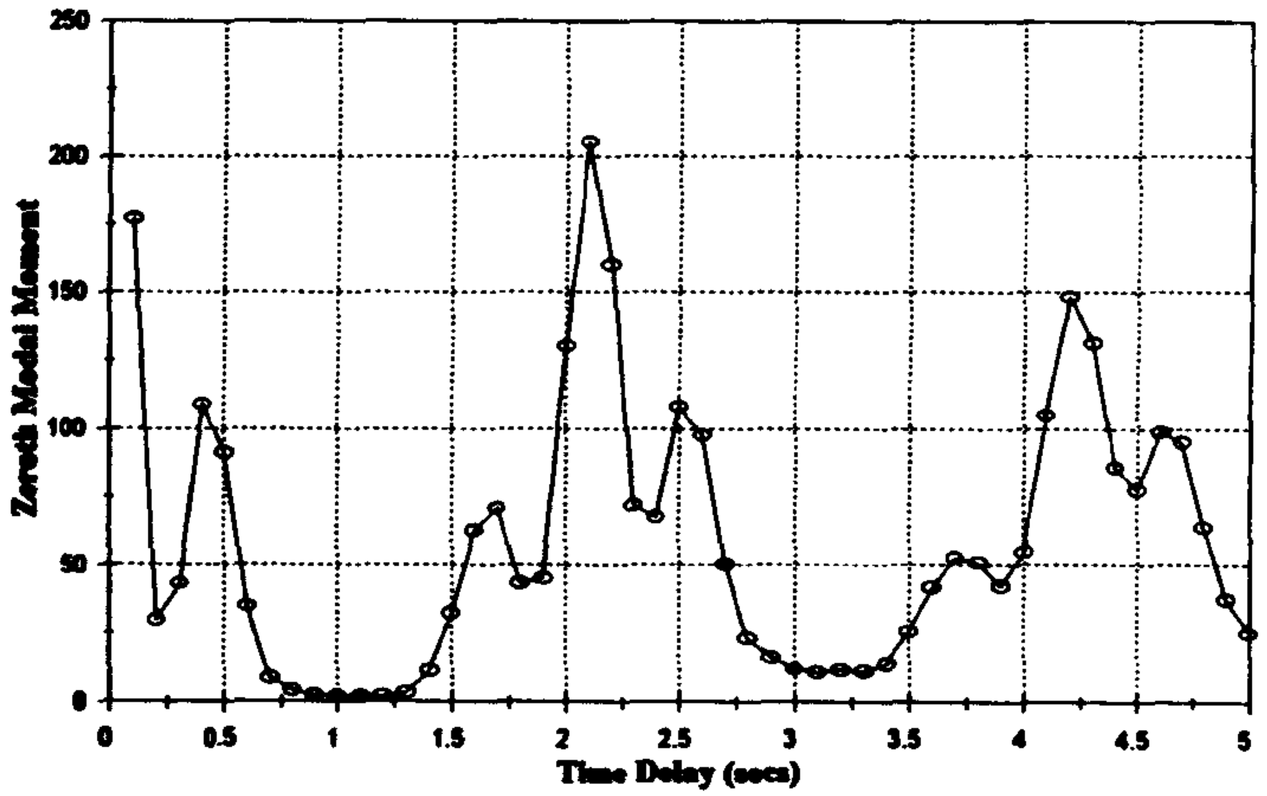

Figure 5.7h -:- Mean Square Response Mode Eight Vertical Excitation

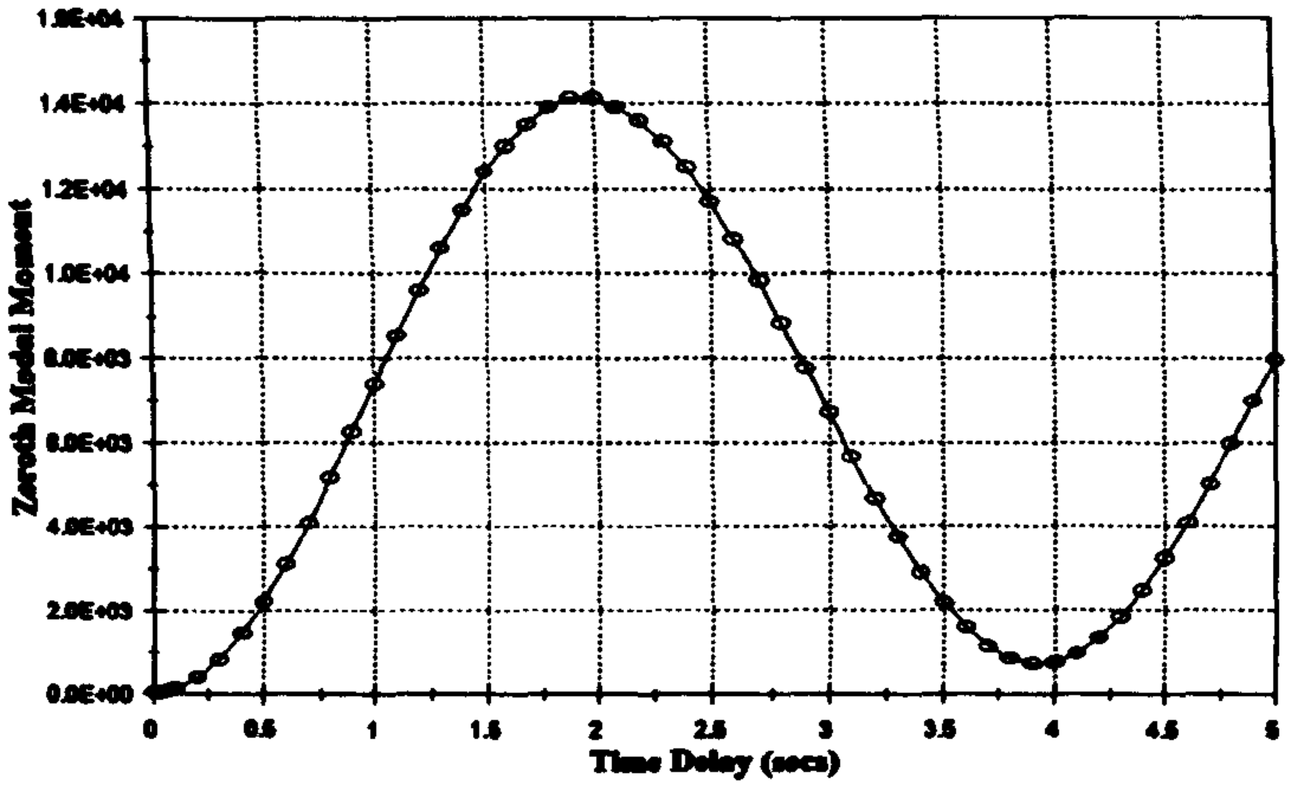

Figure 5.8a -:- Mean Square Response Mode One Horizontal Excitation

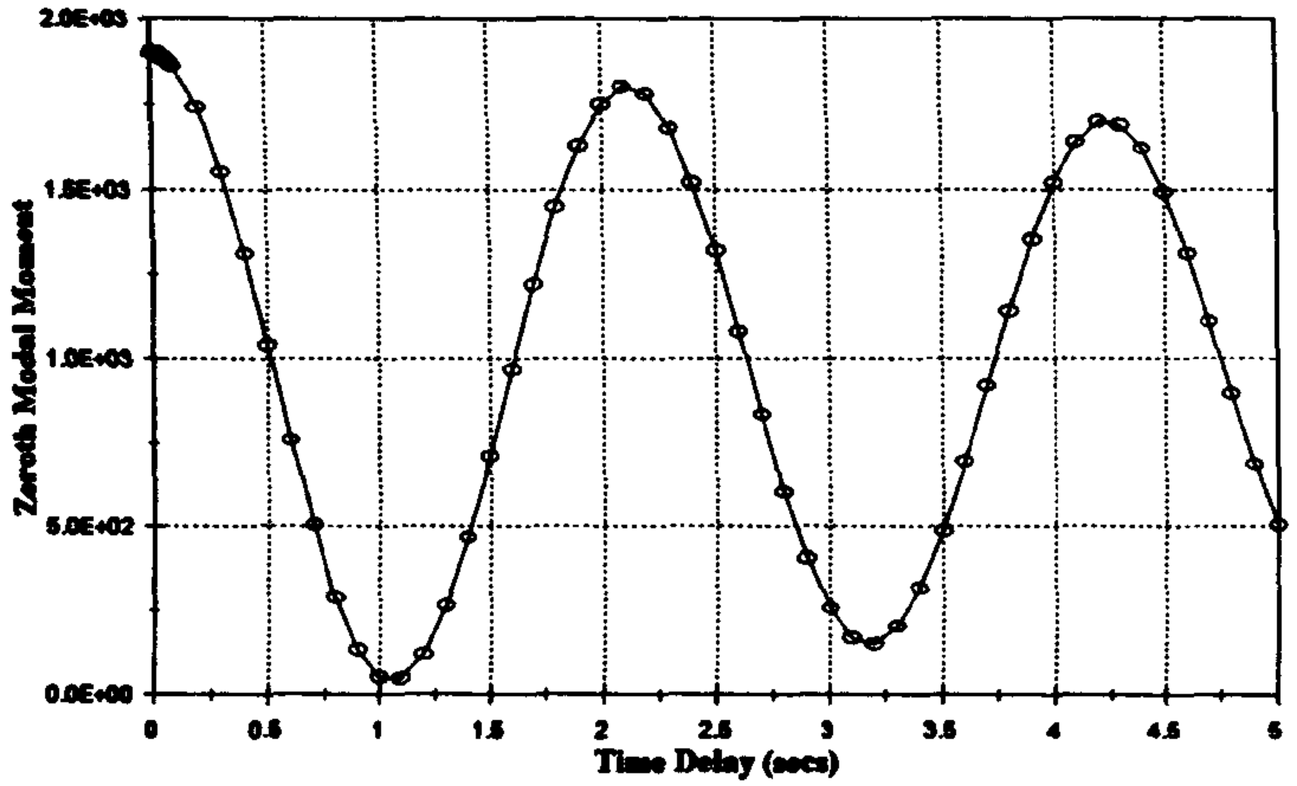

Figure 5.8b -:- Mean Square Response Mode Two Horizontal Excitation

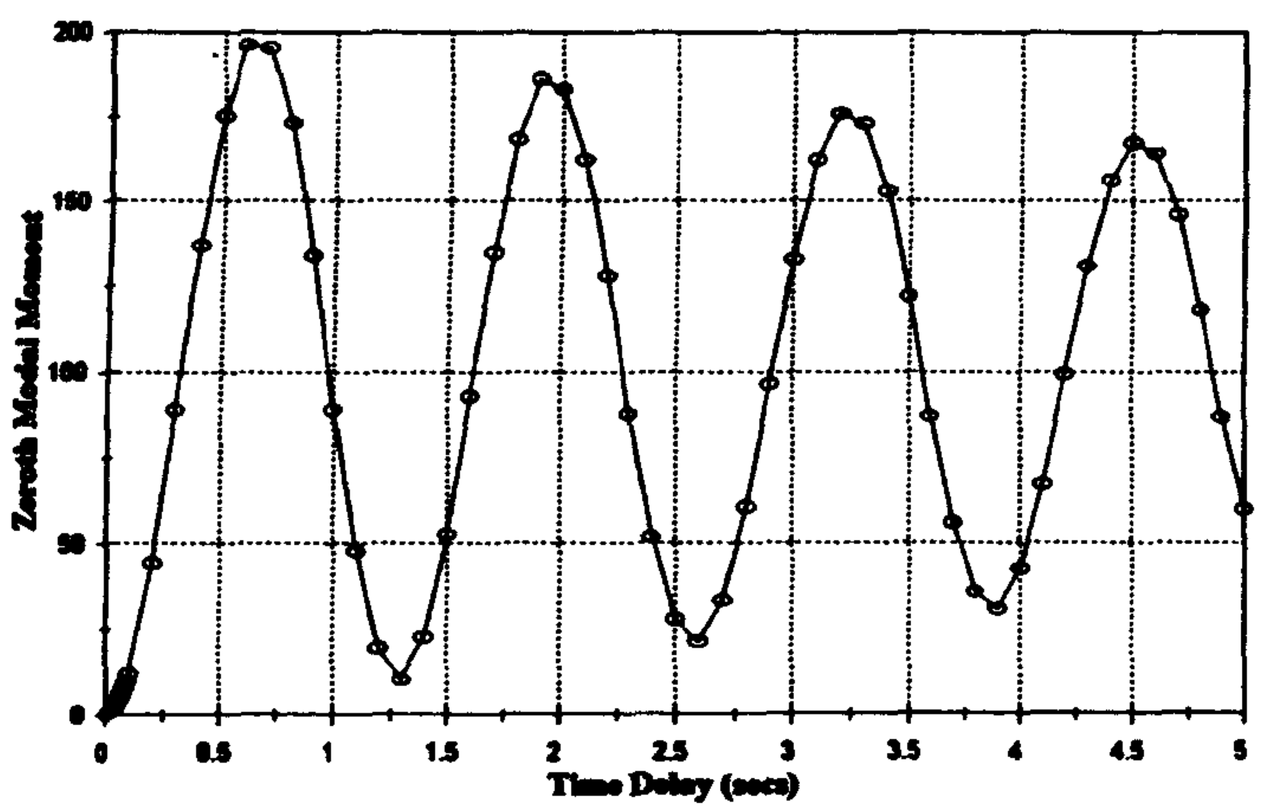

Figure 5.8c -:- Mean Square Response Mode Three Horizontal Excitation

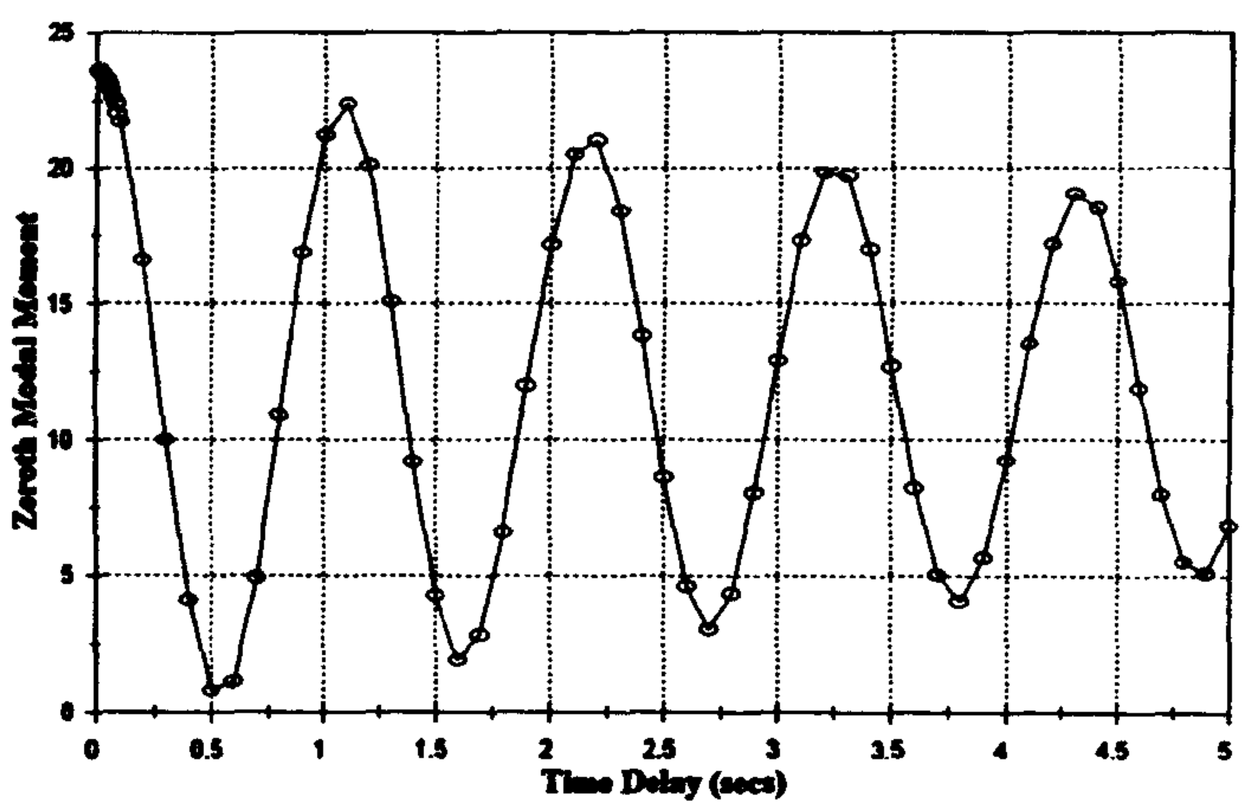

Figure 5.8d -:- Mean Square Response Mode Four Horizontal Excitation

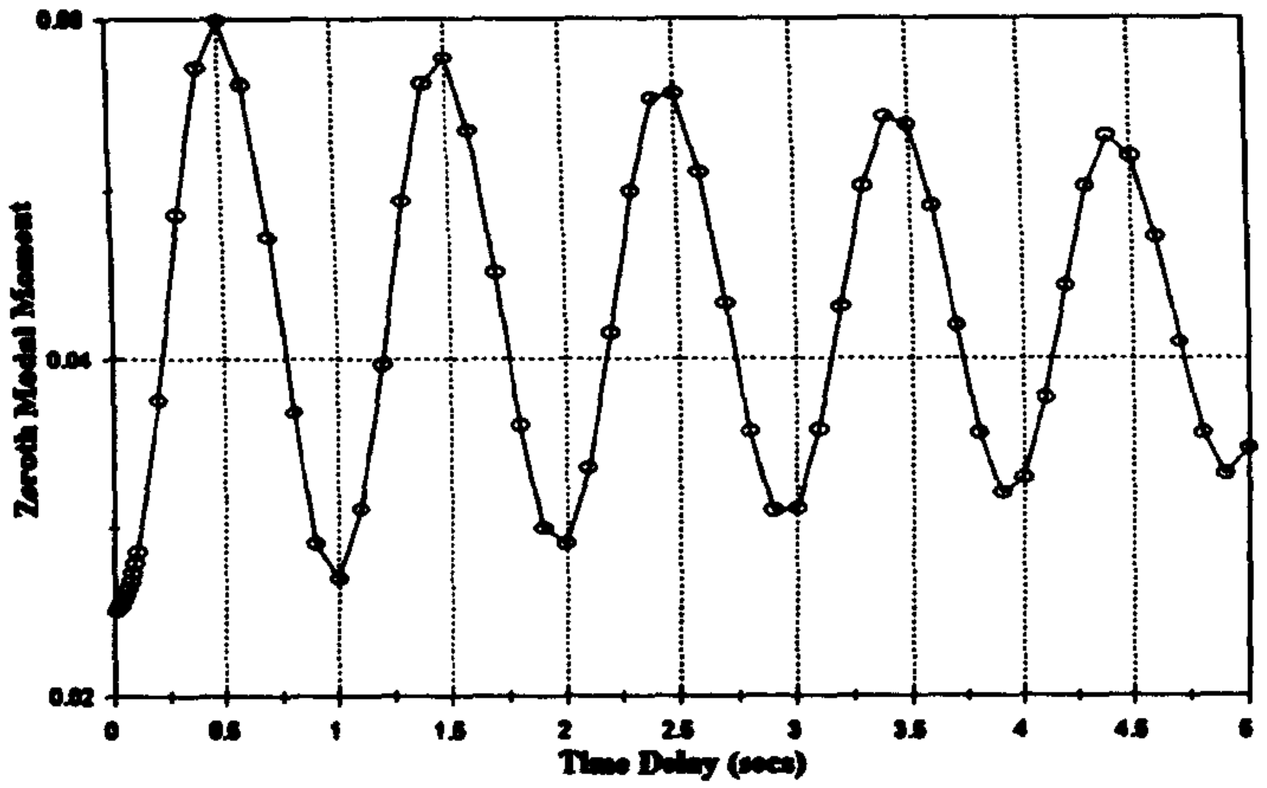

Figure 5.8e -:- Mean Square Response Mode Five Horizontal Excitation

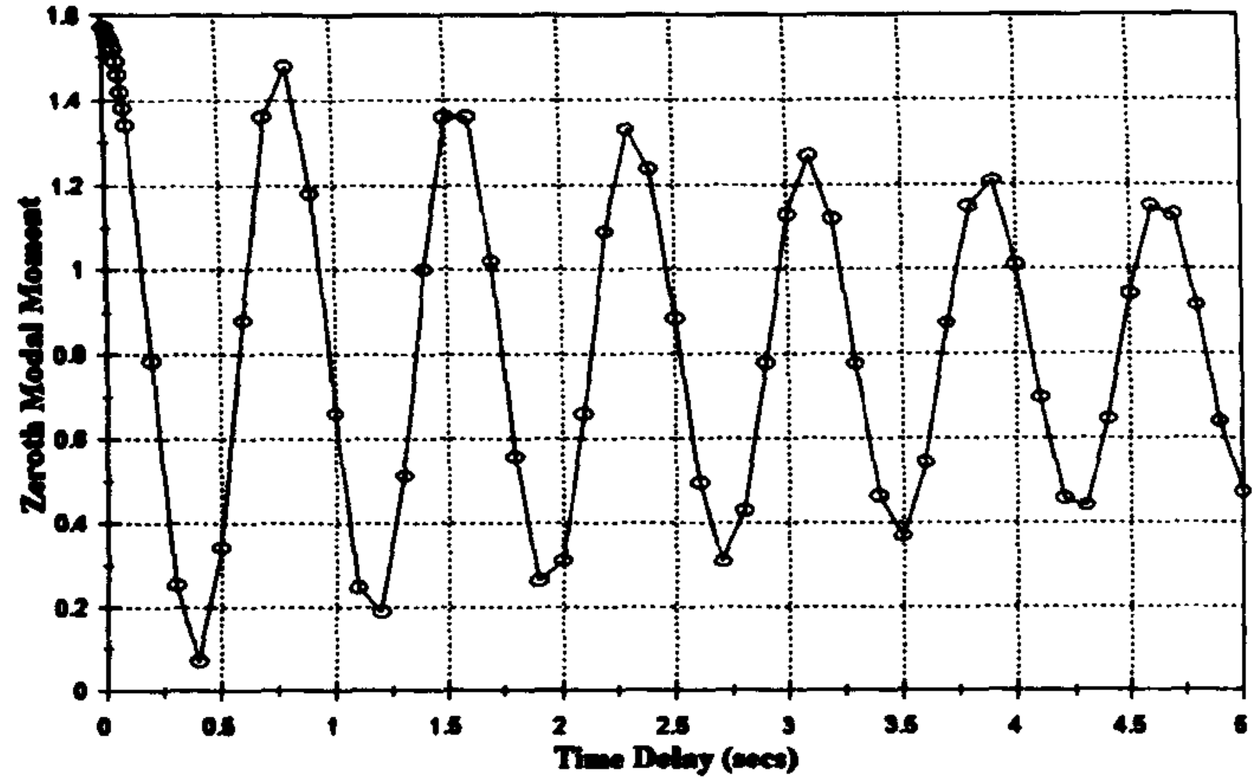

Figure 5.8f -:- Mean Square Response Mode Six Horizontal Excitation

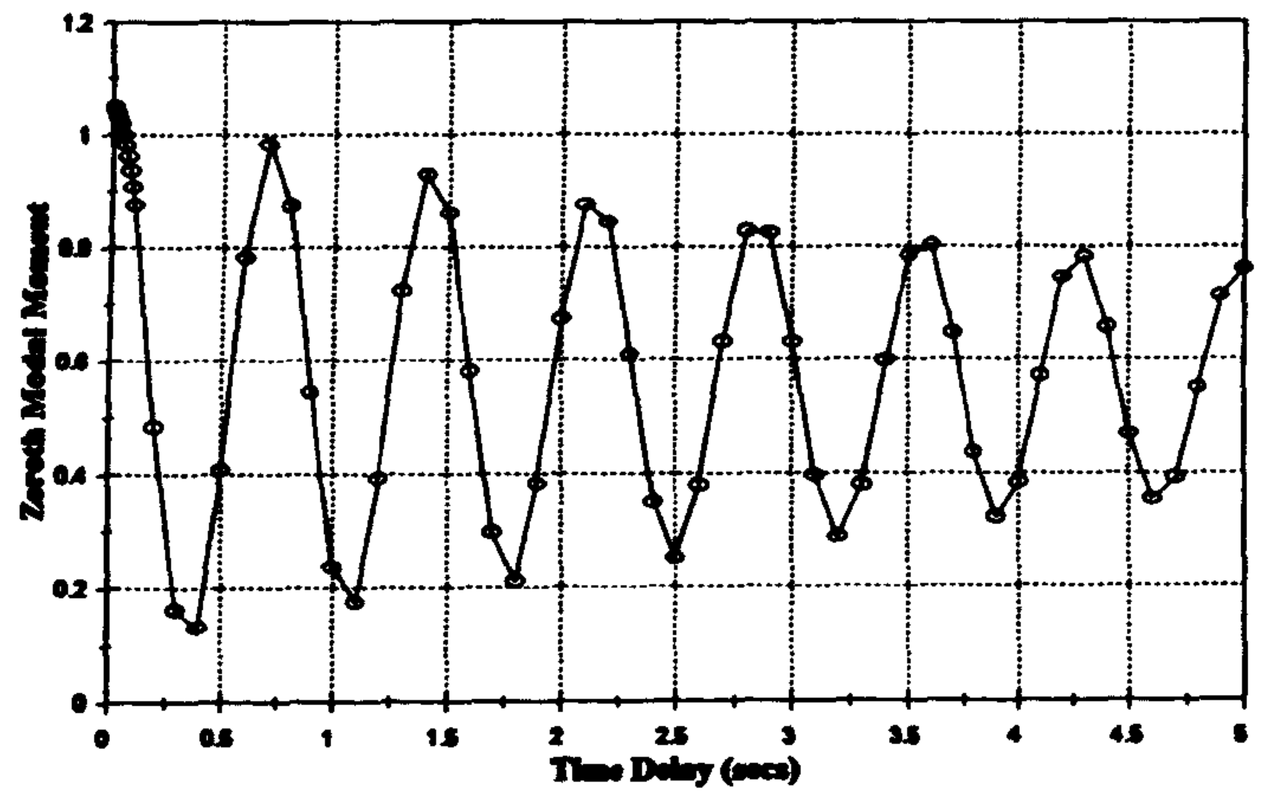

Figure 5.8g -:- Mean Square Response Mode Seven Horizontal Excitation

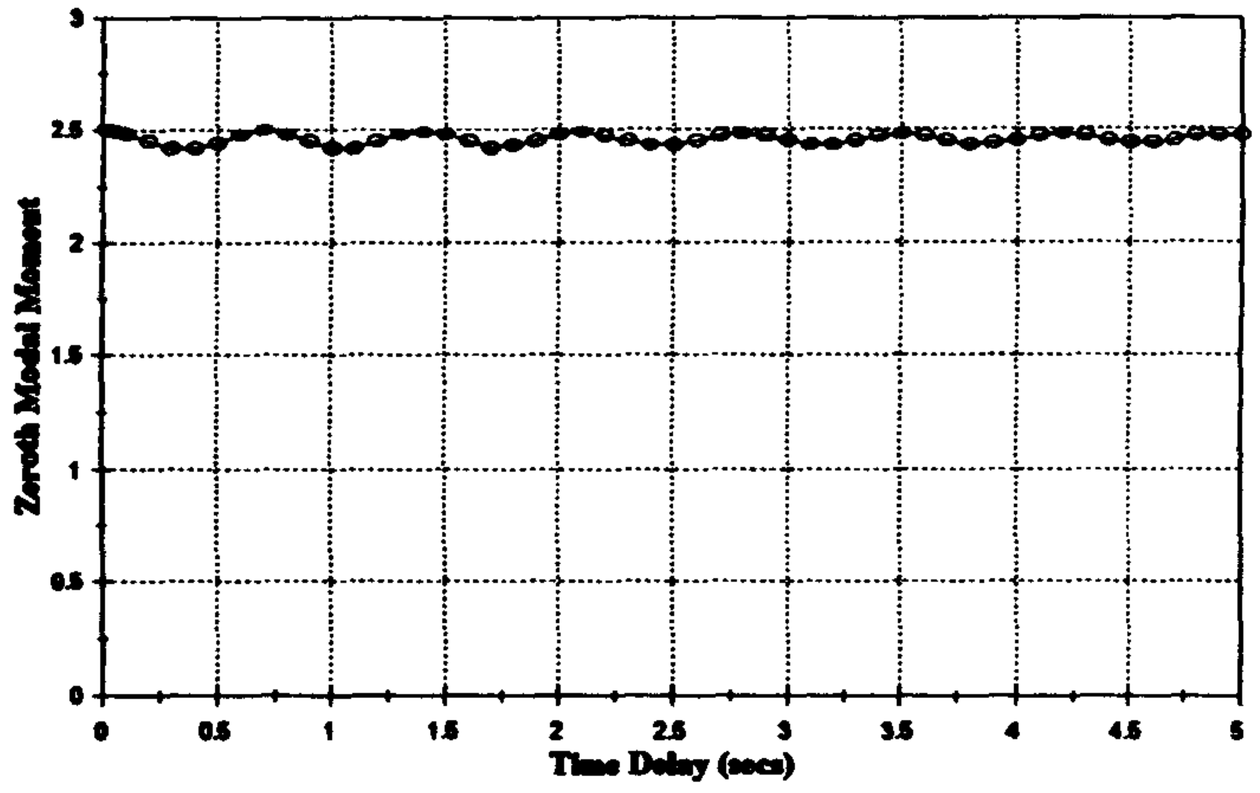

Figure 5.8h -:- Mean Square Response Mode Eight Horizontal Excitation

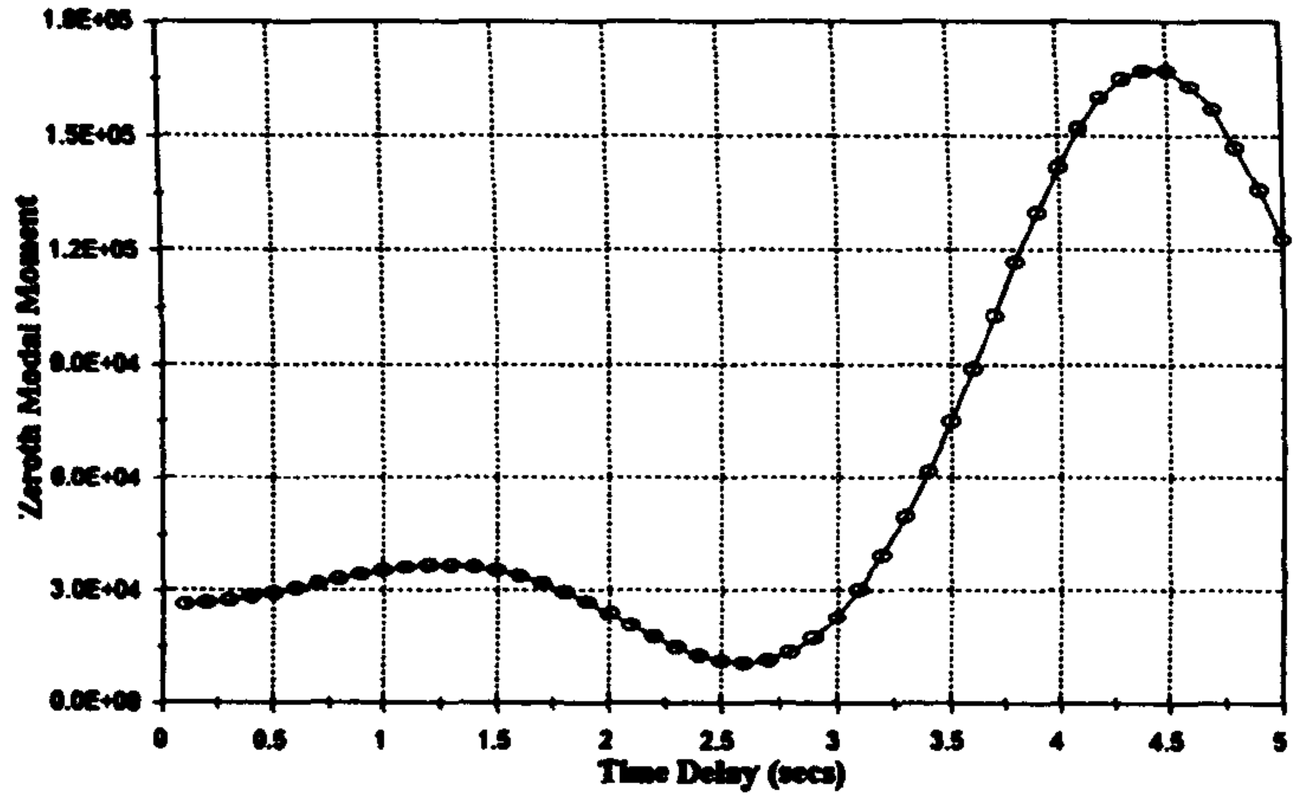

Figure 5.9a -:- Mean Square Response Mode One General Excitation

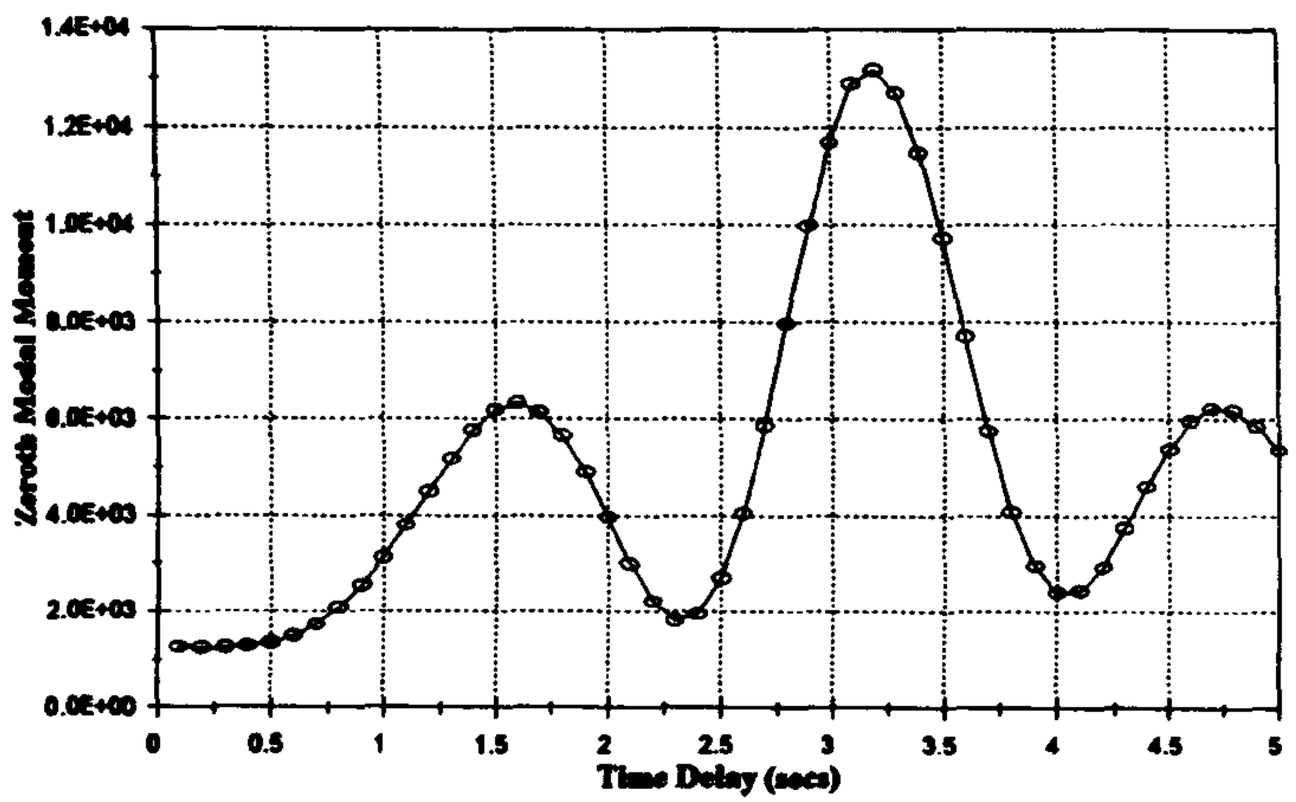

Figure 5.9b -:- Mean Square Response Mode Two General Excitation

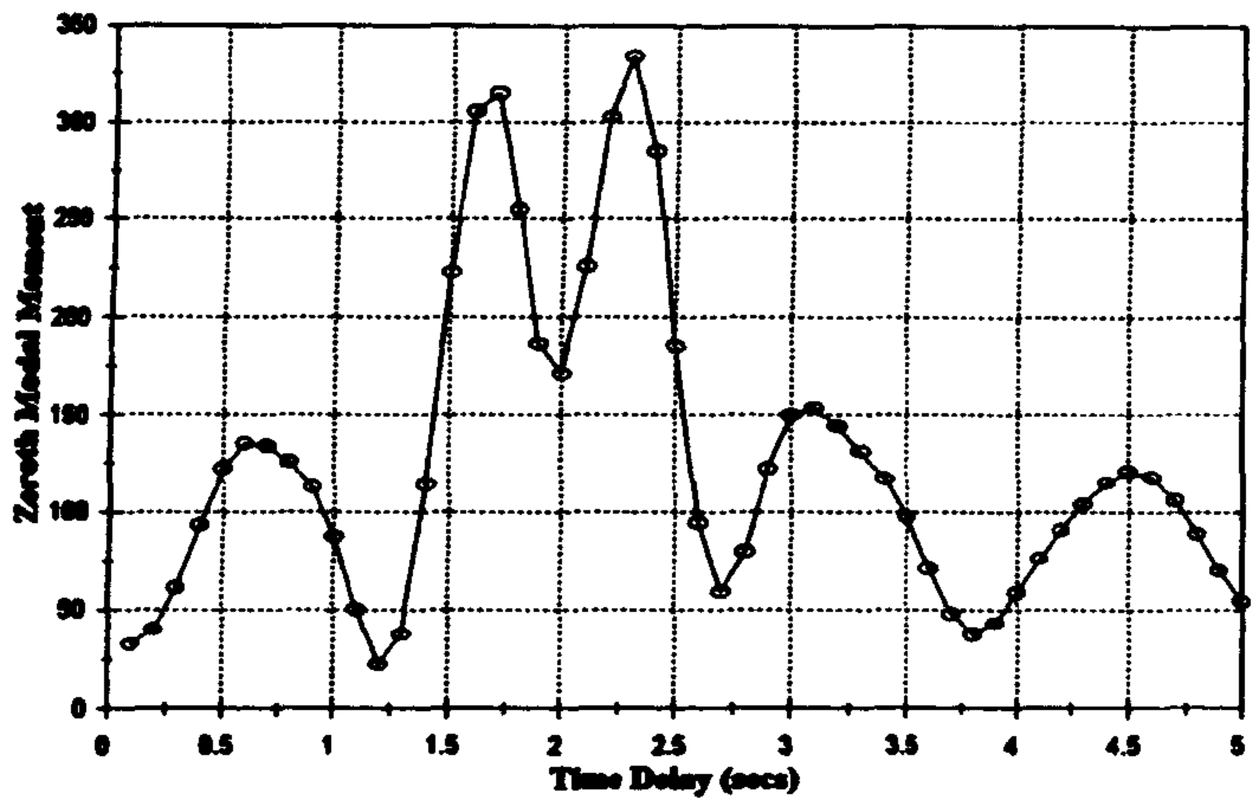

Figure 5.9c -:- Mean Square Response Mode Two General Excitation

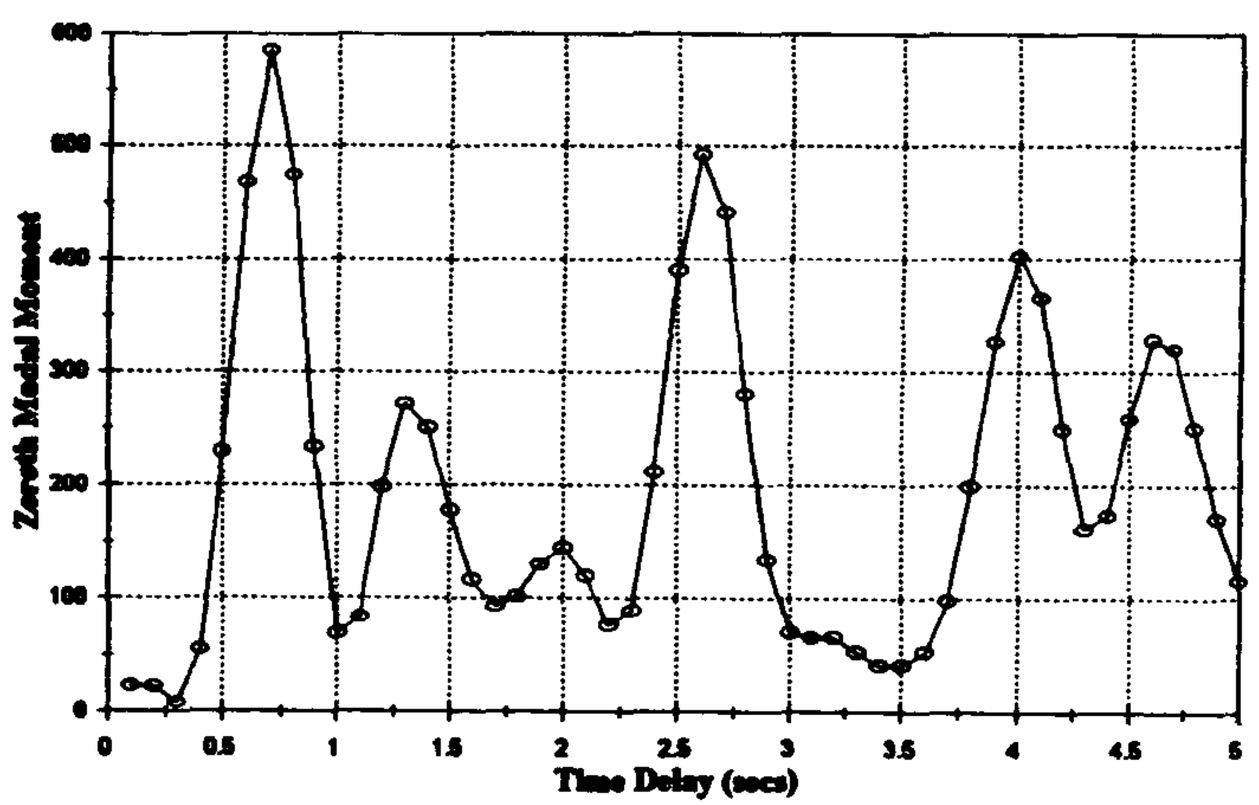

Figure 5.9d -:- Mean Square Response Mode Four General Excitation

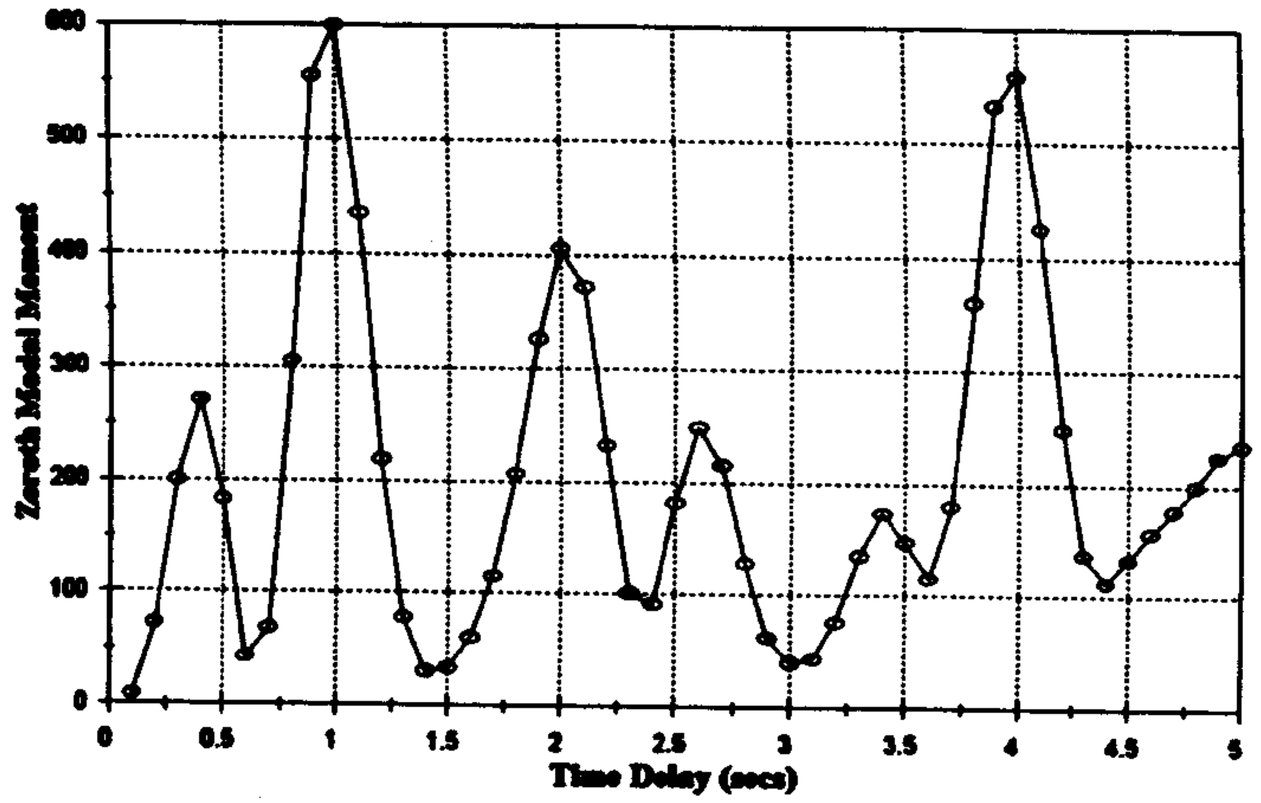

Figure 5.9e -:- Mean Square Response Mode Five General Excitation

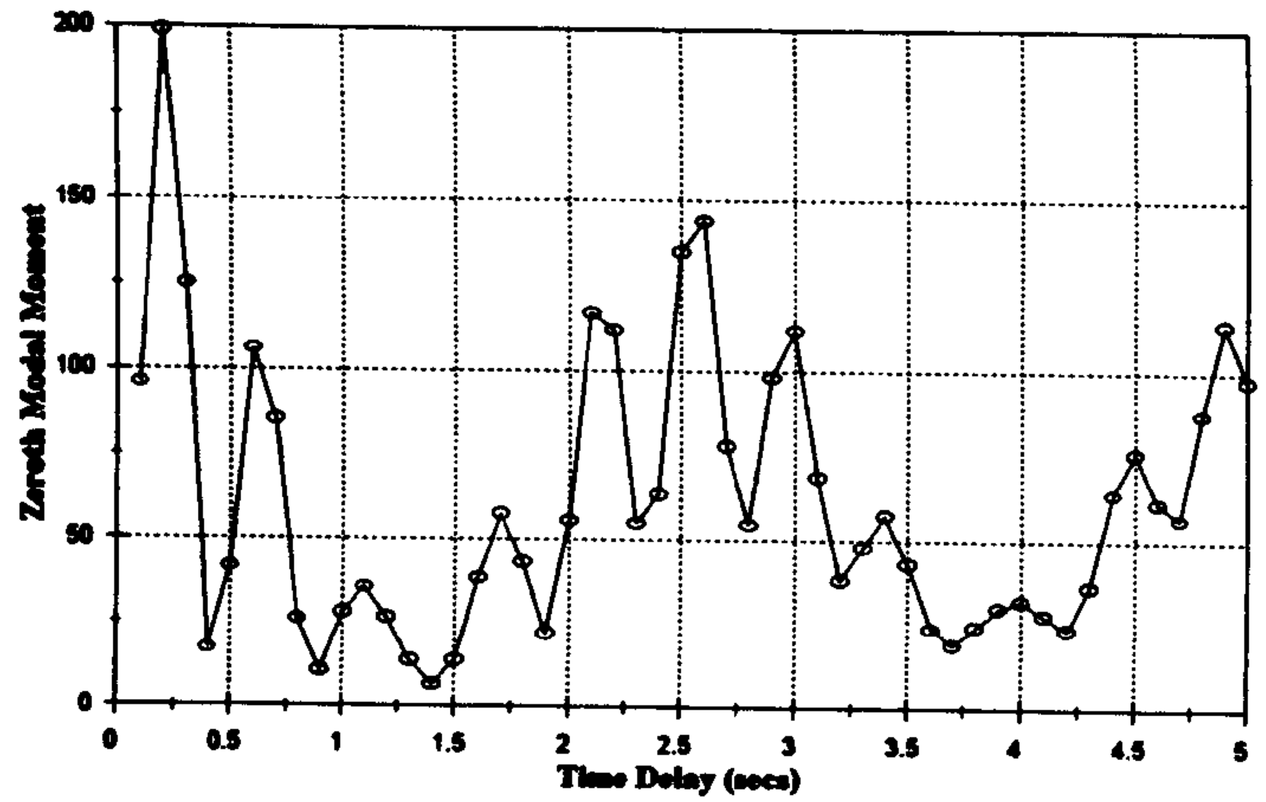

Figure 5.9f -:- Mean Square Response Mode Six General Excitation

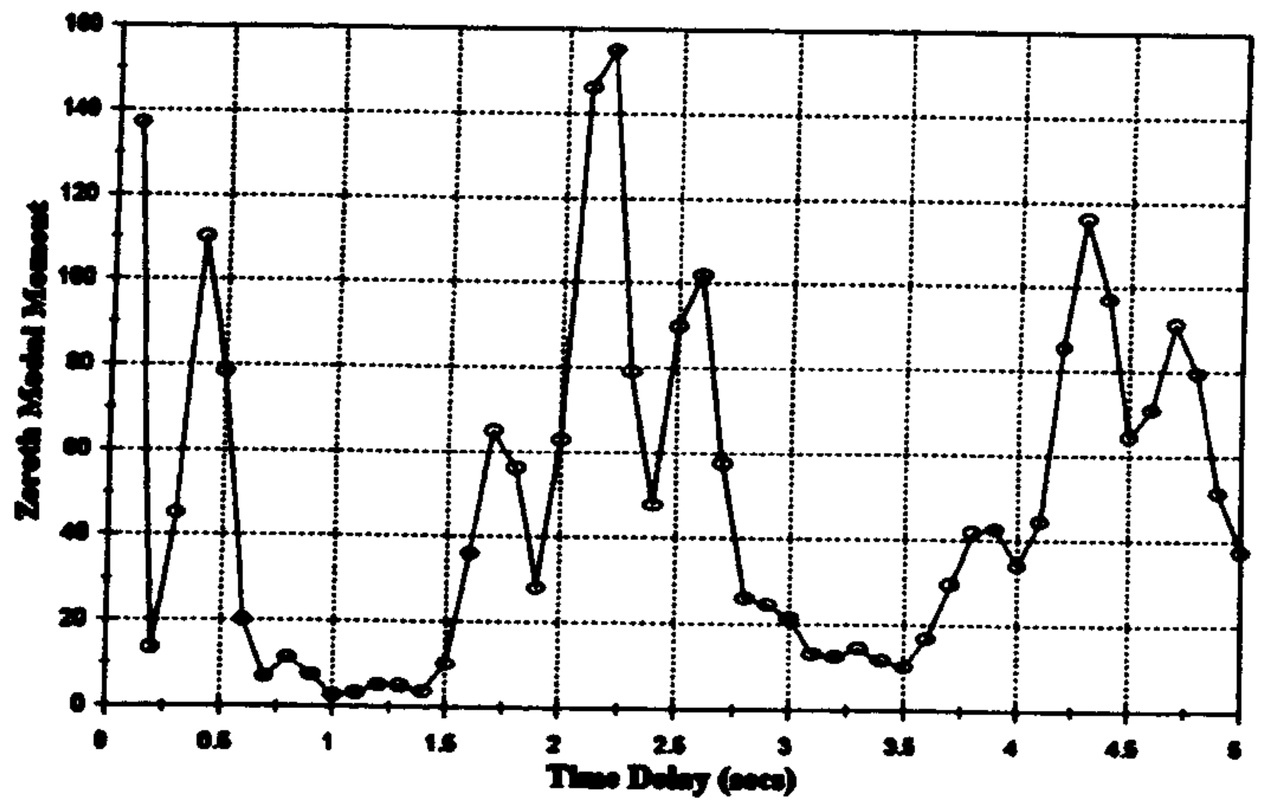

Figure 5.9g -:- Mean Square Response Mode Seven General Excitation

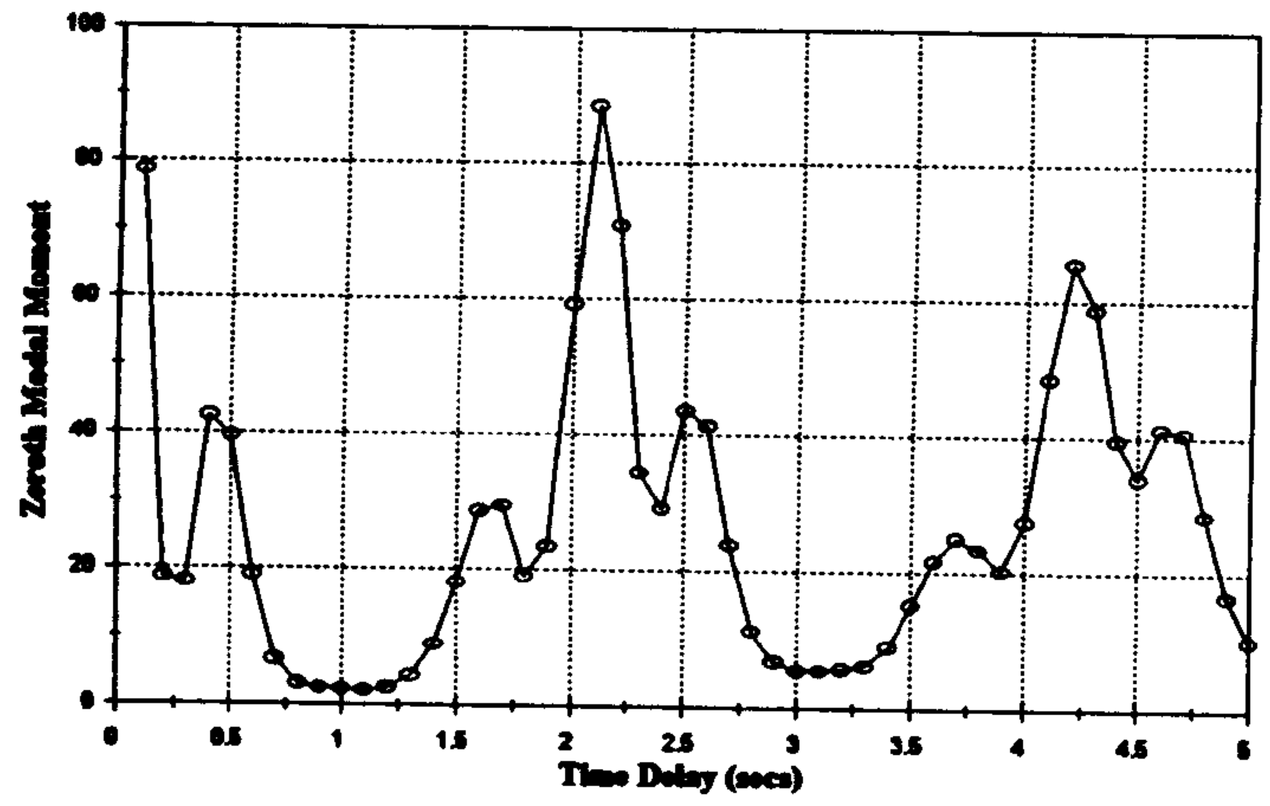

Figure 5.9h -:- Mean Square Response Mode Eight General Excitation

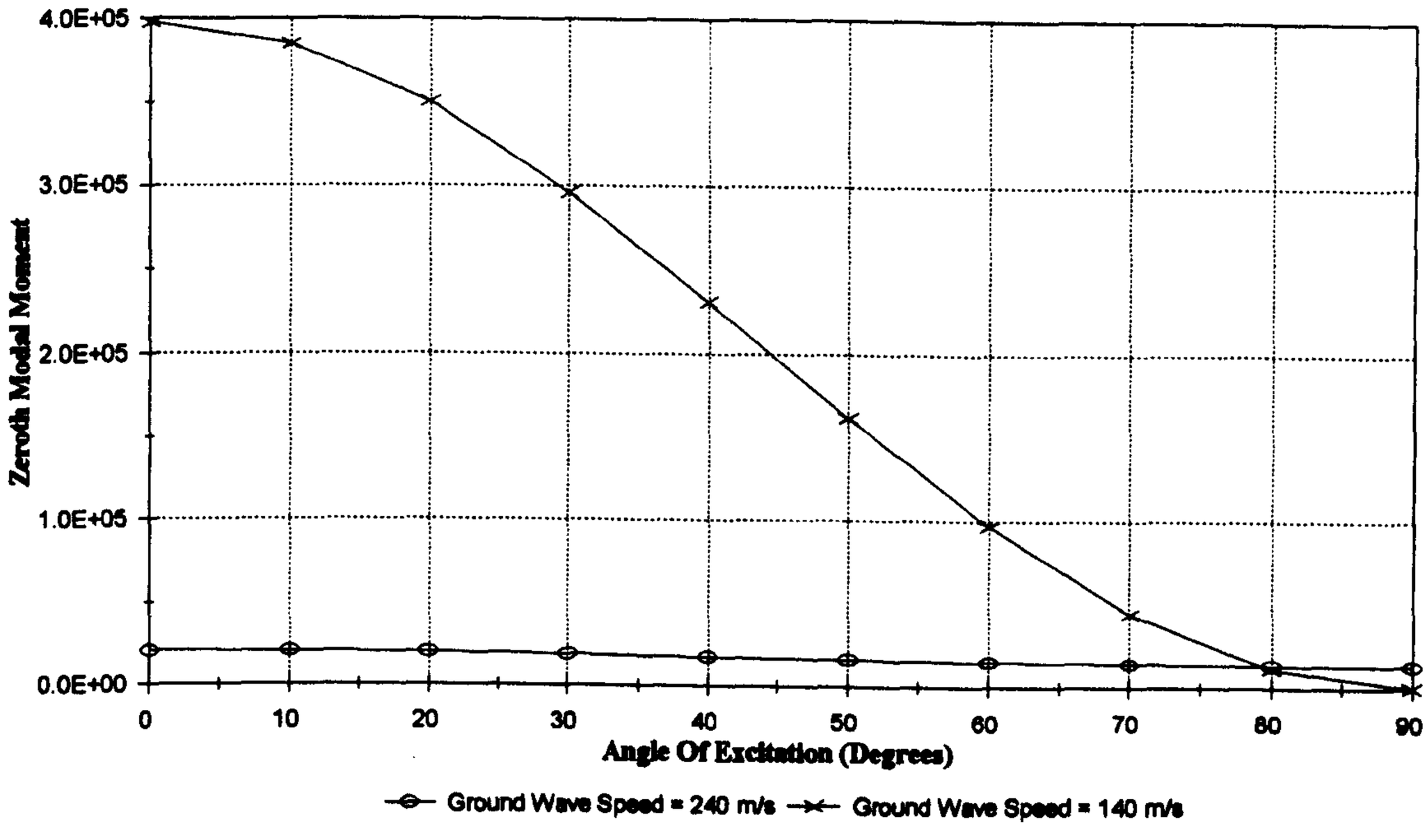

Figure 5.10 -:- Variation Of Mode One Response With Angle Of Excitation

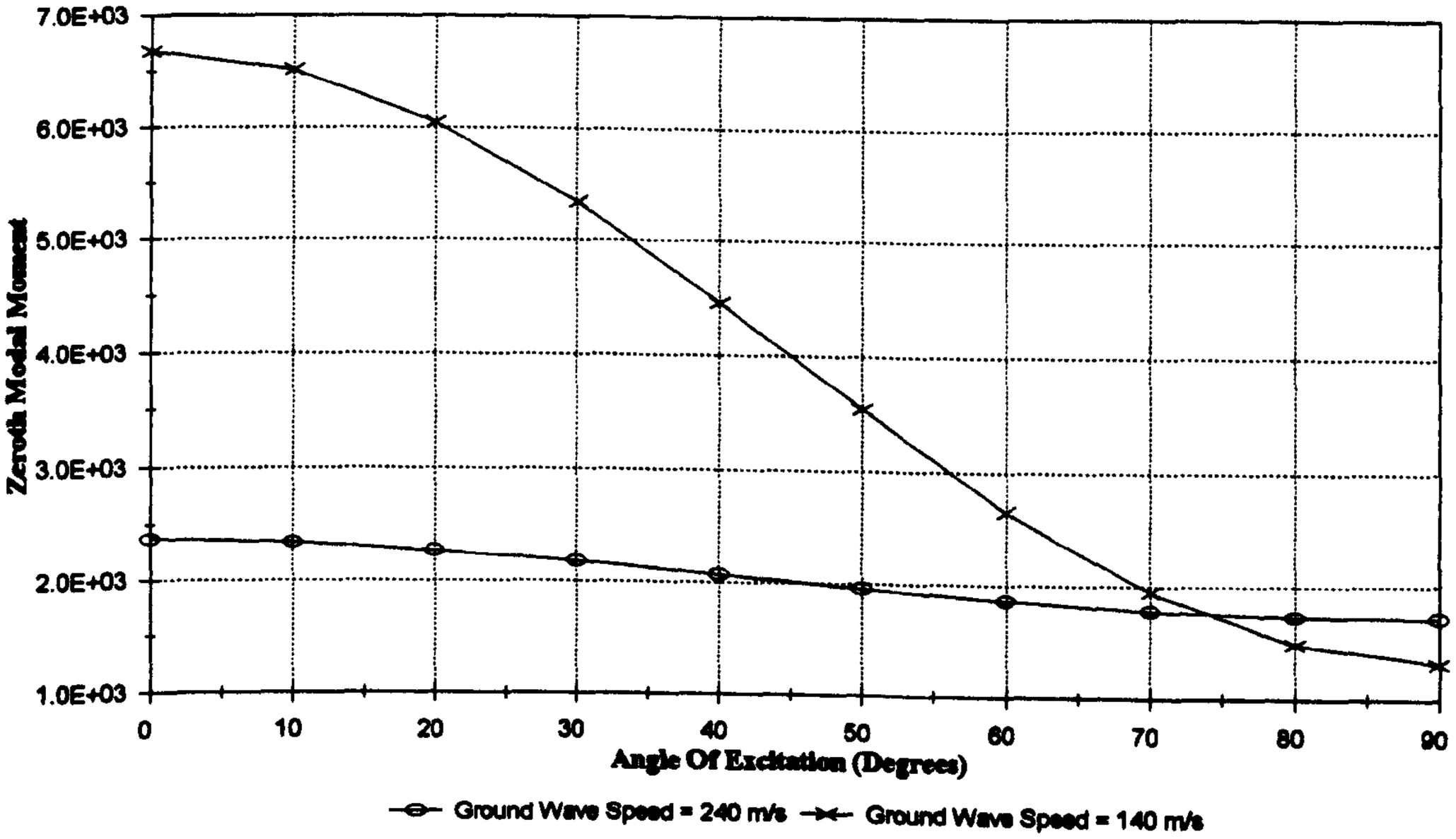

Figure 5.11 -:- Variation Of Mode Two Response With Angle Of Excitation

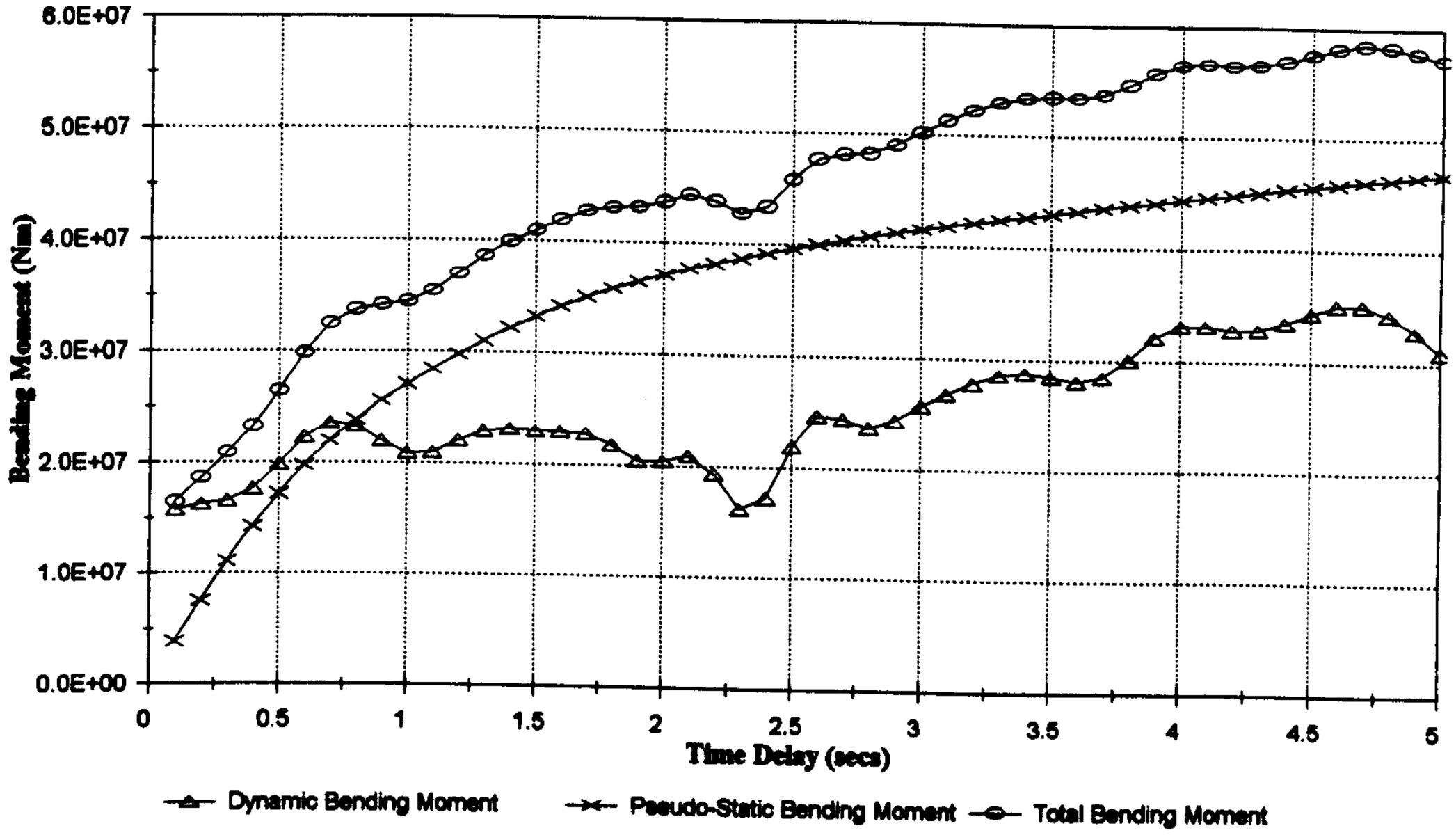

Figure 5.12 -:- RMS Bending Moments In Side Span, Vertical Excitation

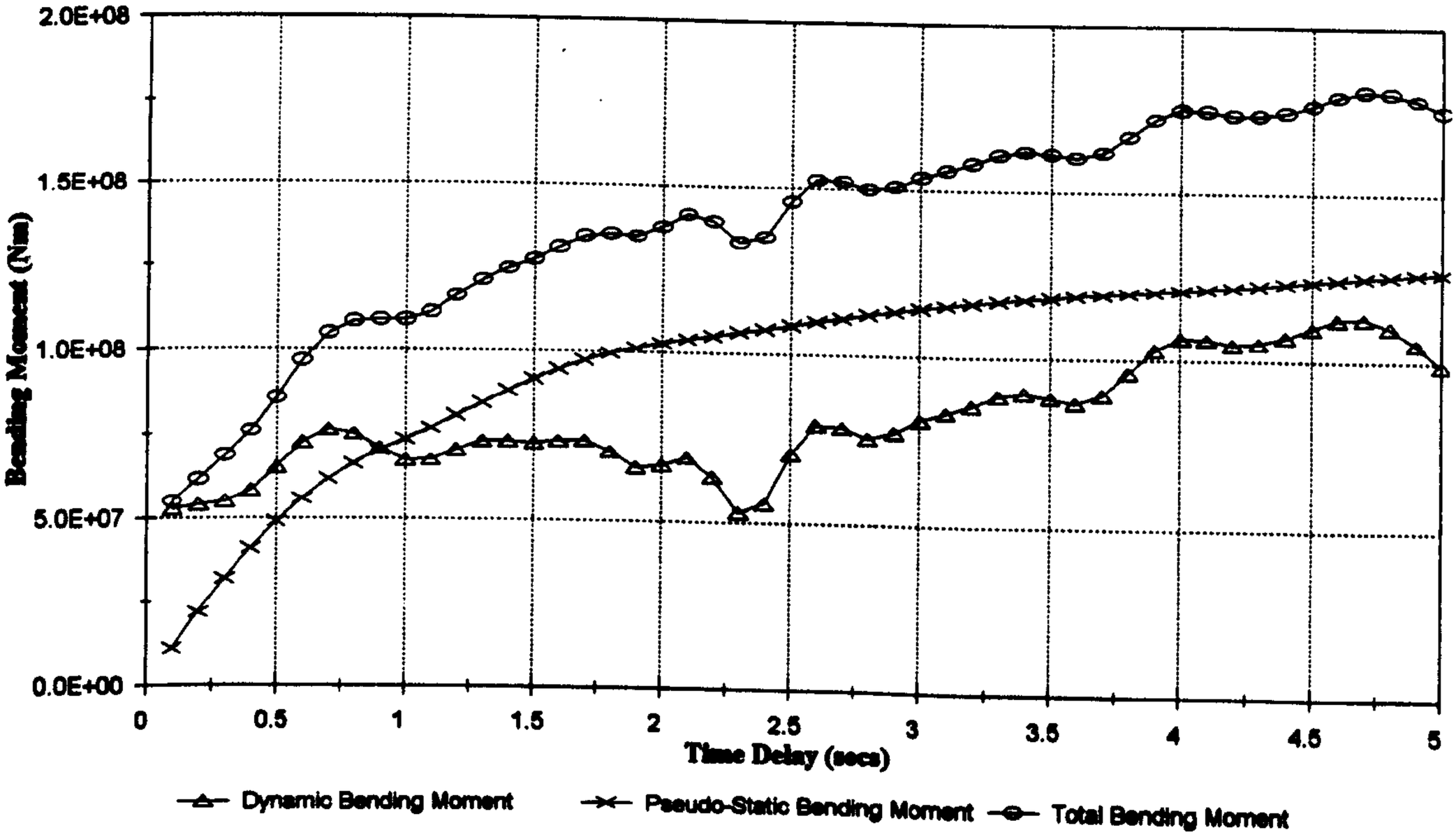

Figure 5.13 -:- Peak Bending Moments In Side Span, Vertical Excitation

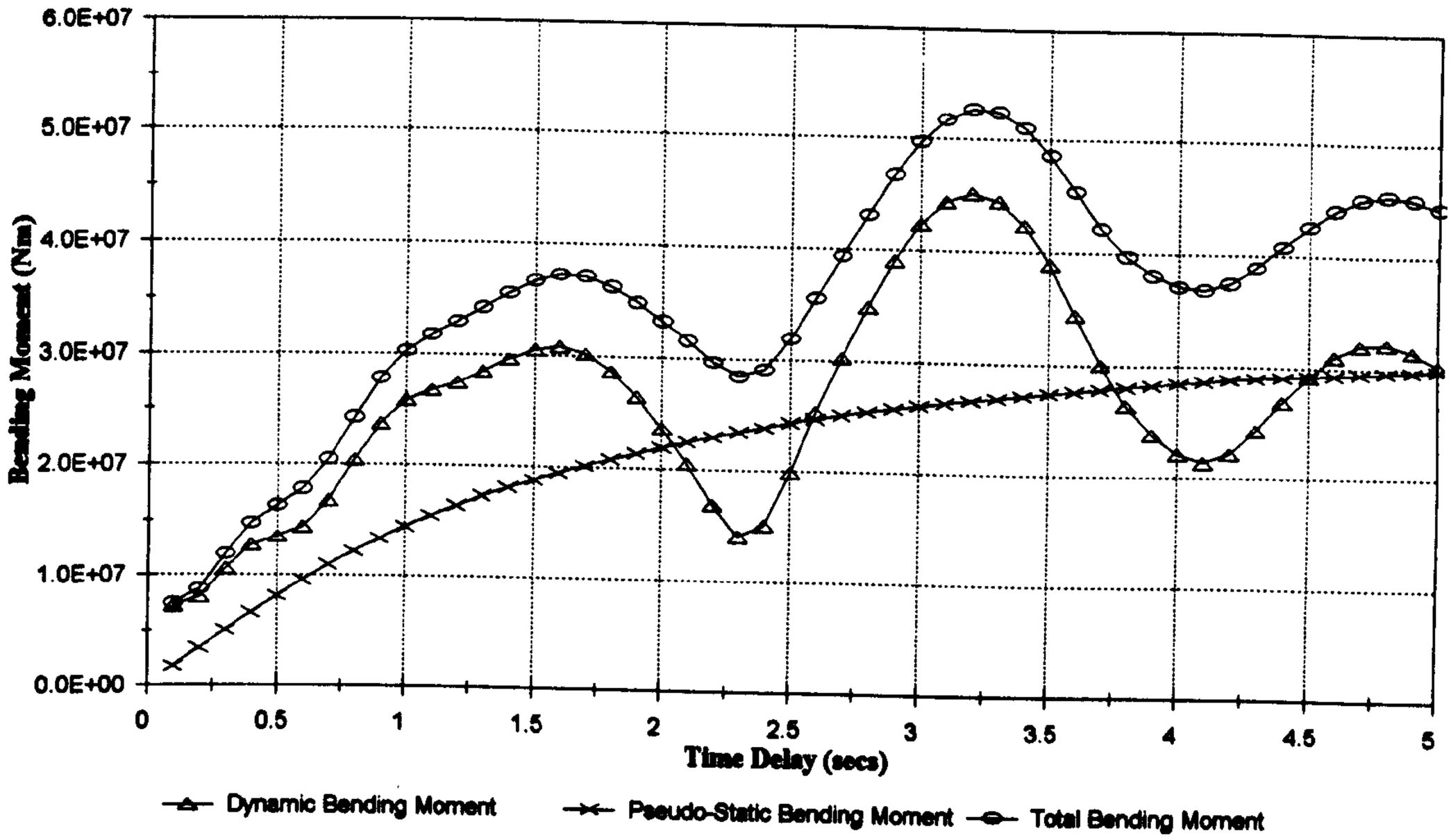

Figure 5.14 -:- RMS Bending Moments At Quarter Point, Vertical Excitation

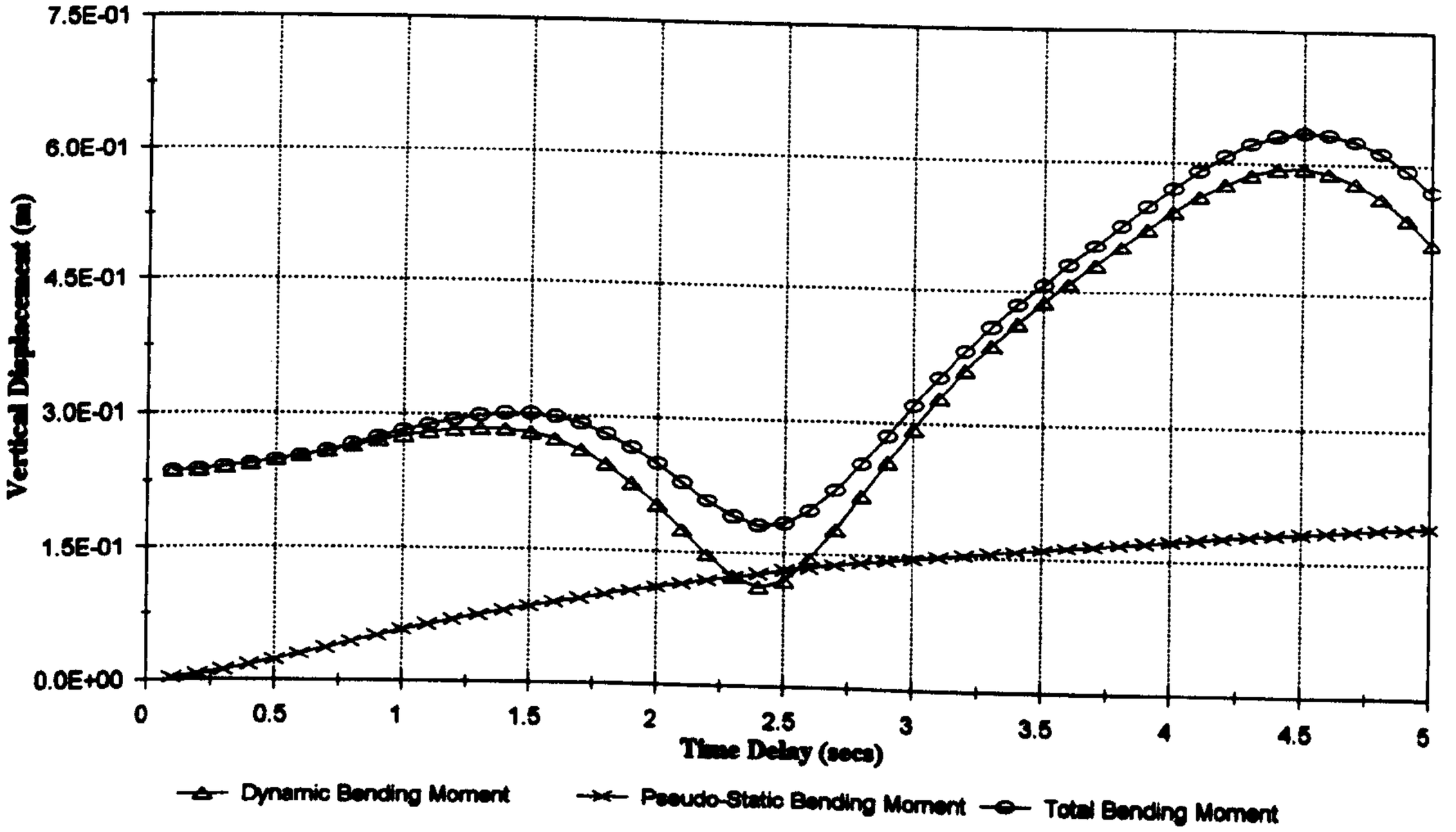

Figure 5.15 -:- RMS Displacements At Quarter Point, Vertical Excitation

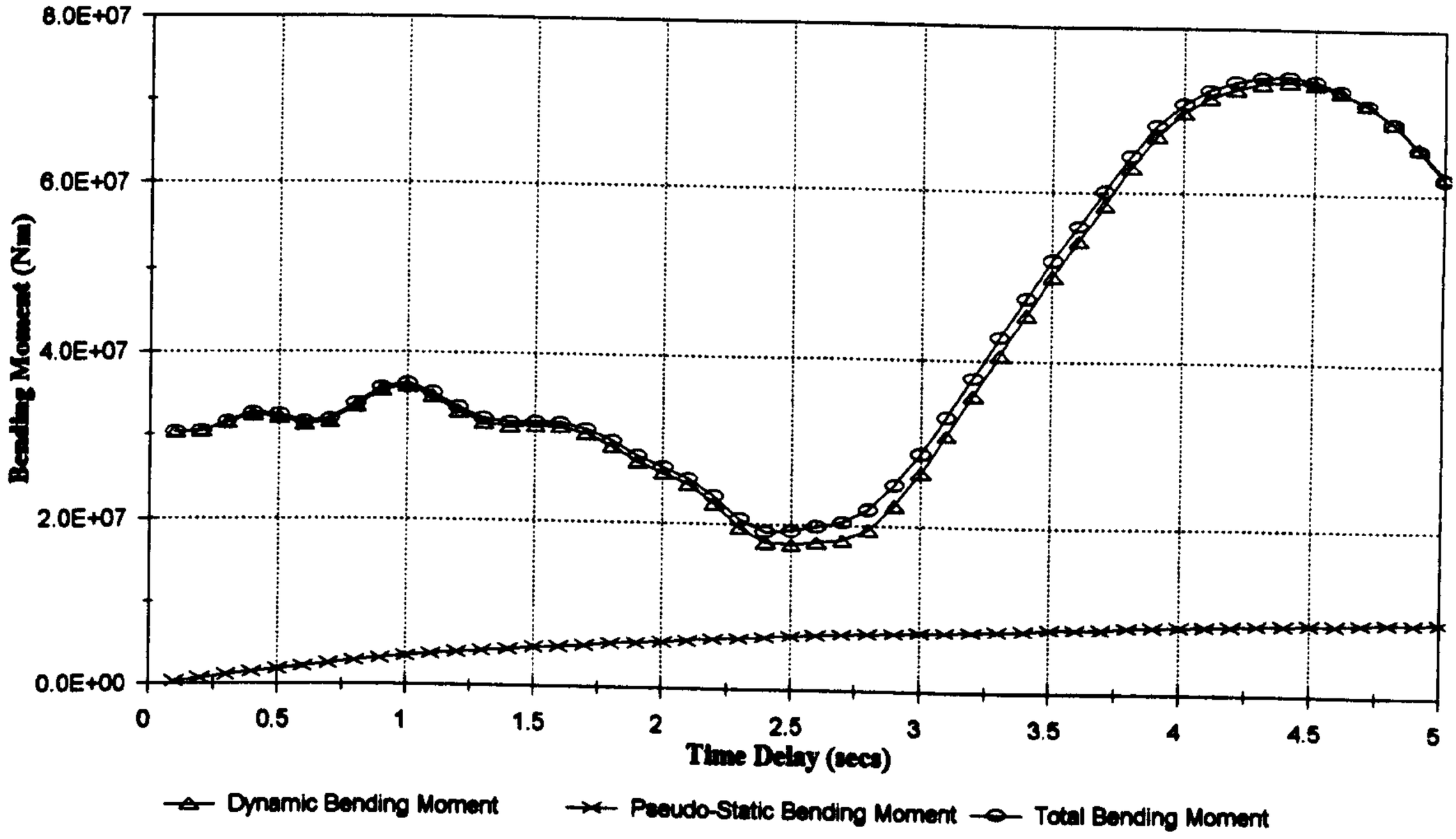

Figure 5.16 -:- RMS Bending Moments At Mid Span, Vertical Excitation

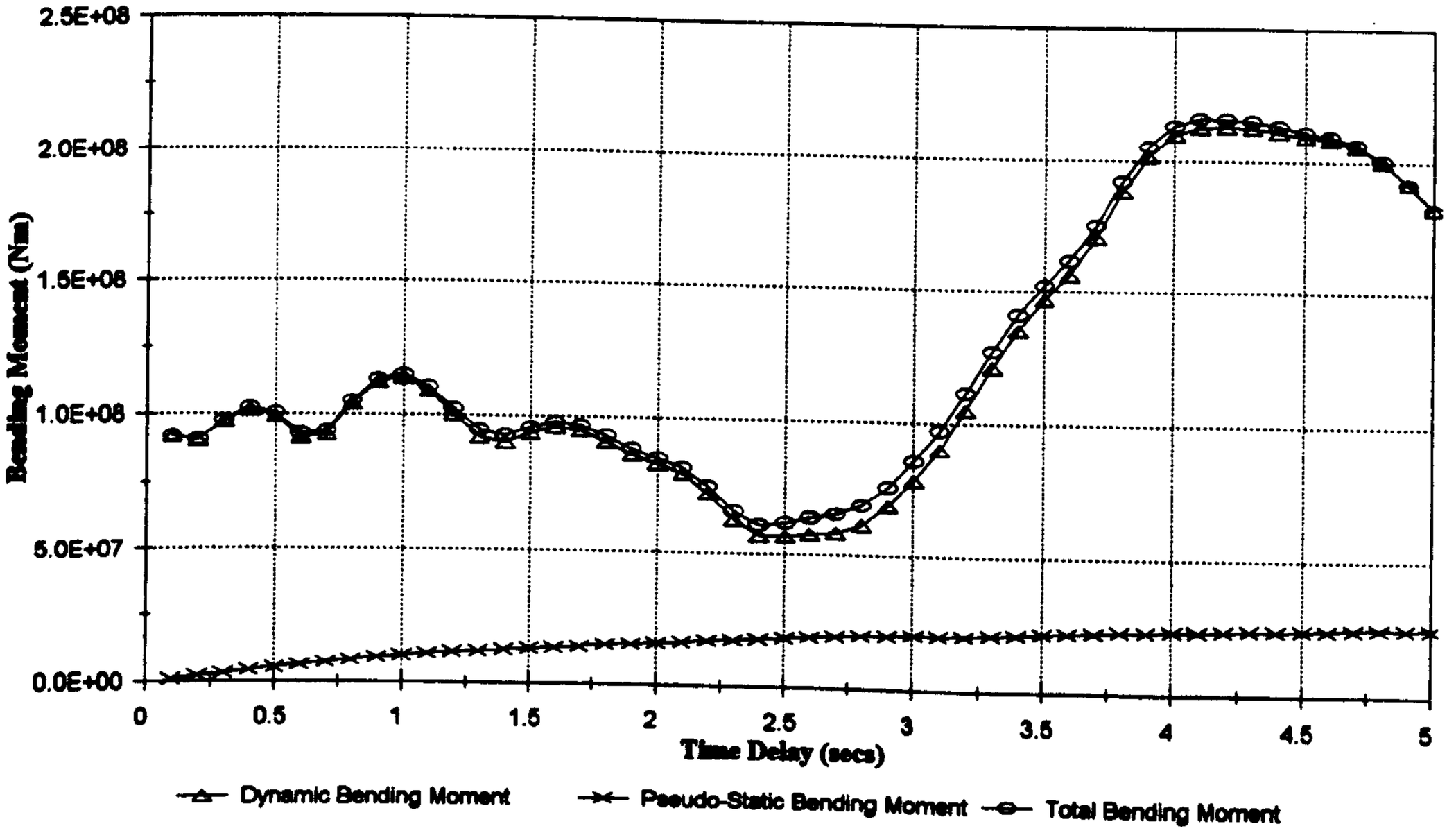

Figure 5.17 -:- Peak Bending Moments At Mid Span, Vertical Excitation

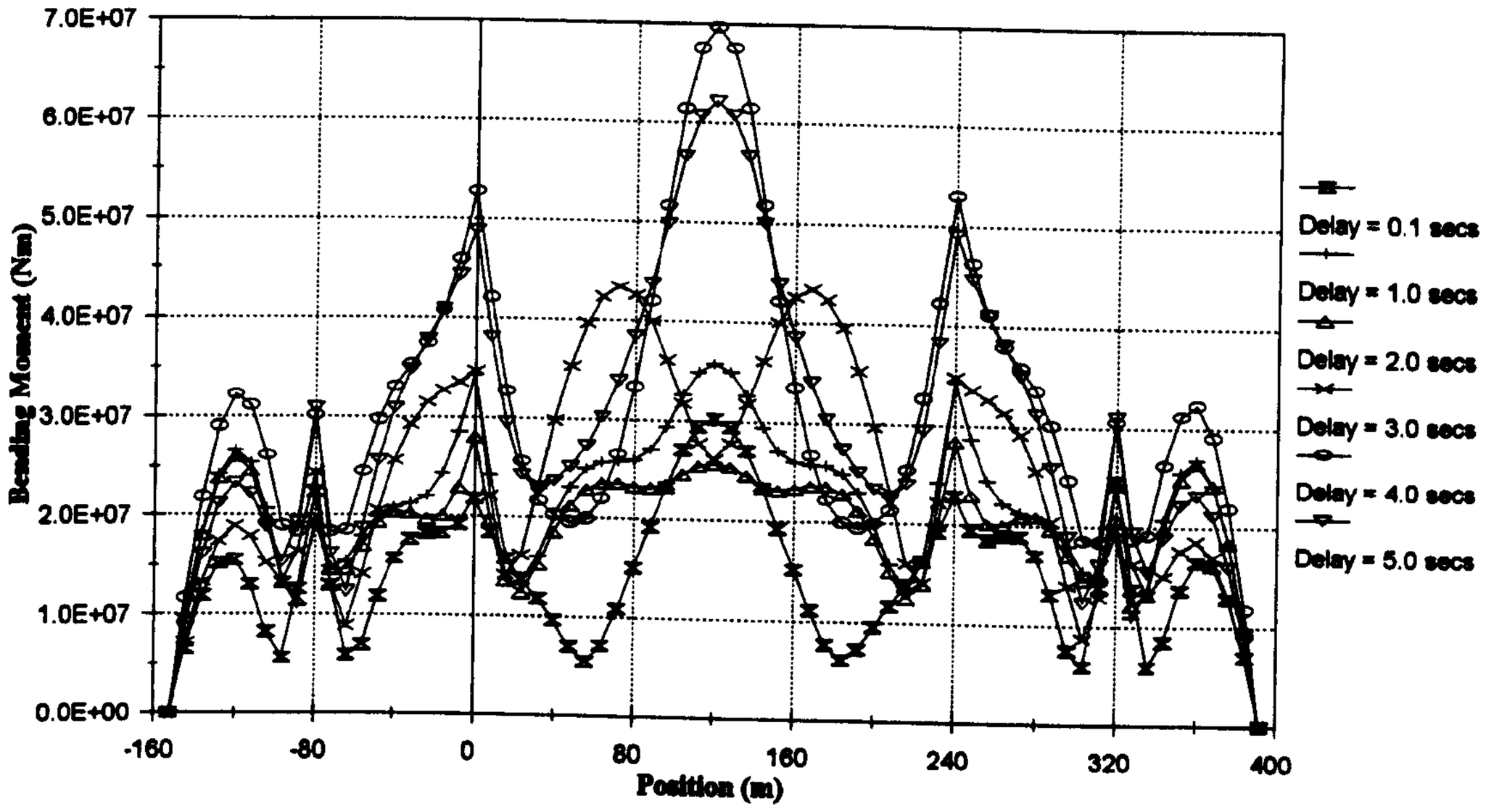

Figure 5.18 -:- RMS Dynamic Bending Moments, Vertical Excitation

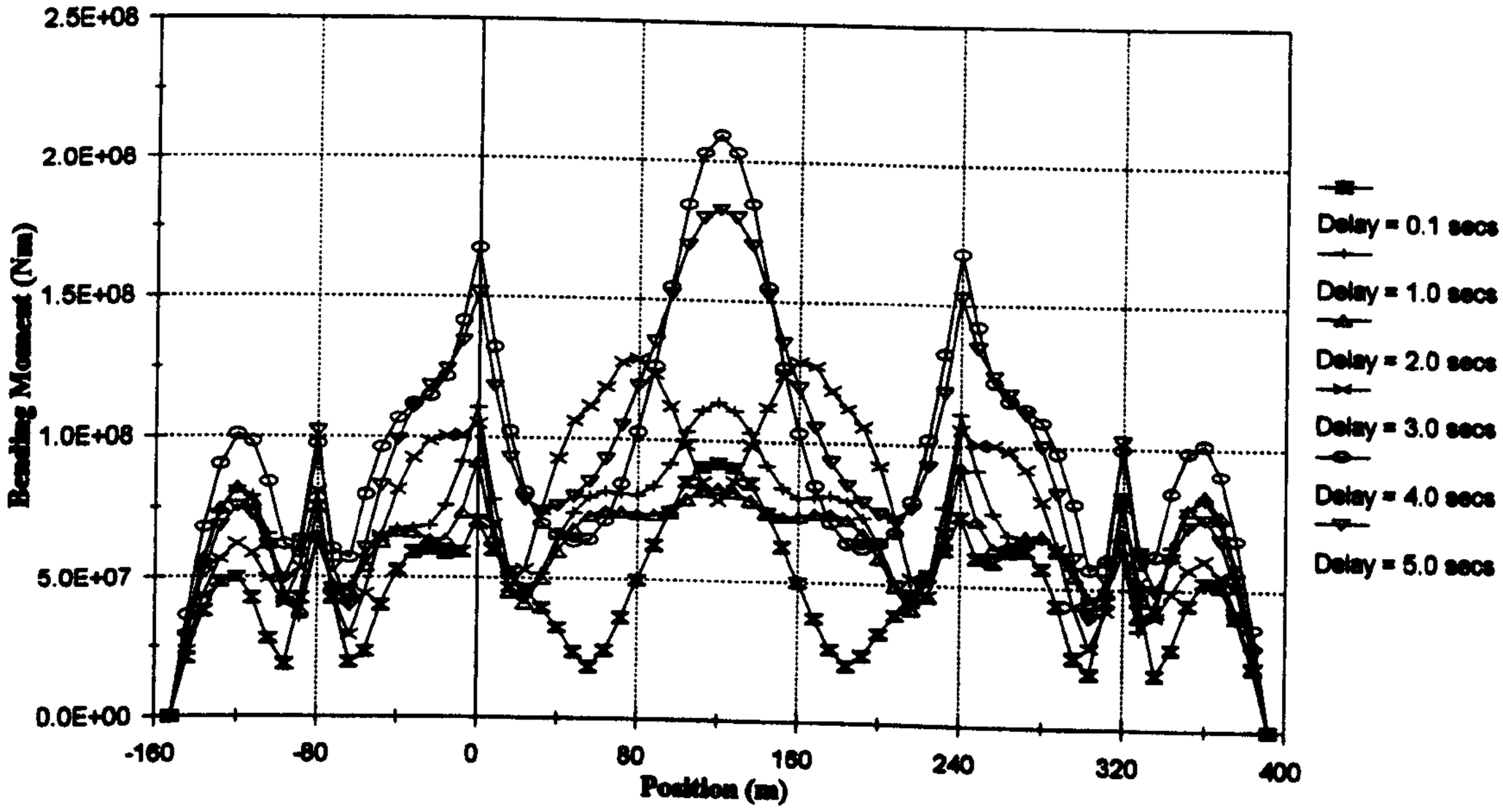

Figure 5.19 -:- Peak Dynamic Bending Moments, Vertical Excitation

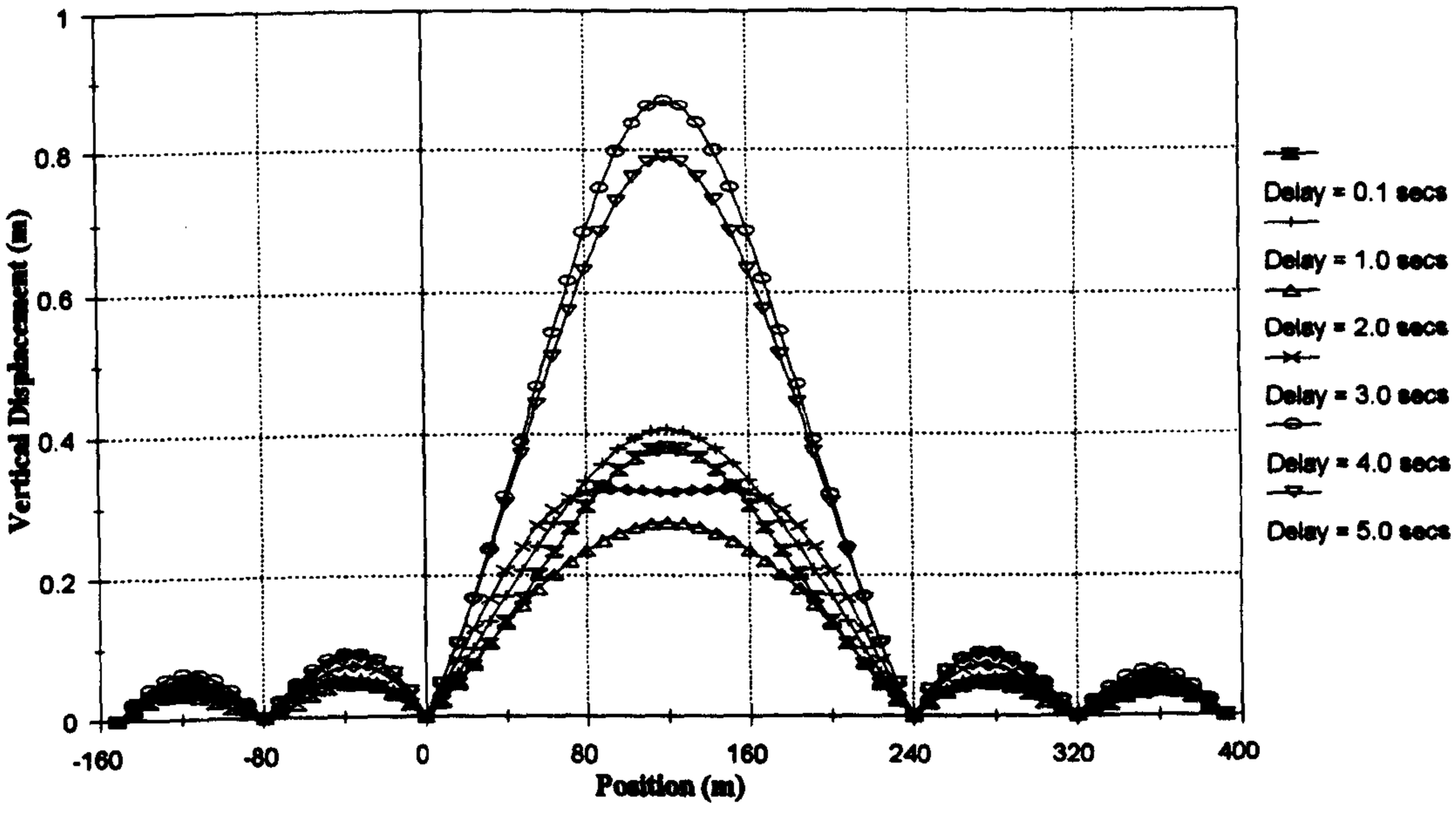

Figure 5.20 -:- RMS Dynamic Deck Displacements, Vertical Excitation

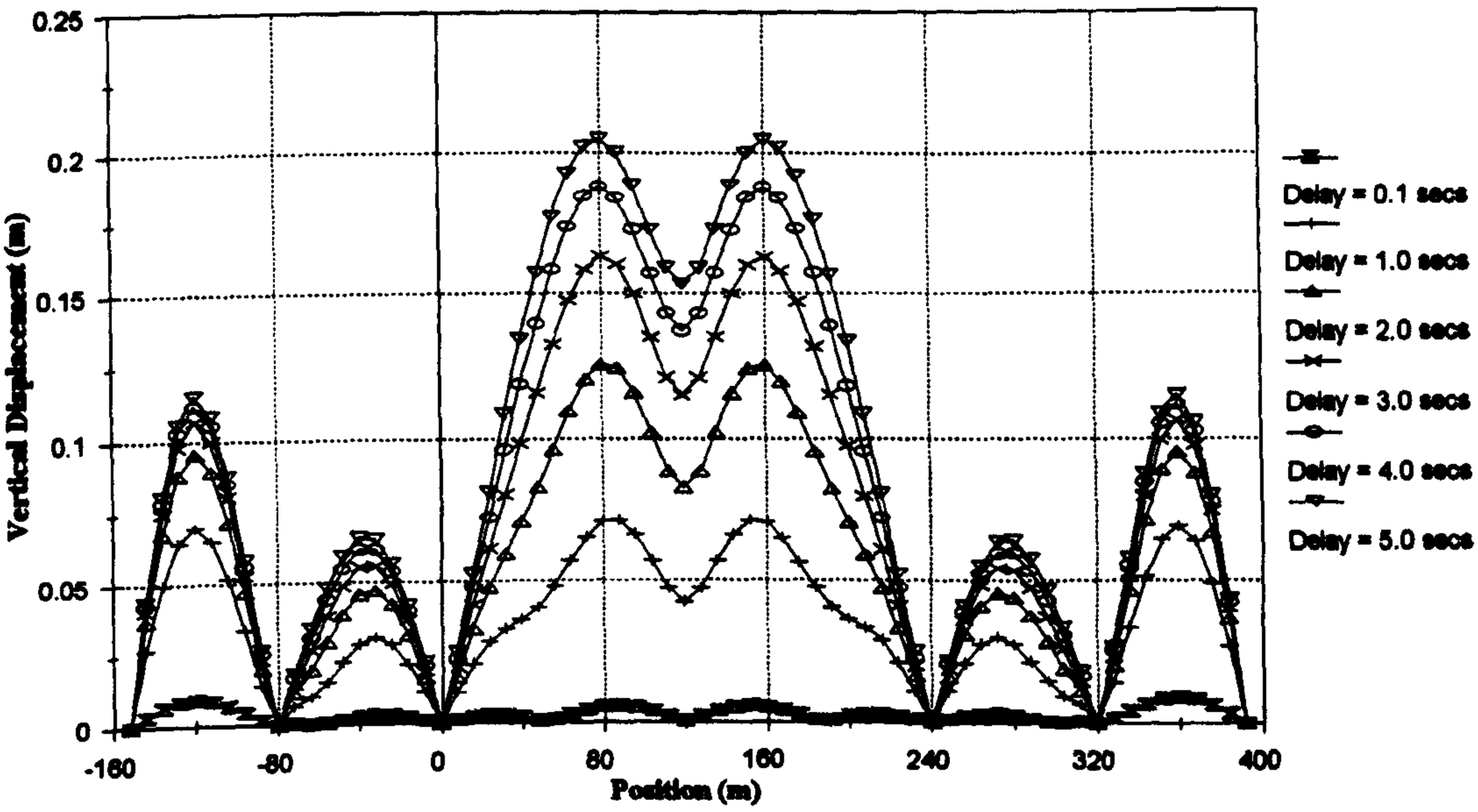

Figure 5.21 -:- RMS Pseudo Static Deck Displacements, Vertical Excitation

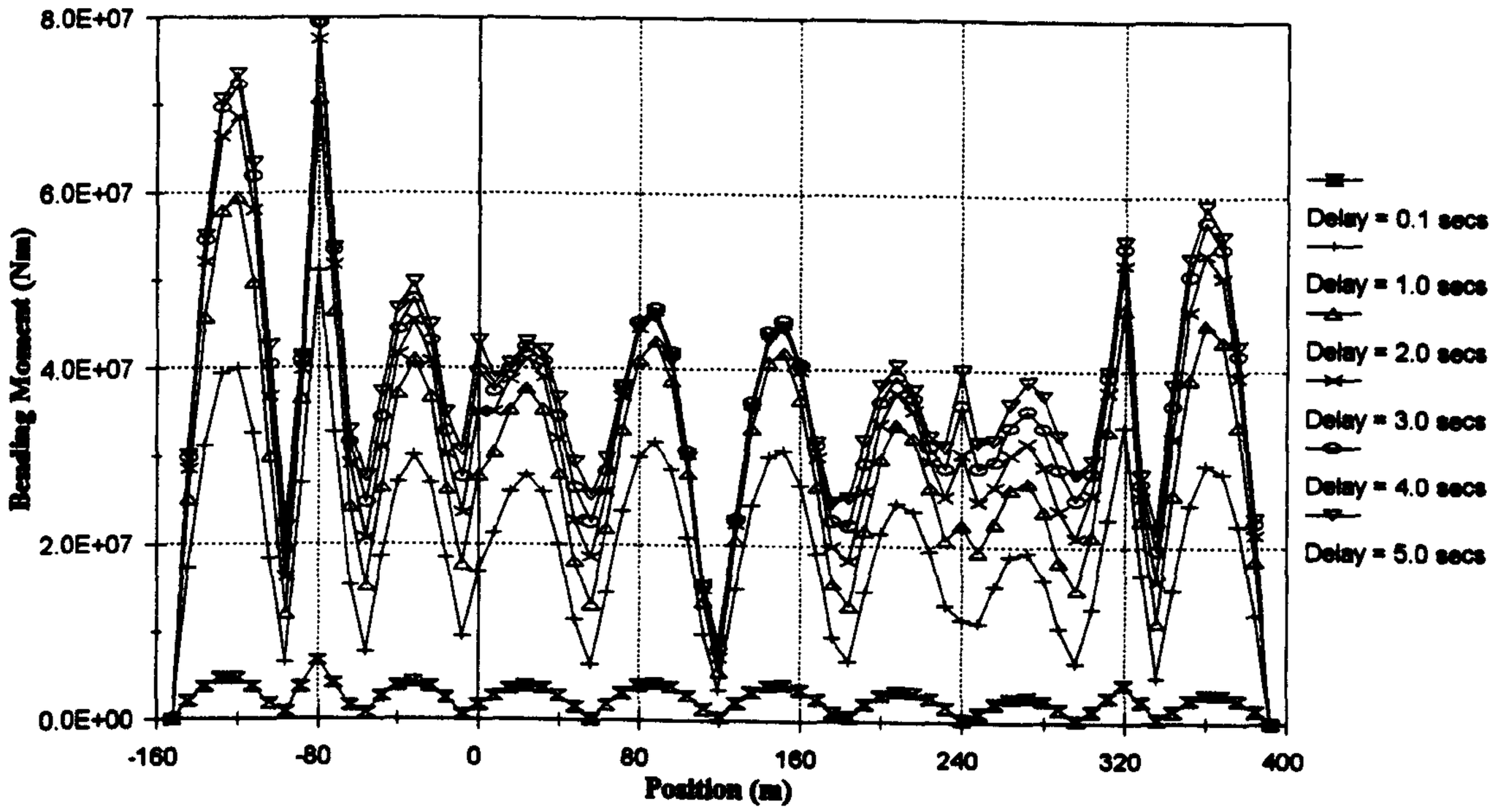

Figure 5.22 -:- RMS Pseudo-Static Bending Moments, Vertical Excitation

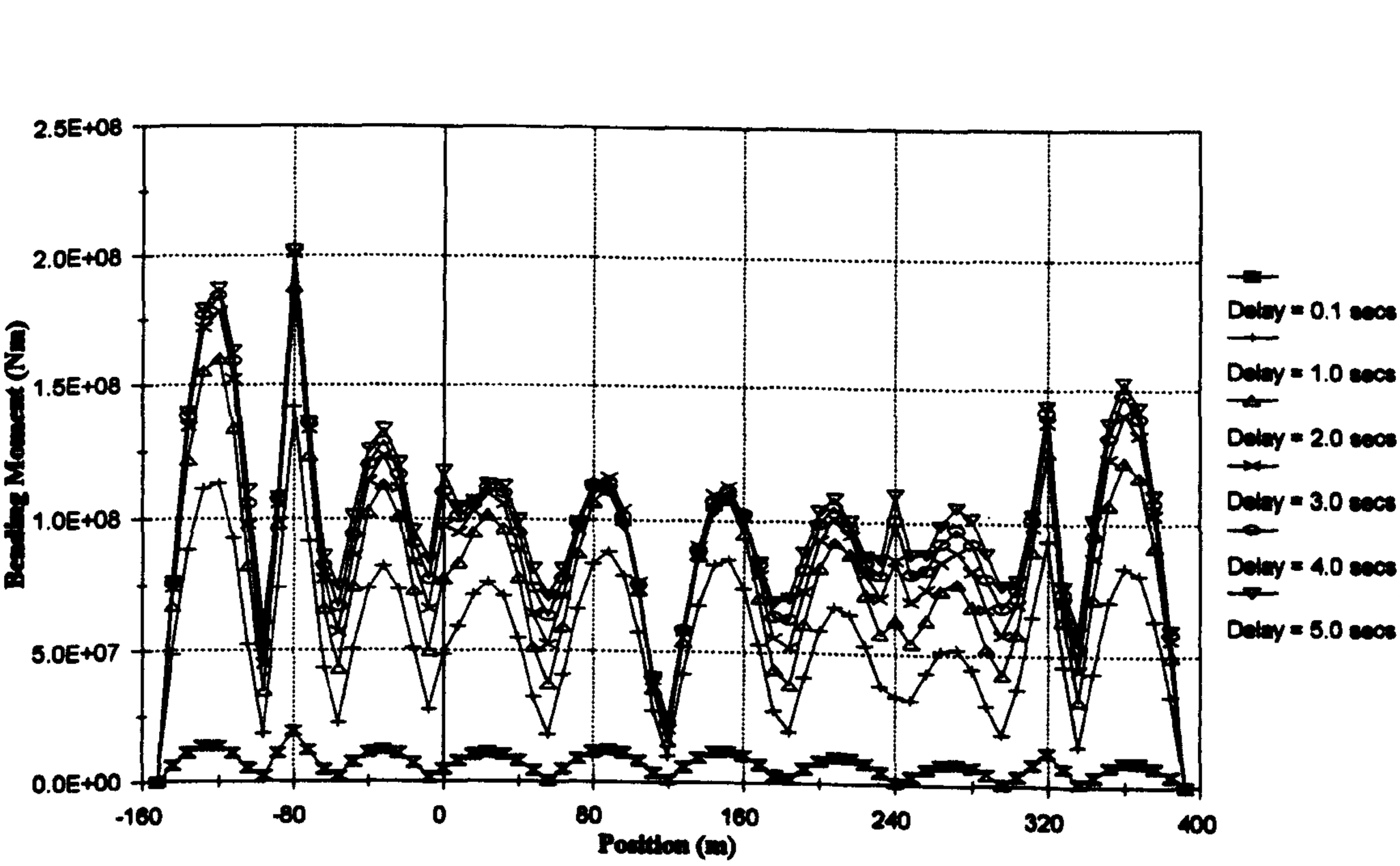

Figure 5.23 -:- Peak Pseudo-Static Bending Moments, Vertical Excitation

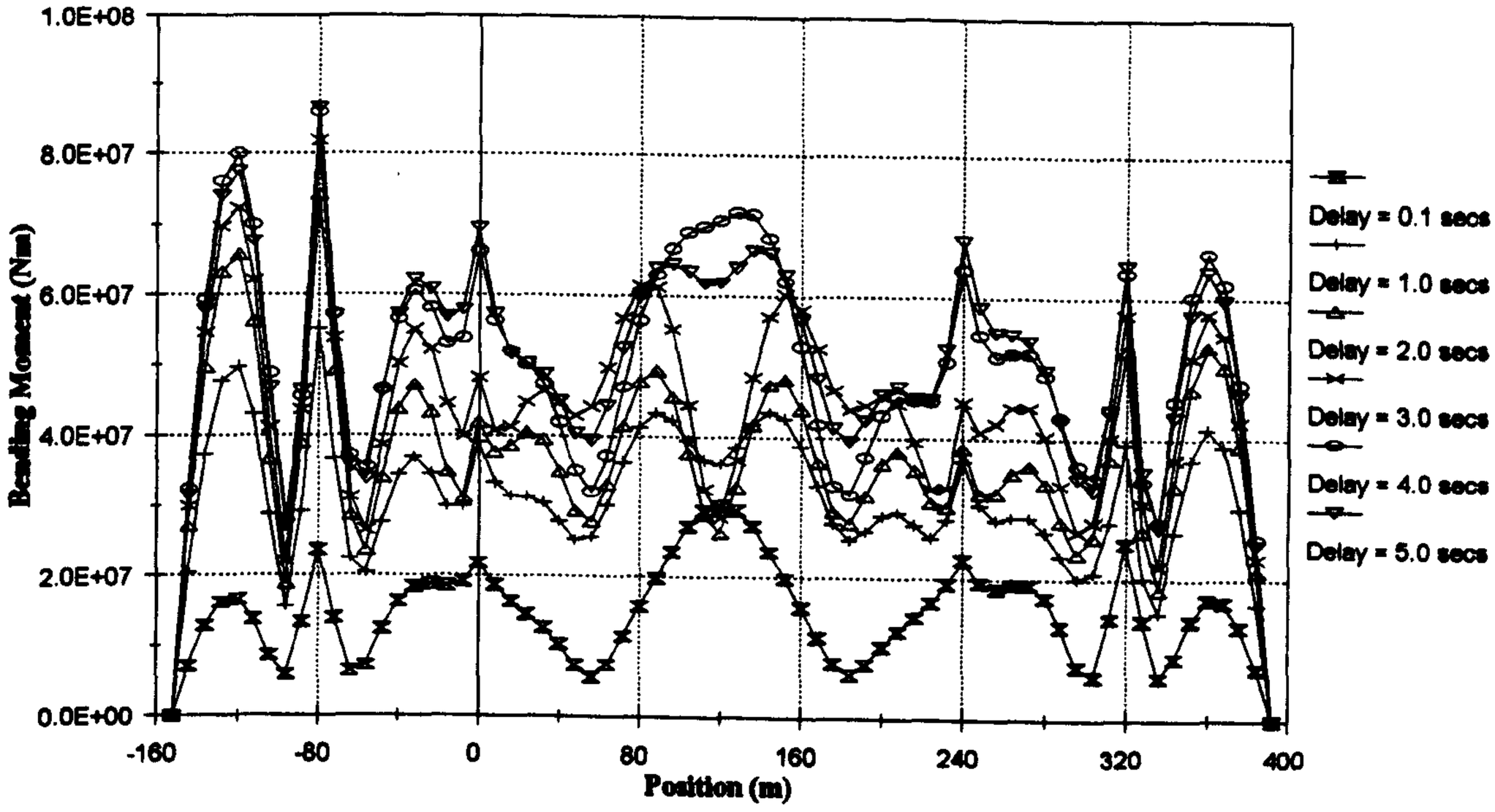

Figure 5.24 -:- RMS Total Bending Moments, Vertical Excitation

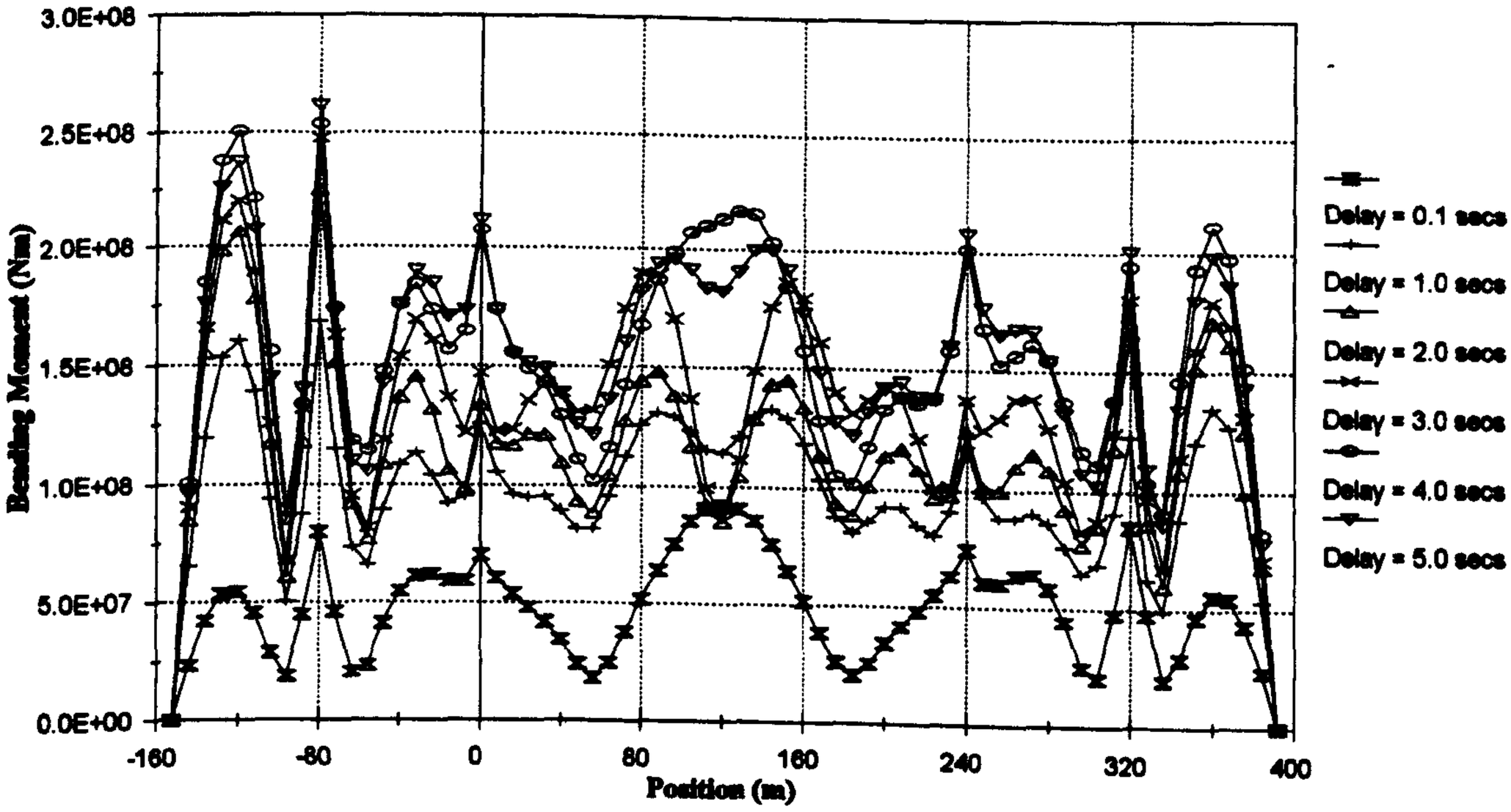

Figure 5.25 -:- Peak Total Bending Moments, Vertical Excitation

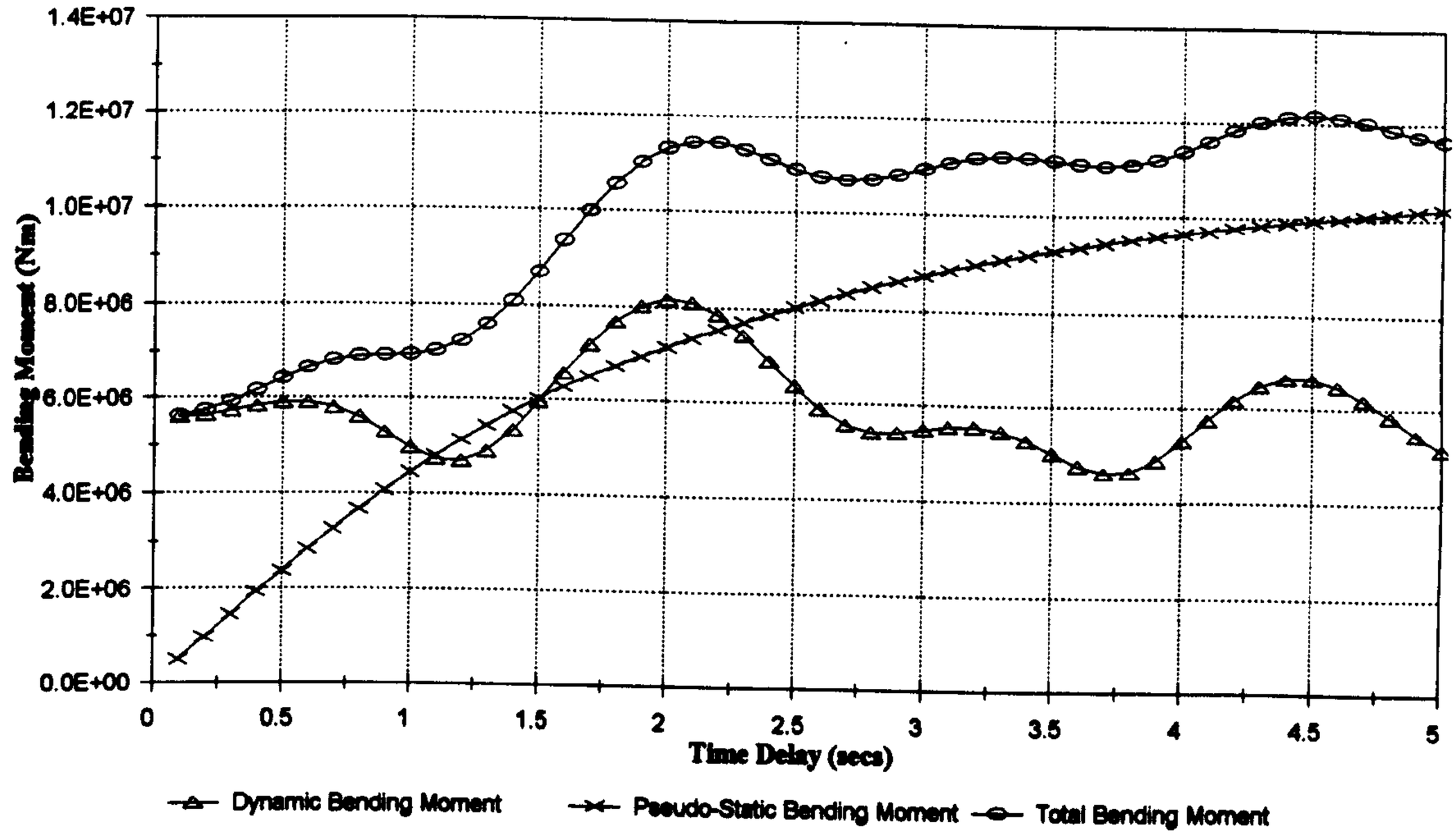

Figure 5.26 -:- RMS Bending Moments In Sidespan, Horizontal Excitation

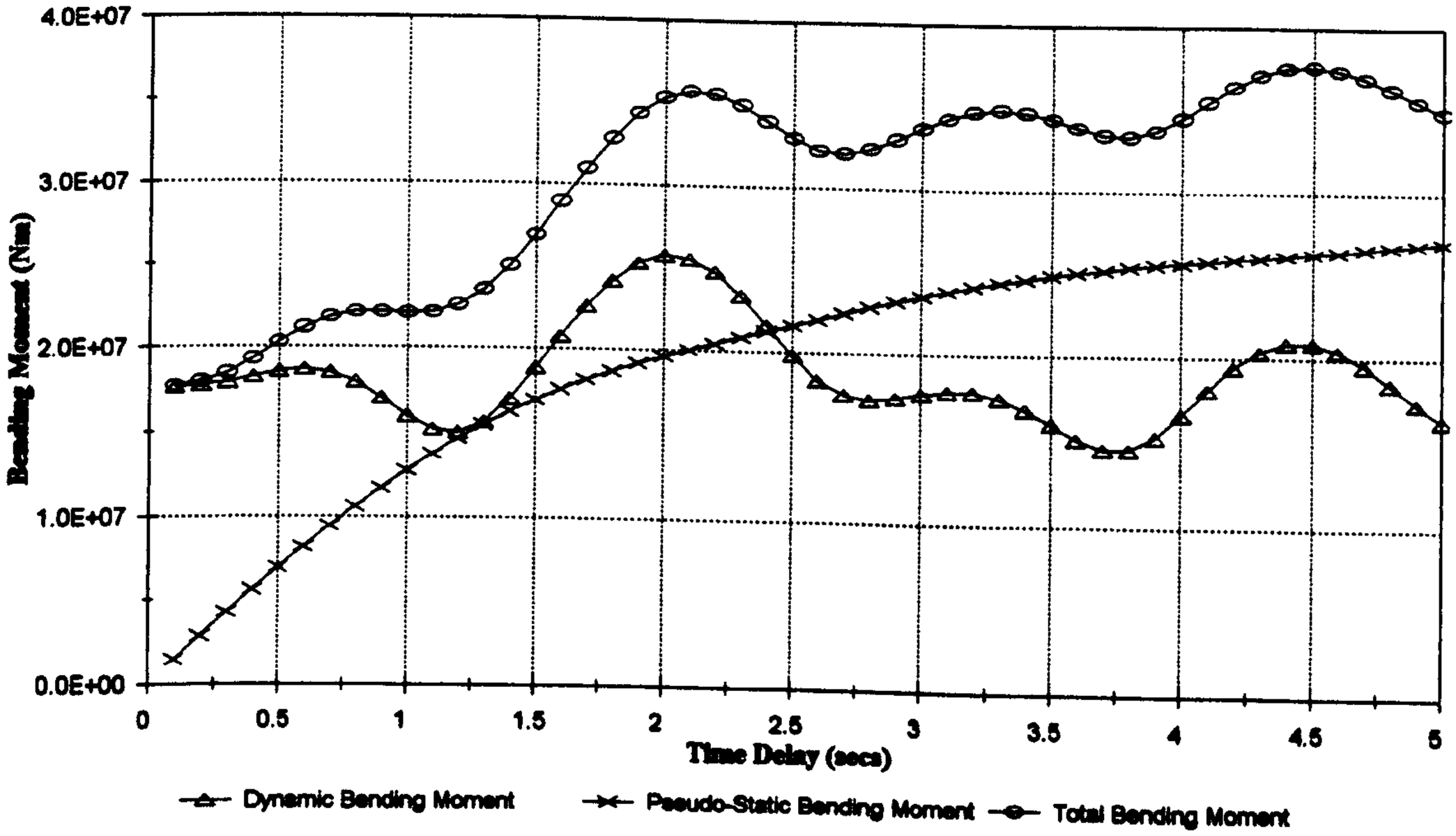

Figure 5.27 -:- Peak Bending Moments In Sidespan, Horizontal Excitation

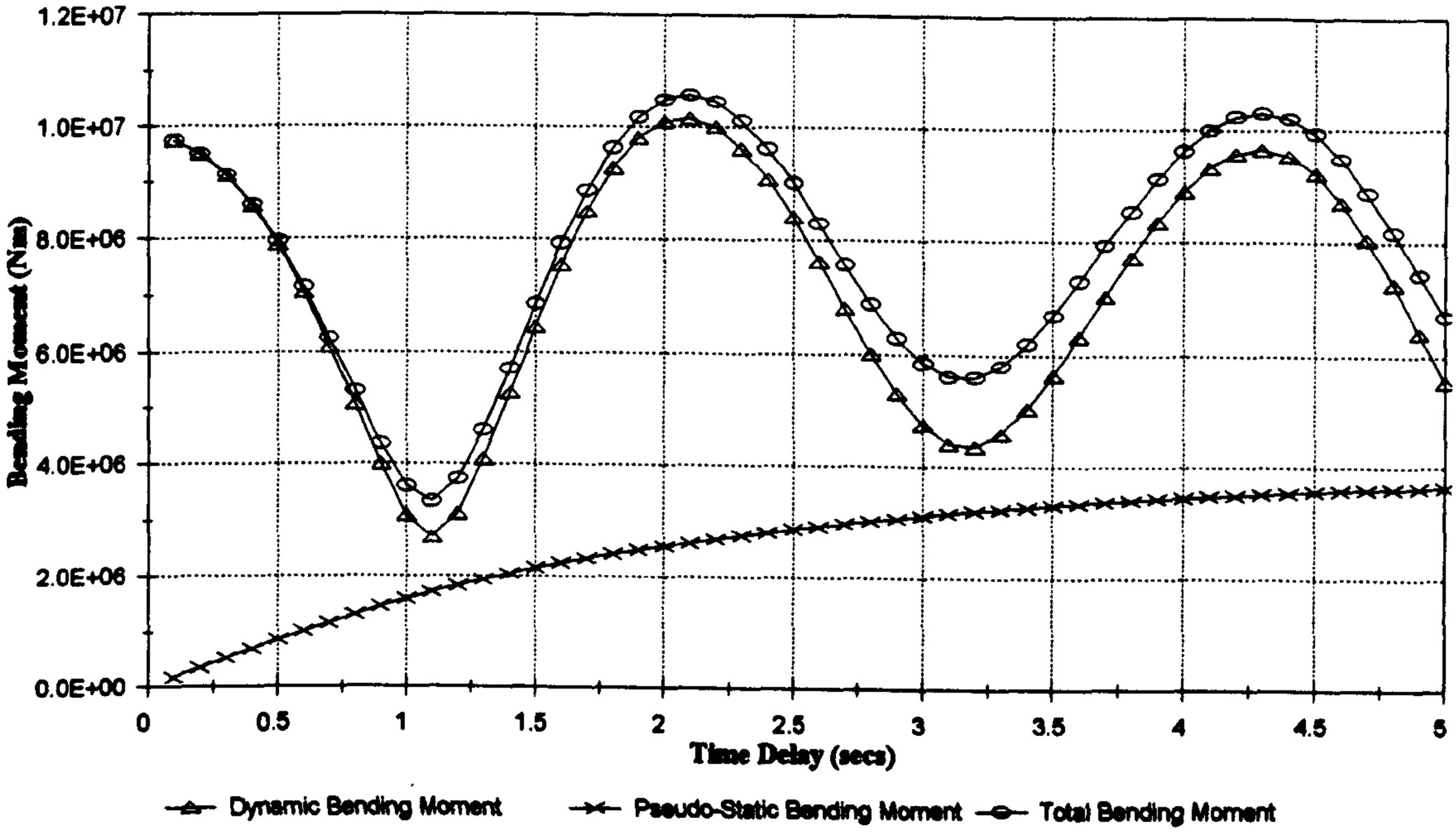

Figure 5.28 -:- RMS Bending Moments At Quarter Point, Horizontal Excitation

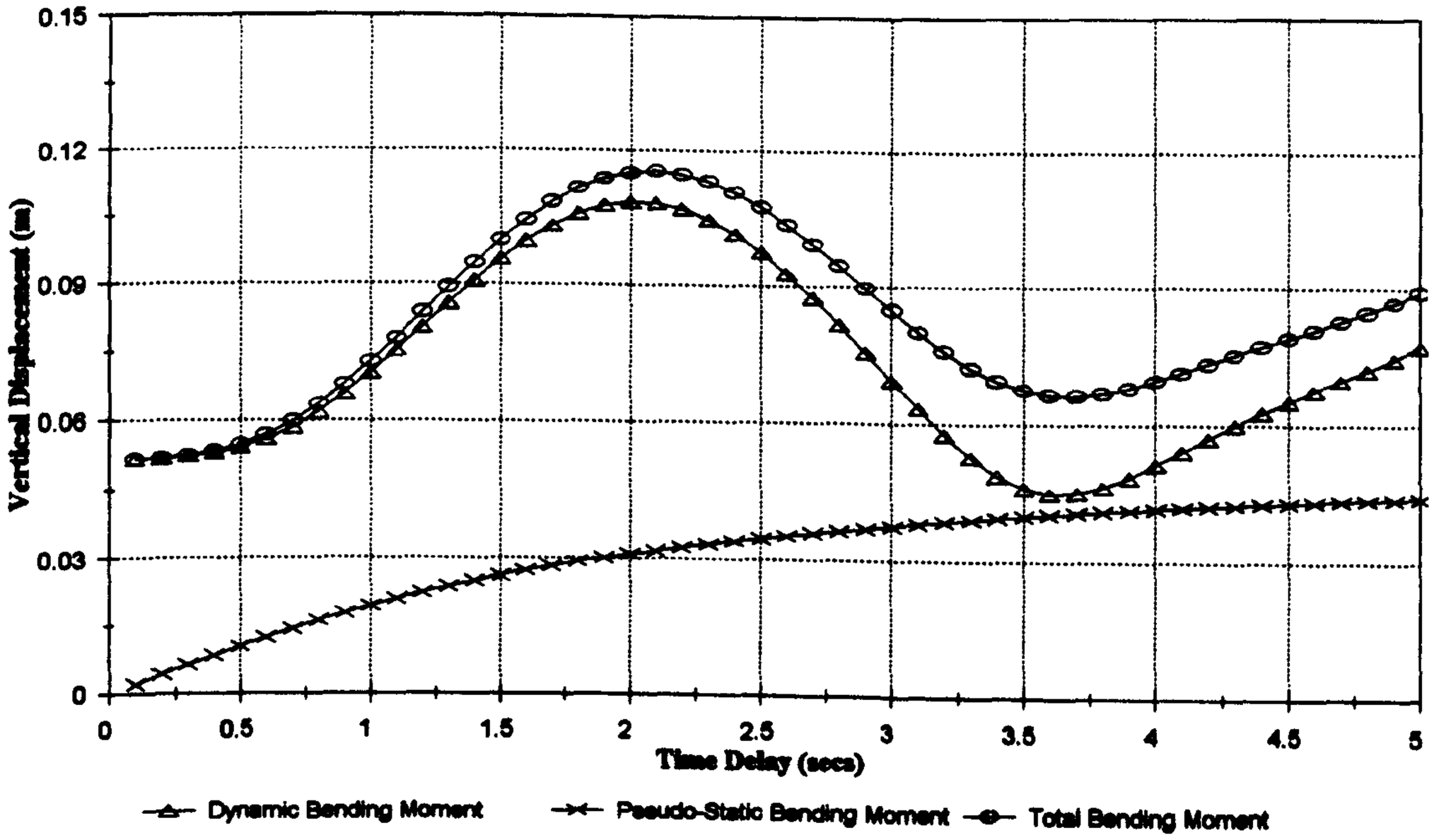

Figure 5.29 -:- RMS Displacements At Quarter Point, Horizontal Excitation

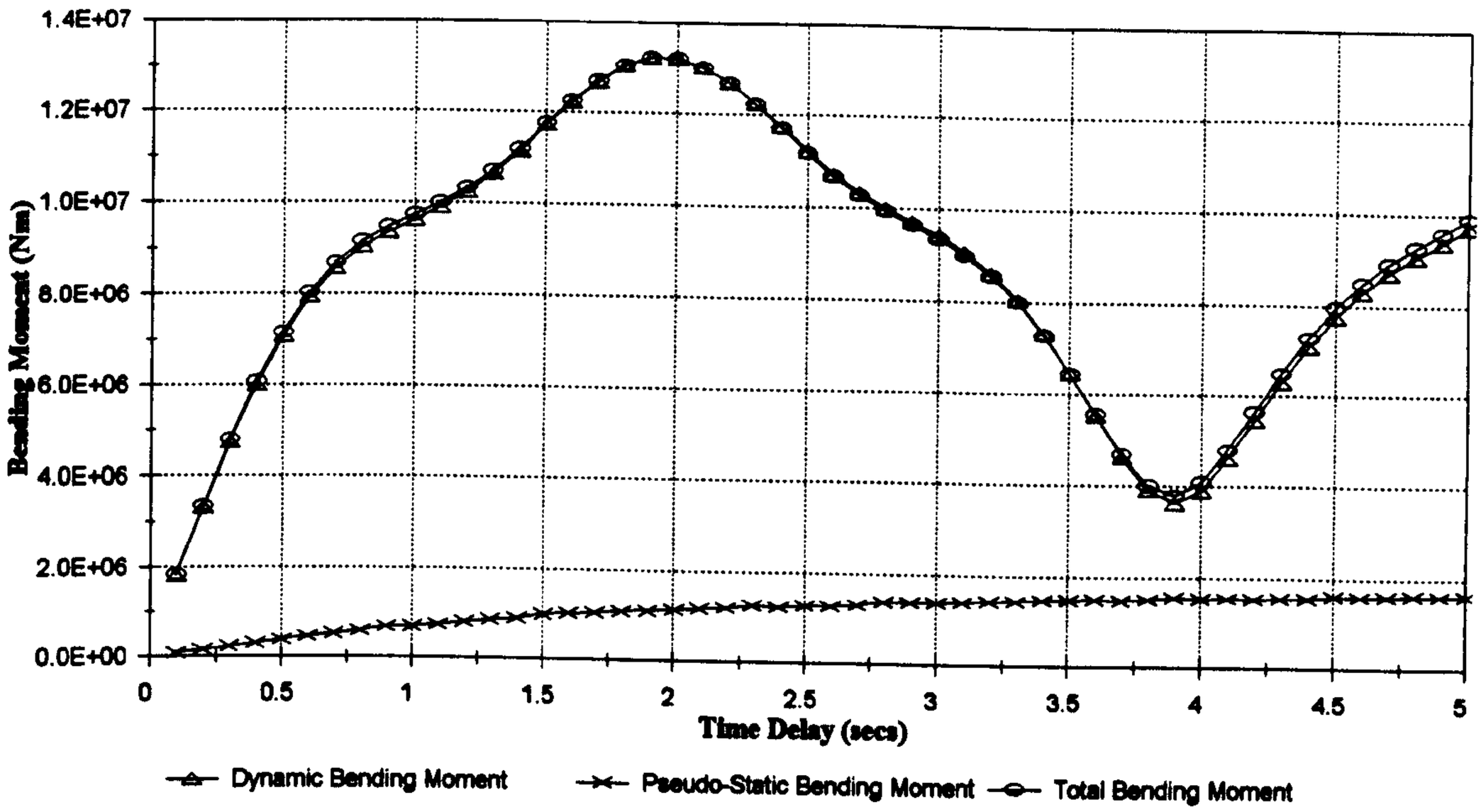

Figure 5.30 -:- RMS Bending Moments At Mid Span, Horizontal Excitation

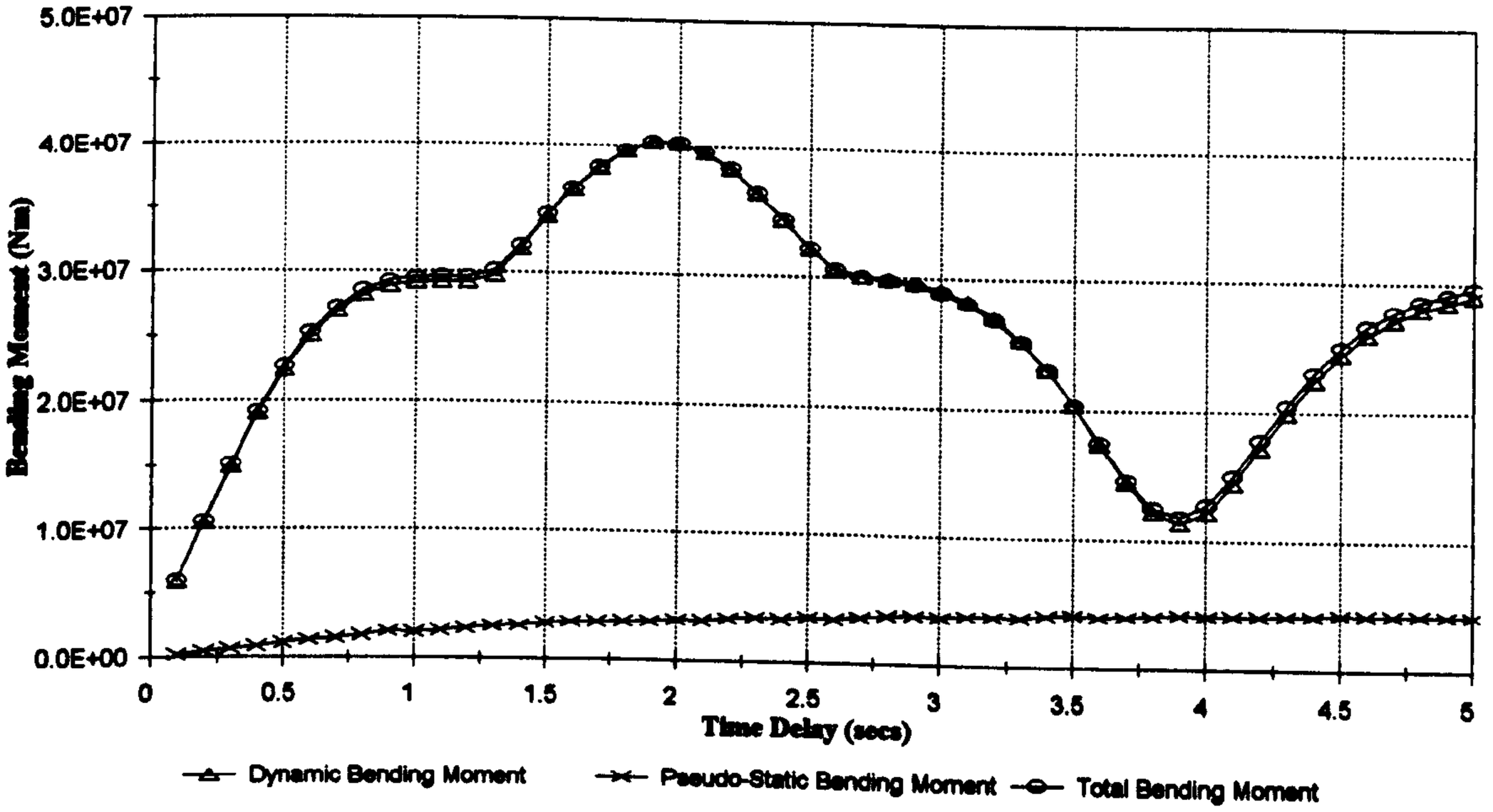

Figure 5.31 -:- Peak Bending Moments At Mid Span, Horizontal Excitation

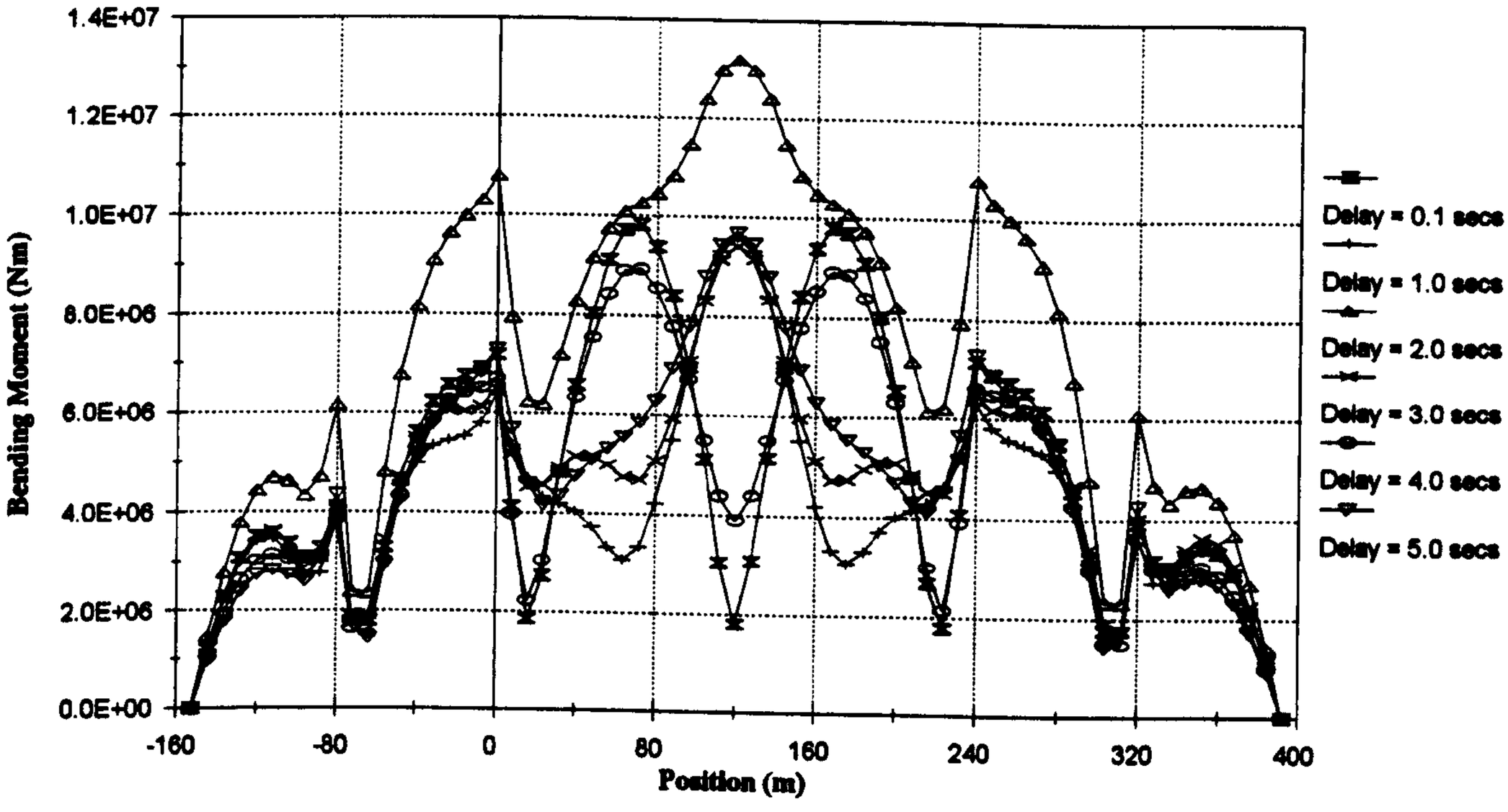

Figure 5.32 -:- RMS Dynamic Bending Moments, Horizontal Excitation

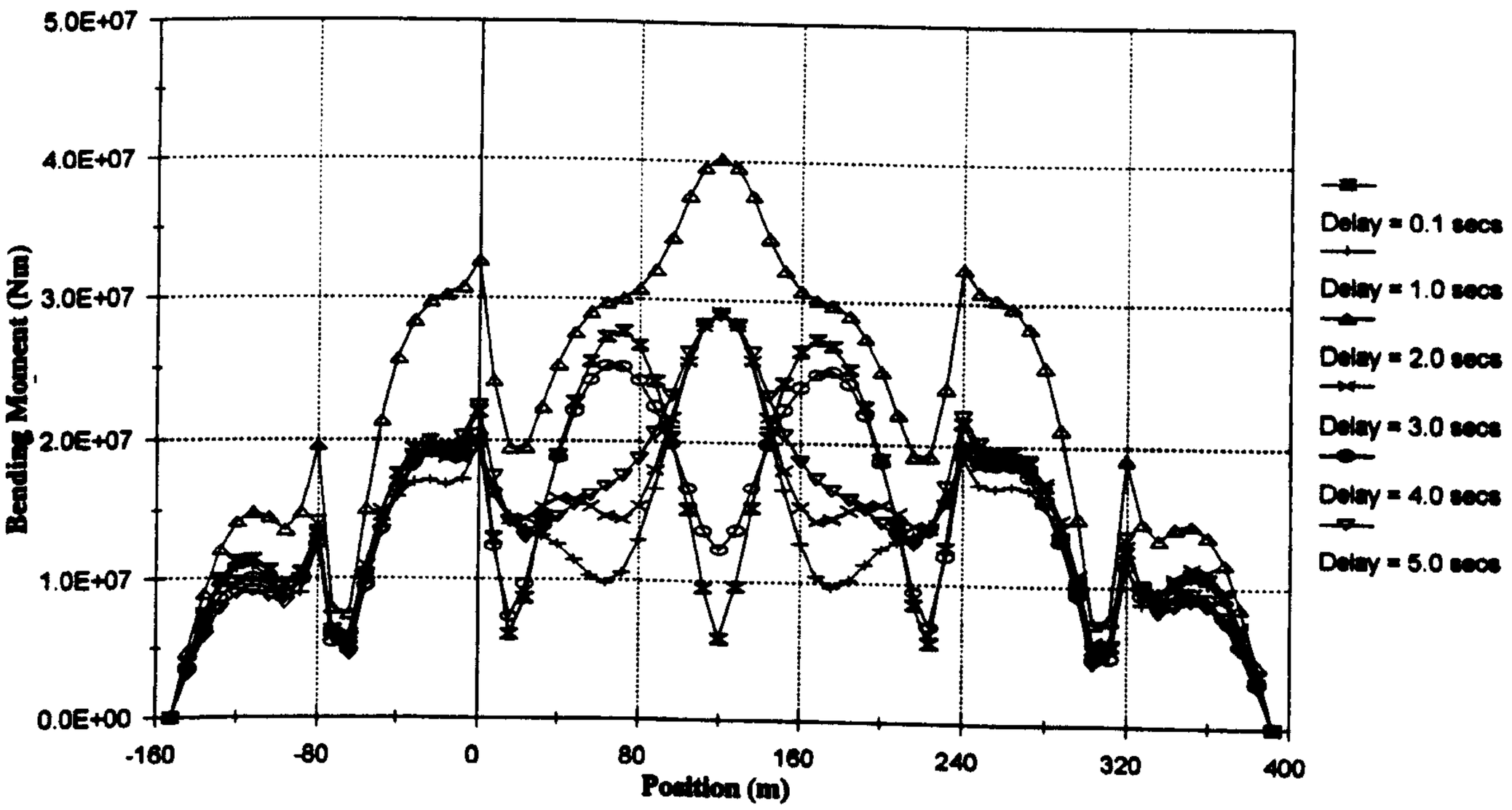

Figure 5.33 -:- Peak Dynamic Bending Moments, Horizontal Excitation

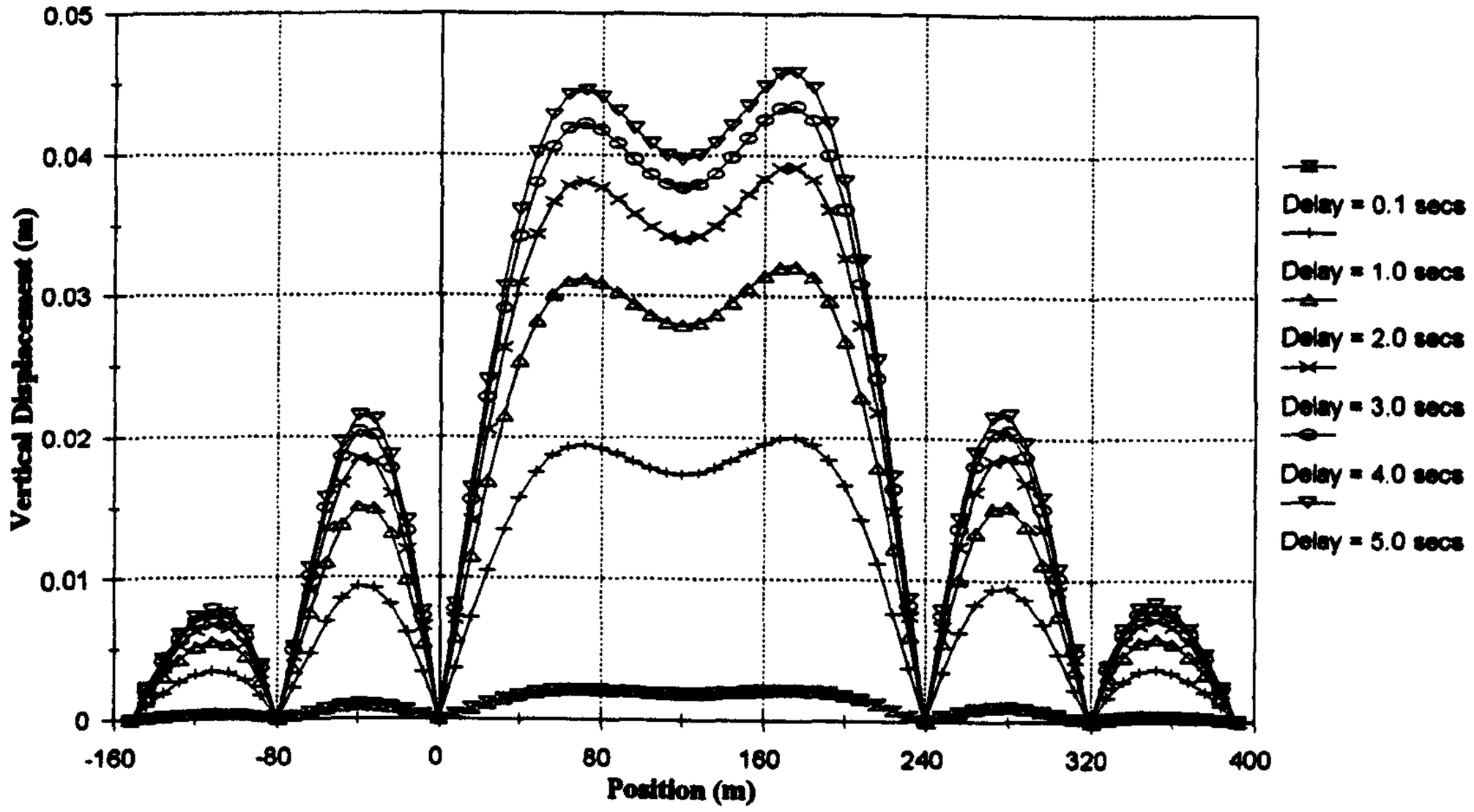

Figure 5.34 -:- RMS Pseudo-Static Deck Displacements, Horizontal Excitation

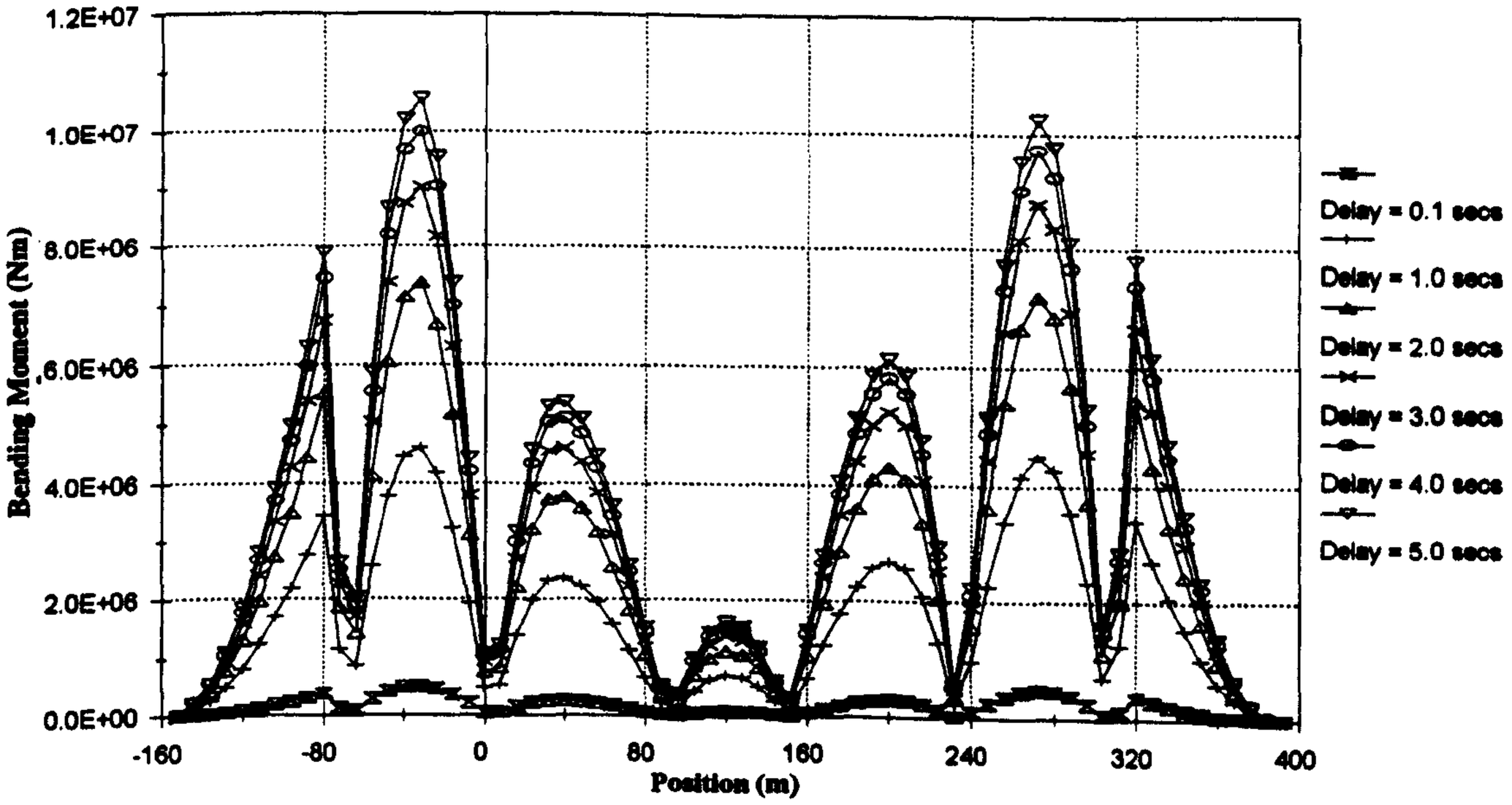

Figure 5.35 -:- RMS Pseudo-Static Bending Moments, Horizontal Excitation

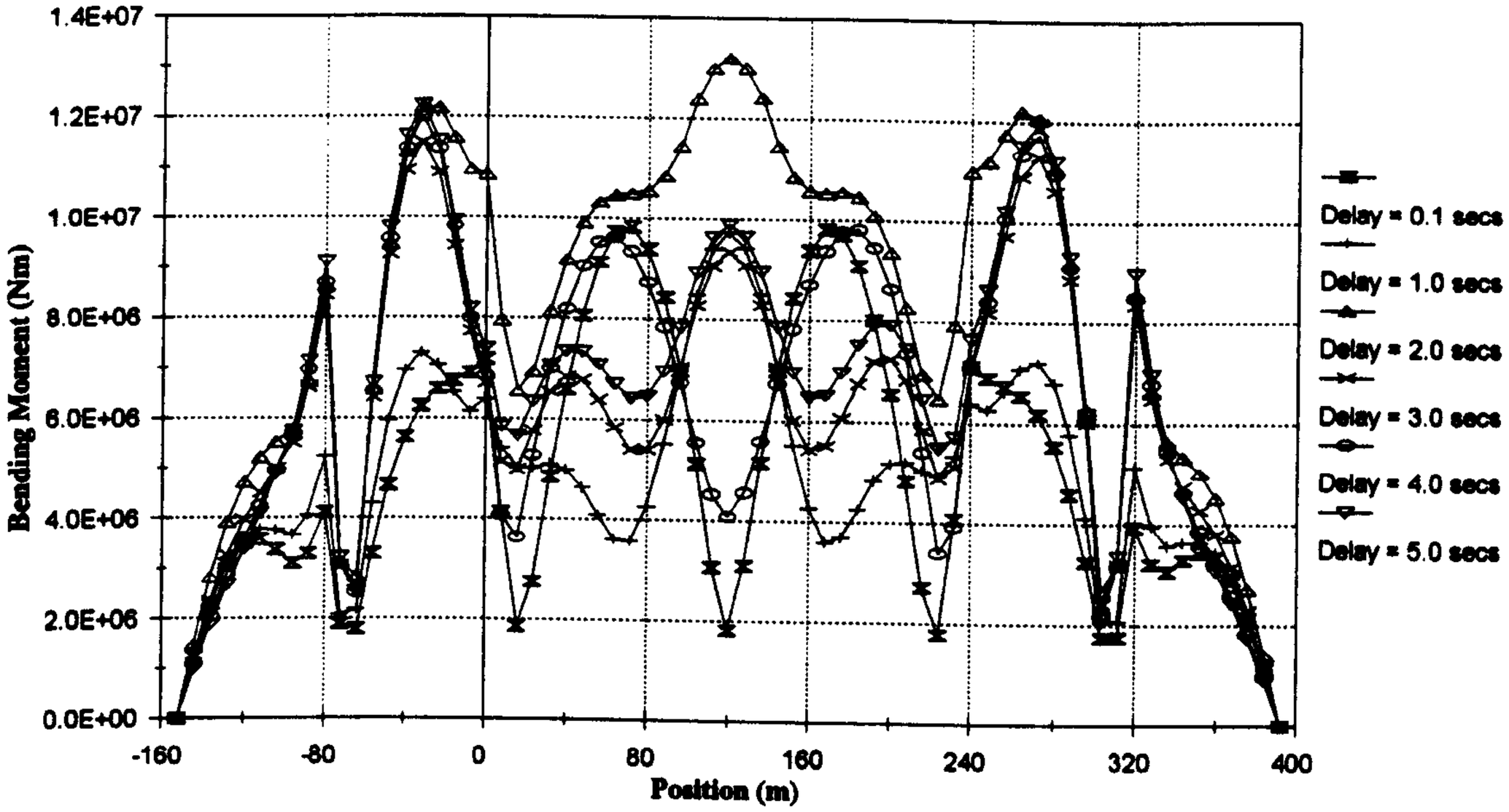

Figure 5.36 -:- RMS Total Bending Moments, Horizontal Excitation

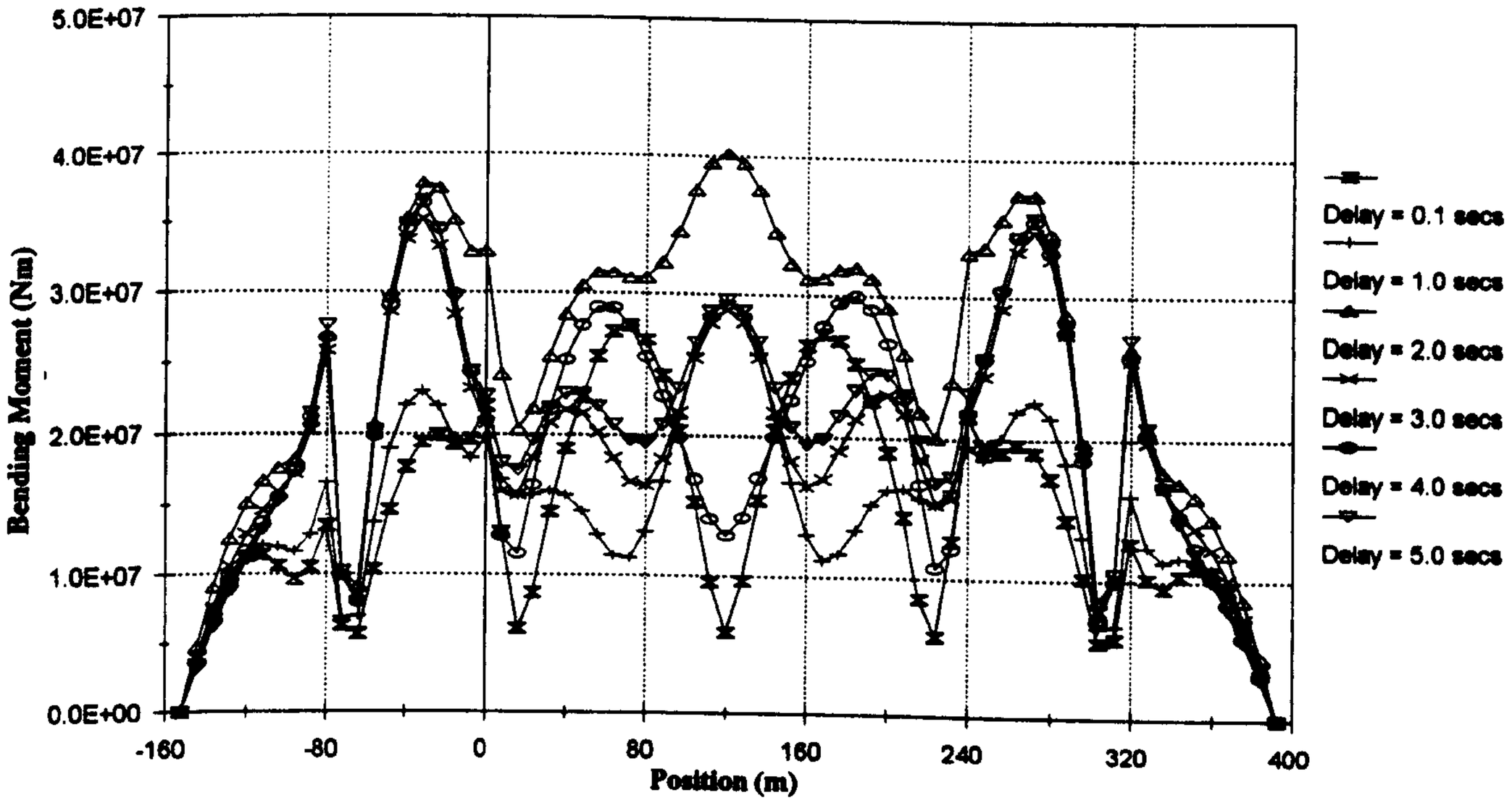

Figure 5.37 -:- Peak Total Bending Moments, Horizontal Excitation

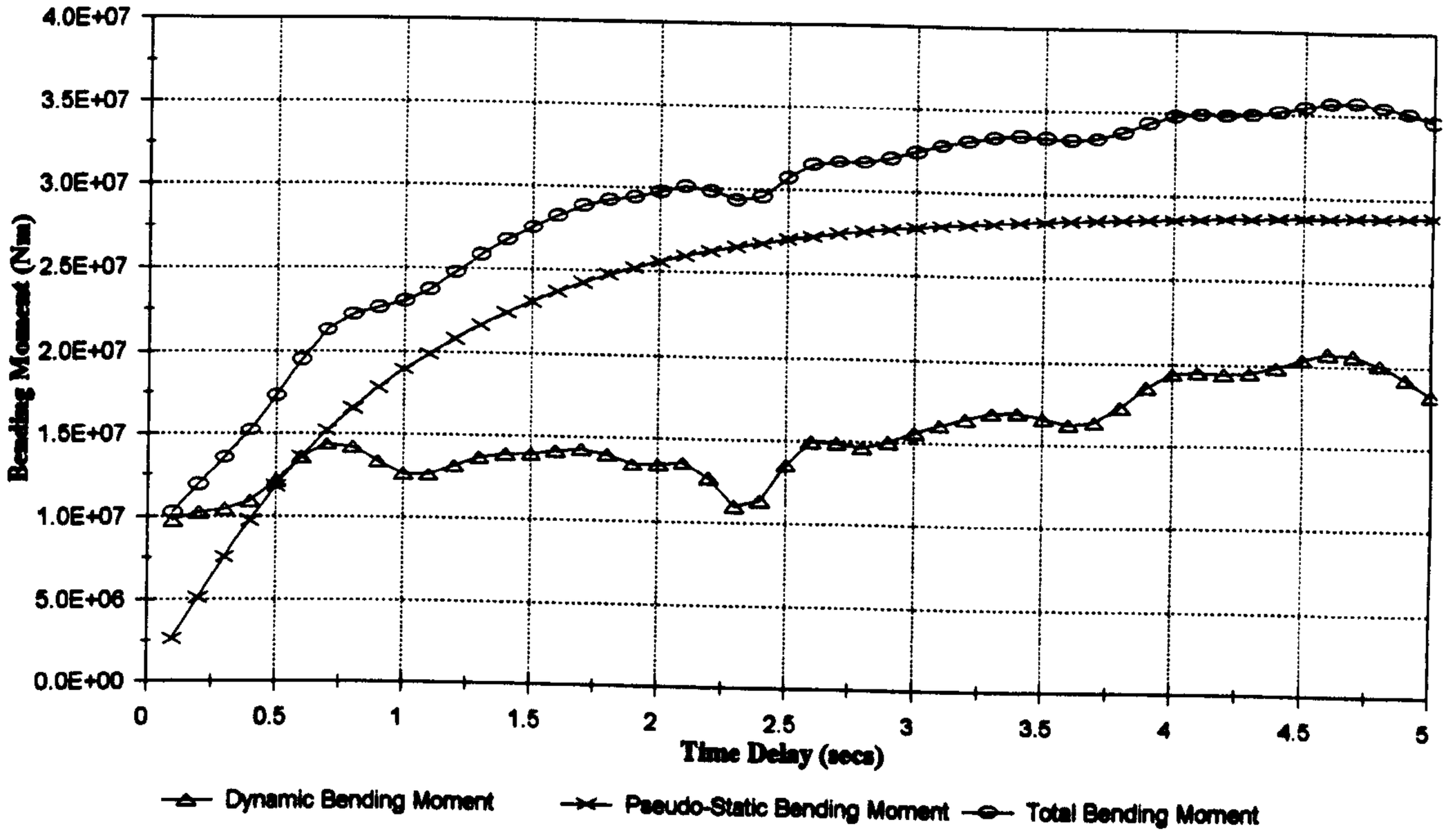

Figure 5.38 -:- RMS Bending Moments In Side Span, General Excitation

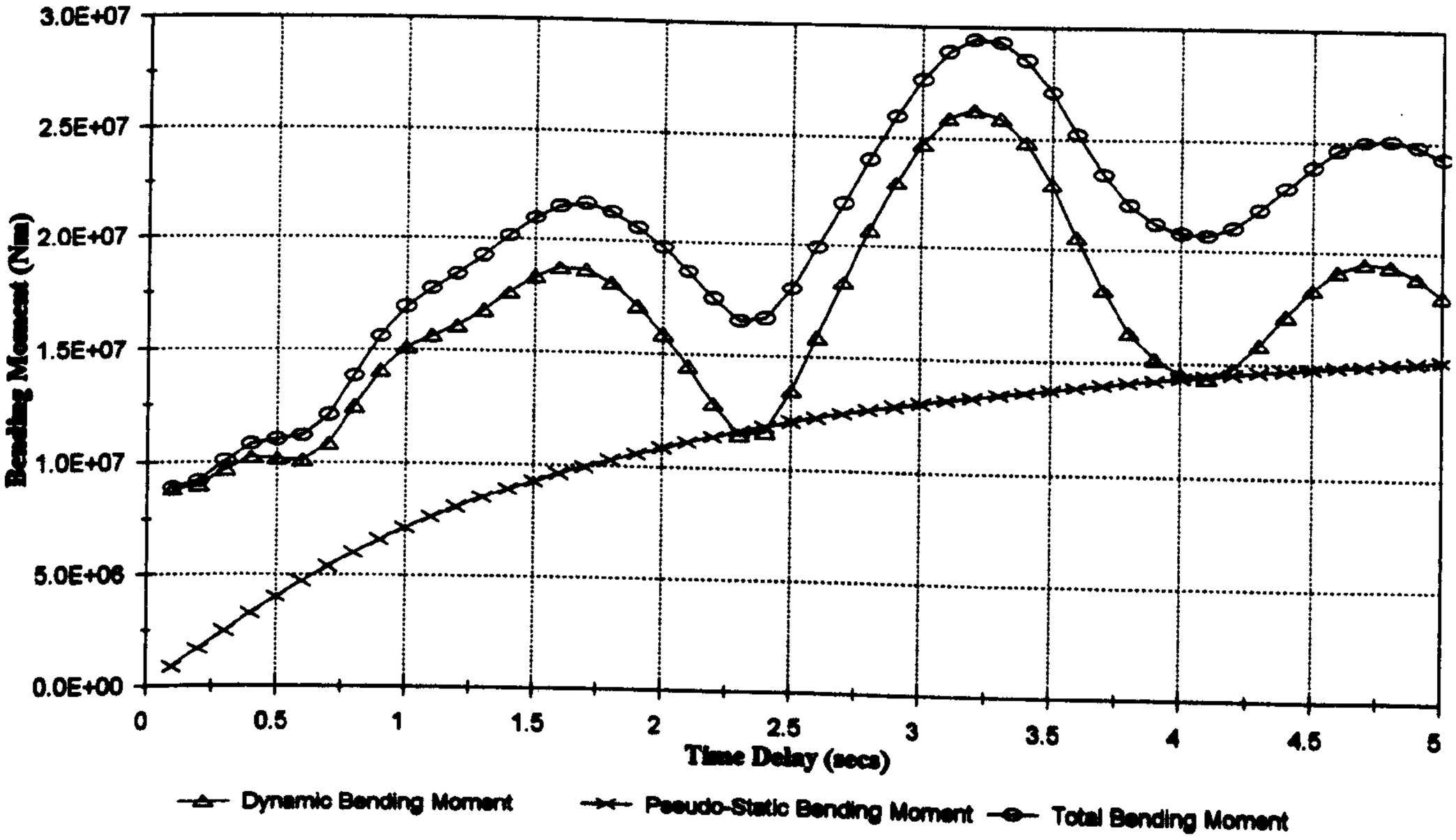

Figure 5.39 -:- RMS Bending Moments At Quarter Point, General Excitation

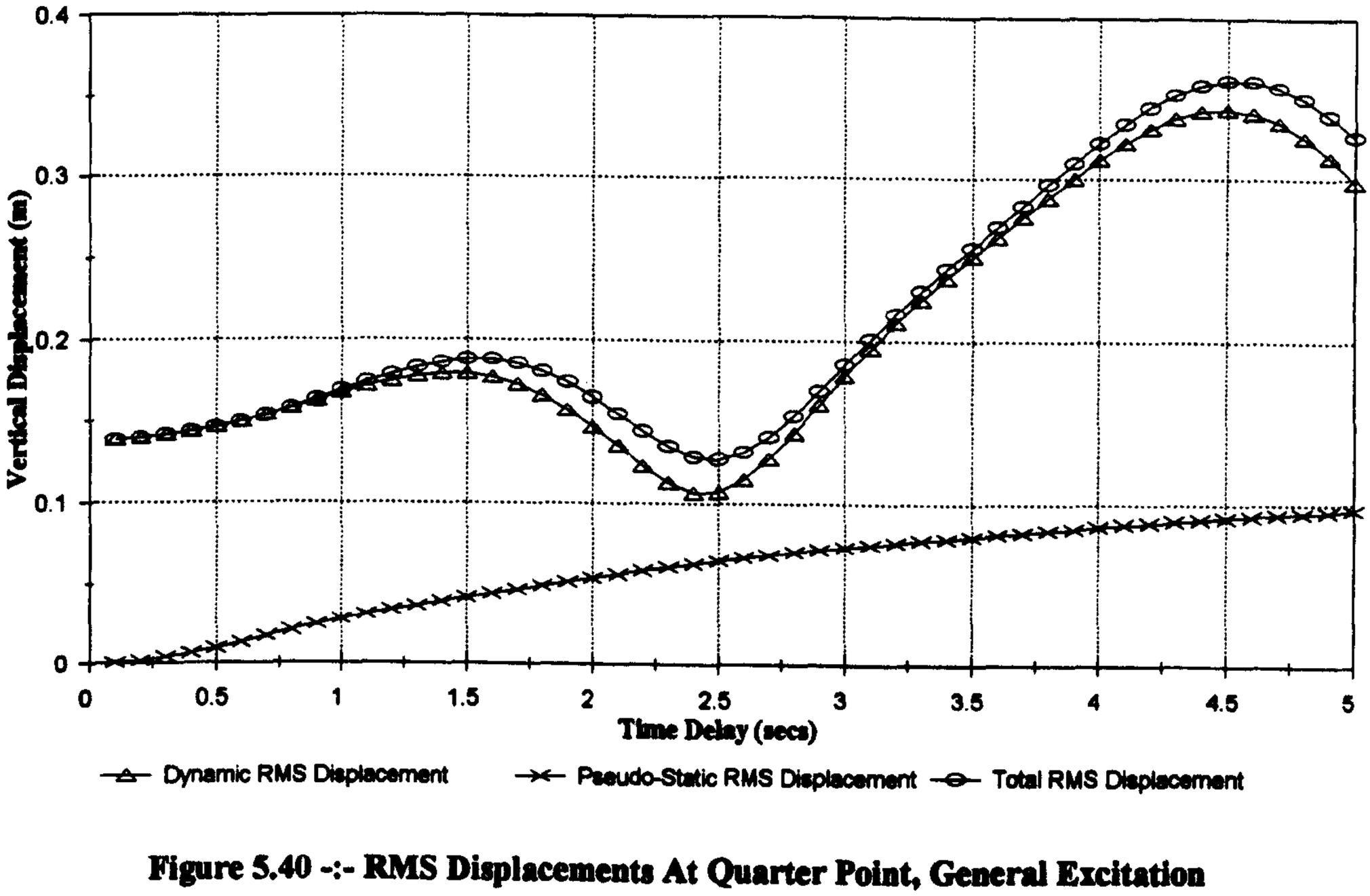

Figure 5.40 -:- RMS Displacements At Quarter Point, General Excitation

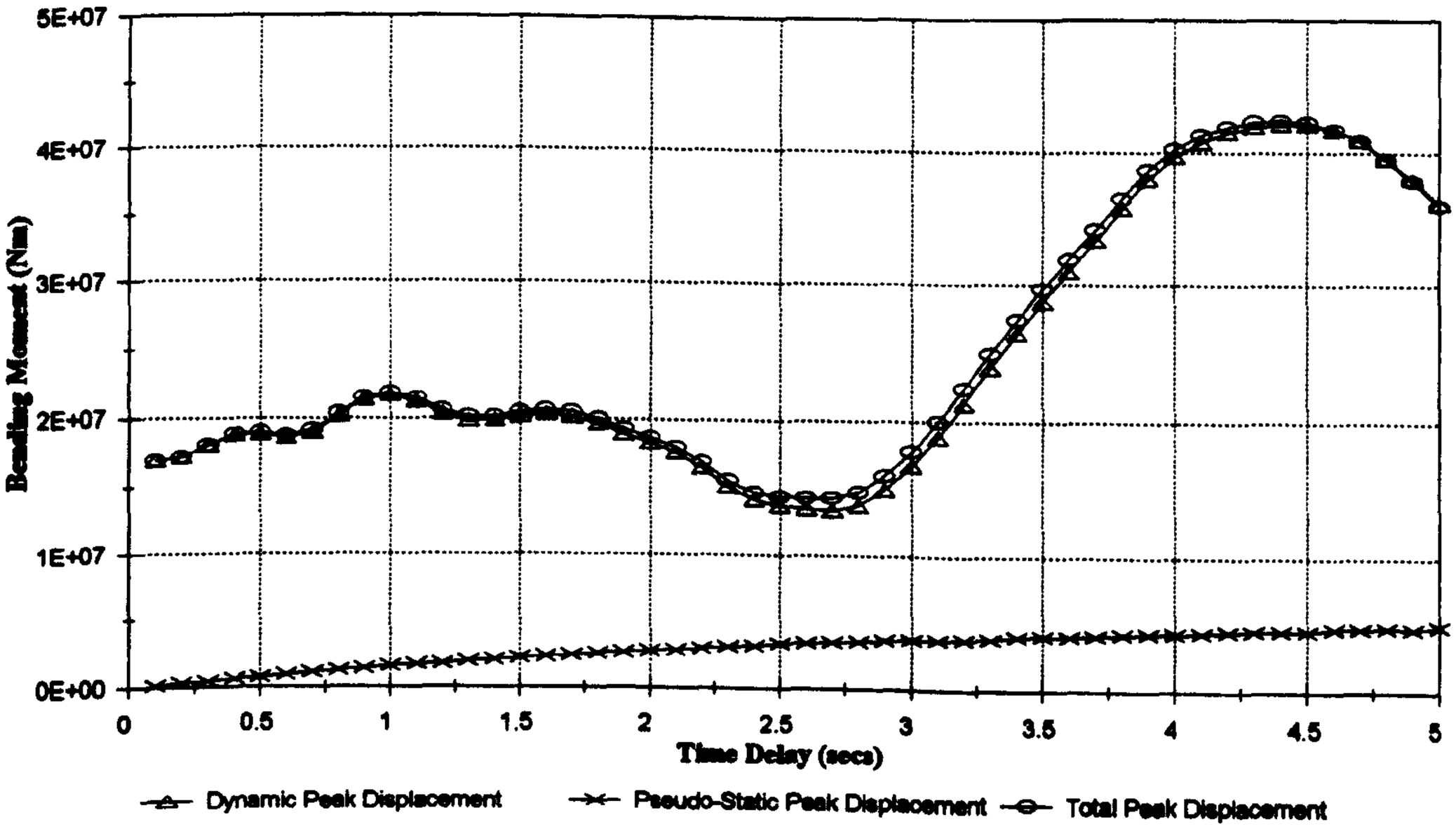

Figure 5.41 -:- RMS Bending Moments At Mid Span, General Excitation

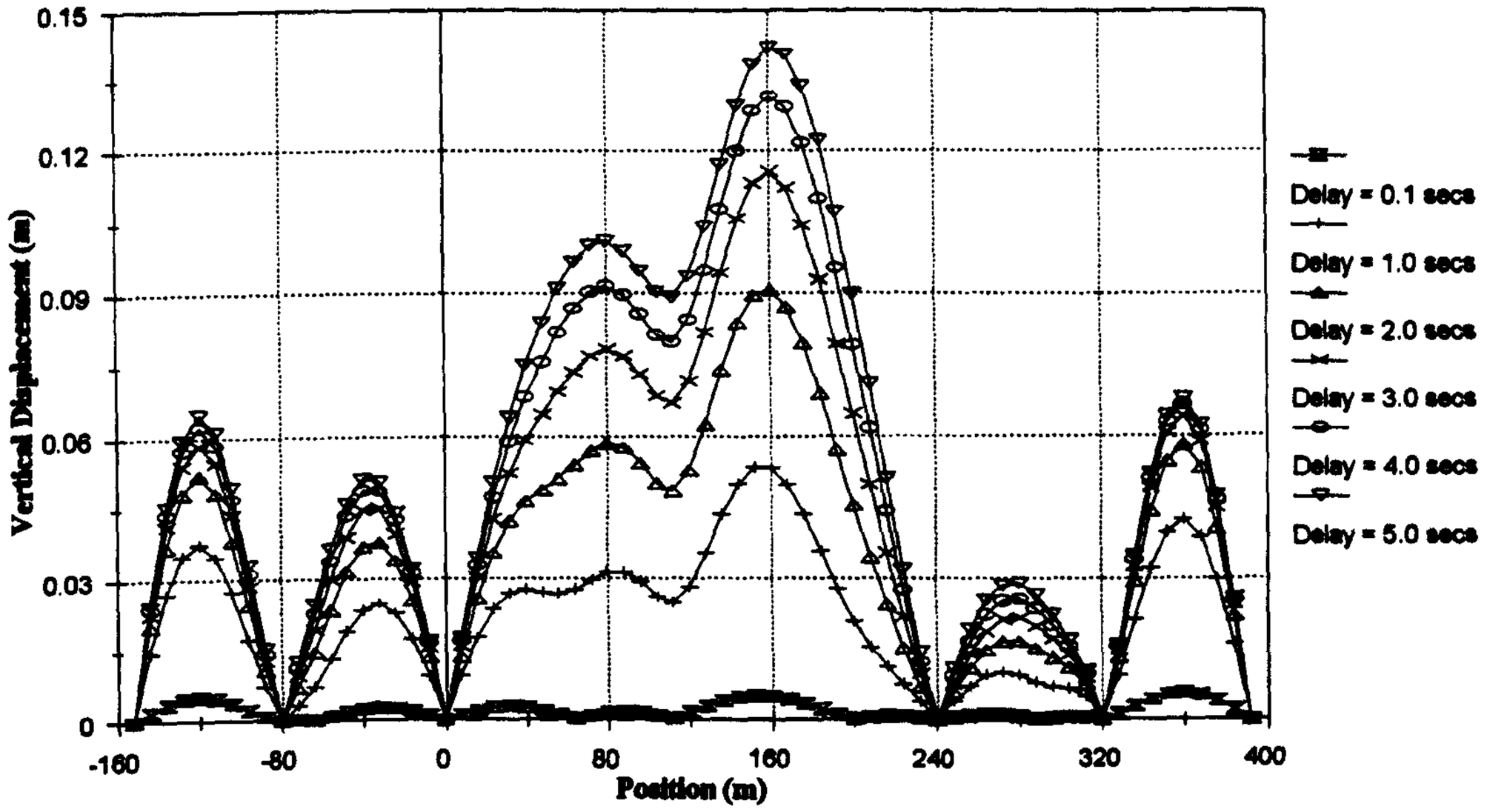

Figure 5.42 -:- RMS Pseudo-Static Deck Displacements, General Excitation

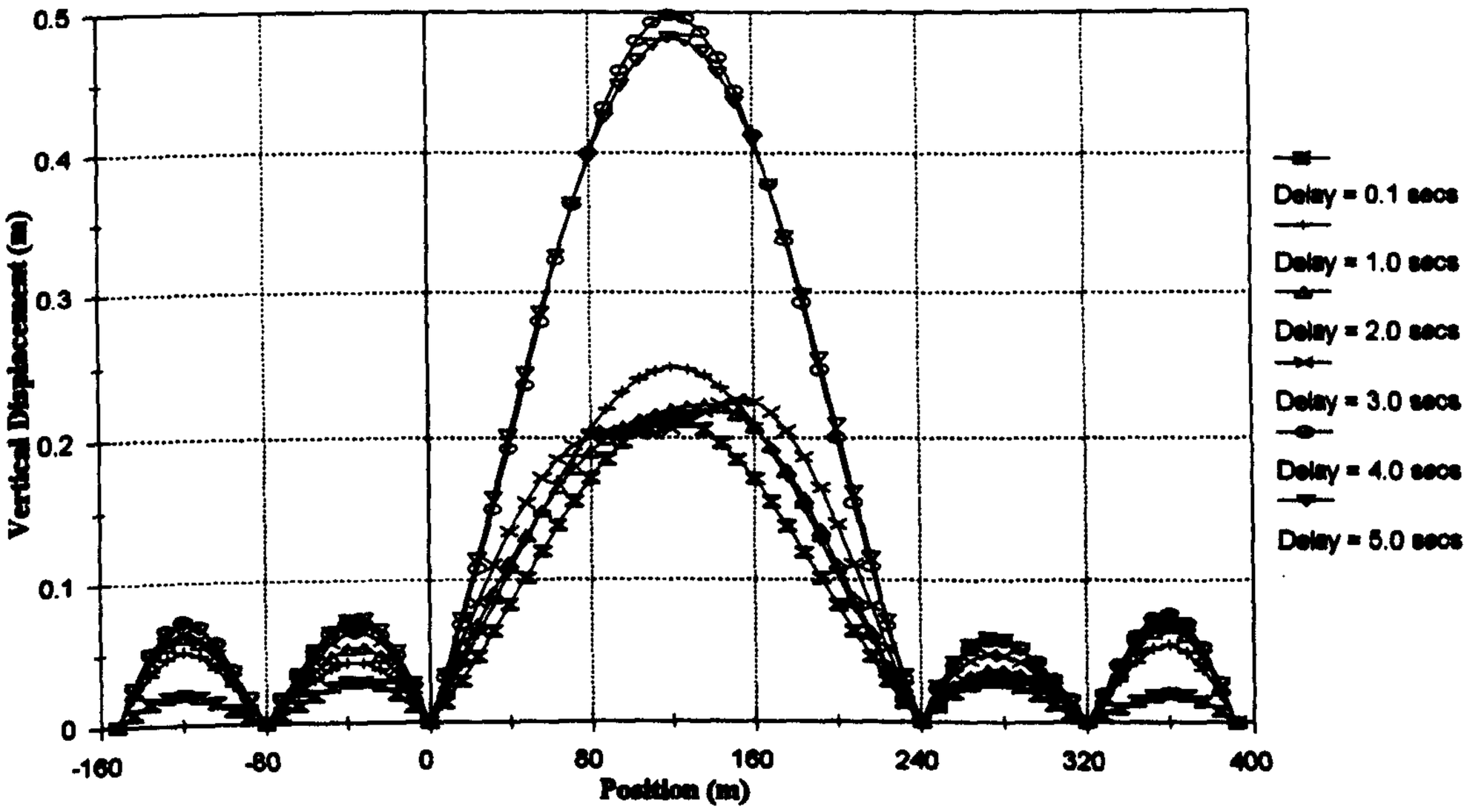

Figure 5.43 -:- RMS Total Deck Displacements, General Excitation

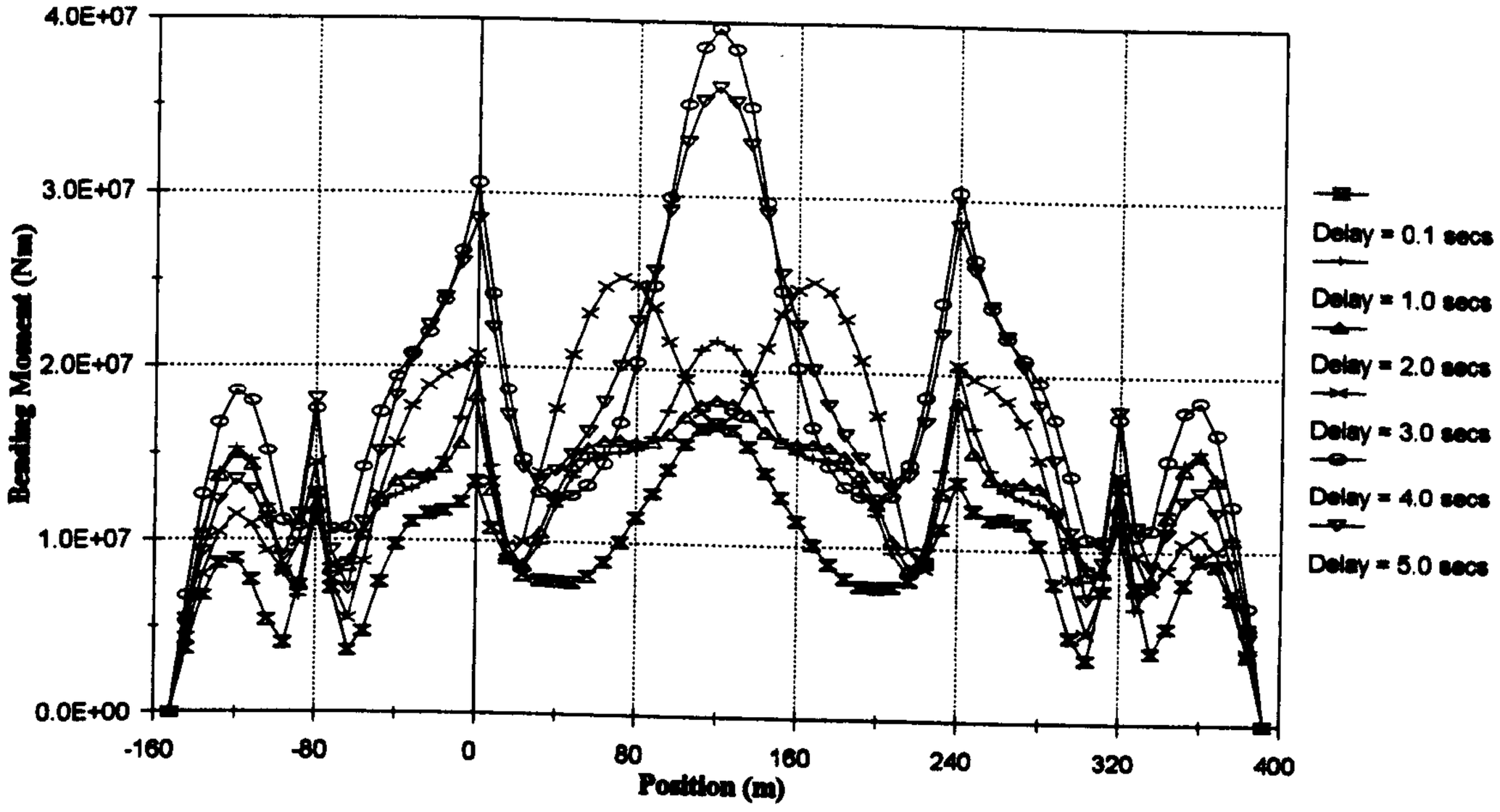

Figure 5.44 -:- RMS Dynamic Bending Moments, General Excitation

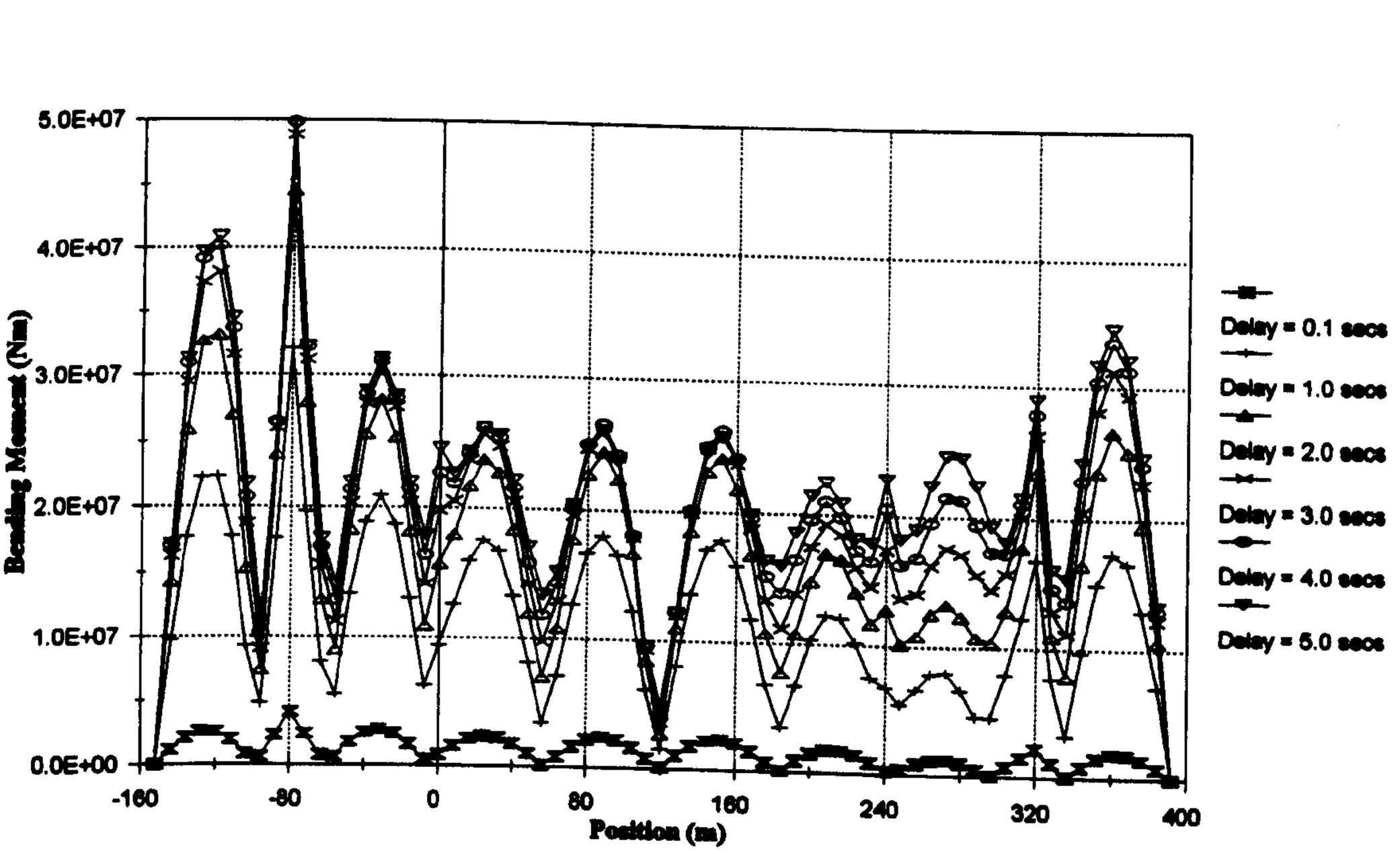

Figure 5.45 -:- RMS Pseudo Static Bending Moments, General Excitation

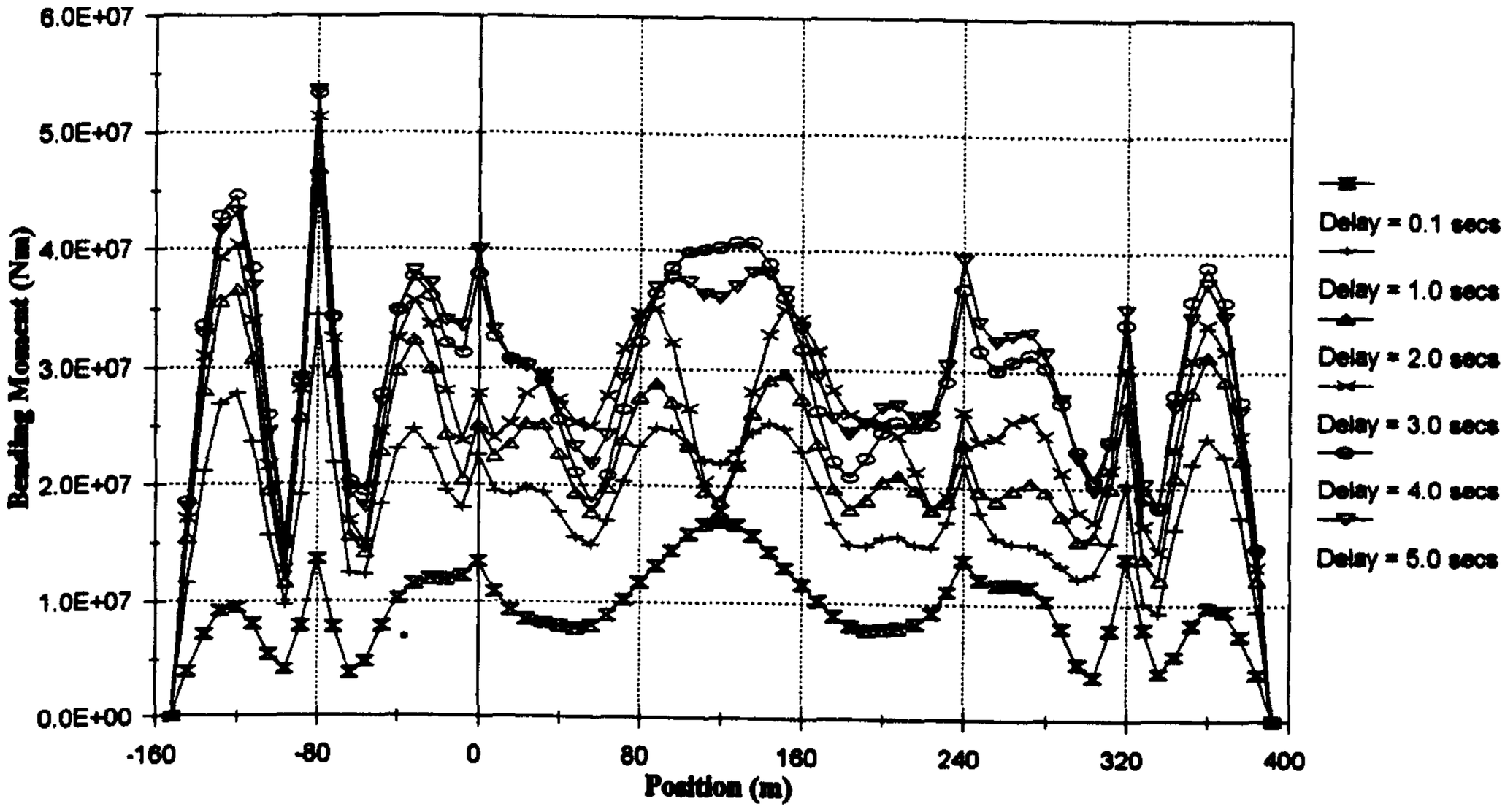

Figure 5.46 -:- RMS Total Bending Moments, General Excitation

Figure 5.47 -:- Peak Total Bending Moments, General Excitation

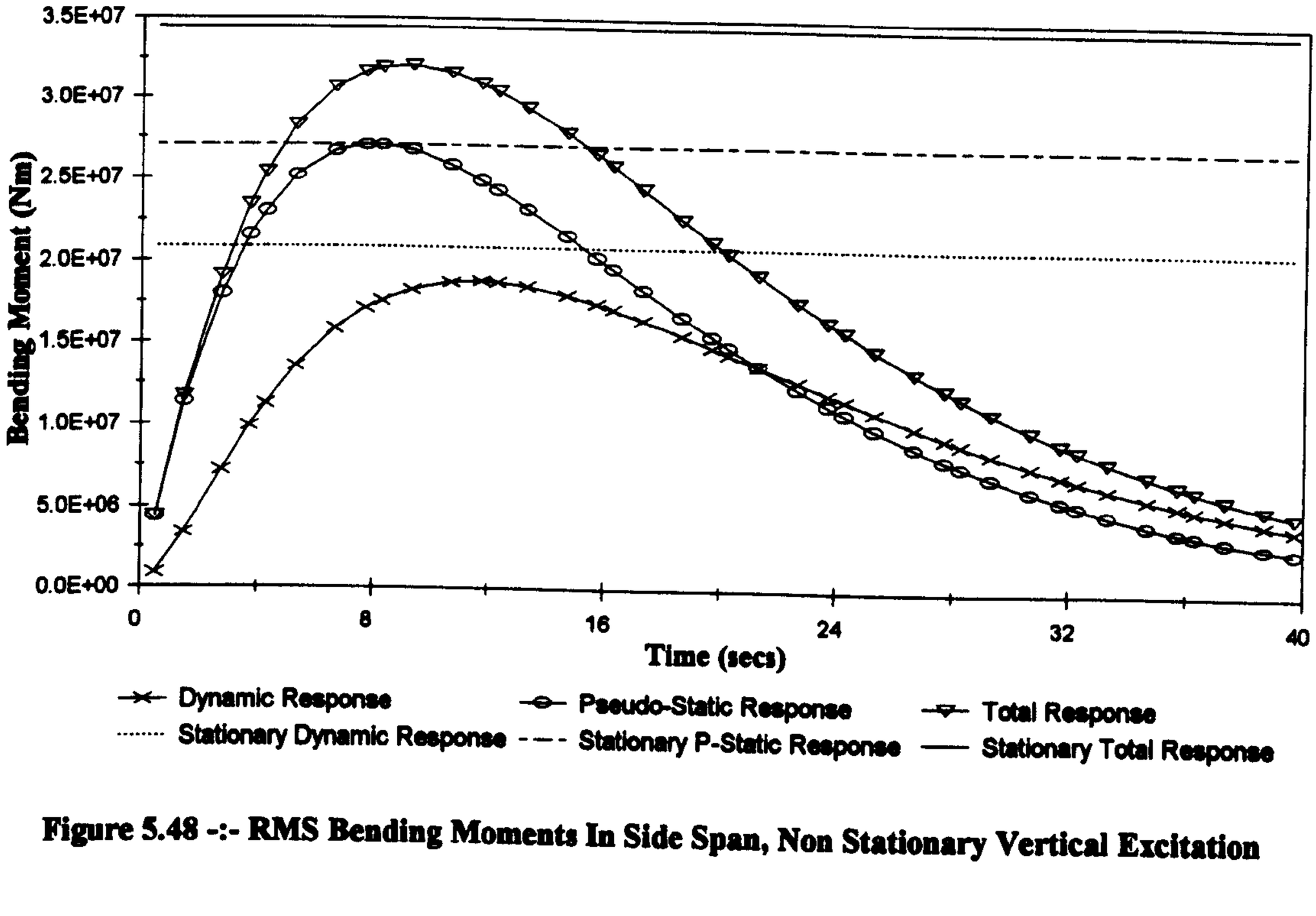

Figure 5.48 -:- RMS Bending Moments In Side Span, Non Stationary Vertical Excitation

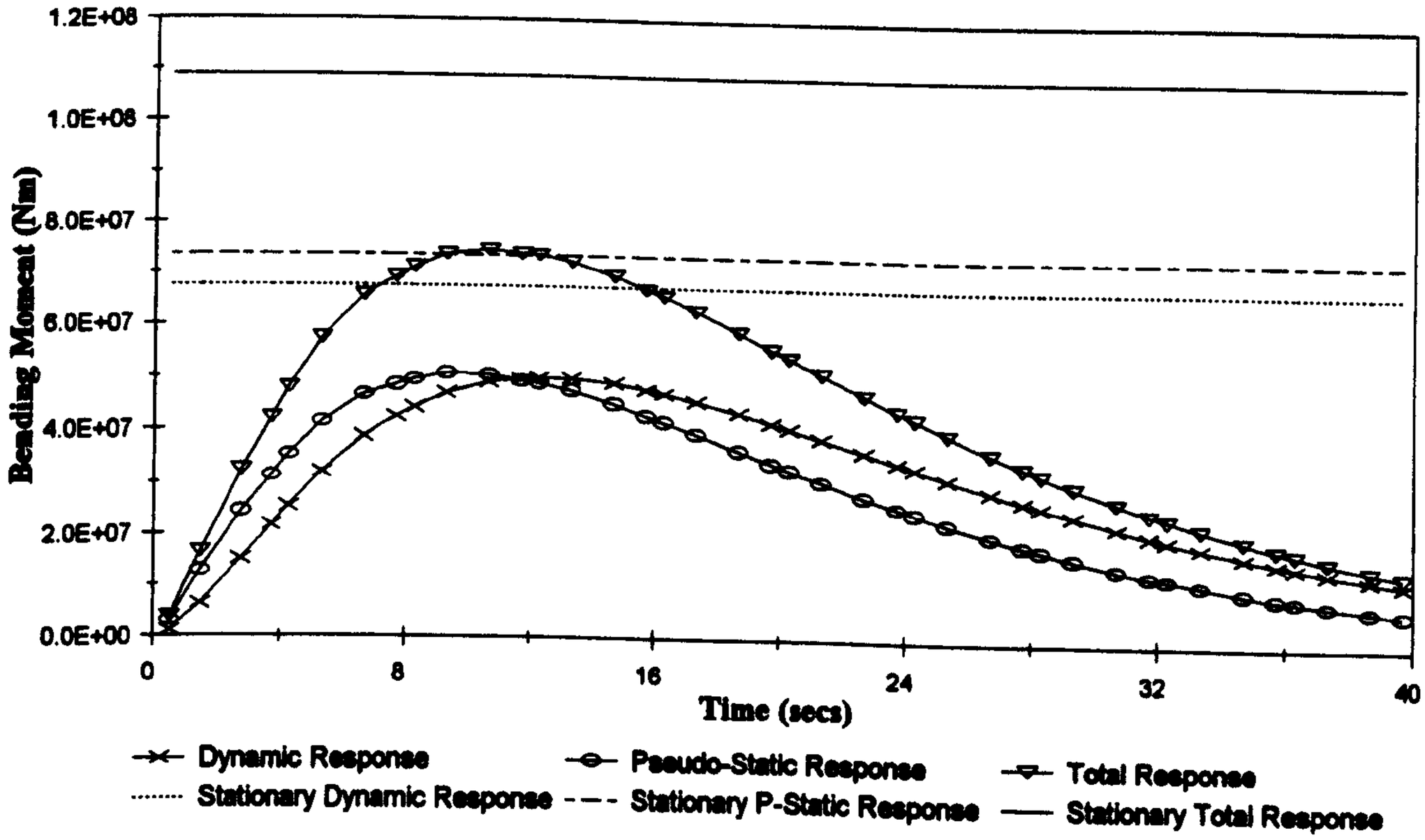

Figure 5.49 -:- Peak Bending Moments In Side Span, Non Stationary Vertical Excitation

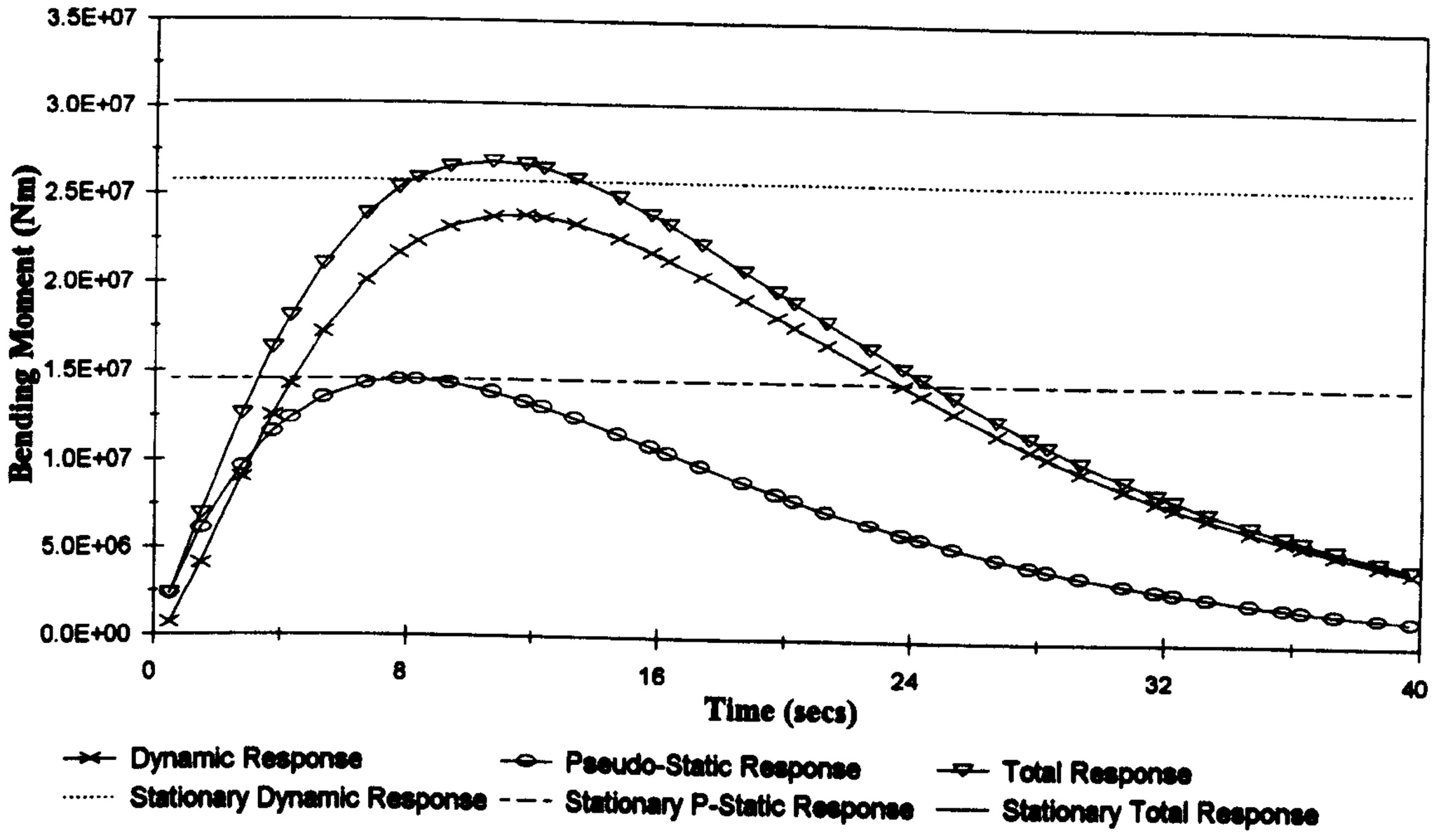

Figure 5.50 -:- RMS Bending Moments At Quarter Point, Non Stationary Vertical Excitation

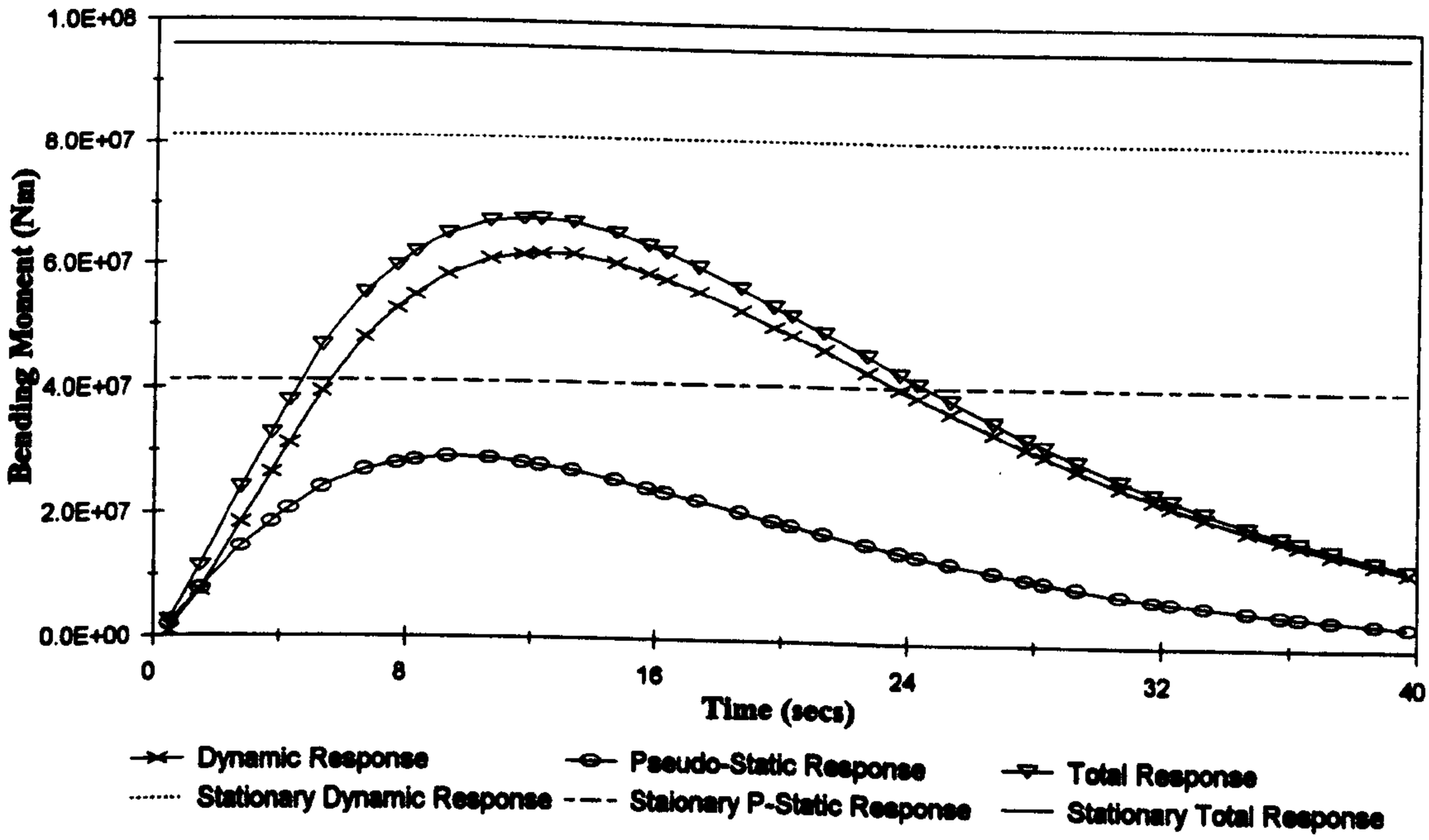

Figure 5.51 -:- Peak Bending Moments At Quarter Point, Non Stationary Vertical Excitation

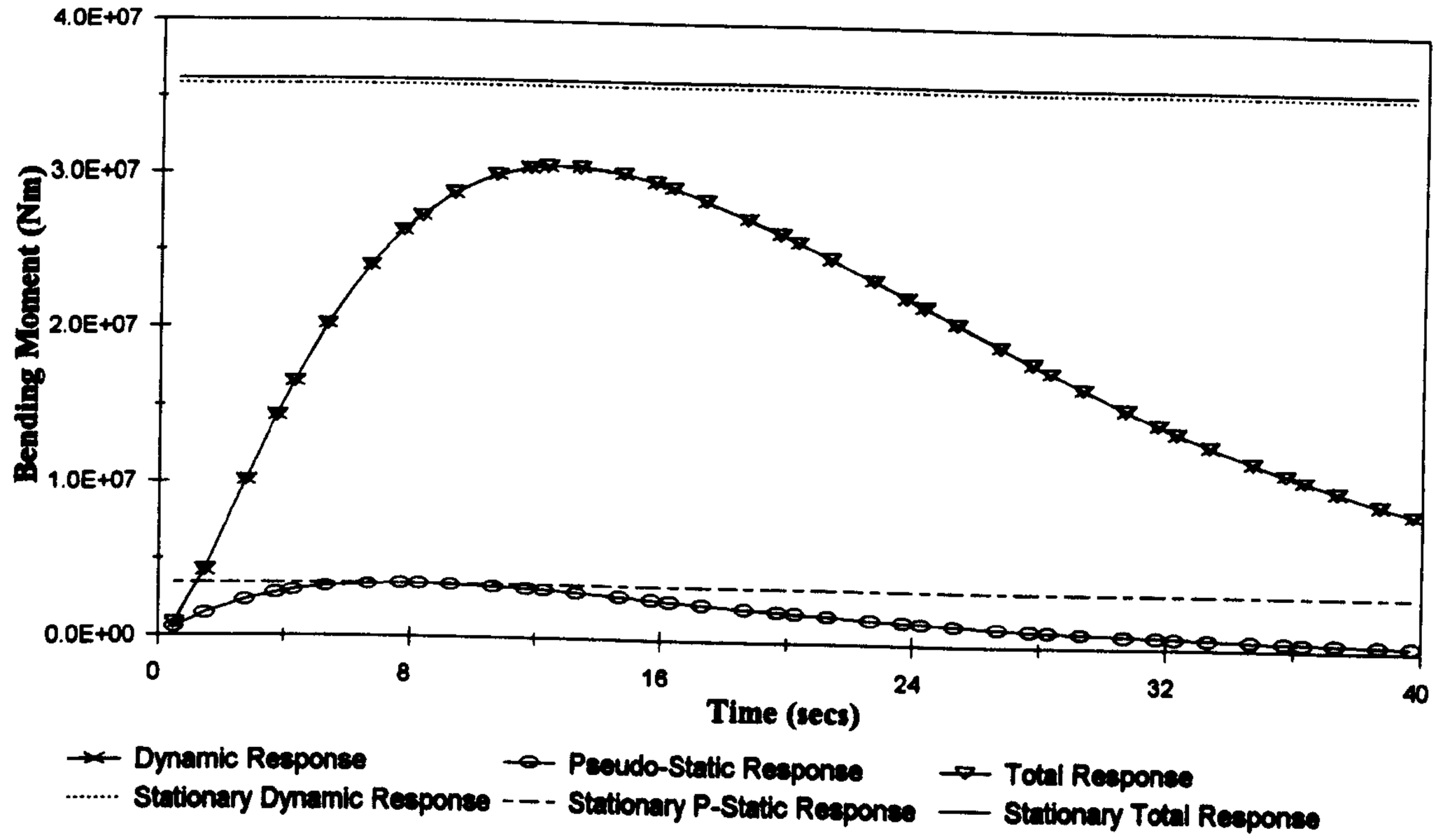

Figure 5.52 -:- RMS Bending Moments At Mid Span, Non Stationary Vertical Excitation

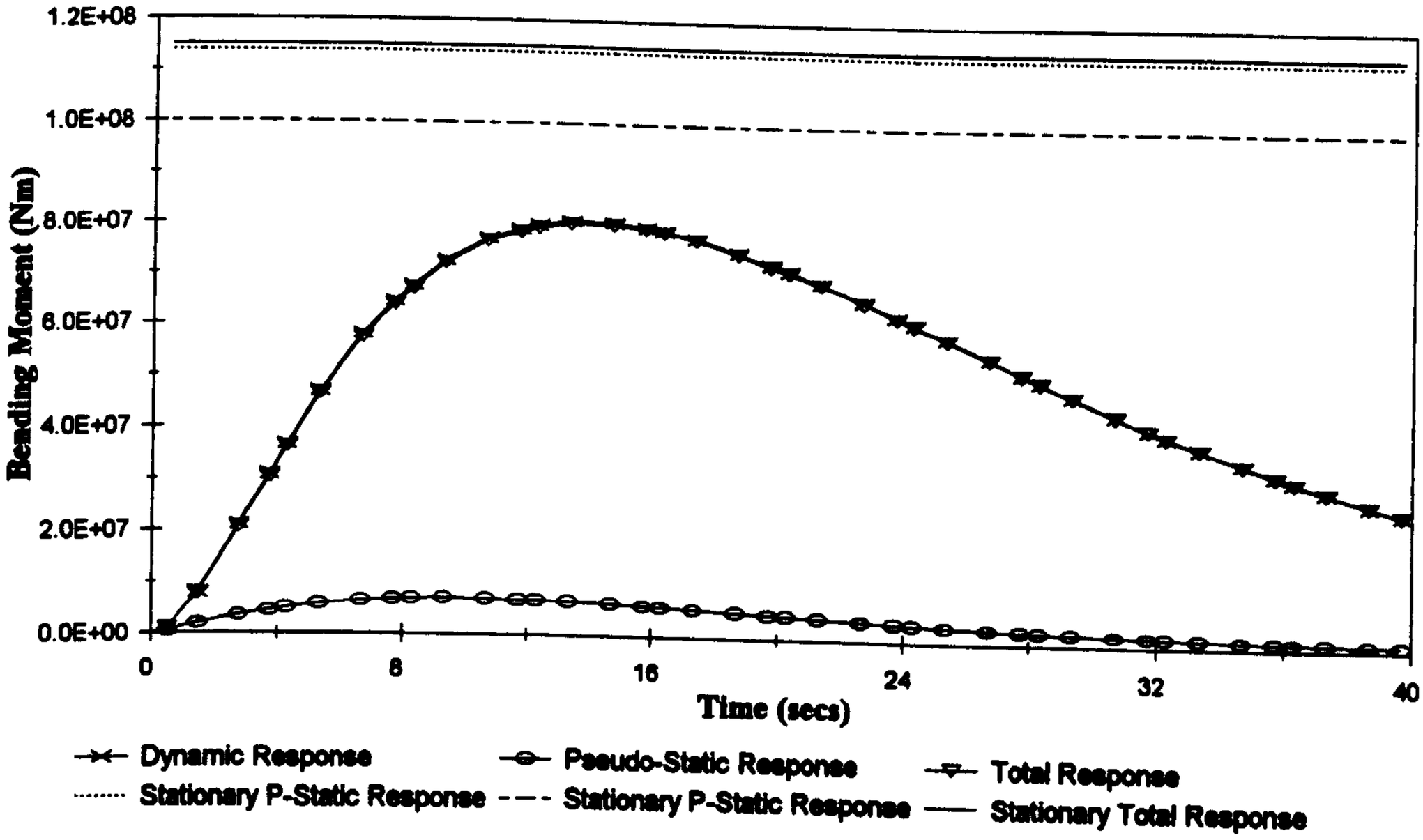

Figure 5.53 -:- Peak Bending Moments At Mid Span, Non Stationary Vertical Excitation

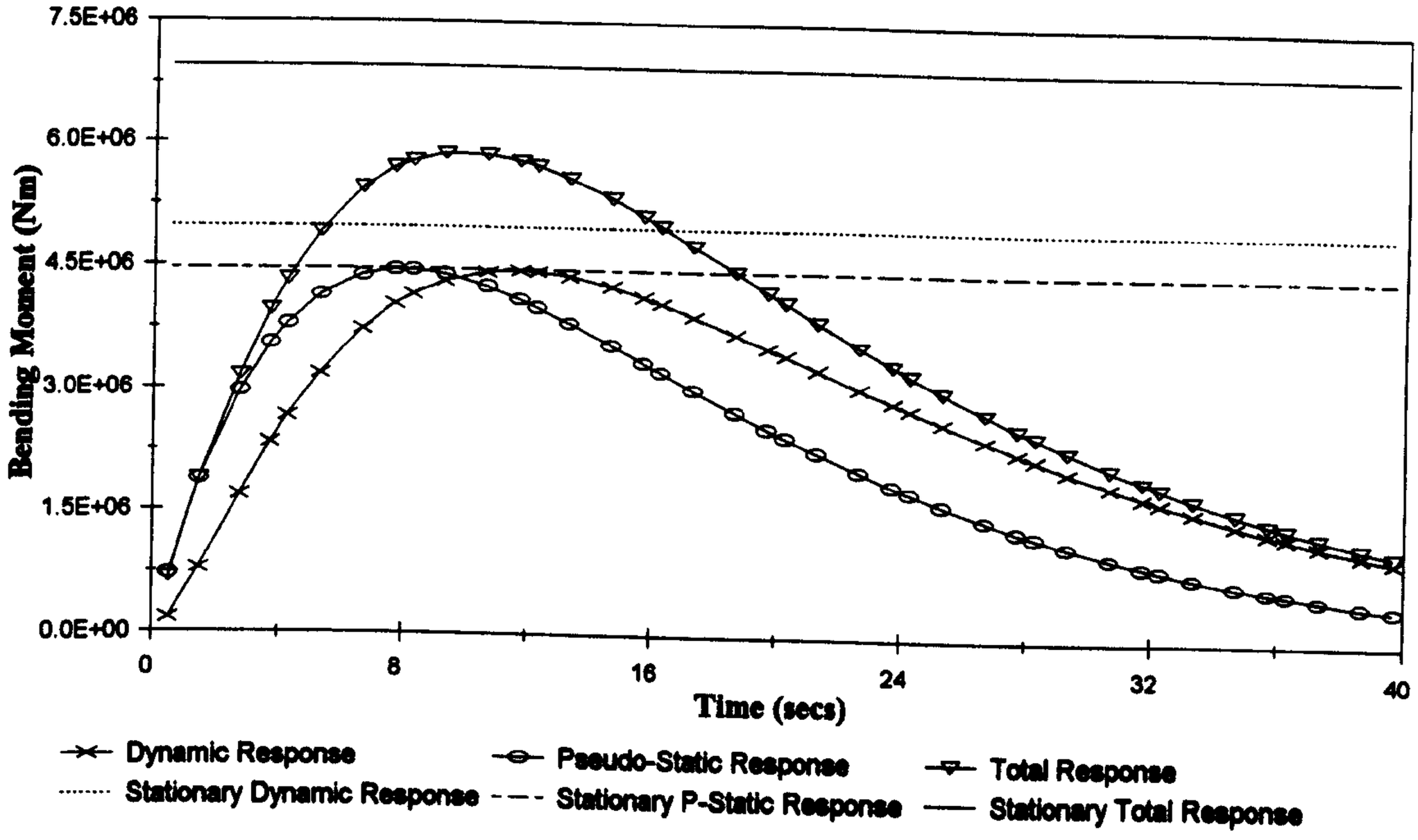

Figure 5.54 -:- RMS Bending Moments In Side Span, Non Stationary Horizontal Excitation

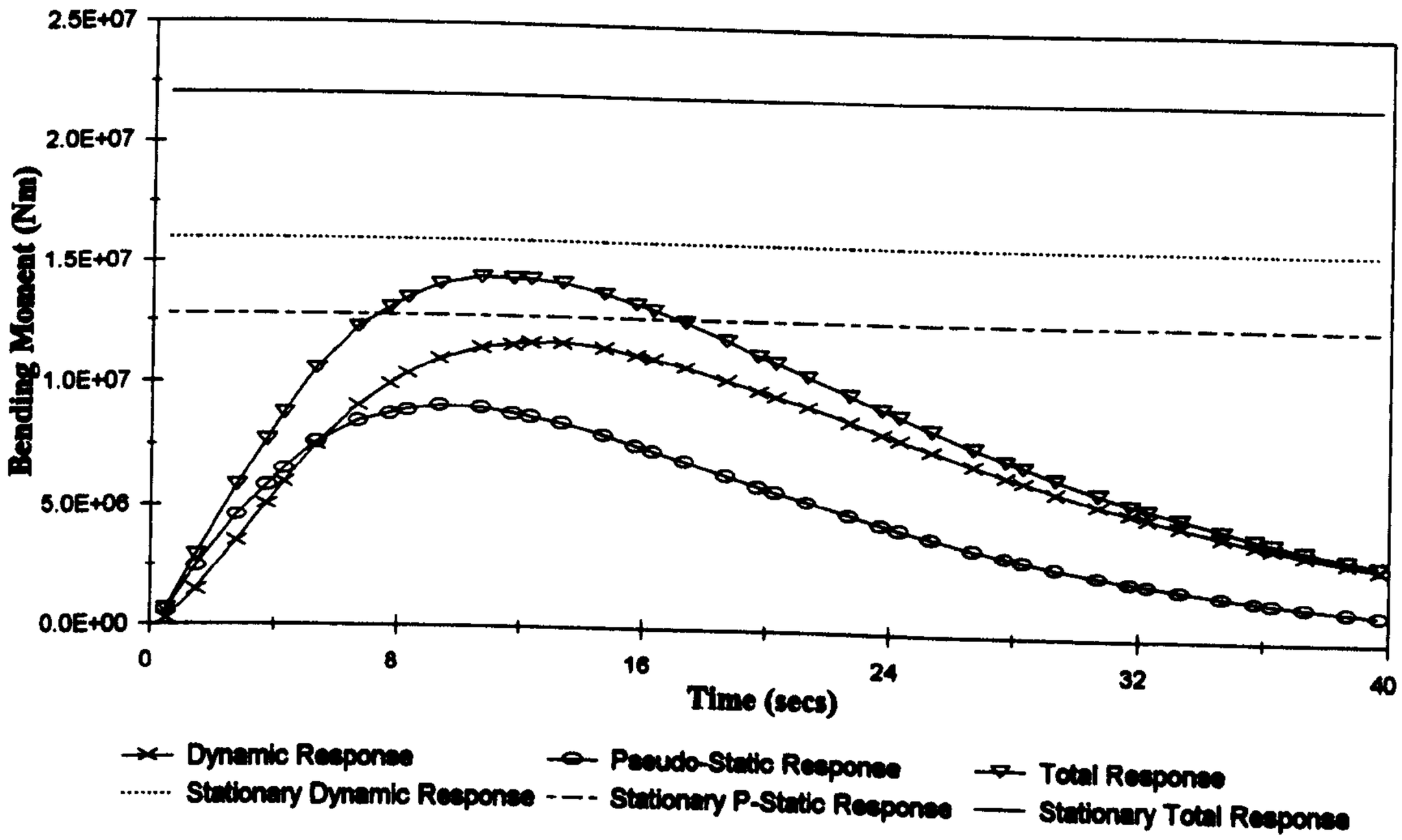

Figure 5.55 -:- Peak Bending Moments In Side Span, Non Stationary Horizontal Excitation

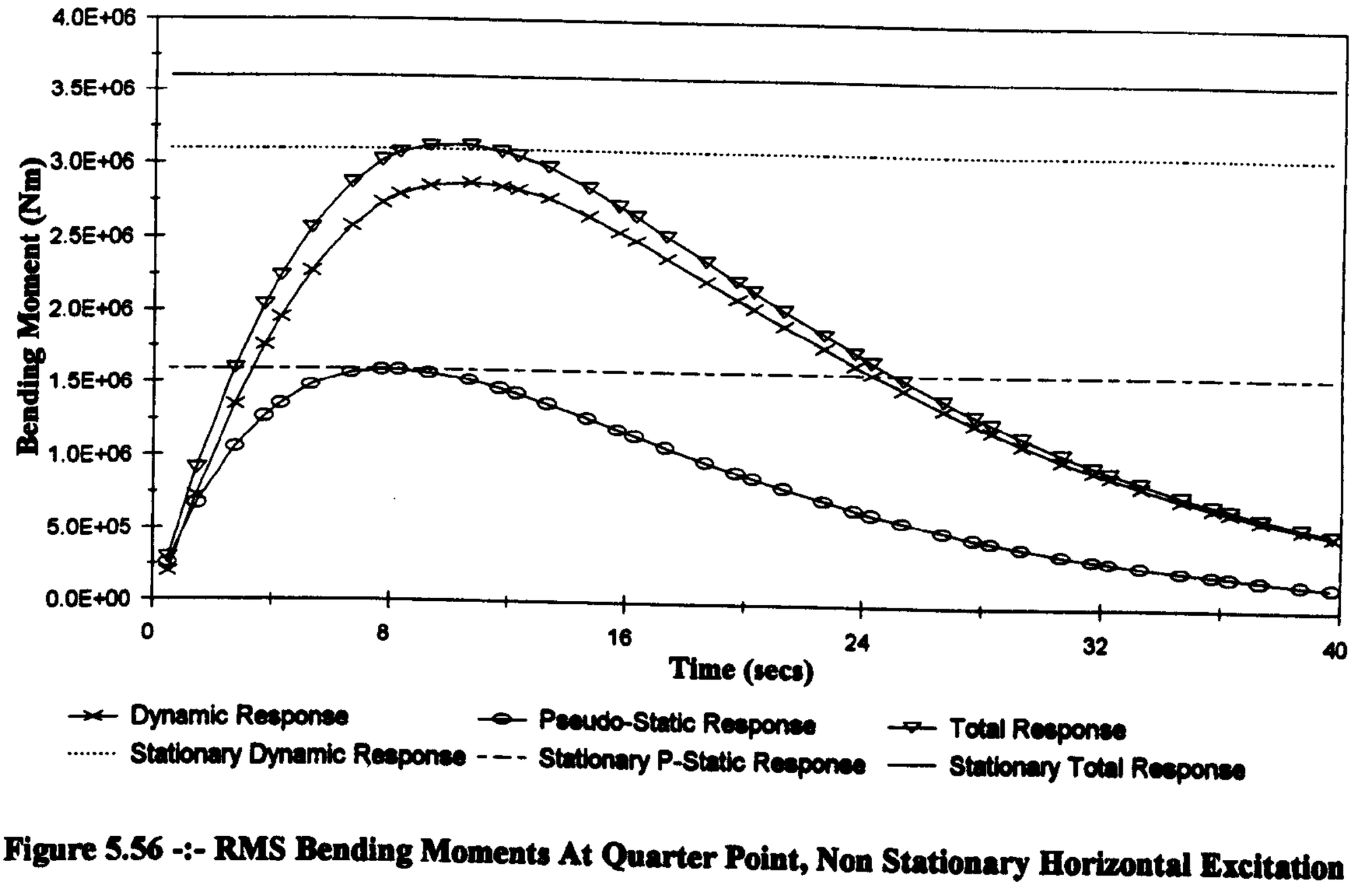

Figure 5.56 -:- RMS Bending Moments At Quarter Point, Non Stationary Horizontal Excitation

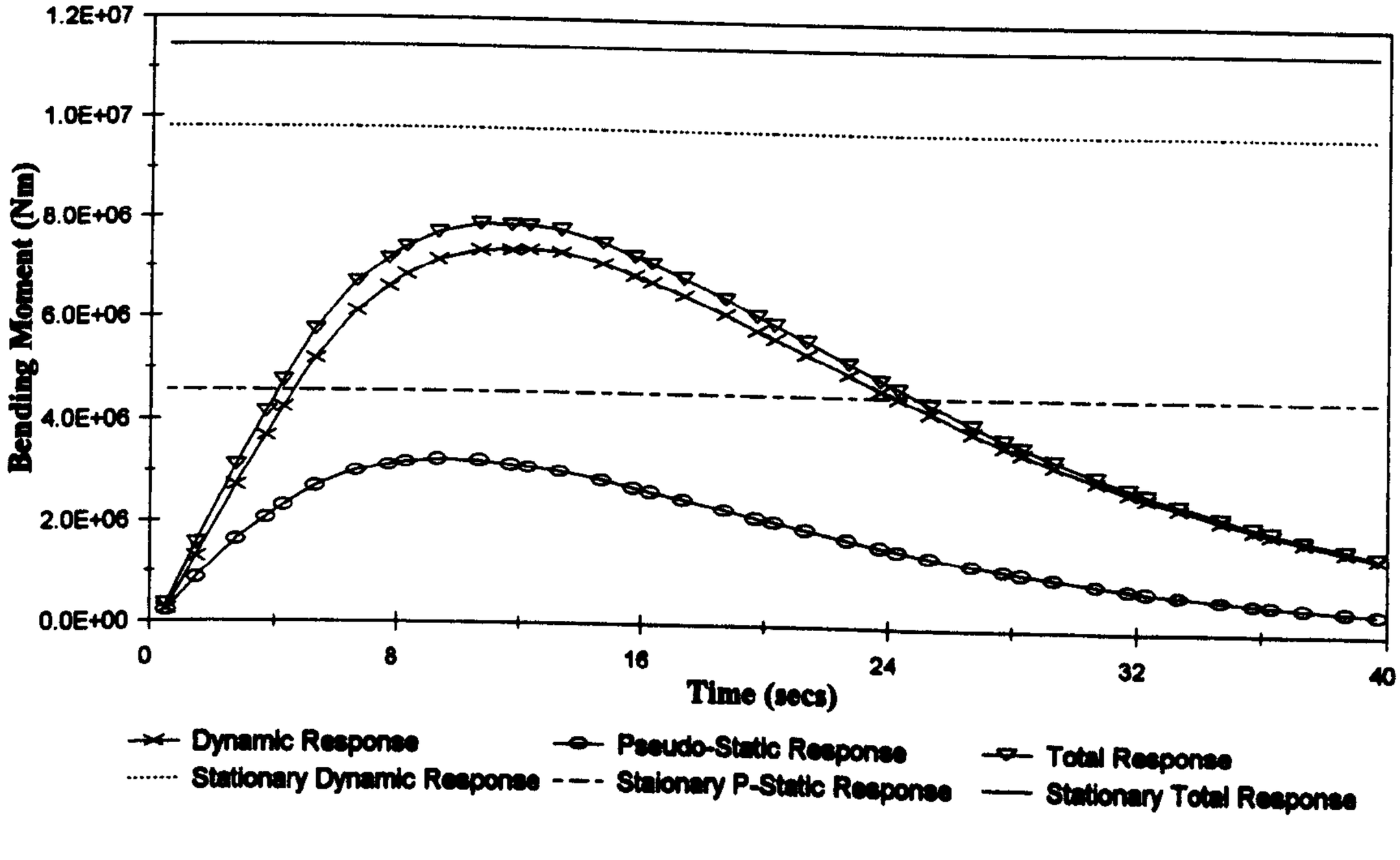

Figure 5.57 -:- Peak Bending Moments At Quarter Point, Non Stationary Horizontal Excitation

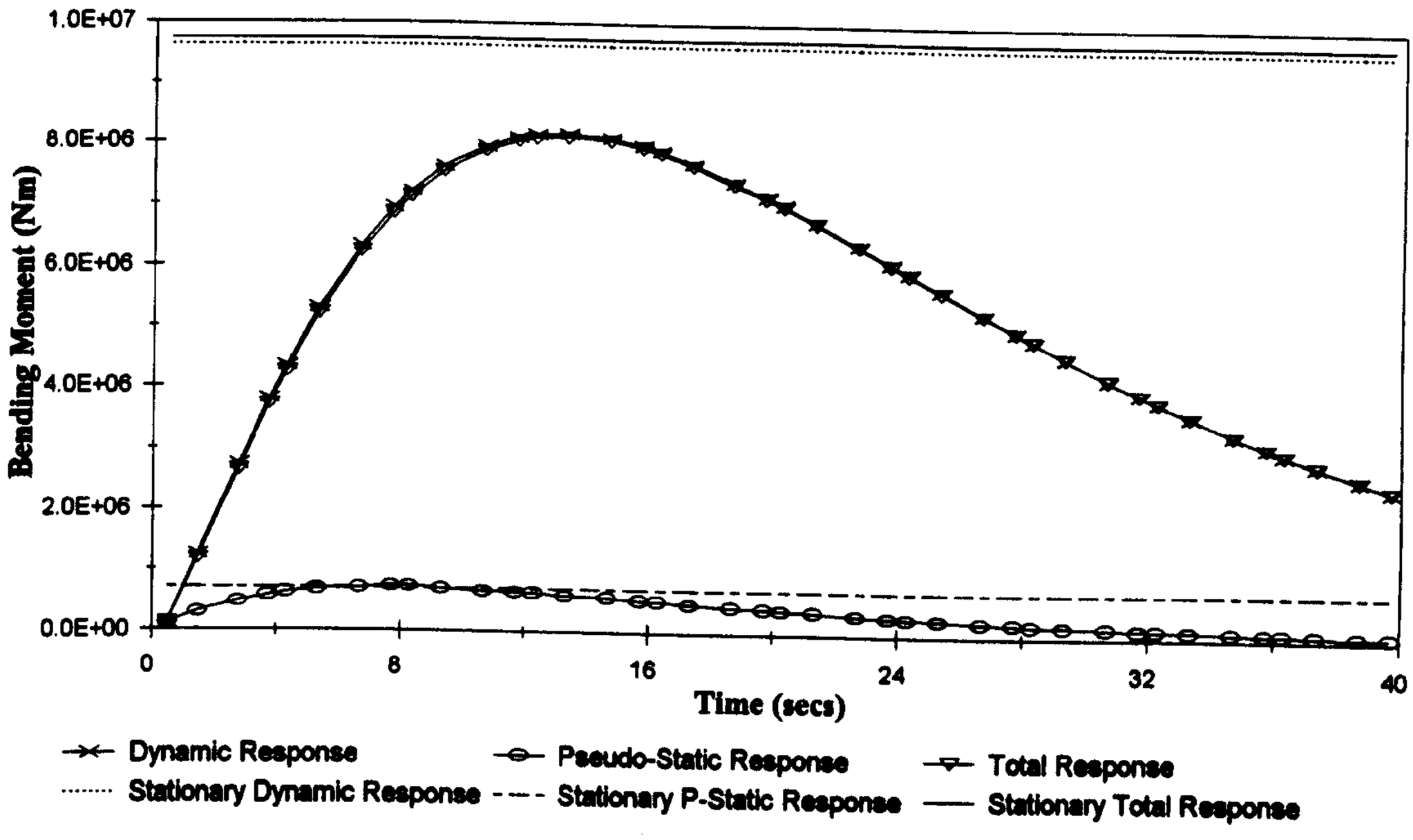

Figure 5.58 -:- RMS Bending Moments At Mid Span, Non Stationary Horizontal Excitation

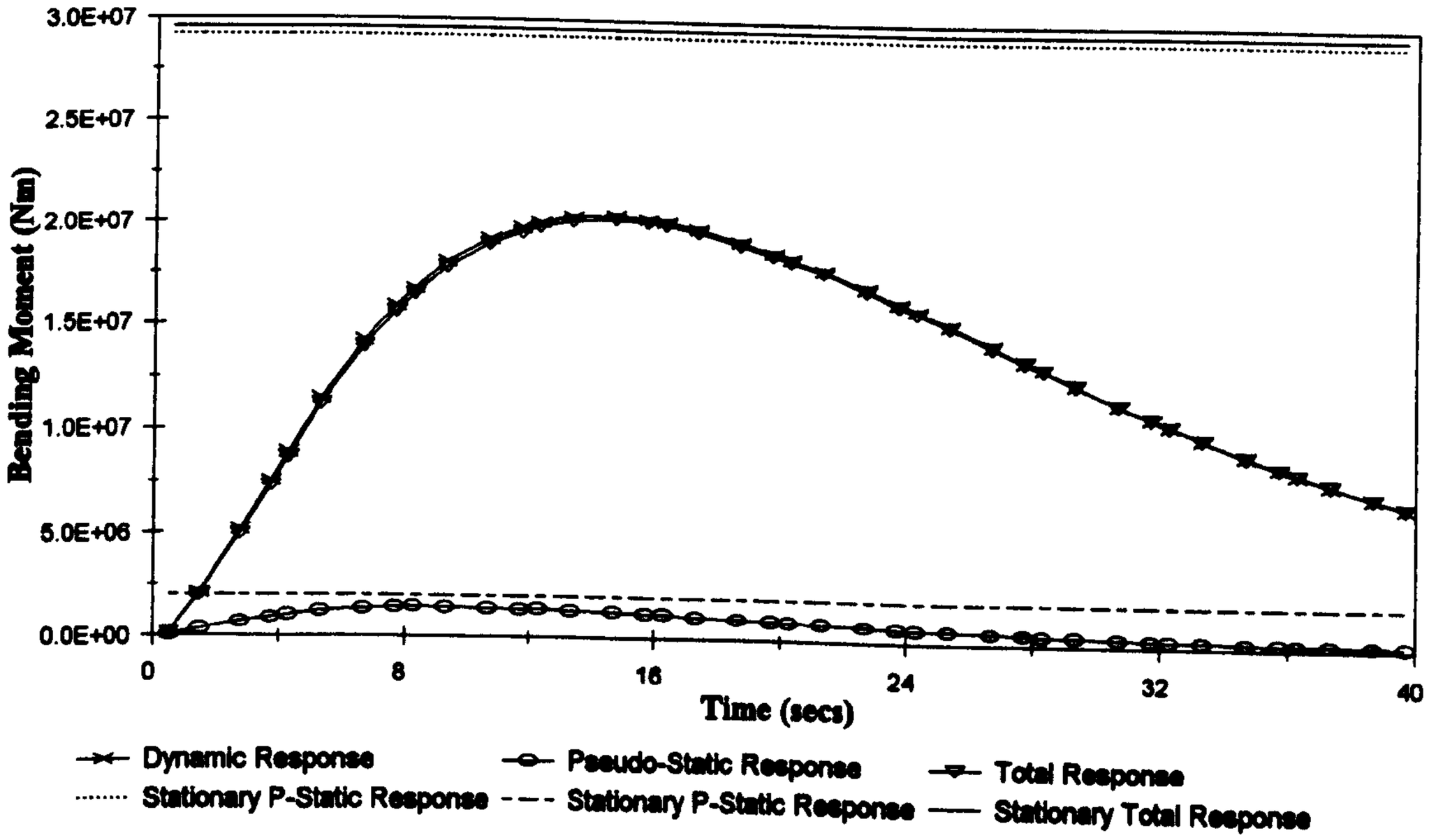

Figure 5.59 -:- Peak Bending Moments At Mid Span, Non Stationary Horizontal Excitation

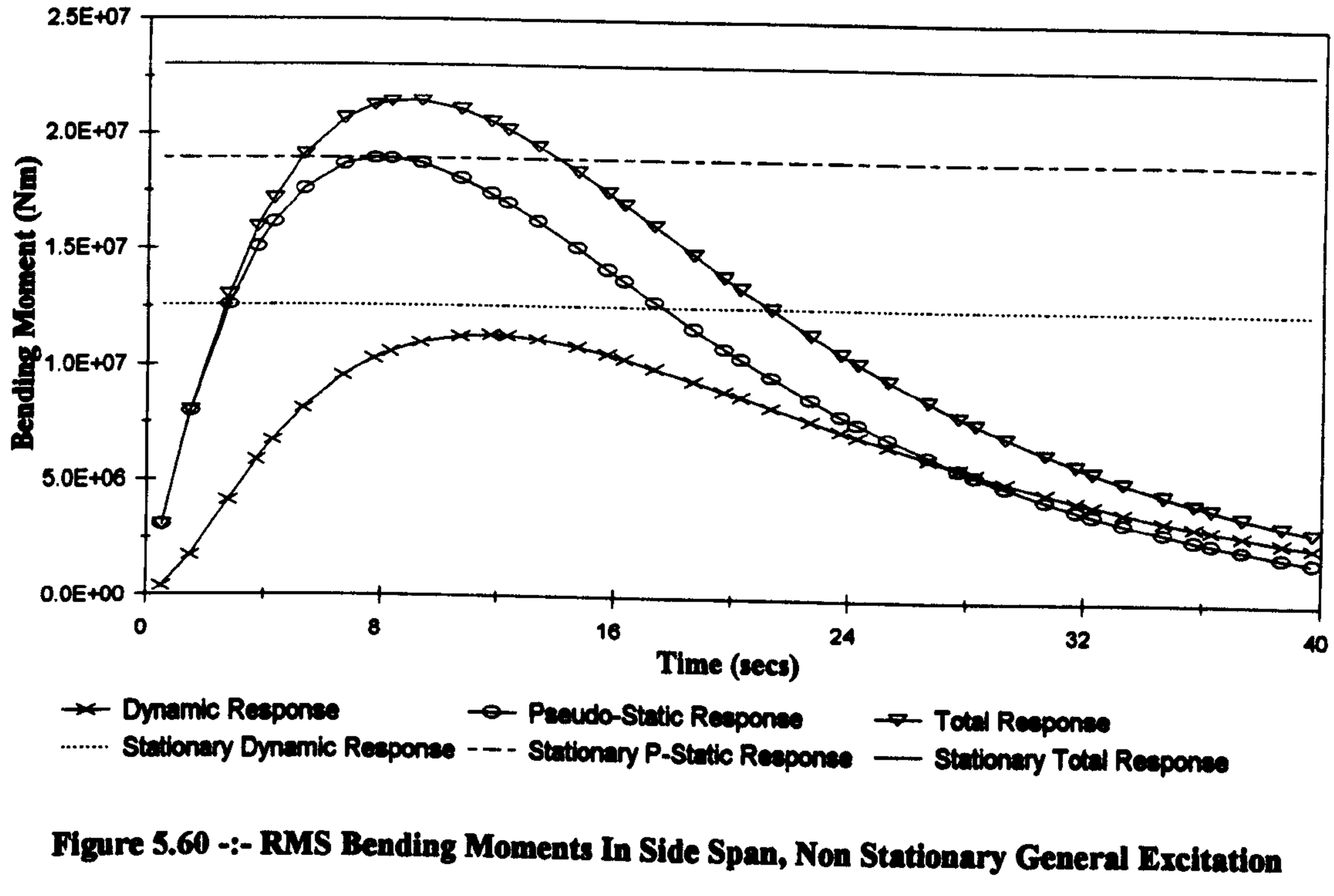

Figure 5.60 -:- RMS Bending Moments In Side Span, Non Stationary General Excitation

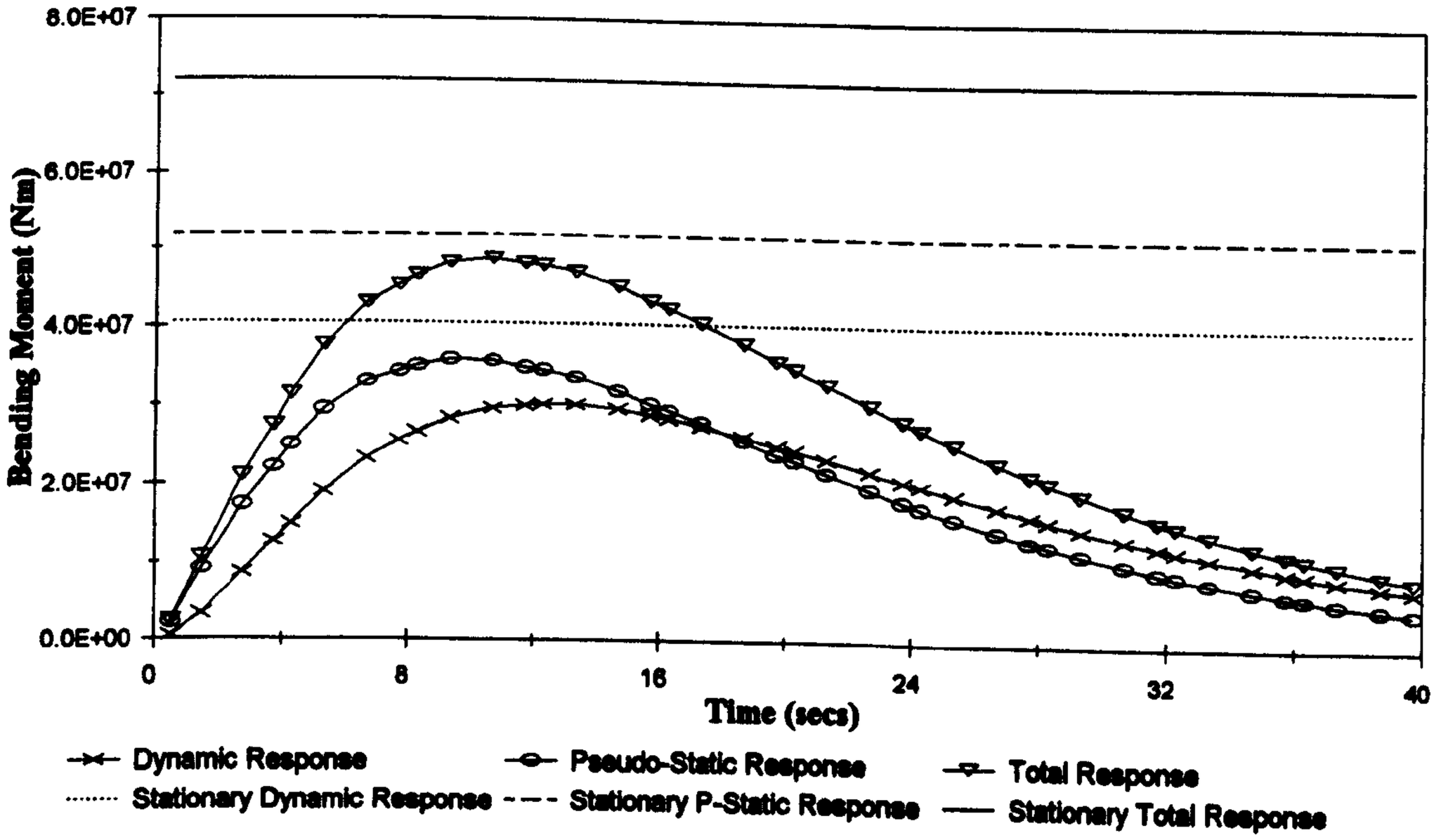

Figure 5.61 -:- Peak Bending Moments In Side Span, Non Stationary General Excitation

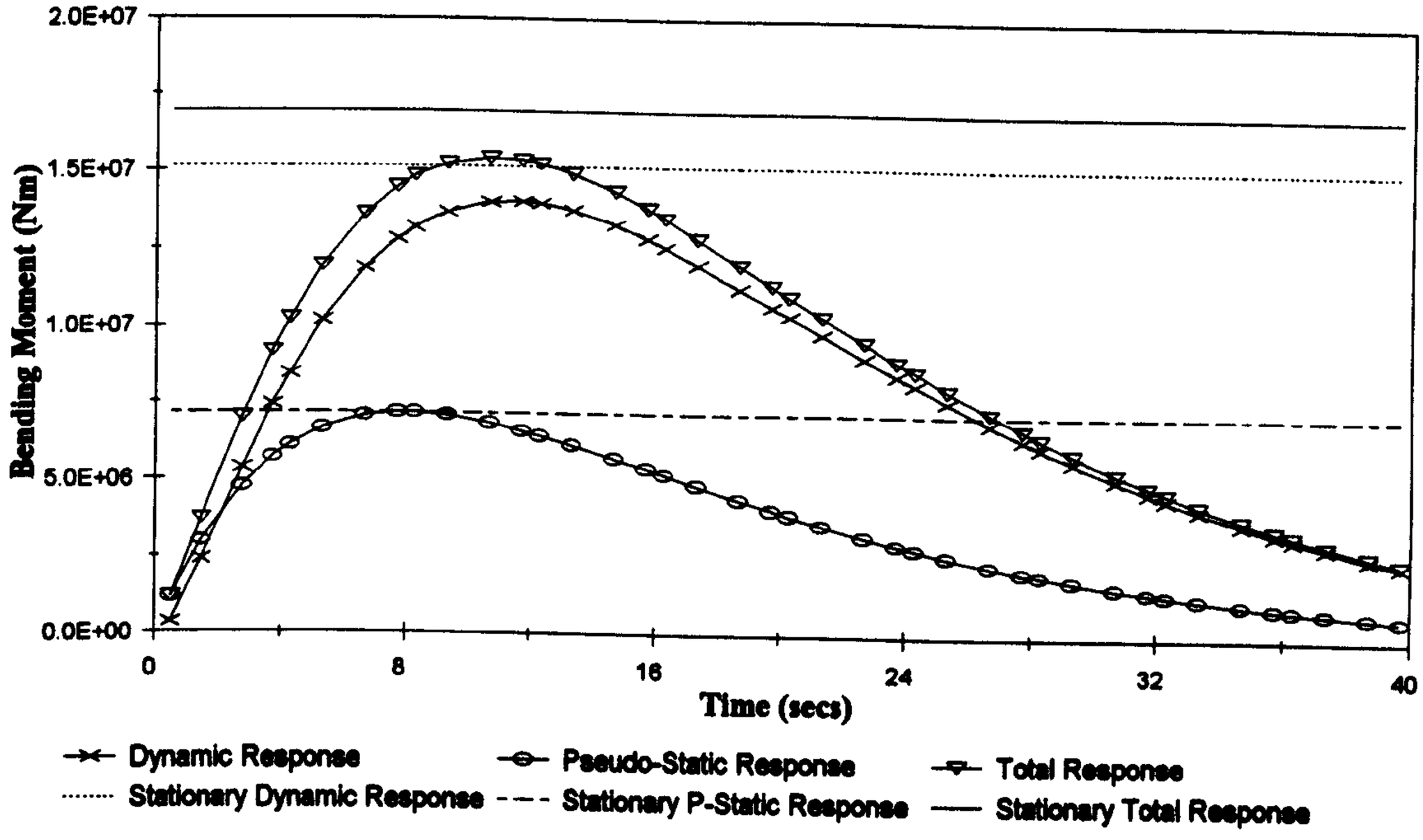

Figure 5.62 -:- RMS Bending Moments At Quarter Point, Non Stationary General Excitation

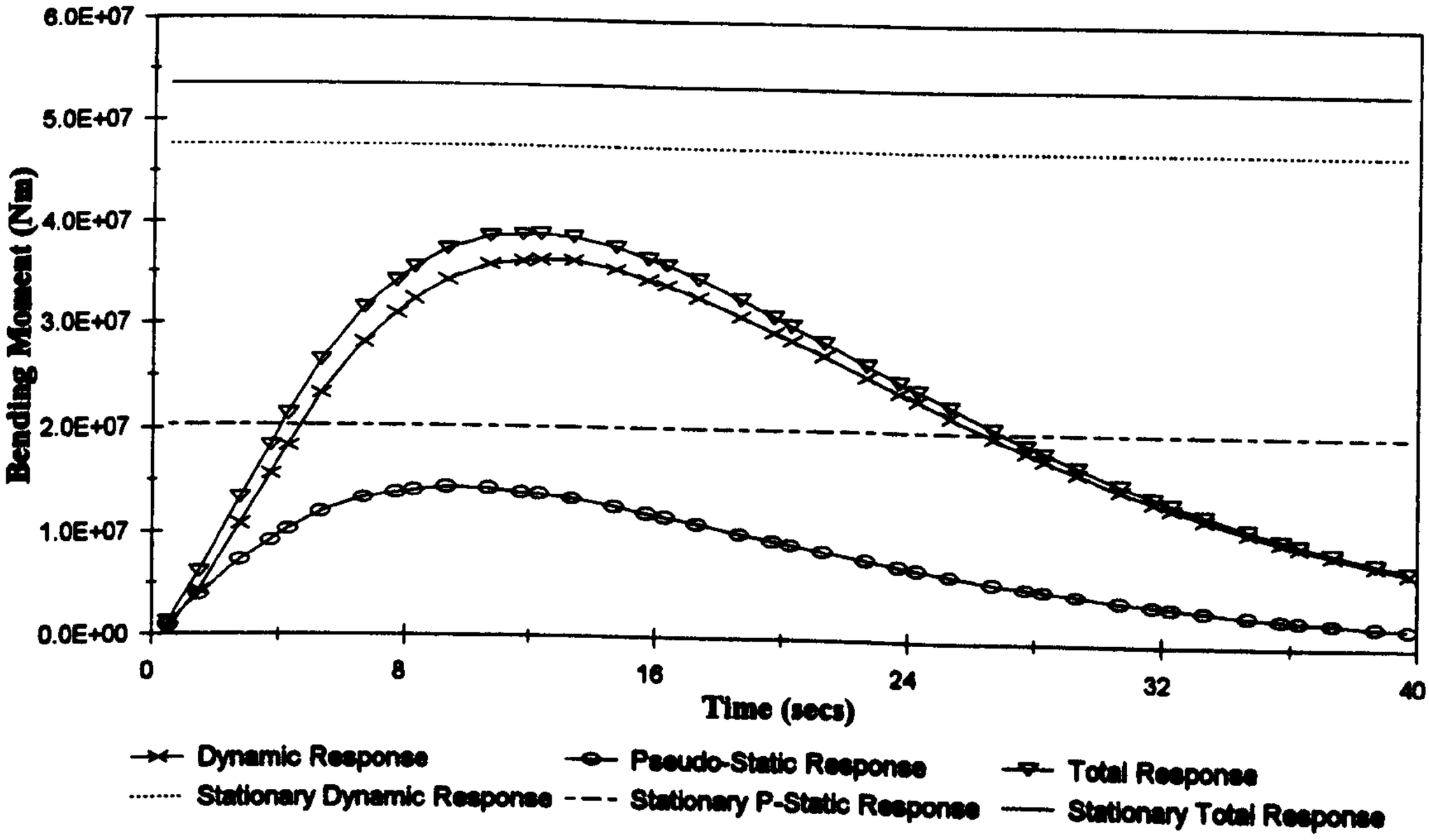

Figure 5.63 -:- Peak Bending Moments At Quarter Point, Non Stationary General Excitation

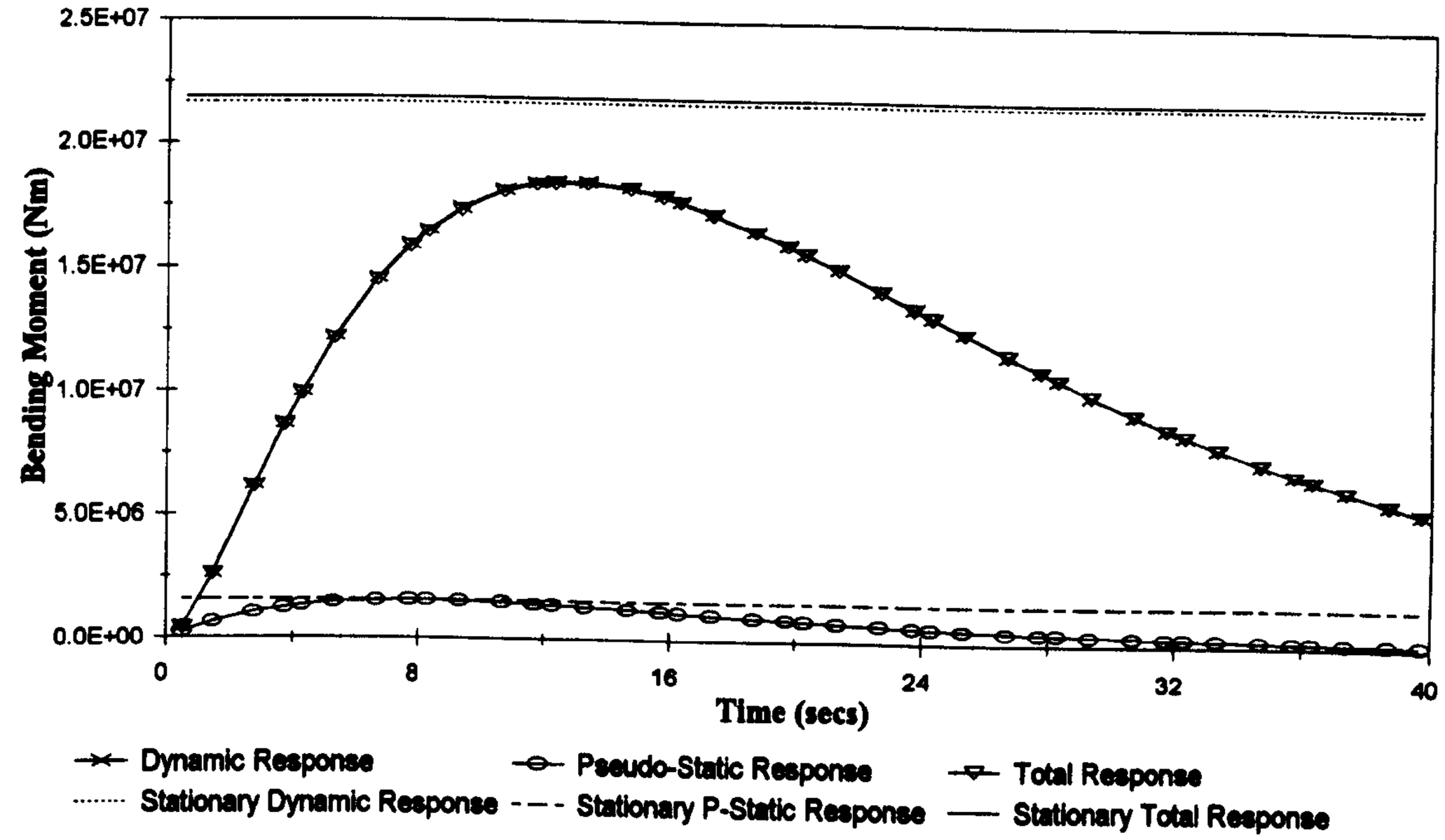

Figure 5.64 -:- RMS Bending Moments At Mid Span, Non Stationary General Excitation

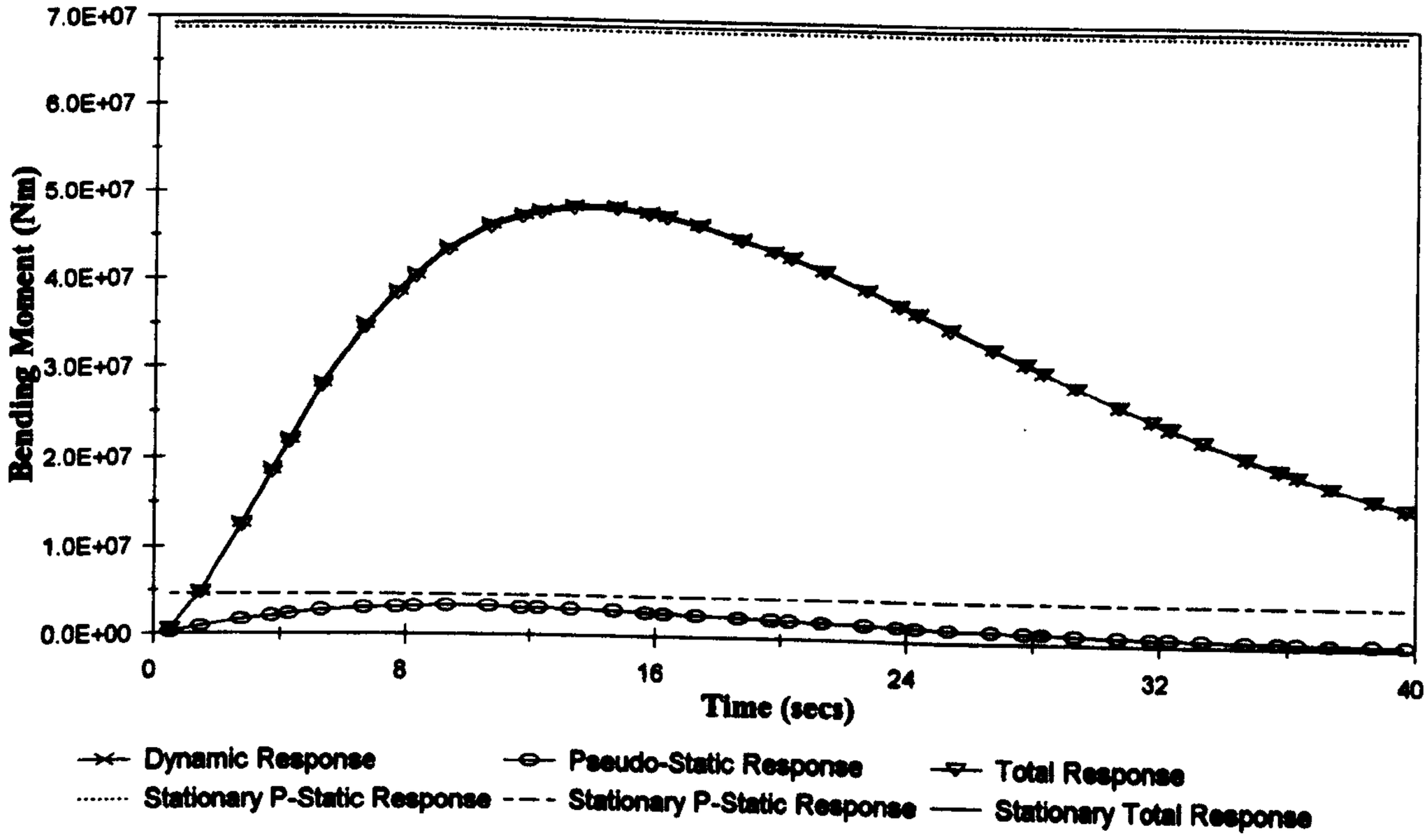

Figure 5.65 -:- Peak Bending Moments At Mid Span, Non Stationary General Excitation

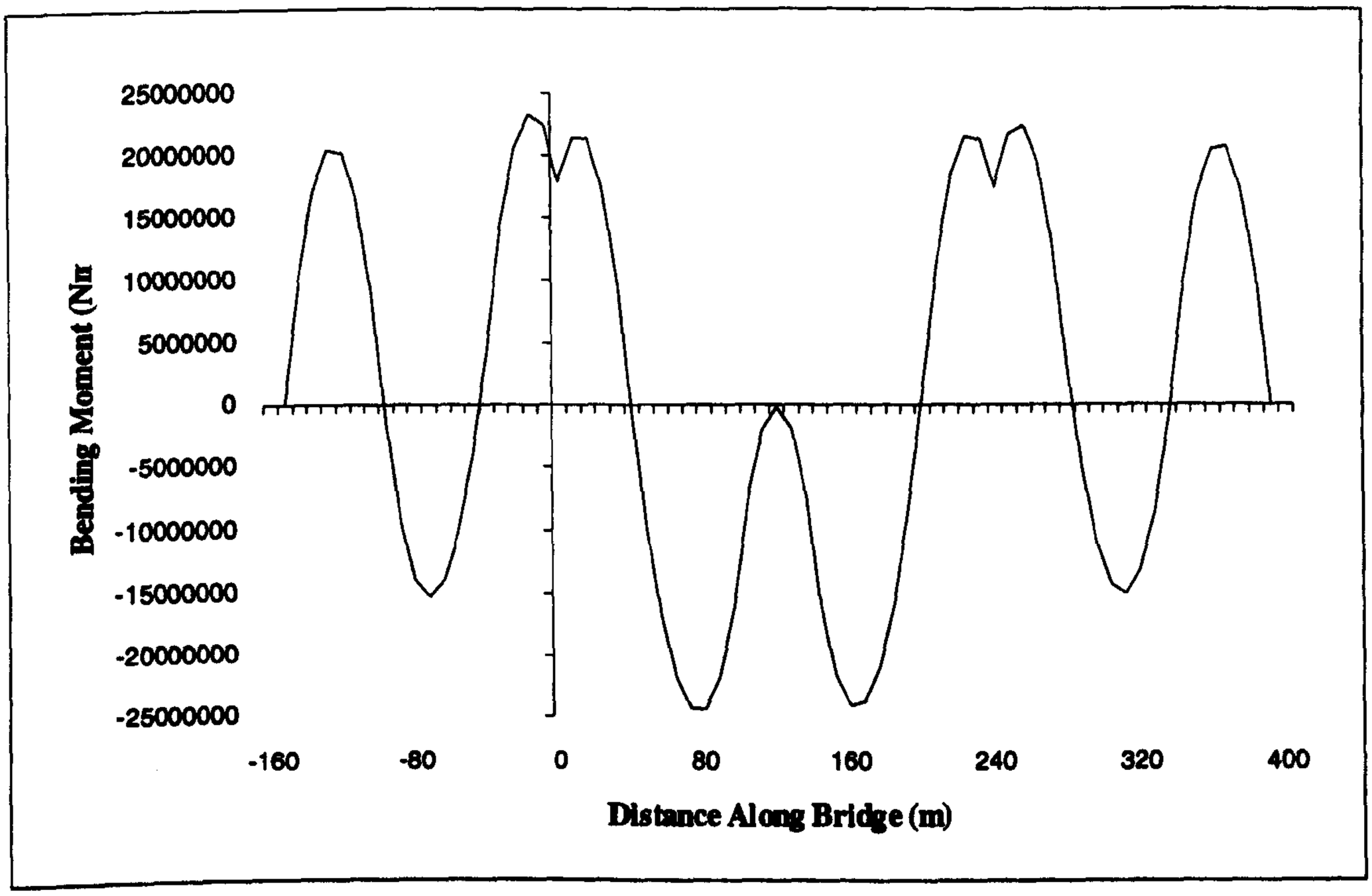

Figure 5.66 : Magnitude of Bending Moment Under Self Weight

Chapter Six

The Response Of Cable-Stayed Bridges To Wind Excitation: An Introduction And Review

6.1 Introduction

The work presented so far in this thesis has concentrated on earthquake excitation and the response of cable-stayed bridges to spatially varying seismic loads. However, one of the conclusions from chapter five was that the power spectral approach developed in chapter three may be more applicable to problems where there is a continuous interface between the load and the structure. For seismic excitation this means structures such as dams and pipelines. For long span bridges other kinds of dynamic excitation which act along the length of the deck, such as wind or traffic loading, could then be considered. In fact this may represent an important extension of the method since earthquakes do not usually pose the most serious threat to long span bridges. Two reasons for this are:

a. The occurrence of major earthquakes is restricted to certain geographic areas and many bridges are built outside these regions.

b. Even in highly active seismic zones, large earthquakes occur at relatively infrequent intervals.

In contrast wind and traffic loading are experienced daily by all bridges irrespective of location, and severe winds occur more frequently than do earthquakes. Wind and traffic therefore represent the more important dynamic loads to be considered in design for both the serviceability and the ultimate limit states.

There are numerous examples of bridges failing, both under traffic loading and under wind. In many cases, such as the Tay Bridge disaster in 1879, failure occurred due to the applied loads exceeding the resistance of the structure, rather than due to dynamic response. However there have been examples where excessive dynamic response under wind loading has lead to damage and even collapse of bridges, especially those with long suspended spans. Several notable failures occurred in Great Britain early in the nineteenth century; Telford's bridge across the Menai Straits was damaged by gales in 1826 and again in 1836 [Provis 1839], and one of the spans of the Brighton chain pier was destroyed in 1836 [Scott-Russell 1841]. Perhaps the most famous example, though, was the Tacoma Narrows bridge which failed soon after completion in 1940 [Farquharson 1950]. This event has had a great influence on the design of long span bridges, and marked a turning point in the battle to achieve yet longer spans [Billington 1977].

The historical examples in the last paragraph show clearly that the dynamic response to wind excitation is an important factor in the design of long span bridges. Therefore, the purpose of this chapter is to extend the approach developed in chapter three for earthquake excitation to the field of wind engineering. It will first briefly outline the factors that influence the response of long span bridges to wind loading. Then it will discuss previous work dealing with the spatial variation of the wind and its influence on bridge response. Finally it will introduce the testing of a prototype cable-stayed bridge in Scotland.

6.2 The Response Of Long Span Bridges To Wind Loading

The purpose of this section is not to give a detailed analysis of wind loading, instead the main concepts shall be outlined so that they can be referred to in more detail as appropriate later on. For a detailed treatment of this subject the reader is referred to Wind Effects On Structures, [Simiu &

Scanlan 1986] from where most of this section has been taken. There are two principal aspects of wind loading which need to be considered, the area of aerodynamics and the area of aeroelasticity. Aerodynamics describes the forces which act on a bridge due to the flow of the air, whereas aeroelasticity describes the interaction of movement of the bridge with the airflow.

6.2.1 Aerodynamic Forces

If a bluff body is placed in a smooth fluid flow, such as a long span bridge deck in a steady wind, then the flow of the fluid around the body will give rise to a pressure on the body. The magnitude of this pressure is determined by Bernoulli's equation:

$$p + \frac{1}{2}\rho U^2 + \rho g h = \text{constant} \quad \text{.....(6.1)}$$

Which reduces to the following form if the flow is horizontal:

$$p + \frac{1}{2}\rho U^2 = \text{constant} \quad \text{.....(6.2)}$$

Here p represents the pressure on the body and U the velocity of the streamline adjacent to the body. However as the velocity varies across the body so will the pressure and p therefore represents a local pressure distribution. Now the pressure acting on the body can also be described in terms of a pressure coefficient, C_P, which is a non dimensional grouping relating the pressure acting on the body, p, to the far upstream pressure, p_0, and the dynamic pressure of the free stream, $\frac{1}{2}\rho U^2$:

$$C_P = \frac{p - p_0}{\frac{1}{2}\rho U^2} \quad \text{.....(6.3)}$$

The forces acting on the body can be found by integrating the pressure over the surface of the body. These are conveniently resolved into two components; the along wind force, known as drag, the across wind force, known as lift (figure 6.1). In addition, because the pressure distribution varies across the body there will also be a resultant moment. Similar coefficients are defined for these terms as for the pressure:

$$C_L = \frac{F_L}{\frac{1}{2}\rho U^2 B} \quad \text{.....(6.4)}$$

$$C_D = \frac{F_D}{\frac{1}{2}\rho U^2 B} \quad \text{.....(6.5)}$$

$$C_M = \frac{M}{\frac{1}{2}\rho U^2 B^2} \quad \text{.....(6.6)}$$

Finally, separation of the flow as it passes over the body can cause vortices to form in the wake (figure 6.2). These vortices are shed periodically and give rise to another aerodynamic force which can be very important for long span bridges. The frequency of vortex shedding is a function of wind velocity and is described by the Strouhal number:

$$\mathcal{S} = \frac{N_s D}{U} \quad \text{.....(6.7)}$$

The aerodynamic forces acting on a bluff body, the lift and drag as well as vortex shedding, are determined by its profile and orientation to the airflow. The choice of the shape for the deck cross section is therefore an important factor in designing long span bridges.

6.2.2 Aeroelastic Effects

The previous section described the aerodynamic forces which act on a bluff body such as a bridge deck, and mentioned how they depend on the shape of the body. However, when these forces act on the body they give rise to displacements, both translations and rotations. For long span cable supported bridges, which are very flexible structures, these deflections can be large and can in turn alter the aerodynamic properties of the bridge deck. This interaction of structure and wind is termed aeroelasticity and can lead to instability under certain circumstances. There are several aeroelastic effects, the more important being galloping, flutter and lock in of vortex shedding.

6.2.2.1 Galloping

Galloping occurs when the aerodynamic forces change with the relative angle of attack. The relative angle of attack is the angle that the body makes with the incident wind (figure 6.3). This depends on the velocity of the wind relative to the deck and hence on the velocity of the body itself (figure 6.4). Consequently, the aerodynamic forces will depend on the across wind velocity of the body, and the equation of motion is given by:

$$m\left(\ddot{v}+2\xi_r\omega_r\dot{v}+\omega_r^2 v\right)=-\frac{1}{2}\rho U^2 B\left(\frac{dC_L}{d\alpha}+C_D\right)_0\frac{\dot{v}}{U} \quad \text{.....(6.8)}$$

The aerodynamic forces can therefore be taken as contributing to the overall damping of the system, a phenomenon termed aerodynamic damping. Instability occurs in a system when the overall damping is less than zero i.e. the damping no longer removes energy from the system. As mechanical damping is almost always positive, instability will only occur in the system described by equation 6.8 if:

$$\left(\frac{dC_L}{d\alpha}+C_D\right)_0<0 \quad \text{.....(6.9)}$$

Furthermore, C_D will also be positive and instability can therefore be identified with a sudden loss of lift, somewhat analogous to the bridge deck stalling.

6.2.2.2 Flutter

Classical flutter arises when two modes, one vertical one torsional, are coupled in an unstable oscillation. Flutter has been known to cause serious problems with long span bridges, and it is important to know the flutter characteristics of a bridge before it is built. These are described by the flutter derivatives, $H_1^*, H_2^*, H_3^*, A_1^*, A_2^*, A_3^*$, which describe the coupling between vertical and torsional modes in terms of the reduced frequency K:

$$L_h = \frac{1}{2}\rho U^2 (2B)\left[KH_1^*(K)\frac{\dot{h}}{U} + KH_2^*(K)\frac{B\dot{\alpha}}{U} + K^2 H_3^*(K)\alpha \right] \quad \text{.....(6.10)}$$

$$M_\alpha = \frac{1}{2}\rho U^2 (2B^2)\left[KA_1^*(K)\frac{\dot{h}}{U} + KA_2^*(K)\frac{B\dot{\alpha}}{U} + K^2 A_3^*(K)\alpha \right] \quad \text{.....(6.11)}$$

where

L_h = aerodynamic lift force

M_α = aerodynamic moment

$$K = \frac{B\omega}{U}$$

The flutter derivatives are usually determined from wind tunnel tests on scale models of the structure during the design process.

6.2.2.3 Vortex Shedding And Lock In

One of the aerodynamic forces acting on a bridge is caused by the periodic shedding of vortices from the deck as the air flows over it (§ 6.2.1). Under most conditions this does not cause major problems, however, when the frequency of vortex shedding approaches the natural frequency of one of the modes of the bridge, interaction between the bridge response and the vortex shedding occurs. Oscillations of the bridge deck cause the vortices to be shed at the natural frequency of the bridge for a range of velocities (figure 6.5). This phenomenon is known as lock in and can give rise to large amplitude response for a narrow range of wind velocities (figure 6.6).

6.3 Atmospheric Turbulence

The discussions in this chapter so far have concentrated on the response of long span bridges to steady fluid flow. However in the real world the wind is very seldom a steady flow of air and the velocity varies with time for two main reasons [Davenport 1965a]:

a. Movement of the large scale pressure systems that give rise to the wind.

b. The influence of the ground surface on the airflow.

A spectrum of the wind velocity shows that these two effects give rise to velocity fluctuations with quite different periods (figure 6.7). Surface induced fluctuations, or turbulence, generally have a period of around 1-2 minutes, whereas velocity fluctuations due to the movement of weather systems have periods of around 4 days. Of these two, the turbulent winds are of particular interest to the designer since gusts can occur at frequencies similar to the natural frequencies of long span bridges and can therefore be a source of dynamic excitation. This excitation is known as buffeting. Other minor peaks occur in figure 6.7 which correspond to daily and seasonal effects. It is also important to

note from figure 6.7 that there is very little energy within the band 5 minutes to 4 hours. This represents the so called spectral gap and is an important factor in determining the procedures for monitoring the response of a bridge to wind loading.

The most important factor influencing the development of turbulence in the airflow is the roughness of the ground. The open sea has little influence on the air flow allowing steady winds to build up with very little turbulence. Flat open countryside also leads to steady winds, but in contrast wooded or urban areas have much greater influence leading to much higher levels of turbulence (figure 6.8) [Davenport 1965a]. Another factor which can influence the build up of turbulence is the topography of the surrounding terrain. Wind tunnel tests on model bridges [Davenport & King 1990] have shown that the presence of hills and canyons influence both the level and spatial variation of turbulence in the wind. Furthermore wind flowing down over steep hills or escarpments can generate so called lee waves. These different factors and their influence on the turbulence of the wind played an important part in selecting Kessock Bridge for the prototype testing presented in chapters seven and eight, as will be outlined in chapter seven.

6.3.1 Descriptions Of Turbulence

Atmospheric turbulence is essentially a random process which means that it is best described using a statistical model. For design purposes, this means that a power spectrum can be used to describe the fluctuating wind and the dynamic analysis can be performed in the frequency domain [Davenport 1961b]. This will of course have the same advantages as outlined in chapter 2 for the power spectral approach for seismic excitation. However, as well as having a tool for design purposes it is also useful to have a measure of turbulence which allows different wind records and sites to be compared. The

power spectra can be used, but several other measures have also been suggested such as the turbulence intensity which is defined as:

$$I_T(z) = \frac{\sigma_{u(z)}}{U(z)} \quad \text{.....(6.12)}$$

This describes the fluctuations in the wind speed as a proportion of the mean speed. Another measure represents the turbulence as large eddies superimposed on the mean flow. The turbulence is then described in terms of the integral lengths:

$$L_u^x = \frac{1}{u^2}\int_0^\infty R_{u_1u_2}(x)dx \quad \text{.....(6.13)}$$

$$L_u^y = \frac{1}{u^2}\int_0^\infty R_{u_1u_2}(y)dy \quad \text{.....(6.14)}$$

$$L_u^z = \frac{1}{u^2}\int_0^\infty R_{u_1u_2}(z)dz \quad \text{.....(6.15)}$$

which represent the size of the eddies in three orthogonal directions, for the longitudinal velocity u. It should be noted here that the along wind integral length is typically larger than the corresponding across wind lengths [Counihan 1975, Duchêne-Marullaz 1980]

6.3.2 Influence On Bridge Response Of Spatial Variations In The Wind

The use of integral scales to describe the atmospheric turbulence conveniently illustrates an important factor for the design of long span bridges. Typical values for linear scales of turbulence can be of the order of 100s of metres [Simiu & Scanlan 1986], which is the same order of magnitude as many medium to long span bridges. It is therefore possible that turbulence in the incident wind will not only cause dynamic excitation, but it will also lead to significant variations in this loading along the span. This can have consequences for the bridge response in a similar way that spatial variations in

the seismic loading influence the response of extended structures. For wind loading there will be no pseudo-static component to the response, but spatial variations in loading could influence the dynamic response by preferentially exciting different modes.

This problem was first addressed by A. G. Davenport during research for his PhD [Davenport 1961a] and in subsequent studies [Davenport 1962, 1965b]. He developed a quantity, the joint mode acceptance, which related the spatial correlation of the fluctuating wind component to a set of generalised coordinates:

$$|J_r(n)|^2 = \frac{1}{N_r^2}\int_0^l\int_0^l \frac{S_{xx'}(n)}{S_{xx}(n)}\varphi_r(x).\varphi_r(x')dxdx' \quad \text{.....(6.16)}$$

The acceptance was then used to modify the power spectrum of the input forces in a standard spectral analysis:

$$S_{p_r}(n) = |J_r(n)|^2 . S_{p_0}(n) \quad \text{.....(6.17)}$$

The spectral approach suggested by Davenport is summarised in figure 6.9. The gust spectrum, or power spectrum of velocity fluctuations in the wind, is related to the force spectrum by the aerodynamic admittance, $|\chi(n)|^2$ and the following equation:

$$S_{ff}(n) = 4F_s^2|\chi(n)|^2 \frac{S_{uu}(n)}{U^2} \quad \text{.....(6.18)}$$

where F_s is the response to a steady state wind U. The force spectrum is then modified by the joint mode acceptance described above (equation 6.17) and combined with the frequency response function of the structure, otherwise known as the mechanical admittance, to give the structural response:

$$S_{rr}(n) = \frac{H_r(n)H_r^*(n)}{K_r^2} S_{p_r}(n) = \frac{H_r(n)H_r^*(n)}{K_r^2} \left|J_r(n)\right|^2 S_{p_0}(n) \quad \text{.....(6.19)}$$

The generalised coordinate system chosen by Davenport in calculating the joint mode acceptance in 6.16 was the mode shapes of the bridge deck. This produced a very neat solution to the problem as it removed the spatially varying component of the wind by expressing it directly in terms of the mode shapes of the structure. Hence, the spatial variations were effectively expressed as functions of frequency and the solution found using a simple frequency domain analysis. Furthermore, because modal coordinates were used the problem was reduced to a set of single degree of freedom systems. However, this approach is not without its drawbacks. Most notably, the bridge is assumed to be a beam and therefore account is not taken of the interaction of the rest of the structure either with the wind or the bridge deck.

Another limitation to this work was that it considered only the spatial variation of the aerodynamic forces; pressure, lift and drag. Perhaps of greater importance to long span bridges is the influence of turbulence and spatial variation of the wind on the aeroelastic effects discussed in section 6.1.3. Investigations into the buffeting response of bridges have shown that buffeting (i.e. the excitation by a turbulent wind) can greatly influence the flutter characteristics of a bridge [Soo & Scanlan 1983]. This observation has been borne out by wind tunnel studies, and it is now the norm to measure the flutter characteristics of proposed bridge decks in a turbulent rather than smooth flow [Davenport & King 1990]. This would indicate that spatial variations of the wind influence the aeroelastic coupling between the vertical and torsional modes. The third aeroelastic phenomenon discussed in section 6.1.3 was lock in of vortex shedding. This however is very sensitive to velocity, and so the large fluctuations in velocity experienced in a turbulent wind are likely to reduce its occurrence. However, the lower the level of turbulence, the longer the integral length will be, and so for long-span bridges

loss of coherence along the deck could be important. Studies have recently been done which have demonstrated ways of tackling this loss of coherence [Ehsan *et al.* 1990].

To summarise this section, spatial variations in the wind loading can have an influence on both the aerodynamic and the aeroelastic response of a bridge. Davenport proposed a neat method of dealing with the spatial variations of the wind loading by expressing the spatial distribution of the loading in terms of the mode shapes of the deck. This, however, has certain limitations due to the assumption that the bridge can be treated as a beam. The method power spectral approach to spatially varying seismic excitation in chapter three was developed from Davenport's model § 3.2.2, but introduced a more comprehensive system of generalised coordinates. This enabled the response to be determined even when the structure was not fully coincident with the loading. It is now necessary to extend Davenport's method in a similar way to apply the ideas from chapter three to wind loading.

6.3.3 Extension Of The Approach Developed In Chapter Three

From the foregoing discussion two factors can be concluded:

a. The wind speed varies both spatially and temporally

b. These fluctuations represent random behaviour

These two factors imply that a two dimensional field representation of the wind structure similar to the earthquake model used in chapter three would be a possible approach to solving the problem. Furthermore, as pointed out in the previous section, the seismic analysis was developed from the model Davenport proposed for wind loading, and therefore an extension of this to wind loading would seem sensible.

Firstly, it must be assumed that the wind loading can be described as a two dimensional random field defined in terms of a space parameter, *s*, and a time parameter, *t*. Then, assuming that the response at a point *x* in the structure can be expressed in terms of an influence line as discussed in § 3.2.2, the response will be given by:

$$v_x = \int_{-\infty}^{\infty} v_x(s)ds = \int_{-\infty}^{\infty} r_x(s).p(t)ds \quad (3.58)$$

This in turn can be transformed to the wavenumber domain:

$$v_x = \int_{-\infty}^{\infty} V_x(\kappa)d\kappa = \int_{-\infty}^{\infty} R_x(\kappa)P(\kappa)d\kappa \quad (3.59)$$

and an expression obtained for the power density spectrum of the response:

$$S_w(\kappa,n) = H(n)H^*(n)R_x(\kappa)R_x^*(\kappa)S_{pp}(\kappa,\omega) \quad (6.20)$$

where the dynamic component has been included. As with the seismic model, a finite element approach to the problem is assumed so that the continuous structure can be approximated by a discrete MDOF system. The terms in equation 6.20 then become matrices and vectors:

$$[\mathbf{S}_w(\kappa,n)] = \{\mathbf{H}(n)\}\{\mathbf{H}(n)\}^{*T}\{\mathbf{R}(\kappa)\}\{\mathbf{R}(\kappa)\}^{*T}S_{pp}(\kappa,n) \quad (6.21)$$

All that remains now is to transform the elements of equation 6.21 to the modal system of coordinates by pre multiplying by the grouping $[\Phi]^T[\mathbf{M}]$. The dynamic response will be orthogonal in the modal coordinates, giving a diagonal frequency response matrix $[\mathbf{H}(\omega)]_r$, though the wavenumber response will include cross correlations between the modes:

$$[\mathbf{S}_w(\kappa,n)]_r = [\mathbf{H}(n)]_r[\mathbf{H}(n)]_r^{*T}[\Phi]^T[\mathbf{M}]\{\mathbf{R}(\kappa)\}\{\mathbf{R}(\kappa)\}^{*T}[\mathbf{M}]^T[\Phi]S_{pp}(\kappa,n) \quad (6.22)$$

It is now useful to compare equations 6.19 and 6.22. Firstly, it should be noted that both equations treat the space and time domains as separable and both have equivalent expressions for the frequency response; the modal stiffness K_r in 6.19 is included in $\{\mathbf{R}(\kappa)\}$ in equation 6.22. Comparing the wavenumber domain response, the first point to note is that when the generalised coordinates in equation 6.16 are changed to complex exponentials defined over an infinite domain, the product in 6.17 becomes the frequency wavenumber power spectrum. Furthermore, as explained in §3.2.2, the modal stiffness, K_r, in equation 6.19 corresponds to the influence lines in 6.22. Therefore, it would appear that the two equations are equivalent. The only difference is that equation 6.22 takes into account the cross correlations between the different modes because the product:

$$[\Phi]^T[\mathbf{M}]\{\mathbf{R}(\kappa)\}\{\mathbf{R}(\kappa)\}^{*T}[\mathbf{M}]^T[\Phi]S_{pp}(\kappa,n)$$

results in off diagonal terms. This should lead to more accurate results although at the expense of computational efficiency.

6.4 The Prototype Testing Of Long Span Bridges

So far this chapter has described the importance of wind loading for long span bridges, and has described some of the aerodynamic and aeroelastic phenomena that cause it. It has also shown that the method developed in chapter three may be used to predict the response of a long span bridge to buffeting by the wind. Now, although this method has been validated by comparing its predictions with the results from other analytical approaches (chapter four), no comparisons have yet been made with measured data. It is usual to compare the results of computer analyses with data obtained either from scale model or prototype structures as this serves as an extra check on the method being used. The nature of the seismic excitation makes it very difficult to make the necessary measurements either

in the lab or in the field. However, wind loading does provide the opportunity to measure both the random excitation and the response of a structure to it over a long period of time. Therefore, wind excitation not only represents an important load case for these bridges, it also presents a means of checking the method against real data obtained from prototype tests. It is now useful to review some of the work which has been done both in dynamic testing, monitoring of the wind and in measuring the response of bridges to wind excitation.

6.4.1 Dynamic Testing

Dynamic testing is often used as an effective and powerful means of validating finite element models of all kinds of engineering systems, from mechanical components to large dams. The dynamic properties; mode shapes, natural frequencies and damping; can be found from a modal survey. Here, the response to a controlled excitation is measured at different points on the structure and the transfer function found. However, although this technique can be used for most engineering systems, including civil engineering structures such as dams [Severn *et al.* 1990] and intake towers [Daniell 1992, Daniell & Taylor 1993], problems can occur when testing full scale long span bridges where ambient excitation from traffic and wind forms the major source of loading. In these cases a modified technique has to be used making use of the ambient excitation; this has proved successful in many studies.

A team of researchers from the University of Bristol have developed finite element models for several long span bridges, including the Humber, Bogazici and Fatih Sultan Mehmet suspension bridges [Dumanoglu *et al.* 1992]. These have then been validated by field measurements of the response to ambient excitation [Brownjohn *et al.* 1987, 1989 & 1992]. Many similar exercises have been carried out on suspension bridges in the United States; these include tests on the Golden Gate Bridge [Abdel-

a + 1985b

Ghaffar & Scanlan 1985] and the St Thomas Bridge [Abdel-Ghaffar & Housner 1978, Abdel-Ghaffar 1978b]. Studies of the ambient vibration of cable stayed bridges include recent work by Wilson [Wilson & Gravelle 1991, Wilson & Tao Liu 1991]. There have also been examples of bridges being tested under forced excitation [Buckland *et al.* 1979] though this is often difficult to control and gives unreliable answers for the reasons discussed above.

6.4.2 Measurements Of Wind Loading

There have been many studies and many reports on the structure of the wind in the Earth's boundary layer, and discussing its effects both from an engineering and a meteorological point of view. Meteorological studies on the spatial distribution of the wind have concentrated on results obtained using arrays of anemometers placed on masts or towers. Teunissen [Teunissen 1980] calculated spatial cross correlations between 15 anemometers on an array of towers. He also calculated values of integral lengths using various techniques and compared the results with formulae given in the ESDU data sheets. Other research [Panofsky *et al.* 1974] has compared the along wind coherence measured over water with measurements over dry land. Berman and Stearns [Berman & Stearns 1976] used the results from an anemometer array set up on the edge of Chesapeake Bay to compare values of measured coherence with theoretical models. These models are based on an exponential decay first proposed by Davenport [Davenport 1961a, 1961b] and have been extended to include several other factors such as atmospheric stability [Ropelewski *et al.* 1973, Panofsky & Mizuno 1975]. However, a review of several sets of data, including data collected over an ice field and on a bridge, has shown that the simple model is adequate in most cases [Kristensen *et al.* 1981].

The studies reviewed in the preceding paragraph have taken a meteorological approach to the problem. Perhaps of more relevance to the work in hand are surveys for more general engineering

applications where data were collected at sites similar to those where long span bridges might be built. Davenport cited the experiment carried out on the old Severn Railway Bridge [Bailey & Vincent 1939] and analysed their data in his thesis [Davenport 1961a]. In this experiment 6 pressure tube anemometers were arranged over a 2412 foot length of the bridge, and the data recorded simultaneously from each for a series of storms. More recently, data have been collected from a similar survey on the Severn road bridge [Harris 1971].

6.4.3 Measured Response Of Bridges To Wind Excitation

Apart from determining the dynamic properties of a bridge, full scale testing also allows the response of the bridge to be related to the incident wind. As with prototype testing in general, and the monitoring of the wind, there are too many examples for an exhaustive bibliography to be cited here. Some important cases studies are presented in a review of the subject by Hay [Hay 1992], and these include monitoring programs on three cable-stayed bridges; the Wye, Erskine and Kessock bridges; as well as the Severn suspension bridge. The recent monitoring of the Humber bridge by groups from the University of Bristol and Politecnico de Milano [Diana *et al.* 1991] has also sought to relate the measured response to the size and distribution of the incident wind. There is however one project which is worthy of special note. This was set up by the Federal Highway Administration in the United States to monitor the response of the Deer Island Bridge which was built in 1939 as a sister bridge of the infamous Tacoma Narrows crossing [Bampton 1986]. This bridge has been known to exhibit large amplitude response to wind excitation on many occasions and consequently it has undergone remedial and strengthening work several times since its initial construction. Obviously its behaviour is of great interest, and so in 1981 it was instrumented with 7 anemometers and 12 accelerometers, as shown in figure 6.10. It is interesting to note that the anemometers measure the wind on both sides of the bridge and hence record the influence of the bridge on the airflow. The

results of the survey have shown that vortex shedding and buffeting have both been responsible for excessive bridge response during the time of the project [Kumarasena *et al.* 1991]. They have also helped to calibrate computer models of the bridge, to assess the efficacy of remedial stiffening work [Kumarasena *et al.* 1989a, Kumarasena *et al.* 1989b] and to suggest improvements in the prediction of buffeting response [Kumarasena *et al.* 1992]. Finally, wind tunnel tests have recently been performed on models of the bridge to try and explain the aerolelastic phenomena observed in the prototype test [Bosch 1990, Kumarasena *et al.* 1991].

6.5 Conclusions And Proposed Monitoring Exercise

The following conclusions can be drawn from the work reviewed in this chapter.

1 Wind loading represents an important load case for bridges with long suspended spans, and has historically proved disastrous.

2. The random nature of atmospheric turbulence makes a stochastic approach essential.

3. The power spectral approach developed for earthquake loading is applicable to wind excitation.

4. As wind represents a major component of the ambient excitation of long span bridges, the response of a prototype bridge to wind excitation can be readily measured.

With these conclusions in mind, the monitoring of a prototype cable-stayed bridge would seem to present a useful way of validating both the method presented for seismic excitation and its extension to cover wind loading. Therefore, an exercise was set up to measure the spatial variation of the incident wind on a bridge and simultaneously monitor the bridge response. This project will be described in chapters seven and eight.

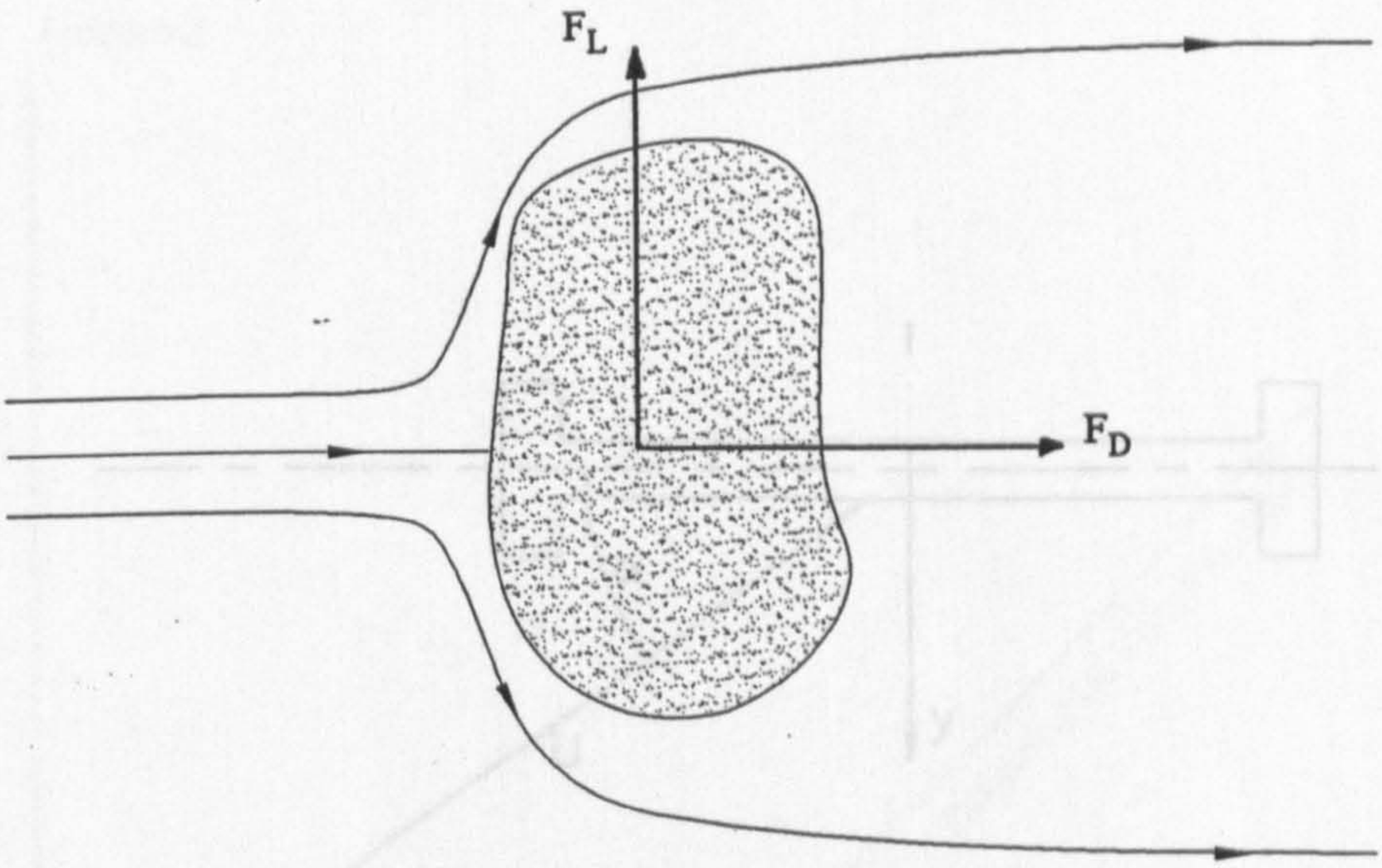

Figure 6.1 -:- Aerodynamic Forces Acting On A Bluff Body

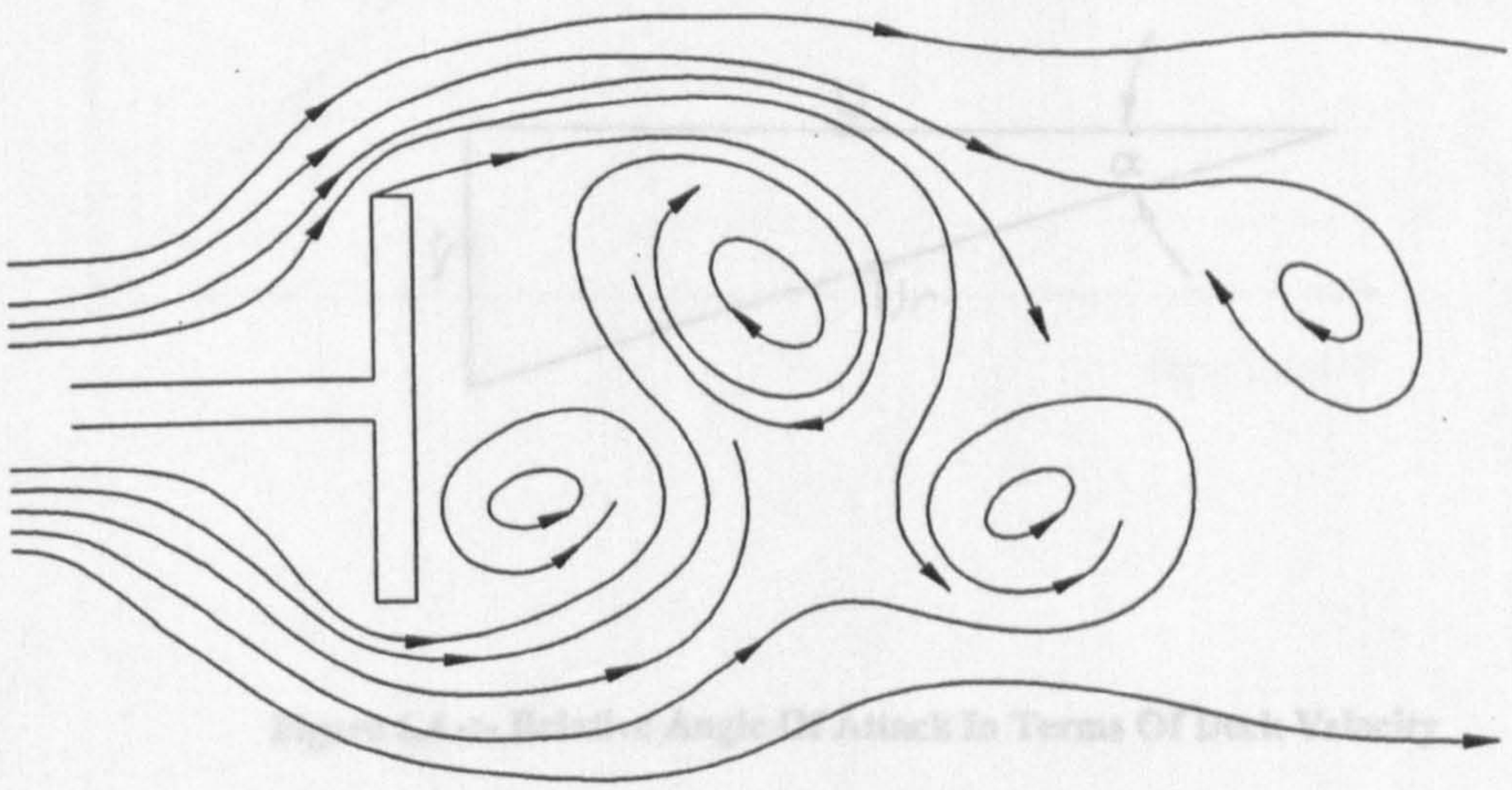

Figure 6.2 -:- Vortex Shedding From Trailing Edge Of Bluff Body

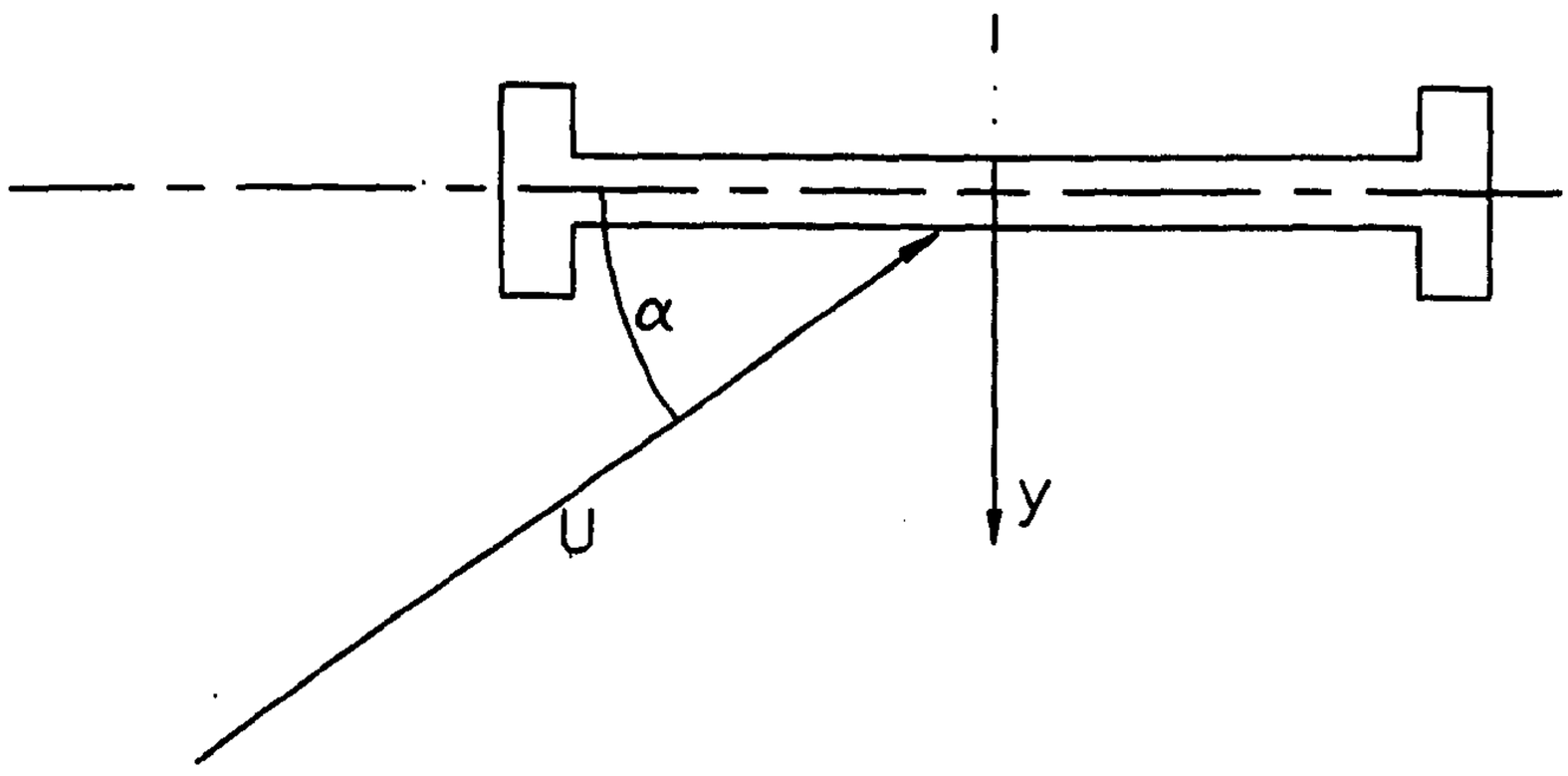

Figure 6.3 -:- Relative Angle Of Attack For Bridge Deck

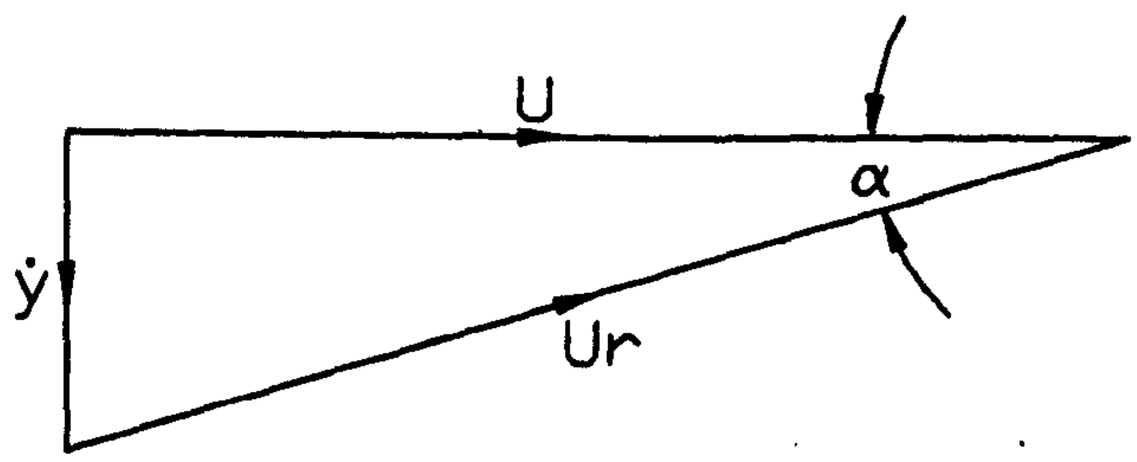

Figure 6.4 -:- Relative Angle Of Attack In Terms Of Deck Velocity

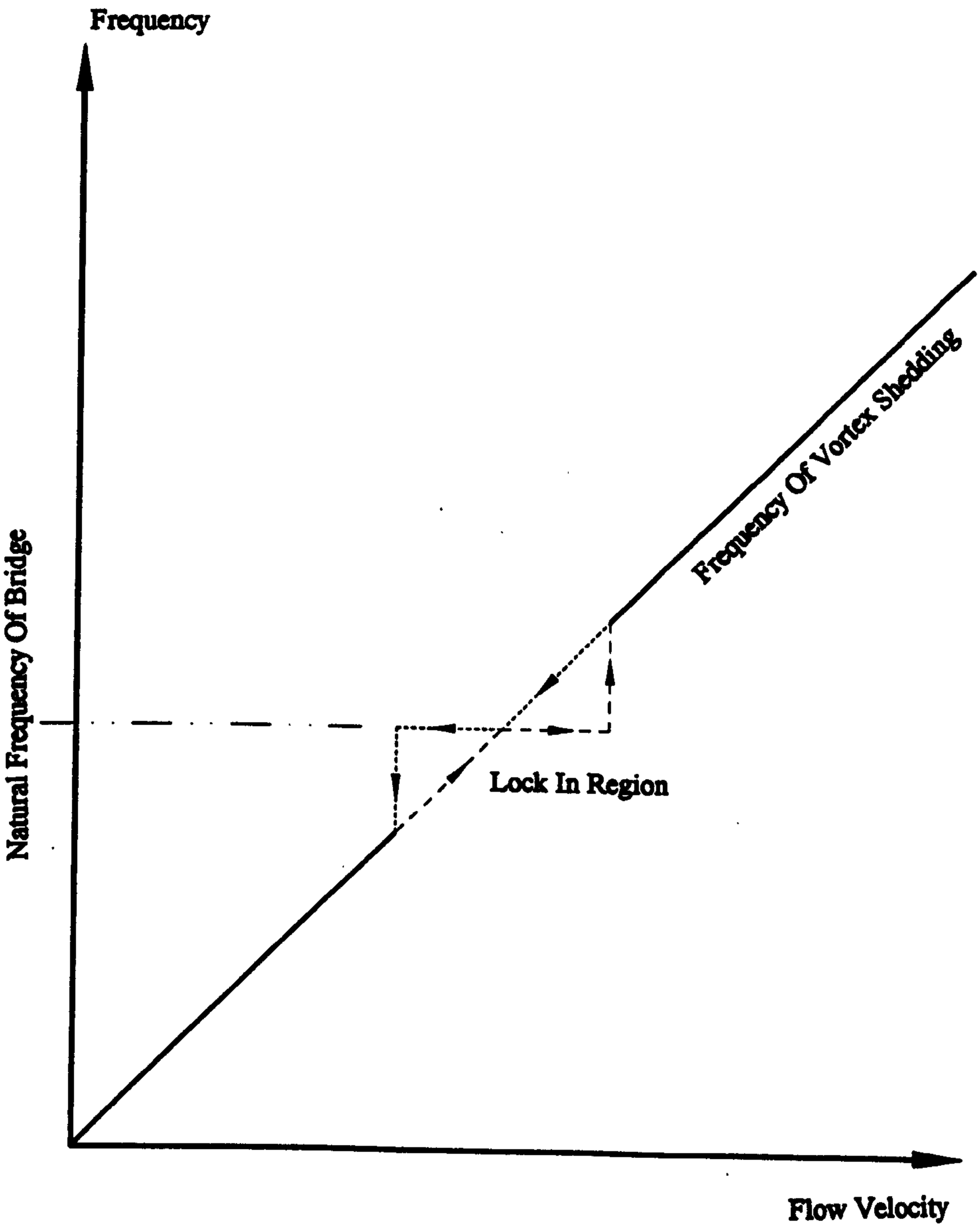

Figure 6.5 -:- Lock In Of Vortex Shedding

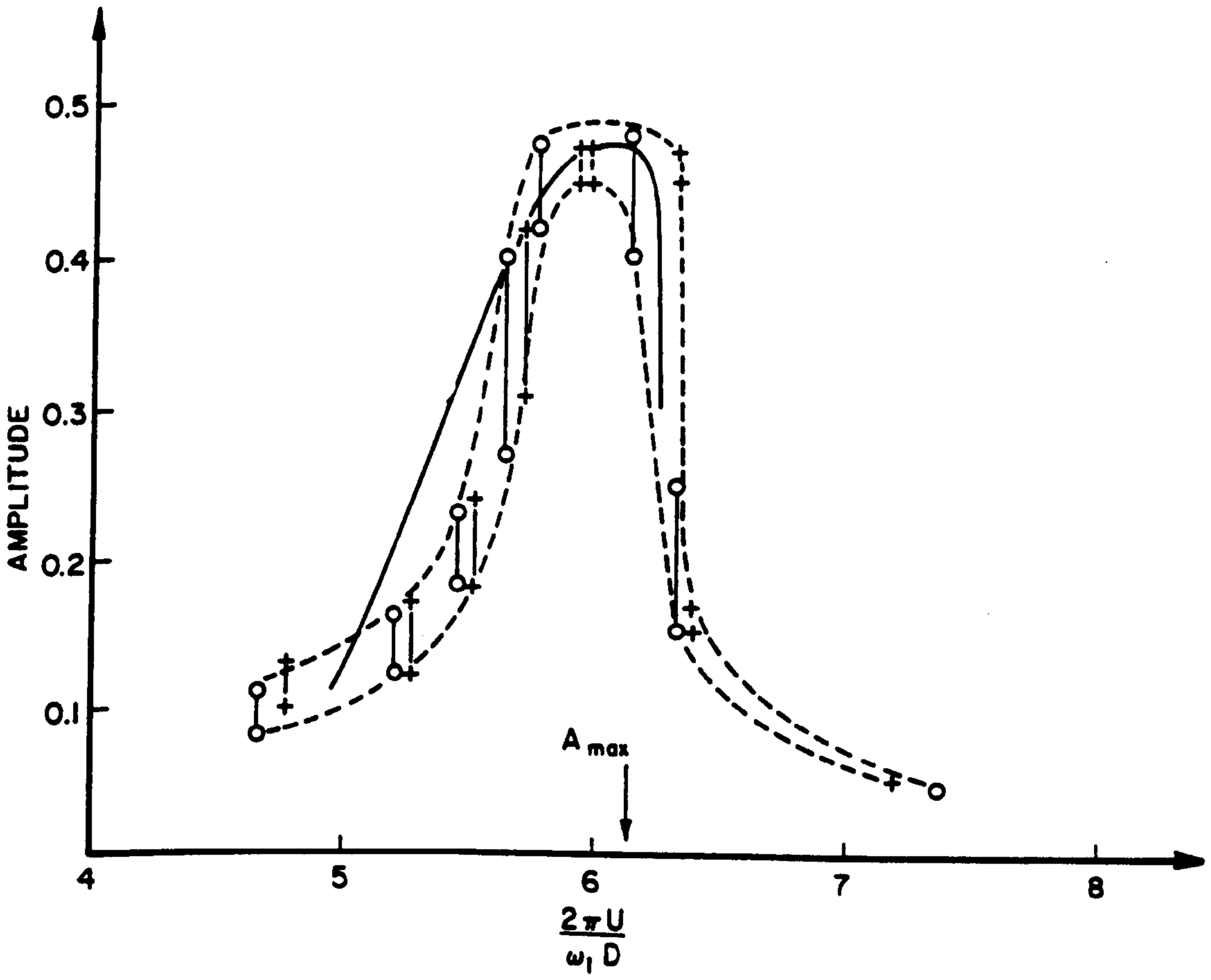

Figure 6.6 : Comparison of Experimental and Theoretical Results Showing Influence of Vortex Lock In on Structural Response (After Simiu & Scanlan 1986)

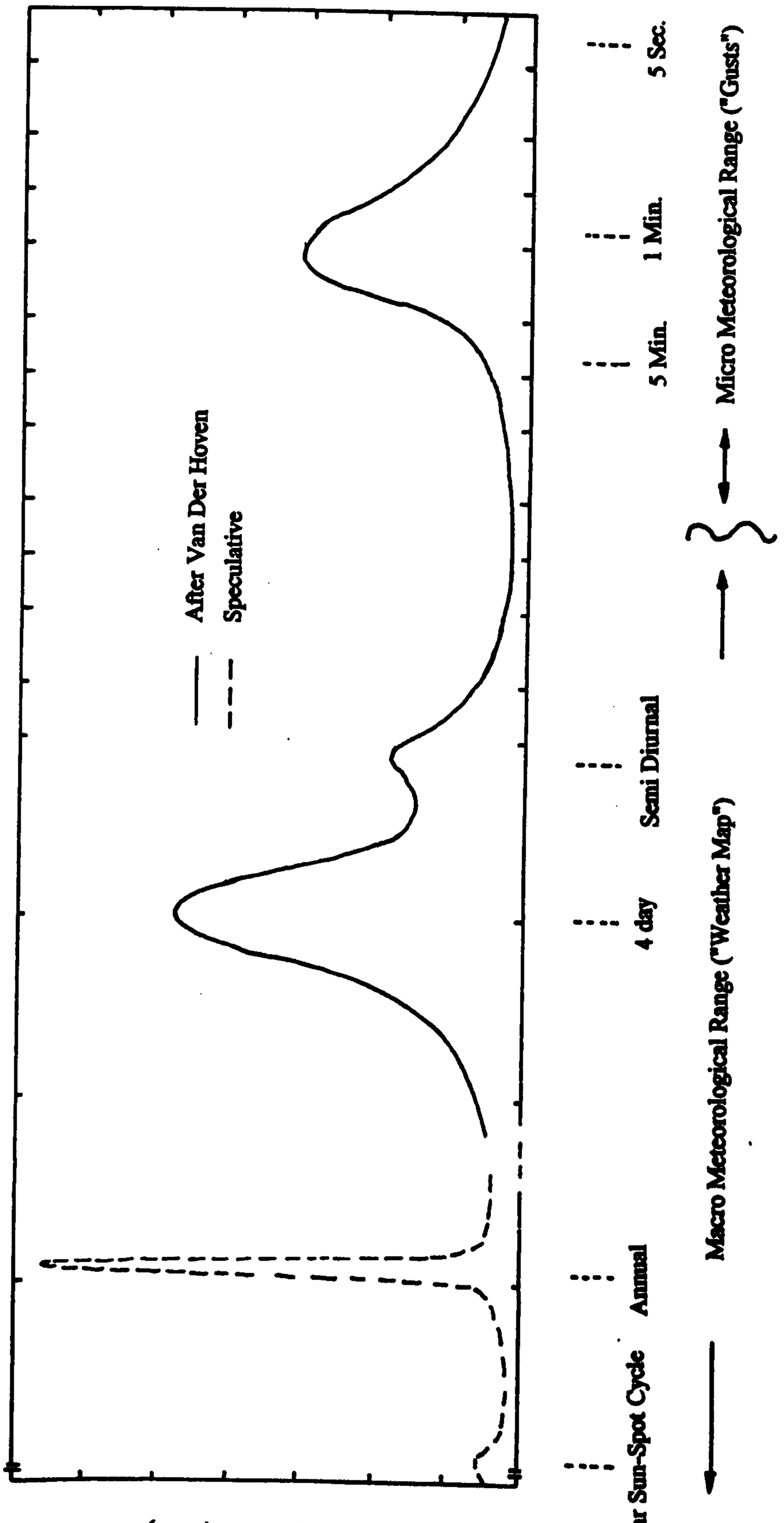

Figure 6.7 -:- Spectrum Of Horizontal Wind Speed Near The Ground
(after Davenport 1965a)

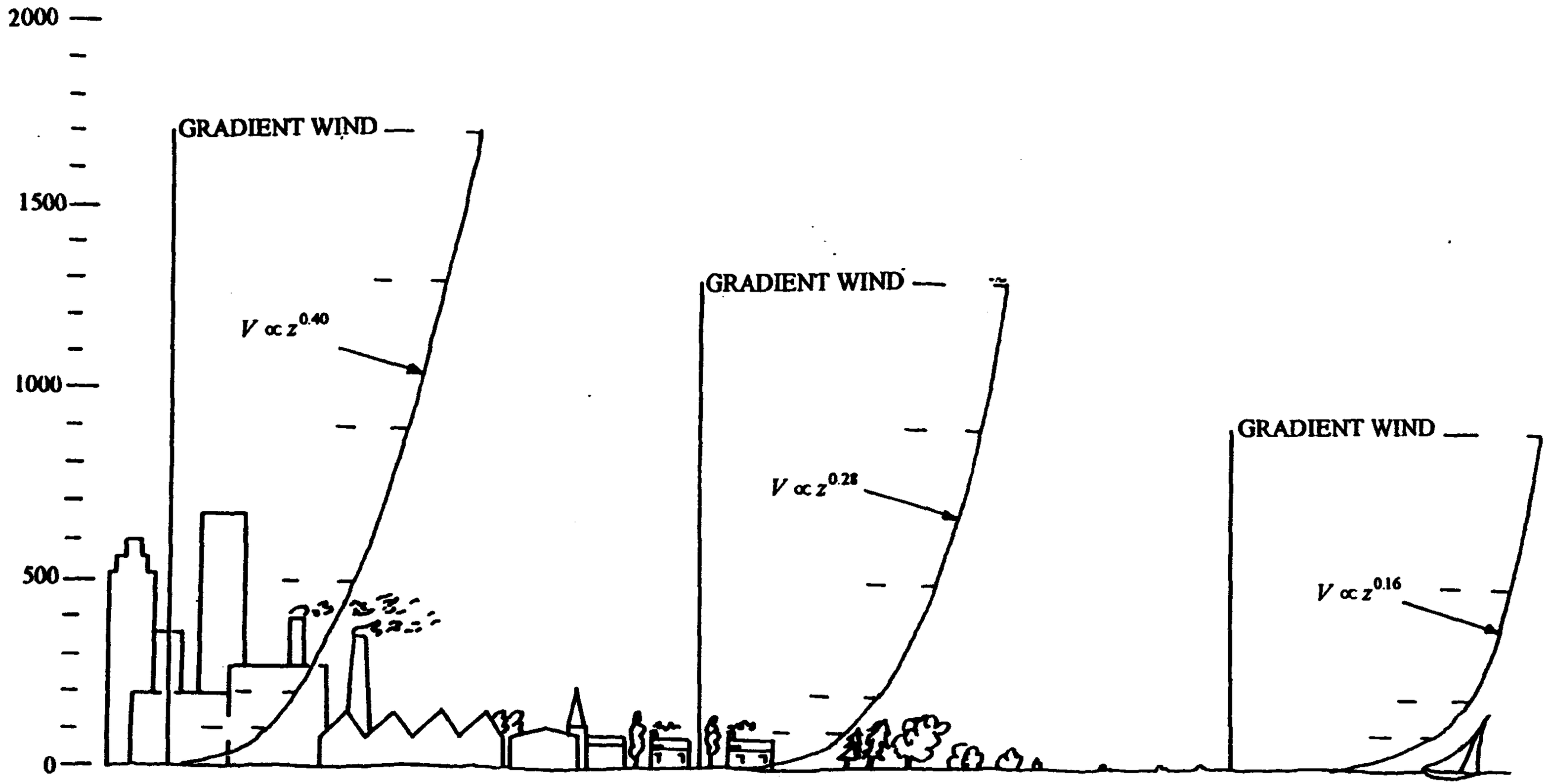

Figure 6.8 -:- Influence Of Ground Roughness On Wind Velocity Profile

(after Davenport 1965a)

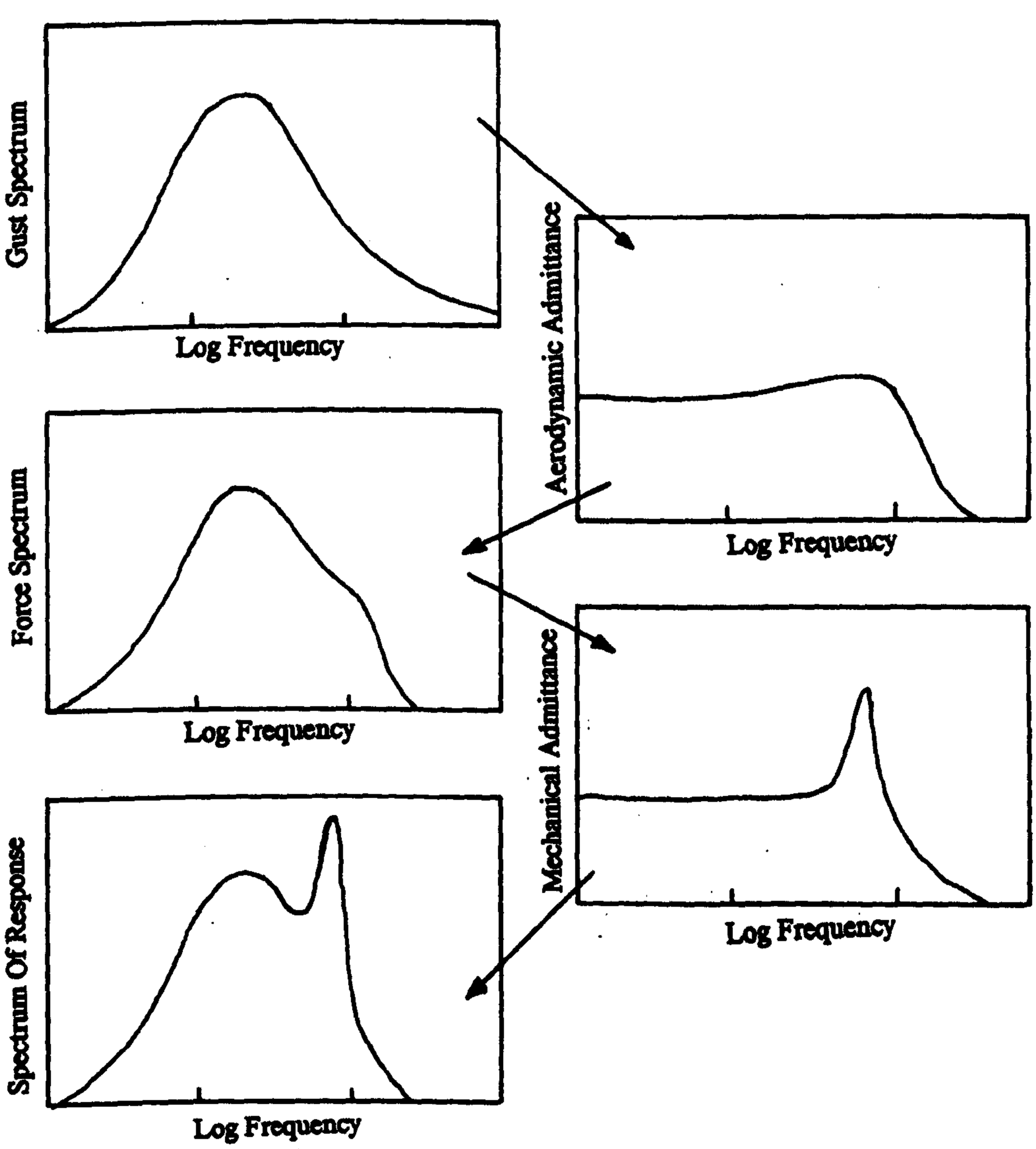

Figure 6.9 -:- Graphical Summary Of Spectral Analysis Of Buffeting

(After Davenport 1962)

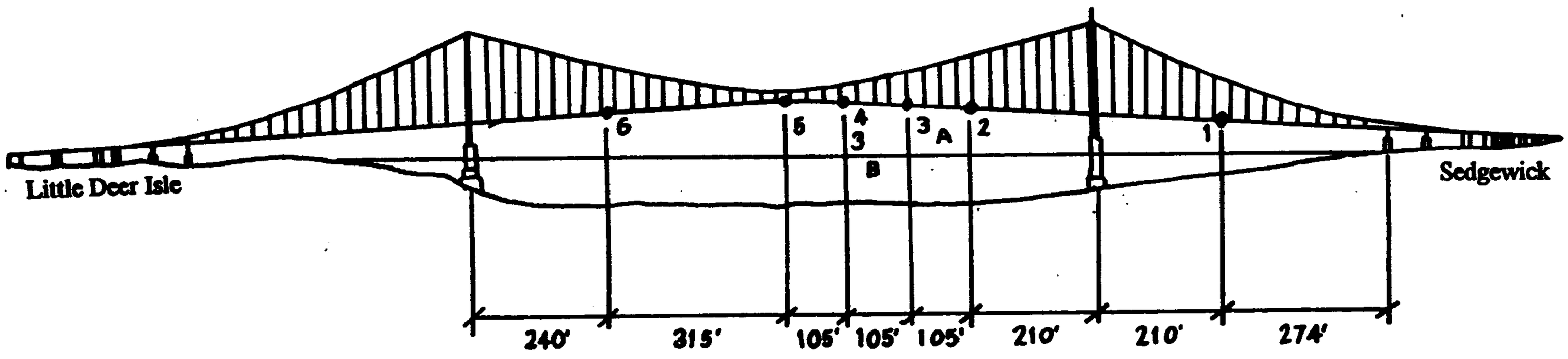

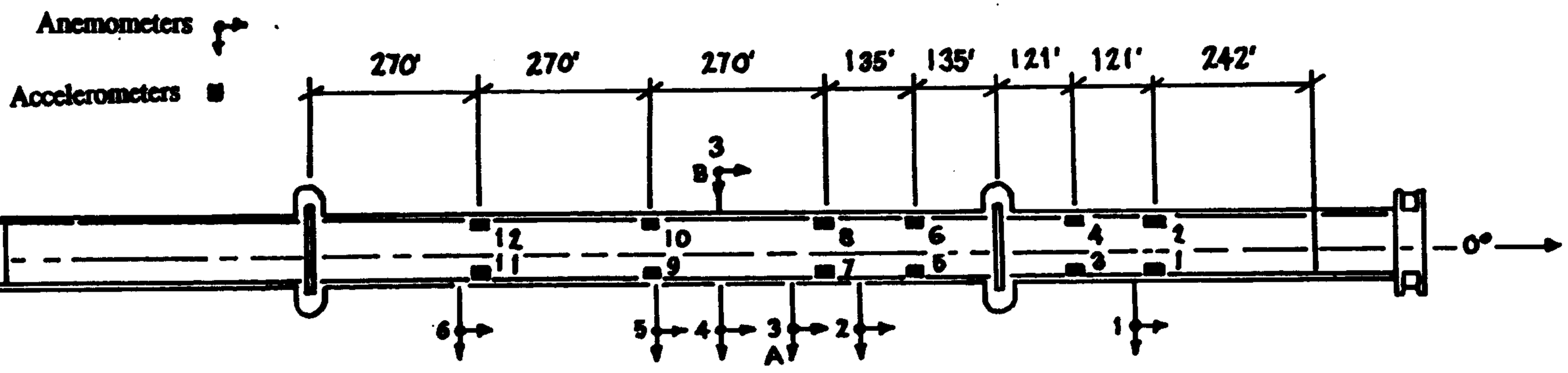

Figure 6.10 -:- Instrumentation On Deer Isle-Sedgewick Bridge

Chapter Seven

The Response Of Cable Stayed Bridges To Wind Excitation: The Prototype Testing of Kessock Bridge

7.0 Introduction

The conclusions drawn from the review presented in chapter six suggested that testing a prototype cable-stayed bridge to measure its response to wind loading would be a suitable way of verifying the approach developed in the earlier chapters of this thesis. Such an exercise would have three aims:

i. To measure the response of the bridge.

ii. To measure the spatial structure of the wind.

iii. To correlate the bridge response with the spatial structure of the wind.

The first step in achieving these aims was to find a suitable bridge. This had to be cable-stayed, and also located somewhere where it was subject to winds of varying strength and turbulence. Once a suitable bridge had been selected, an instrumentation system had to be designed to allow wind and response data to be monitored simultaneously. This instrumentation then had to be installed on the bridge, and left there long enough to record data from a representative selection of different wind regimes. Finally, to help interpret these data, a detailed knowledge of the dynamic properties of the bridge had to be found by finite element modelling and performing a full modal survey.

The purpose of this chapter is to present the planning and execution of the monitoring exercise which was performed on Kessock Bridge, a medium span cable-stayed bridge near Inverness. It will first of all outline the principal reasons for choosing the bridge, and then describe the instrumentation system

which was developed. Next, it will describe the modal survey performed on the bridge and compare the results obtained with predictions made by finite element modelling. Finally, it will describe some of the problems encountered with the execution of the project, and how they were overcome. The results of the exercise will be presented in chapter eight.

7.1 Kessock Bridge

The Kessock Bridge, opened in 1982, carries the A9 dual carriageway across the Beauly Firth to the North of Inverness (figure 7.1). The 1052 m crossing consists of a 240 m cable-supported main span with approach viaducts to the North and South (figure 7.2). The steel deck is continuous along the entire length of the crossing, and is stiffened by plate girders along both edges (figure 7.3). The cables are arranged in an harp configuration in two planes along the outer edges of the deck, and support the central span and two adjacent side spans at each end.

7.1.1 Reasons For Choosing Kessock Bridge

There were three principal reasons why Kessock bridge was chosen to be the subject of this study. Firstly, on several occasions, the bridge had exhibited large amplitude response under certain wind conditions. This had caused concern both for people using the bridge and the Highland Regional Council (HRC) who are responsible for the day to day running of the bridge. As a result, the bridge has been the subject of previous monitoring exercises [Hay 1986, 1992] and dampers have been installed to limit the response [Cullen-Wallace 1985]. In addition, HRC had also approached the Department of Civil Engineering at the University of Bristol with a view to further monitoring of the structure. Therefore, the proposed monitoring of the bridge would be of benefit to both the bridge authorities and ourselves.

The second reason for choosing Kessock bridge, and of particular importance for this project, was its location. Kessock bridge is located on the East coast of Scotland and therefore it will be subject to markedly different wind regimes depending on the direction of the wind [Cullen-Wallace 1985]. Like the rest of the United Kingdom, the prevailing winds at Kessock are from the South West, and therefore they have to pass over the Highlands of Scotland to reach the bridge. As discussed in §6.3, turbulence in the wind is greatly influenced by the terrain and the surface roughness; hence the prevailing South Westerly winds can be expected to be turbulent. In contrast, winds from a North Easterly direction have a long fetch of open sea (figure 7.4), and will be consequently less turbulent. So, Kessock Bridge is subject to both turbulent and steady wind regimes depending upon the wind direction, and it is therefore an ideal structure on which to investigate the effects of spatial variations in the incident wind.

The final reason for choosing Kessock bridge is that it is an example of a modern, medium-span, cable-stayed bridge. Although all bridges have unique features, it is still typical of the many cable stayed bridges which have been built around the World in the last twenty years [Billington & Nazmy 1990].

7.2 Development Of Instrumentation

As outlined in previous chapters there are two other principal sources of dynamic excitation for long span bridges in addition to earthquake, wind and traffic. Initial plans for the project envisaged monitoring both of these, however, because it was not possible to monitor the traffic in sufficient detail within the time and financial constraints, the decision was taken to restrict investigations to wind loading. The importance of traffic loading, and the justification for neglecting it, will be considered in more detail when the processing is presented in chapter 8. As well as monitoring the

wind loading, a detailed knowledge of the structural response was also needed. Therefore, an instrumentation system needed to be developed which had three principal functions:

i To measure the incident wind,

ii. To measure the bridge response,

iii. To log and record the data collected.

7.2.1 The Wind Monitoring System

When measuring the wind it is necessary to know both its speed and direction and the best way of obtaining these is to measure the velocity in three orthogonal directions. This approach allows the velocity of the wind and the cross wind turbulence to be found directly. However, in this project there was an additional requirement - to find the distribution of the wind along the length of the bridge. This meant that a number of anemometers had to be used, located at intervals along the length of the bridge. Therefore, a compromise had to be made between the total cost of the instrumentation and the quality and quantity of data recorded. In the event, eight cup and vane anemometers were installed on the bridge, allowing a large spatial length to be considered, but at the cost of losing data for the vertical and cross wind components in the wind. The significance of losing this data will be discussed in chapter eight.

The anemometer chosen was an off the shelf unit produced by Digitar (figure 7.5). For a cup and vane anemometer, the angular velocity of the cups can be shown to be proportional to the incident wind velocity [Greenway 1977]:

$$\frac{d\theta}{dt} = KU \qquad \text{.....7.1}$$

and so the wind speed can be found by measuring the speed of rotation of the cups. The anemometers contain a reed switch which produces a pulse for each rotation of the cups (figure 7.6). A signal conditioning circuit was designed using a tachometer chip to convert the pulse train produced by each anemometer into a steady voltage proportional to the wind speed. The direction of the wind is found by measuring the orientation of the wind vane which is connected to a variable resistor (figure 7.6). The orientation can then be measured by finding the voltage drop across a resistor placed in series with this variable resistance (figure 7.7) and included in the conditioning circuit (figure 7.8).

Before they were installed on site, the anemometers and signal conditioning circuits had to be calibrated to find the constant of proportionality in equation 7.1. The calibration was carried out in an open section wind tunnel using procedures similar to those described by Greenway and Wood [Greenway 1977, Wood 1982]. Each anemometer in turn was calibrated with its own signal conditioning circuit by setting it up in the centre of the wind tunnel (plate 7.1) The tunnel velocity was then increased in ten increments from the start up velocity of circa 7 m s^{-1} to its maximum of around 40 m s^{-1}. At each increment the output voltage from the conditioning circuit was compared with the tunnel velocity measured using a Betz manometer. The readings were then repeated as the tunnel velocity was decreased. The calibration curve for the anemometer was then produced by plotting the output voltage against tunnel velocity (figure 7.9). The results showed the expected linear relationship for each anemometer, and the resulting calibration constants are given in table 7.1.

As well as finding the calibration curve for each anemometer, it was important to assess their dynamic behaviour since an accurate measurement of the turbulent response is needed. Equation 7.1 describes a first order system which has a step response given by:

$$\frac{d\theta}{dt} = \left(\frac{d\theta}{dt}\right)_s \left[1 - \exp\left(-\frac{t}{\tau}\right)\right] = KU\left[1 - \exp\left(-\frac{t}{\tau}\right)\right] \quad \text{.....7.2}$$

where τ is the time constant. This represents the time taken for the anemometer to reach 63 % of its steady state response. Solving 7.2 for the angular position gives:

$$\theta(t) = KU\left[t - \tau\left(1 - \exp\left(\frac{-t}{\tau}\right)\right)\right] \quad \text{.....7.3}$$

where:

$$\theta_s(t) = KU[t - \tau] \quad \text{.....7.4}$$

is the steady state response. The value of τ can therefore be found by plotting the angular position of the cups as the anemometer starts from rest in a steady wind, and finding the intercept of the asymptote with the time axis. This exercise was performed for one of the anemometers during calibration (figure 7.10). However, as the time constant is a function of the velocity it is usual to quote a distance constant:

$$D = \tau.U \quad \text{.....7.5}$$

which is independent of the wind velocity [Greenway 1977]. For the anemometer tested this was found to be 3.2 m. Finally the frequency response function can be found in terms of the time constant:

$$F(\omega) = \frac{1}{\sqrt{1+\omega^2.\tau^2}} \quad \text{.....7.6}$$

or in terms of a dimensionless frequency defined by the distance constant:

$$F\left(\frac{\omega.D}{U}\right) = \frac{1}{\sqrt{1+\left(\frac{\omega.D}{U}\right)^2}} \quad \text{.....7.7}$$

Figure 7.11 illustrates the frequency response of the anemometers used on the Kessock project. Comparing figure 7.11 with a typical horizontal gust spectrum produced from an empirical formula

(figure 7.12) [Kaimal *et al.* 1972] clearly shows that the anemometers will respond adequately quickly to monitor gust loading.

7.2.1.1 Installation Of Anemometers On The Bridge

An essential requirement of any measurement exercise is that the measuring device does not change the parameter under investigation. In the case of measuring the incident wind on a long span bridge a further complication arises because the bridge itself influences the flow of air around it. There are three factors which may give rise to errors in the readings:

i. The bridge changes the velocity and turbulence of the air flowing around it due to the formation of a boundary layer.

ii. If the bridge is moving significantly, either under wind or traffic loading, then this motion can introduce further turbulence into the airflow.

iii. Because the anemometers are mounted on the bridge, when the bridge moves the anemometers will move. This could possibly give rise to spurious results.

To overcome the first two effects it is necessary to place the anemometers outside the influence of the bridge, and ideally they should be placed some way upstream of the deck (figure 7.13). In the study of the Deer Island Bridge [Bampton *et al.* 1986] anemometers were placed along both sides of the deck allowing both the incident wind and the wake to be measured and hence the influence of the bridge on the airflow. However, in the case of Kessock bridge this was not possible, both because of the limit on the number of anemometers and because there was no means of supporting the anemometers at the extreme edges of the deck. Instead, a compromise was made and seven of the anemometers were mounted on the lamp standards situated along the central reservation (figure 7.14, plate 7.2). These

lamp standards permitted the anemometers to be placed 10 m above the deck, which is three times the depth of the overall section (figure 7.13). The eighth anemometer was mounted on top of the North East Pylon.

Because of the type of anemometers used, the third point mentioned above will only be of significance when motion of the bridge causes horizontal motion of the anemometers. However, the location of the anemometers on top of the lamp-standards means that any torsional motion of the bridge deck will give rise to an amplified horizontal motion of the anemometers. This effect was observed in the results from the Deer Island project, which showed strong peaks in the wind spectra corresponding to the torsional response of the bridge [Kumarasena *et al.* 1990]. Care will therefore have to be used in interpreting the data collected from Kessock bridge to remove any components due to the response of the bridge deck. In addition, when the modal survey was performed measurements were taken to determine the natural frequency of the lamp standards in case their response had a bearing on the anemometer readings.

7.2.2 The Bridge Monitoring System

To fulfil the aims of the monitoring exercise measurements had to be taken of the vertical, lateral and torsional response of the bridge deck. This was achieved by setting up accelerometers on the East side of the deck to measure the vertical response at centre span and at a point 50 m from the North pylons. A third accelerometer was set up on the East side to measure horizontally at the 50 m mark and a fourth vertically at centre span on the West side (figure 7.15).

Four accelerometers were used during the long term monitoring, two Schaevitz LSOC 14 inclinometers and two Sundstrand QA-700 servo accelerometers. Both types of instrument are servo accelerometers which work on the force balance principle. A mass is supported by a system of

springs, designed to be highly linear, and an electrical coil. The position of the mass is continually monitored and the current in the coil adjusted by a servo to keep the mass spring system in its equilibrium position (figure 7.16). Hence, if the mass is subjected to a force or acceleration the current through the coil changes and can therefore be used as a measure of the applied load or acceleration. This system is a very accurate means of measuring acceleration since only very small displacements of the system occur and problems of spring non linearity and hysteresis are avoided. However, there is a disadvantage in using these accelerometers in a long term bridge monitoring exercise. Because the accelerometers are sensitive to any acceleration of the seismic mass, they will also be sensitive to changes in the relative acceleration due to gravity, and in particular the inclination of the instruments. Therefore, the accelerometer readings can be expected to experience long term drift if there are any seasonal trends in the bridge inclination, such as might occur due to temperature changes.

Finally, an important part of the monitoring project was to take readings over a sufficiently long period of time to obtain data for a wide range of wind regimes. Therefore, the instrumentation had to be left in an aggressive coastal environment for several months and so precautions had to be taken to protect the accelerometers and cabling, both from the weather and also from pedestrians on the bridge. To achieve this the accelerometers were sealed in watertight boxes which were then glued to the bridge outside the pedestrian barriers and the cables threaded along the outside of the handrails (figure 7.17). The accelerometers measuring vertically were glued to the handrail stanchion (plate 7.3) and the horizontal instrument to the top flange of the edge girder (plate 7.4).

7.2.3 Data Acquisition System

The final section of equipment needed to complete the test set up was a system to monitor and record the signals produced by the anemometers and accelerometers. As mentioned before, the project was due to run for several months, and so not only would a large amount of data be generated, but it would not be possible to visit the site on a regular basis. Therefore, two refinements to the general data acquisition system were deemed essential. Firstly, to reduce the amount of data storage required, a strategy should be used to select and save only certain data. Secondly, it should be possible to log on to the system remotely so that progress can be monitored. Hence the data acquisition system had to provide the following facilities:

i. Analogue to digital conversion to log the raw data.

ii. Pre-processing to decide on which data should be saved.

iii. Bulk storage to save data.

iv. Remote interrogation

The monitoring system is shown in block diagram form in figure 7.18 and was produced in conjunction with Mr. Andy Vann as part of the development of his system for the intelligent monitoring of civil engineering systems (IMCES) [Vann & Davis 1992, Davis *et al.* 1993, Vann 1993]. The acquisition system was based around a Toshiba P5200 portable PC running Labtech Notebook to handle the analogue to digital conversions and collection of raw data. There were 20 channels of raw data to be collected, 8 anemometer speeds, 8 anemometer directions and 4 accelerometers. These data had to be filtered before sampling to prevent aliasing, and a cascade of two 2-pole Butterworth filters was used on each channel. The filter frequencies and sampling rates chosen were:

Anemometers	Filter at 2.34 Hz.	Sample at 8 Hz.
Accelerometers	Filter at 8.05 Hz.	Sample at 24 Hz.

giving an aggregate sampling rate of 224 Hz. This corresponds to a data acquisition rate of 992 Bytes per second, including a time stamp. The bulk storage of data was provided by an optical disk drive which had a capacity of 540 MBytes per side; hence each disk allowed for approximately 2 weeks of continuous monitoring. This was improved threefold by using a data compression program, PKZIP, to compress the data before the files were stored, but even then it was still necessary to implement a strategy to prevent surplus data being stored. Overall control of the monitoring system and implementation of the data acquisition strategy (see below) was provided by a program written by Mr. Andy Vann.

7.2.3.1 Monitoring Strategy

The previous section has shown that it was not possible to save all the data recorded and so it was necessary to develop a strategy to decide which data should be stored, and which discarded. To implement a working strategy it was necessary to classify the data collected in terms of specific parameters, such as the turbulence intensity of the wind, mean bridge response or time. For this project the data were classified in terms of the mean wind speed and direction averaged over a ten minute period. These parameters were divided into bands, 16 for direction 10 for speed, (figure 7.19) giving a total of 160 cells corresponding to different combinations of wind speed and direction.

The initial strategy is summarised in the flow chart of figure 7.20. Data was collected for a ten minute period, which was chosen so as to fall within the spectral window mentioned in §6.3 to ensure that the wind data would be approximately stationary. The statistics of each record; mean, variance, maximum, minimum and turbulence intensity; were then calculated and saved to disk. These

statistics were kept regardless of whether or not the raw data were saved. Next, the mean wind speed and direction at anemometer 4 (figure 7.14) were used to classify the data, and the decision was then made as to whether or not to store the raw data. The original strategy had been to collect up to 20 records in each cell, and to discard any additional data. However, this threshold was raised during the exercise to reduce the random errors in the data and to maximise the use of available storage. The pre-processing of the data took between one and two minutes, depending on whether data was being stored or not, and so data was logged for approximately 90 % of the monitoring time. The final part of the monitoring strategy was to wait from 18:00 to 18:05 each day to allow the system to be contacted by phone via a modem.

7.3 The Modal Survey

As mentioned in §6.4.1 an important goal in the dynamic testing of any structure is to determine its dynamic properties; natural frequencies, mode shapes and modal damping. Therefore, when the visit was made to Kessock Bridge to install the equipment for the long term monitoring exercise, the opportunity was taken to perform a modal survey by measuring its response to ambient excitation. This survey was then extended and completed during the final visit, when the instrumentation for the long term monitoring program was removed.

7.3.1 Survey Procedure

The standard approach to performing a modal survey on a structure is to measure the response at different points in the structure to a known excitation. The frequency response function (FRF) can then be found by comparing the response with the excitation:

$$H(\omega) = \frac{G_{xy}(\omega)}{G_x(\omega)} \quad \text{.....7.8}$$

where $y(t)$ is the response to an excitation $x(t)$. However, as discussed in §6.4.1, it is often not possible to control the excitation on a structure such as a long span bridge and it is therefore necessary to rely on ambient excitation. This means that the FRF defined by equation 7.8 cannot be measured. Instead, the response at different points on the bridge has to be compared to the response at a reference station:

$$H'(\omega) = \frac{G_{zy}(\omega)}{G_z(\omega)} \quad \text{.....7.9}$$

where $z(t)$ is the response at the reference location. In this case $H'(\omega)$ is not a true FRF, but it does contain information about the relative phase and magnitude of the response which can then be used to plot the mode shapes.

In practice there are two parts to a modal survey; identification of the natural frequencies and modal damping, and plotting the mode shapes; and these lead to conflicting pressures on the survey. An important difference between $H'(\omega)$ and a true FRF is that $H'(\omega)$ does not provide a means of identifying the natural frequencies of the system, whereas a true FRF will always have a phase angle of 90° at a natural frequency. Therefore, when ambient excitation is used the natural frequencies have to be identified from peaks in the auto-power spectra of the response. However, this requires a very fine frequency resolution to distinguish between modes, especially if the natural frequencies are closely spaced. Furthermore, since the frequency resolution is the reciprocal of the monitoring period, a long sampling time has to be used, which is exacerbated by the need to take a large number of averages. In contrast to this, plotting the mode shapes requires data to be collected at many points and so the time available for measurements at each station is limited. Finally, the data collected will

be subject to both random and bias errors and steps have to be taken to minimise these. The random errors can be reduced either by smoothing adjacent spectral estimates, block averaging, or by averaging many sets of readings, ensemble averaging. However, block and ensemble averaging both reduce the information content of the data and lead respectively to loss of frequency resolution and an increase in the monitoring time. Therefore, a balance has to be struck between the frequency resolution achieved, the time taken and the number of averages made. For the modal survey on Kessock bridge the mode shapes were mapped by taking readings during the day with lower frequency resolutions, and the natural frequencies identified from overnight recordings made using a finer frequency resolution.

The modal survey on Kessock bridge was performed by comparing the dynamic response of the bridge at different locations using five servo accelerometers:

Schaevitz LSOC 14 Inclinometers	Nos. I1, I2, & I3
Sundstrand QA-700 Servo Accelerometers	Nos. I4 & I5

One accelerometer was set up as a reference station, and the others were used as travellers at different monitoring locations. A spectrum analyser was then used to form the "FRF", $H'(\omega)$, between the traveller and reference under ambient excitation, and the average of between 50 and 75 readings taken. This process was then repeated for each of the monitoring stations.

7.3.1.1 First Visit

The first part of the modal survey was carried out during the first site visit. A Solartron S1200 spectrum analyser with a resolution of 501 spectral lines was used to measure the "FRF" between the traveller and reference accelerometers using the following frequency ranges:

Frequency Range	**0 - 5 Hz**	**0 - 10 Hz.**	**0 - 20 Hz**
Frequency Resolution	**0.01 Hz.**	**0.02 Hz.**	**0.04 Hz.**

The vertical response was measured on both sides of the deck at 20 m. intervals across the main and side spans. Attempts were also made to measure the lateral motion of the deck and the response of the pylons, but with little success in either case. The stations measured, instruments used and their orientation, and the frequency resolution obtained are shown in table 7.2. During the survey, readings were taken from the spectrum analyser to identify approximately the natural frequencies and mode shapes; however, for detailed processing, the spectral data were transferred to PC.

7.3.1.2 Final Visit

Although successful in identifying the vertical and torsional behaviour of the bridge, the first stage of the modal survey had been unsuccessful in identifying either the horizontal motion of the deck or the dynamic behaviour of the pylons. Therefore further investigations were made when the long term monitoring equipment was removed to find these data, and also to repeat the overnight readings with a yet finer frequency resolution. Once these objectives had been met some additional sets of readings were taken as follows:

a. **Preliminary finite element modelling indicated that the dynamic properties of the approach viaducts could influence the response of the cable-supported spans. Therefore vertical and lateral readings were taken on the approach spans closest to the three central spans.**

b. **Several of the modes in the range 2 - 3 Hz. had low values of the corresponding coherence function, indicating that the reference was close to a node point. therefore**

vertical measurements for the East side of the main span were repeated with the reference moved to the 40 m. mark.

c. A repeat set of readings using a longer sampling period was taken on the main span to improve the frequency resolution and to help distinguish between closely spaced modes.

As during the first visit, the "FRFs" were to be calculated using the Solartron S1200 spectrum analyser. However, this developed a fault during the monitoring period and the readings were completed using an Advantest R9211C analyser. This helped improve the frequency resolution obtained as it provided the option of working with up to 800 spectral lines. A summary of the monitoring stations and instruments used during the final visit is given in table 7.3. As with the first visit, only preliminary processing was performed on site and the data were recorded for detailed processing at a later date.

7.3.2 Processing Of The Modal Survey Data

The modal survey provided raw data on the dynamic response of the bridge, but this then had to be processed to yield the dynamic properties of the structure. This processing fell into two parts, identifying the natural frequencies and modal damping from the power spectra, and plotting the mode shapes using the "FRFs".

7.3.2.1 Identification Of Natural Frequencies

As mentioned in §7.3.1 the natural frequencies can be identified directly from a conventional FRF, and usually curve fitting is used either to fit circles to the data in the complex plane (Nyquist plots), or to find the poles and zeros of the FRF. However, this cannot be applied to a survey based on ambient

excitation and instead peaks in the power spectra have to be used to identify the natural frequencies. There are several approaches which can be used to determine these peaks, for example a rough estimate can be made by eye or the frequency can be found which corresponds to the highest peak in the trace. These methods, though, are not simple as the peaks are often jagged rather than clearly defined. Curve fitting again provides a better approach, though in this case a curve has to be fitted to the power spectrum. The simplest approach is to assume that each peak represents a single degree of freedom system:

$$G(\omega) = \frac{1+\left(\frac{2\xi_r\omega}{\omega_r}\right)^2}{\left[1-\left(\frac{\omega}{\omega_r}\right)^2\right]^2+\left(\frac{2\xi_r\omega}{\omega_r}\right)^2} \qquad \text{.....7.10}$$

and to use a least squares fitting procedure to identify the modal parameters ω_r and ξ_r. Several errors are introduced by this procedure, most notably because peaks are considered individually neglecting the contribution of other modes to the response at that frequency. This is especially important if the modes are closely spaced (figure 7.21). However, the method is simple to use, effective, and produces estimates for modal damping as well as natural frequency directly.

This procedure was adopted in processing the data from Kessock, and a signal processing program, GRAF, was used to perform the curve fitting. Typical traces for the lateral and vertical auto-power spectra for points on the bridge deck are shown in figures 7.22 and 7.23, and the frequencies identified from these are listed in table 7·4.

7.3.2.2 Plotting Of Mode Shapes

In order to plot the mode shapes it is necessary to know the response of different locations on the bridge relative to some reference point. Therefore the mode shapes can be found from the magnitude and phase of the "FRF" at the natural frequencies for each of the monitoring stations. However, in the case of a bridge, a problem arises because the natural frequencies change with time depending on temperature and traffic loading. Ideally, since the different sets of readings were taken over a period of several months, each record should be analysed individually to find the natural frequencies from peaks in the power spectra, and these used to select data from the corresponding "FRFs". However, detailed curve fitting to all the data would be very time consuming and computationally uneconomic. Furthermore, curve fitting would be of little value for the coarser data sets. Therefore, two approaches were used depending on the frequency resolution of the data. Firstly, for the data recorded during the final visit with a frequency resolution of 0.00625 Hz, curve fitting was used to establish the natural frequencies for each record. The nearest frequency quantum was then used to find the magnitude and phase of the "FRF", together with the value of the coherence function. Secondly, for the rest of the data, values of the natural frequencies from the finer records were used as starting points to extract the required information. A band of points either side of these frequencies was then considered, and the data selected depending upon the size of the auto-power spectra and the level of the coherence function.

As discussed earlier, the data contain both bias and random errors and it is important to assess the influence of these on the results. The bias error represents the mean discrepancy between the actual and estimated values:

$$\varepsilon_b = E\left[\hat{H}(\omega) - H(\omega)\right] \quad \text{.....7.11}$$

and the random error the variance in the estimated value:

$$\varepsilon_r = E\left[\left(\hat{H}(\omega) - E\left[\hat{H}(\omega)\right]\right)^2\right] \quad \text{.....7.12}$$

The bias error can occur for various reasons, including the time dependent changes to the system discussed earlier. However, the most likely source of bias error is bias in the power and cross spectral density functions used to calculate the FRF. Following the reasoning of Bendat and Piersol [Bendat & Piersol 1971], an estimate in a spectral density function can be made as follows:

$$\varepsilon_b = b\left[\hat{G}(\omega)\right] \approx \frac{B_e^2}{24} G''(\omega) \quad \text{.....7.13}$$

where the double prime represents differentiation twice in the frequency domain. As $G''(\omega)$ will be very large at peaks in the spectral density functions, i.e. at the natural frequencies, it can be expected that the bias error will be significant in the mode shapes, especially for data collected with a wider resolution, B_e. However, it is not possible to make a quantitative estimate of this error since the value of $G''(\omega)$ is unknown.

In contrast, a quantitative estimate of the random error can be made. This depends on the number of averages taken in a particular set of readings, and the value of the coherence function between the traveller and reference responses. Following Bendat and Piersol again, the confidence limits on the FRF can be found in terms of the F distribution:

$$\hat{r}^2(\omega) = \frac{2}{n-2} \cdot F_{2,n-2;\alpha} \cdot \left[1 - \hat{\gamma}_{xy}^2(\omega)\right] \cdot \frac{\hat{G}_y(\omega)}{\hat{G}_x(\omega)} = \frac{2}{n-2} \cdot F_{2,n-2;\alpha} \cdot \left[1 - \hat{\gamma}_{xy}^2(\omega)\right] \cdot \left|\hat{H}(\omega)\right|^2 \quad \text{.....7.14}$$

where

$$P\left[\left|\hat{H}(\omega)\right| - \hat{r}(\omega) < H(\omega) < \left|\hat{H}(\omega)\right| + \hat{r}(\omega)\right] = 1 - \alpha \quad \text{.....7.15}$$

The data points for each of the mode shapes were plotted using the UNIRAS graphics package on a Silicon Graphics IRIX mini-computer, and the deformed shapes of the deck estimated by fitting a spline through the points. The mode shapes produced are shown in figures 7.24 and 7.25 and summarised in table 7.5. The frequencies in table 7.5 differ from those in table 7.4 because the latter were obtained from data recorded overnight when there was less traffic on the bridge and consequently the total mass of the system was less. Finally, a similar procedure was used to plot the first transverse mode shapes of the Northern pylons (figure 7.26).

7.4 Finite Element Modelling

Another important preliminary to the long term testing was to develop a finite element model of the bridge. This would help both in placing instrumentation, and in understanding the data produced from the long term monitoring and modal survey. In producing the model of the bridge there are four main aspects that need to be considered; deck, pylons, cables and bearings.

7.4.1 Modelling Of The Deck

The model of the bridge deck must accurately represent both the torsional and flexural behaviour of the real structure, which means that values for the transverse and vertical moments of inertia and the torsional constant must be estimated. Furthermore, for a dynamic analysis, nodes in the torsional mode shapes lie in planes where warping is restrained, and so a value of the warping constant must also be found. For Kessock bridge the deck model is complicated further by the lack of symmetry about the horizontal axis (figure 7.3). Several approaches for modelling such bridge decks have been

discussed in the literature. For example, the Quincy Bayview Bridge has a similar non symmetrical cross section (figure 7.27) and this has been modelled using a central spine to supply the flexural and torsional stiffness [Wilson & Gravelle 1991]. In this case the vertical and transverse stiffness of the spine were calculated directly from the full section. The torsional constant was then calculated by considering the deck to be a thin walled open section:

$$J = \sum_{i=1}^{n} \frac{b_i t_i^3}{3} \qquad \text{.....7.16}$$

and the warping constant estimated by approximating the deck as a C section (figure 7.28) using the following formula:

$$\Gamma = \frac{b^2}{4}\left\{ I_{zz} + e^2 A\left(1 - \frac{b^2 A}{4 I_{yy}}\right)\right\} \qquad \text{.....7.17}$$

In order to include this in the model an equivalent torsional constant J_{eq}, defined as follows:

$$T = GJ\Phi' - E\Gamma\Phi''' = GJ_{eq}\Phi' \qquad \text{.....7.18}$$

was found by assuming that the torsional modes shapes were sine functions:

$$\Phi(x) = B\sin\left(\frac{n\pi}{L}x\right) \qquad \text{.....7.19}$$

Substituting into equation 7.18 then yields:

$$J_{eq} = J + \frac{E\Gamma}{G}\left(\frac{n\pi}{L}\right)^2 \qquad \text{.....7.20}$$

Finally the mass of the deck was modelled by lumping the mass at the outer edges of the deck. To model the interaction of the lateral and torsional modes these masses were placed below the axis of the spine, at a depth equal to the height of the shear centre (figure 7.29).

Although this approach was successfully used by Wilson to model the Quincy Bayview Bridge, it does introduce some problems. Most notably, because there is a different equivalent torsional constant for each mode, a mean value has to be used and so the warping is not adequately modelled. This is especially important for the type of open cross sections being considered in this study since warping dominates normal torsional behaviour. Kumarasena used an alternative approach to modelled the deck of the Deer Island Suspension Bridge, which again has an non symmetrical cross section (figure 7.30) [Kumarasena *et al.* 1989]. In this study the torsional, vertical and warping behaviour of the structure were modelled using separate elements. The torsional stiffness was supplied by a central spine which had no transverse or vertical stiffness. For the vertical analysis, the vertical stiffness was supplied by edge beams which represented the girders of the non symmetrical deck. For the torsional studies these beams were then replaced by a different set of beams which modelled the warping of the deck. Here they assumed that warping of a length of deck δx gave rise to a bending deflection α (figure 7.31) defined by:

$$\alpha = \frac{b}{2}\frac{d^2\Phi}{dx^2}\delta x \qquad \text{.....7.21}$$

The moment associated with this deflection is:

$$M = EI_{ZZ}\frac{\alpha}{\delta x} = \frac{EI_{ZZ}b}{2}\left(\frac{d^2\Phi}{dx^2}\right) \qquad \text{.....7.22}$$

which leads to the following expression for the strain energy:

$$\delta U_s = \frac{M^2}{2EI_{ZZ}}\delta x = \frac{1}{2}E\Gamma\left(\frac{d^2\Phi}{dx^2}\right)^2 \delta x \quad \text{.....7.23}$$

Equation 7.23 equates the strain energy due to warping with the strain energy due to bending of the edge beam, and allows the inertia of the edge beams representing warping to be found:

$$I_{ZZ} = \frac{4\Gamma}{b^2} \quad \text{.....7.24}$$

This approach has an advantage over the method used by Wilson in that the modelling of the warping constant is consistent for all modes. However, this method does not allow the torsional and vertical behaviour to be modelled simultaneously, nor does it account for the effects of the position of the shear centre.

In the event two finite element models of the bridge were produced using sectional properties supplied by the bridge engineers. In the first of these, the whole of the crossing was modelled using the approach of Kumarasena, and the deck was represented as a grillage of beams (figure 7.32). However, calculating values of torsional and warping constants using equations 7.16 and 7.17, showed that the torsional behaviour would be dominated by the warping constant. In fact normal torsion contributed less than 1 % and so the spine beam was neglected. Furthermore to allow the vertical and torsional behaviour to be modelled in the same analysis the vertical second moment of area of the edge beams was made the same for both warping and flexure. Therefore this meant that the distances between the edge beams had to be different for different cross sections, the width being given by:

$$b = \sqrt{\frac{4I_{ZZ}}{\Gamma}} \quad \text{.....7.25}$$

Finally the cross sectional area of the edge beams was chosen so as to correctly represent the transverse second moment of area of the complete section:

$$A = \frac{2I_{YY}}{b^2} \qquad \text{.....7.26}$$

The cross beams in the grillage were defined using the properties of the cross beams on the real bridge.

The model just described was adequate for representing the vertical and torsional behaviour of the deck, but still did not account for the interaction of the horizontal and torsional response. In an effort to model this coupling, a more detailed three dimensional model was produced using a combination of shell and beam elements (figure 7.33). The deck plate and the webs of the edge beams were modelled using 4 noded shell elements. Both these components have orthotropic stiffeners on the real bridge to prevent localised buckling, but, because only global effects were being considered, it was assumed that these could be adequately modelled by uniformly increasing the thickness of the shell elements. It was also assumed that the road surface, hand rails and crash barriers made no contribution to the stiffness of the deck. However, the mass of the hand rails and crash barriers was included, and the density of the shells representing the deck plate was increased to model the added mass of an asphalt layer 75 mm thick.

Stiffening of the cross section is provided by yokes formed by the cross beams and vertical stiffeners, and by the bottom flanges of the edge beams. Each of these components was modelled using two noded beam elements as shown in figure 7.33. An added advantage of this approach to modelling the bridge deck now becomes apparent. The maximum bending moments, and hence the designed section properties of the bridge deck, vary along the deck, and these changes in section were achieved by changing the thickness of the bottom flanges of the edge beams. Therefore, these variations can be

taken account of very simply in this model without having to recalculate the section properties of the whole deck for each change in cross section.

The beam shell model correctly represents all the aspects considered earlier, but because of the large number of elements involved it is considerably more expensive both to produce and to analyse. Therefore only the five cable-supported spans were modelled using this approach.

7.4.2 Modelling Of The Pylons

The pylons on the Kessock Bridge are 45 m high and are formed from rectangular box sections (figure 7.34) 2.20 by 1.60 m. in cross section. The wall thickness varies from 28 mm at the base to 8 mm at the top. These pylons were modelled with linear beam elements using section properties obtained from the engineers' calculations. At their bases, the pylons are continuous with the edge girders of the deck section which provide rotational restraint in the longitudinal direction. Therefore, the same nodes were used to define the base of the pylons and the edge beams. Restraint in the transverse direction is provided by the cross boxes (figure 7.35), which are box girders running across the width of the bridge between the bases of the pylons. These were represented by beam elements in both of the models. In the beam shell model two beams were used to represent each cross box, one at the top and one at the bottom of the edge girders.

7.4.3 Modelling Of The Cables

As discussed in chapter two, cable-stayed bridges exhibit several types of non-linearity which will have a bearing both on the creation of the model and the type of analysis performed. One source of non-linearity is the sag in the cables and therefore it is important to choose appropriate models for the cable behaviour. However, several authors [Fleming & Egesli 1982, Nazmy & Abdel-Ghaffar 1990

a&b] have shown that a full non-linear dynamic analysis is not required, and that a linear dynamic analysis following a non-linear static analysis is sufficient. More recent research [Wilson and Gravelle 1991] achieved close agreement between the measured mode shapes of a prototype bridge and finite element predictions using a purely linear model. Therefore, it was decided that a linear model would be satisfactory, and the cables were represented with truss elements. Some account of the cable sag was made by using an equivalent modulus of elasticity given by the formula:

$$E_{eq} = \frac{E_c}{\left\{1+(wH)^2 \frac{AE}{12T^3}\right\}} \qquad \text{.....7.27}$$

The value of the tension, T, used in this equation was again obtained from the engineers' calculations.

7.4.4 Modelling Of The Bearings

The bearings on Kessock Bridge have two main functions, to support the weight of the bridge, and to control the movement of the deck in the horizontal plane. The horizontal restraint provided varies between the different points of support and is shown in figure 7.36. These restraints can be modelled by selecting corresponding boundary conditions to be fixed in the finite element analysis. Figure 7.36 shows that the restraint in the longitudinal direction is provided at only one set of supports. This has important consequences in developing the grillage finite element model because warping will not be fully restrained and so the value of the warping constant discussed above may need to be modified. However, for a modal analysis the warping can be taken to be restrained by the nodal planes as mentioned above. Therefore, by selecting a set of boundary conditions consistent with the bridge bearings and using the full value of the warping constant, an accurate prediction of the mode shapes and natural frequencies can be made. In contrast, this grillage model would not be suitable for modelling the torsional behaviour of the bridge under static loading because the bearings do not fully

restrain warping of the cross section. The beam shell model, of course, does not rely on calculated values of the section properties and so can be applied equally well to both static and dynamic problems.

7.4.5 Analysis Procedures

Eigen value analyses were performed on the two models described above using the SOLVIA finite element package. For the grillage model a fully linear analysis was performed using a consistent mass matrix. The predicted mode shapes and natural frequencies for this model are shown in figures 7.37 a - i. For the beam shell model, the analysis was repeated using three different techniques to investigate the influence of the analysis technique on the results:

i. Fully linear analysis

ii. Large displacement analysis

iii. Large displacement preliminary static analysis prior to dynamic analysis.

The fully linear analysis assumes that only small displacements occur whereas the large displacement analysis takes into account any geometrical non linearities that arise. The preliminary static analysis allows the stiffness matrix to be modified to take account of displacements of the bridge under its self weight, and hence the beam column effects which arise due to the compressive force in the deck and pylons. Each of the analyses was performed using both lumped and consistent mass matrices and the predicted natural frequencies are shown in table 7.6. Clearly, the type of analysis has little influence on the results and this supports the published findings cited earlier on the importance of non linearities in cable stayed bridges. However, using a lumped mass matrix has a significant influence on the predicted frequencies of the torsional modes. This is to be expected since a lumped mass matrix will concentrate the mass at the edges of the deck and consequently increase the rotational

inertia of the system. The mode shapes and natural frequencies predicted by large displacement analysis following a preliminary static analysis are shown in figures 7.38 a - j.

7.5 Comparison Of Predicted And Measured Modal Properties

The natural frequencies measured in the modal survey and predicted by the finite element modelling are compared in table 7.5. The discrepancies between the figures are approximately 5 % for the vertical modes and 10 % for the torsional modes, indicating that the finite element model is not a good representation of the real structure. However, several mitigating factors need to be considered. Firstly, the frequencies measured on the bridge varied with time by up to ± 4 %. Secondly, the finite element model was based on data obtained from the engineers' calculations which were based on design assumptions. Therefore, any discrepancies between these figures and the bridge as built could lead to errors in the predicted frequencies. Thirdly, educated guesses had to be made for the dimensions of some of the non structural elements not included in the engineers' figures. The results could apparently be improved by adjusting these estimates, but this would not necessarily represent an improvement in the model unless there was a sound basis for the changes. Bearing these factors in mind, the finite element results represent a reasonable prediction of the structure's natural frequencies. Figures 7.39 a - c show the finite element predictions for the first three mode shapes superimposed on the results from the modal survey. These figures show that there is a reasonable agreement between the measured data and the finite element results, and also illustrate the large discrepancies between readings taken on the different visits to the bridge.

Before drawing any conclusions, several further comments need to be made on the results. Firstly, the measured power spectra contain groups of closely spaced peaks which make it difficult to determine accurately the natural frequencies and mode shapes in these areas. By comparing the response on

opposite sides of the deck it is possible to separate out the torsional and vertical components (figure 7.40). This indicates that it is the torsional modes which appear in groups, whereas the vertical modes are more clearly defined, a conclusion which is borne out by the results in table 7.5. It is important now to determine whether these groups of peaks represent single modes, or whether they correspond to families of similar modes. This is because closely spaced modes could lead to an unstable coupled response such as flutter. Comparison with the finite element modelling gives conflicting results. The beam shell finite element model failed to predict any closely spaced or multiple modes indicating that the measured data really represent a single mode. The multiple peaks therefore represent deficiencies in the measuring system. However, the simpler grillage model did predict some multiple torsional modes (e.g. figures 7.37b & c) with the major differences in the mode shapes occuring in the pylon behaviour and their relative base motion. With such conflicting results, further work needs to be done to investigate the possible causes of the multiple peaks in the measured data.

Secondly, the measured lateral behaviour of the bridge did not yield well-defined mode shapes (figure 7.41). However, most of the peaks in the lateral power spectra (7.22) coincide with torsional modes measured from the vertical response. Since the cross section of the deck is an inverted U shape, the shear centre lies above the level of the deck and does not coincide with the centre of mass. Therefore lateral dynamic excitation will always give rise to torsional displacement, and it is likely that the lateral and torsional motion of the deck will be closely coupled. Furthermore there will be no purely lateral modes. This view is supported by the second finite element model which does not predict any lateral modes and shows that the torsional modes contain significant lateral displacements (figure 7.38). The processing of the long term data provided the opportunity to calculate the coherence between the horizontal and vertical accelerations of the bridge deck, and this confirmed that the

vertical and lateral response are closely correlated at frequencies corresponding to the torsional modes (figure 7.42).

Thirdly, the first finite element model, which included the full approach viaducts, showed that several modes gave similar deflected shapes in the cable supported spans. These modes corresponded to different side spans vibrating in their fundamental modes and could explain why some of the measured vertical modes appear to be repeated, for example modes 21 and 26. Another interesting result from the finite element modelling is that the second model showed that the higher torsional mode shapes were often dominated by large deflections of the bottom flanges of the edge girders (figures 7.43 and 7.44). As the flange is only restrained laterally by the stiffness of the web, this type of response does not appear unlikely. Unfortunately no measurements could be taken on site to investigate and confirm this phenomenon because there was no access over the side of the bridge.

Finally, it has to be noted that the investigations into the pylon behaviour were only successful in producing an estimate for the first transverse mode where the natural frequency and mode shape agreed with finite element predictions (figure 7.45). However, the finite element analysis predicted that the pylons would move together, but poor coherence between the response at the top of adjacent pylons (figure 7.46) indicated that this does not occur in the real structure. No clearly defined modes were found in the longitudinal direction, although at low frequencies there appears to be some correlation with the vertical movement of the bridge deck (figure 7.47).

7.6 The Long Term Monitoring Exercise

The equipment for the long term monitoring was installed on the bridge in late September 1991. Initially the exercise had been planned to last for just one month after the instrumentation had been

set up. However, several difficulties were encountered once the equipment had been installed and it was therefore necessary to extend the monitoring period. These problems included:

i. Damage to the accelerometer cables,

ii. Loss of meaningful signals from the anemometer 8 on top of the North pylon,

iii. Intermittent faults in the signal conditioning,

iv. Failure of the control system.

These problems were of course exacerbated by the large distance between Inverness and Bristol which meant that all attempted diagnostics had to be carried out via the telephone link. Fortunately the employees of Highland Regional Council were very co-operative and helped by repairing the damaged cables and rebooting the PC when the control system crashed. Eventually most of the teething problems were overcome, with the exception of the loss of anemometer 8 and the unreliable signal conditioning. Because of this, an unscheduled trip to Inverness had to be arranged. This revealed that the anemometer had become unserviceable because of water ingress, and the fault in the signal processing was traced to a faulty power supply to the filters. These pieces of equipment were brought back to Bristol for repair and returned to the bridge by courier. One further problem arose during this visit which caused the loss of the signals from accelerometer 2. Since this accelerometer was the only one measuring the response on the West side, this was very significant as it meant that it was no longer possible to measure the torsional behaviour of the deck directly. Unfortunately, this fault was not noticed until after the employees of HRC had reinstalled the filters in the bridge and it was then too late to solve it. When the monitoring restarted everything was functioning as planned with the exception of the anemometer 8 and accelerometer 2 on the west side of the deck, which were no longer working.

These problems had caused a delay of about two months and so it was decided to extend the exercise until the end of May 1992. During this time the equipment functioned well and a large amount of data was collected. However, as the equipment was left in a hostile environment for longer than had been intended significant wear and tear had occurred by the time the final visit was made. When the equipment was decommissioned, inspection showed:

i. Anemometers 2 and 3 had ceased to function because the cables had severed,

ii. The other anemometer cables were all badly worn in places,

iii. Accelerometer 4 had become detached from the bridge deck.

Fortunately, the recorded data showed exactly when the instruments were damaged, and that this was in the last few weeks of the project, and so the consequences were limited. Finally, the fault on accelerometer two was traced to a short circuit on one of the outputs from the conditioning amplifiers.

7.7 Conclusions

This chapter has described the planning and execution of a testing program on the Kessock Bridge near Inverness. As a result of this program the following conclusions can be drawn.

1. The modal survey of the bridge was successful in identifying 27 possible natural frequencies and mode shapes.

2. Measurements of the lower modes confirmed predictions made by two finite element models and therefore show that these models are a reasonable representation of the bridge.

3. Both the modal survey and the computer modelling indicate that there is strong interaction between lateral and torsional vibrations.

4. The modal survey indicated that the torsional behaviour of the deck is typified by families of similar mode shapes with closely spaced natural frequencies.

5. More than five months of data have been recorded detailing the wind loading at seven points across the bridge, and the vertical and horizontal response of the deck. These data now need to be used to correlate the bridge response with the spatial structure of the wind.

Table 7.1 : Anemometer Calibration Constants

Anemometer	Constant	Coefficient
1	0.881	45.92
2	1.695	45.92
3	0.0615	44.09
4	1.012	44.39
5	1.531	45.99
6	2.313	46.15
7	0.974	40.76
8	-0.280	46.54

Table 7.2 : Monitoring Locations First Visit

Reference			Traveller				
Location	**Instrument**	**Orientation**	**Location**	**Instrument**	**Orientation**	**Analyser**	**Resolution**
East 60 m.	I 5	Vertical	East 300 m.	I 1	Vertical	S1200	0.04
East 60 m.	I 5	Vertical	East 280 m.	I 1	Vertical	S1200	0.04
East 60 m.	I 5	Vertical	East 260 m.	I 1	Vertical	S1200	0.04
East 60 m.	I 5	Vertical	East 220 m.	I 4	Vertical	S1200	0.04
East 60 m.	I 5	Vertical	East 200m.	I 4	Vertical	S1200	0.04
East 60 m.	I 5	Vertical	East 180 m.	I 4	Vertical	S1200	0.04
East 60 m.	I 5	Vertical	East 160 m.	I 4	Vertical	S1200	0.04
East 60 m.	I 5	Vertical	East 150 m.	I 4	Vertical	S1200	0.04
East 60 m.	I 5	Vertical	East 150 m.	I 4	Vertical	S1200	0.02
East 50 m.	I 5	Vertical	East 150 m.	I 4	Vertical	S1200	0.01
East 60 m.	I 5	Vertical	East 140 m.	I 4	Vertical	S1200	0.04
East 60 m.	I 5	Vertical	East 120 m.	I 4	Vertical	S1200	0.04
East 60 m.	I 5	Vertical	East 100 m.	I 4	Vertical	S1200	0.04
East 60 m.	I 5	Vertical	East 90 m.	I 4	Vertical	S1200	0.04
East 60 m.	I 5	Vertical	East 80 m.	I 4	Vertical	S1200	0.04
East 60 m.	I 5	Vertical	East 70 m.	I 4	Vertical	S1200	0.04
East 60 m.	I 5	Vertical	East 60 m.	I 4	Vertical	S1200	0.04
East 60 m.	I 5	Vertical	East 40 m.	I 4	Vertical	S1200	0.04
East 60 m.	I 5	Vertical	East 20 m.	I 4	Vertical	S1200	0.04
East 60 m.	I 5	Vertical	East -20 m.	I 4	Vertical	S1200	0.04
East 60 m.	I 5	Vertical	East -20 m.	I 4	Vertical	S1200	0.01
East 60 m.	I 5	Vertical	East -40 m.	I 4	Vertical	S1200	0.04
East 60 m.	I 5	Vertical	East -60 m.	I 4	Vertical	S1200	0.04
East 60 m.	I 5	Vertical	West 300 m.	I 1	Vertical	S1200	0.04
East 60 m.	I 5	Vertical	West 280 m.	I 1	Vertical	S1200	0.04
East 60 m.	I 5	Vertical	West 260 m.	I 1	Vertical	S1200	0.04
East 60 m.	I 5	Vertical	West 220 m.	I 1	Vertical	S1200	0.04
East 60 m.	I 5	Vertical	West 200 m.	I 1	Vertical	S1200	0.04
East 60 m.	I 5	Vertical	West 180 m.	I 1	Vertical	S1200	0.04
East 60 m.	I 5	Vertical	West 160 m.	I 1	Vertical	S1200	0.04
East 60 m.	I 5	Vertical	West 140 m.	I 1	Vertical	S1200	0.04
East 60 m.	I 5	Vertical	West 120 m.	I 1	Vertical	S1200	0.02
East 60 m.	I 5	Vertical	West 100 m.	I 1	Vertical	S1200	0.04
East 60 m.	I 5	Vertical	West 80 m.	I 1	Vertical	S1200	0.04
East 60 m.	I 5	Vertical	West 60 m.	I 1	Vertical	S1200	0.04
East 60 m.	I 5	Vertical	West 40 m.	I 1	Vertical	S1200	0.04
East 60 m.	I 5	Vertical	West 20 m.	I 1	Vertical	S1200	0.04
East 60 m.	I 5	Vertical	West -20 m.	I 1	Vertical	S1200	0.04
East 60 m.	I 5	Vertical	West -40 m.	I 1	Vertical	S1200	0.04
East 60 m.	I 5	Vertical	West -60 m.	I 1	Vertical	S1200	0.04
East 50 m.	I 5	Vertical	West 120 m.	I 2	Vertical	S1200	0.01

Table 7.3 : Monitoring Locations Final Visit

Reference			Traveller				
Location	Instrument	Orientation	Location	Instrument	Orientation	Analyser	Resolution
West 338 m.	I 3	Transverse	East 374 m.	I 1	Transverse	Advantest	0.025
East 60 m.	I 5	Transverse	East 356 m.	I 1	Transverse	Advantest	0.025
East 60 m.	I 5	Transverse	East 338 m.	I 1	Transverse	Advantest	0.025
East 60 m.	I 5	Transverse	East 300 m.	I 1	Transverse	Advantest	0.025
East 60 m.	I 5	Transverse	East 280 m.	I 1	Transverse	Advantest	0.025
East 60 m.	I 5	Transverse	East 260 m.	I 1	Transverse	Advantest	0.025
East 60 m.	I 5	Transverse	East 220 m.	I 4	Transverse	S1200	0.04
East 60 m.	I 5	Transverse	East 200m.	I 4	Transverse	S1200	0.04
East 60 m.	I 5	Transverse	East 180 m.	I 4	Transverse	S1200	0.04
East 60 m.	I 5	Transverse	East 160 m.	I 4	Transverse	S1200	0.04
East 60 m.	I 5	Transverse	East 140 m.	I 4	Transverse	S1200	0.04
East 60 m.	I 5	Transverse	East 120 m.	I 4	Transverse	S1200	0.04
East 60 m.	I 5	Transverse	East 100 m.	I 4	Transverse	Advantest	0.025
East 60 m.	I 5	Transverse	East 80 m.	I 4	Transverse	Advantest	0.025
East 60 m.	I 5	Transverse	East 60 m.	I 4	Transverse	Advantest	0.025
East 60 m.	I 5	Transverse	East 40 m.	I 4	Transverse	Advantest	0.025
East 60 m.	I 5	Transverse	East 20 m.	I 4	Transverse	Advantest	0.025
East 60 m.	I 5	Transverse	East -20 m.	I 4	Transverse	Advantest	0.025
East 60 m.	I 5	Transverse	East -20 m.	I 4	Transverse	Advantest	0.025
East 60 m.	I 5	Transverse	East -40 m.	I 4	Transverse	Advantest	0.025
East 60 m.	I 5	Transverse	East -60 m.	I 4	Transverse	Advantest	0.025
East 60 m.	I 5	Transverse	East -98 m.	I 4	Transverse	Advantest	0.025
East 60 m.	I 5	Transverse	East -116 m.	I 4	Transverse	Advantest	0.025
East 60 m.	I 5	Transverse	East -134 m.	I 4	Transverse	Advantest	0.025
East 60 m.	I 5	Vertical	East -98 m.	I 4	Vertical	Advantest	0.025
East 60 m.	I 5	Vertical	East -116 m.	I 4	Vertical	Advantest	0.025
East 60 m.	I 5	Vertical	East -134 m.	I 4	Vertical	Advantest	0.025
East -98 m.	I 5	Vertical	West -98 m	I 2	Vertical	Advantest	0.025
East -98 m.	I 5	Vertical	West -116 m	I 2	Vertical	Advantest	0.025
East -98 m.	I 5	Vertical	West -134 m	I 2	Vertical	Advantest	0.025
East 60 m.	I 5	Vertical	East 338 m	I 1	Vertical	Advantest	0.025
West 338 m	I 3	Vertical	East 356 m	I 1	Vertical	Advantest	0.025
West 338 m	I 3	Vertical	East 374 m	I 1	Vertical	Advantest	0.025
East 338 m	I 1	Vertical	West 338 m	I 3	Vertical	Advantest	0.025
East 338 m	I 1	Vertical	West 356 m	I 3	Vertical	Advantest	0.025
East 338 m	I 1	Vertical	West 374 m	I 3	Vertical	Advantest	0.025
East 60 m.	I 5	Vertical	East 220 m.	I 4	Vertical	Advantest	0.0625

Table 7.3 Continued

East 60 m.	I 5	Vertical	East 200m.	I 4	Vertical	Advantest	0.0625
East 60 m.	I 5	Vertical	East 180 m.	I 4	Vertical	Advantest	0.0625
East 60 m.	I 5	Vertical	East 160 m.	I 4	Vertical	Advantest	0.0625
East 60 m.	I 5	Vertical	East 140 m.	I 4	Vertical	Advantest	0.0625
East 60 m.	I 5	Vertical	East 120 m.	I 4	Vertical	Advantest	0.0625
East 60 m.	I 5	Vertical	East 100 m.	I 4	Vertical	Advantest	0.0625
East 60 m.	I 5	Vertical	East 80 m	I 4	Vertical	Advantest	0.0625
East 60 m.	I 5	Vertical	East 40 m	I 4	Vertical	Advantest	0.0625
East 60 m.	I 5	Vertical	East 20 m	I 4	Vertical	Advantest	0.0625
East 40 m.	I 5	Vertical	East 210 m.	I 4	Vertical	Advantest	0.025
East 40 m.	I 5	Vertical	East 190m.	I 4	Vertical	Advantest	0.025
East 40 m.	I 5	Vertical	East 170 m.	I 4	Vertical	Advantest	0.025
East 40 m.	I 5	Vertical	East 150 m.	I 4	Vertical	Advantest	0.025
East 40 m.	I 5	Vertical	East 130 m.	I 4	Vertical	Advantest	0.025
East 40 m.	I 5	Vertical	East 108.5 m.	I 4	Vertical	Advantest	0.025
East 40 m.	I 5	Vertical	East 80 m.	I 4	Vertical	Advantest	0.025
East 40 m.	I 5	Vertical	East 70 m	I 4	Vertical	Advantest	0.025
East 40 m.	I 5	Vertical	East 50 m	I 4	Vertical	Advantest	0.025
East 40 m.	I 5	Vertical	East 30 m	I 4	Vertical	Advantest	0.025
East 40 m.	I 5	Vertical	West 20 m.	I 4	Vertical	Advantest	0.00625
East 40 m.	I 5	Vertical	West 40 m.	I 4	Vertical	Advantest	0.00625
East 40 m.	I 5	Vertical	West 80 m.	I 4	Vertical	Advantest	0.00625
East 40 m.	I 5	Vertical	West 100 m	I 4	Vertical	Advantest	0.00625
East 40 m.	I 5	Vertical	West 120 m	I 4	Vertical	Advantest	0.00625
East 40 m.	I 5	Vertical	West 140 m	I 4	Vertical	Advantest	0.00625
East 60 m.	I 5	Vertical	East 180 m	I 4	Vertical	Solartron	0.002
East 60 m.	I 5	Vertical	East 100 m.	I 4	Vertical	Advantest	0.0025
East 60 m.	I 5	Vertical	East 80 m.	I 4	Vertical	Solartron	0.002
East 60 m.	I 5	Vertical	East -98 m.	I 4	Vertical	Advantest	0.00125
East 60 m.	I 5	Vertical	West 60 m	I 2	Vertical	Advantest	0.0025
East 40 m.	I 5	Vertical	West 60 m	I 2	Vertical	Advantest	0.0025
East 40 m.	I 5	Vertical	West 80 m	I 2	Vertical	Advantest	0.0025
East 60 m.	I 5	Transverse	East 160 m	I 2	Transverse	Advantest	0.0025
East 60 m.	I 5	Transverse	East 100 m	I 2	Transverse	Advantest	0.0025

Table 7.3 Continued

Pylons

East 60 m	I 5	Vertical	NE 1	I 4	Longitudinal	Advantest	0.025
East 60 m	I 5	Vertical	NE 2	I 4	Longitudinal	Advantest	0.025
NE 1	I 5	Longitudinal	NE 2	I 4	Longitudinal	Advantest	0.025
NE 1	I 5	Longitudinal	NE 3	I 4	Longitudinal	Advantest	0.025
NE 1	I 5	Longitudinal	NE 4	I 4	Longitudinal	Advantest	0.025
NE 1	I 5	Longitudinal	NE 5	I 4	Longitudinal	Advantest	0.025
NE 1	I 5	Longitudinal	NE 6	I 4	Longitudinal	Advantest	0.025
NE 1	I 5	Longitudinal	NE 7	I 4	Longitudinal	Advantest	0.025
NE 1	I 1	Transverse	NE 1	I 3	Transverse	Advantest	0.025
NE 1	I 1	Transverse	NE 2	I 3	Transverse	Advantest	0.025
NE 1	I 1	Transverse	NE 3	I 3	Transverse	Advantest	0.025
NE 1	I 1	Transverse	NE 4	I 3	Transverse	Advantest	0.025
NE 1	I 1	Transverse	NE 5	I 3	Transverse	Advantest	0.025
NE 1	I 1	Transverse	NE 6	I 3	Transverse	Advantest	0.025
NE 1	I 1	Transverse	NW 1	I 3	Transverse	Advantest	0.025
NE 1	I 1	Longitudinal	NW 1	I 3	Longitudinal	Advantest	0.025
NW 1	I 3	Longitudinal	NW 6	I 1	Longitudinal	Advantest	0.025
NW 1	I 3	Longitudinal	NW 5	I 1	Longitudinal	Advantest	0.025
NW 1	I 3	Longitudinal	NW 4	I 1	Longitudinal	Advantest	0.025
NW 1	I 3	Longitudinal	NW 3	I 1	Longitudinal	Advantest	0.025
NW 1	I 3	Longitudinal	NW 2	I 1	Longitudinal	Advantest	0.025
NW 1	I 3	Longitudinal	NW 1	I 1	Longitudinal	Advantest	0.025
NW 1	I 3	Transverse	NW 1	I 1	Longitudinal	Advantest	0.025
NW 1	I 3	Transverse	NW 1	I 1	Transverse	Advantest	0.025
NW 1	I 3	Transverse	NW 2	I 1	Transverse	Advantest	0.025
NW 1	I 3	Transverse	NW 3	I 1	Transverse	Advantest	0.025
NW 1	I 3	Transverse	NW 4	I 1	Transverse	Advantest	0.025
NW 1	I 3	Transverse	NW 5	I 1	Transverse	Advantest	0.025
NW 1	I 3	Transverse	NW 6	I 1	Transverse	Advantest	0.025

Table 7.4 : Measured Frequencies

Vertical Frequencies.	Vertical Damping %	Lateral Frequencies.	Lateral Damping %
0.510	1.8	-	-
0.712	0.7	0.712	0.3
0.747	0.7	0.755	0.9
0.812	0.8	-	-
-	-	0.985	0.3
0.992	0.8	-	-
-	-	1.007	0.7
-	-	1.047	0.9
1.072	0.3	1.072	2.2
1.088	0.3	-	-
-	-	1.112	0.9
1.116	0.4	-	-
1.224	1.4	-	-
-	-	1.230	0.9
-	-	1.417	1.5
-	-	1.465	4
1.472	1.2	-	-
1.532	1	-	-
1.590	0.8	1.585	0.5
1.772	1.7	-	-
1.889	1.4	-	-
1.978	0.7	-	-
2.08	6	-	-
2.14	1.5	-	-
2.24	-	-	-
2.414	2.4	-	-
-	-	2.68	1.3
-	-	2.891	0.6
-	-	3.155	0.9
-	-	3.376	1
3.578	-	-	-
3.854	5	3.85	0.4
4.012	3	-	-
4.282	3	-	-
4.761	5	-	-

Table 7.5 : Measured Modes Of Kessock Bridge

Mode Number	Frequency / Hz.	Damping / %	FEM Estimate / Hz	Description
1	0.51	3	0.526	V1
2	0.72	-	-	T1
3	0.74	1	0.756	T1
4	0.81	1	0.835	V2
5	1.04	3	-	T2
6	1.06	1	-	T2
7	1.07	2	-	T2
8	1.10	-	1.14	T2
9	1.20	1	1.21	V3
10	1.48	1	-	T3
11	1.52	1	-	T3
12	1.56	2	1.65	T3
13	1.74	3	-	V3
14	1.87	2	-	V4
15	1.98	2	-	-
16	2.04	1	-	T4
17	2.14	2	-	T4
18	2.40	-	-	T4
19	2.66	-	-	T4
20	2.85	2	-	V5

Table 7.6 : Comparison Of Natural Frequencies Predicted By Different Analysis Methods

	Consistent Mass Matrix			Lumped Mass Matrix		
Mode	Restart Analysis	Large Displacements	Small Displacements	Restart Analysis	Large Displacements	Small Displacements
1st Vertical	0.526	0.539	0.529	0.524	0.536	0.526
1st Torsional	0.756	0.769	0.754	0.673	0.682	0.670
2nd Vertical	0.835	0.854	0.845	0.829	0.848	0.839
2nd Torsional	1.144	1.160	1.144	1.016	1.029	1.015
3rd Vertical	1.207	1.240	1.236	1.195	1.227	1.223
3rd Torsional	1.652	1.673	1.666	1.484	-	1.496

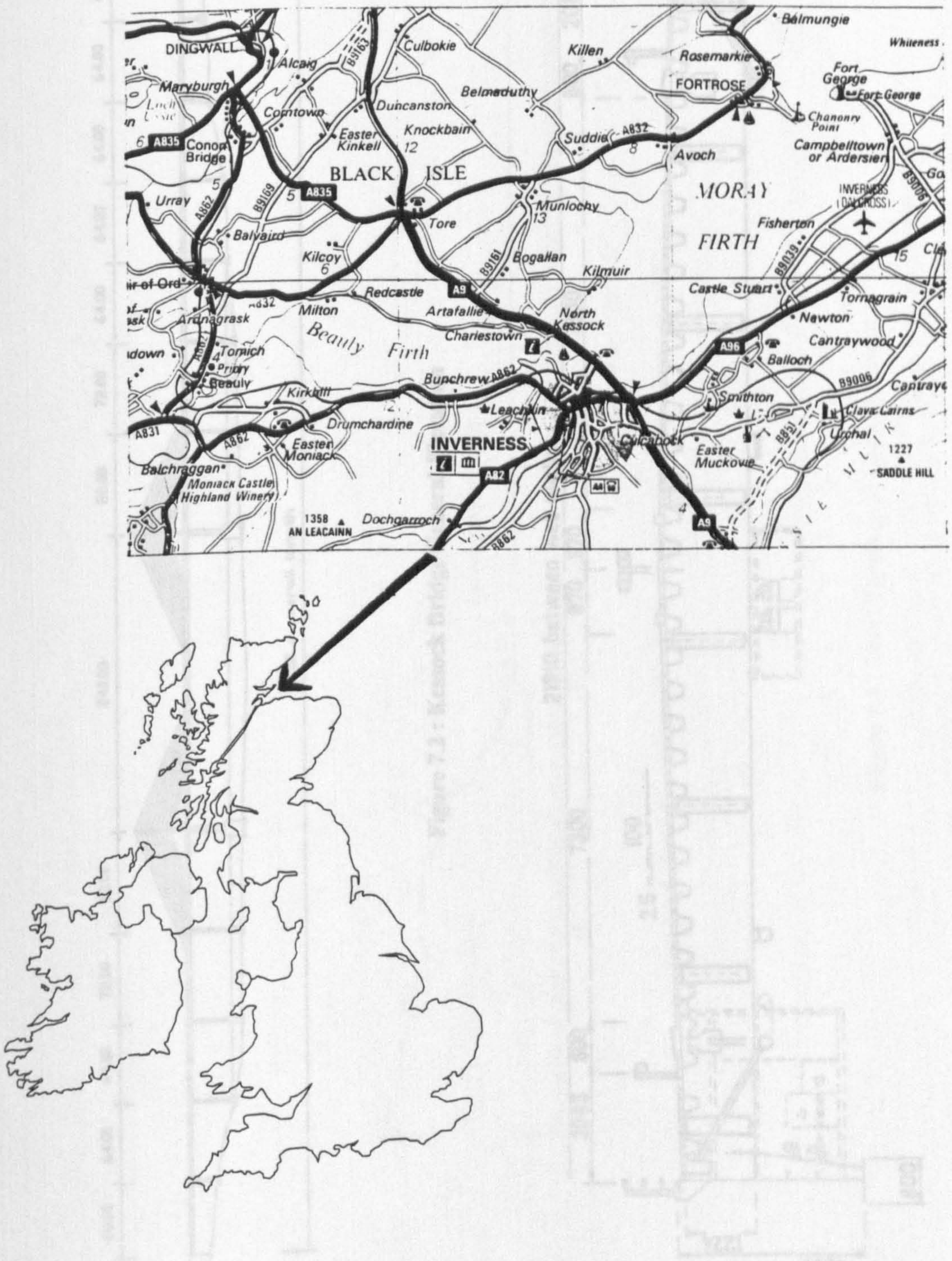

Figure 7.1 : The Location of Kessock Bridge

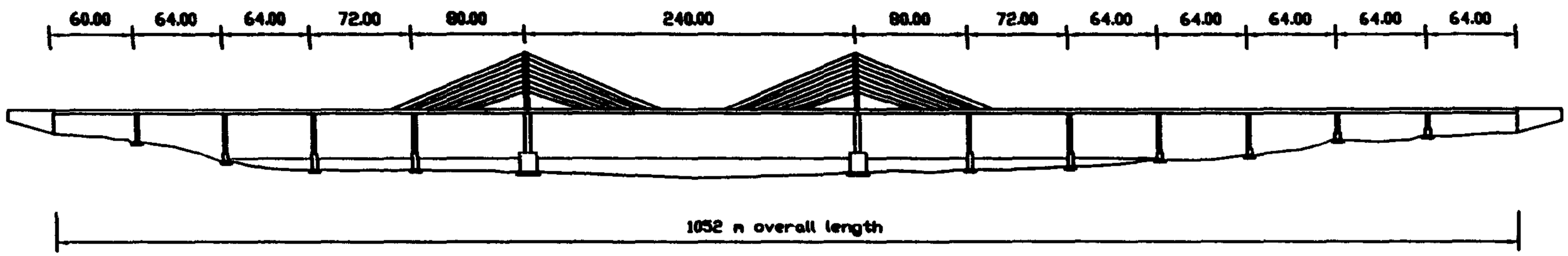

Figure 7.2 : Kessock Bridge General Elevation

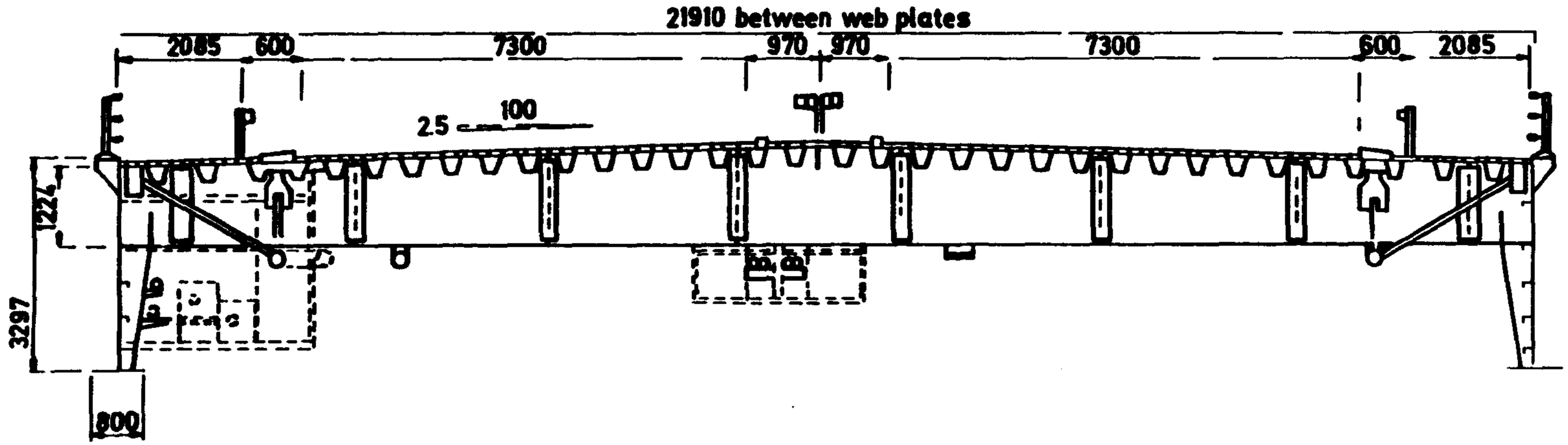

Figure 7.3 : Kessock Bridge Deck Cross Section

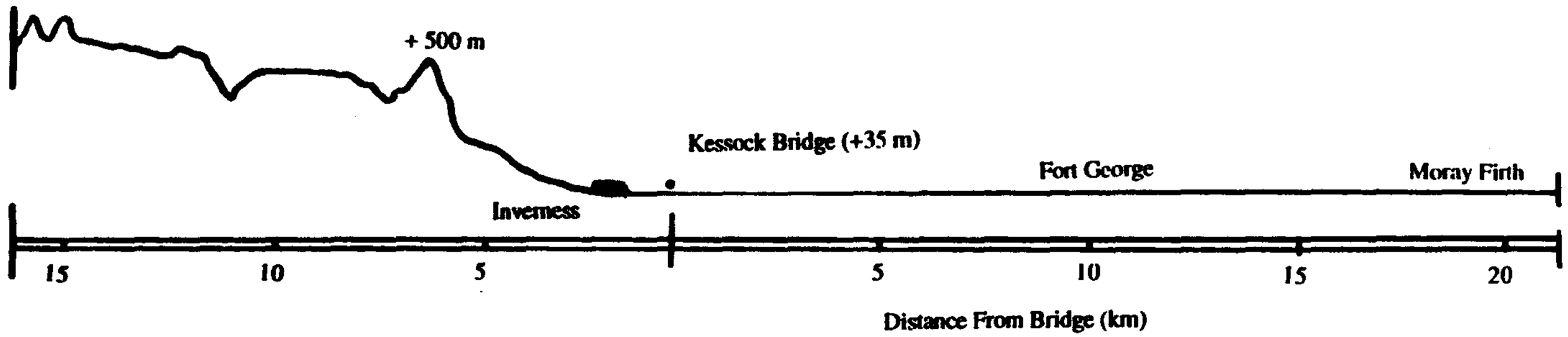

Cross Section Normal to bridge Axis (After Cullen-Wallace 1985)

Figure 7.4 : Local Topology at Kessock Bridge

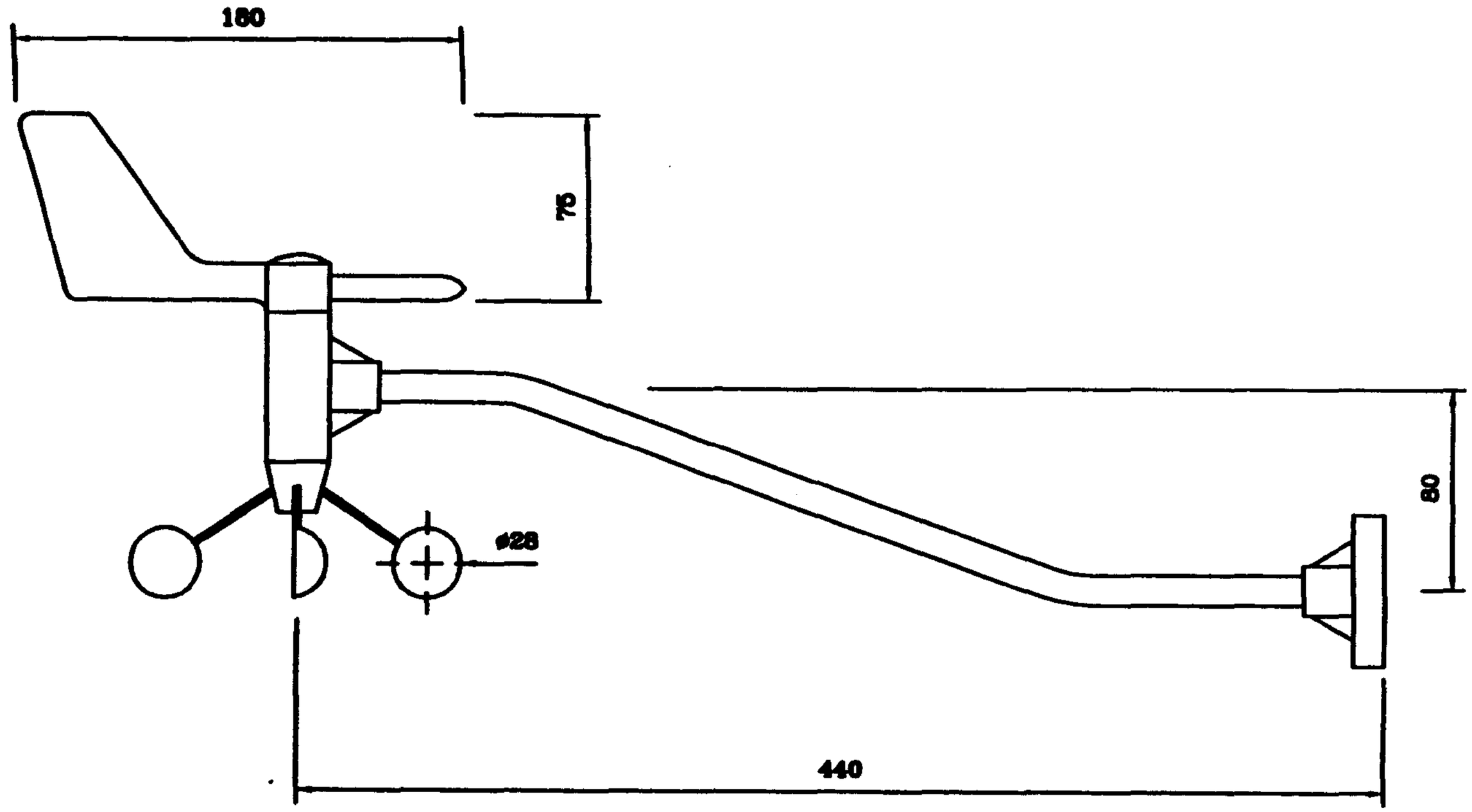

General Arrangement of Anemometer (not to scale)

Figure 7.5 : Digitar Cup and Vane Anemometer Used on Kessock Bridge

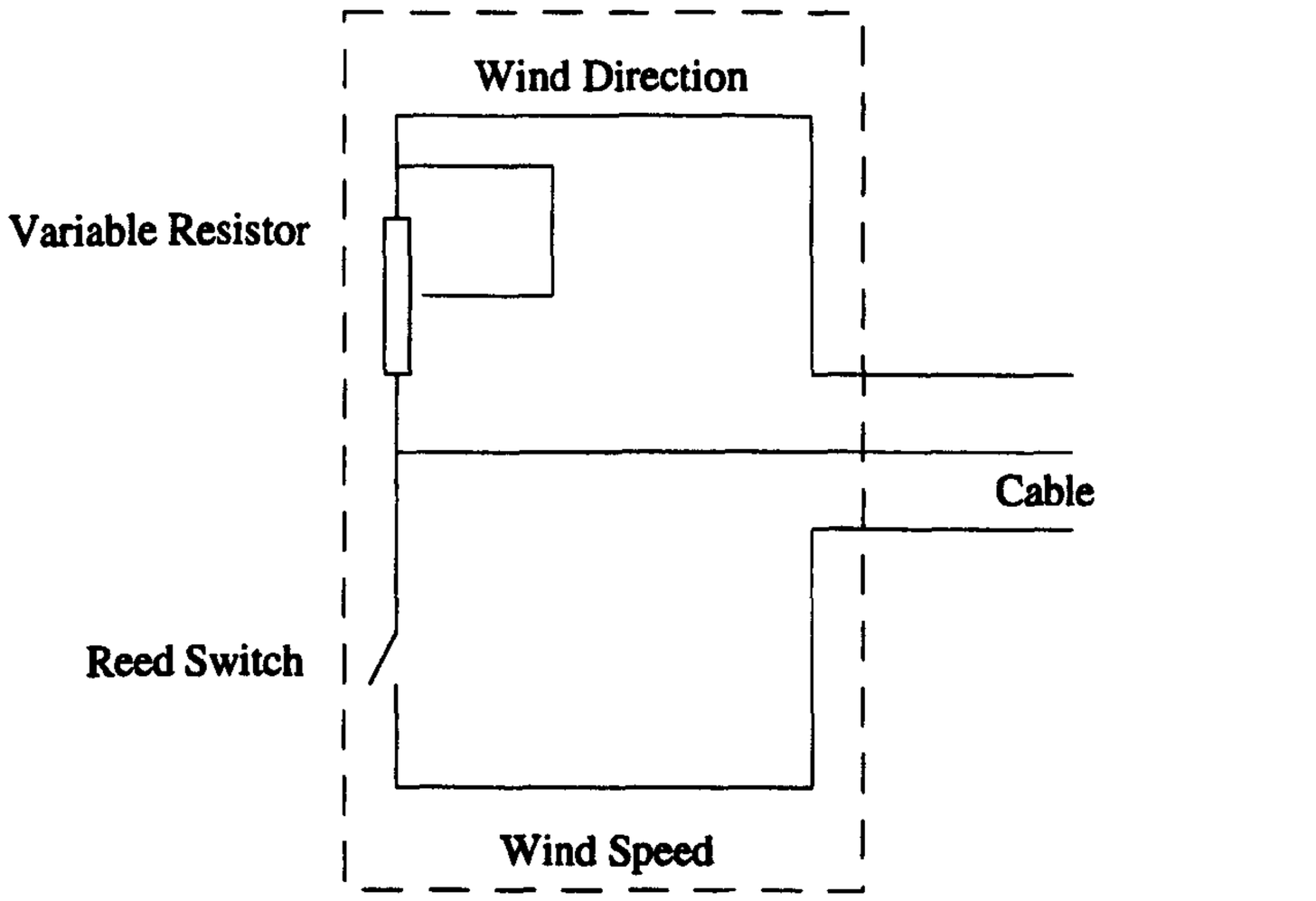

Figure 7.6 : Wiring Inside Cup and Vane Anemometer

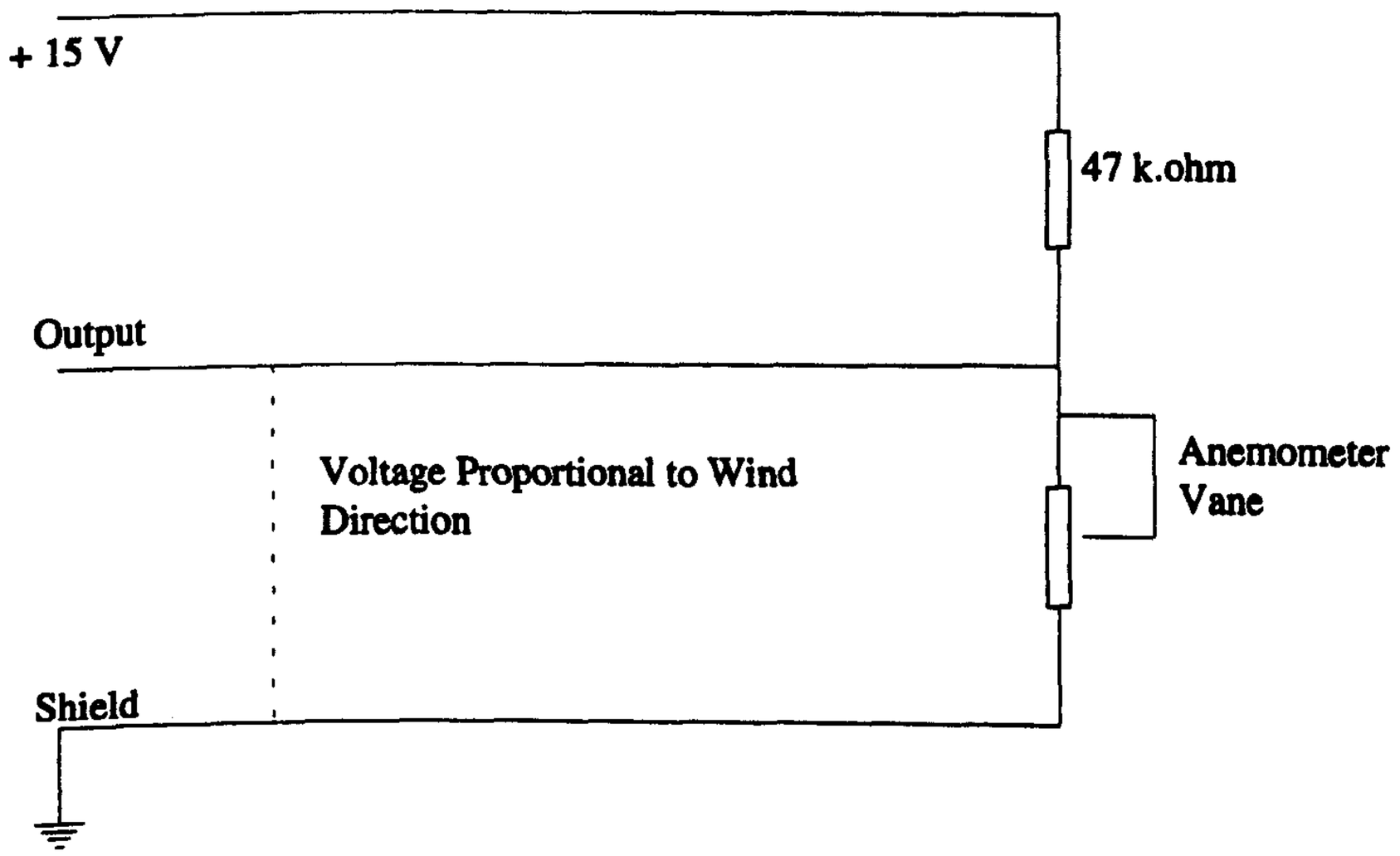

Figure 7.7 : Circuit for Wind Direction Measurement

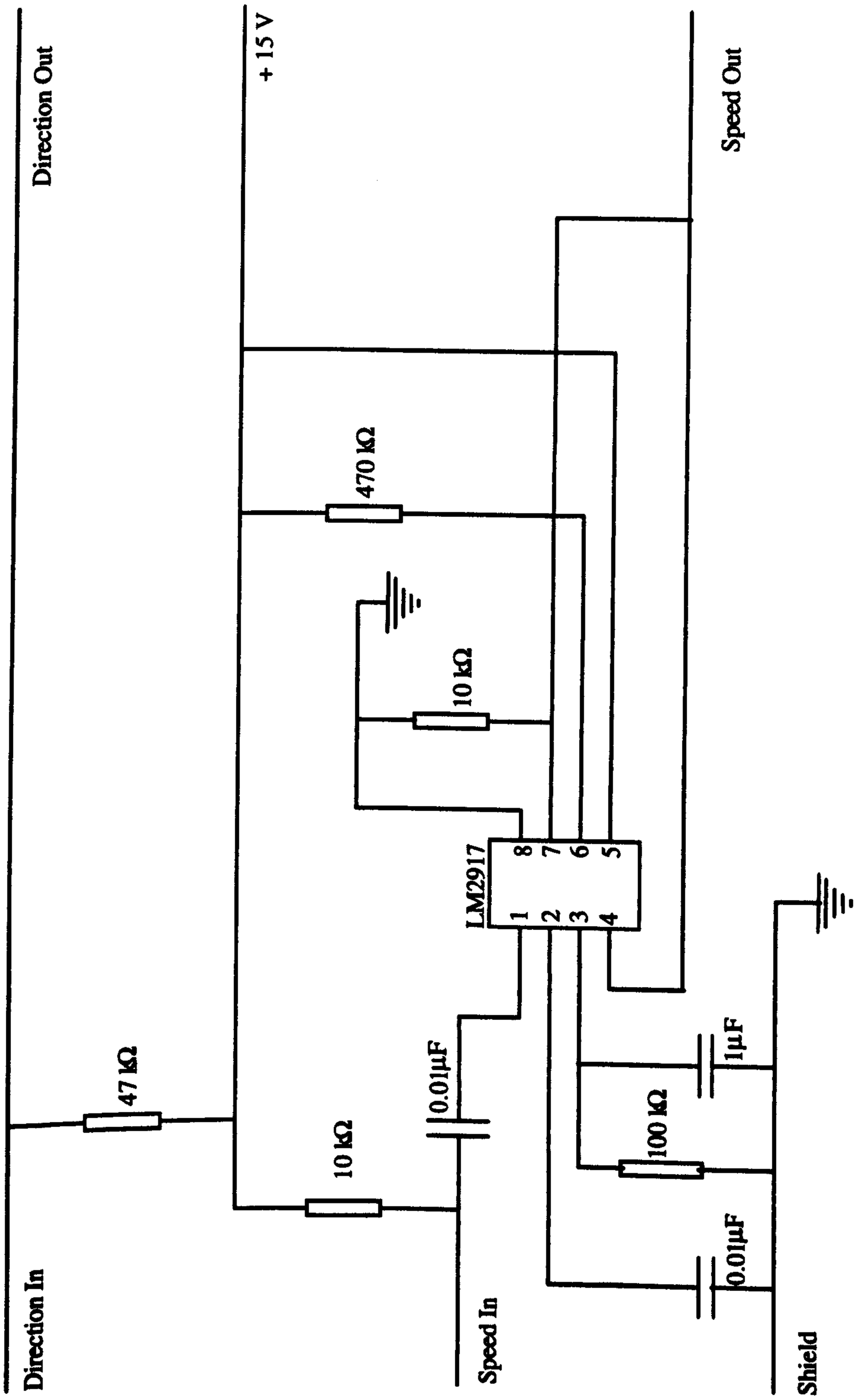

Figure 7.8 : Anemometer Signal Conditioning Circuit

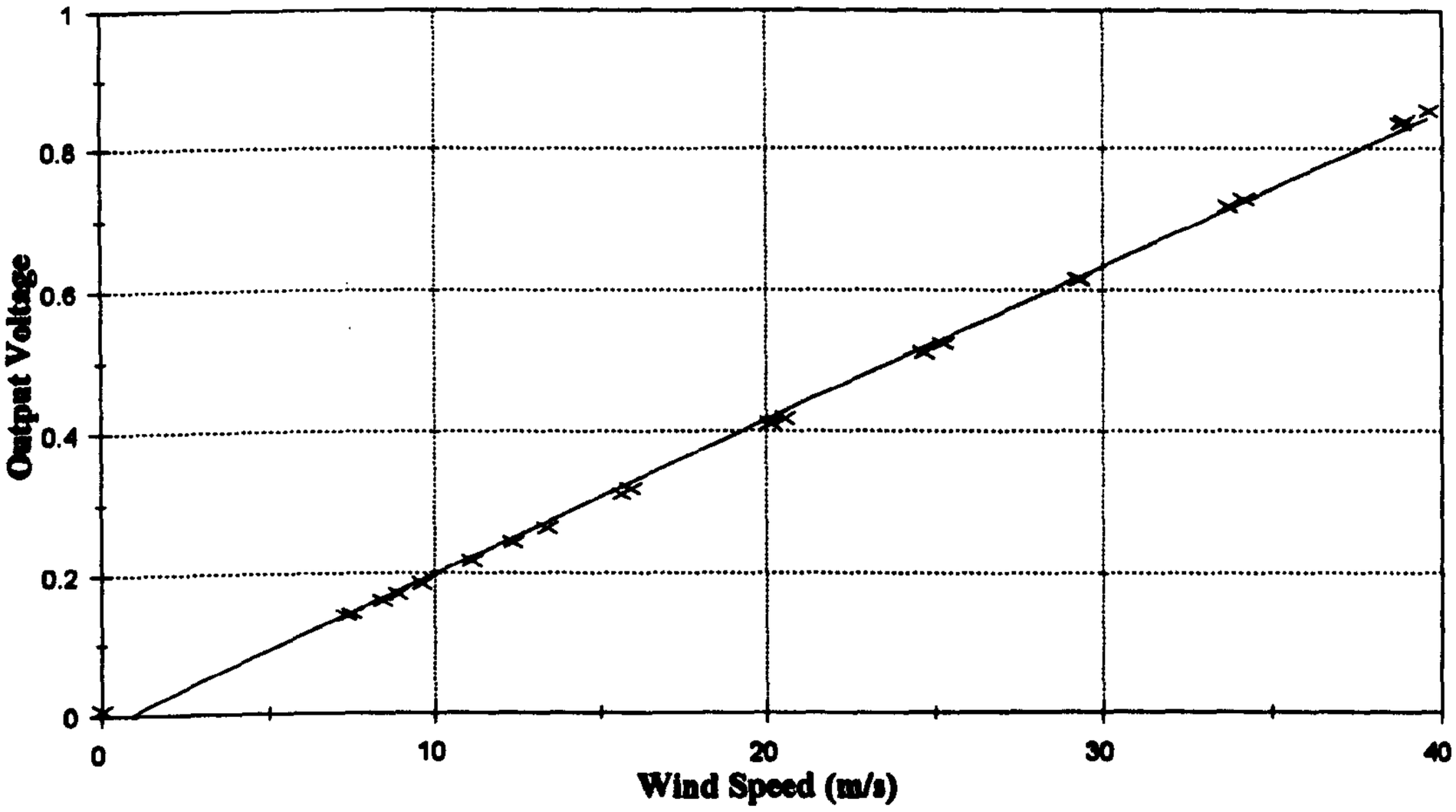

Figure 7.9 -:- Typical Calibration Curve For Anemometer In Wind Tunnel

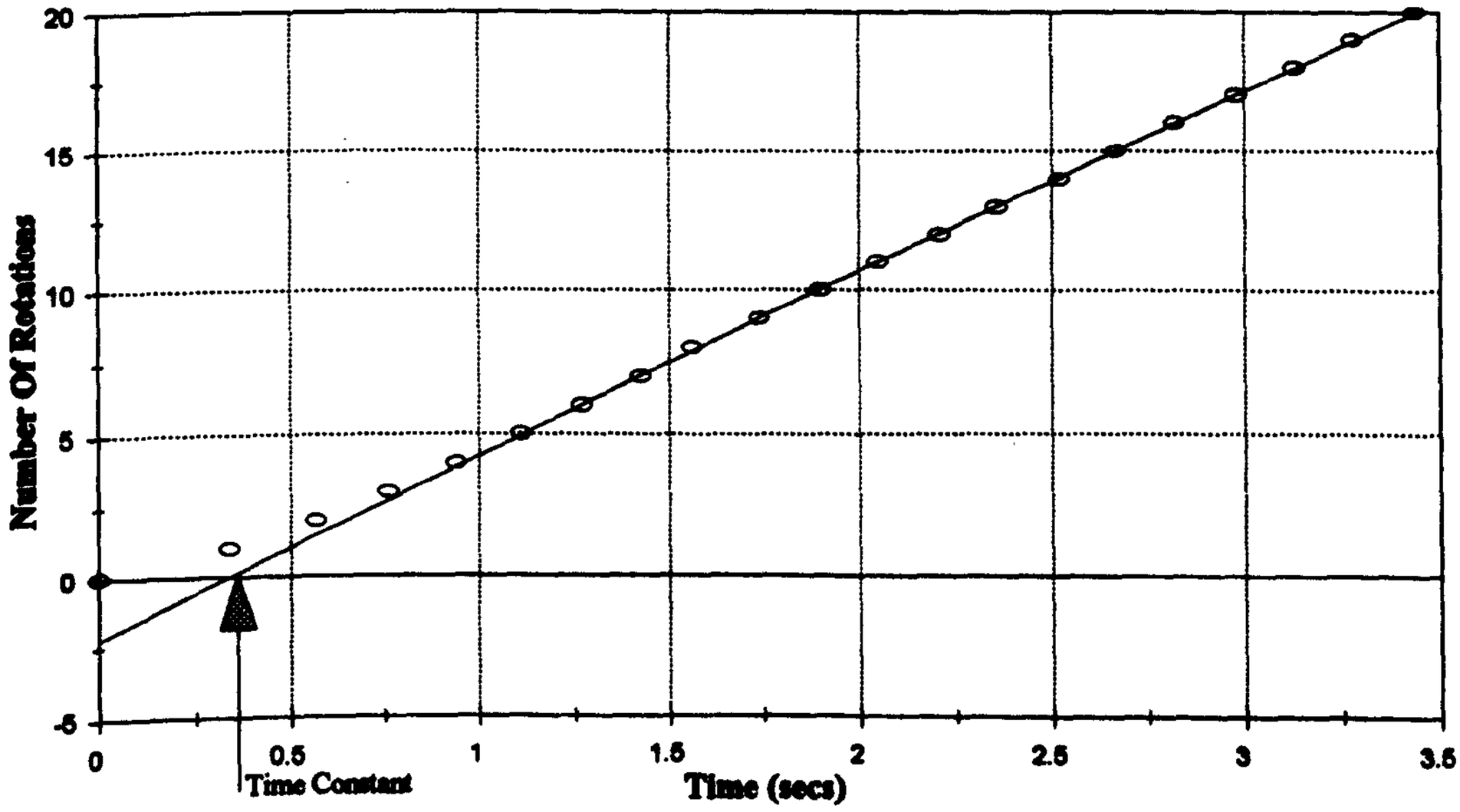

Figure 7.10 -:- Measurement Of Anemometer Time Constant, Typical Curve

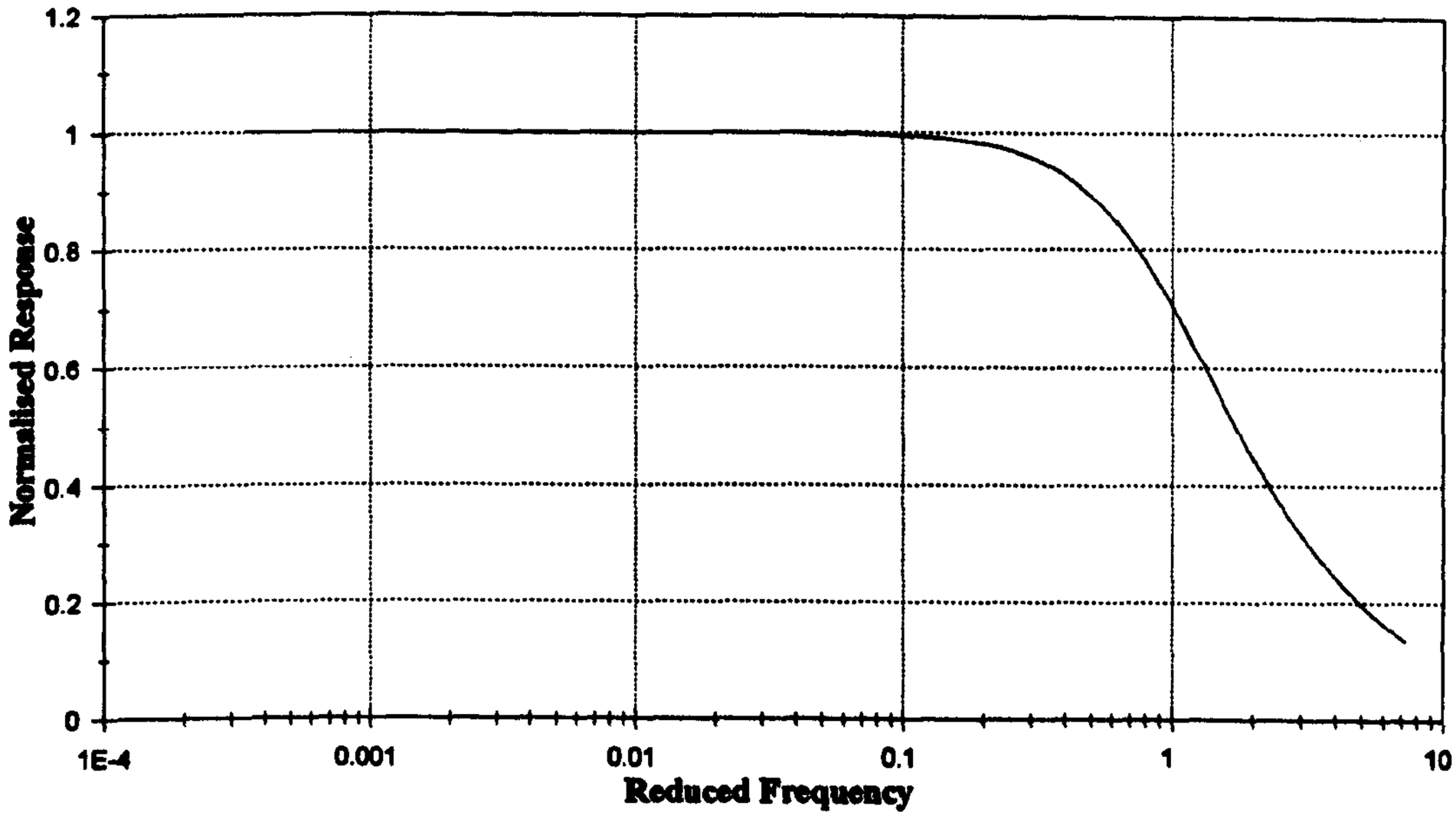

Figure 7.11 -:- Typical Frequency Response Function For Digitar Anemometer

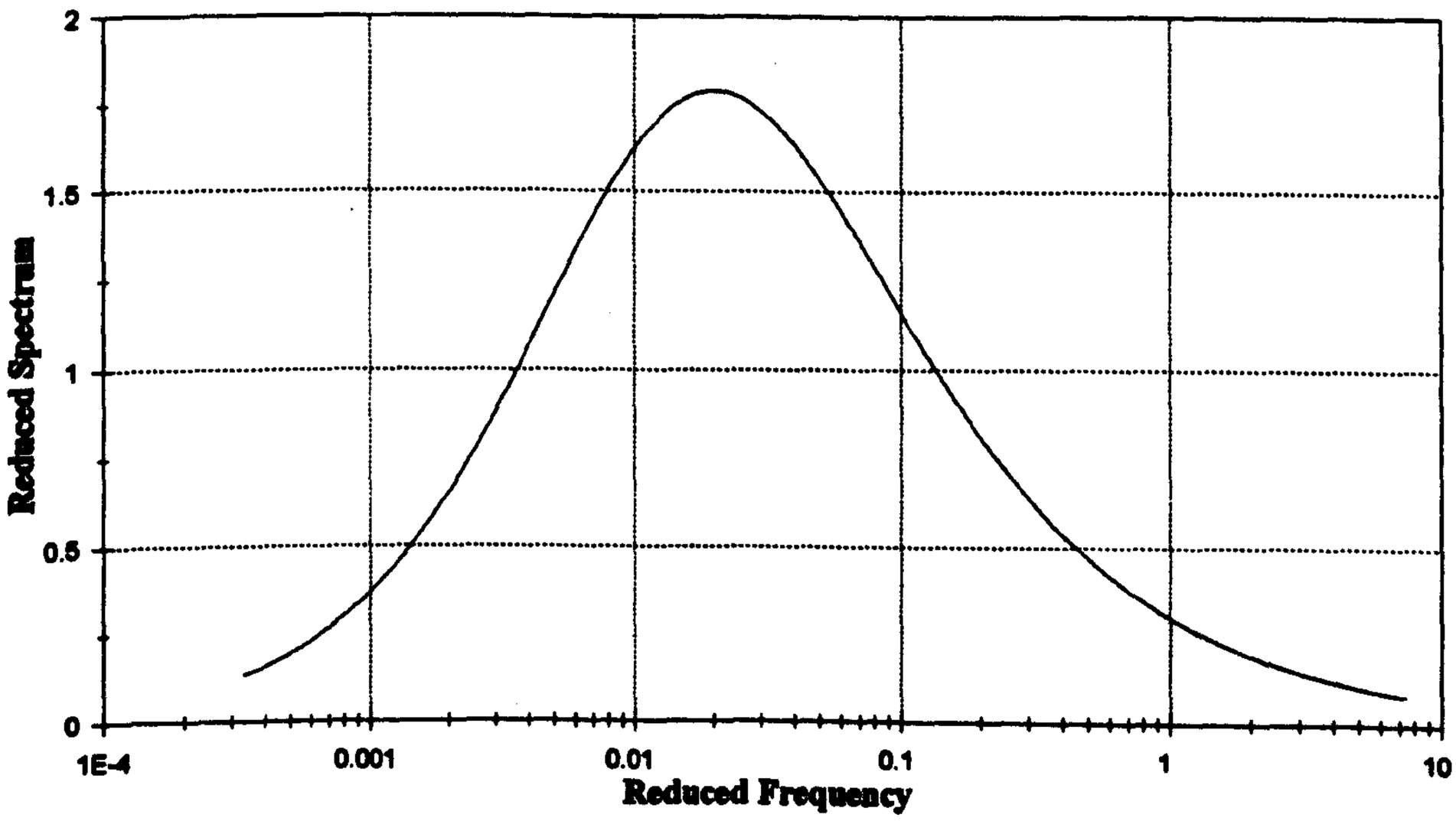

Figure 7.12 -:- Kaimal Model Of Horizontal Gust Spectrum

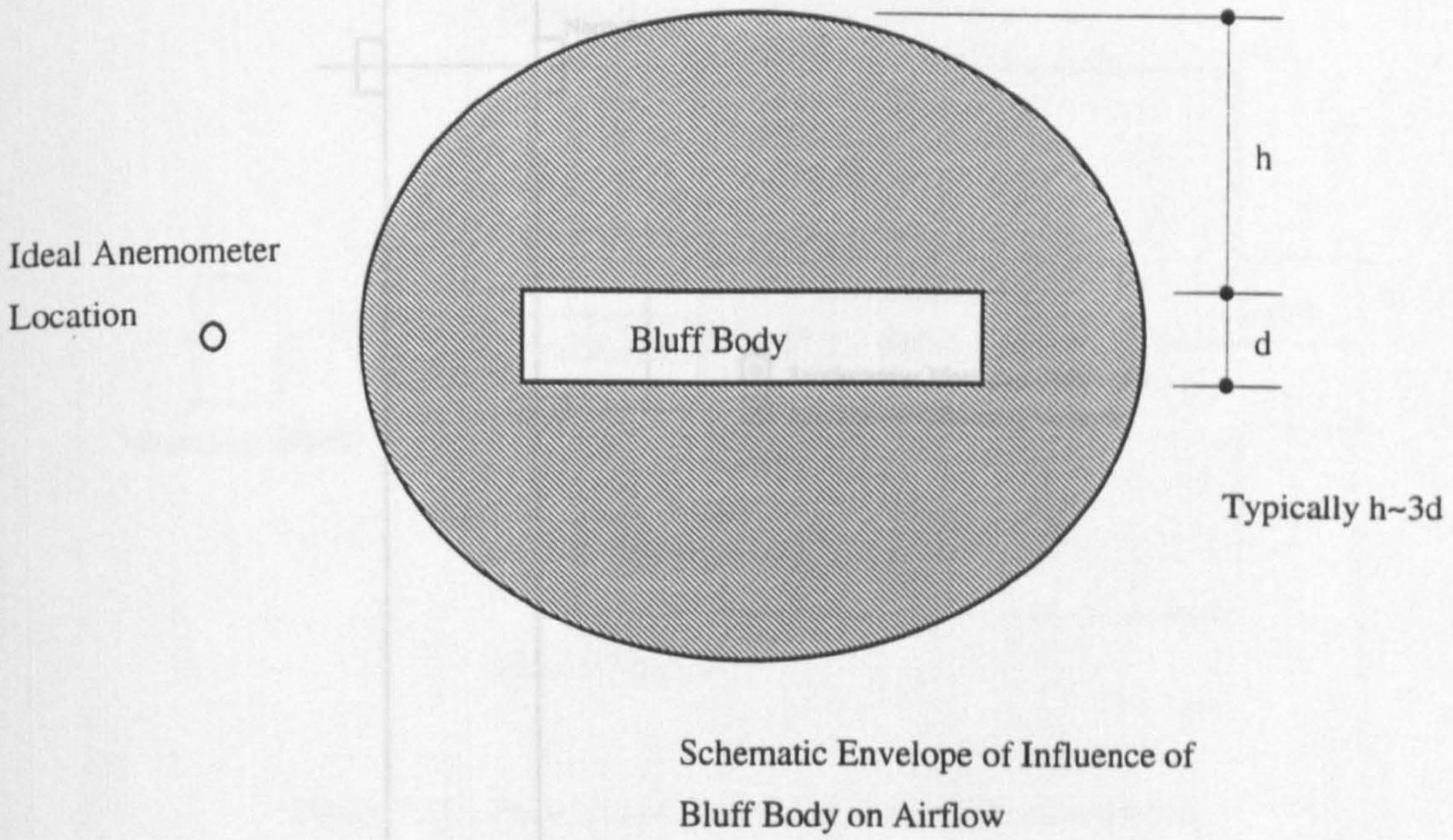

Figure 7.13 : Ideal Location of Anemometers Outside Influence of Bridge on Wind

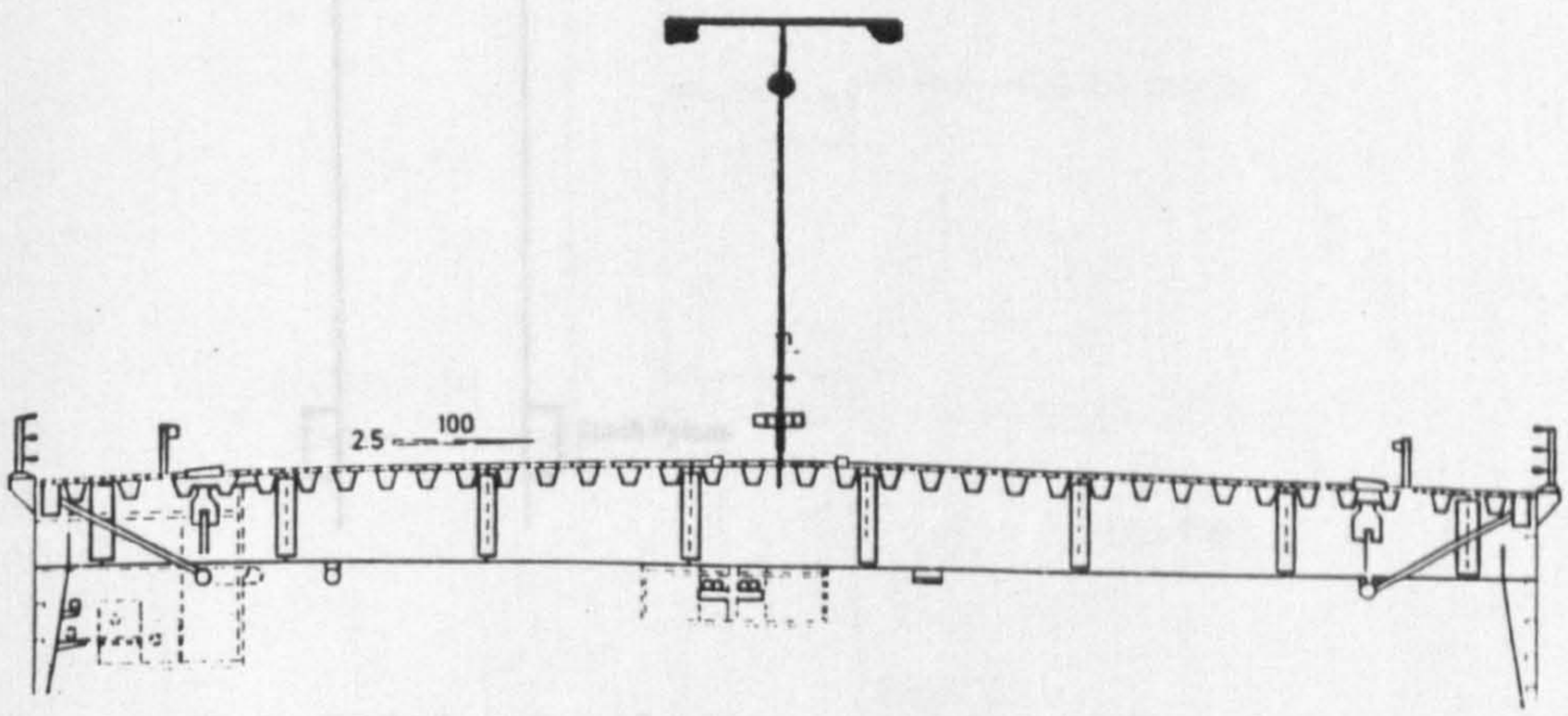

Figure 7.14 : Location of Anemometers on Kessock Bridge

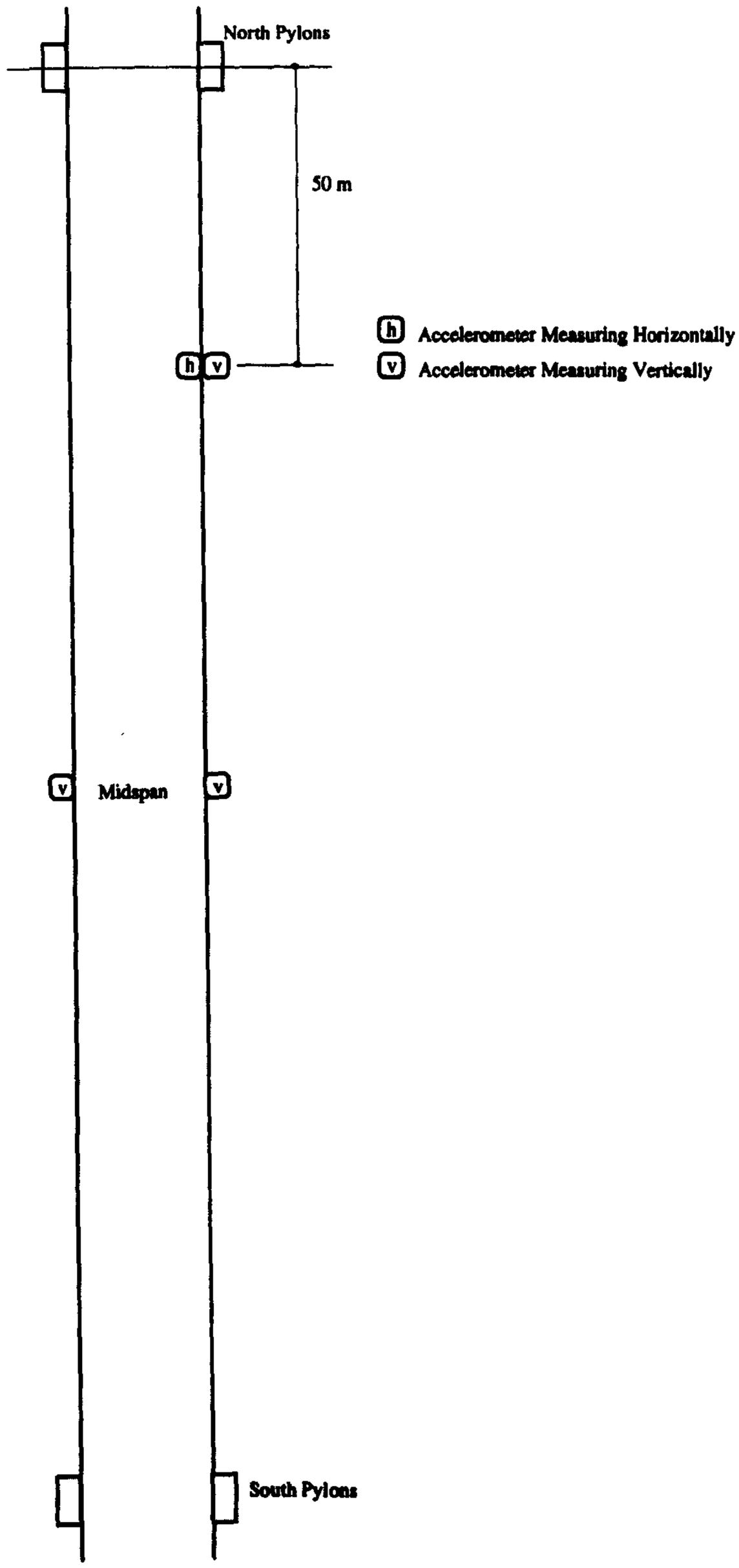

Figure 7.15 : Location of Accelerometers for long Term Survey

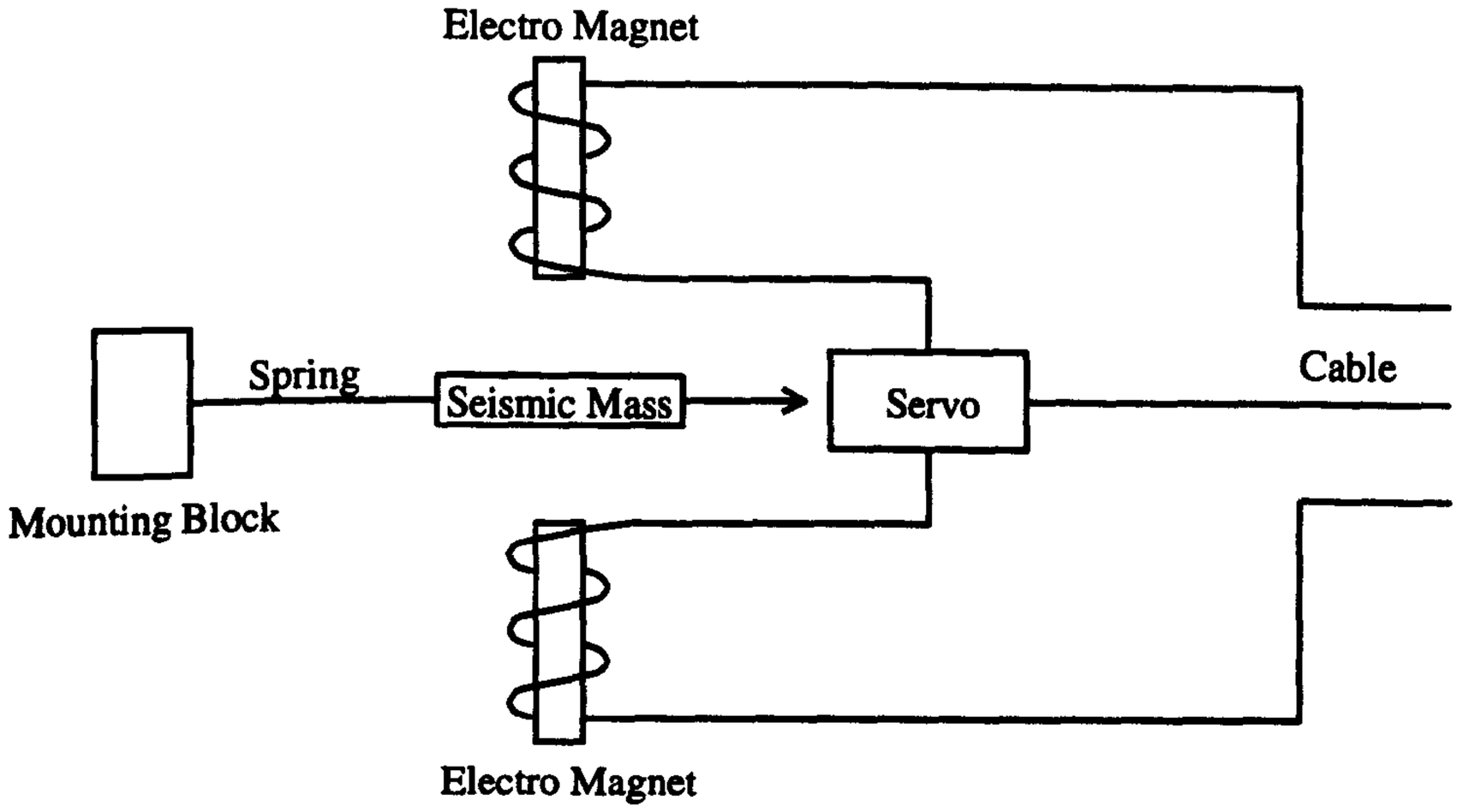

Figure 7.16 : Principal of Operation of Servo Accelerometer

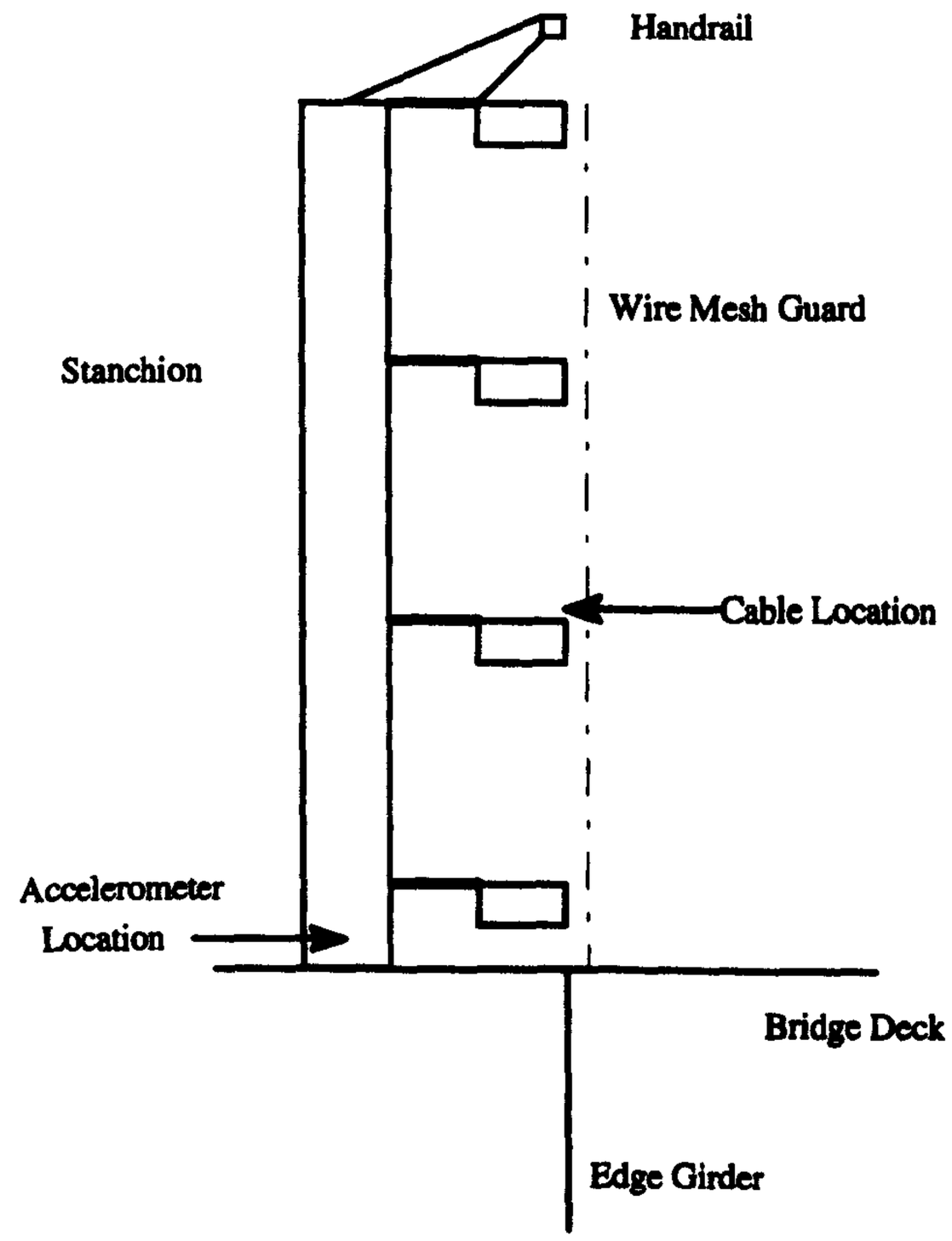

Figure 7.17 : Mounting of Accelerometers and Cabling on Bridge Deck

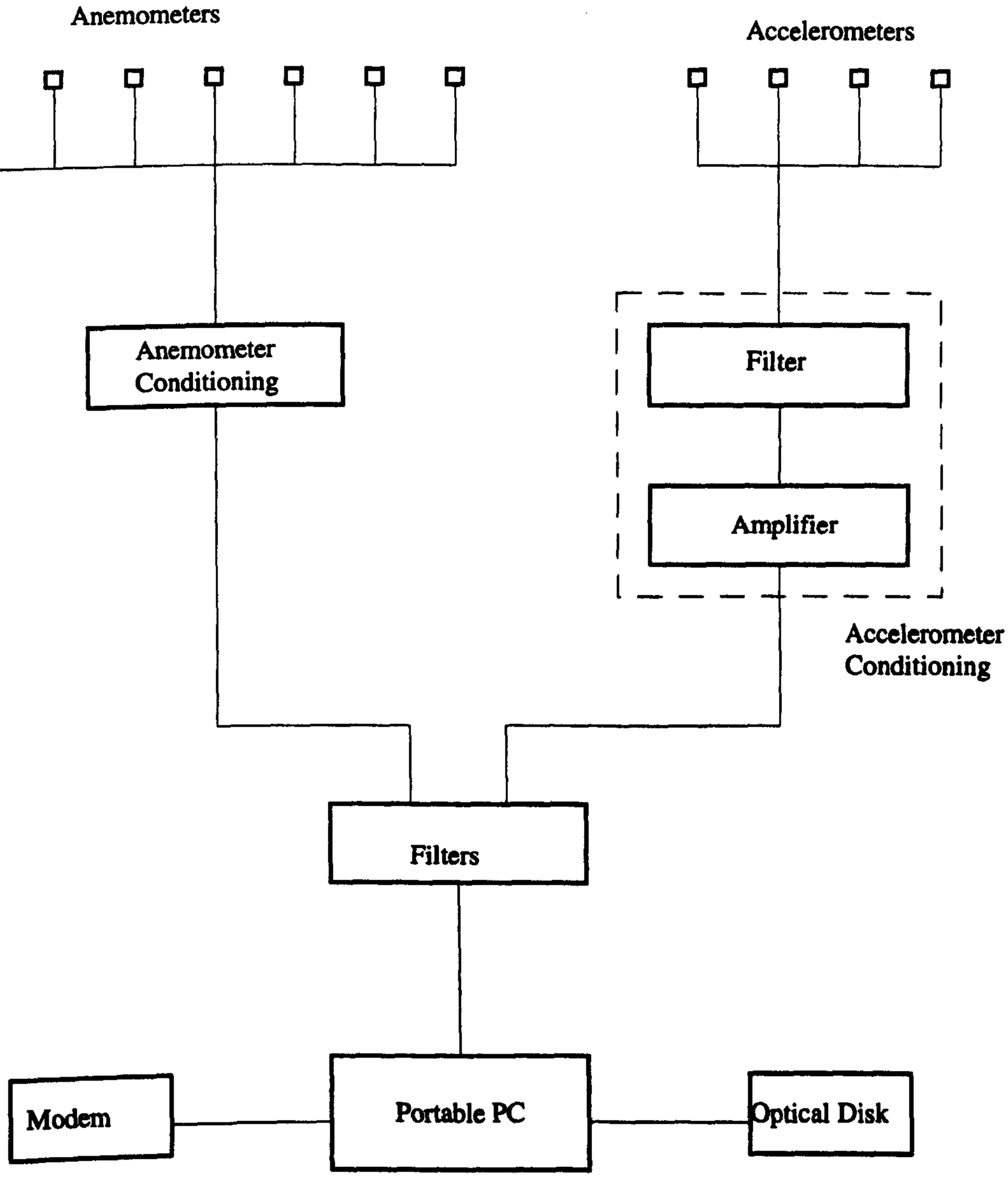

Figure 7.18 : Block Diagram of Data Acquisition System

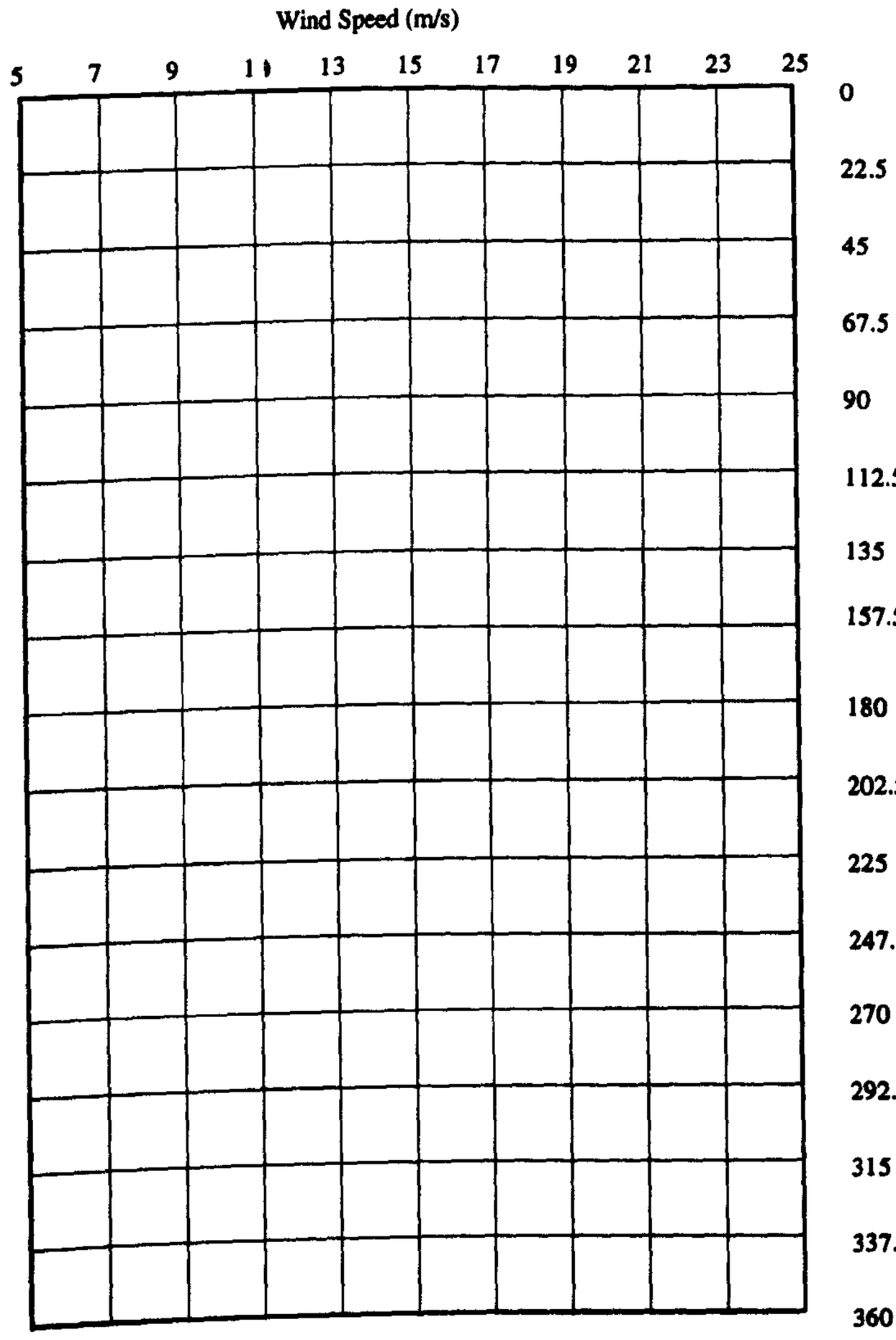

Figure 7.19 : Data Acquisition Cells

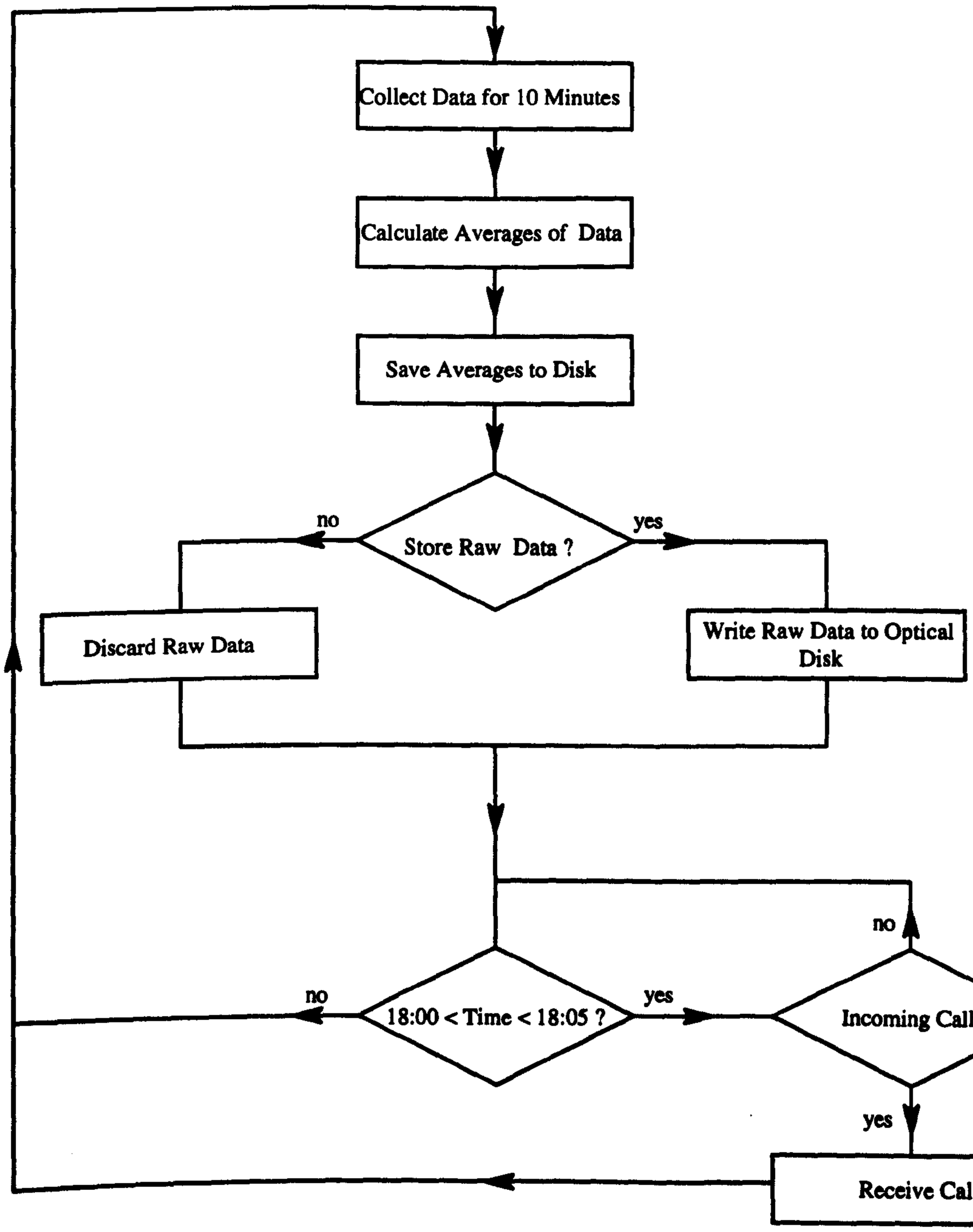

Figure 7.20 : Flow Chart of Data Acquisition Strategy

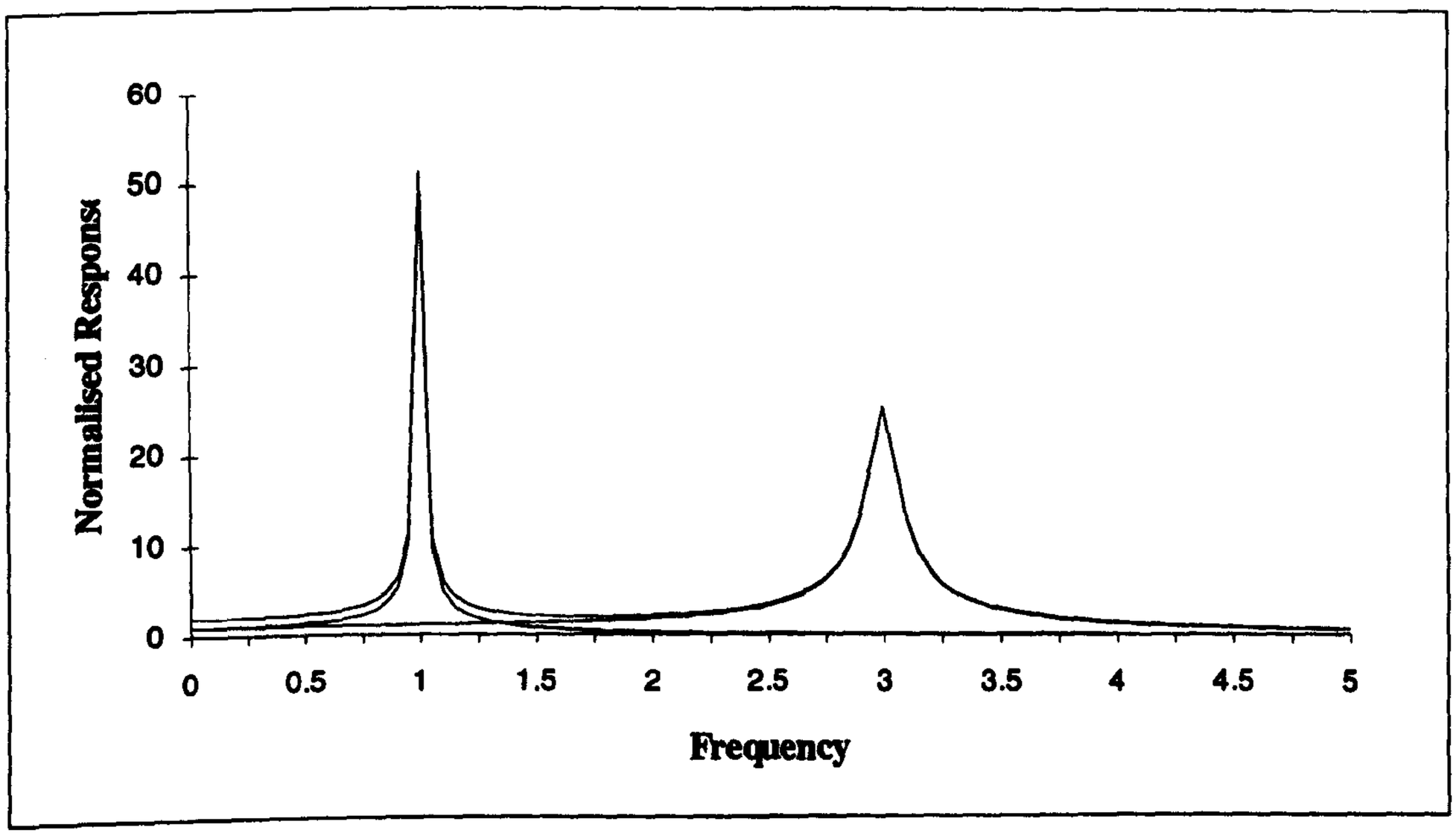

Figure 7.21a : Well Spaced Modes

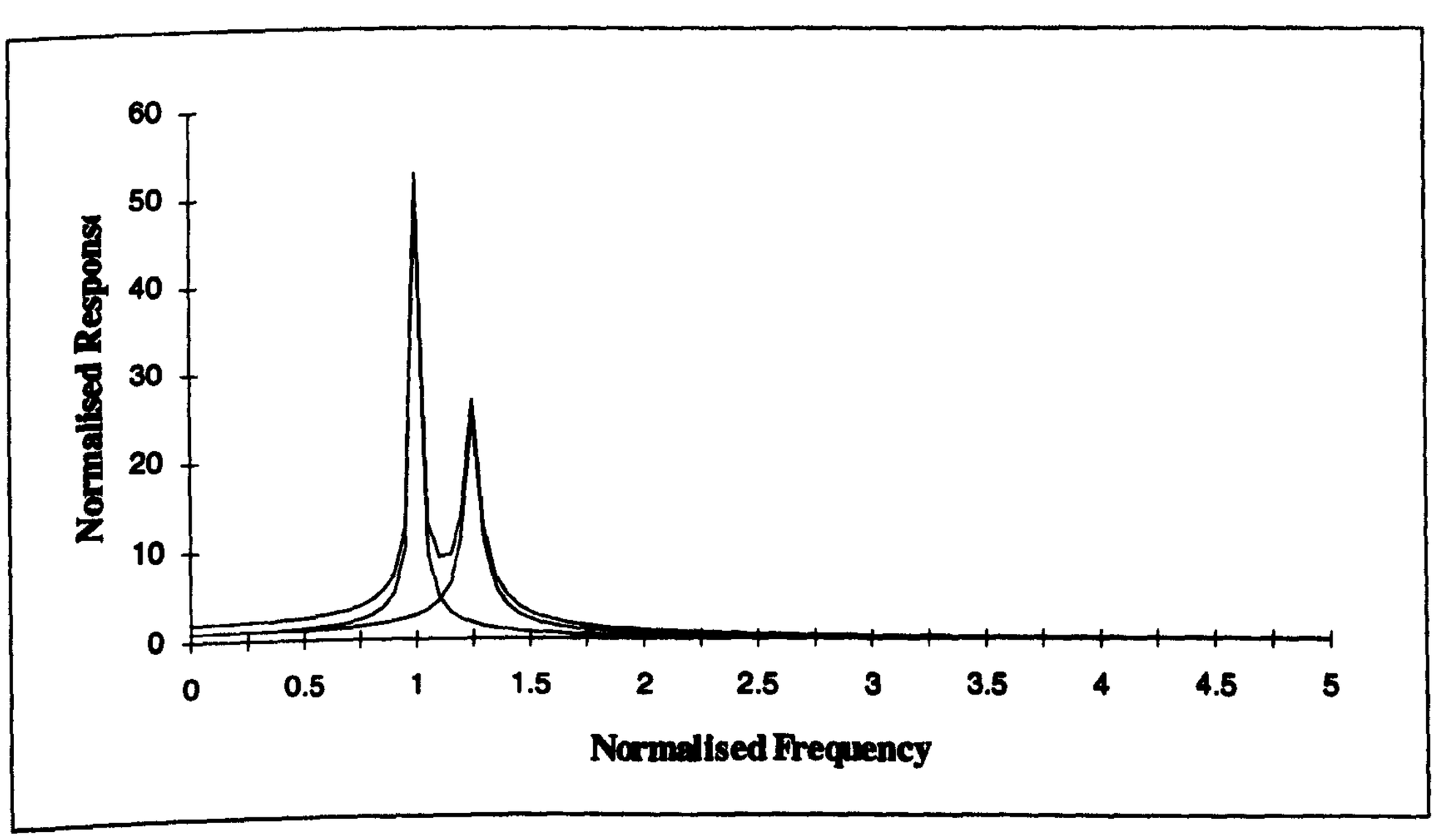

Figure 7.21b : Closely Spaced Modes

Figure 7.21 : Illustration of Errors in Curve Fitting to Closely Spaced Modes

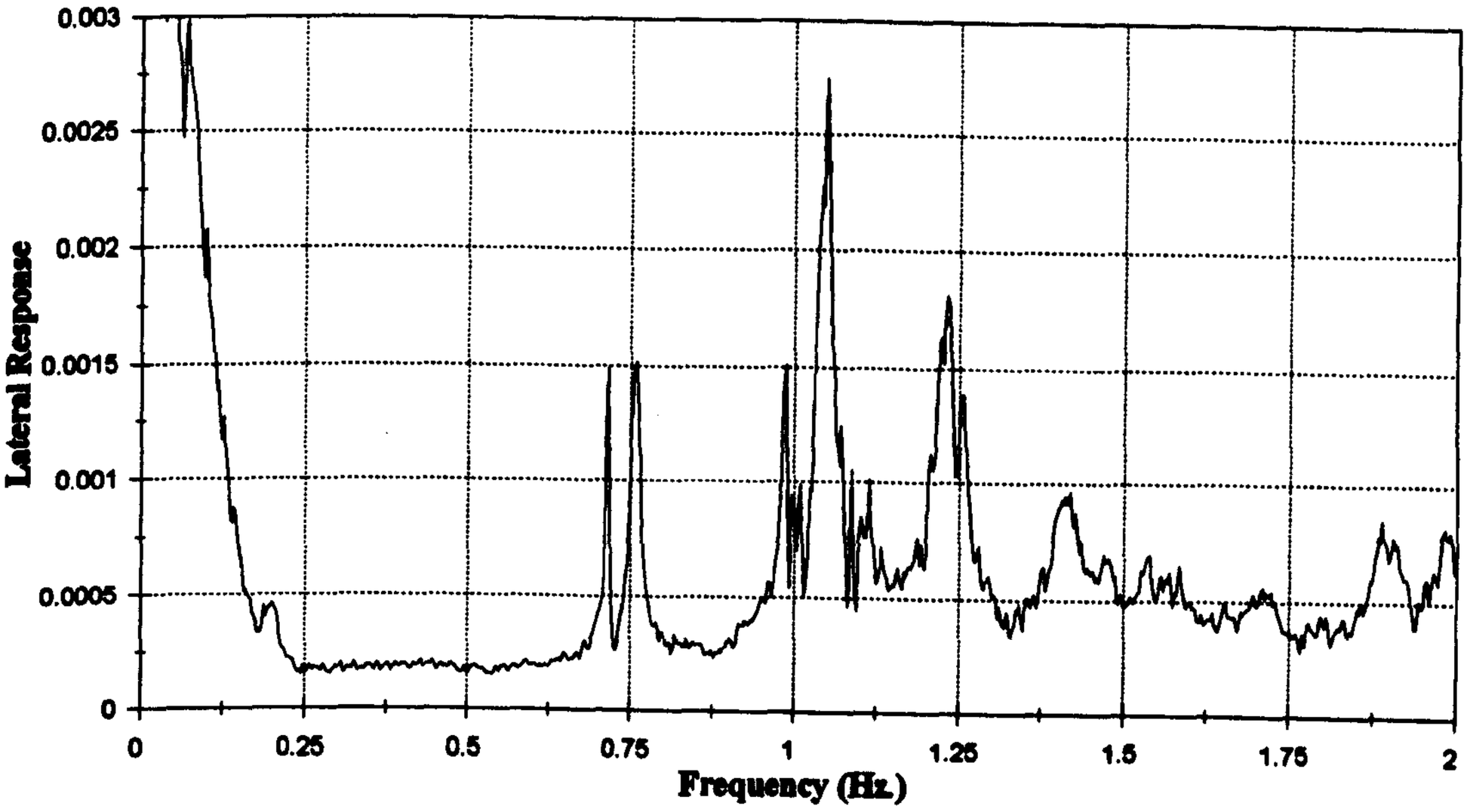

Figure 7.22 -:- Typical Auto Power Spectrum for Lateral Deck Acceleration

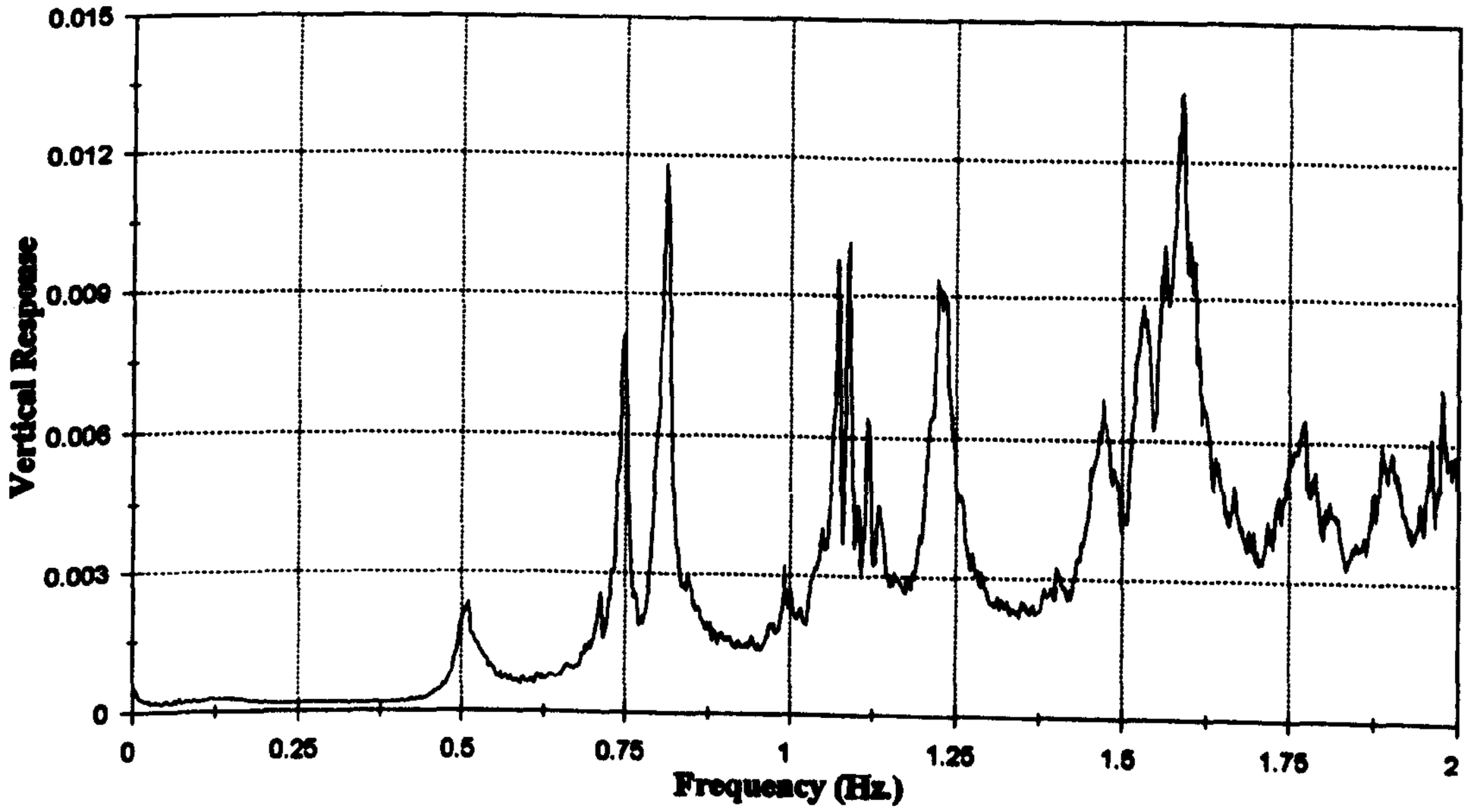

Figure 7.23 -:- Typical Auto Power Spectrum for Vertical Deck Acceleration

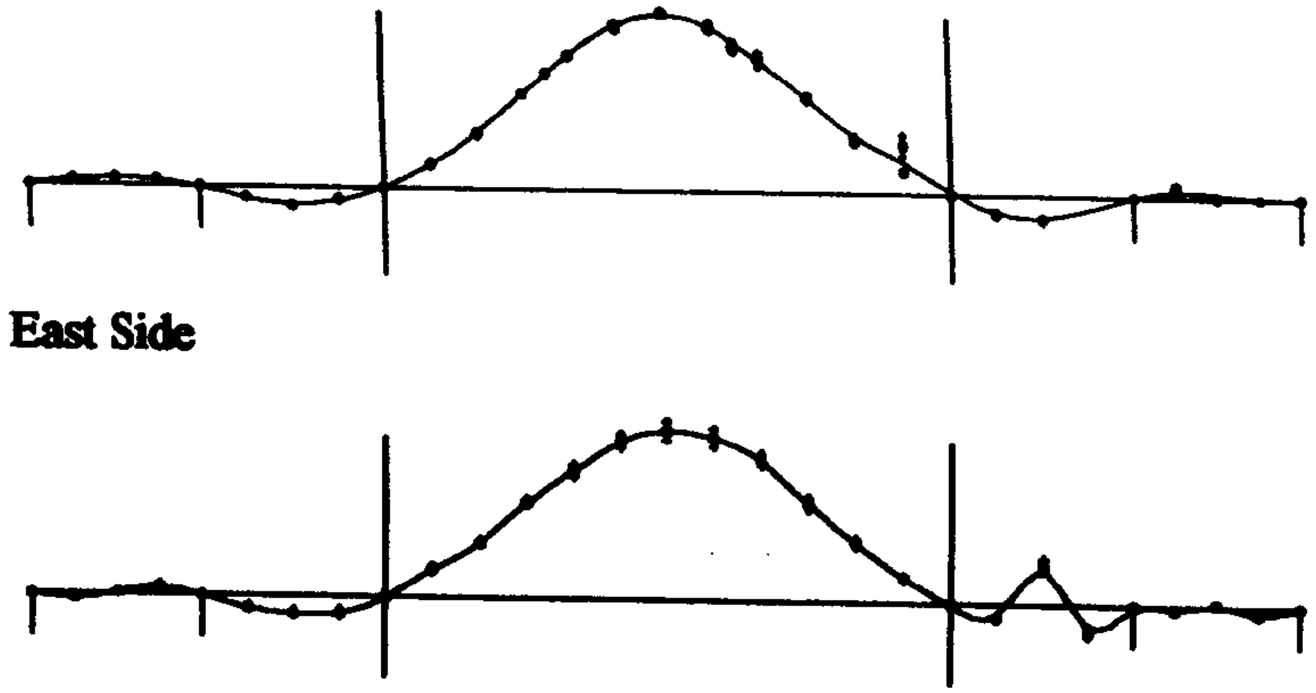

Figure 7.24 -:- Measured Mode Shapes of Deck, Reference at 60 m Point

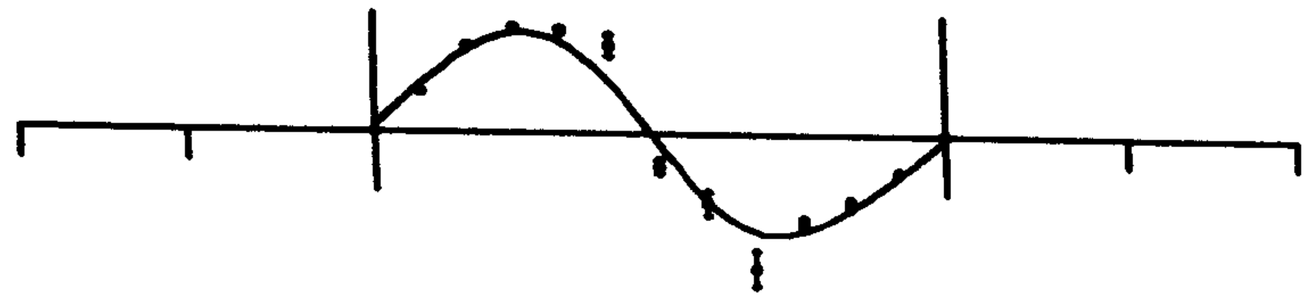

East Side

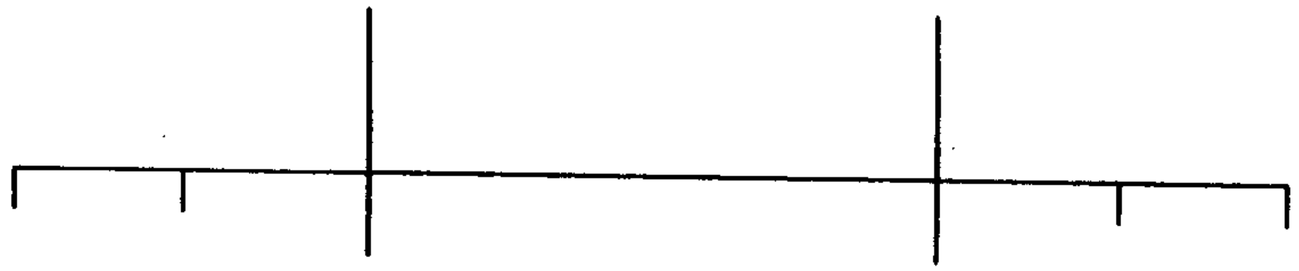

West Side

Mode 5

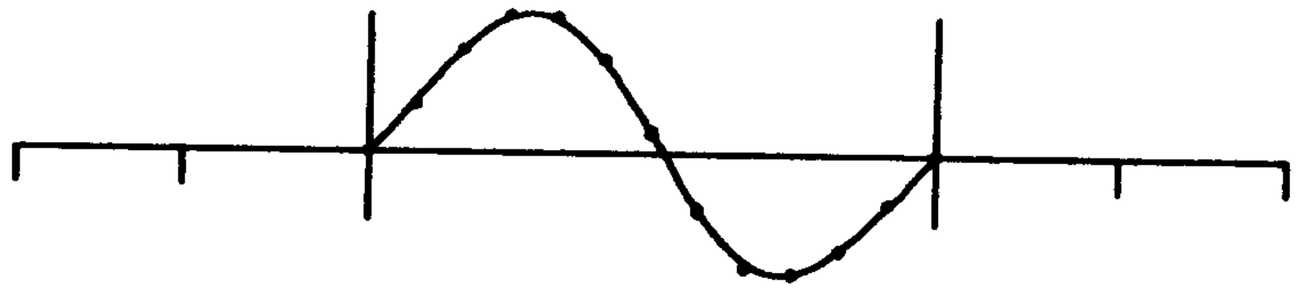

East Side

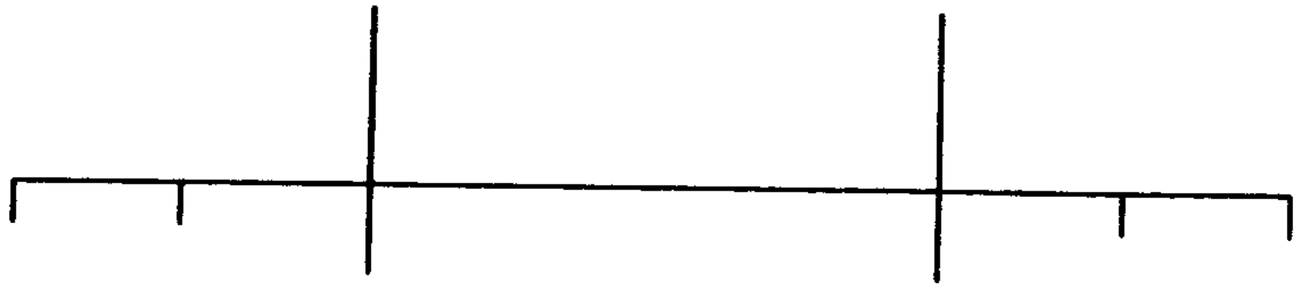

West Side

Mode 6

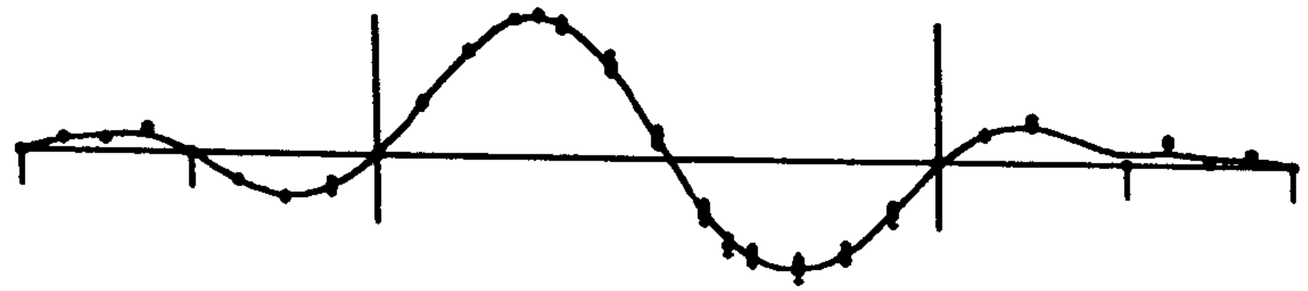

East Side

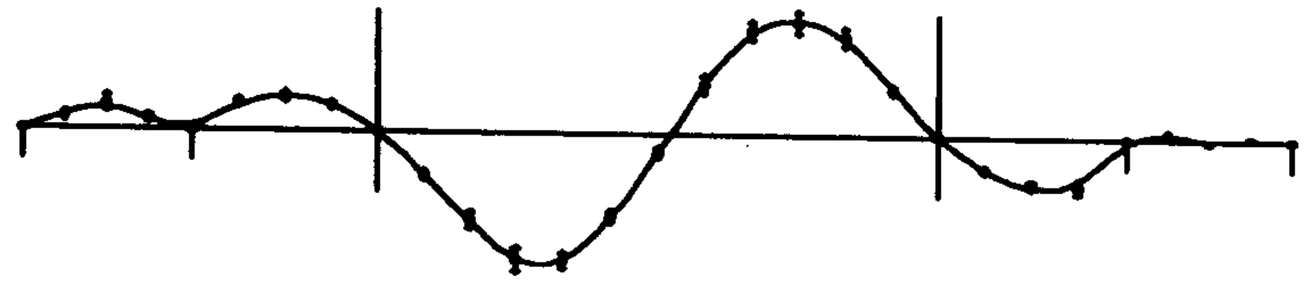

West Side

Mode 7

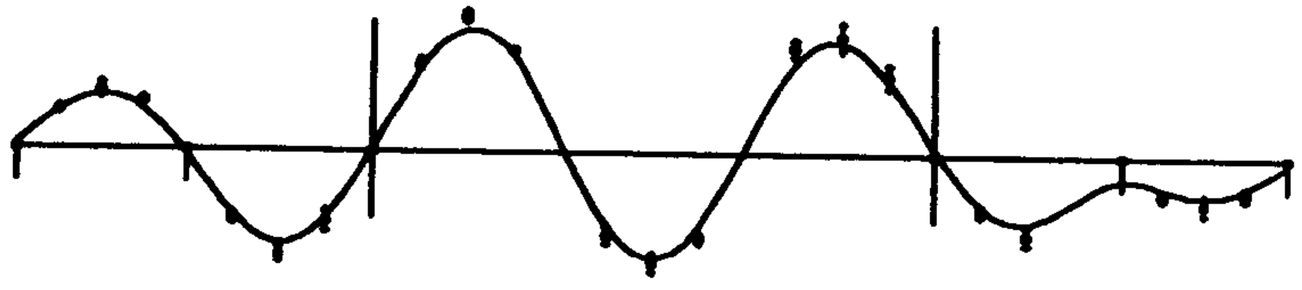

East Side

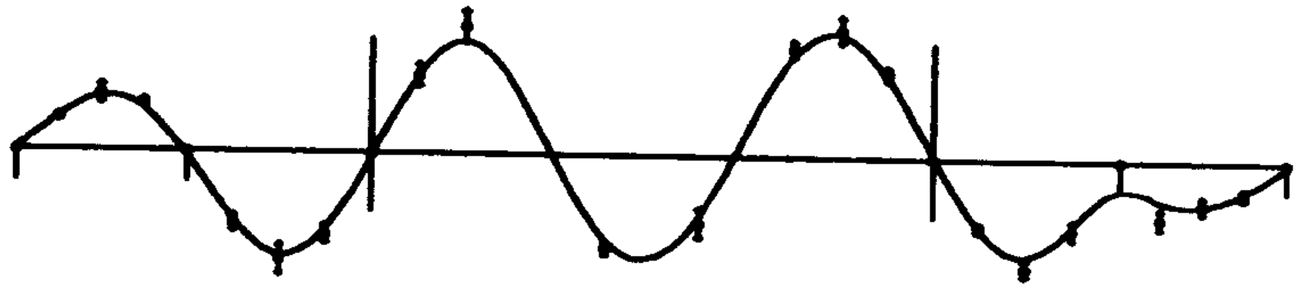

West Side

Mode 8

Figure 7.24 (cont.) -:- Measured Mode Shapes of Deck, Reference at 60 m Point

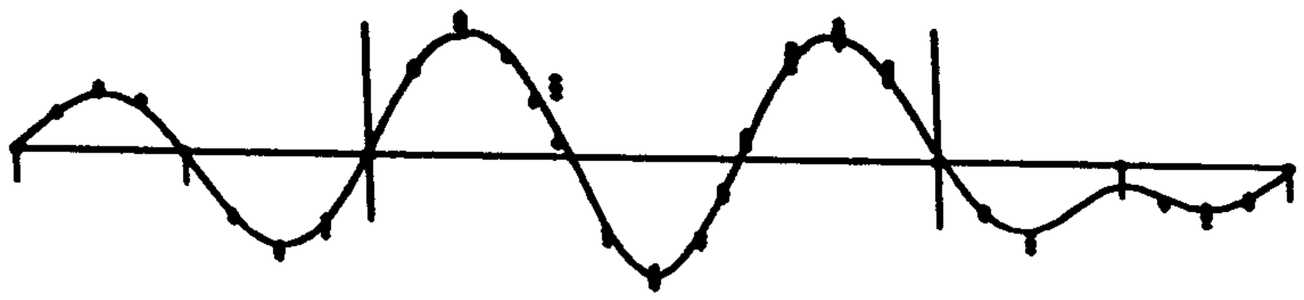

East Side

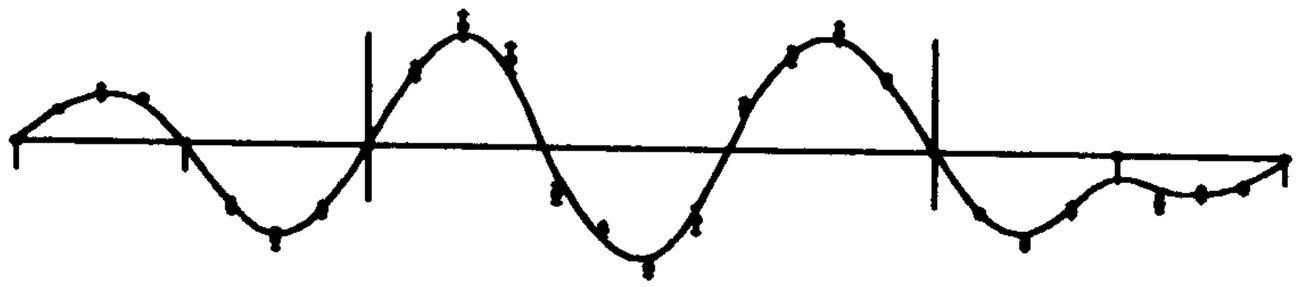

West Side

Mode 9

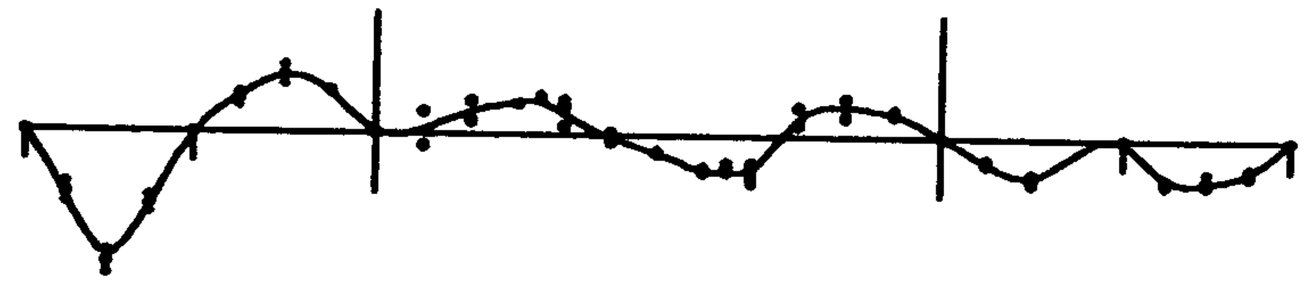

East Side

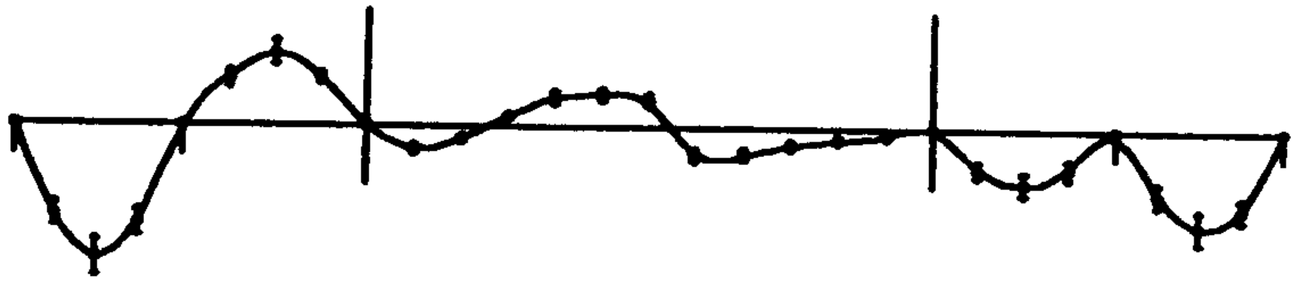

West Side

Mode 10

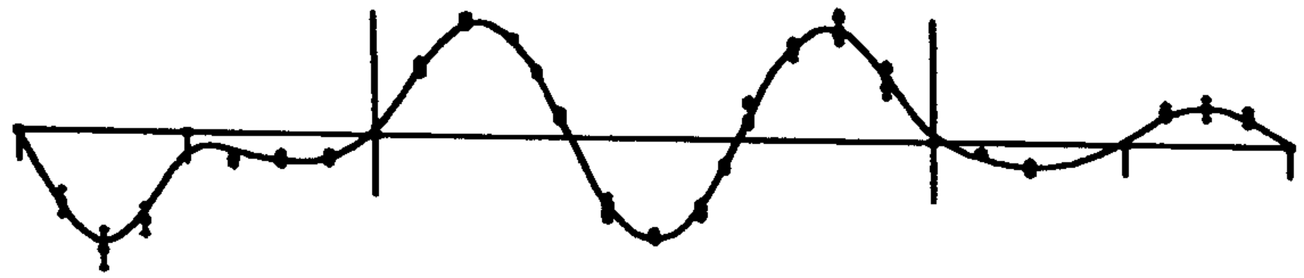

East Side

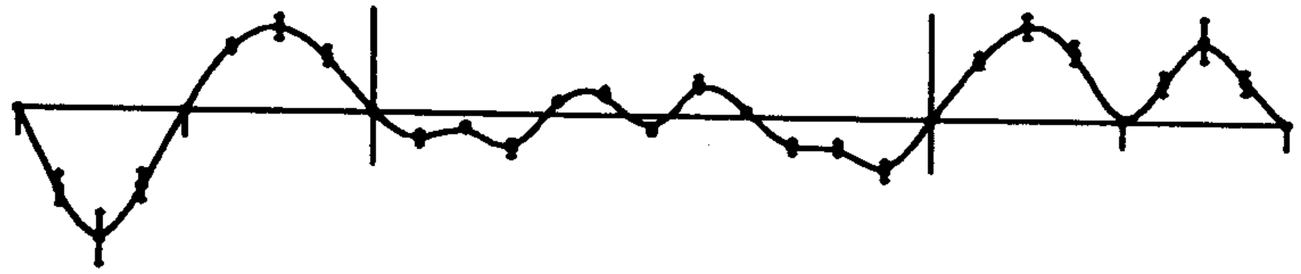

West Side

Mode 11

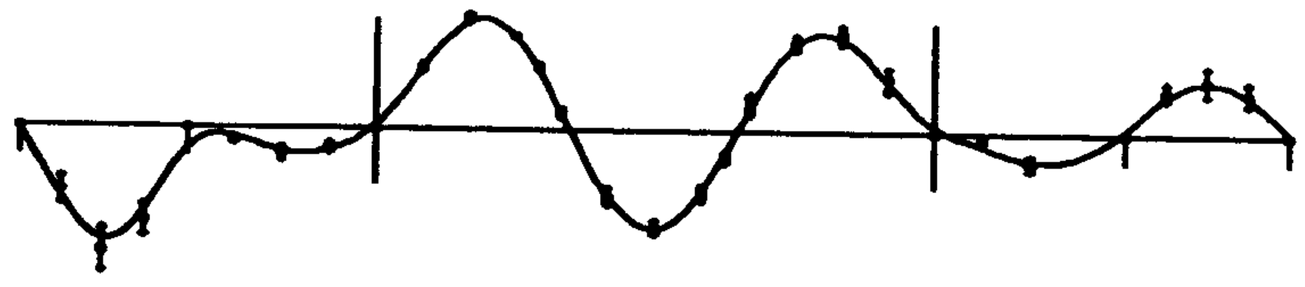

East Side

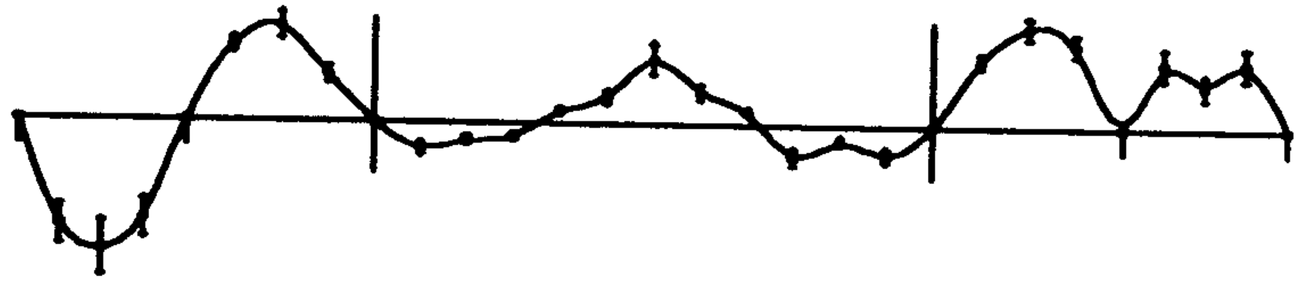

West Side

Mode 12

Figure 7.24 (cont.) -:- Measured Mode Shapes of Deck, Reference at 60 m Point

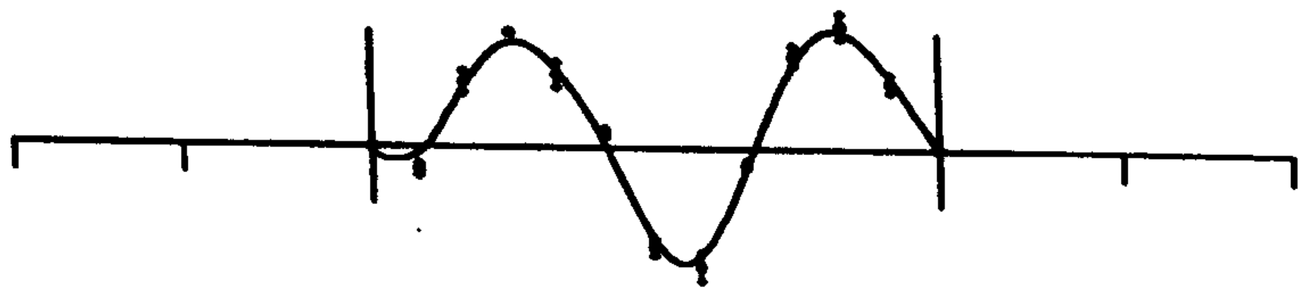

East Side

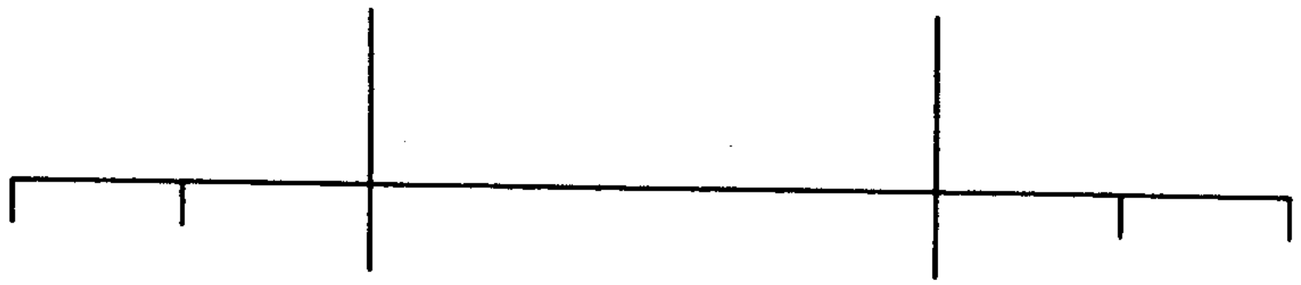

West Side

Mode 13

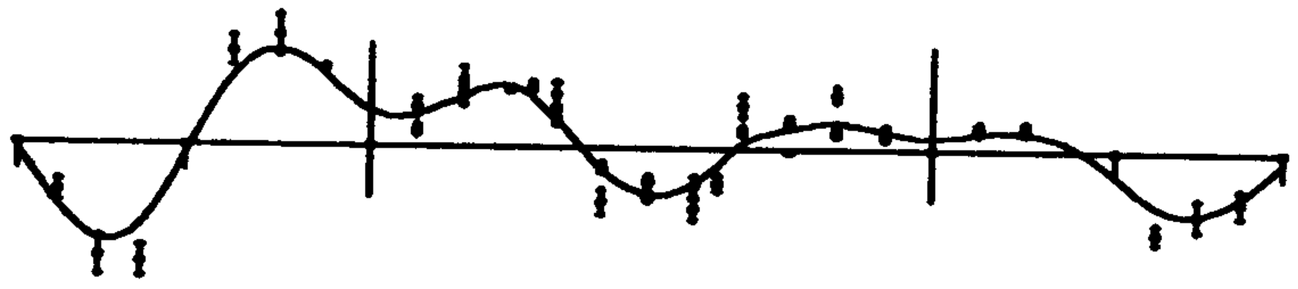

East Side

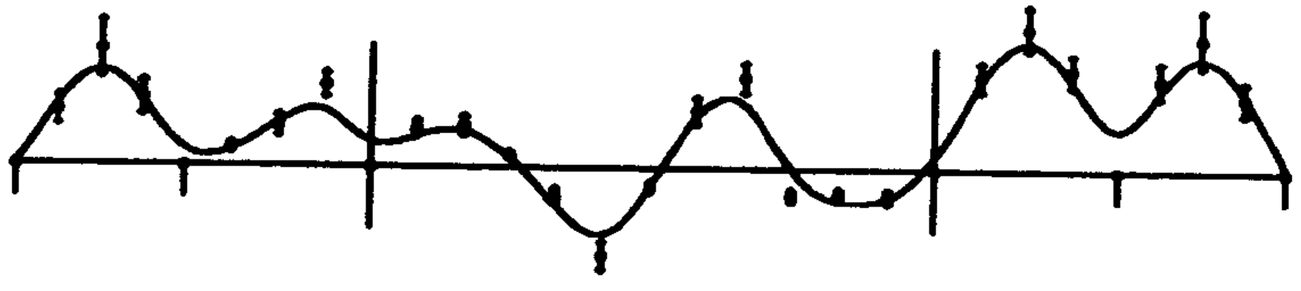

West Side

Mode 14

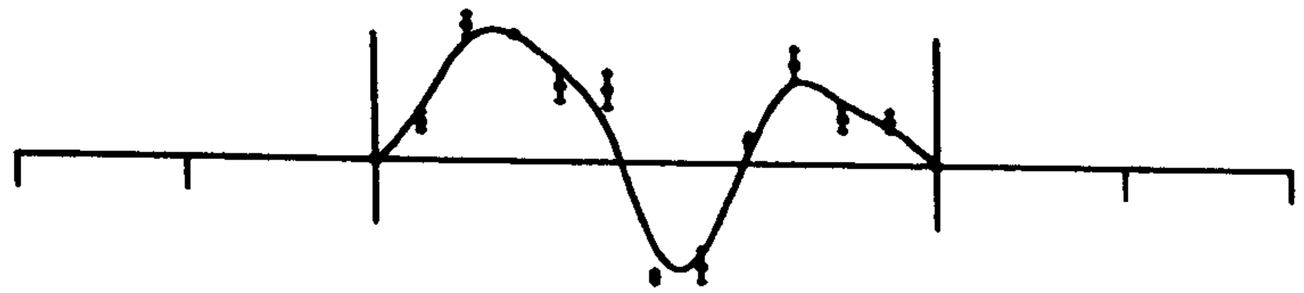

East Side

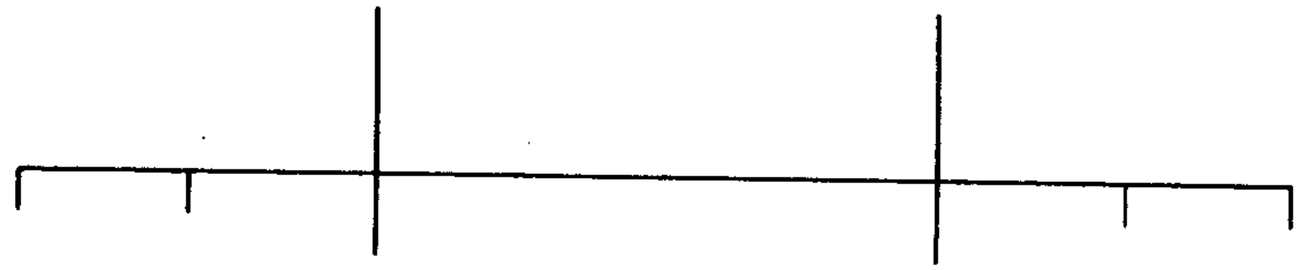

West Side

Mode 15

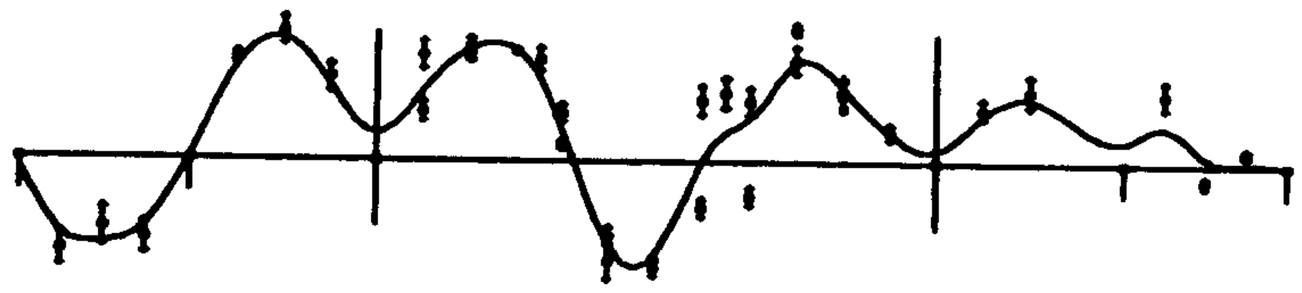

East Side

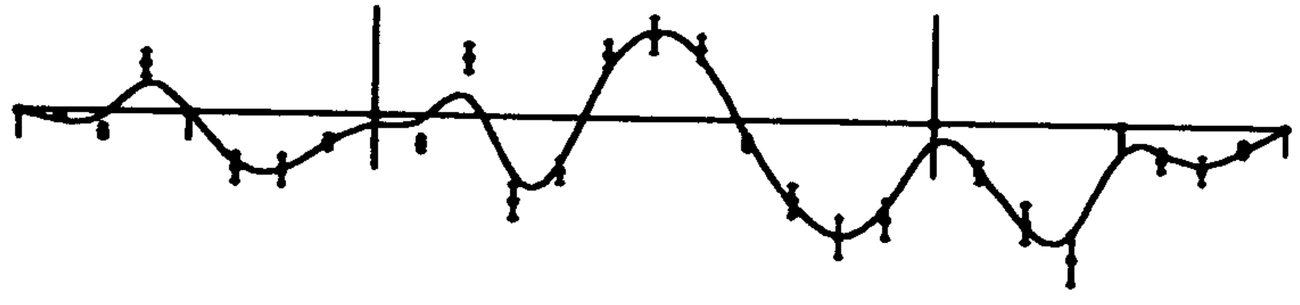

West Side

Mode 16

Figure 7.24 (cont.) -:- Measured Mode Shapes of Deck, Reference at 60 m Point

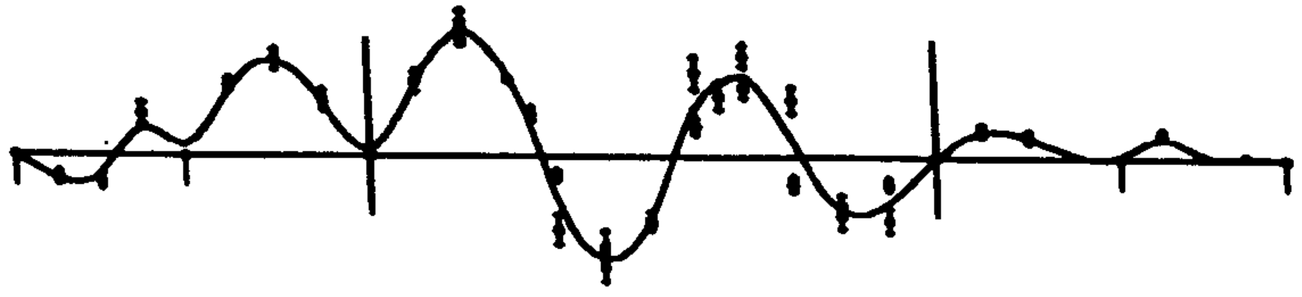

East Side

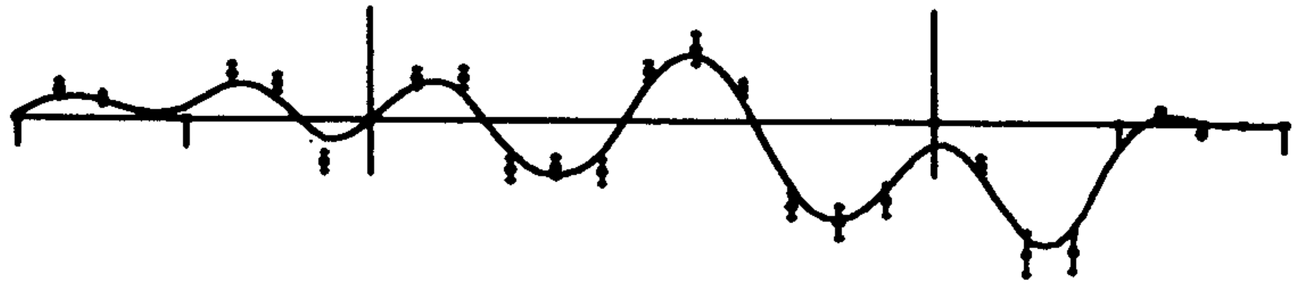

West Side

Mode 17

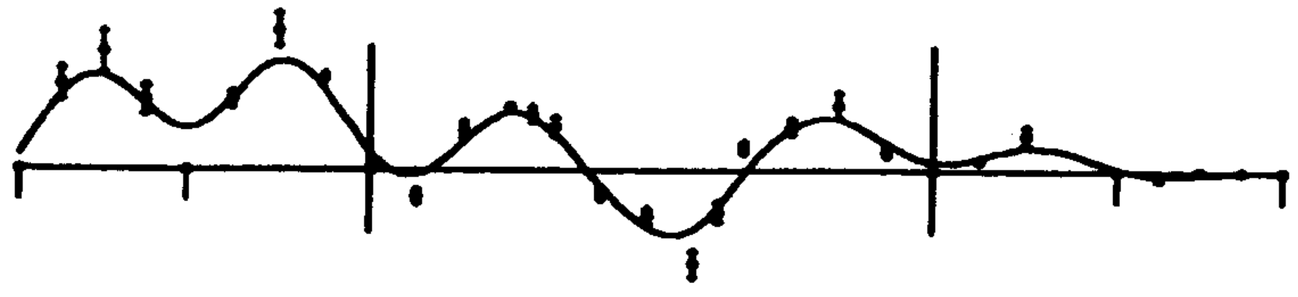

East Side

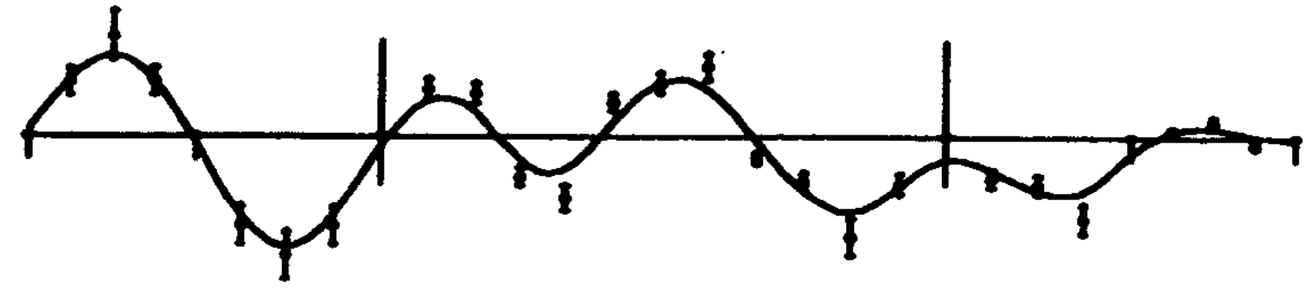

West Side

Mode 18

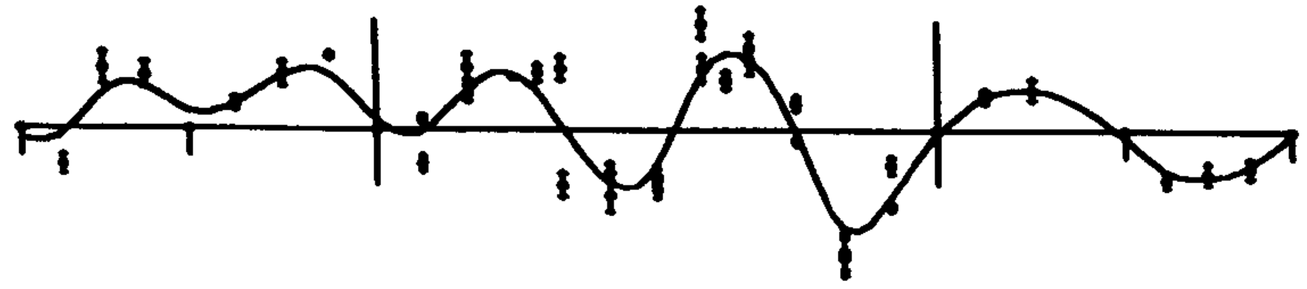

East Side

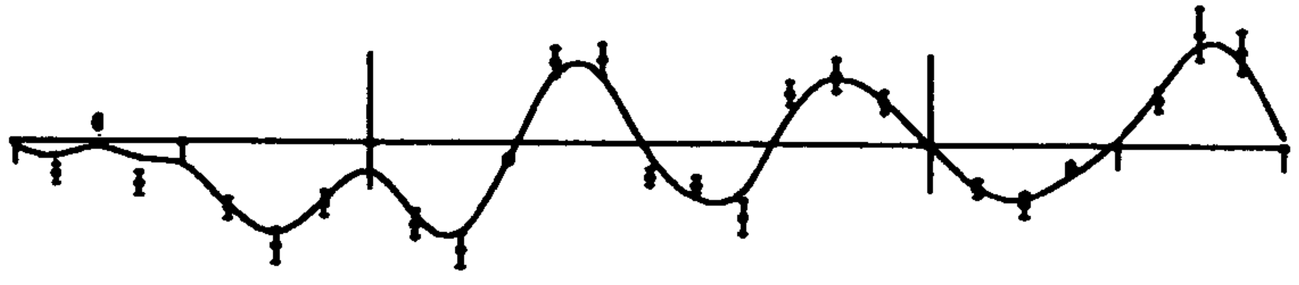

West Side

Mode 19

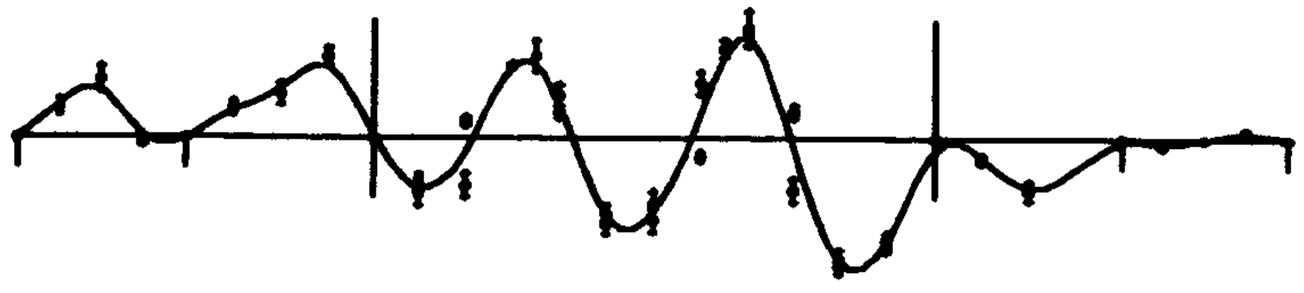

East Side

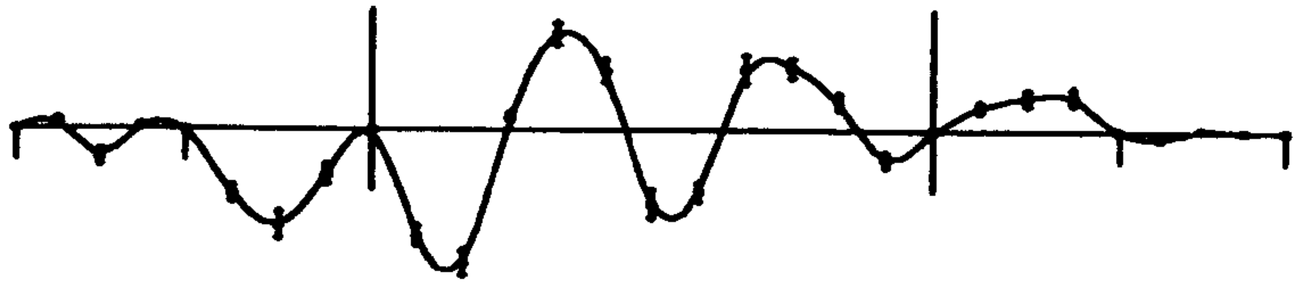

West Side

Mode 20

Figure 7.24 (cont) -:- Measured Mode Shapes of Deck, Reference at 60 m Point

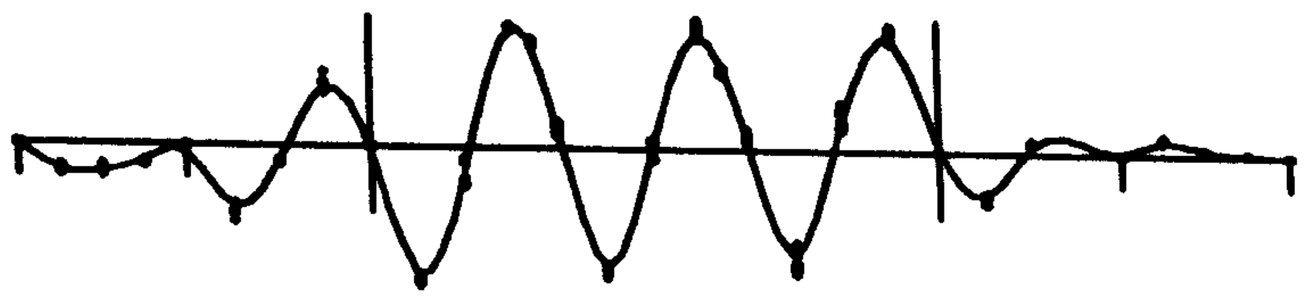

East Side

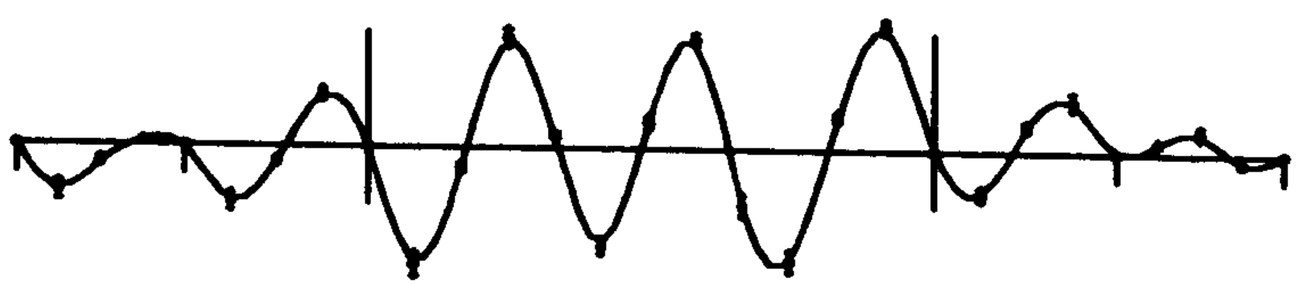

West Side

Mode 21

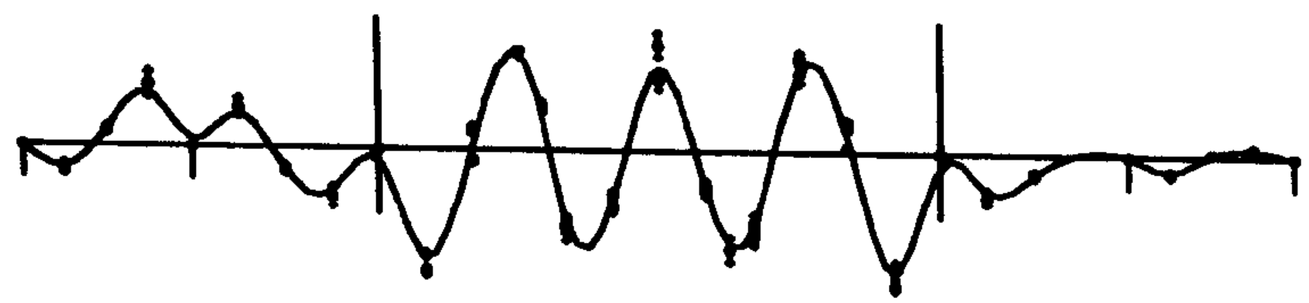

East Side

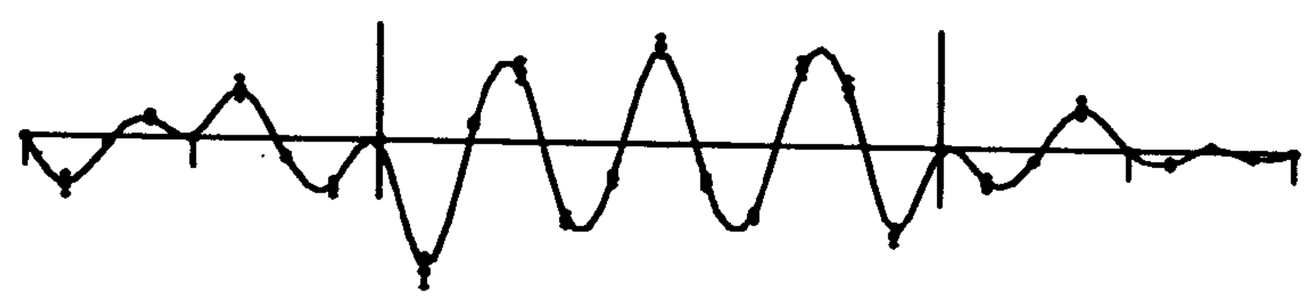

West Side

Mode 23

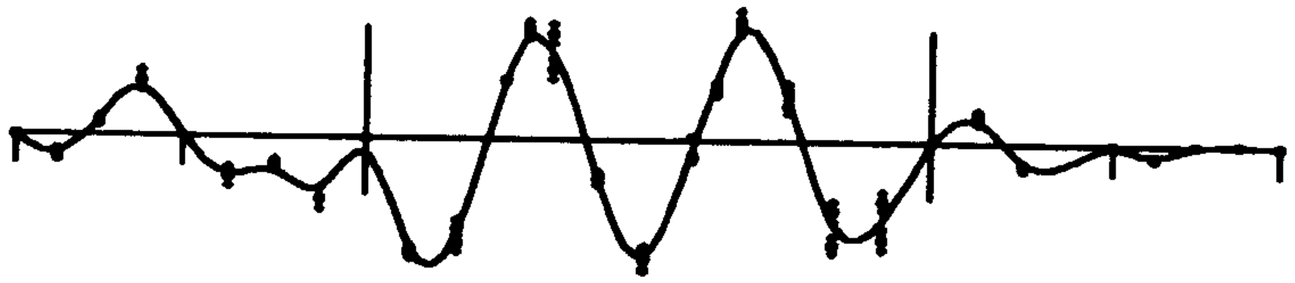

East Side

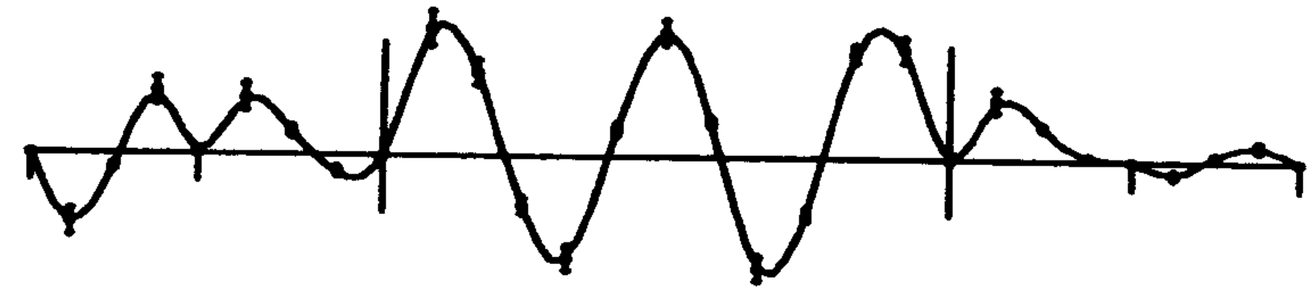

West Side

Mode 22

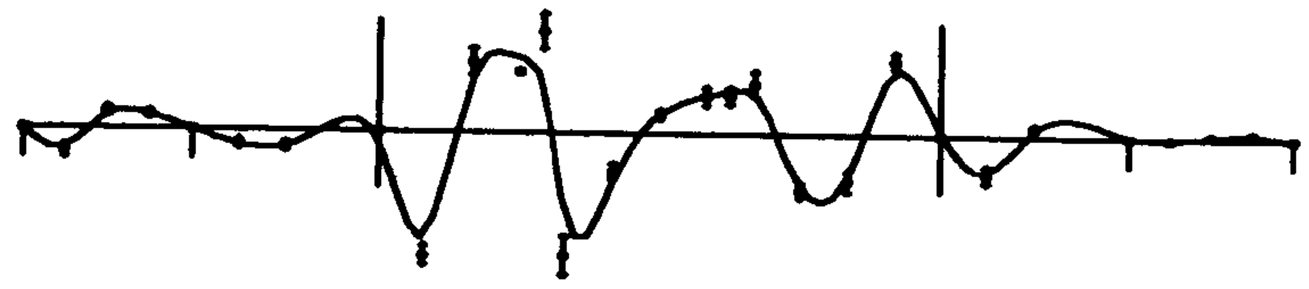

East Side

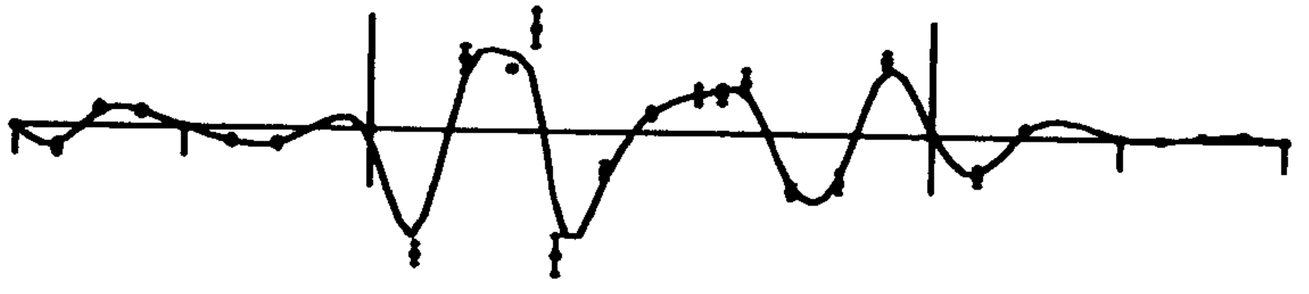

West Side

Mode 24

Figure 7.24 (cont.) -:- Measured Mode Shapes of Deck, Reference at 60 m Point

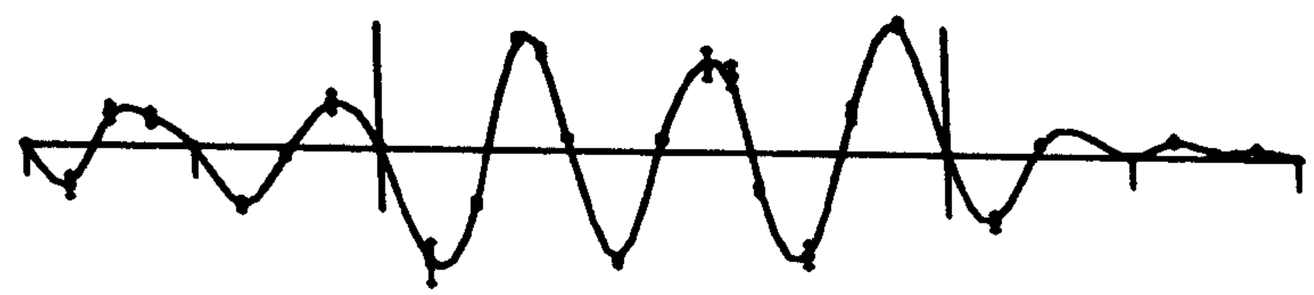

East Side

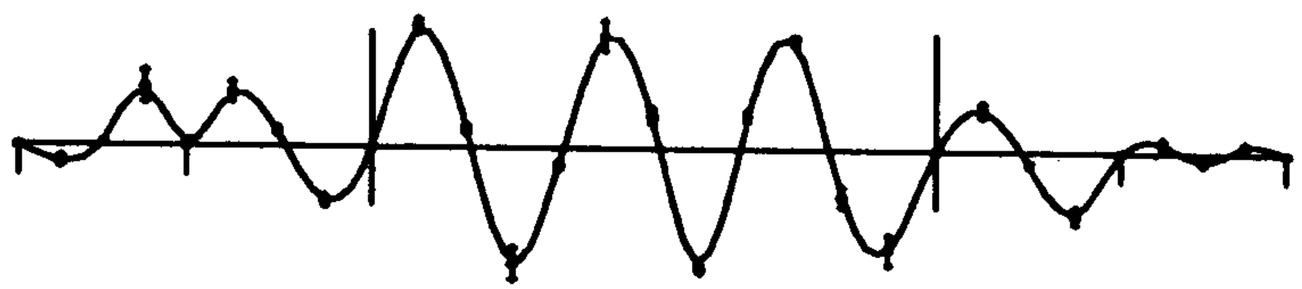

West Side

Mode 25

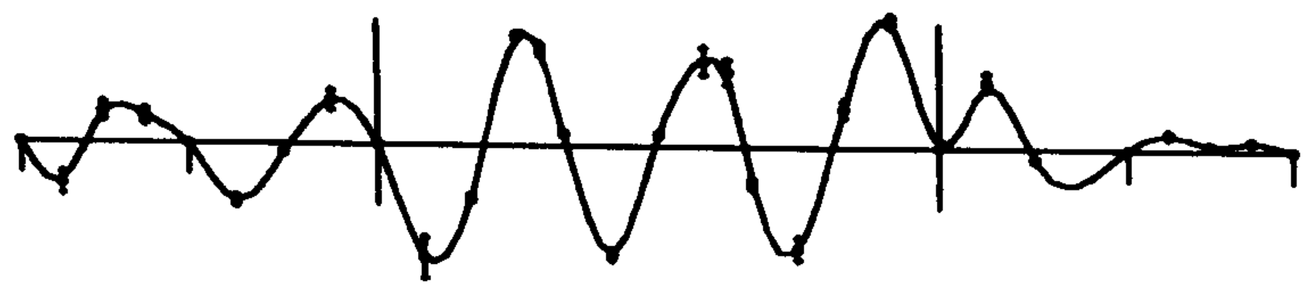

East Side

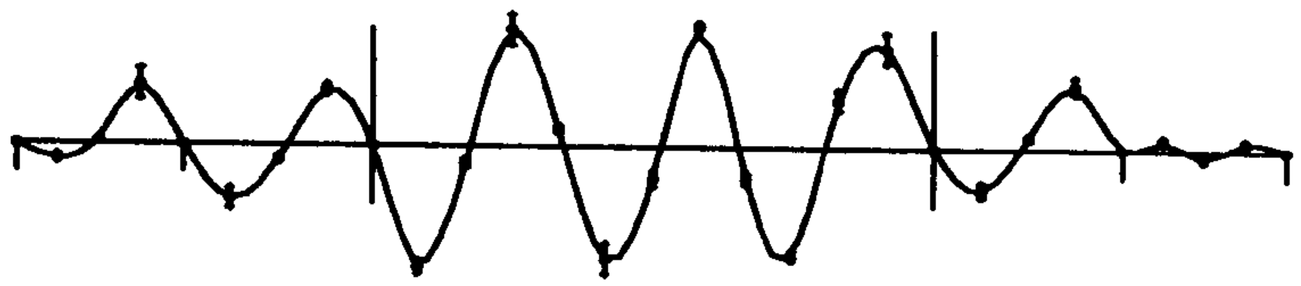

West Side

Mode 26

Figure 7.24 (cont.) -:- Measured Mode Shapes of Deck, Reference at 60 m Point

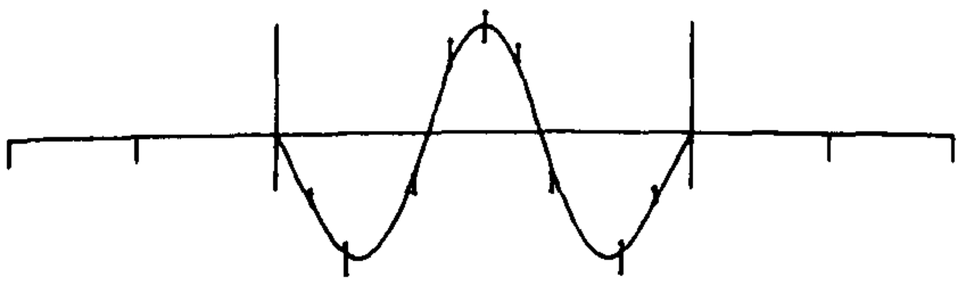

Mode 10, West Side

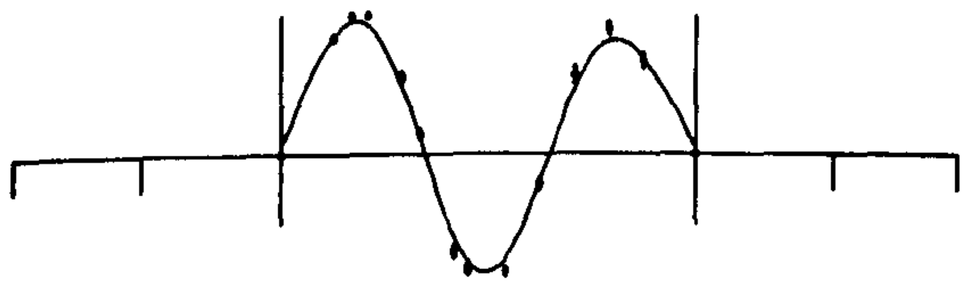

Mode 11, East Side

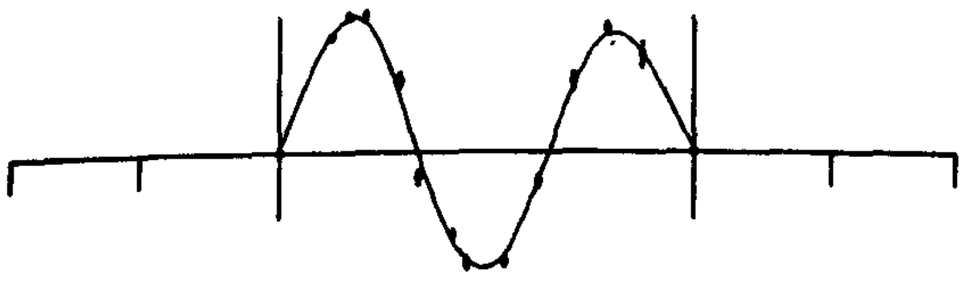

Mode 12, East Side

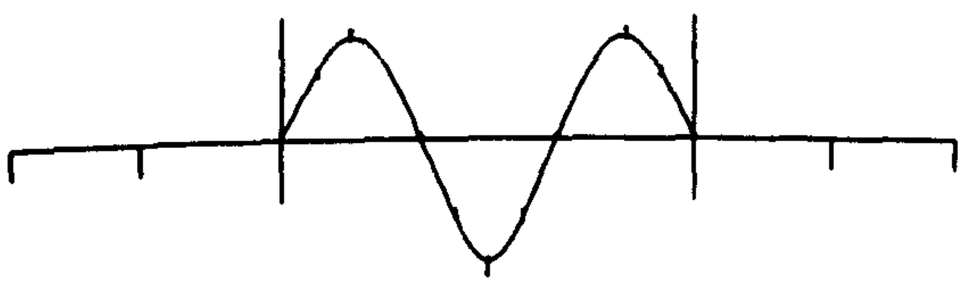

Mode 13, West Side

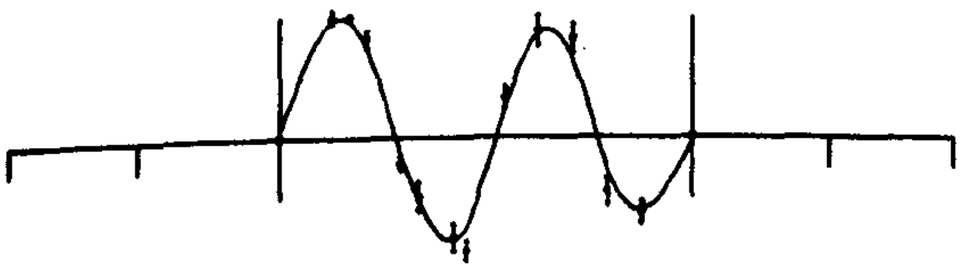

Mode 14, East Side

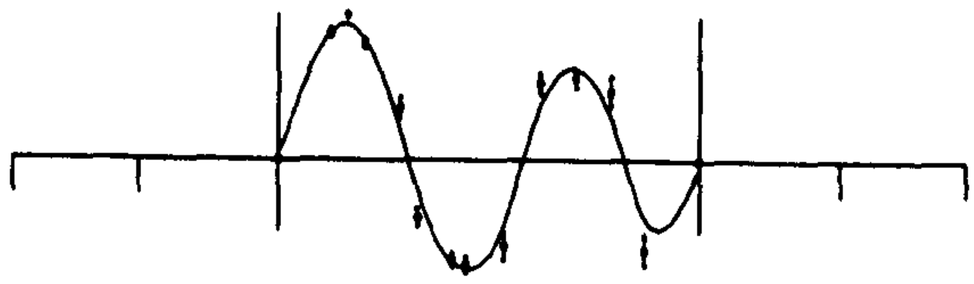

Mode 16, East Side

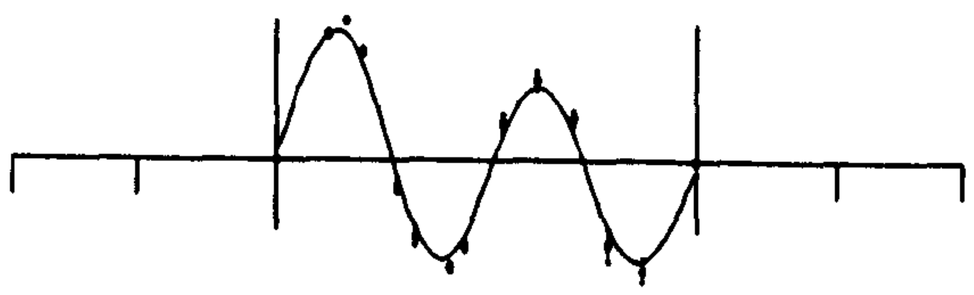

Mode 17, East Side

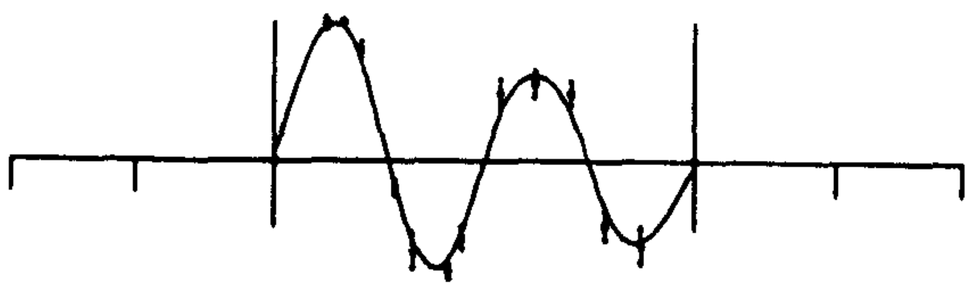

Mode 18, East Side

Mode 19, East Side

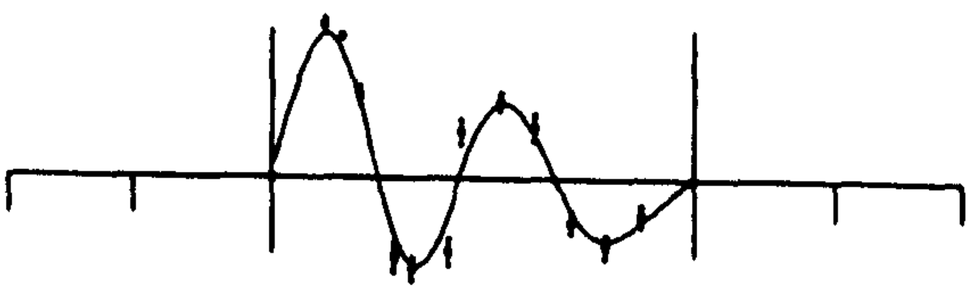

Mode 20, East Side

Figure 7.25 -:- Measured Mode Shapes of Deck, Reference at 40 m Point

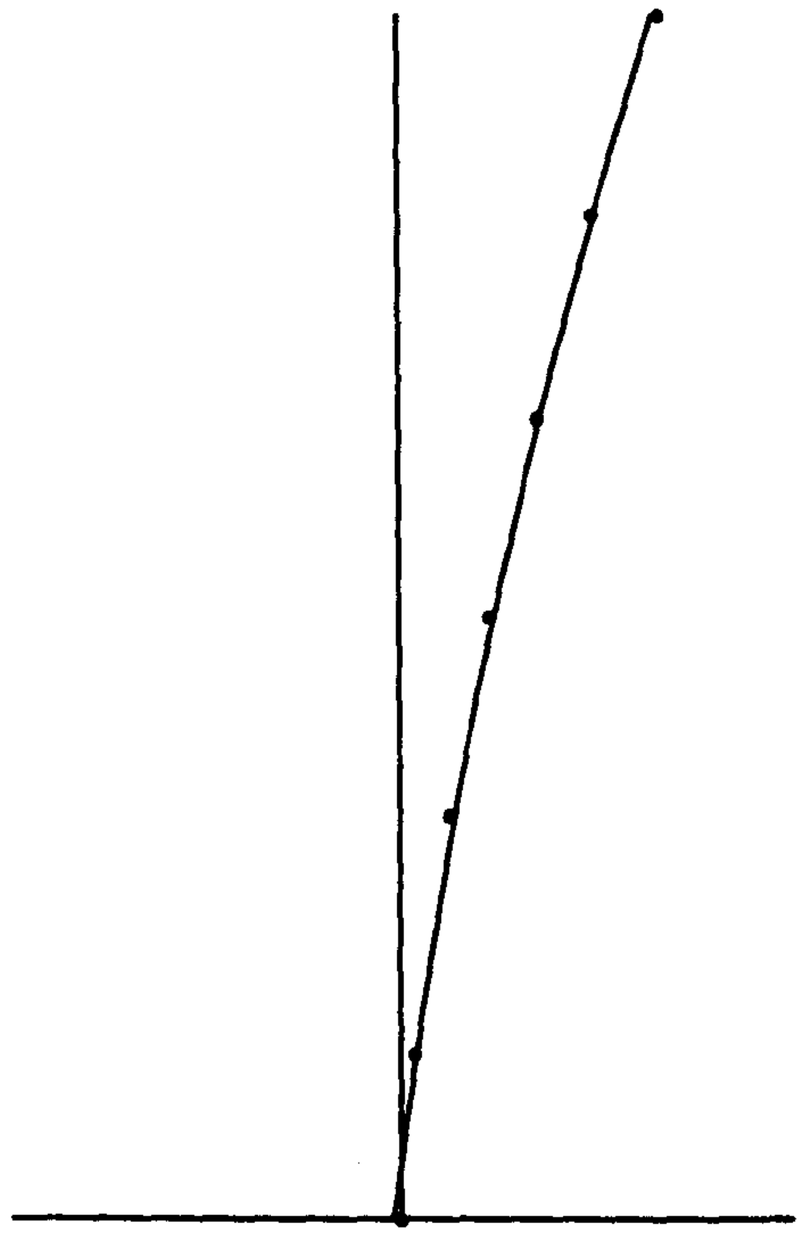

Figure 7.26a -:- Transverse Mode Shape of North East Pylon (0.70 Hz.)

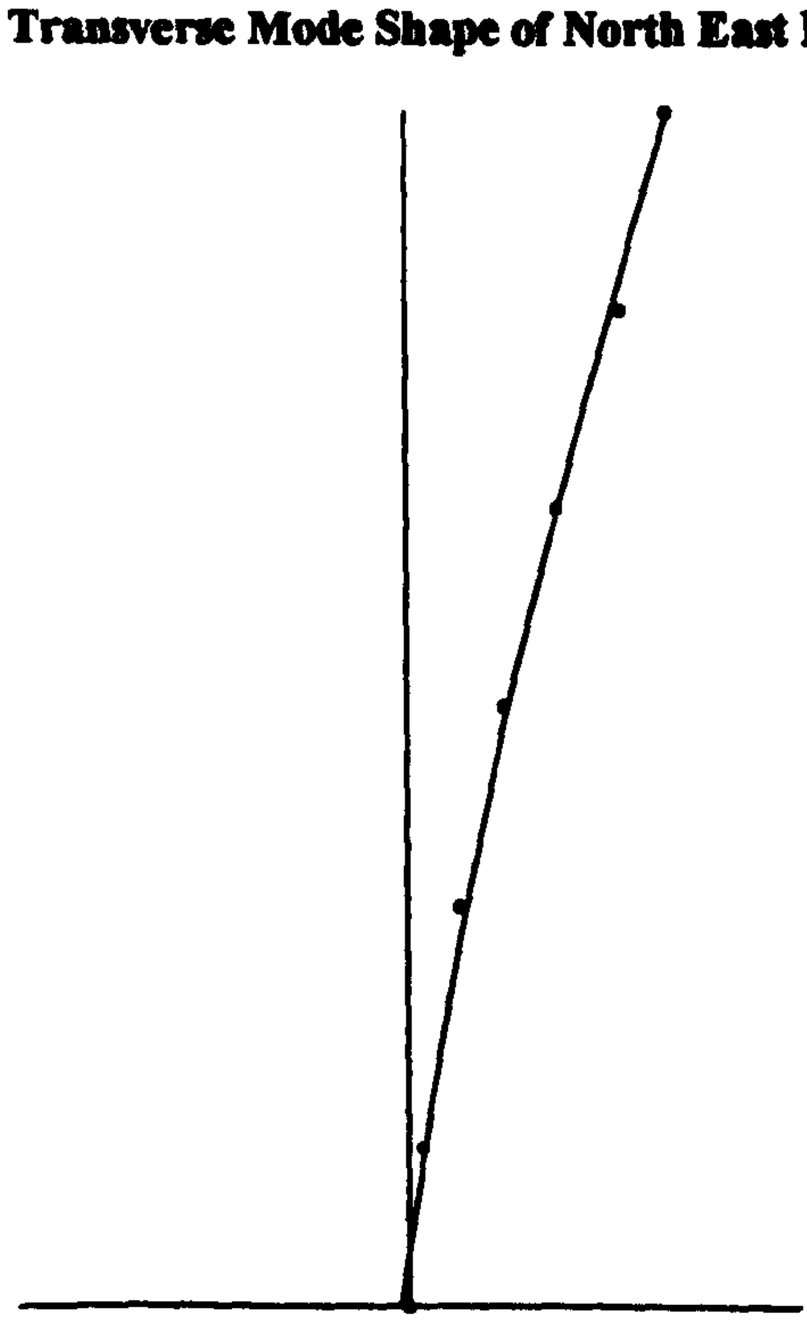

Figure 7.26b -:- Transverse Mode Shape of North West Pylon (0.70 Hz.)

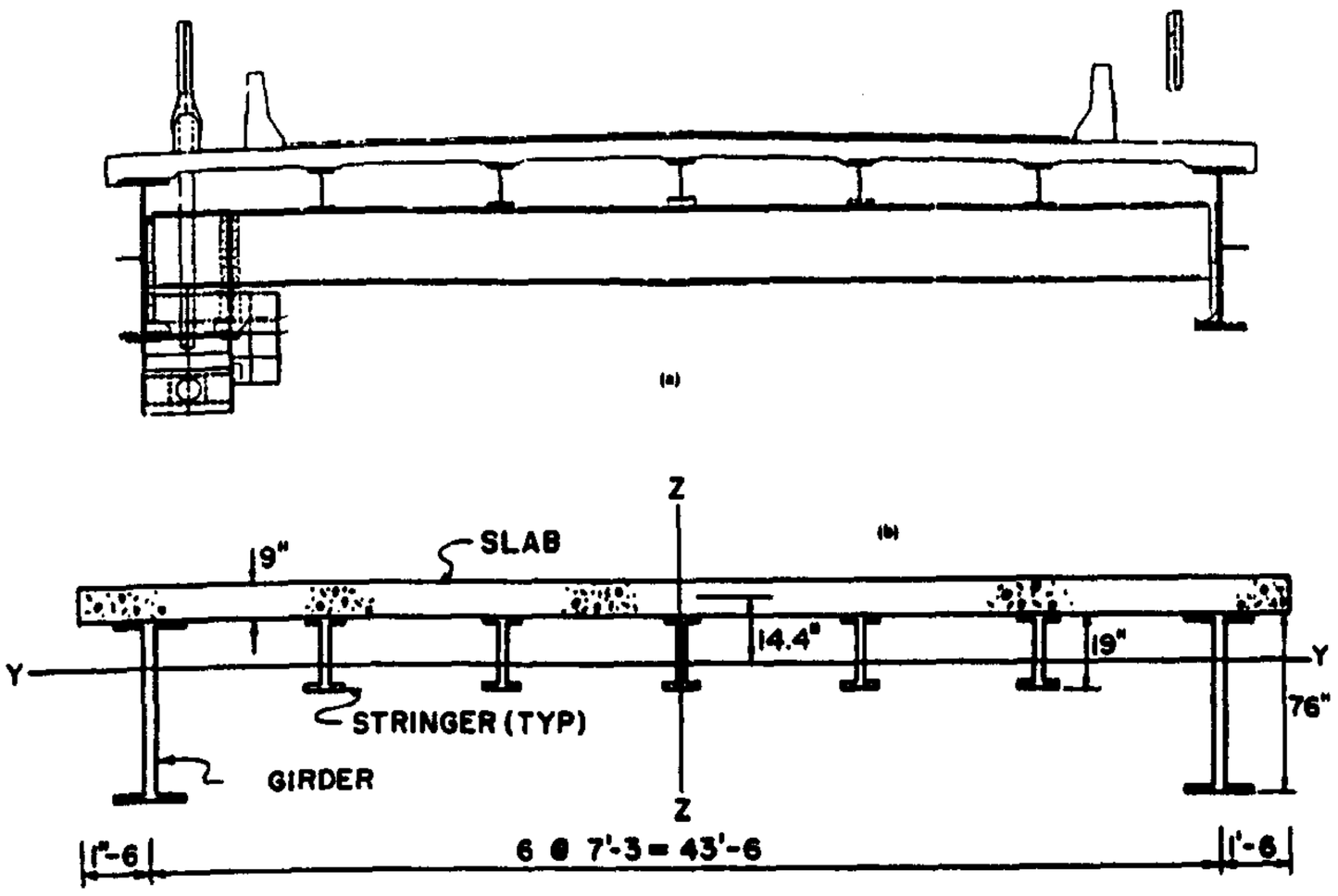

Figure 7.27 : Cross Section Of Quincy Bayview Bridge (Wilson & Gravelle 1991)

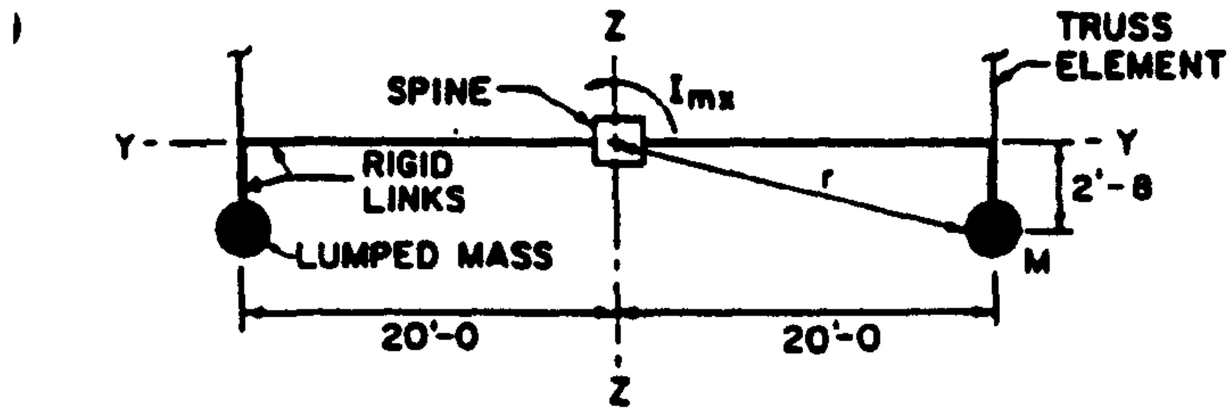

Figure 7.28 : Modelling of Deck Section of Quincy Bayview Bridge (Wilson & Gravelle 1991)

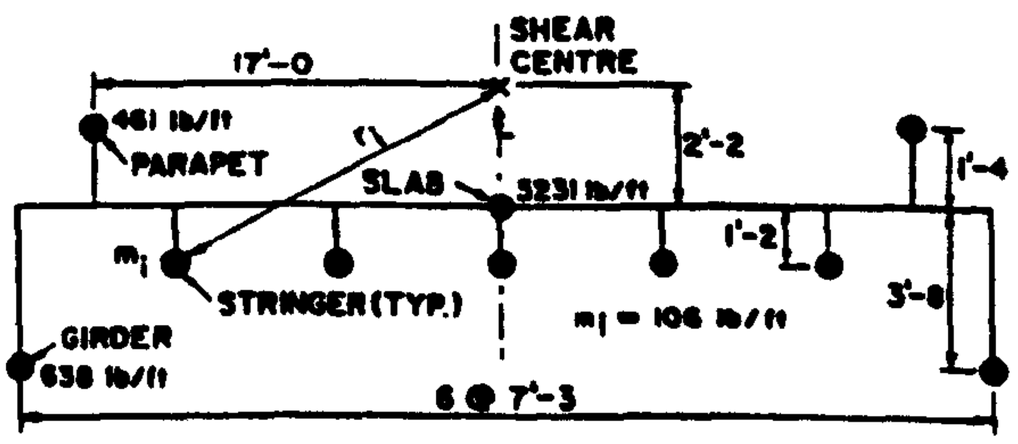

Figure 7.29 : Modelling of Mass Distribution of Quincy Bayview Bridge (Wilson & Gravelle 1991)

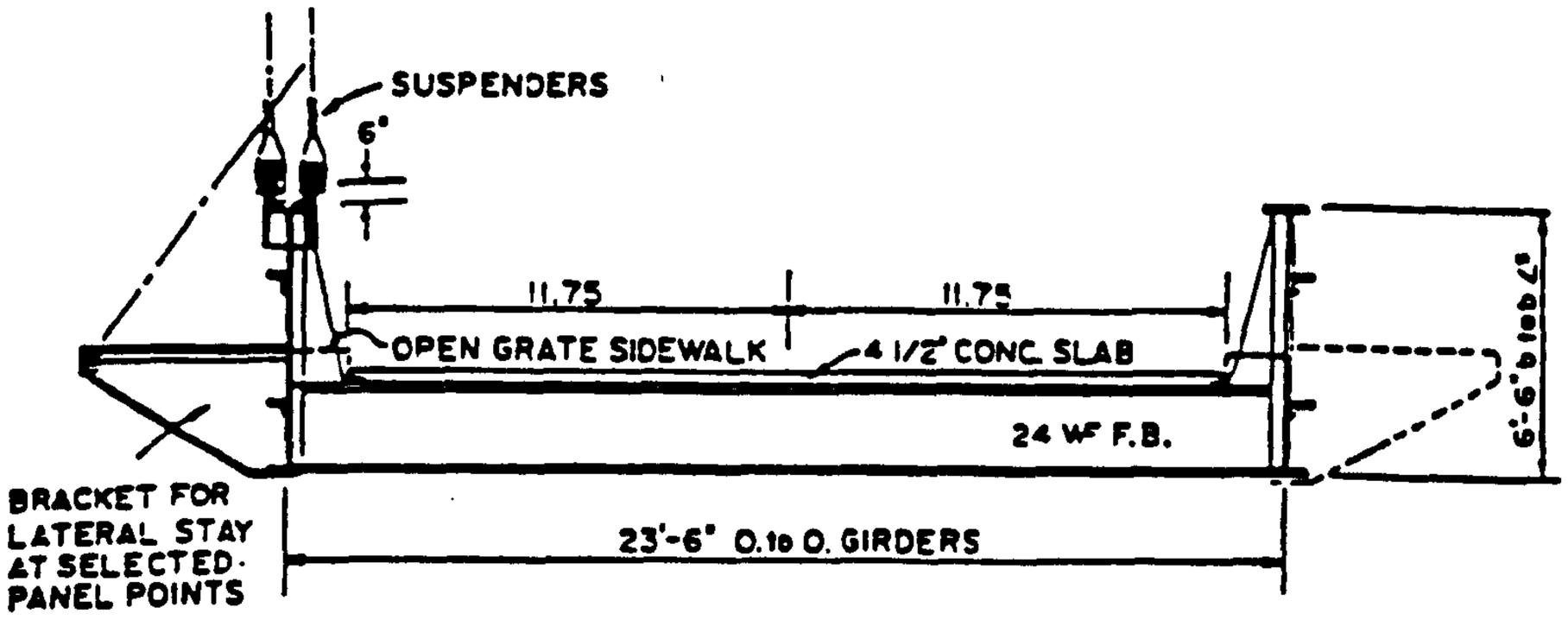

Figure 7.30 : Deck Cross Section of Deer Isle Bridge (Kumarasena et al 1989a)

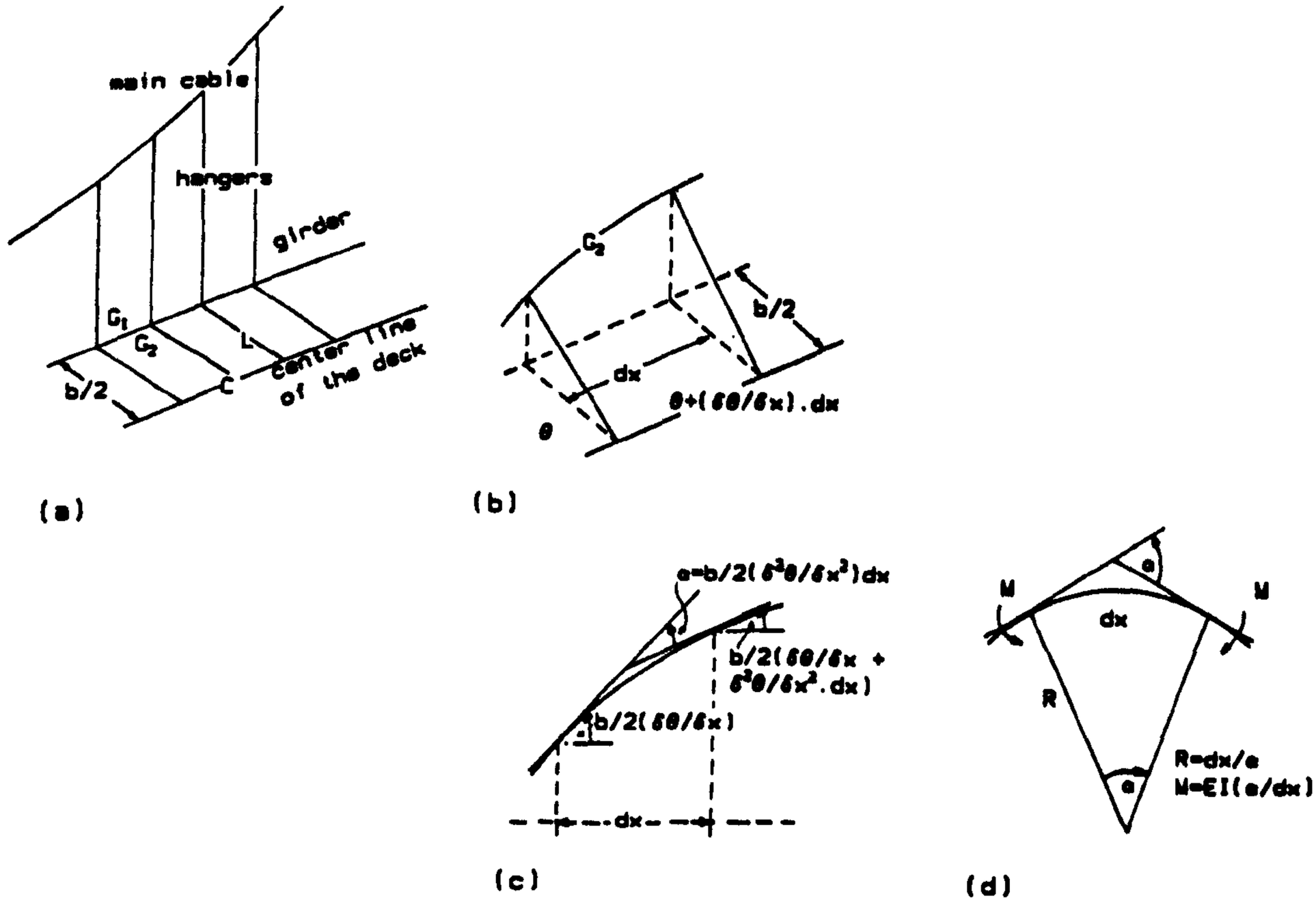

Figure 7.31 : Modelling of Warping Stiffness Using Edge Beams(Kumarasena et al 1989a)

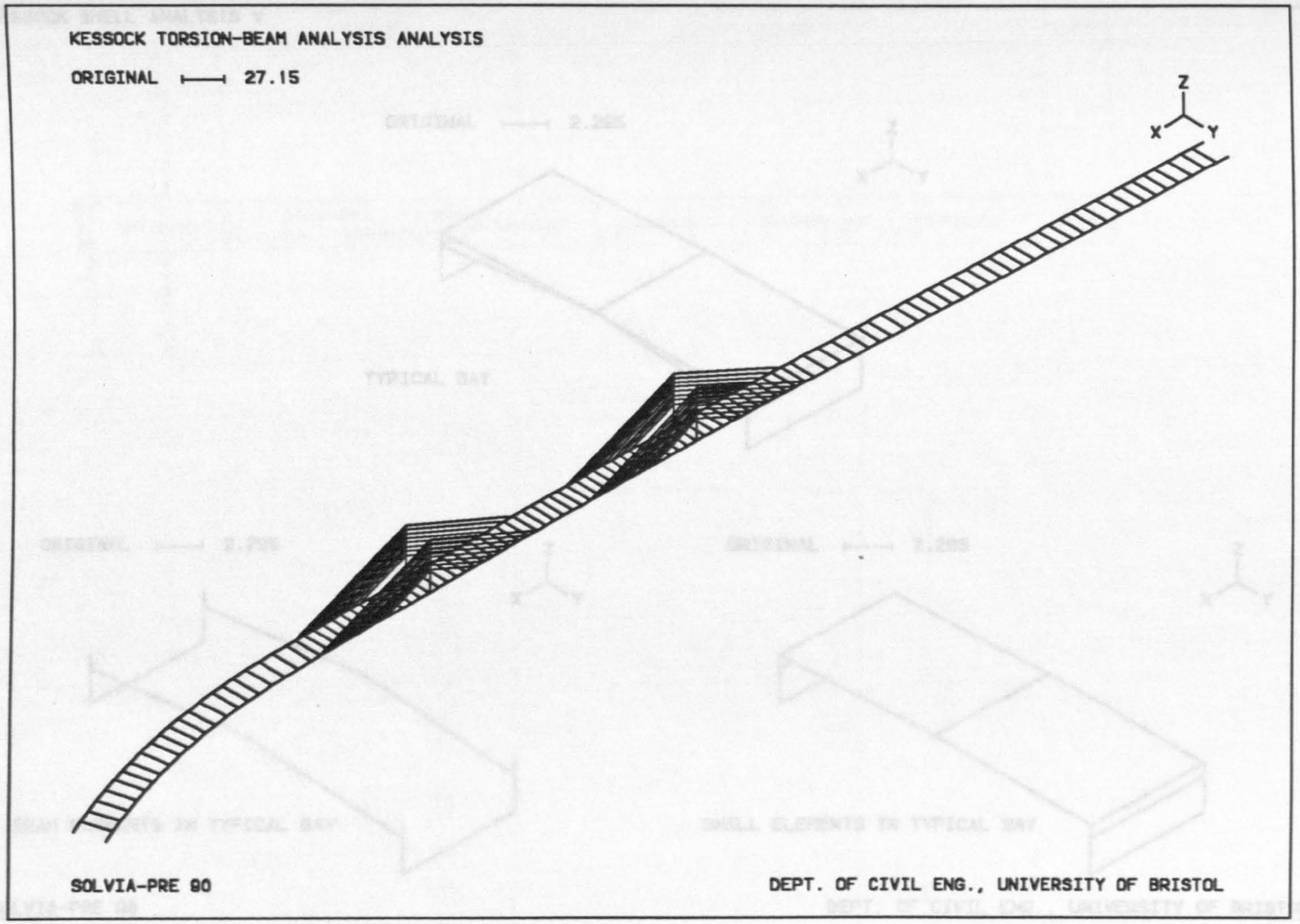

Figure 7.32 -:- Grillage Model Of kessock Bridge

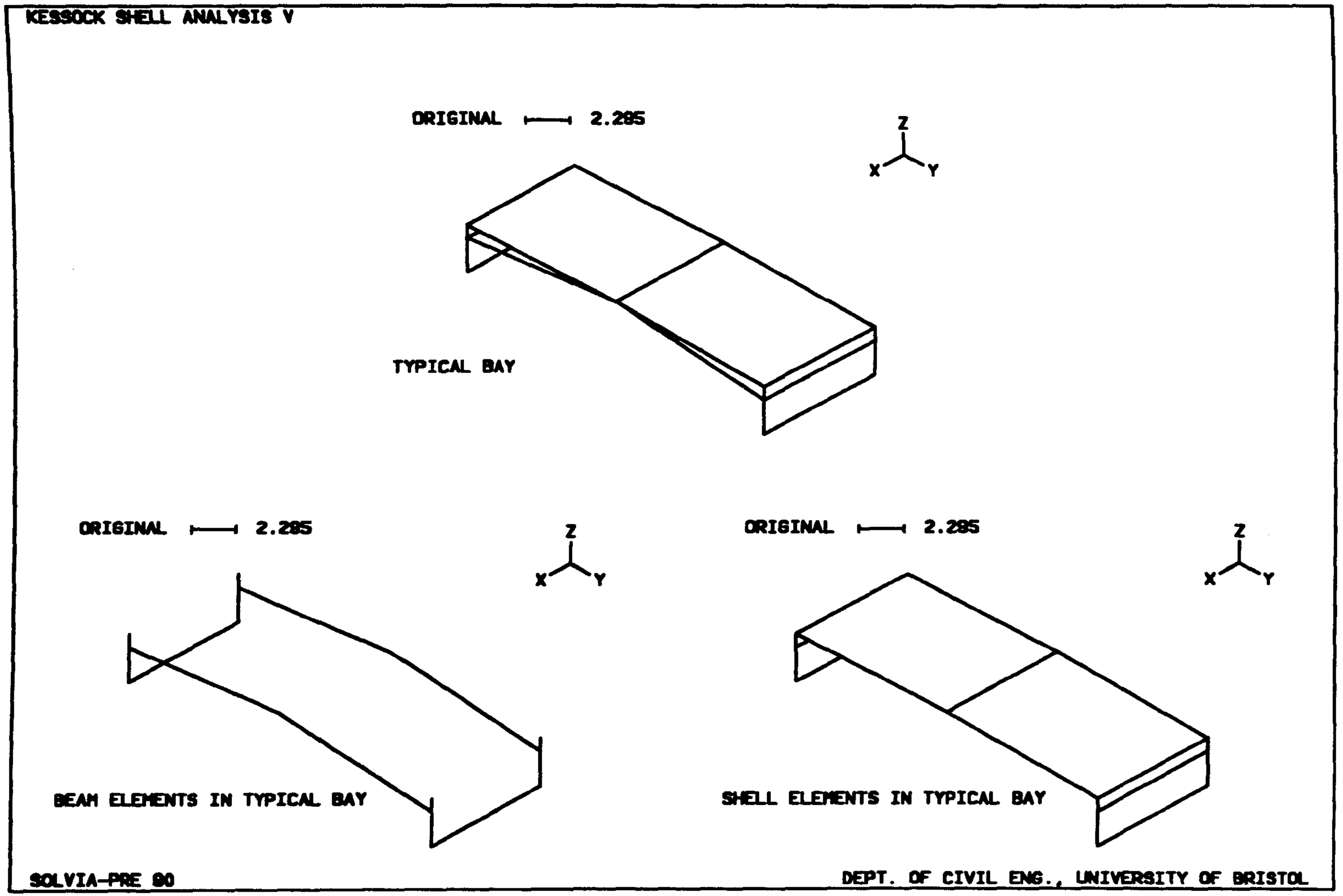

Figure 7.33 -:- Details Of Beam Shell Model Of Kessock Bridge

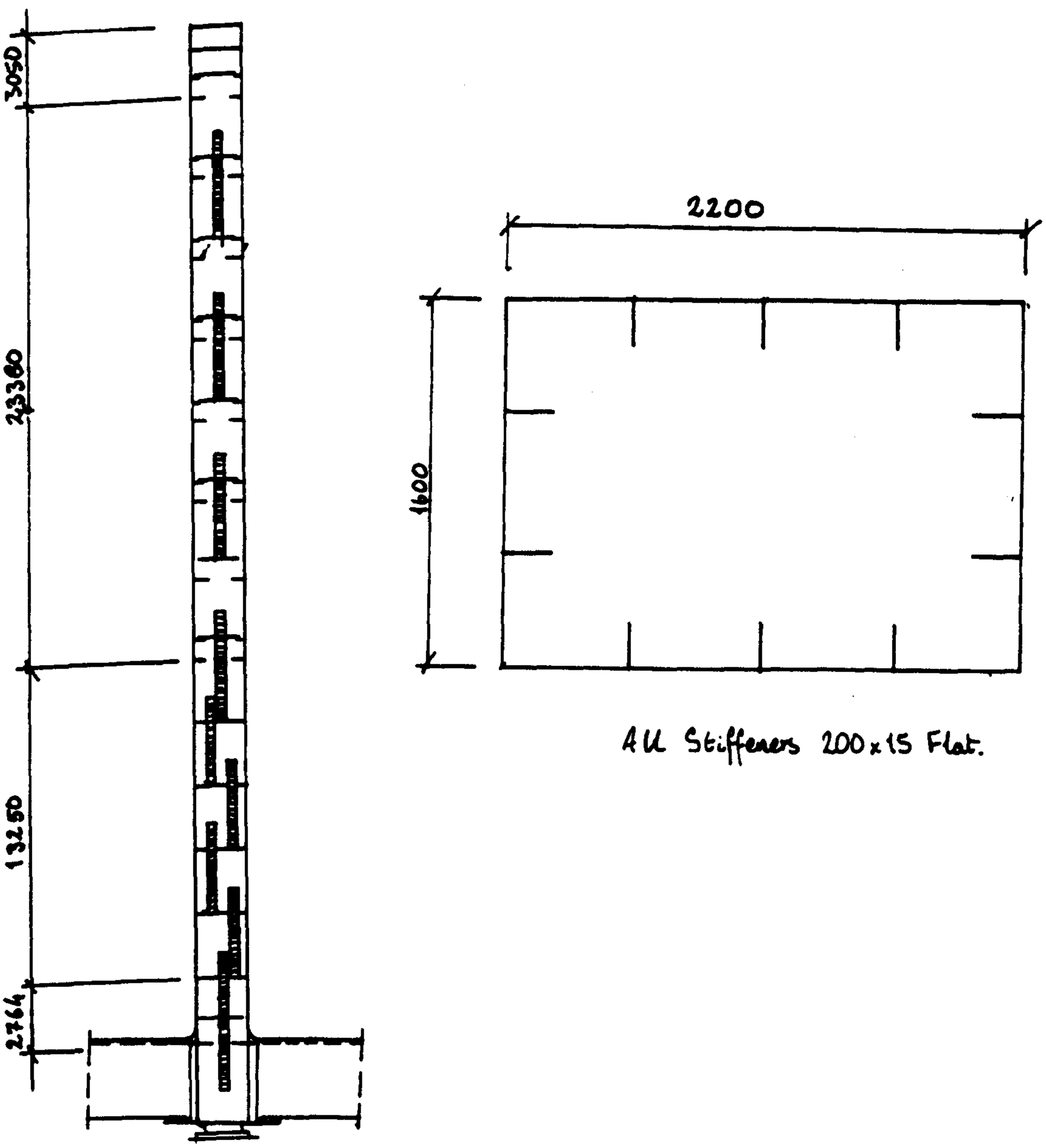

All Stiffeners 200 x 15 Flat.

Figure 7.34 : Structural Details of Pylons

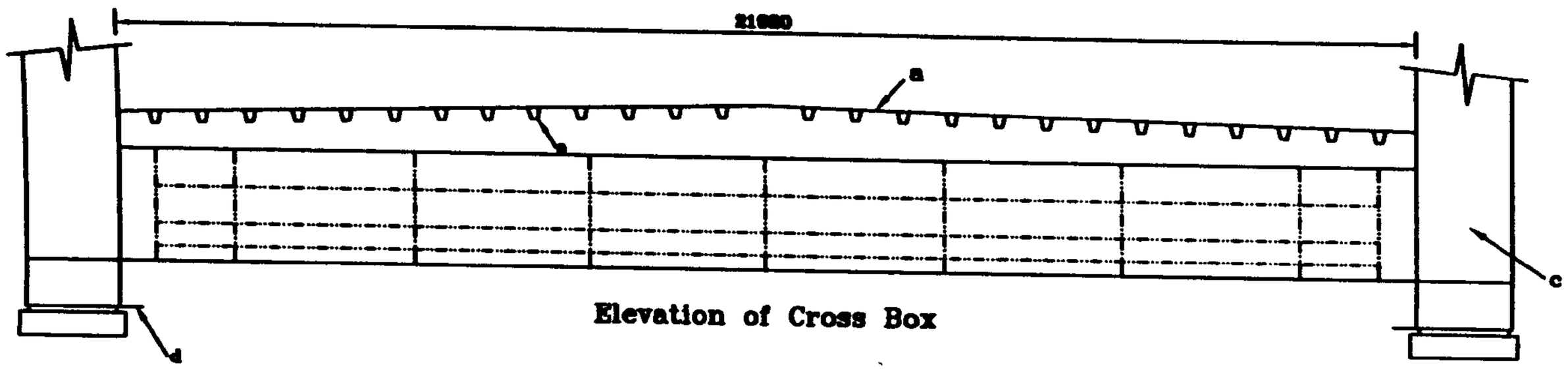

Elevation of Cross Box

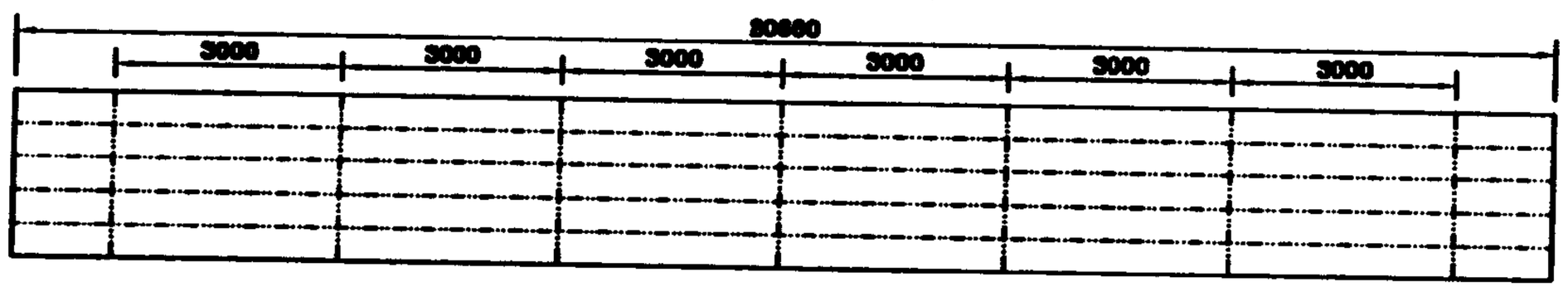

Plan of Cross Box

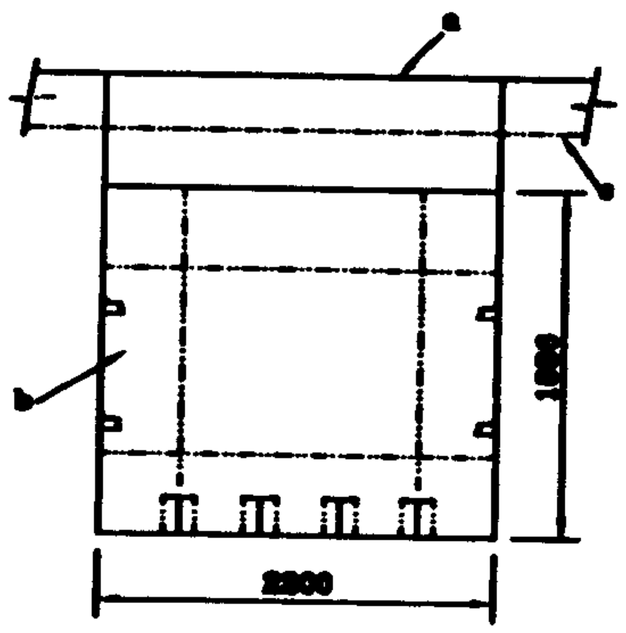

Section of Cross Box

Notes
a. Deck Plate
b. Internal Diaphragm
c. Pylon Base
d. Lower Flange of Edge Girder
e. Orthotropic Trough Stiffener

Figure 7.35 : Structural Details of Cross Box

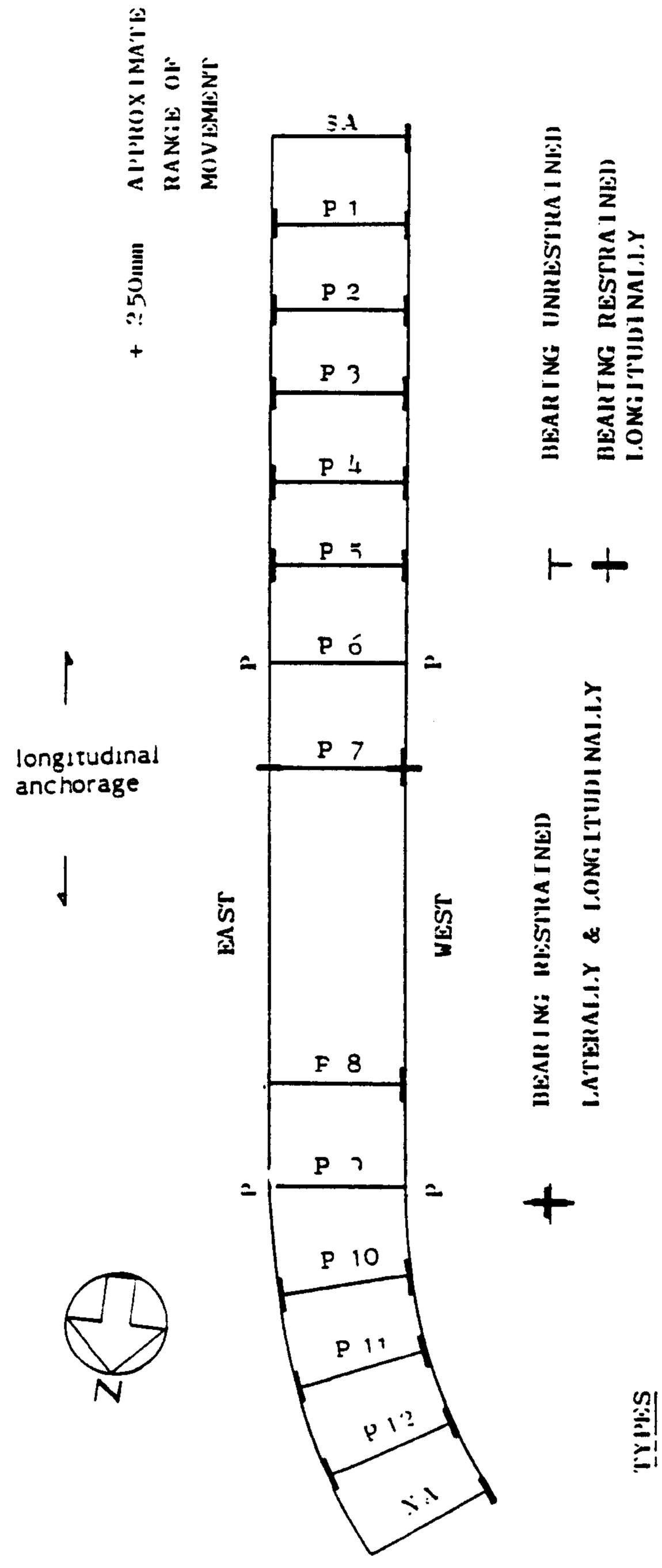

Figure 7.36 : Boundary Conditions at Kessock Bridge Bearings

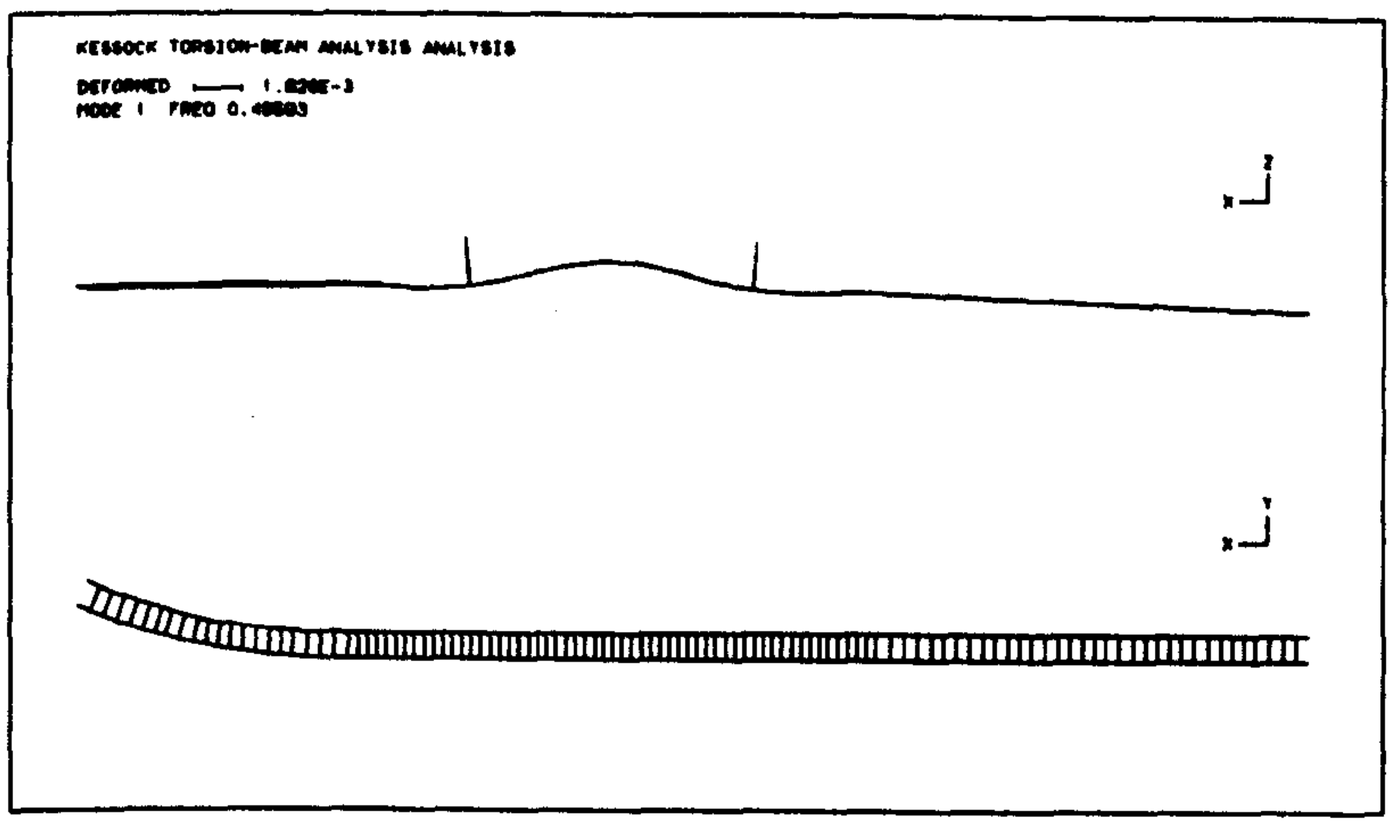

Figure 7.37a -:- Predicted First Vertical Mode, Grillage Model

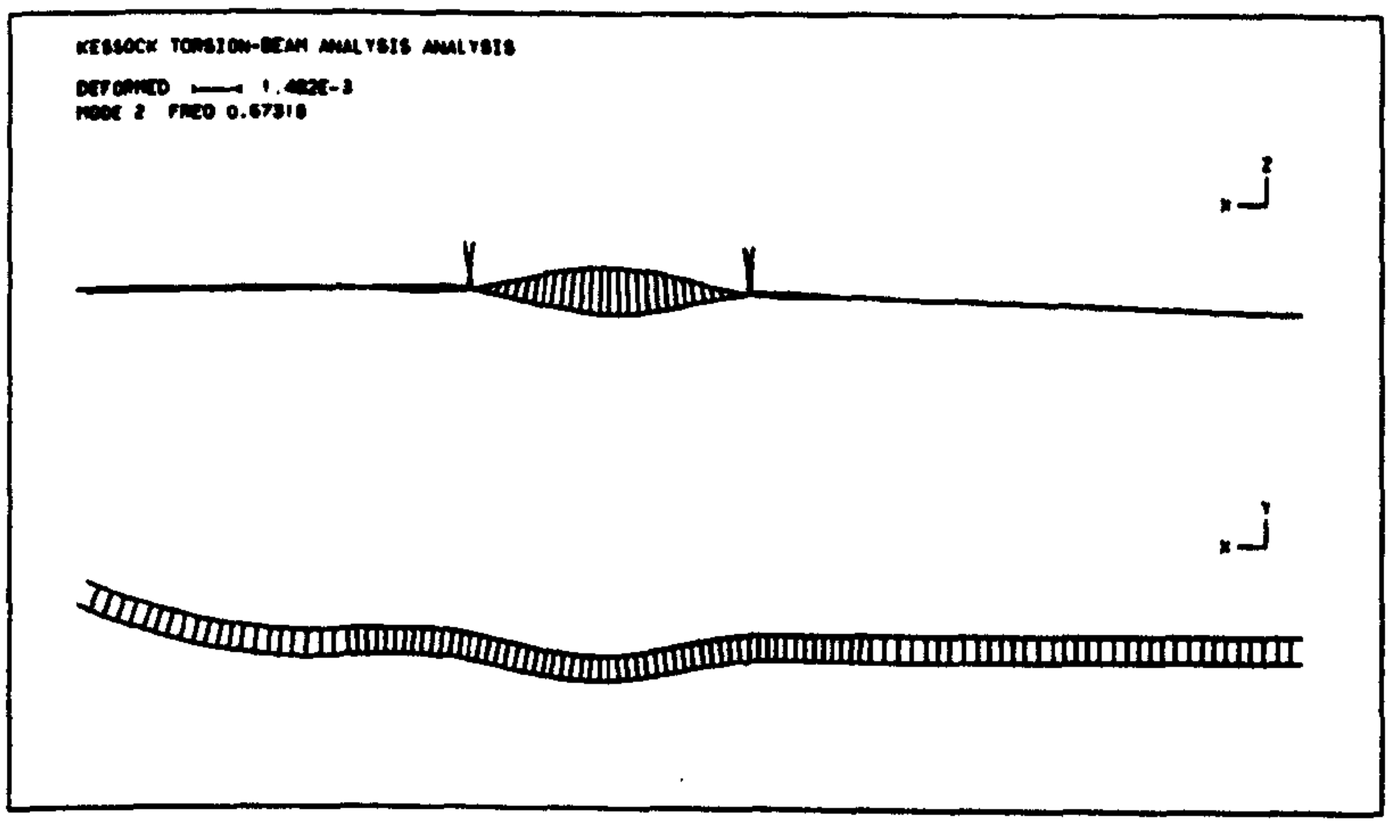

Figure 7.37b -:- Predicted "First" Torsional Mode, Grillage Model

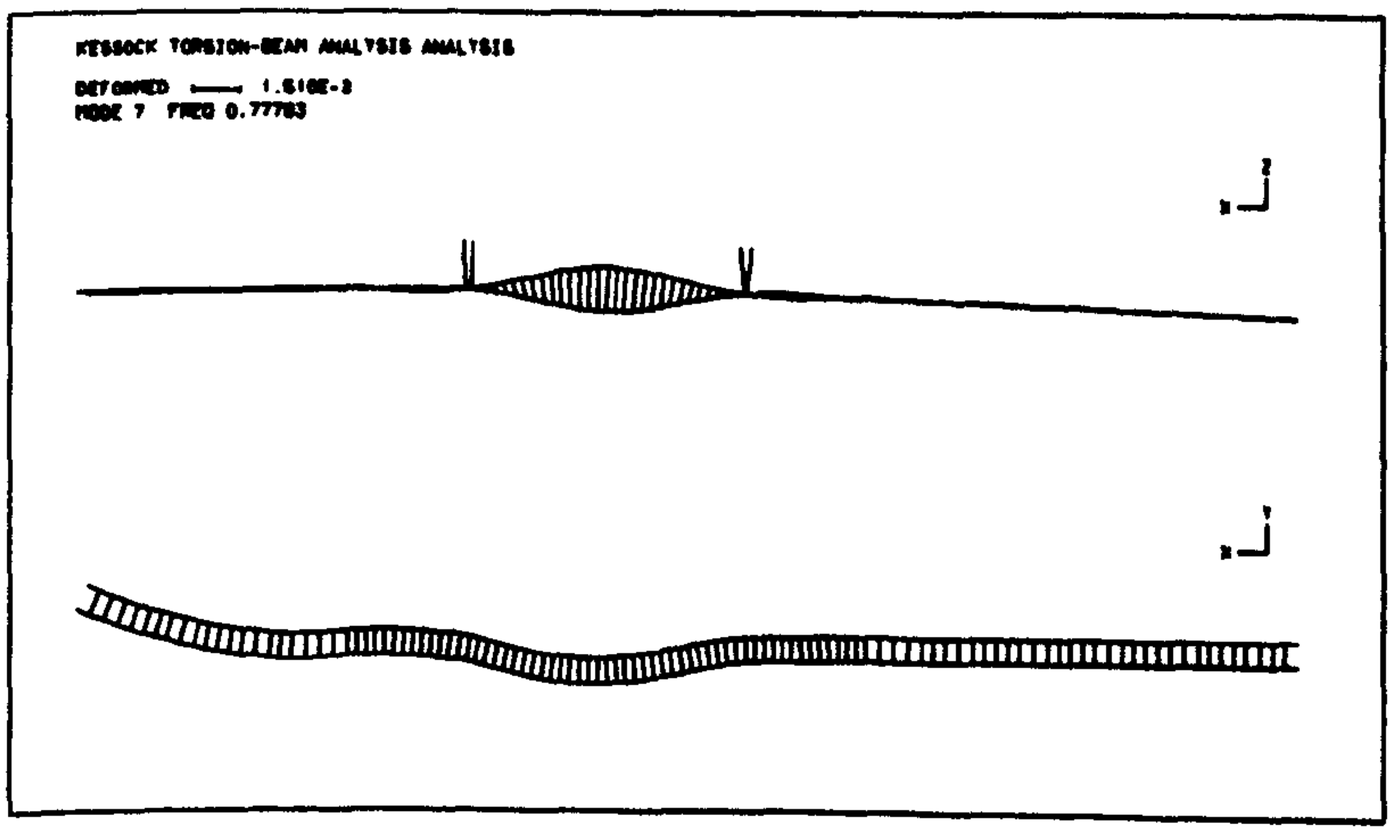

Figure 7.37c -:- Predicted "First" Torsional Mode, Grillage Model

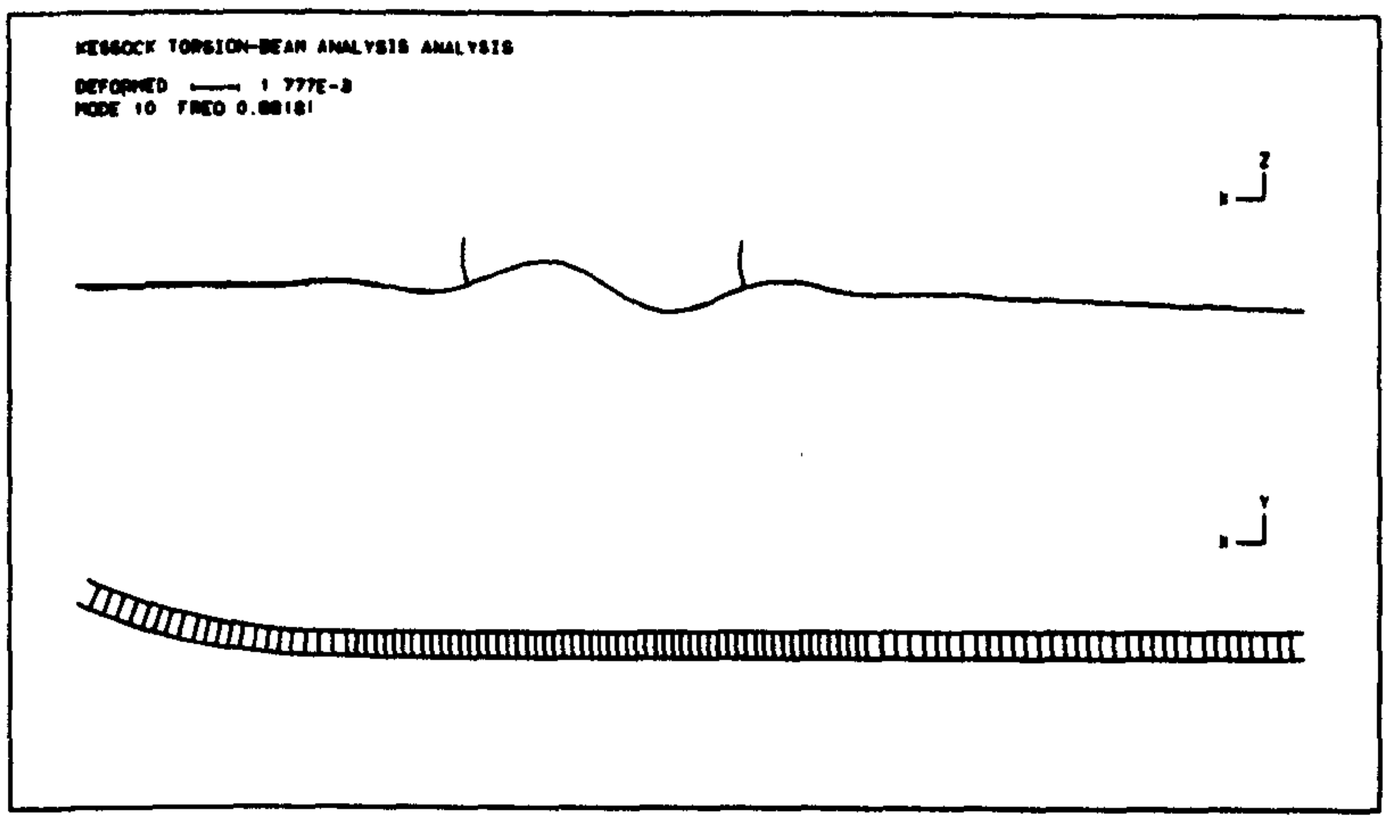

Figure 7.37d -:- Predicted Second Vertical Mode, Grillage Model

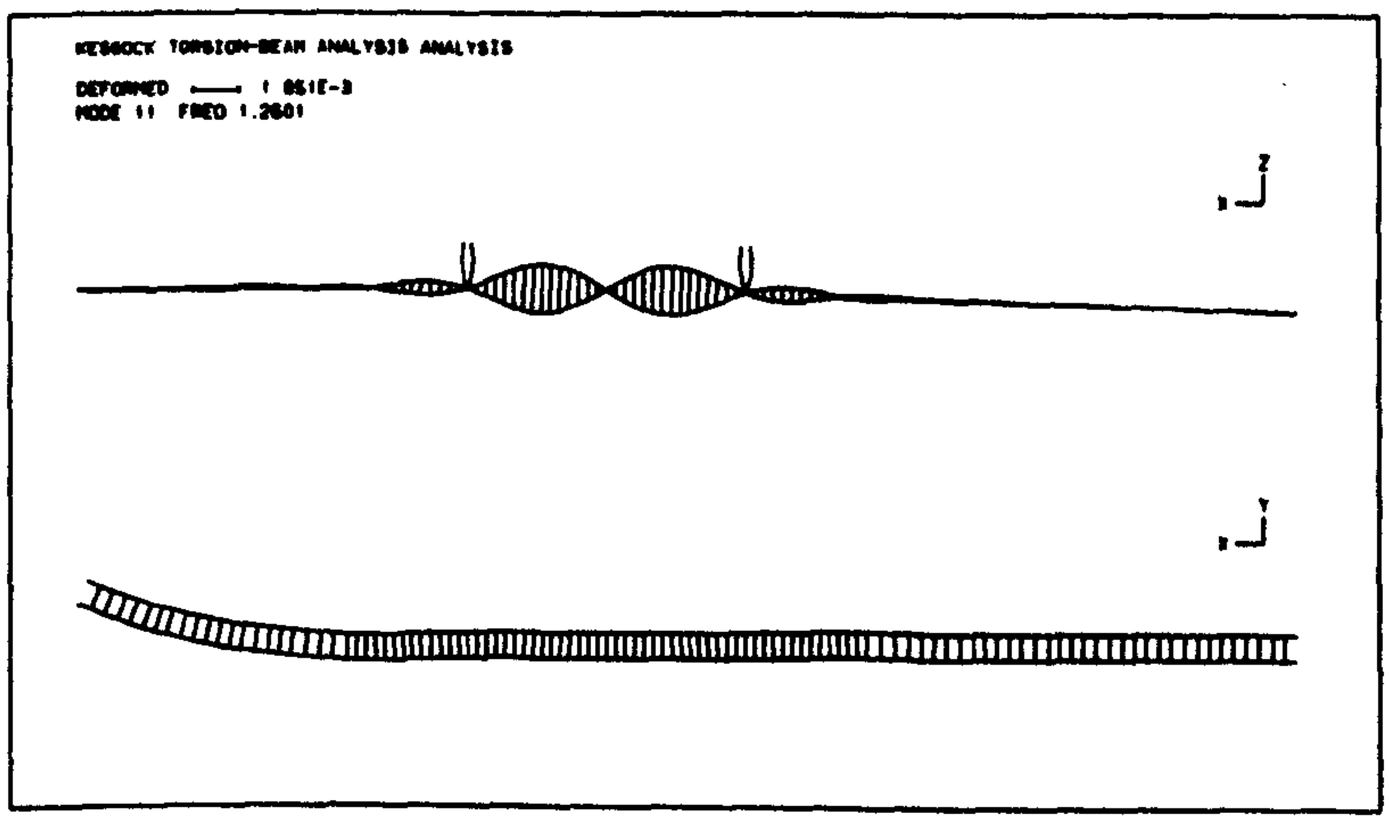

Figure 7.37e -:- Predicted Second Torsional Mode, Grillage Model

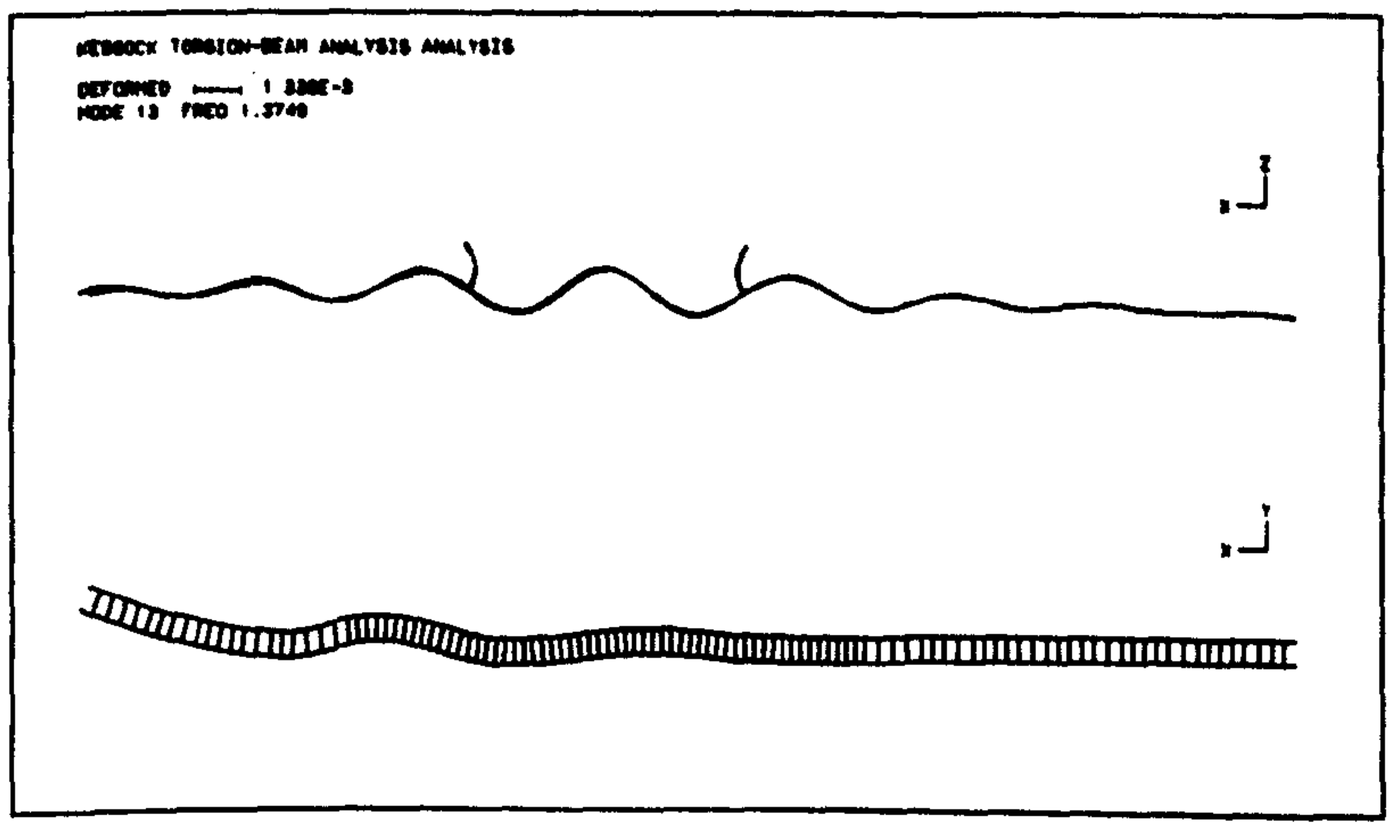

Figure 7.37f -:- Predicted Third Vertical Mode, Grillage Model

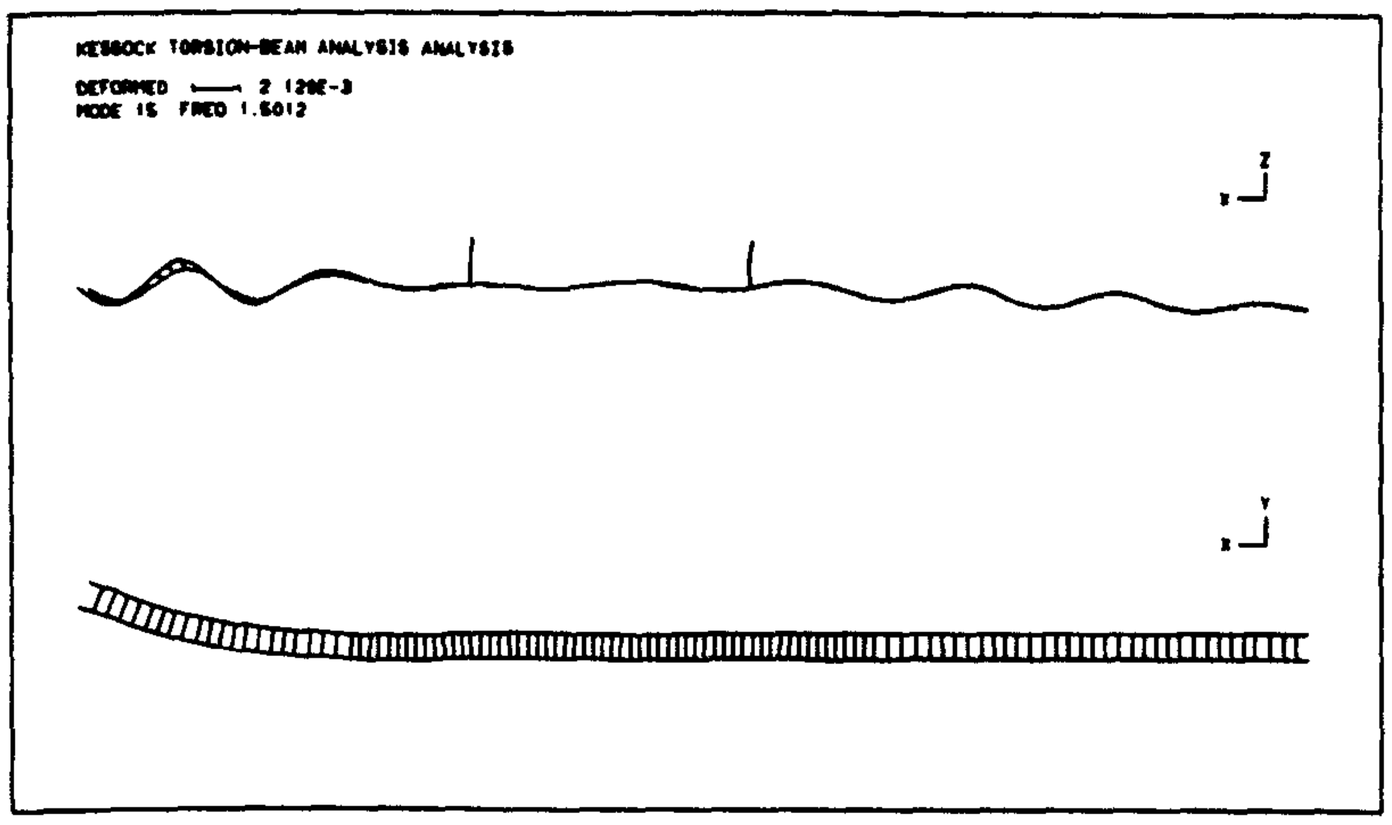

Figure 7.37g -:- Predicted Side Span Mode, Grillage Model

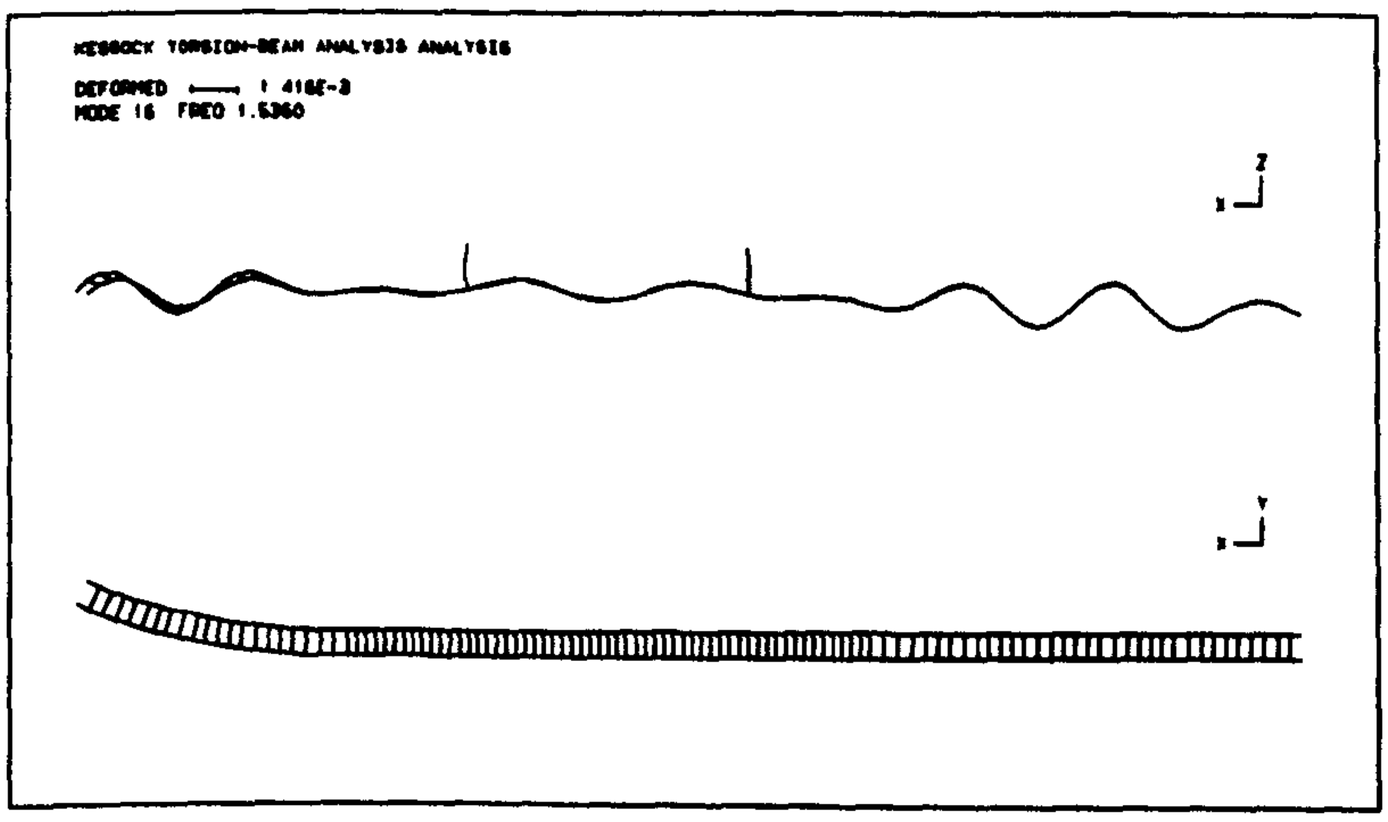

Figure 7.37h -:- Predicted Side Span Mode, Grillage Model

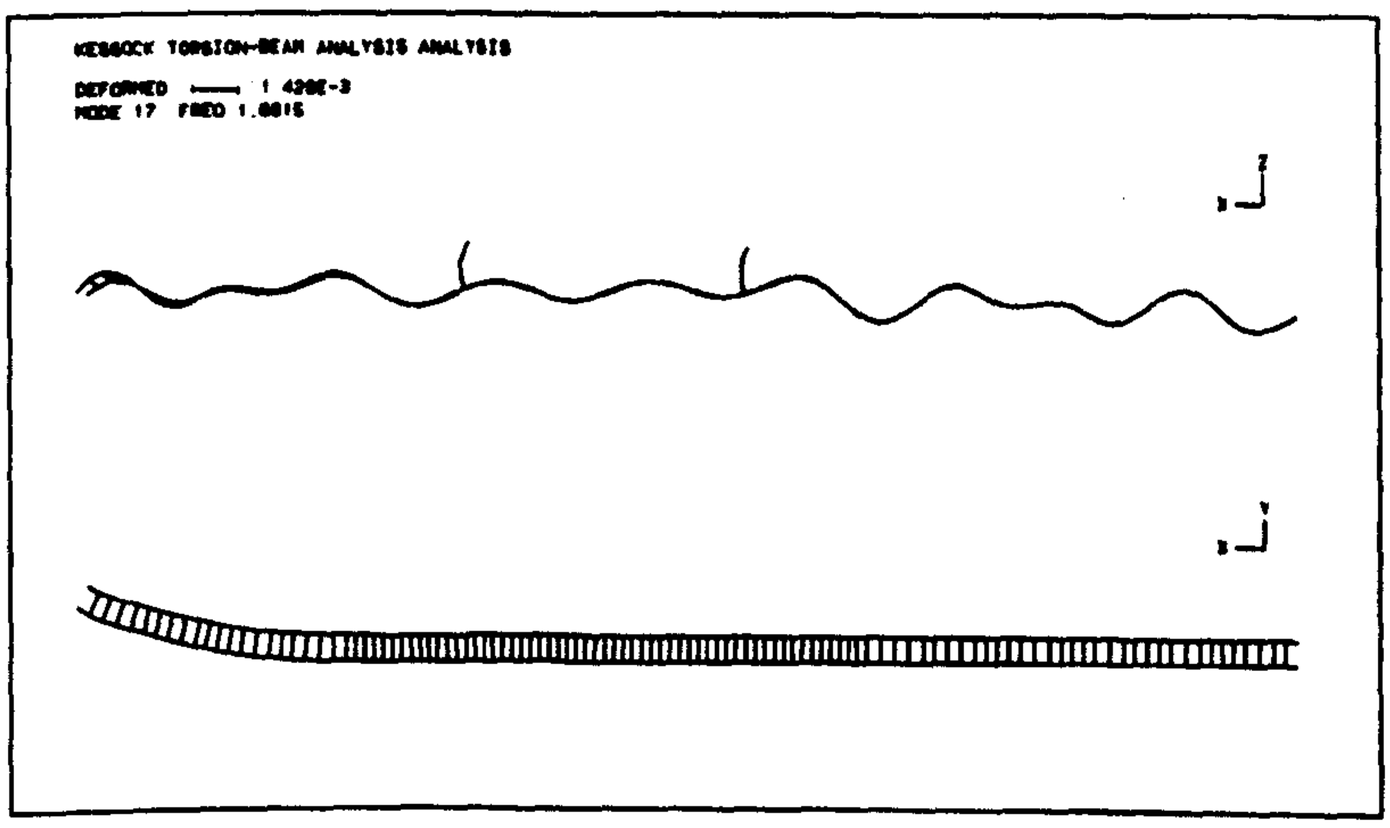

Figure 7.37i -:- Predicted Side Span Mode, Grillage Model

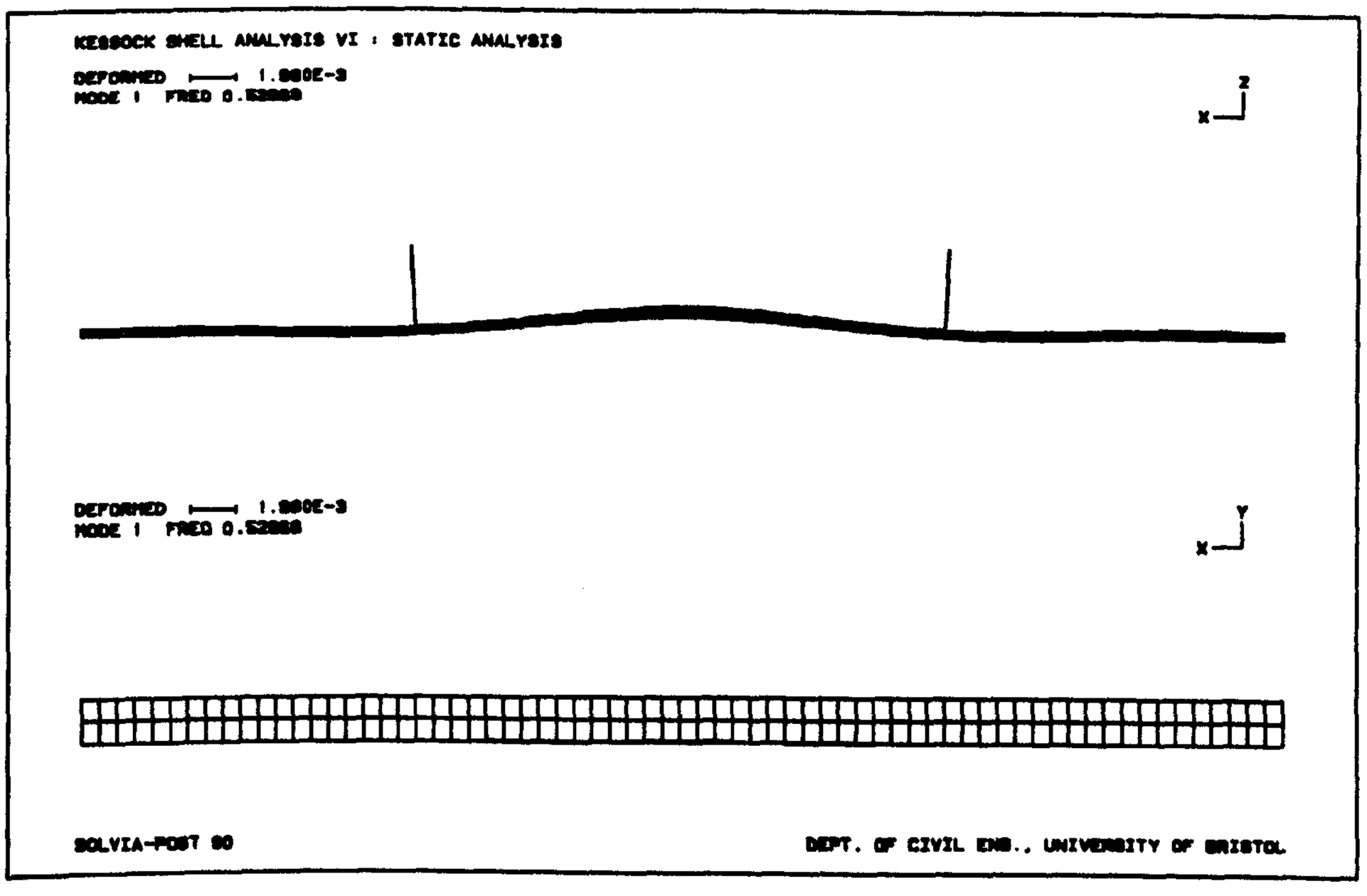

Figure 7.38a -:- Predicted First Vertical Mode And Natural Frequency, Beam Shell Model

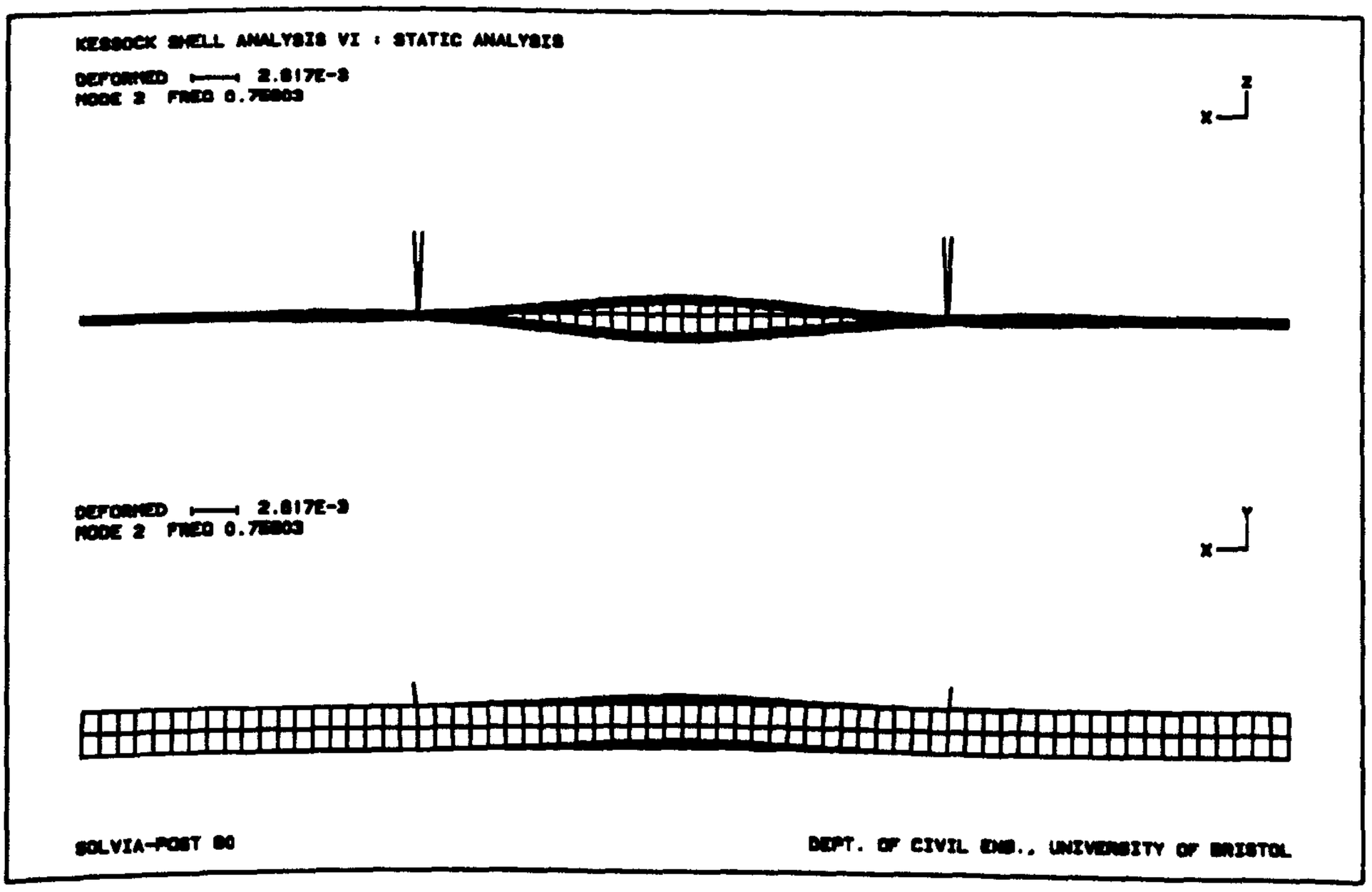

Figure 7.38b -:- Predicted First Torsional Mode And Natural Frequency, Beam Shell Model

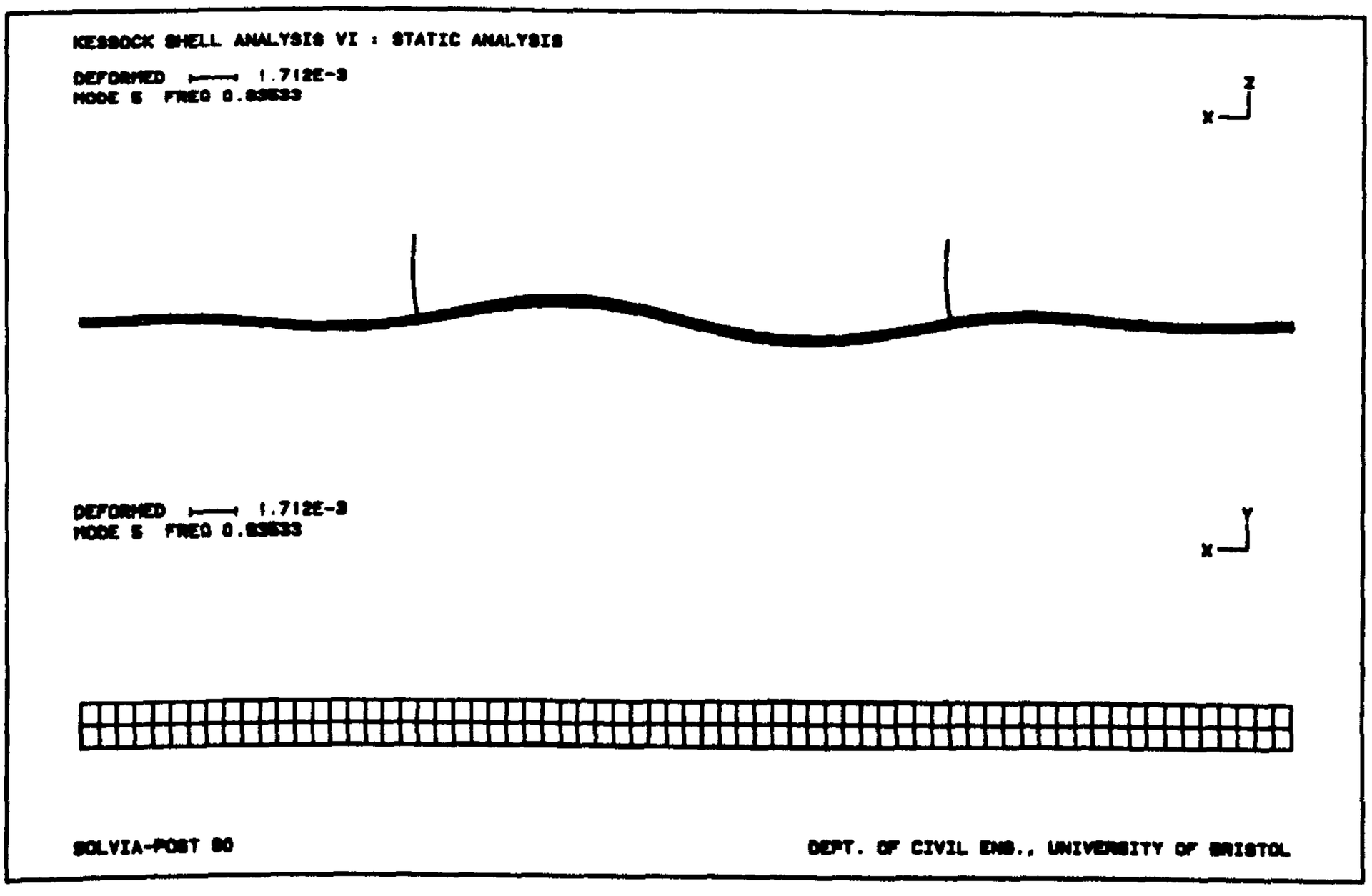

Figure 7.38c -:- Predicted Second Vertical Mode And Natural Frequency, Beam Shell Model

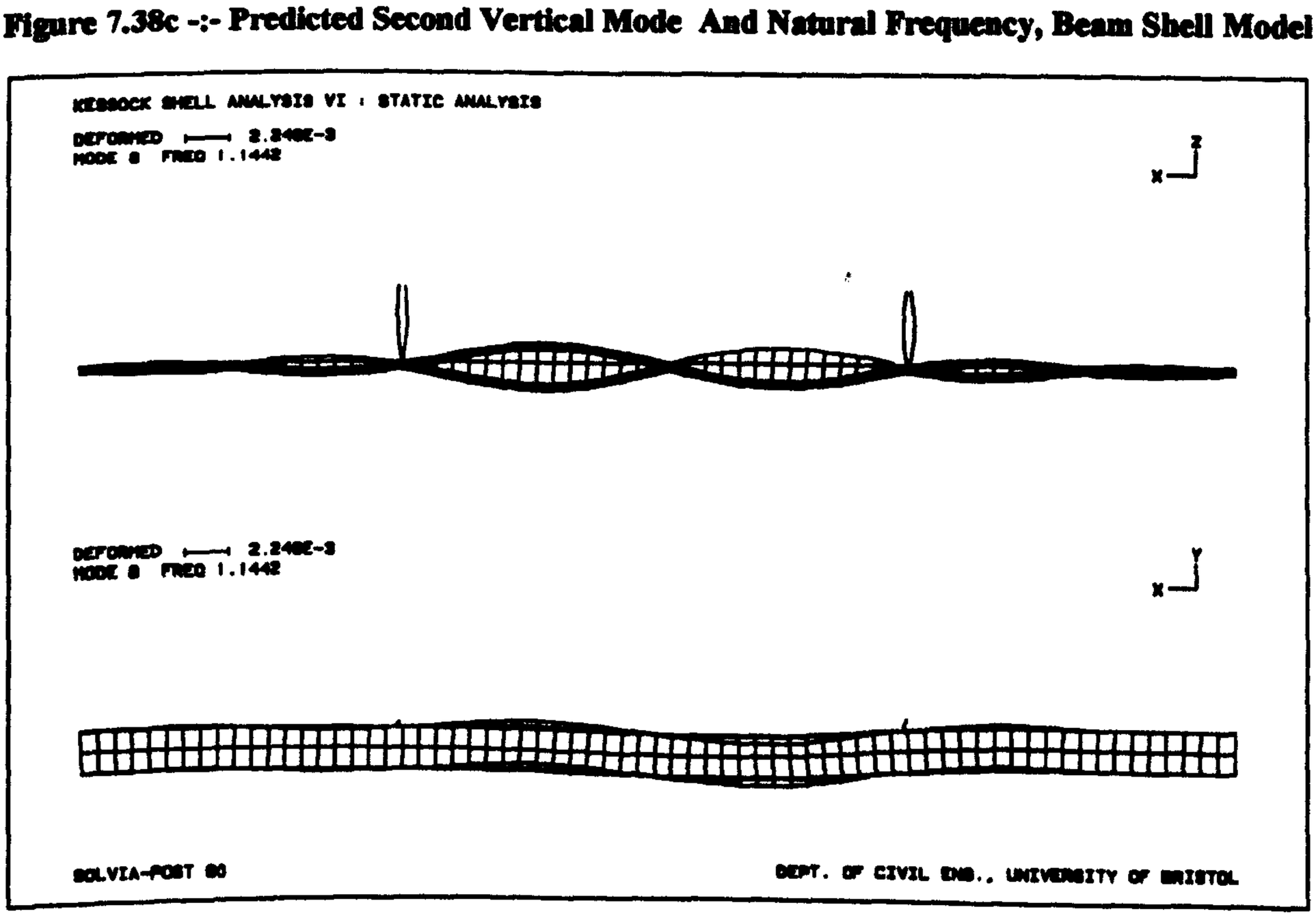

Figure 7.38d -:- Predicted Second Torsional Mode And Natural Frequency, Beam Shell Model

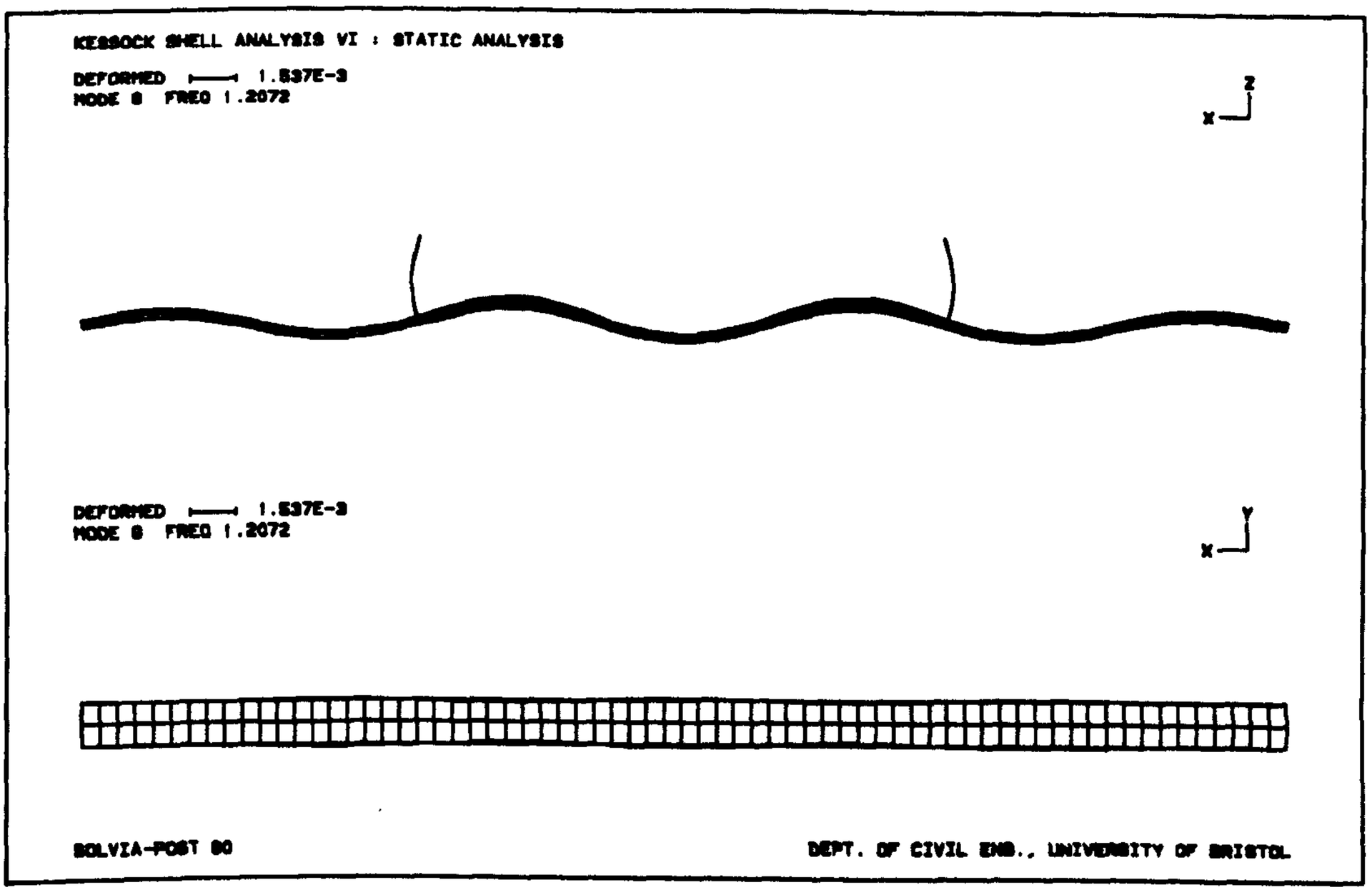

Figure 7.38e -:- Predicted Third Vertical Mode And Natural Frequency, Beam Shell Model

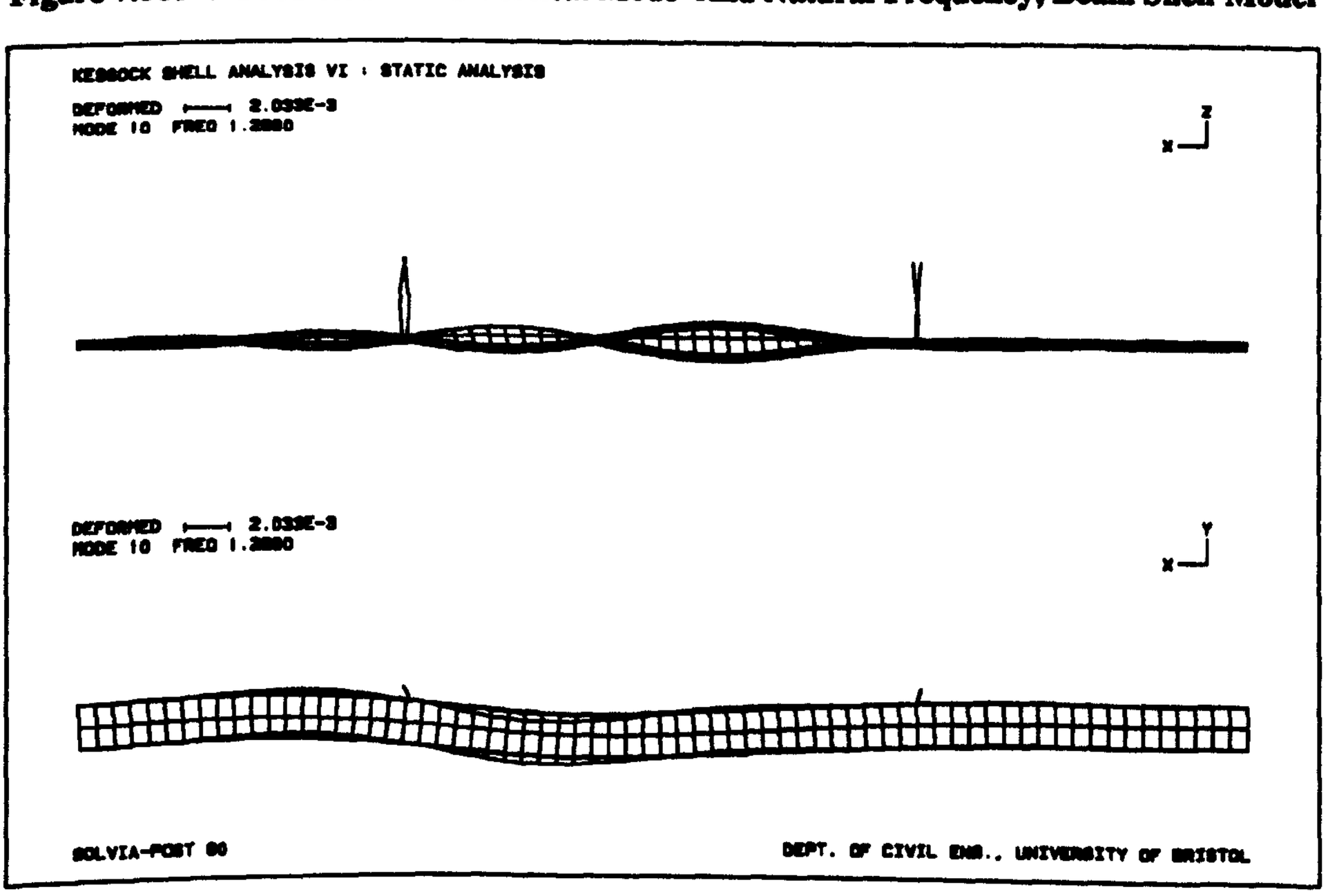

Figure 7.38f -:- Predicted Torsional Mode And Natural Frequency, Beam Shell Model

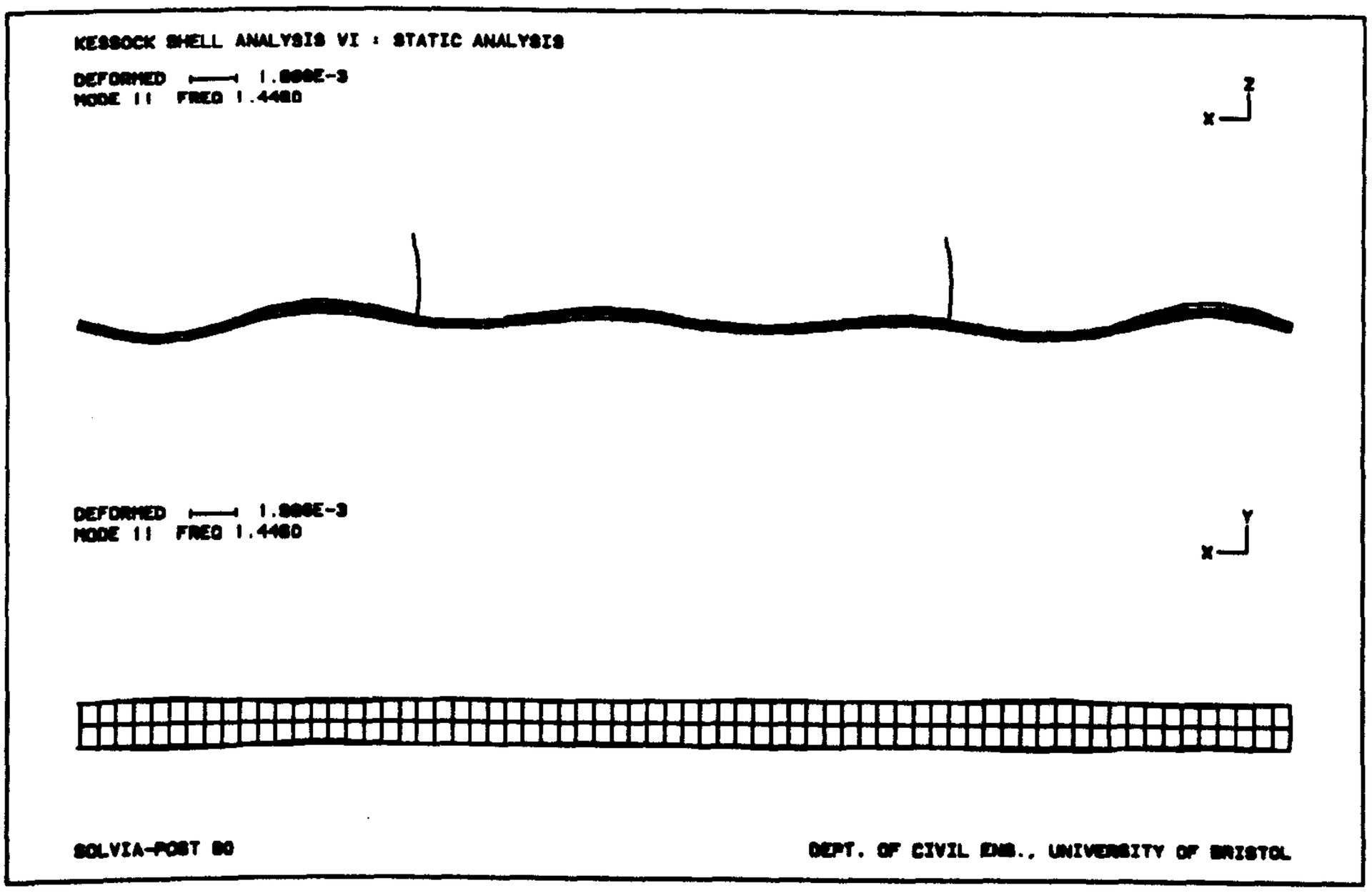

Figure 7.38g -:- Predicted Vertical Mode And Natural Frequency, Beam Shell Model

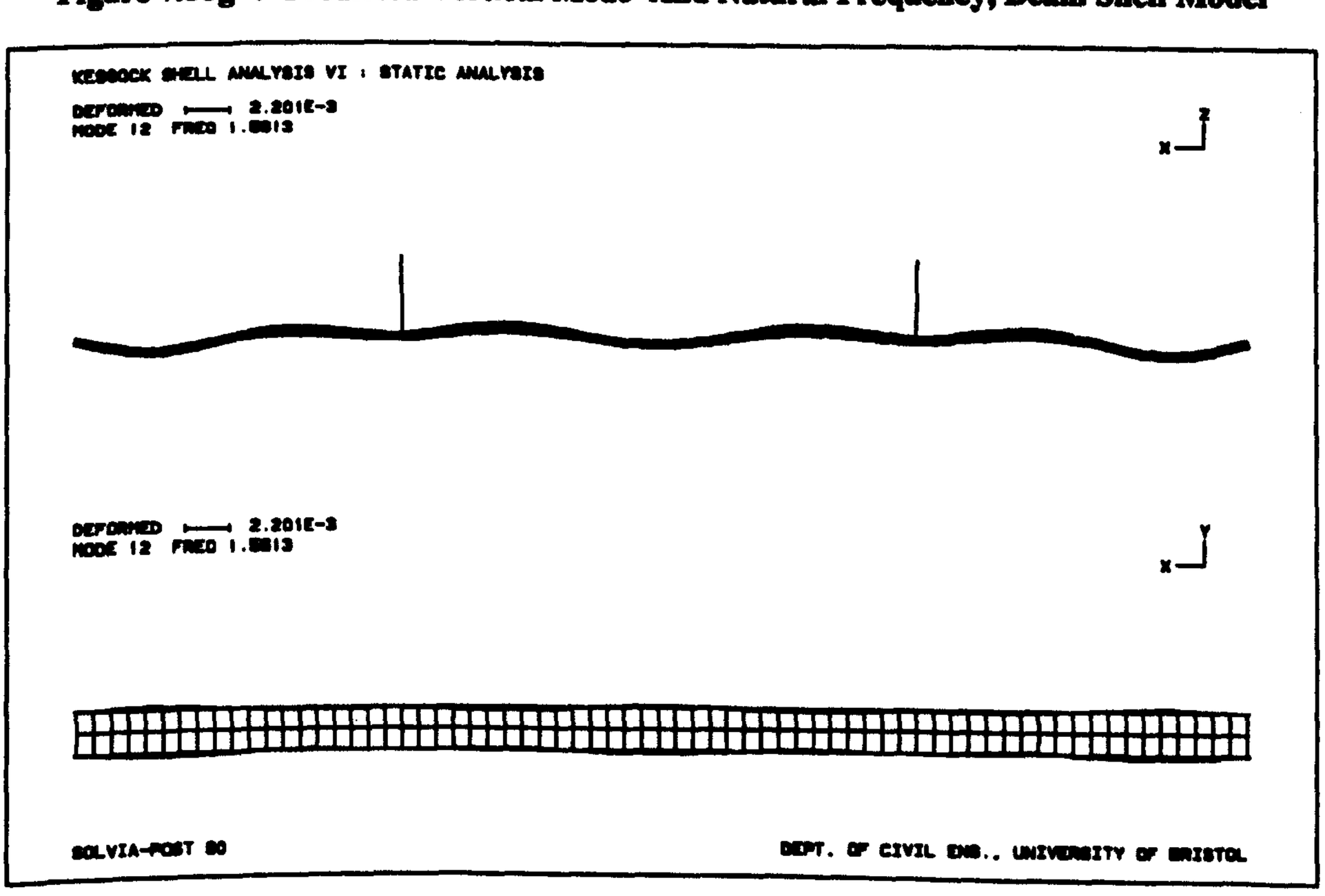

Figure 7.38h -:- Predicted Vertical Mode And Natural Frequency, Beam Shell Model

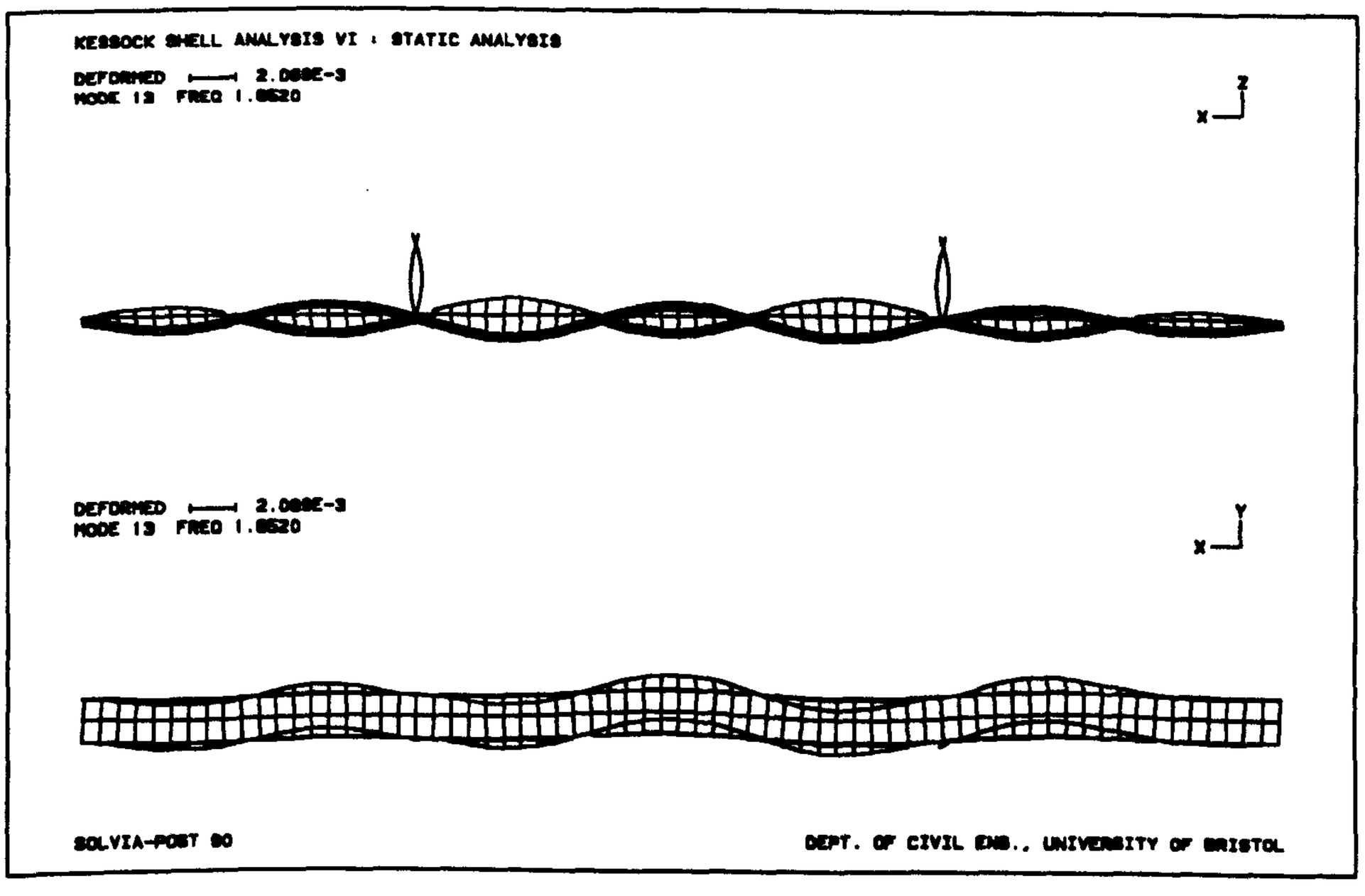

Figure 7.38i -:- Predicted Third Torsional Mode And Natural Frequency, Beam Shell Model

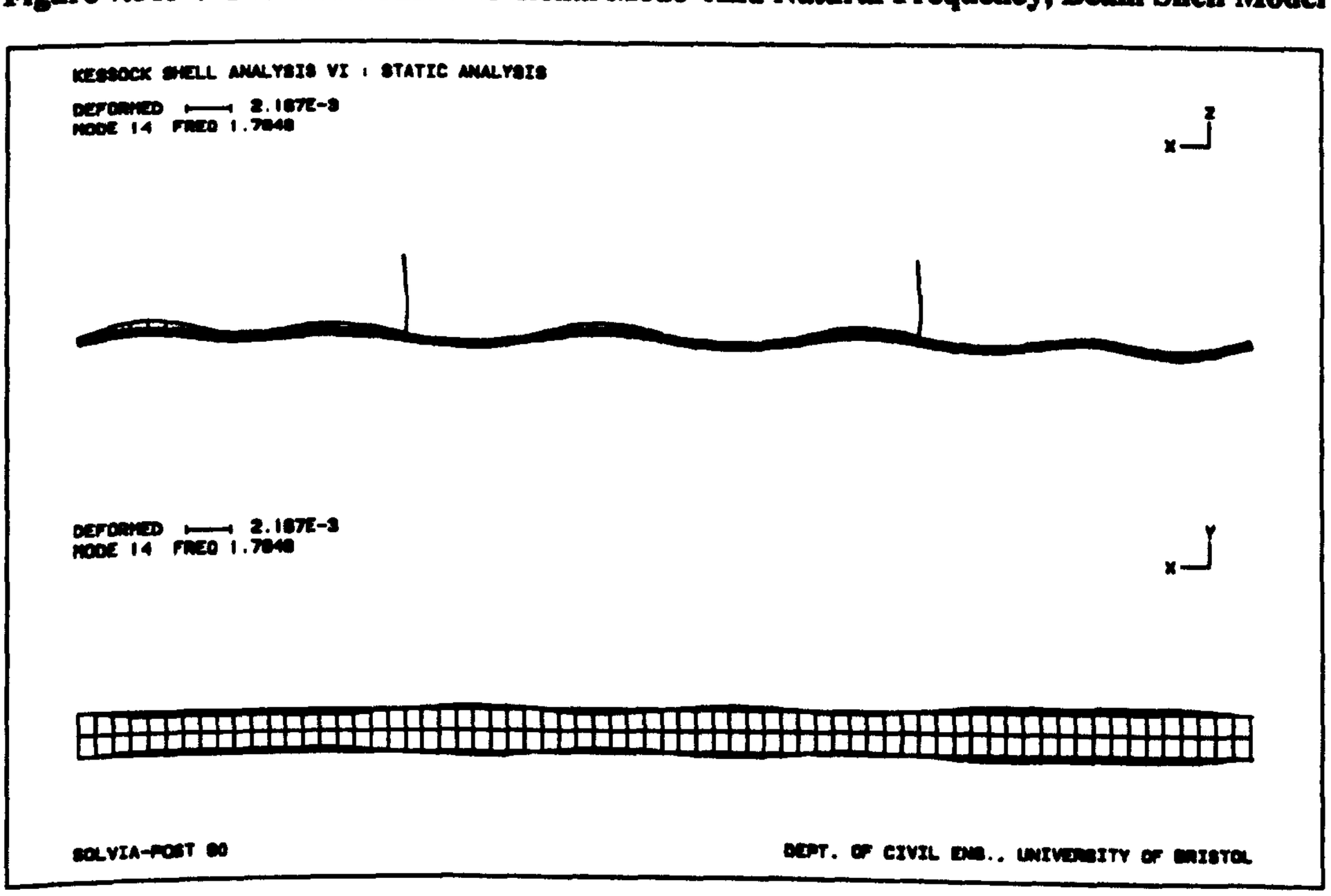

Figure 7.38j -:- Predicted Fourth Vertical Mode And Natural Frequency, Beam Shell Model

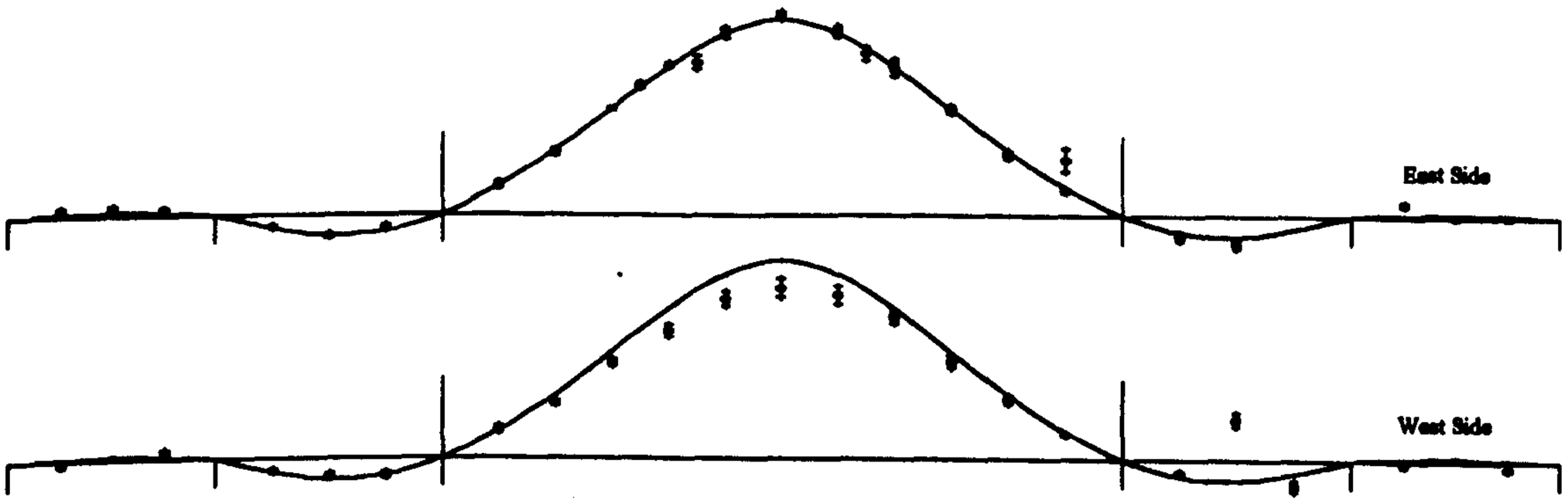

Figure 7.39a -:- Comparison Of Measurements And Predictions For Mode One

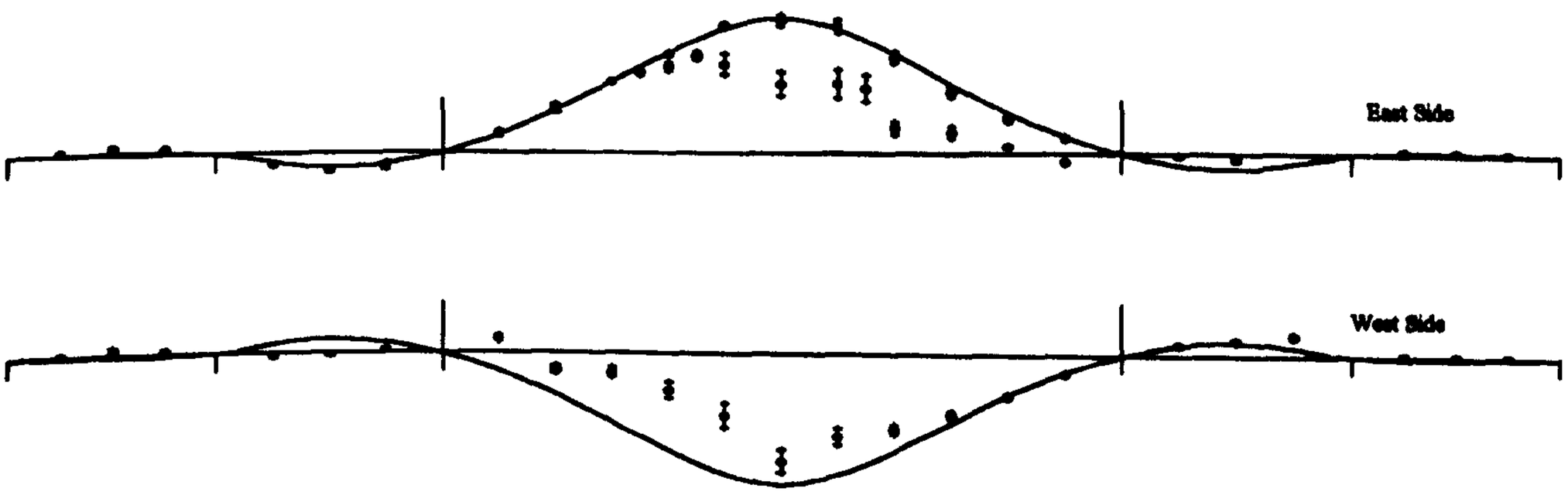

Figure 7.39b -:- Comparison Of Measurements And Predictions For Mode Two

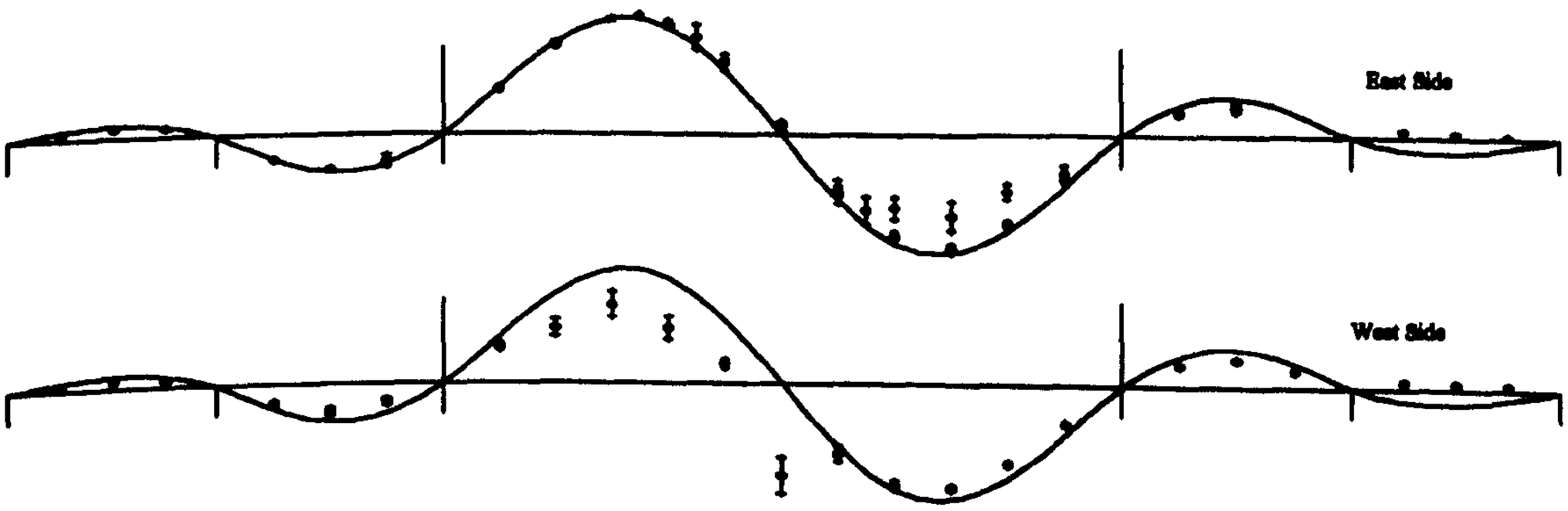

Figure 7.39c -:- Comparison Of Measurements And Predictions For Mode Three

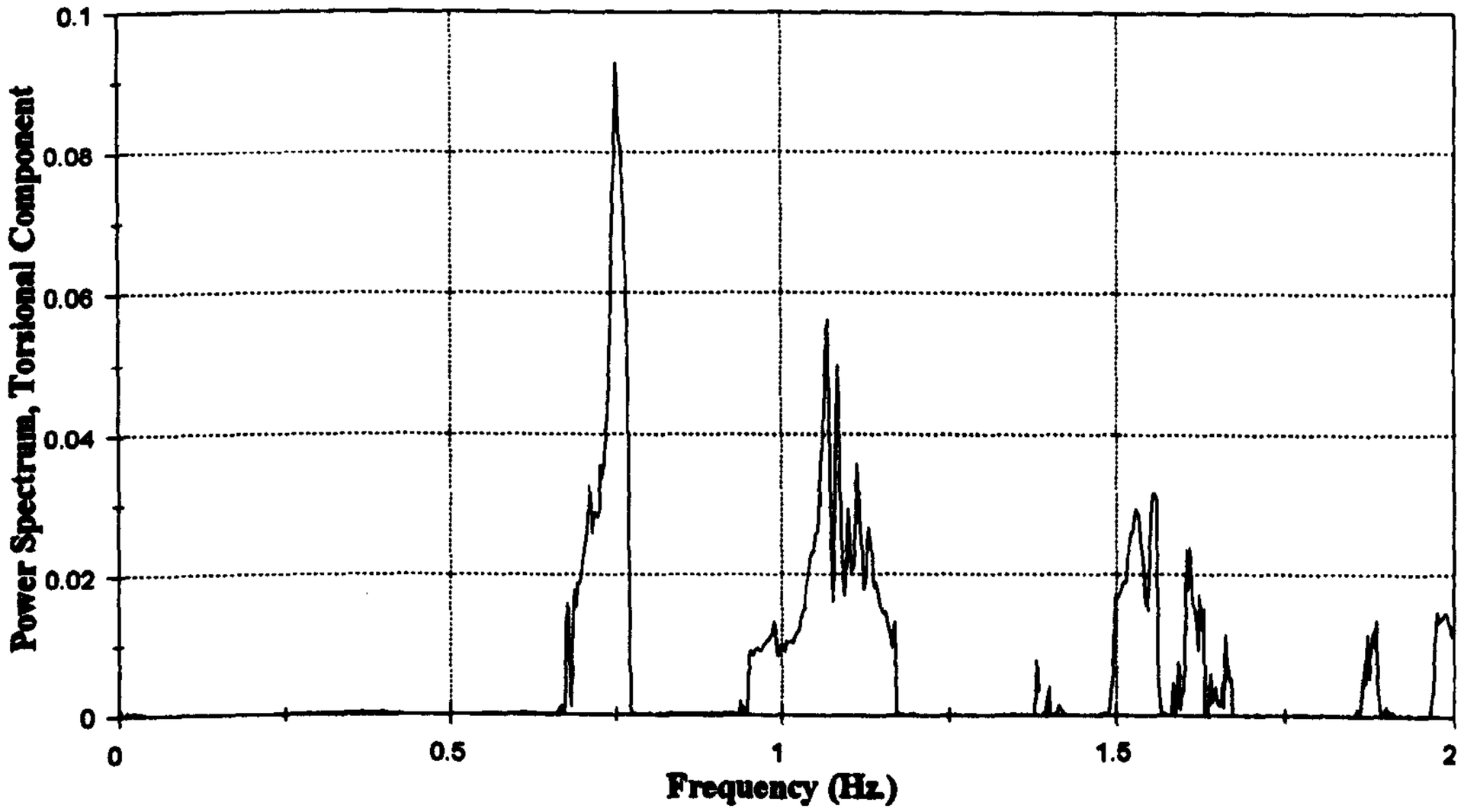

Figure 7.40a -:- Torsional Component Of Deck Response

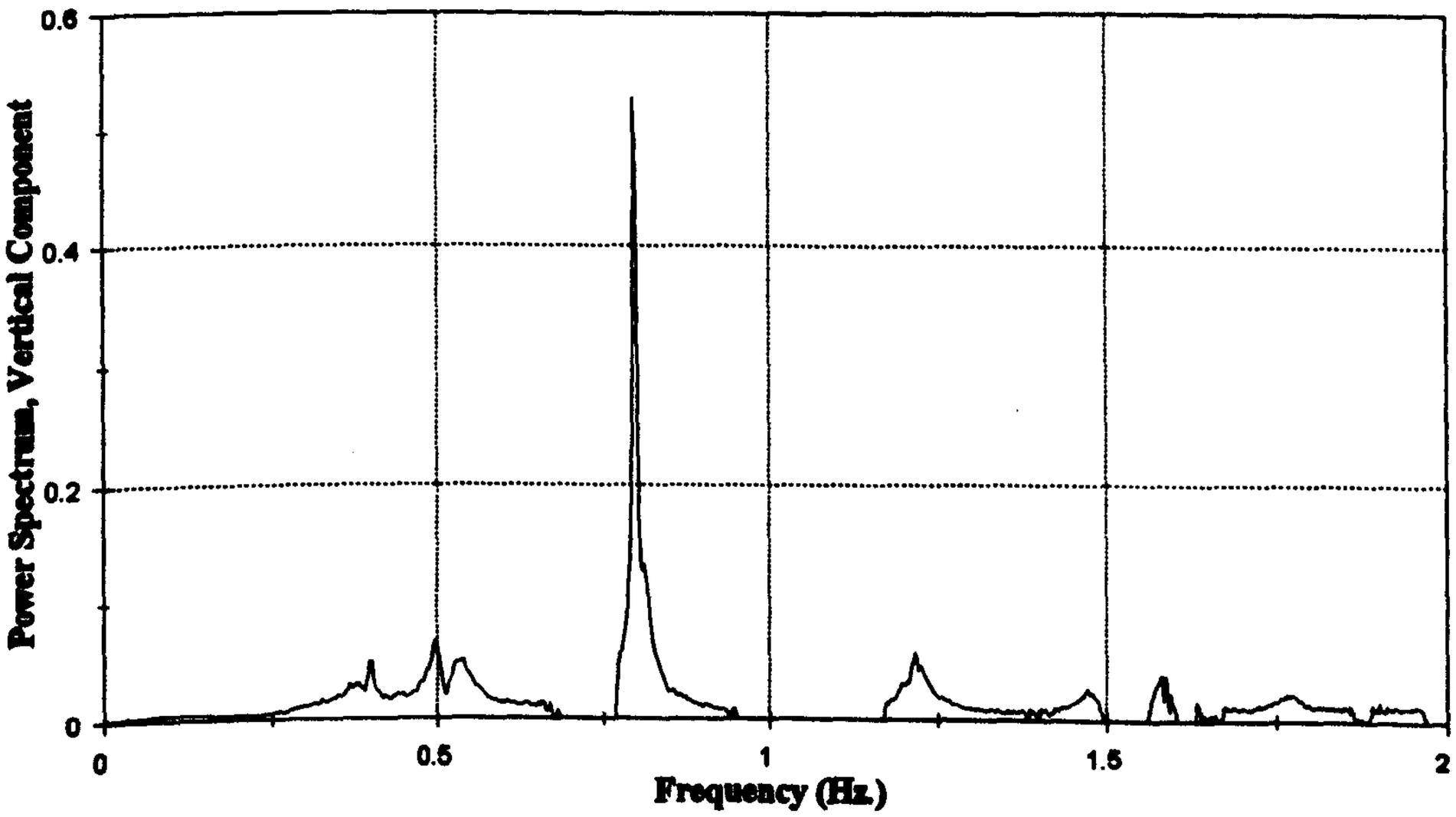

Figure 7.40b -:- Vertical Component Of Deck Response

Figure 7.83

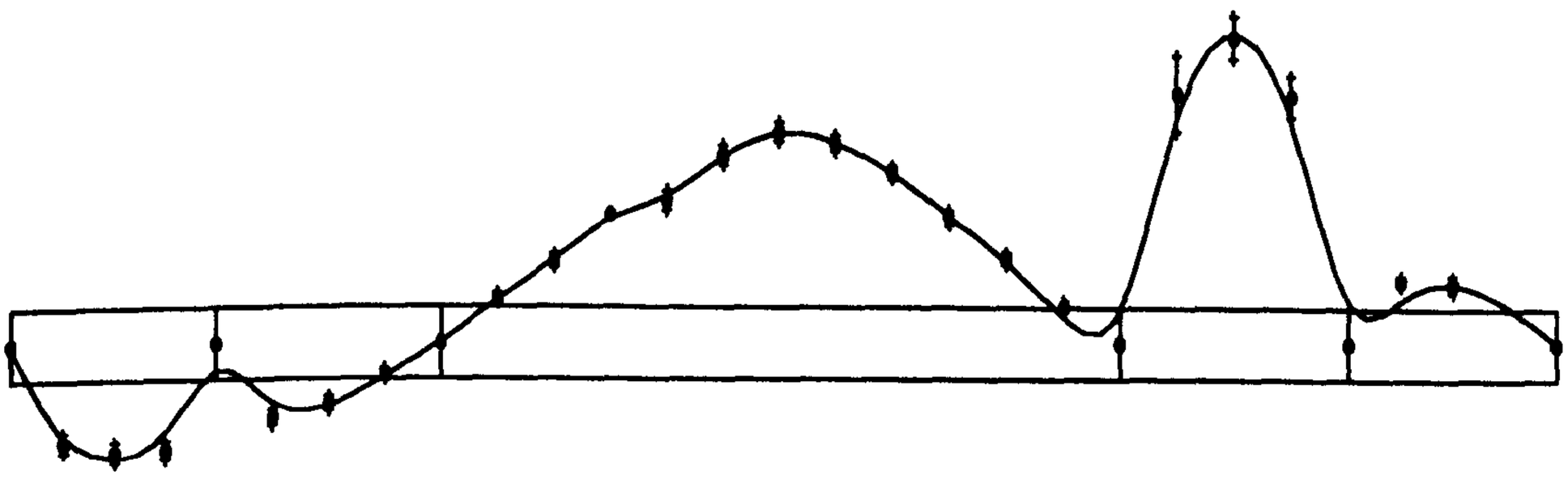

Figure 7.41 -:- Typical Measured Lateral Mode Shape

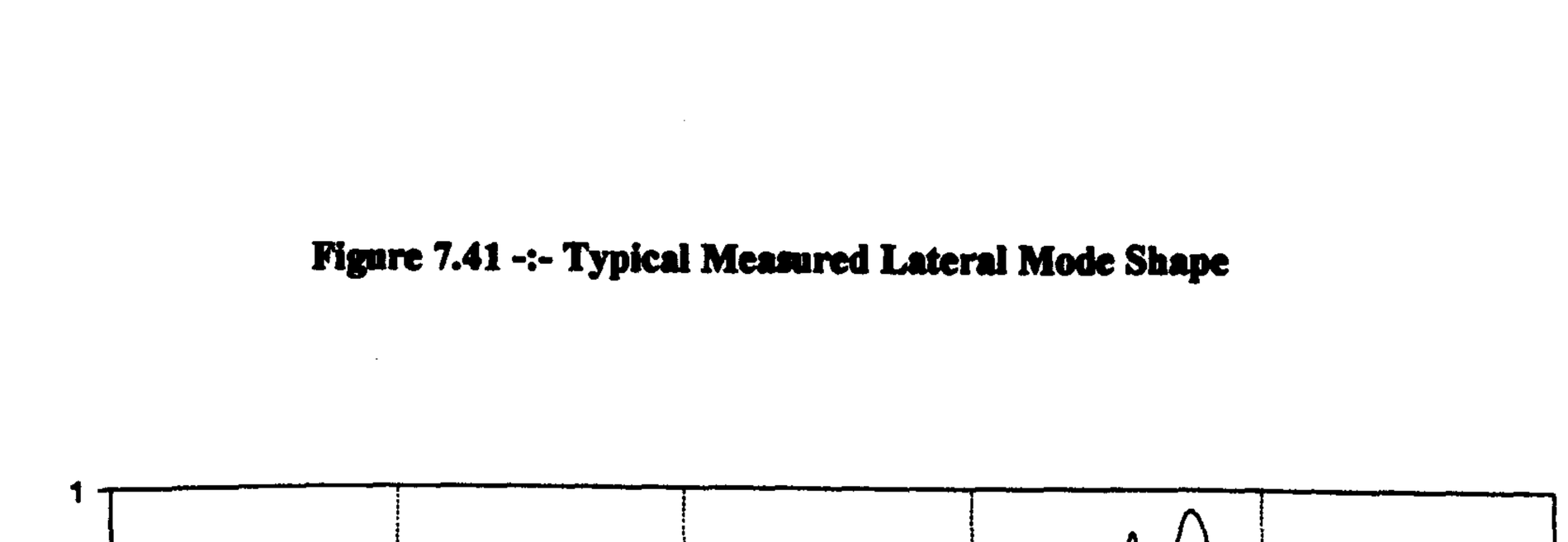

Figure 7.42 -:- Coherence Spectrum Between Horizontal And Vertical Response

Figure 7.84

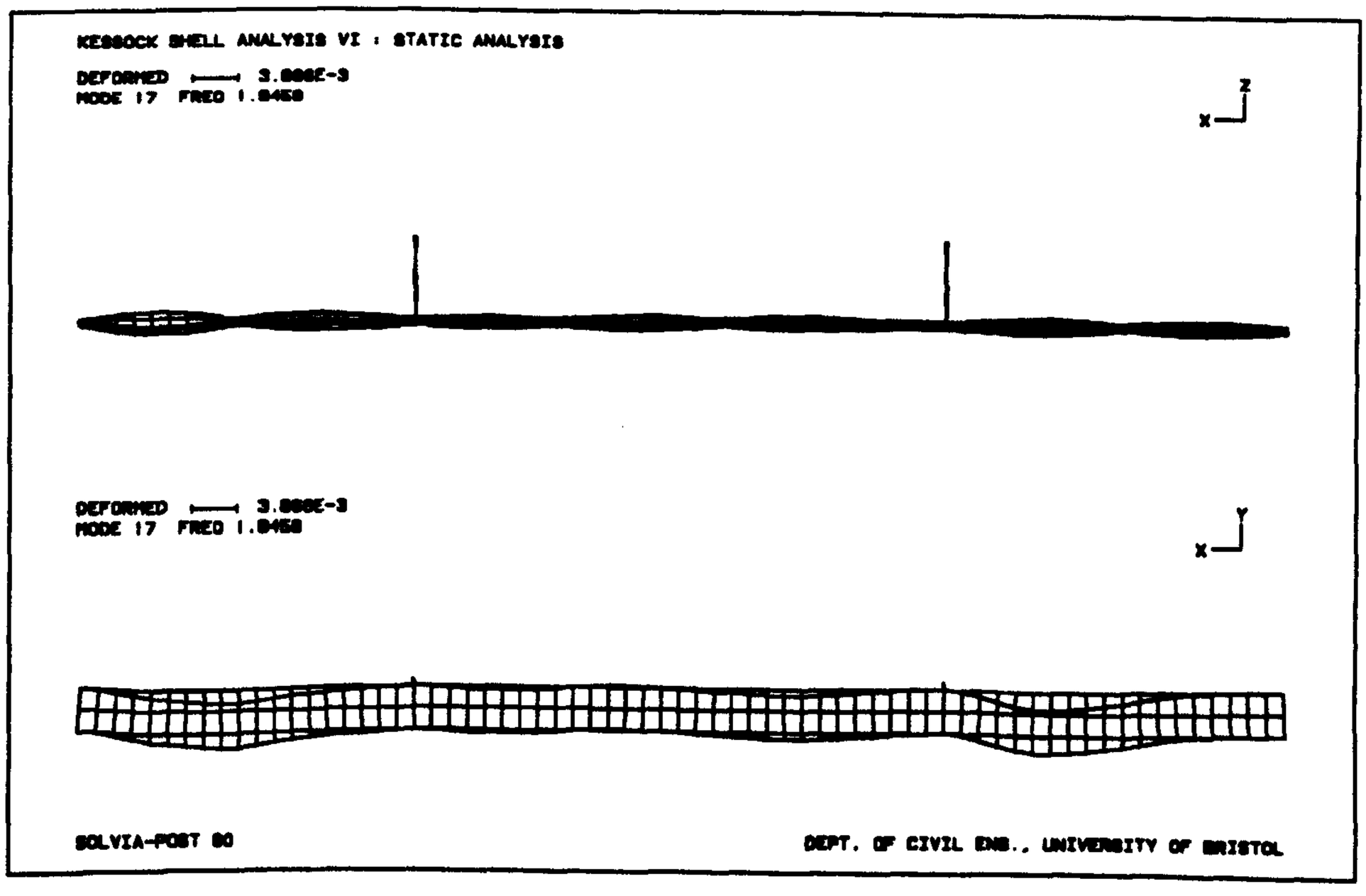

Figure 7.43 -:- Typical "Flapping" Of Lower Flange In Higher Modes

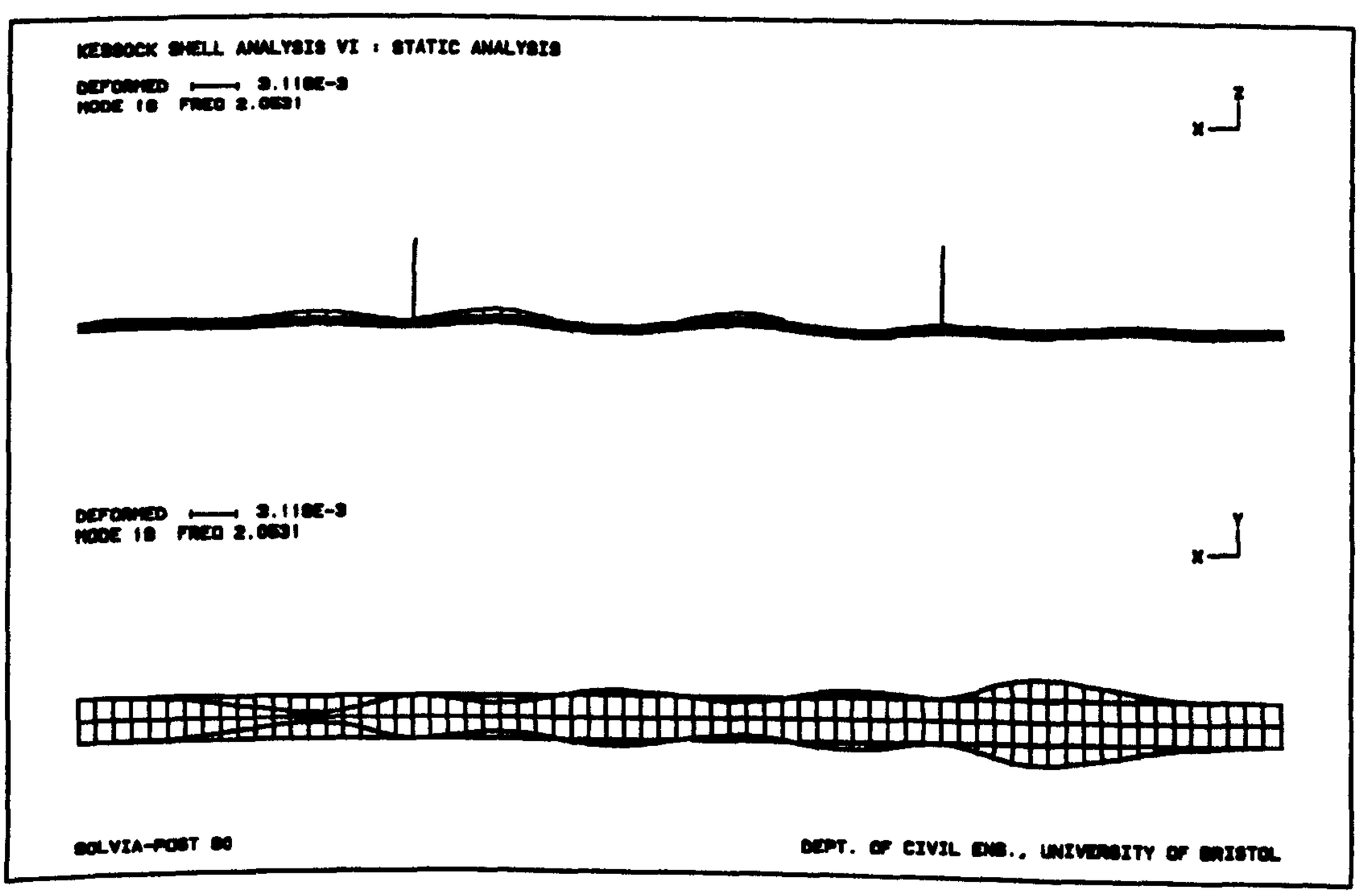

Figure 7.44 -:- Typical "Breathing" Of Lower Flange In Higher Modes

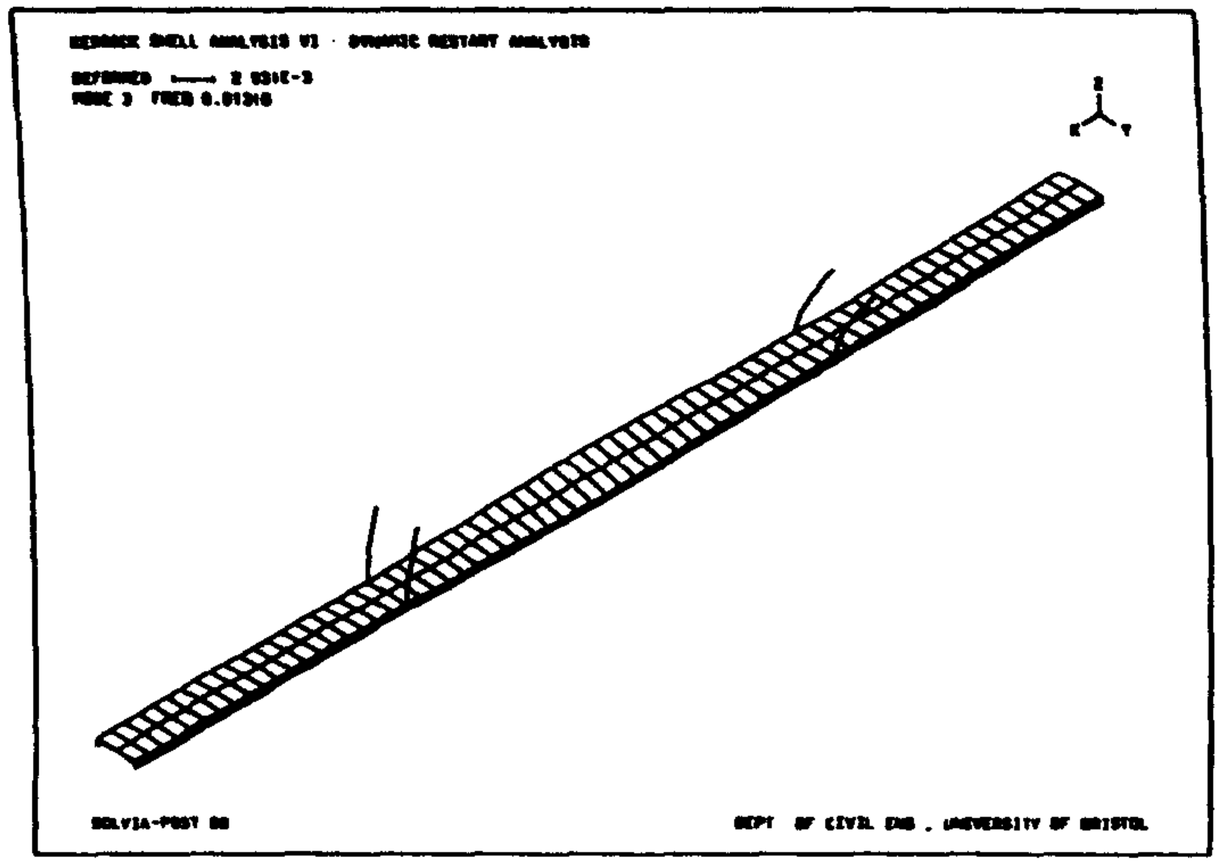

Figure 7.45a : Predicted First Pylon Mode

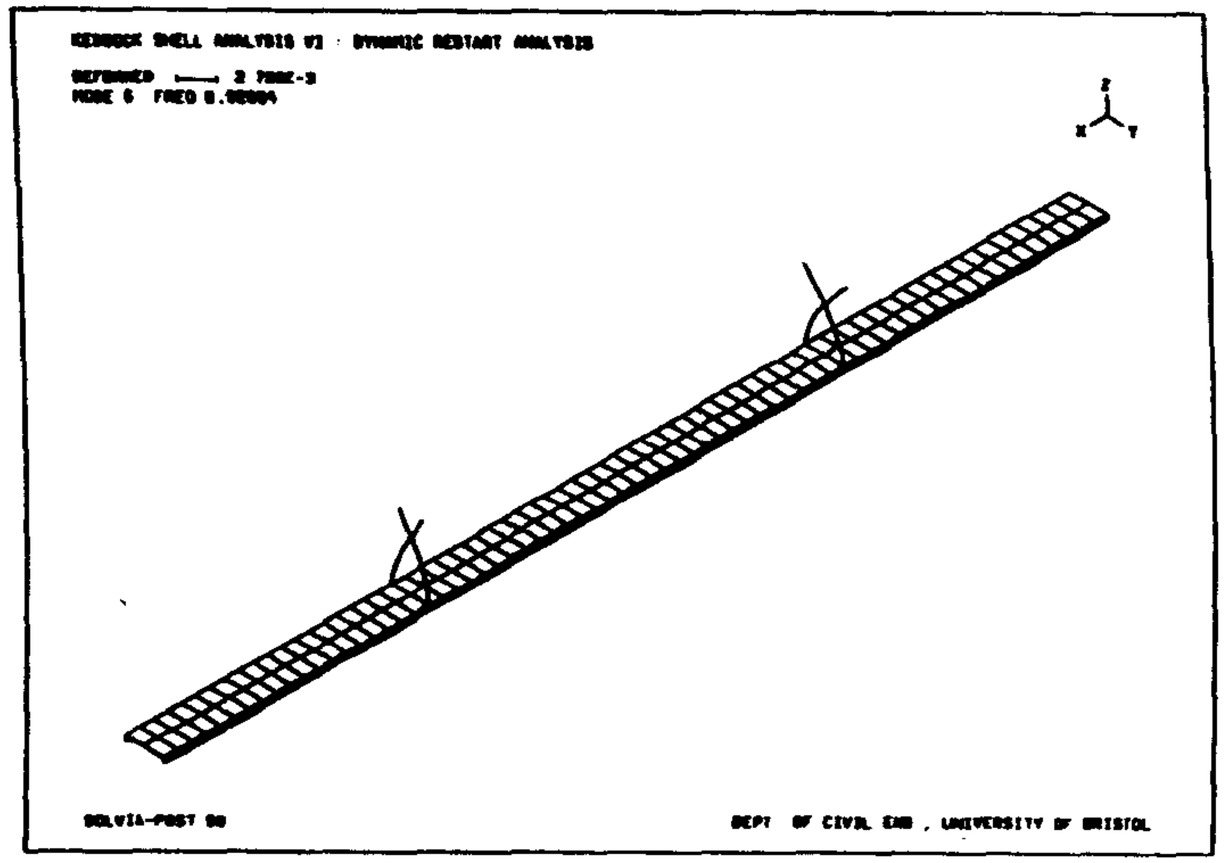

Figure 7.45c : Predicted Third Pylon Mode

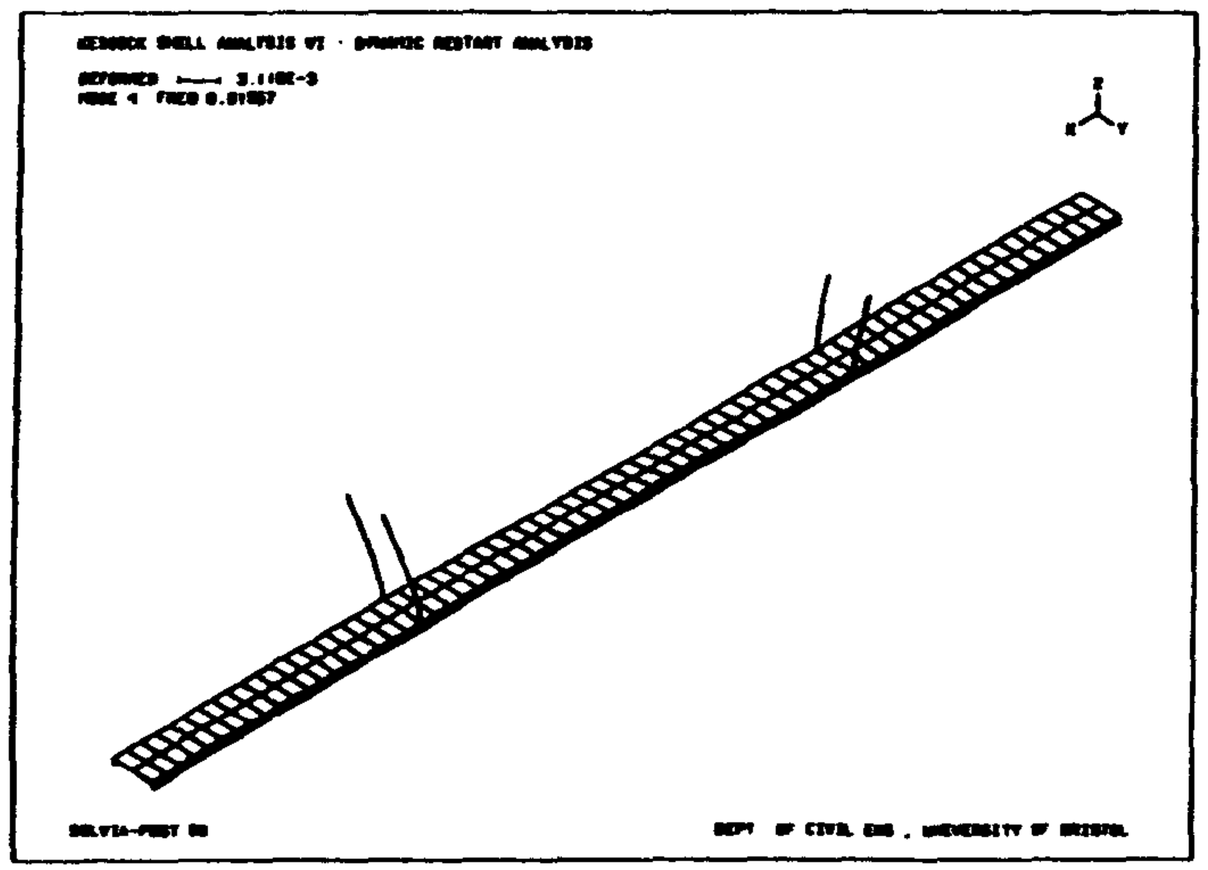

Figure 7.45b : Predicted Second Pylon Mode

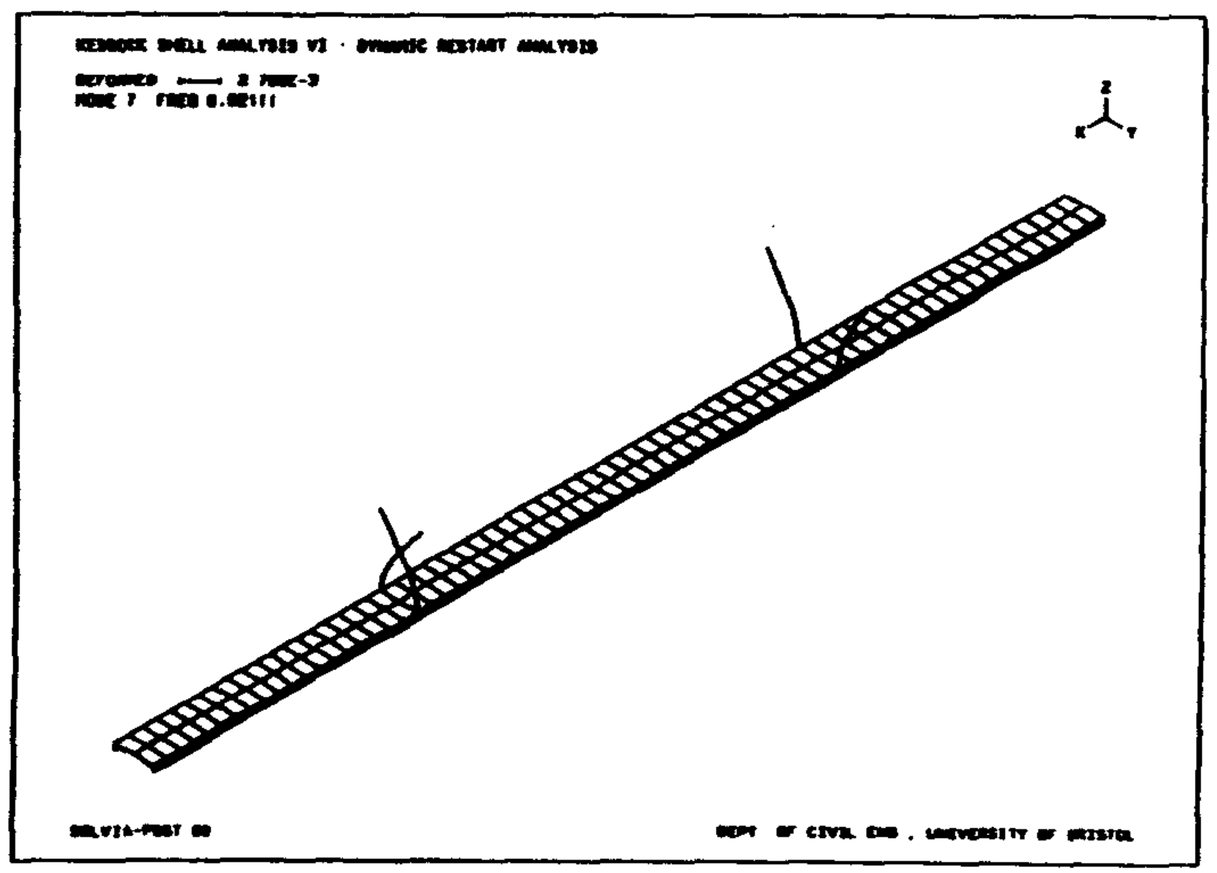

Figure 7.45d : Predicted Fourth Pylon Mode

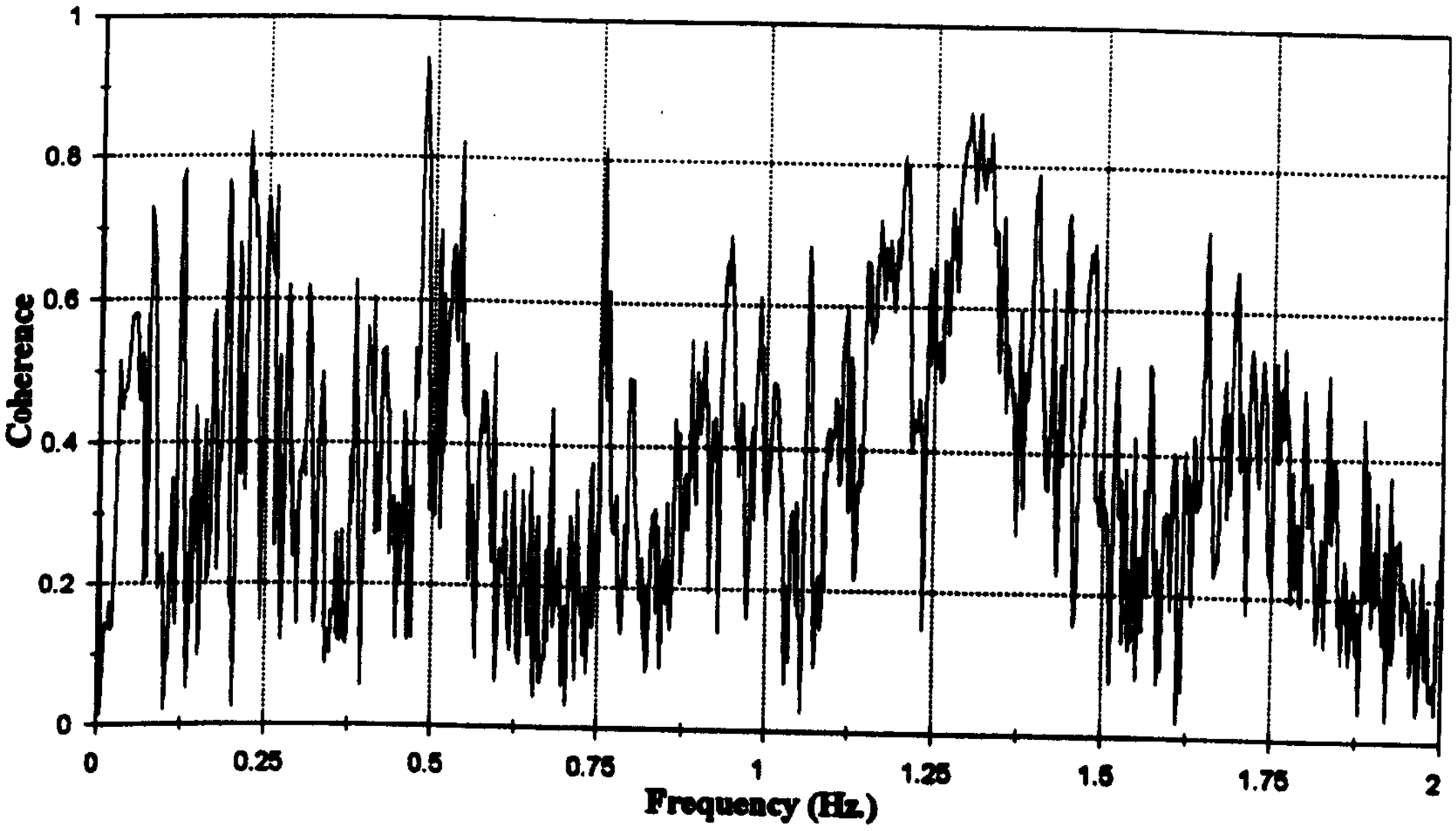

Figure 7.46 -:- Coherence Spectrum Between Transverse Acceleration At Pylon Tops

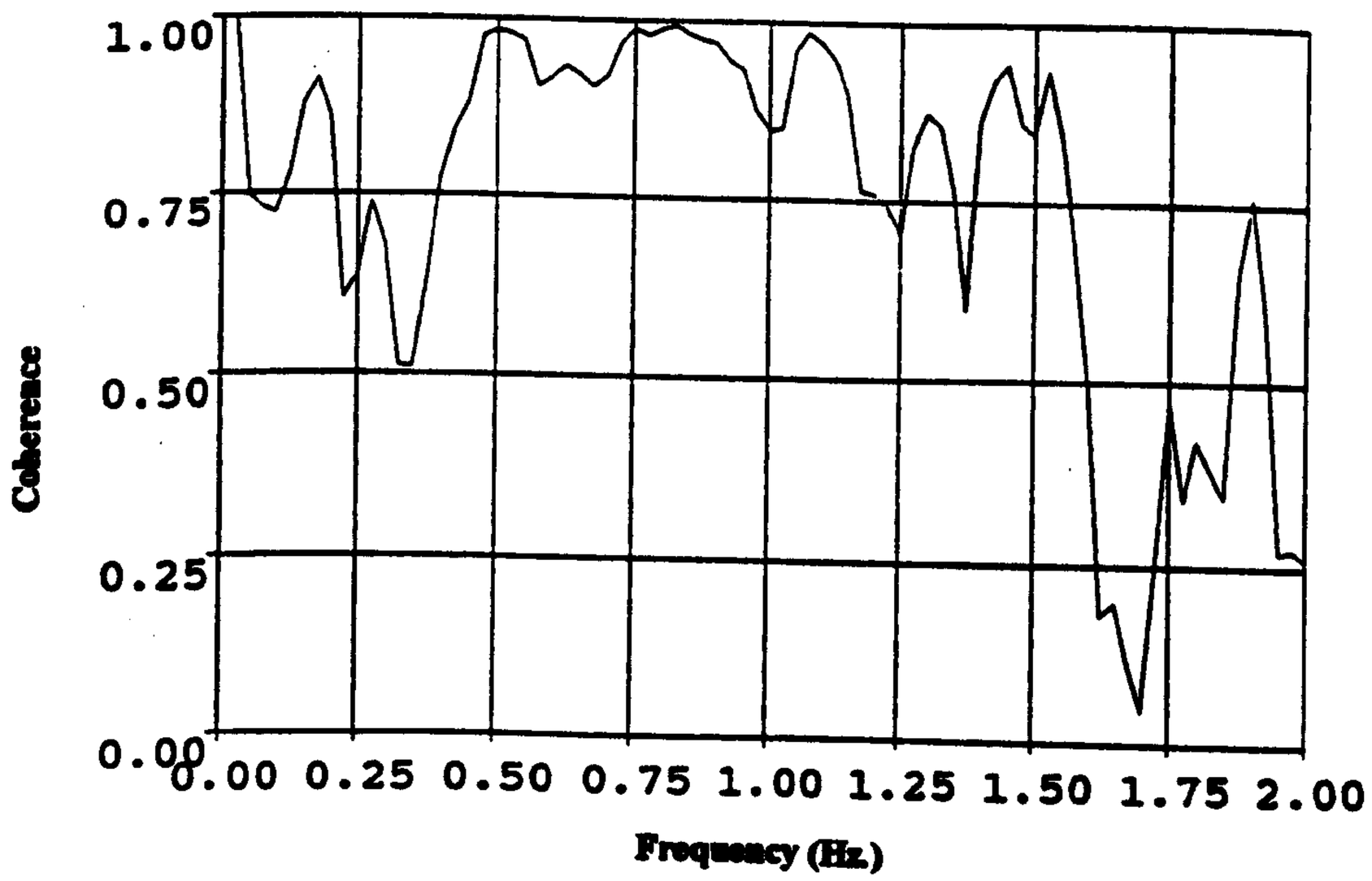

Figure 7.47 -:- Coherence Spectrum Between Longitudinal Pylon and Deck Responses

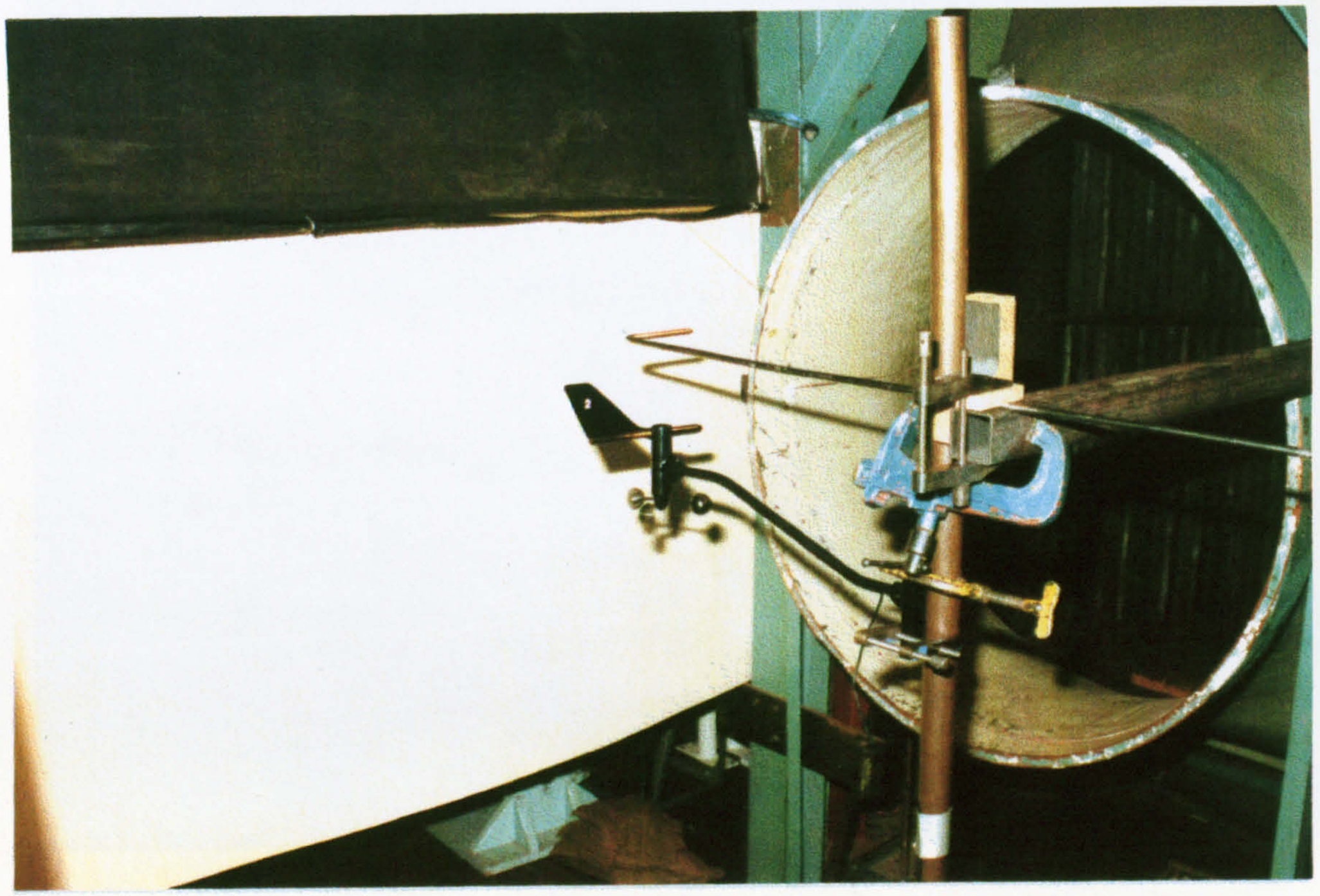

Plate 7.1 : Anemometer Set up in Open Section Wind Tunnel for Calibration

Plate 7.2 : Anemometer Mounted on Lamp Standard

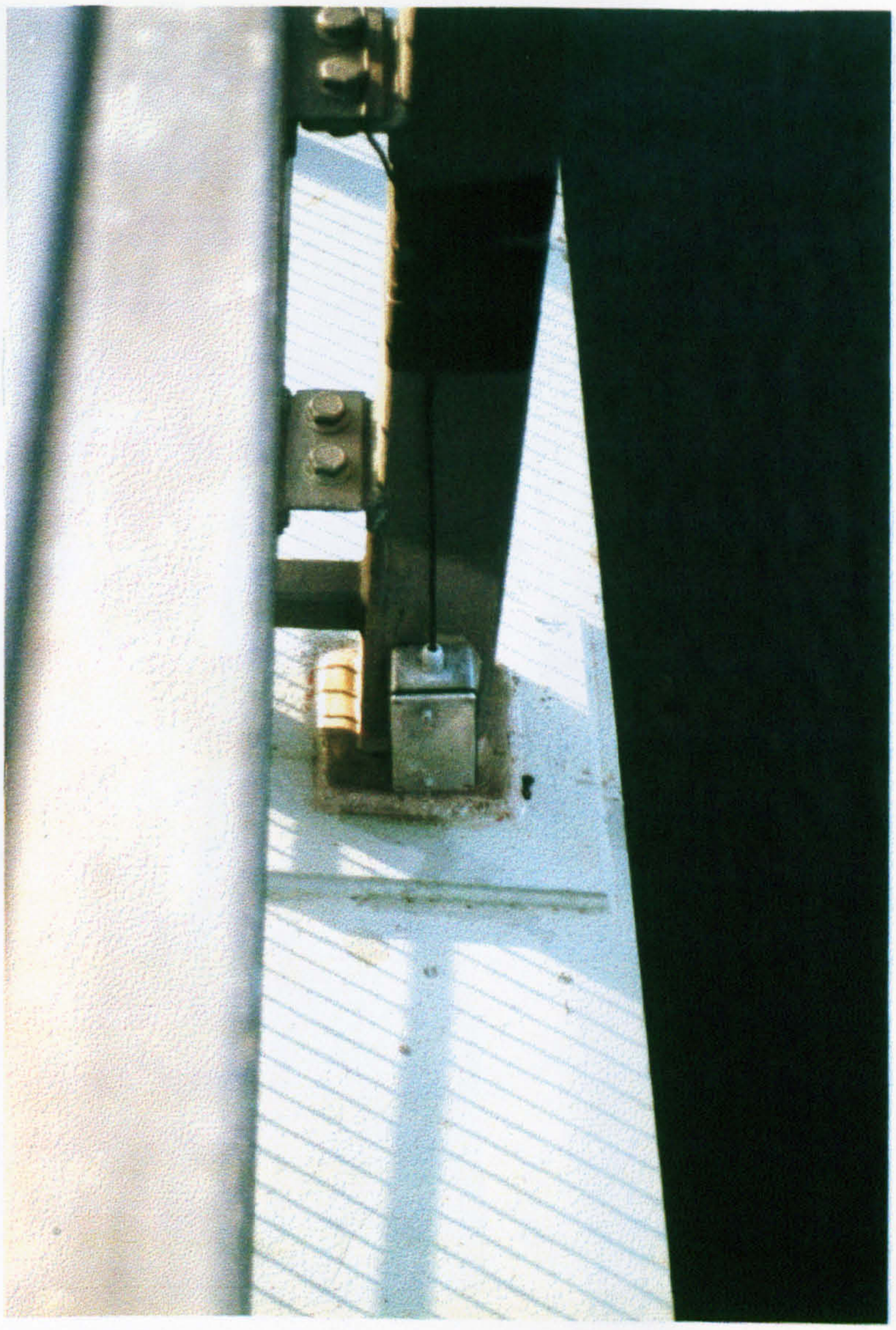

Plate 7.3 : Accelerometer Mounting to Measure Vertically at Mid Span

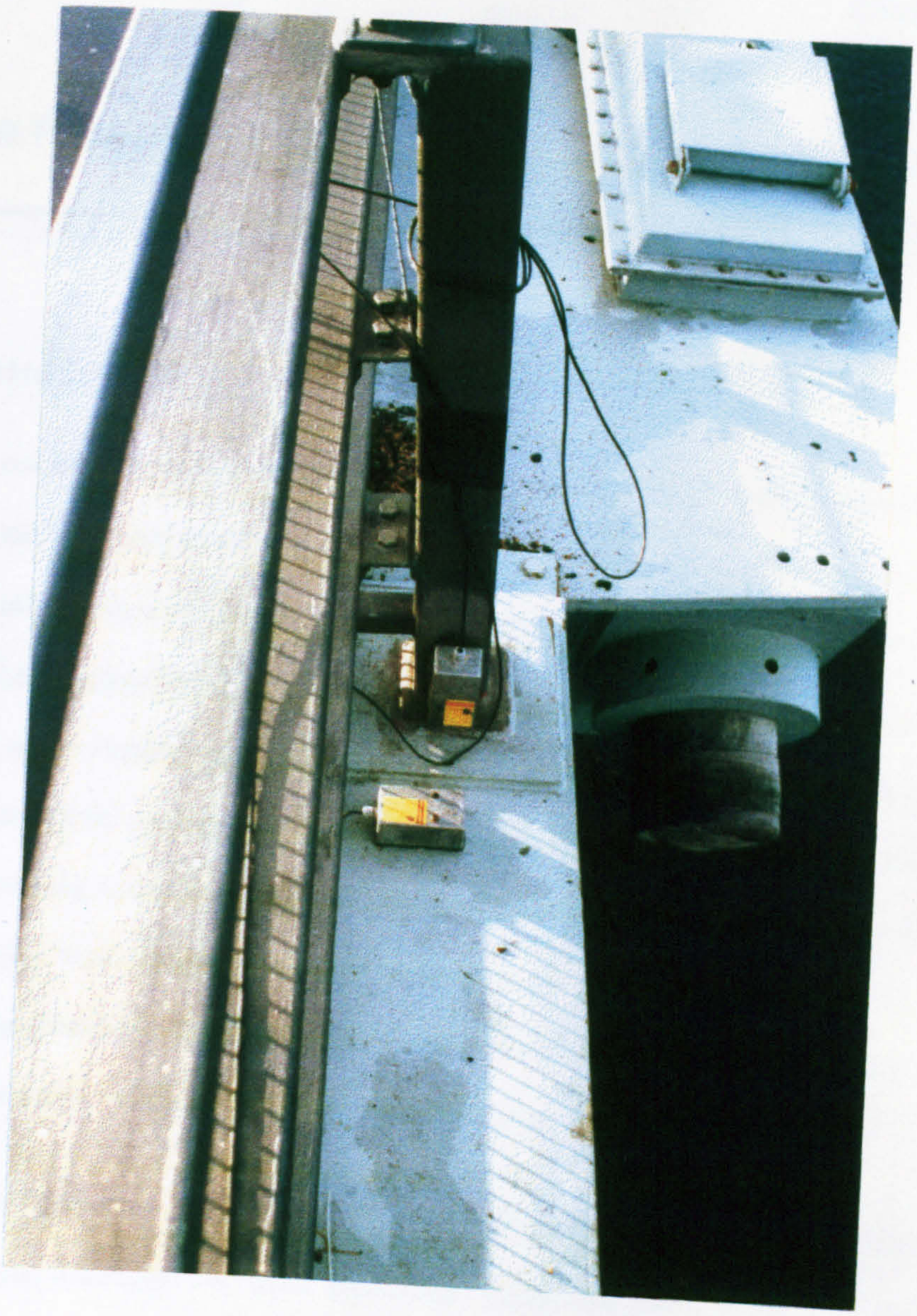

Plate 7.4 : Accelerometer Mountings at 50 m Point

Chapter Eight

The Response Of Cable Stayed Bridges To Wind Excitation: Results Of Prototype Testing

8.0 Introduction

Chapter seven has described the prototype testing of Kessock bridge which involved both a modal survey and the long term monitoring of the response of the bridge to wind excitation. The long term monitoring of the bridge was successful in recording wind and bridge response data continuously for 5 months, yielding approximately 4.5 GBytes of raw data. It is now necessary to process these data, making use of the dynamic properties measured during the modal survey, to obtain usable results. One of the aims of the exercise was to validate the power spectral approach to analysing the response to spatially varying dynamic excitation. Therefore, the goal of the data processing is to typify the spatially varying wind excitation as a two dimensional power density spectrum and to correlate this with the bridge response. As a step towards this, it is useful to find simpler measures of the spatial structure of the wind which can then be correlated with the bridge response.

The purpose of this chapter is to present the data processing which has been performed to date, and to outline areas and techniques for further processing. Firstly, the trends in the average data recorded during the exercise will be described in order to present an overview of the wind regime on the bridge. The techniques used for processing the raw data will then be discussed, and the results from some of the records presented to show whether spatial variations in the wind excitation are important. Finally, several periods of large amplitude response which occurred during the exercise due to vortex shedding

will be described, and the consequences of these discussed, both for the work presented to date and for the bridge itself.

8.1 Processing of the Average Data

The monitoring strategy described in §7.2.3.1 involved performing a small amount of processing on site to decide whether or not to save the raw data collected during a given 10 minute period. The averages calculated during this processing; the mean wind speed and direction, the turbulence intensity, and the mean and variance of the bridge response; were saved to disk regardless of whether or not the raw data itself was saved. Hence, these averages form a record of the general wind regime and bridge response for the complete monitoring period. They also provide useful information about the effectiveness of the monitoring strategy and the validity of the assumptions which underlie the processing of the raw data. Therefore, it is important to consider the trends in these data and their implications.

8.1.1 Distribution of Wind Speed and Direction

Figure 8.1 shows the distribution of all the events recorded during the monitoring exercise plotted against the wind speed and direction. Clearly the wind regime is dominated, as expected, by the westerly and south westerly winds which represent the prevailing airflow in the United Kingdom. Of course, not every one of these records was stored during the exercise, and the distribution of those that were is shown in figure 8.2. This shows that the monitoring strategy was successful in storing a more uniform distribution of records, yet the data stored were still dominated by the prevailing winds. It also indicates that the wind tended to follow the direction of the Firth, there were very few occurrences of the wind coming either from the north or south because of the shelter provided by local

hills. Therefore, the wind was nearly always approximately normal to the bridge axis. Figures 8.1 and 8.2 also illustrate the reduction of data storage achieved by applying the strategy; only one third of the recorded events were stored. Even with this amount of reduction the cost of storing and managing the data was high compared with the additional information obtained. It must therefore be concluded that some kind of monitoring strategy is not only helpful but essential if problems of having too much data are to be avoided.

It is also informative to consider the distribution of the mean wind speed (figure 8.3) and direction (figure 8.4) with time; on average between 130 and 140 events were recorded each day, and so the record number represents a rough measure of time. These figures indicate that the winds on the bridge were generally light and predominantly from a westerly direction. The average wind speed over the whole monitoring period was only 7.73 m s^{-1} and there were even periods of several days when there was almost no wind at all. However, it is also important to note that the higher, and therefore more critical, wind speeds occurred for short periods, often less than a day. A typical one of these "storms" occurred on 24/12/91 (figures 8.5 and 8.6) and during this storm peak wind speeds were maintained for only a few hours; the whole storm is contained within records 6800 to 6950 and therefore lasted less than a day. Comparing figures 8.5 and 8.6 it can also be seen that the wind direction swings abruptly through 90° from an approximately westerly to a northerly direction at the end of the period of highest wind speeds. This indicates that a low pressure system (cyclone) has passed to the north of the bridge. The occurrence of large storms, and their effect on the structure could be important factors in determining future monitoring strategies and this will be discussed further in § 8.1.4.

8.1.2 Variations in Turbulence Intensity

One of the averages stored for each of the 10 minute events was the turbulence intensity as defined by equation 6.12, and since turbulence is a principal cause of spatial variations in the wind this is very relevant to the work in hand. Furthermore, as discussed in §7.1.1, one of the reasons for choosing Kessock bridge was the expected variations in turbulence with wind direction. The values of turbulence intensity calculated during the monitoring are shown in figure 8.7 plotted against wind direction. There is no discernible trend in this figure since there are so very few readings from easterly winds. However, smoothing the data by averaging points in 1 degree bands reveals that easterly winds are indeed noticeably less turbulent than westerlies (figure 8.8). The averages also show that there appeared to be little correlation between the turbulence intensity and the wind velocity (figure 8.9) which is in keeping with the findings of other researchers [Bocciolone *et al.* 1991]. However, a key assumption in the monitoring strategy was that spatial variations in the wind, and hence turbulence, would be the similar for winds with the similar speeds and directions. Figures 8.8 and 8.9 indicate that this assumption is not valid and the implications of this will be discussed in §8.1.4 and in the account of the detailed processing.

8.1.3 Variations and Trends in the Bridge Response

The average data saved during the monitoring exercise also included the mean and variance of each of the accelerometer channels, and these data can now be used to identify some of the more general trends in the bridge response. Each of the accelerometer records has mean and fluctuating components (figure 8.10). The mean acceleration signal ought to be zero, but, as mentioned in §7.2.2, long term movements of the bridge can cause a drift in the output from the servo accelerometers. Typical smoothed traces for the mean accelerometer signals show clear periodic trends in both vertical

and lateral directions (figure 8.11) with a period of c. 132 records. As noted above, between 130 and 140 records were recorded each day and these trends were therefore probably caused by daily temperature fluctuations between day and night. These are superimposed on much longer term trends (figure 8.12) which were caused by several factors including seasonal variations in temperature. It is interesting to note that these long term trends are most significant for the horizontal accelerometer and, because of the orientation of the instrument, this indicates that these trends are predominantly due to a twisting of the bridge deck.

The variance of the accelerometer signals represents the mean square dynamic response of the bridge and is of greater interest and importance for the study in hand. The variation of the dynamic response with time (figure 8.13) shows that events with a larger response occur as spikes in an otherwise flat trace. Typically these spikes represent the response to storms such as that described earlier (figure 8.14) though some do represent the response to vortex excitation and these will be considered separately in §8.4. Looking at the response for periods between storms, there was a clear daily cycle in the bridge response (figure 8.15) which corresponds to the day night cycle of traffic loading. (It is interesting to note that weekends, when the density of traffic is much lighter, can be identified from figure 8.15). However, the response of the bridge to traffic loading was significantly less than the response to high winds. Indeed, the variation of the bridge response with wind speed shows a steep rise above 10 m s^{-1} (figure 8.16) which is even more apparent when the data is smoothed (figure 8.17). The trend of rising response is broken by a scatter of points with very high response in the range 20 - 23 m s^{-1}; these represent the response to vortex excitation mentioned above and will be discussed in more detail in §8.4. The variation of response with wind speed has two important consequences for the detailed processing of the raw data records; for all events where the response to

wind excitation is significant it is acceptable to neglect both the response to traffic and the stability of the atmosphere. This second point will be discussed in more detail below.

Finally, it should be noted that it is not possible to relate trends in the response of the bridge to the direction of the wind (figure 8.18) even when the data is smoothed (figure 8.19). The peaks in these figures merely correspond to the directions where the higher wind speeds occurred. However, it should be noted that the highest response was to winds which came from the east, and this will be discussed below when the large amplitude response is considered.

8.1.3.1 Stability of the Atmosphere

In general there are two factors which influence the formation and decay of turbulence in fluid flow, the viscosity and the inertia of the fluid, and turbulence is dependent upon the Reynolds number, which relates these two quantities. However, in the atmosphere other factors can also influence the turbulence of the wind. Since turbulence involves some vertical mixing of the atmosphere the buoyancy and gravitational forces acting on the air have to be considered as well. The effect of vertical movements in the airflow will depend on the relative values of the environmental and adiabatic lapse rates. The environmental lapse rate is the variation of actual air temperature with height and for a given location will vary both from day to day, as the weather changes, and with time of day. The adiabatic lapse rate is a theoretical model of the temperature change that would occur if a pocket of air changed height with no change in its thermal energy. There are three scenarios. If the adiabatic lapse rate is greater, then the density of a pocket of air rising in the atmosphere will increase relative to the surrounding atmosphere, the buoyancy force will be reduced and the air pocket will return to its original height. This represents a stable atmosphere. If the lapse rates are the same then the temperature and density change at the same rate as the surroundings and the forces acting on the

pocket will remain the same. This represents a neutrally stable atmosphere and the body of air will remain in its new location until acted upon by another force. Finally, if the temperature of the pocket changes less rapidly than the surrounding air then the density relative to the surrounding air will reduce with height and the net buoyancy force will increase. In this case the atmosphere is described as unstable.

The stability of the atmosphere is very important and gives rise to several meteorological effects, such as localised temperature inversions. Therefore, when taking dynamic atmospheric readings it is important to have some measure of the atmospheric stability. This is usually achieved using the Richardson number which is a dimensionless grouping of gravitational, inertial and buoyancy forces. This in turn is influenced by the temperature and the humidity since the adiabatic lapse rate is different for dry and saturated air. However, it is generally accepted that for higher wind speeds, typically those above 10 m s^{-1}, the inertia forces are sufficiently high to dominate the turbulent behaviour and the atmosphere can be assumed to be neutrally stable. Since the response of Kessock bridge to wind excitation is small for wind speeds less than 10 m s^{-1} it is safe to neglect the stability considerations.

8.1.4 Comments on the Monitoring Strategy

Having discussed the general trends in the wind regime and bridge response, it is now useful to appraise the effectiveness of the monitoring strategy employed at Kessock and consider the implications for developing future strategies. Although the results of the detailed processing will also give important feedback on the monitoring strategy, it is important that the monitoring strategy is discussed at this juncture since it must involve as little processing as possible in order to be viable.

The monitoring strategy was based on two key assumptions. Firstly, that the spatial structure of the wind would be influenced predominantly by the wind speed and direction, and secondly, that the variations between records in the same speed and direction cell would be tolerably small. The second assumption is especially important since spectral analysis requires the data to be stationary. This means that not only must each record be stationary, but there must not be any variations in the statistics of the records within each ensemble to be averaged. However, it is clear from processing the average data that the turbulence, and hence the spatial variation in the wind, was not constant across each of the cells. This processing has also revealed that it was unnecessary to save data when the wind speed was less than 10 m s^{-1}, since the bridge behaviour for these wind speeds was dominated by the response to traffic. Furthermore, these higher wind speeds occur in storms, and it might therefore be better to classify the wind data in terms of these storms which could then typify design events. These factors are clearly relevant to the monitoring strategy but they were not known before the monitoring project actually started; the results of the monitoring were needed to decide which data should be recorded.

Clearly, the answer to this kind of problem is to introduce feedback to the system so that data which has already been recorded is used to amend the strategy; in effect the system will learn what to look for. To a limited extent, a crude form of feedback was implemented during the Kessock monitoring by manually adjusting the logging strategy, however, it would be far more efficient to make this an integral part of the system. To do this it would be necessary to consider the bridge response in the decision making algorithm, so no data is collected when the bridge response is small, and to use the turbulence intensity as well as the speed and direction to classify the wind.

Two further points need to be made regarding the monitoring strategy. Firstly, it would be useful to be able to write larger amounts of data to temporary storage, allowing them to be both re-read and

erased if necessary. The bulk storage during the Kessock project did not permit this since data stored on the optical disk could not be erased. Secondly, the strategy could be implemented more efficiently by using a second PC to process the results continuously whilst fresh data is logged, thus reducing the dead time which occurs because it is not possible to process and acquire data simultaneously. Of course this problem could be overcome by using a more powerful computer, but this has consequent cost implications.

The amendments mentioned above have been incorporated in a modified monitoring strategy shown by the flow diagram in figure 8.20. In this system, data collection continues whilst the pre-processing is performed, either on a second PC or by using a more powerful machine allowing multi-tasking. The decision whether or not to store the data is made using both the wind data and the bridge response, and the thresholds are adjusted after each cycle to provide the necessary feedback.

The preceding comments need to be qualified by stating that the data that have been collected are far from useless, as will be seen from the rest of this chapter; the aim of this section has just been to highlight some lessons which can be learnt so that they can be applied to future exercises.

8.2 Procedures for the Detailed Processing of the Raw Data

Having looked at the more general description of the wind regime and the bridge response it is now possible to move on and consider the large amount of raw data that was collected during the project. There were two factors which influenced the processing of these data, and these had a bearing both on the logistics of the approach and the numerical methods employed. Firstly, because the project had generated such a large amount of data, and this was stored in a compressed format on more than one disk, a reliable data management system was required. This had to allow the data to be selected,

according to criteria specified by the user, recovered from the disk, and processed, all automatically. Therefore the system needed a detailed knowledge of the average data for each record stored, and to allow data to be selected, either according to these averages or the time it was recorded. Secondly, as became apparent from the processing of the average data, wind speed and direction were not the best measures to classify the data. Hence, a different classification had to be found which was better suited to the aims of the project. This in turn had an effect on the assumptions on which the signal processing was based.

8.2.1 The IMCES Signal Processing System

An important element of the IMCES package being developed by Vann (§7.2.3) is a system that can manage the data collected and perform any signal processing that is required. As in the data collection phase of the project, the development of IMCES was complementary to the work which had to be done to process the data from the Kessock project. Kessock served as a guinea pig for IMCES, providing a set of raw data which could be used to try out the system as it was developed. Conversely, IMCES provided a tool which allowed for flexible, repeatable processing of the large amount of data collected from Kessock. Therefore, since it was mutually beneficial, it was decided to continue the cooperation started during the monitoring phase of the project. It is inappropriate to give a detailed description of IMCES here, however, it is useful to present a brief overview of the main features of the system. A more detailed introduction is given by the system' s designer [Vann 1994].

At the heart of IMCES is an object oriented program written using the KAL programming language which is part of the KAPPA knowledge based system tool kit [Intellicorp 1991]. Since KAPPA is a Windows application, it can link to other Windows applications using Dynamic Data Exchange (DDE) making the complete system potentially very powerful. IMCES makes use of this facility to

incorporate standard packages to perform different aspects of the processing; the database files are stored in dBase format and are managed using ObjectVision [Borland 1991], and the signal processing is performed with the FAMOS package [IMC Meßsysteme GmbH 1992]. The result is a single system which links several commercial packages, each tackling a step of the data processing, from the data management through the signal processing to the final presentation of the results (figure 8.21)

Each of the raw data channels, 4 accelerometer and 16 anemometer, forms a possible input to the system known as a primary data stream. Any process, or combination of processes, can be applied to these data streams ranging from calibrations, to convert the signal voltage to engineering units, through simple arithmetic and statistical operations to more complicated spectral analysis routines. Each of these processes can either be written in C, called from another windows application or developed as a FAMOS sequence; the last allowing full use to be made of the signal processing and mathematical routines available in FAMOS. Using this methodology a signal processing tree can be produced for each of the primary data streams (figure 8.22) on which each node represents an object in itself which can either be processed further or examined as an output. In order to calculate cross correlations it is necessary to process objects from two or more data streams. This is made possible by defining processes which connect together objects from different trees.

There were several advantages gained from using IMCES to process the Kessock data, apart from the convenience factor mentioned in the opening paragraph of the section. Firstly, the system was very flexible, the processing trees could easily be amended so that different procedures could be tried. It was also possible to apply the same tree repeatedly to many different data sets. Again, this lead to greater flexibility and allowed the system to be automated so that large blocks of data could be processed over night. However, the fact that IMCES was still very much in the early stages of

development was a major disadvantage for this project. This meant that not only did the processing have to be developed, but so did the system to perform it. Furthermore, as more complicated signal processing procedures were tried out, greater demands were placed on the system revealing the shortcomings of the KAPPA toolbox. Quite often problems with the software caused major delays to the analysis.

8.2.1.2 Archiving of Data

Before starting on the detailed signal processing, a complete backup of the raw data was made. There were two principal reasons for doing this. Firstly, the data represent the product of much work and expenditure, and are consequently of great financial (and emotional) value. Therefore, it was extremely important to produce a backup of the data so that they would not be lost should any damage occur to the disks. Secondly, the data had been written to the optical disks in the order in which they were recorded; it was not possible to do otherwise. However, this made it difficult to automate the processing of the data because data with similar wind criteria could be stored on different disks; though it is possible to automate the processing it is not yet easy to automate turning disks over in the drive. To overcome both these problems the data were backed up to two new optical disks, and during the backing up they were reordered and stored in order of wind speed. The second set of disks was then used for the signal processing and the originals stored in a safe place.

8.2.2 Data Processing Assumptions

The data processing both of the bridge response and the wind data relied on power spectral techniques. However, for such a spectral approach to be applied there is an axiomatic assumption that the data is stationary, power spectra are not defined for non stationary data (cf. §3.1.3.1). It is

therefore important to be able to justify this assumption otherwise the results obtained from the analysis will have little real meaning. At this point it is useful to remember that the monitoring period of 10 minutes was chosen to fall in the spectral gap (§6.3 & §7.2.3.1) to maximise the likelihood that the wind data would be stationary, although this will not necessarily ensure stationarity. The question of stationarity immediately brings in another key assumption and questions the whole ethos on which the data processing is based. As discussed in §7.3.1 the data will contain errors both due to system effects, bias errors, and due to random variations, random error. The method used to reduce the effect of the random error for the modal survey was to average together several sets of spectral results, so called ensemble averaging. In this approach the results of processing many different records are averaged together assuming that the records represent stationary samples of an ergodic random process. Therefore, if ensemble averaging is to be applied the stationarity condition must hold not only for each of the records, but across the whole of the ensemble.

8.2.2.1 The Run Test

A simple means of assessing the stationarity of the raw data is to use a run test [Bendat & Piersol 1971]. The sample data is divided into a set of N equal time intervals and a given statistic calculated for each interval - in this case the RMS value was used. The median value of these statistics is then found and the observations divided into two classes depending on whether they are above or below the median. The number of runs relative to this median is then calculated, where a run is defined as a sequence of identical observations (i.e. either greater than or less than the median) that is preceded and followed by a different observation or no observation at all. This number of runs is then compared with the expected number for a stationary random process.

A FAMOS sequence was written to perform a run test on a set of data and this was then applied to the wind data records from the Kessock project. Each wind record was divided into twenty 30 second lengths, and the number of runs calculated. For the stationary hypothesis to hold at the 5 percent confidence limit the number of runs must then lie between 6 and 15 inclusive [Bendat & Piersol 1971]. The results of this test showed that, for the runs processed, the majority of the data was indeed stationary as indicated in table 8.1. Typical results are shown for anemometers 4 (figure 8.23) and 7 (figure 8.24).

Two further points should be made regarding the results of the run test. Firstly, it was noted that records which were stationary for one anemometer were not necessarily stationary for all the others. This had an important influence on the processing of the data since calculation of cross correlations between pairs of anemometers assumes that both sets of data are stationary. Secondly,. the run test applied here did not prove to be very robust. Indeed, the stationarity of a given record often appeared to depend on the parameters chosen for the run test. This could explain the discrepancies just noted.

8.2.3 Evolution of the Signal Processing System

The initial intention had been to consider each of the data collection cells defined by the ranges of wind speed and direction as a set of data to be processed using an ensemble averaging technique. However, it soon became apparent that not only were the differences between the records in the cells too great for the different records to be considered part of the same random process, but as outlined in the earlier discussion the trends in turbulence intensity showed that there was a significant variation in the spatial structure between records within a given cell. An attempt was made to process the data using much finer cells, though still defined using wind speed and direction, though even then it was still not possible to obtain reasonable results using the ensemble averaging technique. Therefore, a

change in approach had to be considered and the switch was made to the block averaging procedure. This a smoothing technique that reduces the influence of random errors in spectral analysis by averaging adjacent spectral estimates. Ensemble and block averaging both lead to the same reduction in error [Bendat & Piersol 1971] and are compared schematically in figure 8.25.

The use of block averaging gave rise to a problem in the processing because the length of time that the data had been recorded was only ten minutes. This gave a frequency resolution of only 0.001667 Hz. and so at most six adjacent spectral estimates could be averaged together whilst still maintaining an adequate frequency resolution. This therefore had a limited effect on reducing the random component of the error in the signals. Finally, as time was running out, the decision was made only to process the data which was collected for winds within ± 15° of the bridge beam axis. This reduced the amount of data to be processed and restricted the records considered to those which would have the greatest effect on the bridge.

8.3 The Results of Processing the Raw Data

Having looked at the evolution of the scheme for performing the detailed processing of the raw data it is now possible to look at some of the results. Two aspects will be examined the spatial structure of the wind and the influence that this has on the bridge response. The methods used in processing the data were based almost exclusively on spectral analysis techniques and followed the following basic scheme. First, a calibration was applied to each record to convert voltage values into engineering units. The records were then resampled to give waveforms with 2^n data points so that use could be made of the efficient Fast Fourier Transform (FFT) algorithm. (This step could have been avoided if more thought had been given to choosing the original data sampling rate). Once the FFT had applied the resulting frequency domain wave form was manipulated algebraically as described below.

8.3.1 Frequency Content of Raw Data

The frequency content of the wind can readily be found by calculating the power spectrum from the raw data. However, to compare spectra from winds of different speeds it is usual to normalise the data so that dimensionless quantities are plotted. Several methods have been suggested for normalising the wind power spectra, and for the current discussion a reduced spectral quantity defined by:

$$\text{reduced spectrum} = \frac{nS(n)}{\sigma_u^2} \qquad \text{.....6.1}$$

will be used. A similar reduced frequency will be used defined by:

$$f = \frac{nl}{\overline{U}} \qquad \text{.....6.2}$$

In equation 6.2, l represents a typical linear dimension which is typically chosen to be either the anemometer height or the along wind integral scale. The former allows wind speeds at different heights to be compared, the latter, used by Von Karman, takes account of turbulence. There are two reasons why it is inappropriate to use the anemometer height to normalise the Kessock data. Firstly, the presence of the bridge deck has a marked influence on the turbulence structure of the wind which will therefore correspond neither to the free flow turbulence at the full height (c. 50 m) nor to the height of the instruments above the bridge deck (c. 10 m). Secondly, if the height is measured from the ground, the actual value will vary with the state of the tide which has a range of several metres. However, when an attempt was made to fit the Von Karman spectrum:

$$\frac{nS(u)}{\sigma_u^2} = \frac{4f}{(1+70.8f^2)^{5/6}} \quad : \quad f = \frac{nL_u^x}{\overline{U}} \qquad \text{.....6.3}$$

to the wind data, a very poor correlation was obtained. This was because there were insufficient readings at the low frequency end of the spectrum, indicating once more that the data records were too

short. Hence, the reduced frequencies had to be calculated using an approximate value for the anemometer height, which was taken to be 50 m.

The reduced spectrum was calculated for two records with westerly winds and for one easterly, selected so that the data from each anemometer were stationary. The spectra for each anemometer were averaged together and a block averaging procedure was applied. The spectra obtained are shown in figures 8.26, 8.27 for the westerly winds and 8.28a for the easterly wind. Unfortunately, the lack of low frequency data made it difficult to make comparisons with any of the accepted empirical models for wind spectra.

Although the spectra for individual anemometers are not shown, there was reasonable agreement between the different instruments. However, one point worthy of note is the extra peak which occurs in the response for anemometer 3 for the easterly wind (figure 8.28b). We were informed during installation that the lamp standard on which anemometer three is mounted is often subject to large torsional response; more repairs have had to be made to this lamp than any of the others. This happens because the lamp standard is in the wake of the north pylons. It is therefore probable that the peak in the wind spectrum corresponds to the response of the lamp standard in its torsional mode.

8.3.2 Spatial Coherence of Raw Data

One of the methods for measuring spatial variations in the wind structure is to calculate the coherence spectrum of the wind between records from the different anemometer pairs. It should be remembered from the seismic work in chapter three that the coherence spectrum can be used to obtain a two dimensional power spectrum. Hence, the calculation of the coherence spectrum represents a useful step towards the aim stated in the introduction. This approach was suggested by Davenport and he

proposed an exponential relationship for the spatial cross correlation spectrum (§6.4.2) [Davenport 1961a]:

$$D_{xy}(n) = \frac{G_{xy}(n)}{\sqrt{G_x(n)G_y(n)}} = \exp\left(-\frac{kn\xi}{\overline{U}}\right) \quad \text{.....8.4}$$

where the spatial cross correlation spectrum is related to the coherence by:

$$\gamma^2_{xy}(n) = \frac{\left|G_{xy}(n)\right|^2}{G_x(n)G_y(n)} = \left|D_{xy}(n)\right|^2 \quad \text{.....8.5}$$

By calculating the coherence spectrum for each anemometer pair it should be possible to find a value for the exponential decay factor in equation 8.4 which can then be used to compare the results with the bridge response.

The spatial cross-correlation spectrum defined in equation 8.4 was calculated for each of the records lying within ±15° of the beam axis of the bridge. An exponential decay curve was then fitted to this data using a least squares approach to obtain a value for the exponential decay factor. The results should be a function of both the wind speed and the spatial separation of the anemometers:

$$D_{xy}(n) = \exp\left(-\frac{kn\xi}{\overline{U}}\right) = \exp(bn) \quad \Rightarrow \quad b = f(\xi, \overline{U}) \quad \text{.....8.6}$$

However, when the exponential factors were plotted against the wind speed, the only discernible trend occurred for the closest anemometer pairing (figure 8.29). As the distance between the anemometers increased the data became less well correlated and it was not possible to detect any trend (figure 8.30). This indicates that the spatial separation of the anemometer was too large compared with the eddy structure of the airflow. These results imply that such a phenomenon is unlikely to be important here since, if lateral variations in the wind loading are important, it is the larger eddy sizes which are

likely to influence the bridge response. However, it should be noted that the reduced frequency resolution mentioned above could make it difficult to detect larger eddies and so it is useful to consider the size of eddies actually measured.

8.3.3 Integral Length Scales

As mentioned in chapter six, another measure of the spatial distribution and turbulence of the wind is to calculate the integral length. Teunissen [Teunissen 1980], suggested three approaches for calculating the spectral length from raw data. Firstly, the Von Karman spectral model is defined in terms of the spectral lengths, hence by fitting a curve to the reduced spectrum an estimate of the spectral length can be found. The problems discussed in §8.3.1 regarding the anemometer heights make this method inappropriate for this study. The second approach is to integrate the cross correlation curves directly. This requires extrapolation of the curves to zero, which, as Teunissen points out, is of necessity rather subjective. The third approach is to fit an exponential curve to the normalised spatial correlation coefficient data. This provides an objective extrapolation to zero but ignores the actual shape of the curve. The integral length is then found as the separation distance at which the curve has decayed to 0.368 (i.e. e^{-1}). This third approach was adopted in this study as the most objective approach available.

The covariance function between two processes $X(t)$ and $Y(t)$is defined by:

$$\kappa_{xy}^2 = E\left[(x(t)-\mu_x)(y(t)-\mu_y)\right] = E\left[x(t)y(t)\right]-\mu_x\mu_y \quad \text{.....8.7}$$

The normalised version of this is known as the cross correlation coefficient:

$$\rho_{xy} = \frac{\kappa_{xy}^2}{\sigma_x\sigma_y} = \frac{R_{xy}(0)}{\sigma_x\sigma_y} \quad \text{.....8.8}$$

and as shown is equal to the normalised cross correlation function at zero time, for mean zero processes. Here it should be noted that the mean value of the wind at each location were removed during the spectral analysis so that this simplification could be used. The most effective way of calculating $R_{xy}(0)$ is from the cross spectral density function, G_{xy}:

$$\rho_{xy} = \frac{\int_0^\infty G_{xy}(n)dn}{\sigma_x \sigma_y} \quad \text{.....8.8}$$

The cross correlation coefficients were calculated for each pair of anemometers, ignoring any data which were non stationary. This produced a maximum of 15 sets of results for each record, which could then be plotted against the spatial separation of the anemometer pairs (figure 8.31). A least squares curve fitting procedure was then used to fit the exponential curve through these data points and these then used to calculate the integral lengths as described above. The values calculated were then plotted against wind speed (figure 8.32) and against turbulence intensity (figure 8.33). However, there was no discernible trend in either case. These results were repeated with the easterly winds (figures 8.34 and 8.35) but there was so little data from this quarter that no realistic conclusions can be drawn.

Bearing in mind the discussion of the results from the coherence spectrum analysis it is useful to consider the range of integral lengths calculated for the wind data. The majority of records showed lengths between 20 and 60 m and hence it is not surprising that there were poor results in §8.3.2. However, there were certain records with lengths over 100 m and these could well have an influence on the bridge response.

8.3.4 The Influence of the Spatial Structure of the Wind on the Bridge Response

To measure the influence of the spatial structure on the bridge response it is necessary to find some means of describing the bridge response which will be affected by changes in the spatial structure of the wind. Since one of the likely effects of spatial distributions in the loading is the preferential excitation of different modes, it was decided to use the ratio of the response in different modes to typify the bridge response. In particular the ratios of the response in the first mode to the second and the third modes were used. These were calculated by integrating the power spectra of the response between the appropriate frequencies found from the modal survey and simply dividing the result for mode one by the result from the other modes. However, three qualifications need to be noted. Firstly, since there is a relationship between frequency and acceleration, care has to be taken in making quantitative comparisons between the response in different modes. Secondly, because fixed limits were used in the integration, and because, as pointed out in chapter seven, the natural frequencies do vary, there is inevitably going to be some level of error in the integration. Thirdly, the location of the accelerometer has a key influence on the relative response measured in each mode; therefore, comparisons between the first and second modes were made using the response at mid span, and between the first and third modes using the response at the 50 m point. These ratios were calculated for each of the chosen records in the westerly and easterly directions and the results were then plotted against three factors, the turbulence intensity, the integral length and the wind speed.

For the westerly winds the ratios showed no clear trend, either with the integral length (figures 8.36 & 8.37) or the turbulence intensity (figures 8.38 & 8.39). However, the variations with the wind speed were much less random, especially for the ratio between the response in the first and third modes (figures 8.40 & 8.41). There appear to be peaks in both these figures in the region 15 to 20 m s^{-1}, indicating that there is a much stronger response in the first mode for this range of wind speeds.

Above this band, the ratios appear to decay again, though with a much less clearly defined trend. However, there is still significant spread in these results, and it is not possible to propose a model to fit to these data.

One reason why trends in the curves presented are not well defined is that the response ratios are a function of several parameters, wind speed, wind direction and integral length. Furthermore, as the along and across wind integral lengths are related, the wind speed and integral length must be related to the frequency content of the wind. The diagrams presented above have shown that the wind speed seems to have the greatest influence on which modes are excited. However, to get a fuller picture of the behaviour it is necessary to account for the other influences as well, which can be done by plotting the response coordinate against several parameters at the same time. Since the data has been selected for winds within ±15° of the beam axis, the data were plotted against the wind speed and the integral length only.

The ratio of response in modes one and two is shown in figure 8.42 as a function of both integral length and wind speed. A fitting package was then used to fit a surface to these points using a bilinear interpolation algorithm (figure 8.43). A great deal of caution has to be employed in drawing any conclusions from this surface; the paucity of the data, especially for the higher values of integral length which are of interest, makes the fit unreliable and this is exacerbated by the need to use a very high smoothing factor to avoid over emphasising individual data points. However, the surface fit provides the only means of identifying trends in the data. Clearly, for all values of integral length, there are certain wind speeds which favour response in the first mode. It appears from figure 8.43 that for longer integral lengths, that is larger eddy sizes, the wind speed for peak response in the first mode is greater than for lower integral lengths. This trend is even more apparent in the ratios between the first and third modes (figures 8.44 & 8.45). This is to be expected since the first and

third modes are the first two vertical modes and are most likely to demonstrate preferential excitation due to spatial variations in the loading.

The amount of data for the easterly winds was even less than that available for the westerly winds. The raw data for the first and second modes is shown in figure 8.46 and the fitted surface in figure 8.47. Again the comment has to be made that the paucity of data means that the surface is only a very crude representation of the trends. The ratios in the first and third mode are shown in figures 8.48 & 8.49.

8.4 Large Amplitude Response of Kessock Bridge

It was mentioned in chapter seven that Kessock bridge has experienced very large amplitude response in the past due to vortex excitation. As has been noted earlier, the results of the long term monitoring described in this chapter have also indicated that large amplitude response occurred on several occasions during this monitoring exercise. It is therefore important to look at these events and to investigate their implications both for the spectral methods developed in this thesis and for the bridge itself.

8.4.1 Historical Overview

The deck section chosen for the Kessock Bridge has several factors in common with the ill fated Tacoma Narrows Bridge and runs counter to recommendations made for the aerodynamic design of bridge decks [Institution of Civil Engineers, 1981]. Therefore, even before the bridge was built, problems of aerodynamic instability were being predicted. However, despite these warnings, the bridge was constructed as originally designed, and in October 1982, soon after opening, the bridge

experienced large oscillations in response to a north easterly wind of approximately 22 m s^{-1}. The amplitude of these oscillations ranged from 90 to 200 mm, which is in excess of the 50 mm adopted in designing the lower flange of the main girder against fatigue [Cullen-Wallace 1985]. In an attempt to limit the amplitude of future oscillations to 12 mm, eight tuned mass dampers were added to the bridge at the centre of the main span. However, these dampers seem to have had only a limited influence on the bridge response [Hay 1986], and indeed a further set of large amplitude vibrations occurred in January 1988. Following this later set of vibrations the mass dampers were inspected and found to be in a poor state of repair [Crouch and Hogg 1988].

8.4.2 Processing of Large Amplitude Response Data

The first stage in the processing of the large amplitude response data was to identify the records which contained the large amplitude response. As, in the general processing of the long term data, the data to be processed were selected using the IMCES system. However, the selected records were then processed to extract the required statistical data and spectra of the events using FAMOS. The aim of the processing was to obtain the peak acceleration during the event, and from this to estimate the peak displacements. It was also to obtain an estimate of the type of response going on.

8.4.3 Results and Discussions

As expected from previous observations and reports large amplitude response occurred when the wind speed was between 20 and 22 m s^{-1}. There were several periods during the time of the monitoring project when the wind speed reached this level, but for the main part the bridge response did not show any untoward behaviour. However on three occasions during the Spring of 1992 large amplitude vibrations were measured and recorded. These occurred as short periods of large amplitude response

during longer periods when the wind speed held around 22 m s^{-1}. Each of these three events will now be discussed in turn by considering the two records with the largest RMS response for each event.

8.4.3.1 April 1 1992.

The first, and most extreme, large amplitude response occurred on the morning of April 1 1992. The power spectra for the vertical response are shown in figures 8.50 and 8.51, and these indicate that the response is concentrated in the first vertical mode of the deck, at a frequency of around 0.5 Hz (cf. §7.3.2.1). By integrating the power spectra, it is possible to estimate the distribution of energy between each of the response modes (Table 8.2). The details of the bridge response and the incident wind are given in table 8.3, and time histories for the wind speed and deck acceleration are shown in figures 8.52 and 8.53. It should be noted here that for several instances in these records the response was so high that the peak acceleration exceeded the limits of the signal processing amplifiers and it is therefore only possible to estimate a lower bound to the true peak acceleration. Because the response is concentrated in the first mode it is possible to estimate displacements by dividing accelerations by the square of the angular natural frequency. This gives a lower bound estimate of the peak displacement as ±110 mm, much larger than the 50 mm limit assumed in the design.

Examining all the recorded traces containing large amplitude response on April 1, it is clear that the large amplitudes are intermittent. In an hour of records (figure 8.54), the maximum duration of large amplitude motion is about 3 minutes, and outside these times the response is very much reduced. This has two implications. Firstly, it indicates the sensitivity of this large amplitude response to other factors, such as wind speed and direction. Secondly, it means that the response is non-stationary, and therefore a detailed spectral analysis will be inappropriate for these records. Indeed, because the most

significant response of the bridge occurs in this way it also means that the power spectral approach may not be suitable for the design of the bridge.

8.4.3.2 May 12 1992

The second period of large response occurred at about lunch time on May 12. The power spectra (figures 8.55 and 8.56), again indicate that the response is concentrated in the first vertical mode. The wind data and response are summarised in table 8.5, and the time histories are shown in figures 8.57 and 8.58. There are several differences between this event and that of April 1 that need to be noted. Firstly the wind is from a westerly direction, rather than easterly, and is consequently more turbulent. Secondly the duration of the large amplitude response is much shorter as shown by the lower values of the RMS acceleration for the ten minute records. This is probably due to the more turbulent nature of the wind, and will be discussed later.

8.4.3.3 May 15 1992

The third set of readings were recorded on the morning of Friday May 15. This set of readings is of special interest because during this morning restrictions had to be placed on traffic crossing the bridge. Men working on the bridge noted that the bridge was responding strongly, and in a torsional manner which had not been noted previously. The power spectra for the two records considered are shown in figures 8.59 and 8.60. These show that the response on this morning was not concentrated in the first vertical mode; indeed for the earlier record the response is instead dominated by the first torsional mode and contains a significant contribution from the second vertical mode. The wind and response data are summarised in table 4. As on May 12, the wind is from a westerly direction, however, it is more turbulent than both the easterly winds of April 1, and the westerly winds of May

12. The time histories shown in figures 8.61 and 8.62 indicate that the two records represent two very different types of response. The first record shows a more consistent, but less intense response. The second record is very similar to the response on May 12 with steady low accelerations and a short pulse of large amplitude response.

8.4.4 Causes of Response

The most likely cause of the behaviour observed on April 1 and May 12 is vortex shedding. This was predicted by the initial wind tunnel tests performed by Glasgow University [Cullen-Wallace 1985], and explains some of the differences between the records for easterly and westerly winds. The frequency of vortex shedding is sensitive to the wind velocity, and resonance with the first mode at Kessock bridge occurs for a velocity of c. 22 m s^{-1}. For more turbulent winds, such as the westerly winds of May 12, this resonance can occur, but cannot be sustained due to large changes in velocity. This explains the short duration of large amplitude response on May 12. However, the records show that for the less turbulent easterly winds this effect can be sustained for much longer periods, even for several minutes as on April 1.

The behaviour on May 15 is more difficult to explain. The second record shown for this date seems to indicate vortex shedding as the probable cause, but this would not explain the presence of the torsional response in the first record. Vortex excitation of the first torsional mode would occur for wind speeds around 33 m s^{-1}. These speeds were reached during this record but were not sustained for any appreciable time, whereas the response appears consistent throughout the record. A different explanation for the response in this record is flutter. Classical flutter, however, would seem unlikely as the first two natural frequencies are well separated. Furthermore the wind tunnel tests predicted a critical velocity for flutter of 61.5 m s^{-1}, far in excess of anything experienced on the day in question.

There is though some evidence that the flutter response of bridges can be influenced by turbulence and the wind during this record was extremely turbulent. The response on this day is important as it caused concern for those using the bridge, but an explanation will require further processing of the available records in order to find the cause.

8.4.5 Performance of the Added Mass Dampers

The added mass dampers were installed on the bridge to limit the dynamic displacement of the deck to 12 mm. From the observations made during the monitoring of the bridge it is clear that they were not fulfilling this aim during the Spring of 1992. Immediately following the events of May 15, the dampers were found to be in a very poor state of repair. Most had lost all of their damping fluid, some showed signs of physical damage, and several had been displaced so far that the central piston no longer remained within the cylinder. Estimates of the damping factor made from readings taken in September 1991 and May 1992 show damping in the first mode was less than 3 % (cf. results of modal survey) which is lower than would be expected if the dampers were functioning properly.

The added mass dampers have yet to show that they are effective in reducing the response of the bridge to acceptable levels. Since the large amplitude vibrations are almost exclusively vortex induced, some measures to prevent vortex shedding might prove more successful in reducing the response. The addition of vanes to the edge of the bridge has been suggested [Cullen-Wallace 1985], and experiments have shown that venting the bridge deck can dramatically reduce the response to vortex shedding [Kumarasena et al. 1992].

8.5 Appraisal of the Long Term Monitoring and Its Implications

As mentioned in the introduction, the purpose of this chapter has been to present the results from preliminary analysis of the data collected during the monitoring of Kessock bridge, and to suggest approaches for further data processing. Having presented the results of the data processing, it is now time to step back and review the monitoring exercise as a whole, to summarise what has been learnt and to identify the next step in the data processing.

Judged against its primary aim of typifying the wind excitation in the form of a two dimensional power spectrum, and thus verifying the analytical work developed in earlier chapters, the monitoring exercise has not been a success. There are two principal reasons for this. Firstly, the size of the eddies recorded on the bridge was significantly smaller than the array of anemometers that had been installed. Therefore, the data recorded was not suitable for calculating a two dimensional power spectrum as intended. This observation must be qualified by pointing out that the smaller eddies observed are unlikely to have the expected influence on the bridge, and only a very few eddies were recorded which were of the same order of magnitude as the bridge. At this point it is useful to ask the question why so few larger eddies were recorded, was it because they were not present or was it because the monitoring system missed them? As explained in §8.2.3 the switch to a block averaging approach to processing the raw data resulted in a loss of frequency resolution and hence a loss of information at the low frequency end of the spectrum. If Taylor's hypothesis holds, then the larger eddies will correspond to lower frequencies, and this gives a possible explanation to why they could have been missed. However, this must again be qualified by reference to the structure; the frequency associated with these eddies will be less than 0.01 Hz. which is much less than the first natural frequency of the bridge. They will therefore have little influence on its dynamic behaviour.

The second reason for the lack of success was that there were not sufficient similar data to derive meaningful conclusions. Despite collecting a very large amount of raw data, there were so many variables that influenced the wind data, wind speed, direction and turbulence for example, that the data set contained very few records that were sufficiently similar. This problem was exacerbated by the fact that it was not known beforehand exactly which data needed to be recorded (cf. §8.1.4). With hindsight it would have been better to monitor the bridge for a much longer period, preferably several years, and to have been far more selective when recording raw data.

Although the monitoring project did not succeed in its primary aim, it has provided valuable information on the factors that can influence the bridge response, and also highlighted factors that need to be considered when developing future monitoring systems. The processing of the raw data has indicated, although tenuously, that the larger eddies do have an influence on the bridge response. The aim of the next step in processing the raw data must be to pursue this issue further, to isolate those records which correspond to the larger integral lengths and to develop a more refined measure of the bridge response. However, the most striking observation is that the response of the bridge to buffeting forces is negligible compared to the response to vortex excitation. Even after remedial measures had been taken the response was still an order of magnitude greater with vortex excitation. This raises two questions, is the detailed processing of the buffeting response relevant? and can the approach be applied to the analysis of vortex induced response? The answer to the first question is yes, and for two main reasons. Firstly, Kessock bridge is somewhat anomalous in having a bridge deck which is peculiarly susceptible to vortex excitation at a low wind speeds, most well designed modern bridges should not have such major problems. Secondly, figures 8.16 and 8.17 indicate that the bridge response rises very rapidly as the wind speed increases. Since the monitoring period only lasted a matter of months, it is unlikely that any unusually high winds were observed, and so it is

probable that higher winds will occur that may give a response to buffeting which is at least as great as caused by vortex shedding. In answer to the second question, investigations have recently been made into the influence of spatial variations on vortex excitation [Ehsan *et al.* 1990] and this is an obvious area for further research. However, the results from this monitoring exercise indicate that the response is intermittent, therefore non stationary and hence unsuitable for a power spectral approach.

8.5.1 Data Processing, the Next Step

The data processing presented in this thesis, has, because of the limited time available, only been able to look superficially at a limited amount of the data recorded. It is essential that the data recorded should not be wasted, and so it is useful to suggest further avenues to explore. As mentioned in the preceding section, the aim of future processing must be to concentrate on examining the influence of the records with larger integral lengths on the bridge response. Further processing could include:

a. Calculation of the along wind integral lengths for these records

b. Using a finer classification by wind direction

c. Examining those records which lie outside ±15°

d. Correcting non stationary data so it can be included in the processing.

8.5.2 Proposal for a New Monitoring Scheme

Having, processed some of the raw data and examined some of the problems that have arisen, it is useful at this point to pick up the discussion of §8.1.4 and consider how the monitoring scheme could be improved. Two simple improvements can be suggested immediately, extend the monitoring period, preferably to several years, so that more usable data is collected and extend the time taken for each

record to be made. The latter suggestion will improve the frequency resolution of the data and allow the block averages to be made over a wider range making it more effective at removing the random errors. A more radical change to the system would be to process the data as it was recorded, using the parallel system suggested in §8.1.4. In this way it would be possible to calculate the integral length and the bridge response parameter for each record and then discard the raw data. This would save tremendously on the amount of storage required, and would allow the surfaces presented in figures 8.42 to 8.49 to be built up as the project proceeds. In the light of the small eddies observed in the current study, it would also be useful to reduce the spacing of the anemometers along the bridge. However, the two drawbacks to this are the expense for more anemometers and the lack of suitable place to mount them.

8.6 Conclusions

1 The wind regime on Kessock Bridge is dominated by the prevailing south westerly winds. These are more turbulent than winds from the east.

2 For low wind speeds the bridge response is dominated by traffic, for winds above 10 m s^{-1} the response to wind excitation rises rapidly.

3 The wind speed is the dominant factor in determining the response to buffeting, although the results indicate that larger values of the cross wind integral length may influence the response.

4 Kessock Bridge exhibits displacements in excess of ±110 mm in response to winds of c. 22 ms^{-1}. This response is caused by vortex excitation, and occurs for both easterly and westerly winds, although the response is more marked for easterlies because they are less turbulent.

5 The response on May 15 showed a strong component in the first torsional mode. This needs to be investigated further to determine the cause and the consequences of a repeat occurrence.

Table 8.1

Summary of Results of Run Test for Stationarity

	West		East	
Anemometer	**No. Stationary**	**%**	**No. Stationary**	**%**
1	192	25	27	23
2	185	25	30	25
3	221	30	30	25
4	170	23	34	28
5	157	21	35	29
6	158	21	38	32
7	166	22	30	25

Table 8.2

Modal Contributions To Bridge Deck Response

		Mid Span		50 m	
April 1		**10:27**	**11:44**	**10:27**	**11:44**
1st Vertical	0.51 Hz.	92 %	94 %	74%	79 %
1st Torsional	0.74 Hz.	1 %	-	-	-
2nd Vertical	0.81 Hz.	-	-	-	2 %
May 12		**12:19**	**13:05**	**12:19**	**13:05**
1st Vertical	0.51 Hz.	78 %	86 %	51 %	62 %
1st Torsional	0.74 Hz.	5 %	5 %	2 %	-
2nd Vertical	0.81 Hz.	-	-	6 %	11 %
May 15		**09:37**	**10:58**	**09:37**	**10:58**
1st Vertical	0.51 Hz.	17 %	72 %	5 %	22 %
1st Torsional	0.74 Hz.	50 %	8 %	28 %	7 %
2nd Vertical	0.81 Hz.	-	-	24 %	26 %

Table 8.3

Wind And Bridge Response Statistics, April 1

		10:27	11:44
	Turbulence Intensity	0.06	0.07
Wind Speed	Mean	21.79 m s^{-1}	21.34 m s^{-1}
	Minimum	17.70 m s^{-1}	16.72 m s^{-1}
	Maximum	25.83 m s^{-1}	24.74 m s^{-1}
Wind Direction*	Mean	308°	308°
	Minimum	293°	290°
	Maximum	324°	323°
Mid-Span Accel	RMS	0.43 m s^{-2}	0.47 m s^{-2}
	Peak	1.11 m s^{-2}	1.12 m s^{-2}

Table 8.4

Wind And Bridge Response Statistics, May 12

		12:19	13:05
	Turbulence Intensity	0.09	0.10
Wind Speed	Mean	19.96 m s^{-1}	22.25 m s^{-1}
	Minimum	15.10 m s^{-1}	16.94 m s^{-1}
	Maximum	25.18 m s^{-1}	28.21 m s^{-1}
Wind Direction*	Mean	125°	127°
	Minimum	100°	105°
	Maximum	151°	156°
Mid-Span Accel	RMS	0.14 m s^{-2}	0.23 m s^{-2}
	Peak	0.76 m s^{-2}	1.11 m s^{-2}

Table 8.5

Wind And Bridge Response Statistics, May 15

		12:19	13:05
	Turbulence Intensity	0.14	0.12
Wind Speed	Mean	24.72 m s^{-1}	22.10 m s^{-1}
	Minimum	15.97 m s^{-1}	15.10 m s^{-1}
	Maximum	35.15 m s^{-1}	30.16 m s^{-1}
Wind Direction*	Mean	84°	87°
	Minimum	66°	67°
	Maximum	-	-
Mid-Span Accel	RMS	0.17 m s^{-2}	0.17 m s^{-2}
	Peak	0.80 m s^{-2}	0.95 m s^{-2}

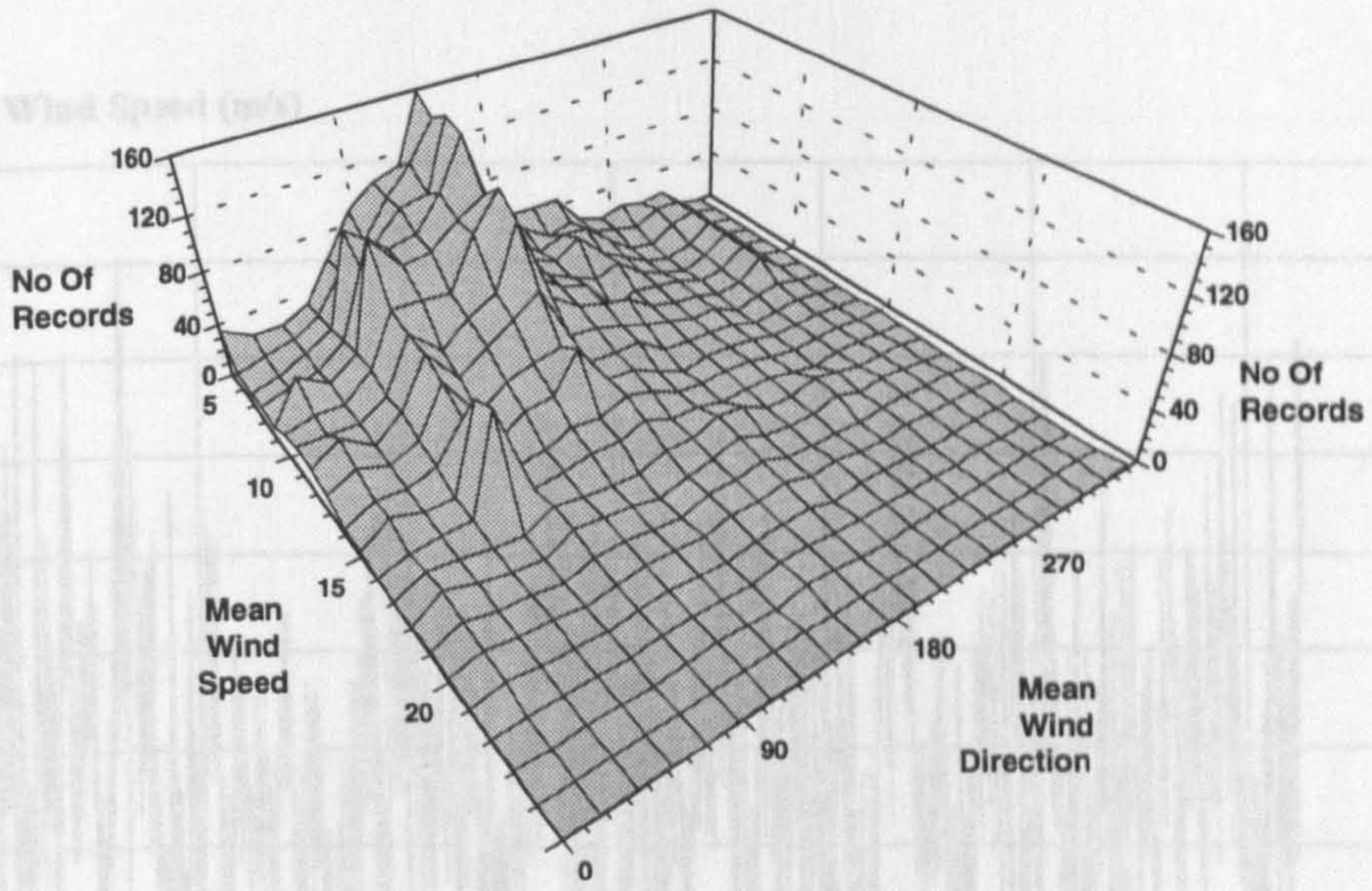

Figure 8.1 : Records Seen During Kessock Bridge Monitoring Programme

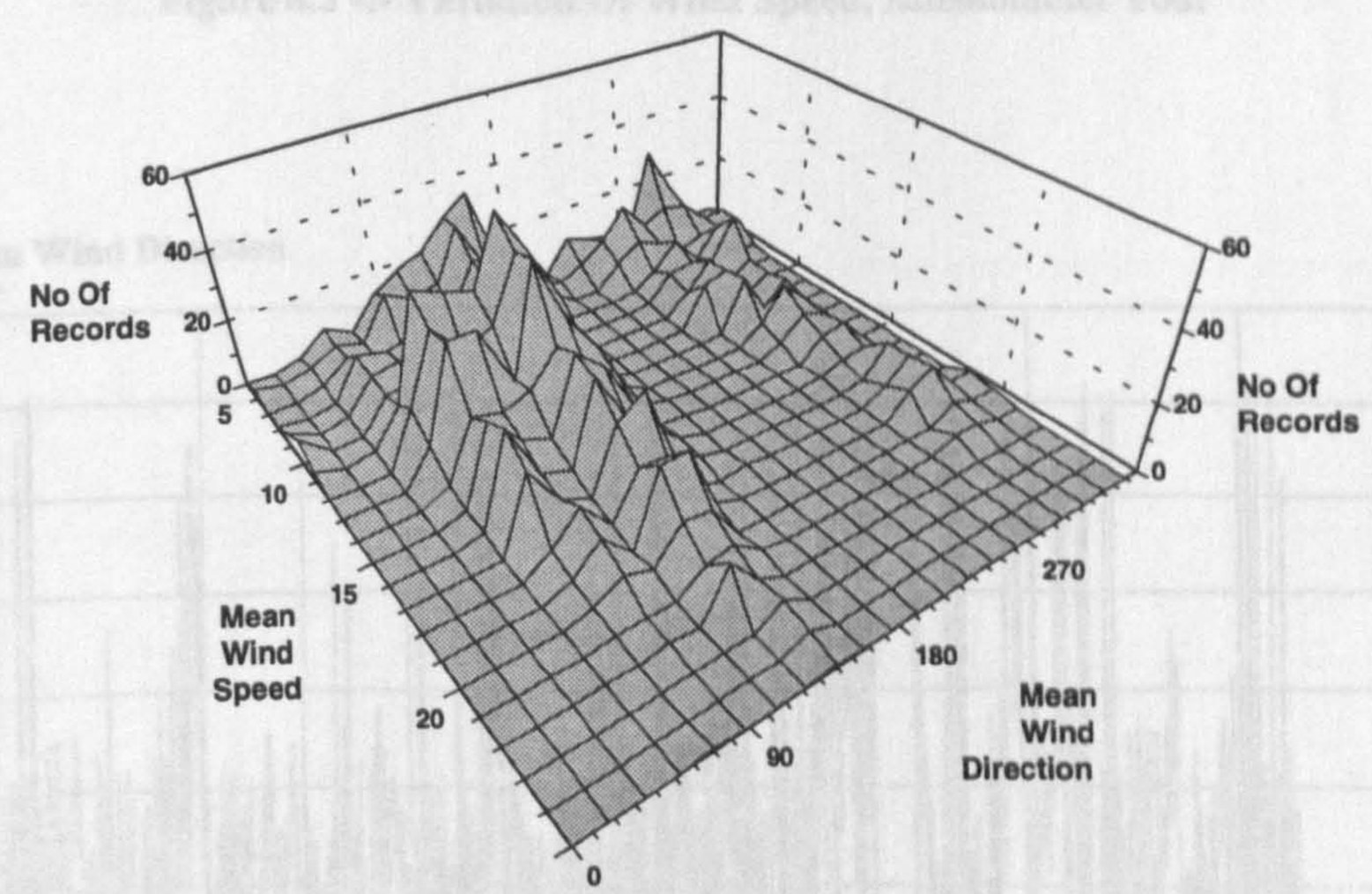

Figure 8.2 : Records Stored During Kessock Bridge Monitoring Programme

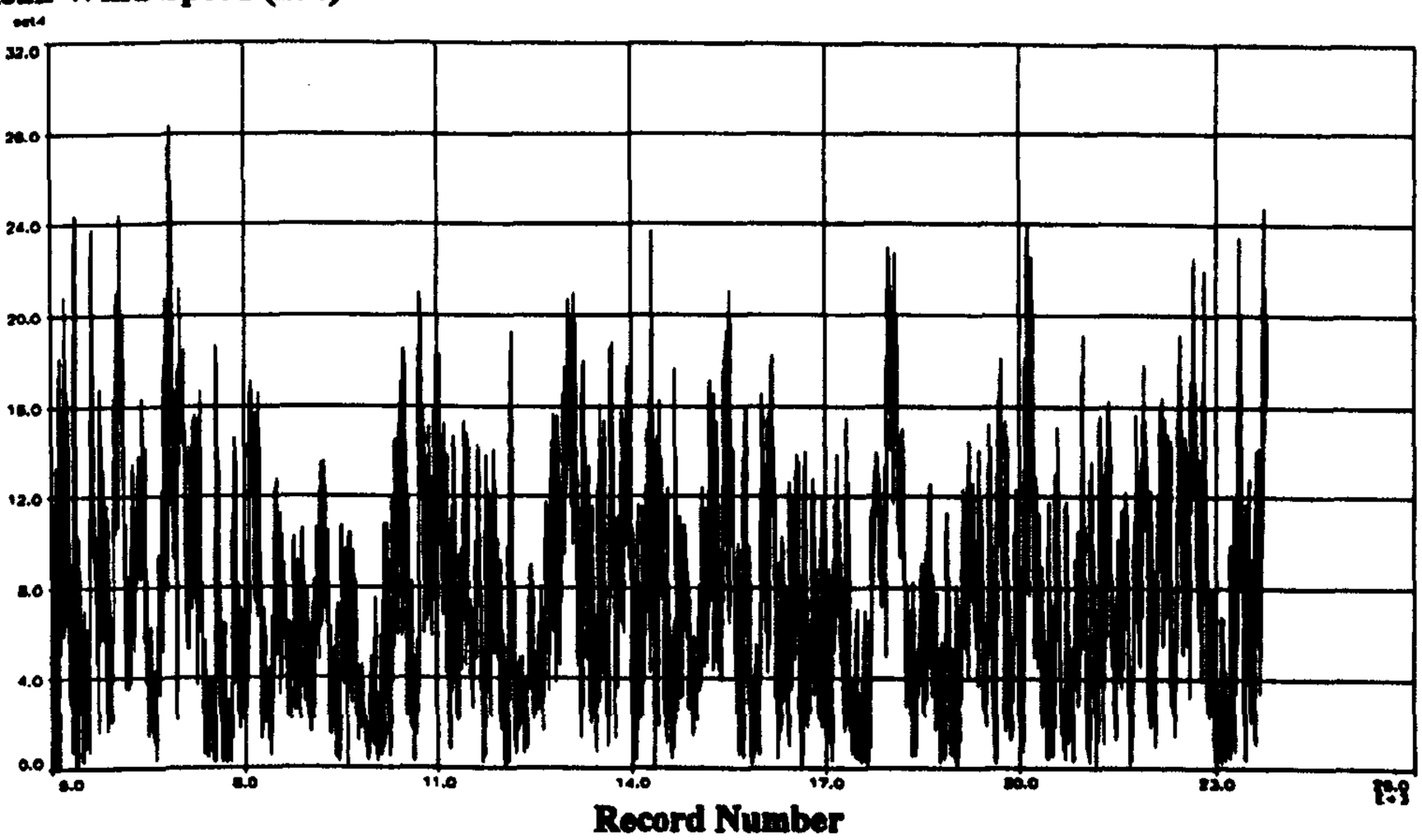

Figure 8.3 -:- Variation Of Wind Speed, Anemometer Four

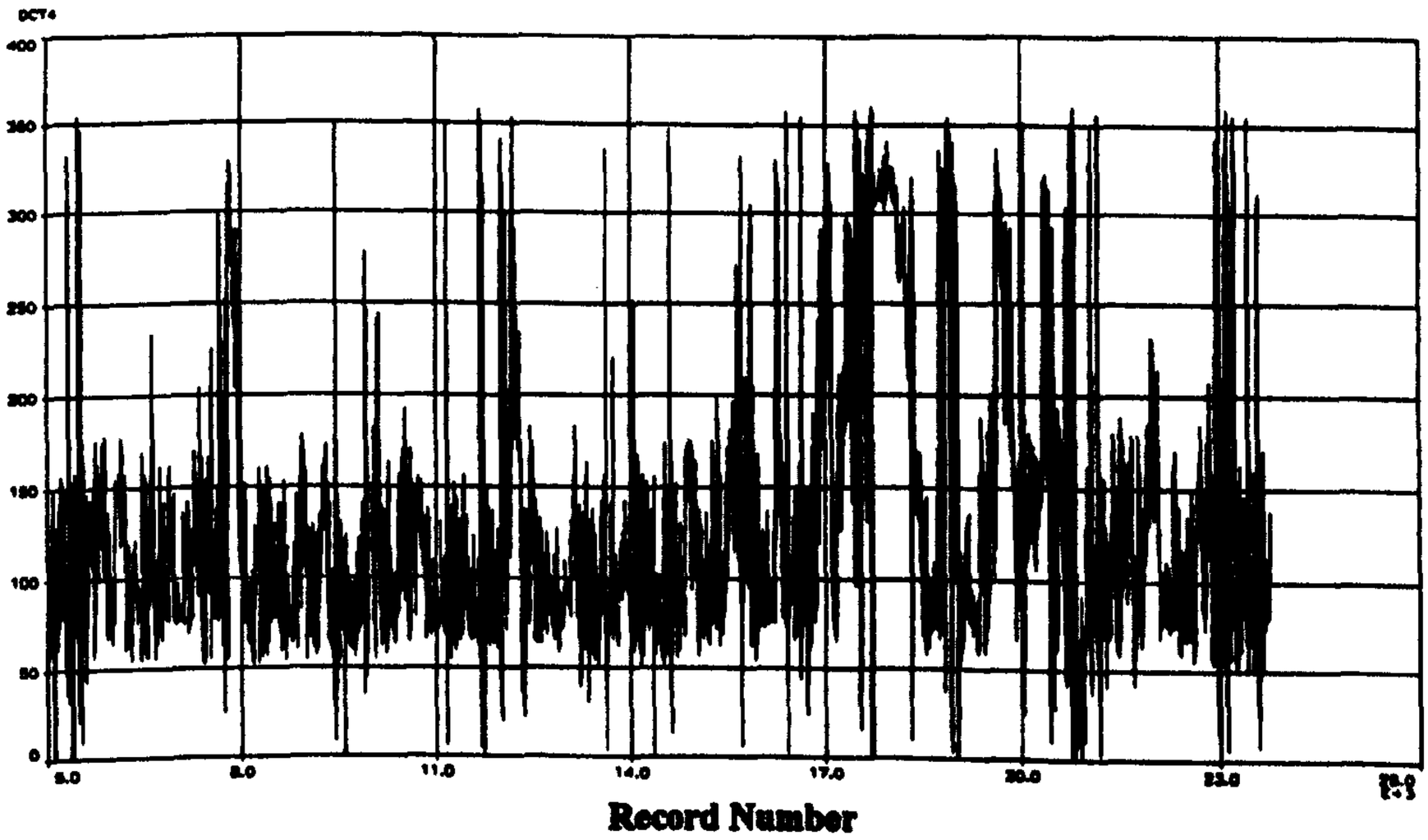

Figure 8.4 -:- Variation Of Wind Direction, Anemometer Four
(Wind direction is measured in degrees, clockwise from Southerly axis of the bridge)

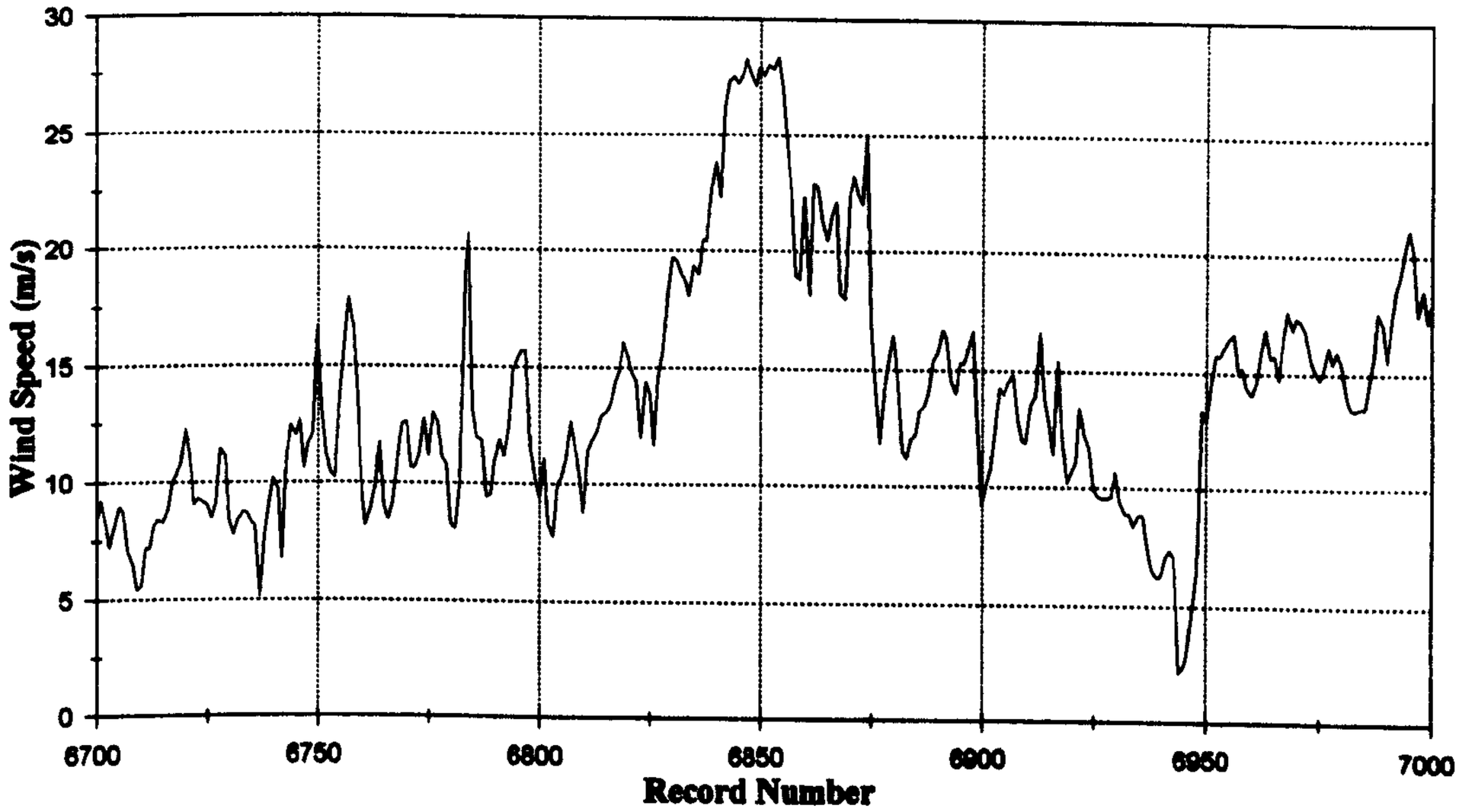

Figure 8.5 -:- Variation Of Wind Speed With Time For Typical Storm

Figure 8.6 -:- Variation Of Wind Direction With Time For Typical Storm
(Wind direction is measured in degrees, clockwise from Southerly axis of the bridge)

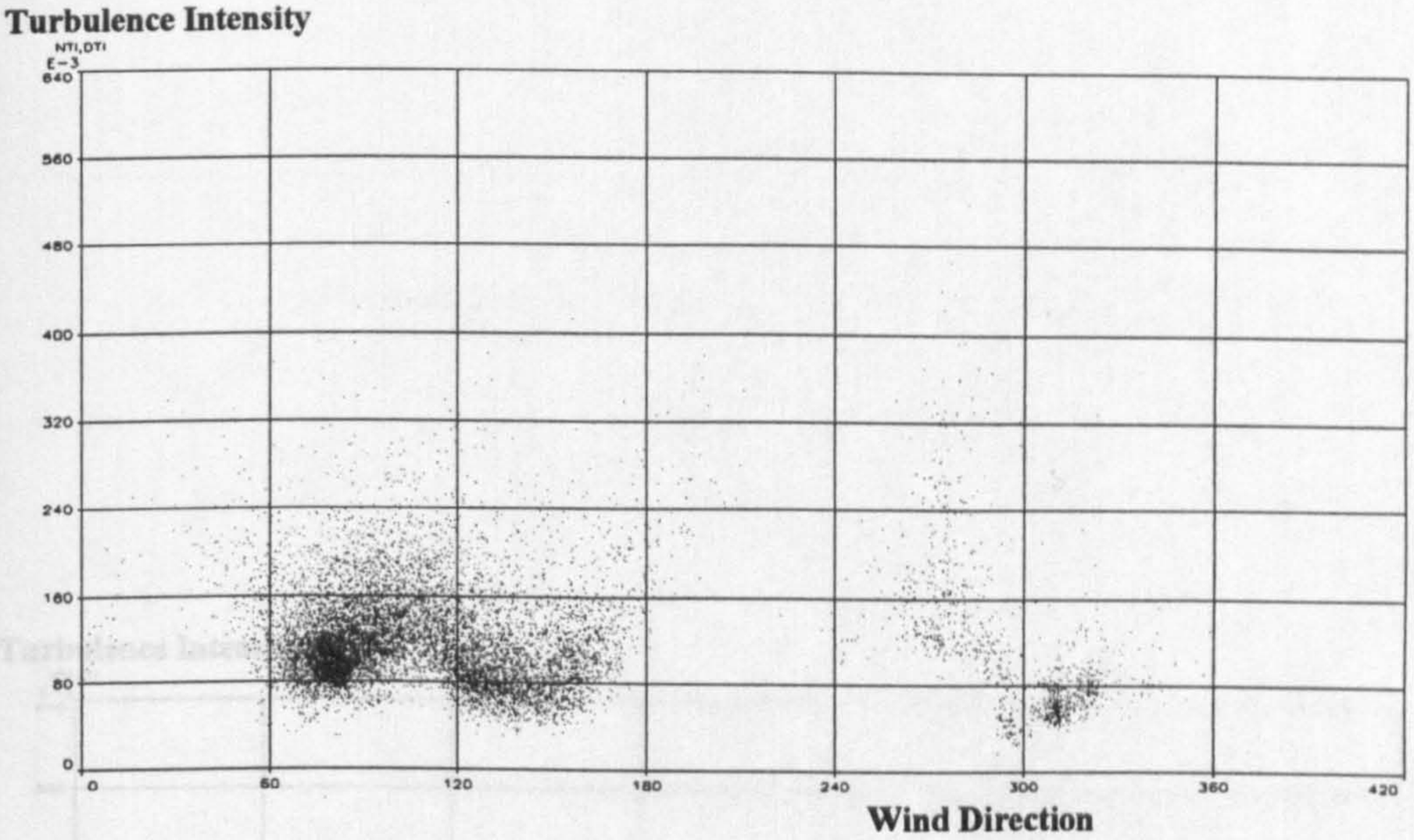

Figure 8.7 -:- Variation Of Turbulence Intensity With Wind Direction
(Wind direction is measured in degrees, clockwise from Southerly axis of the bridge)

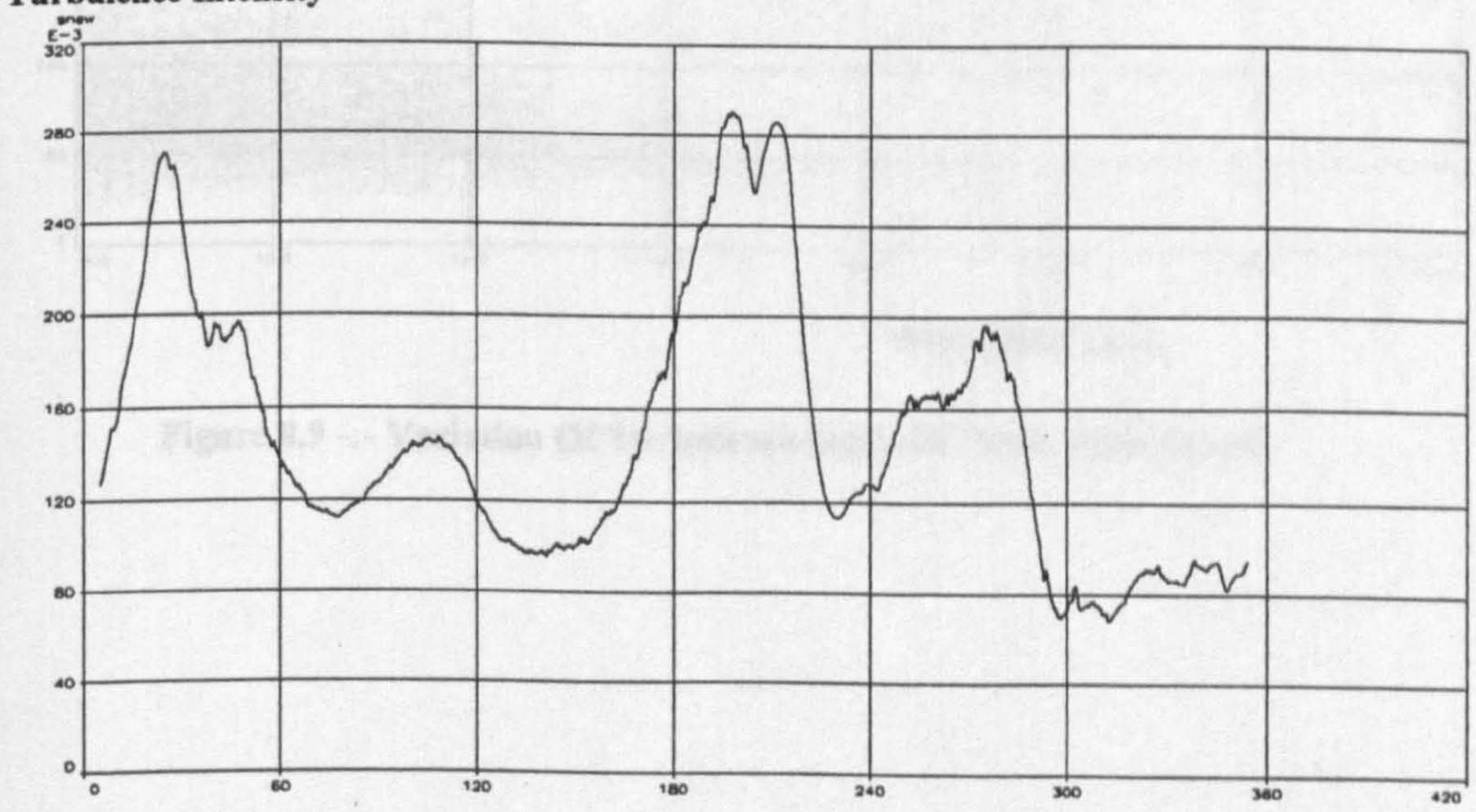

Figure 8.8 -:- Smoothed Variation Of Turbulence Intensity With Wind Direction
(Wind direction is measured in degrees, clockwise from Southerly axis of the bridge)

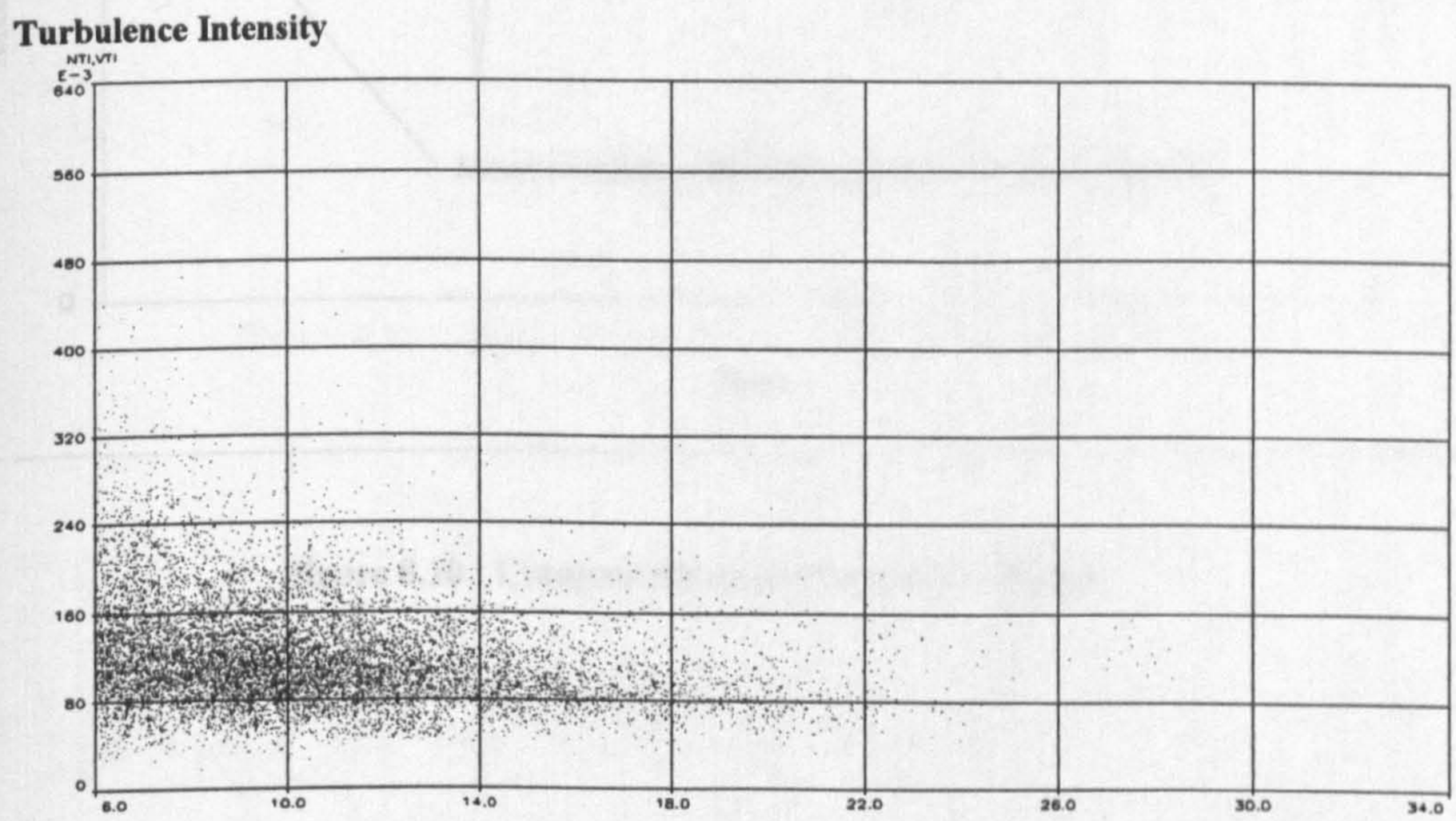

Figure 8.9 -:- Variation Of Turbulence Intensity With Wind Speed

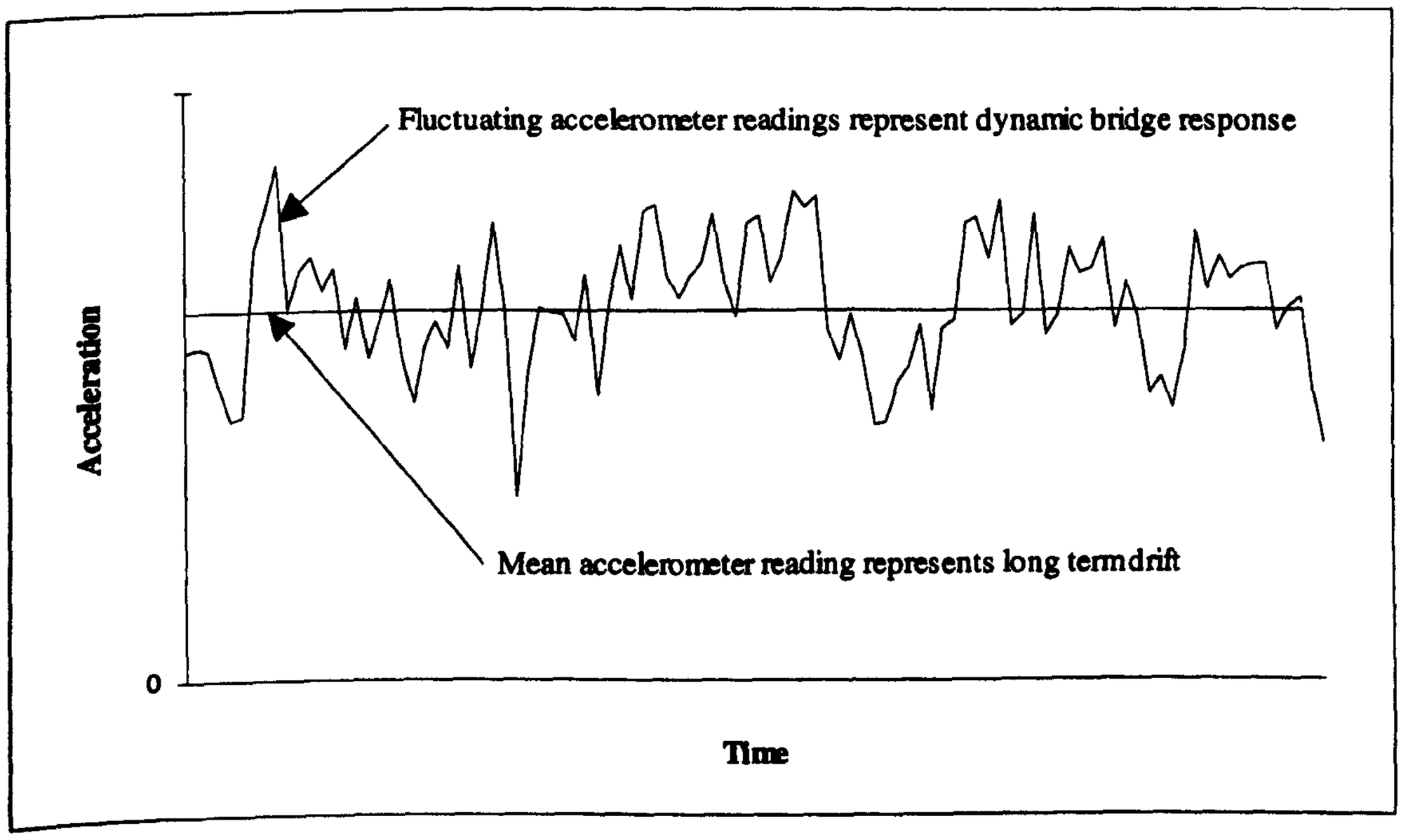

Figure 8.10 : Components of Accelerometer Signal

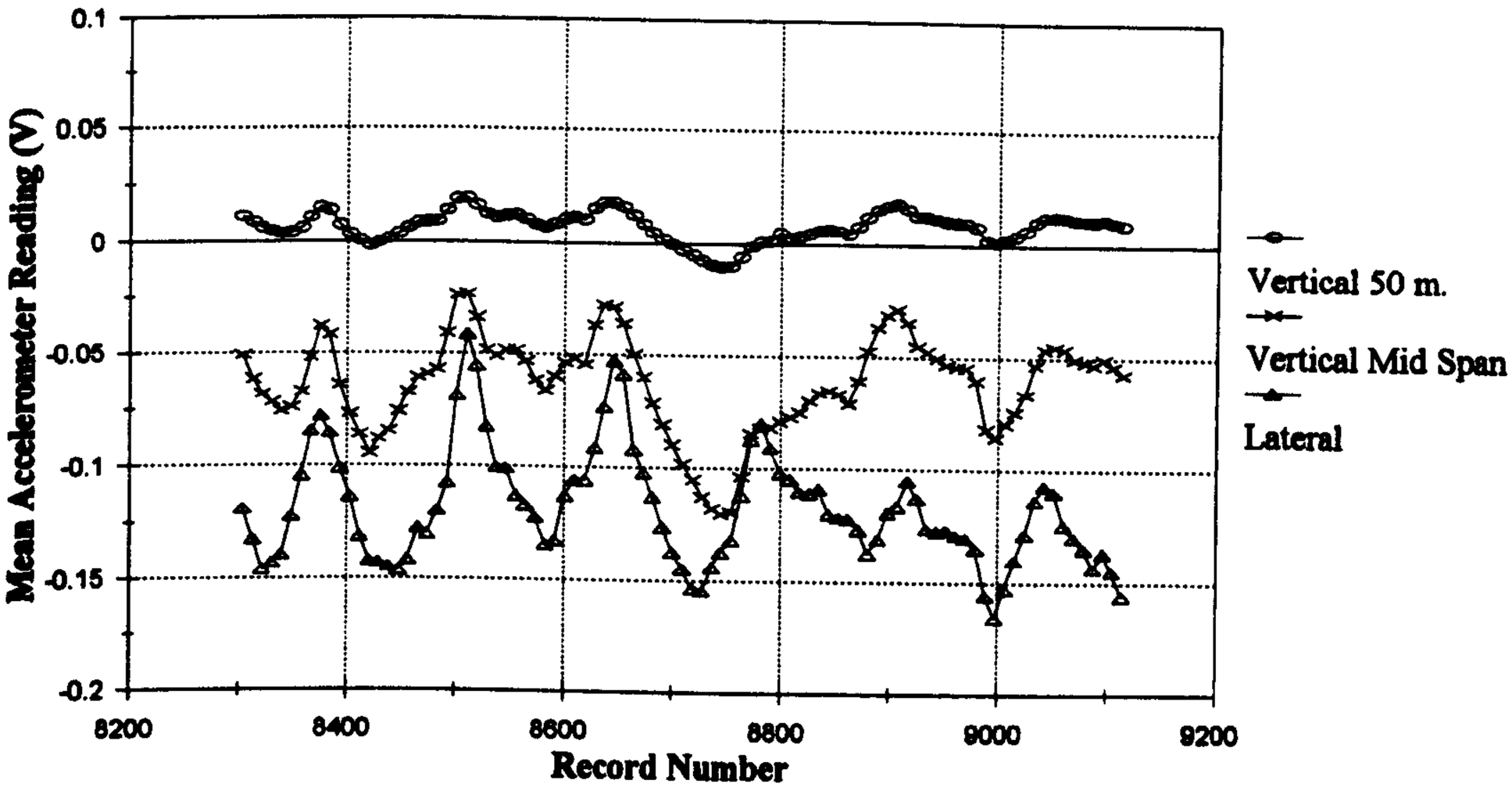

Figure 8.11 -:- Daily Trend In Mean Accelerometer Reading

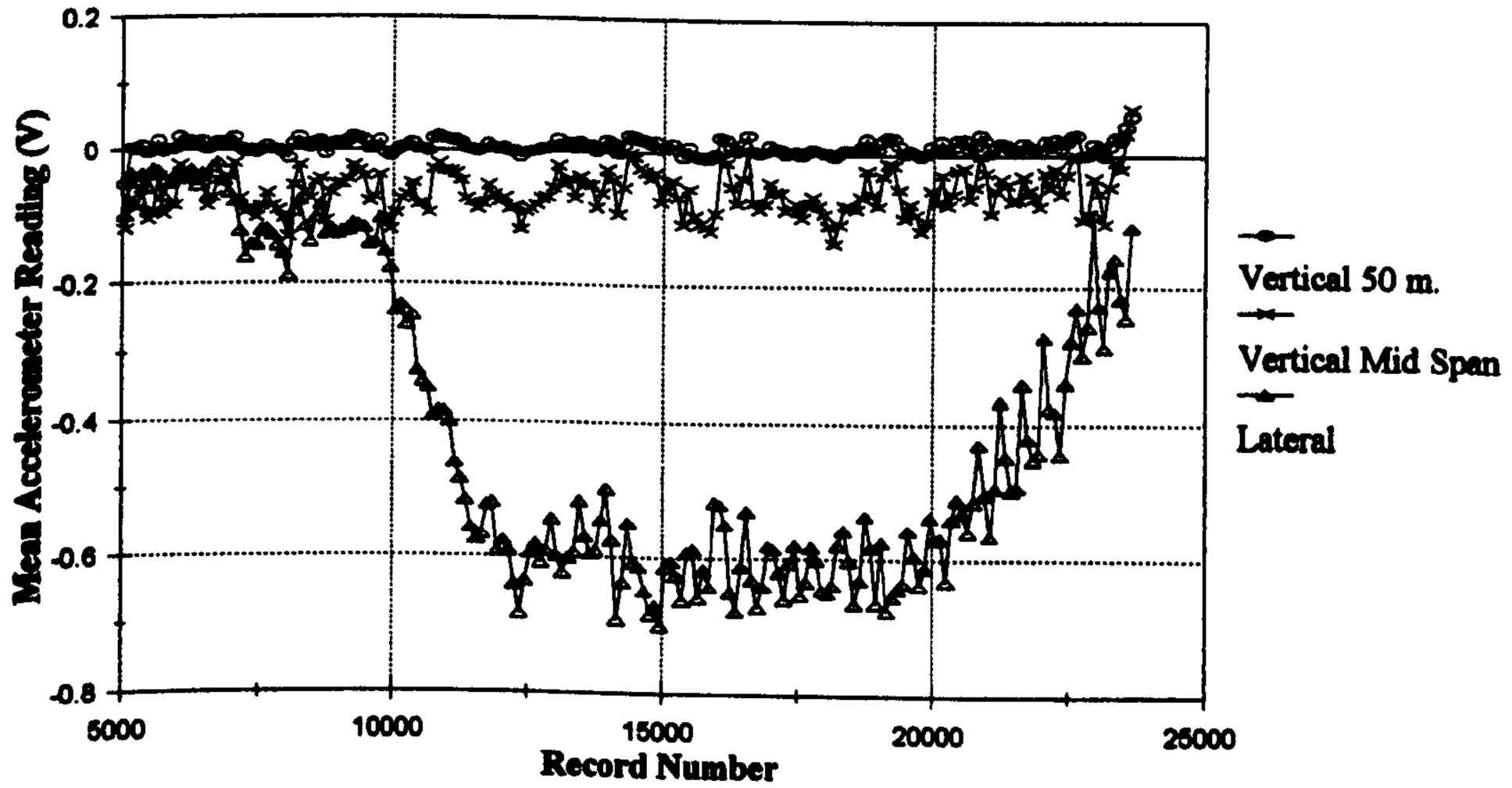

Figure 8.12 -:- Long Term Trend In Mean Accelerometer Reading

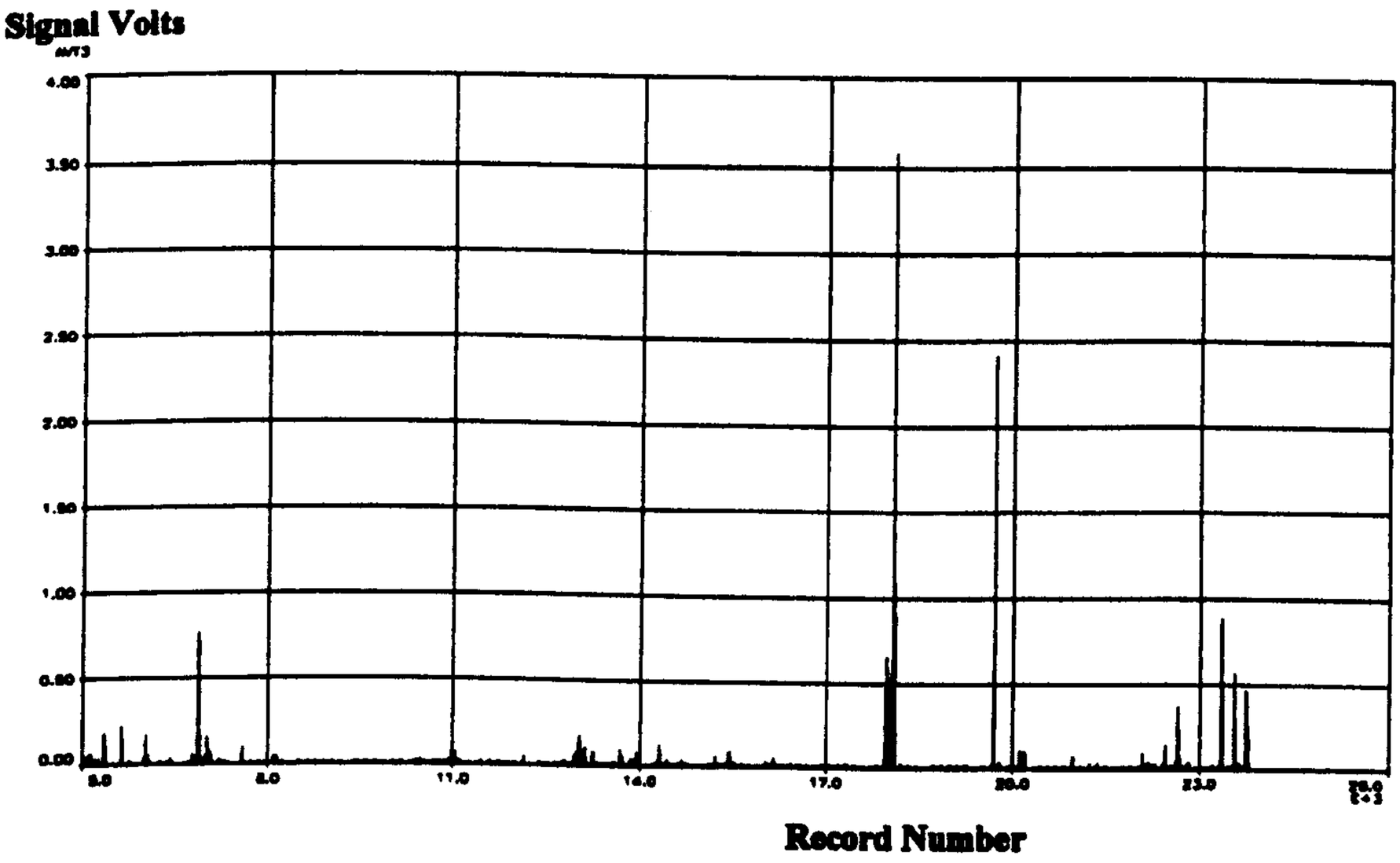

Figure 8.13 -:- Long Term Trends In Response At Mid Span

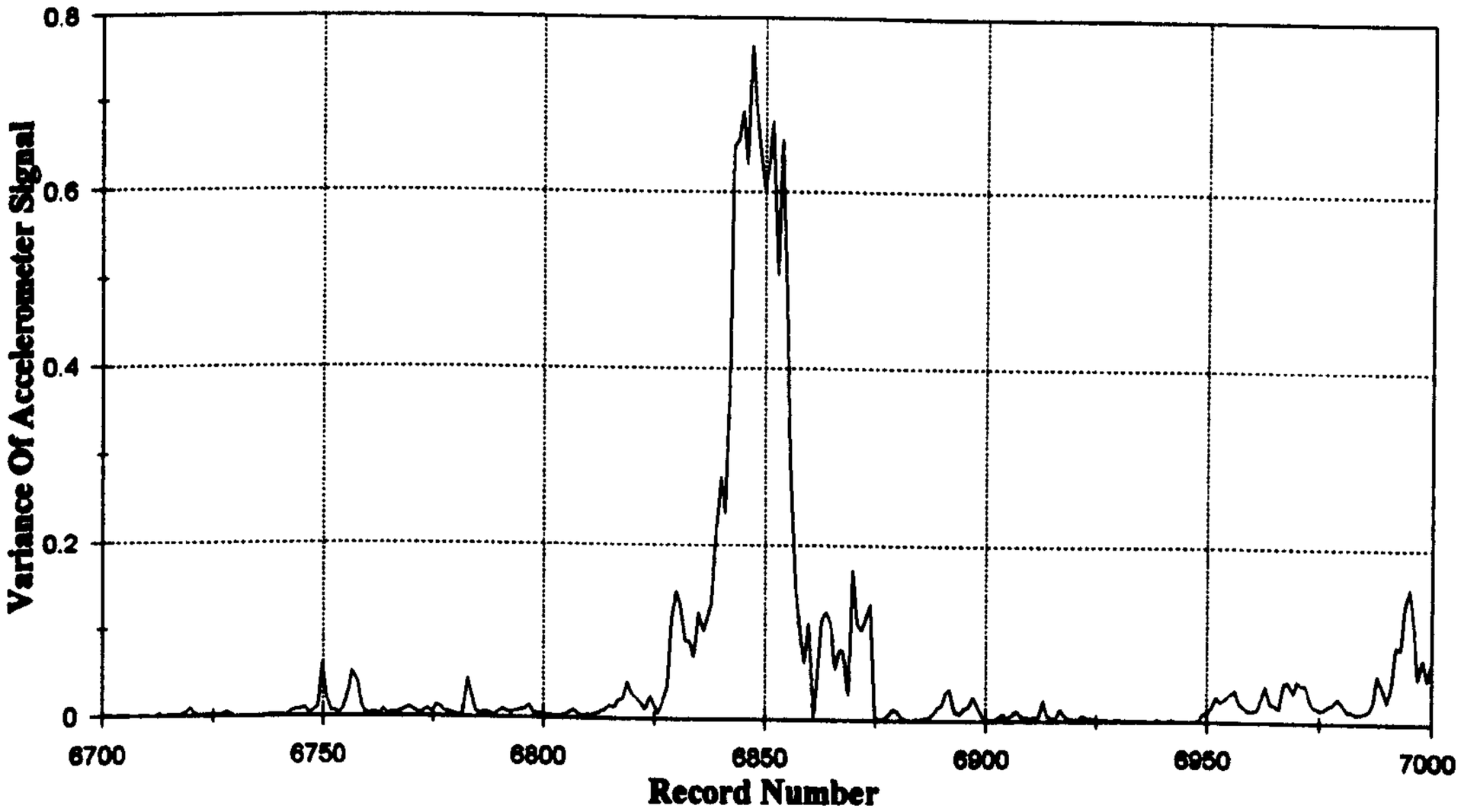

Figure 8.14 -:- Response Of Bridge At Centre Span For Typical Storm

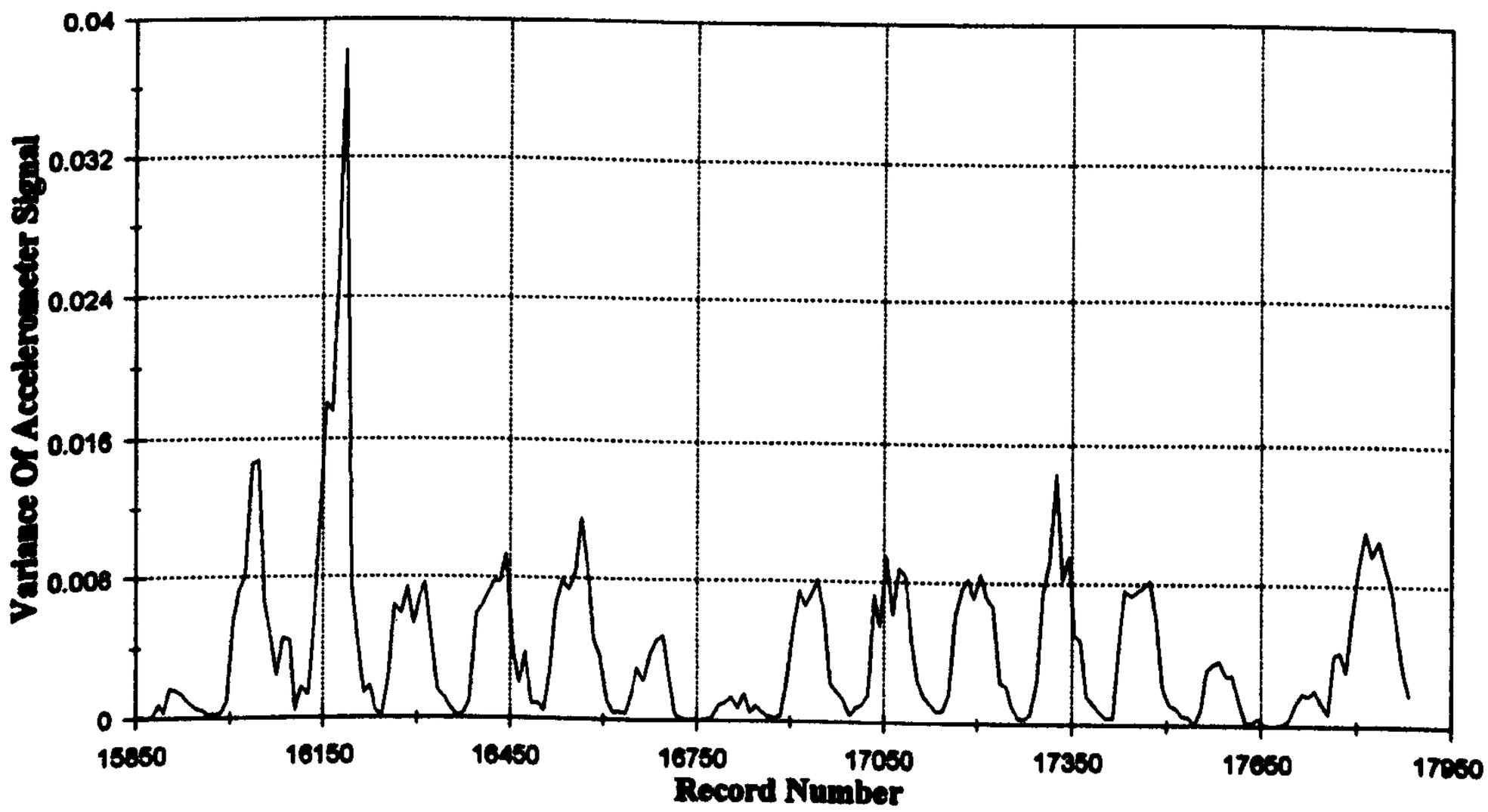

Figure 8.15 -:- Daily Trend In Bridge Response At Centre Span

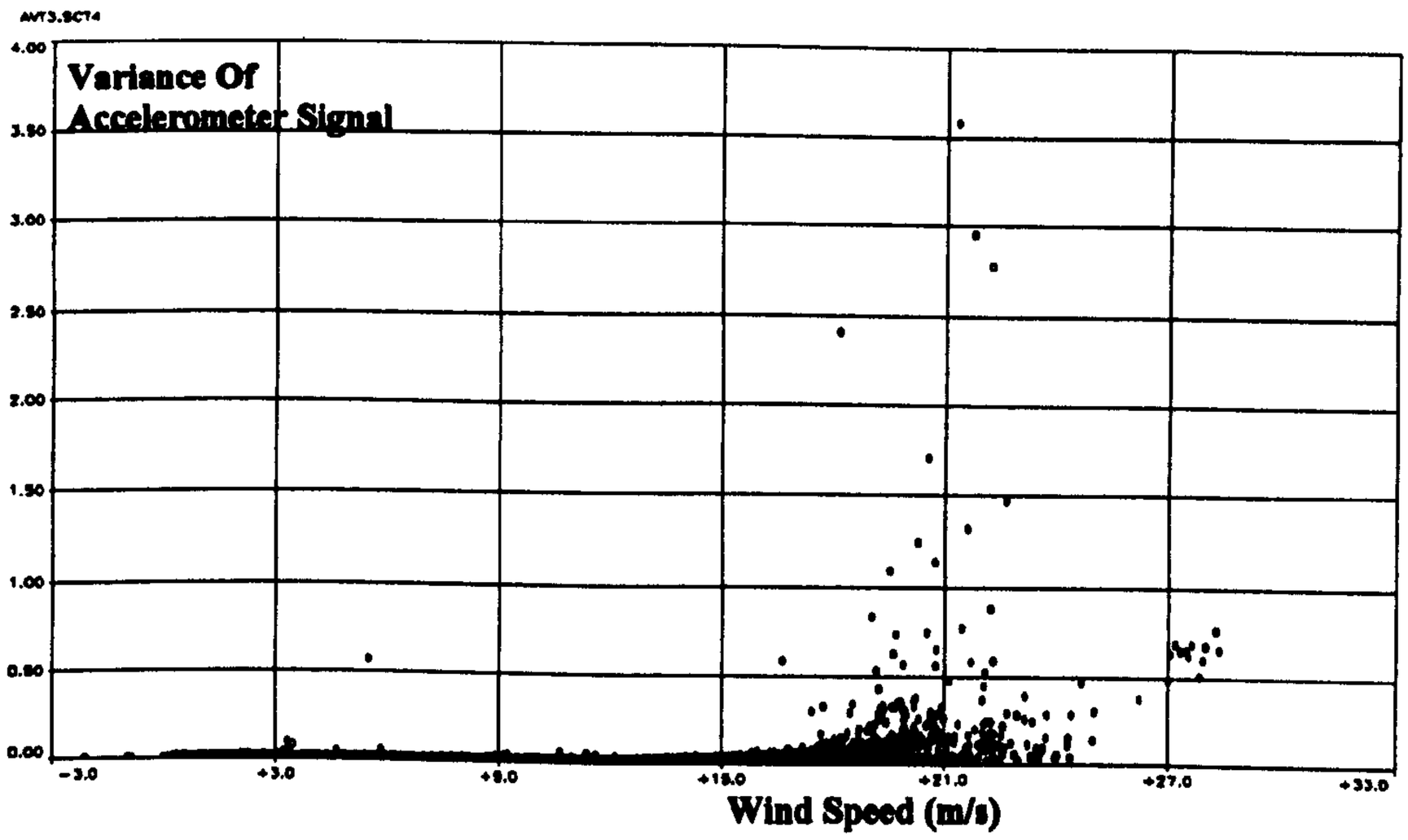

Figure 8.16 -:- Variation Of Response At Mid Span With Wind Speed

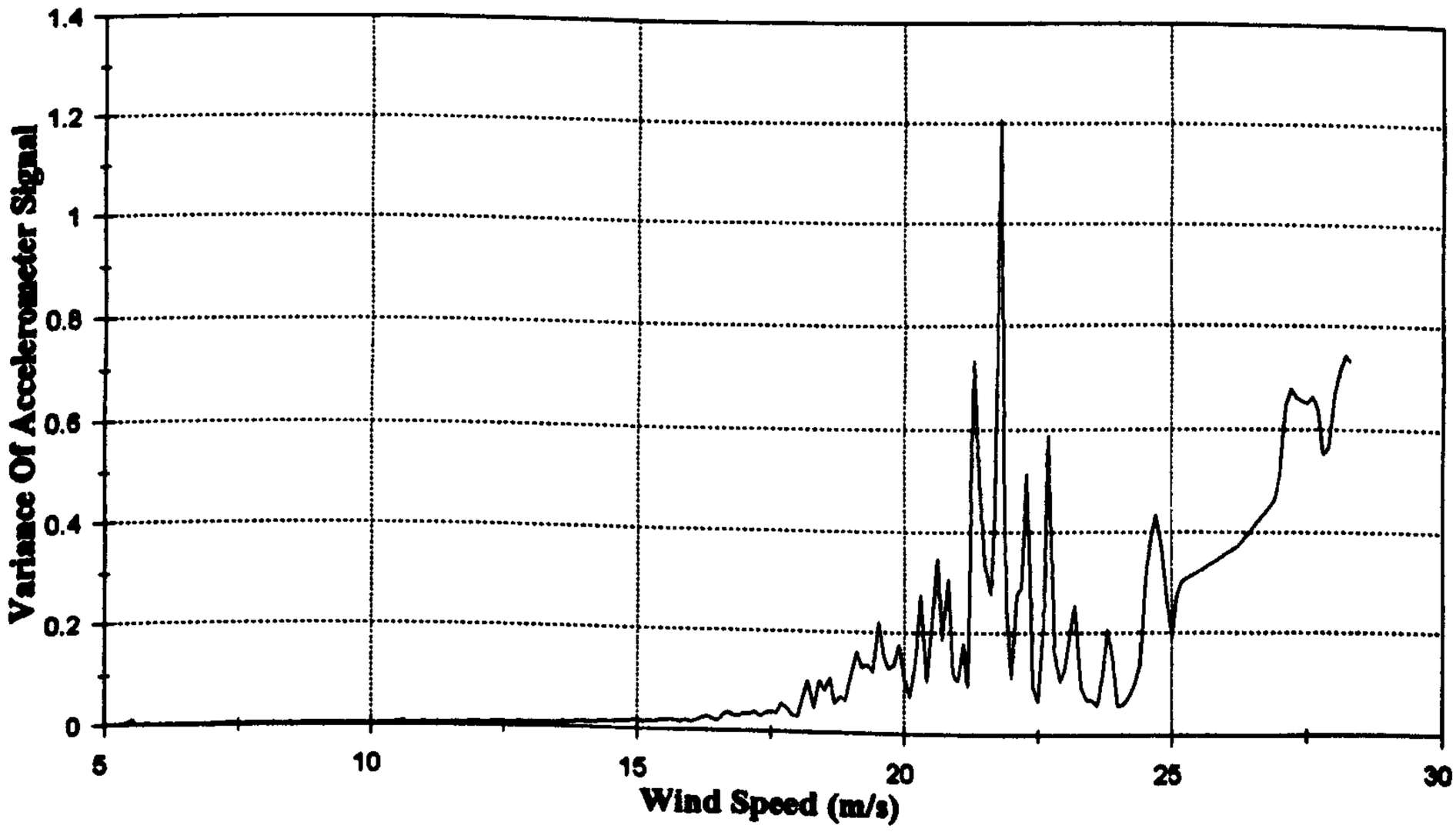

Figure 8.17 -:- Smoothed Variation Of Response At Mid Span With Wind Speed

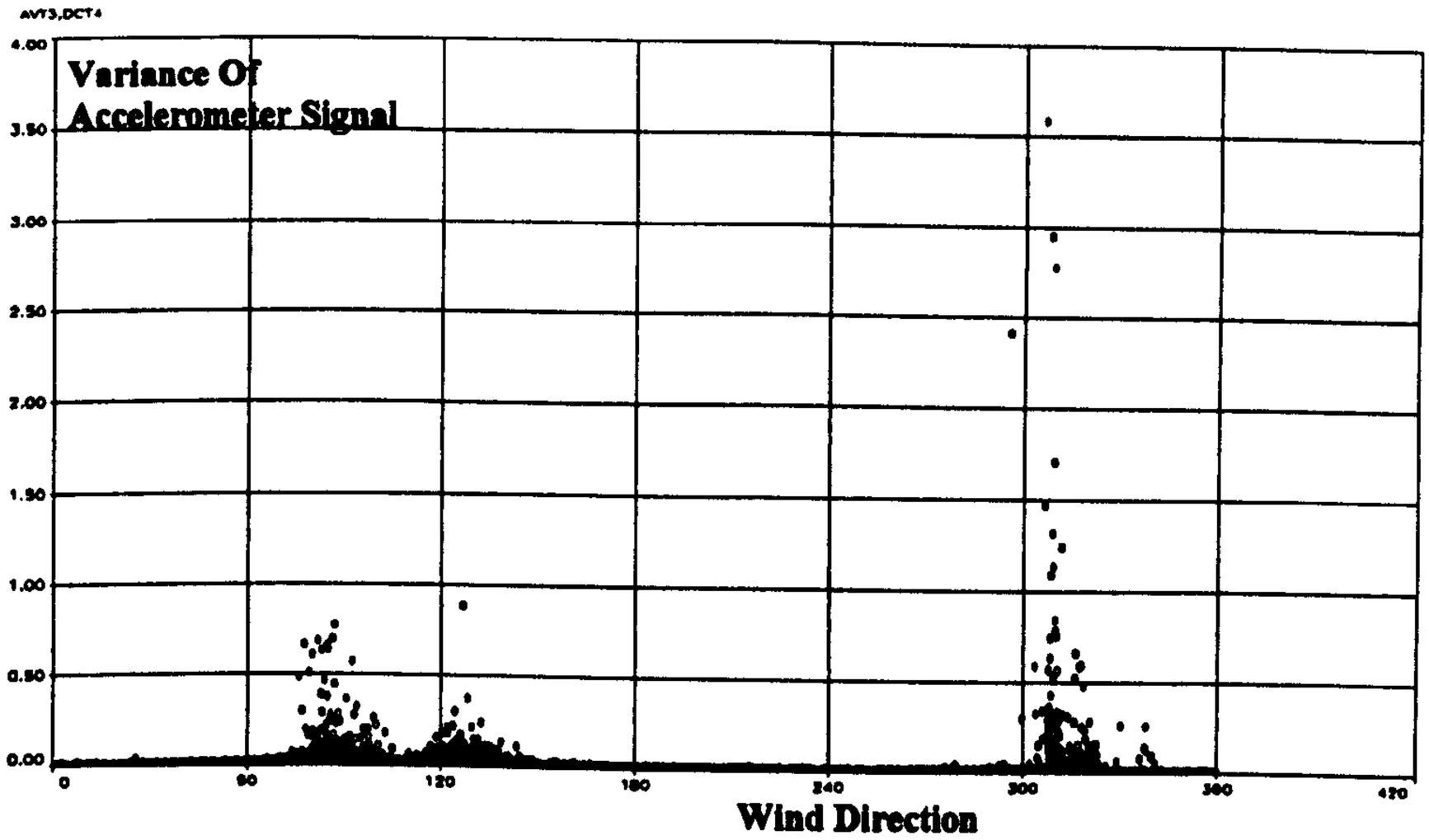

Figure 8.18 -:- Variation Of Response At Mid Span With Wind Direction
(Wind direction is measured in degrees, clockwise from Southerly axis of the bridges)

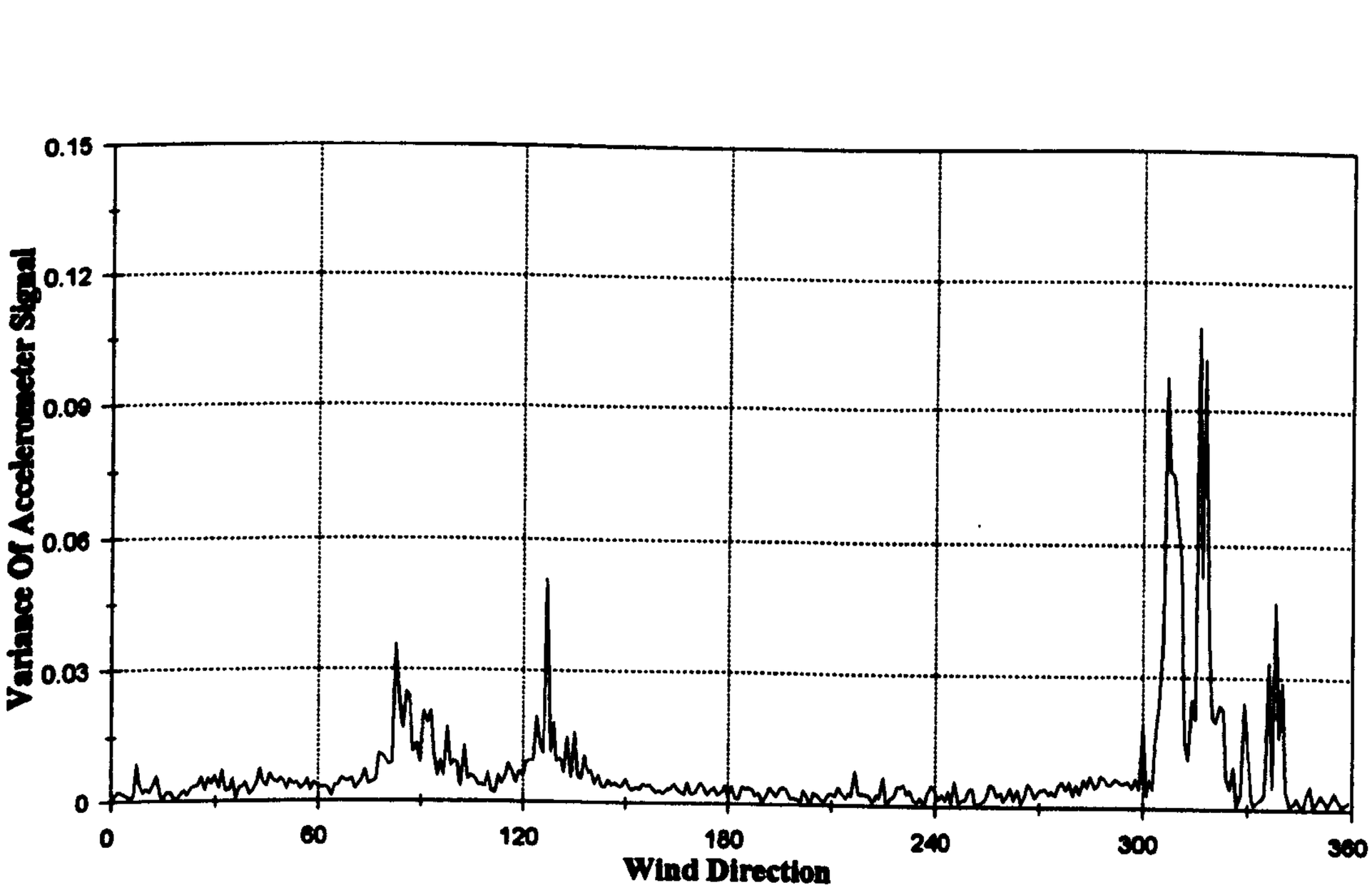

Figure 8.19 -:- Smoothed Variation Of Response At Mid Span With Wind Direction
(Wind direction is measured in degrees, clockwise from Southerly axis of the bridges)

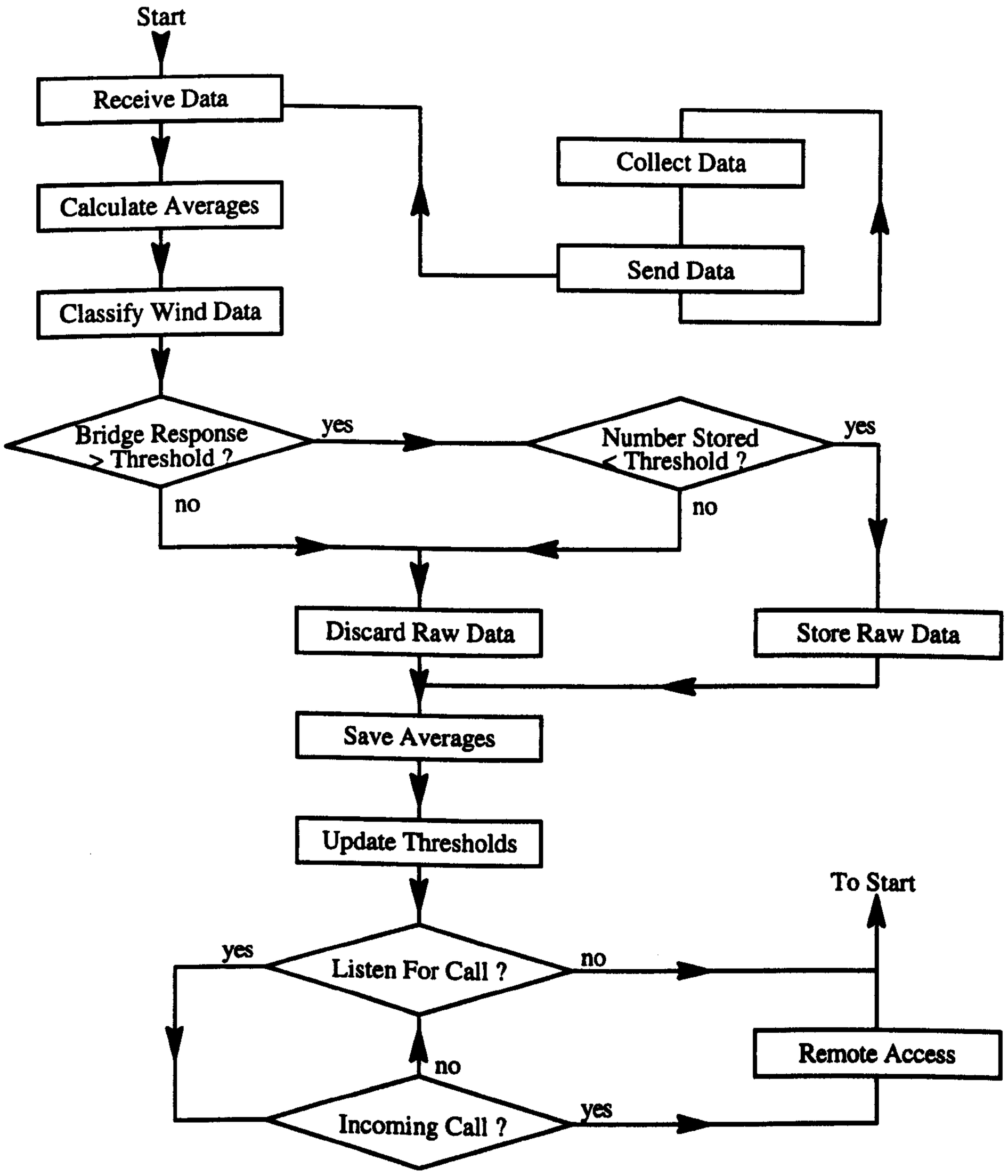

Figure 8.20 : Flow Chart of Modified Monitoring Strategy

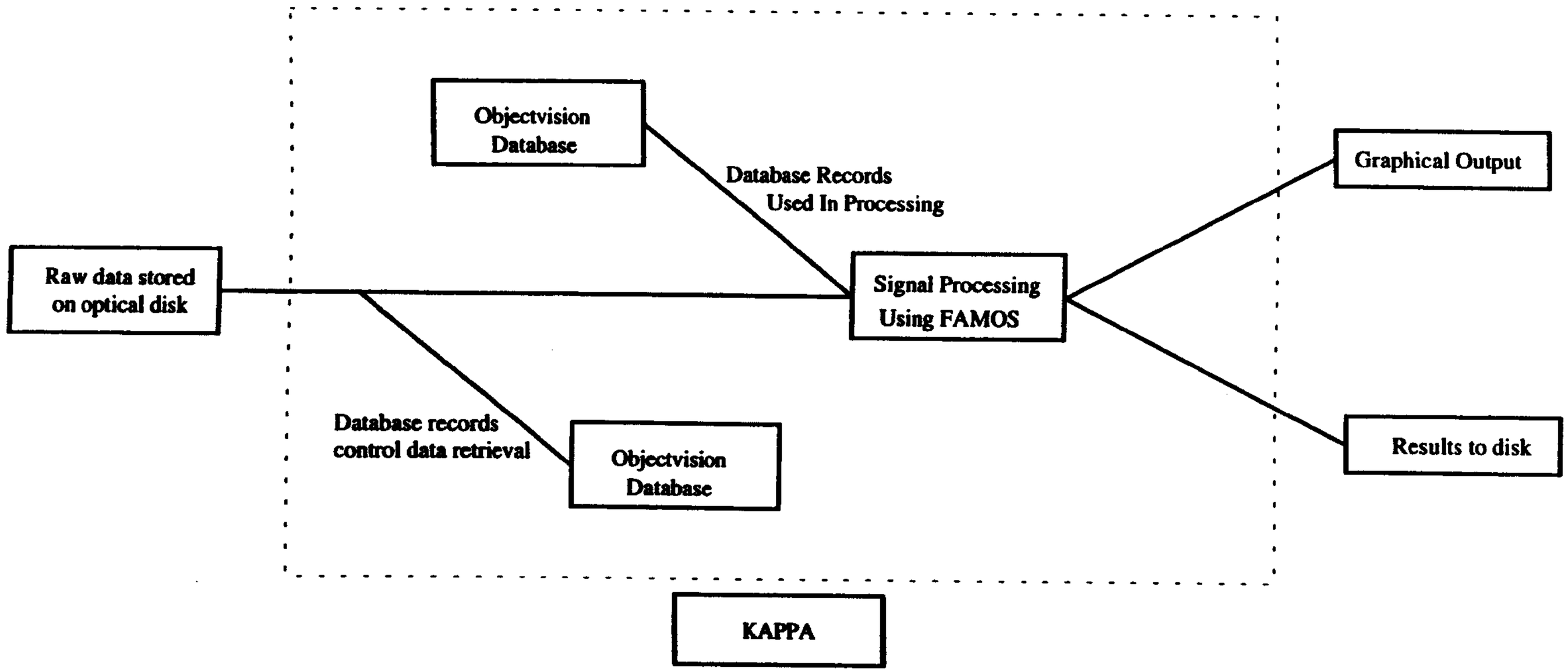

Figure 8.21 : Block Diagram of IMCES Program

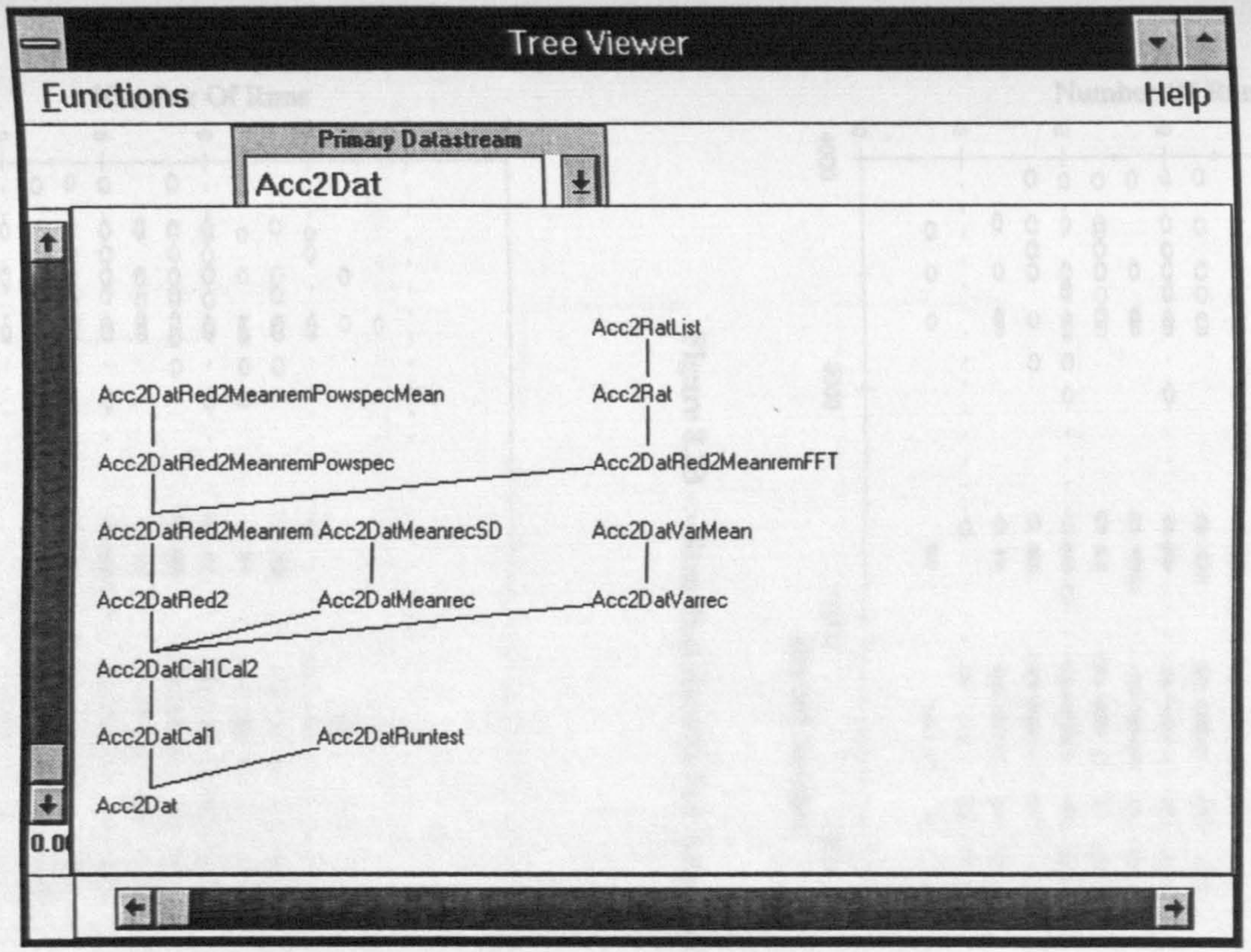

Figure 8.22 : Typical Signal Processing Tree

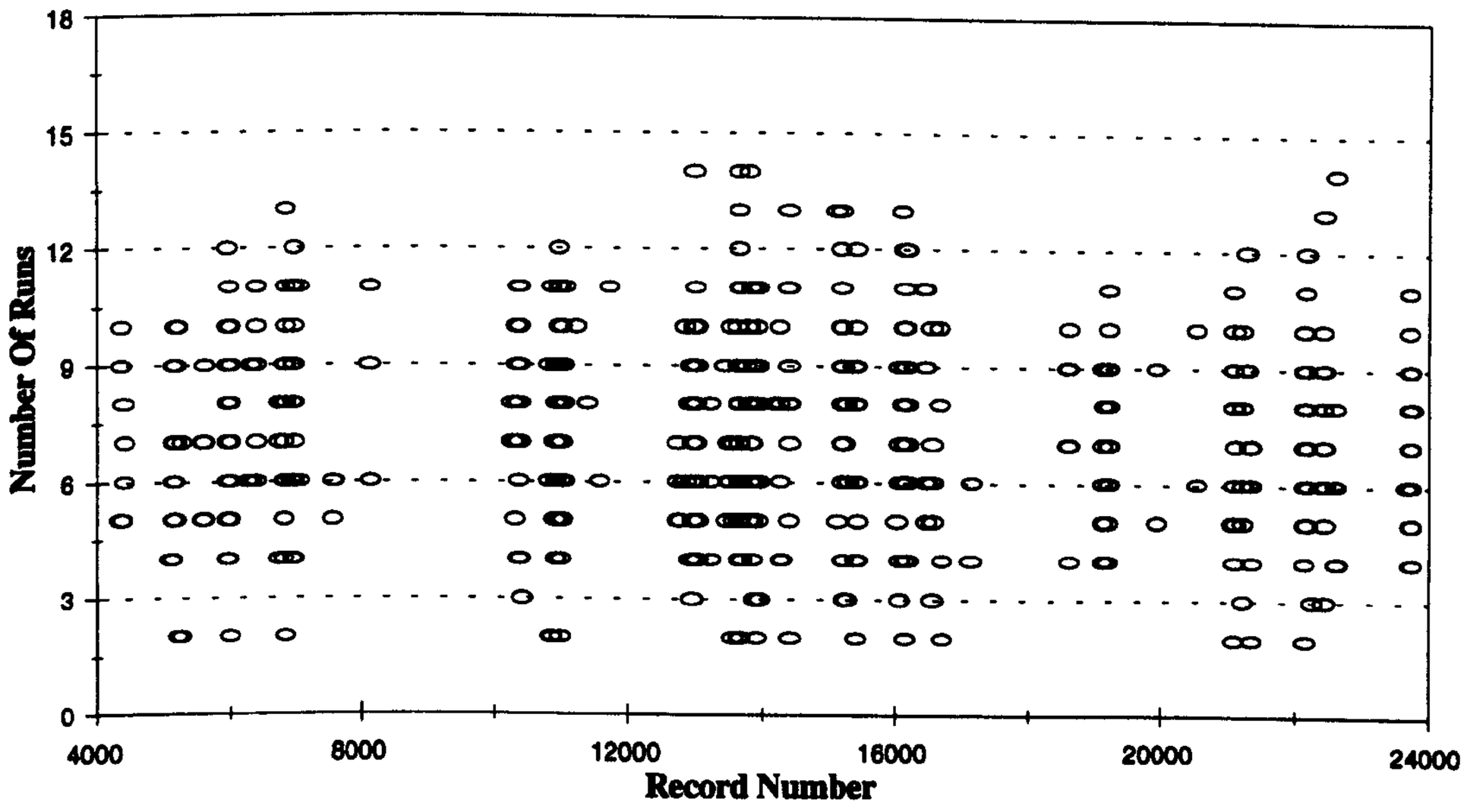

Figure 8.23 -:- Run Test Results For Anemometer Four

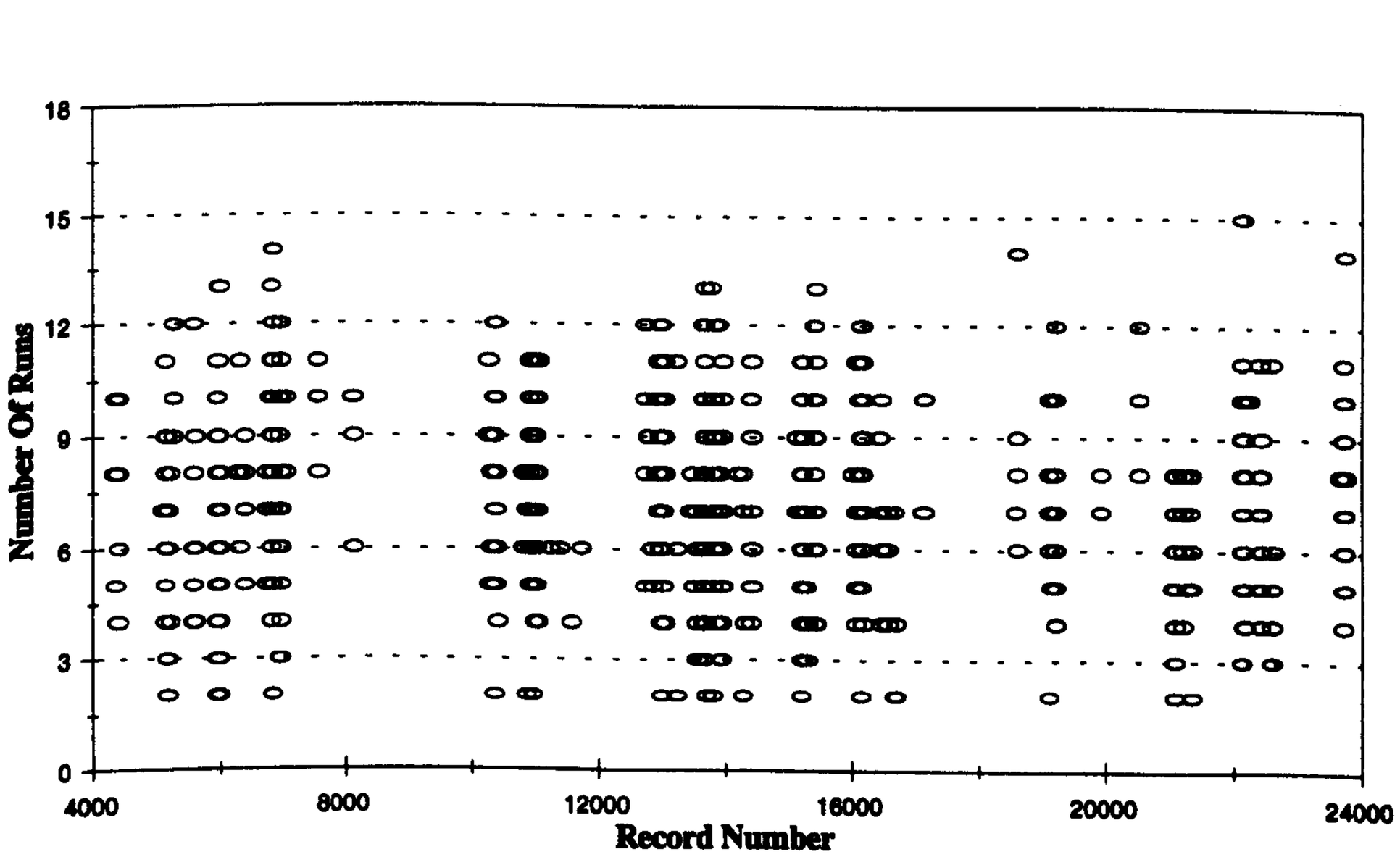

Figure 8.24 -:- Run Test Results For Anemometer Seven

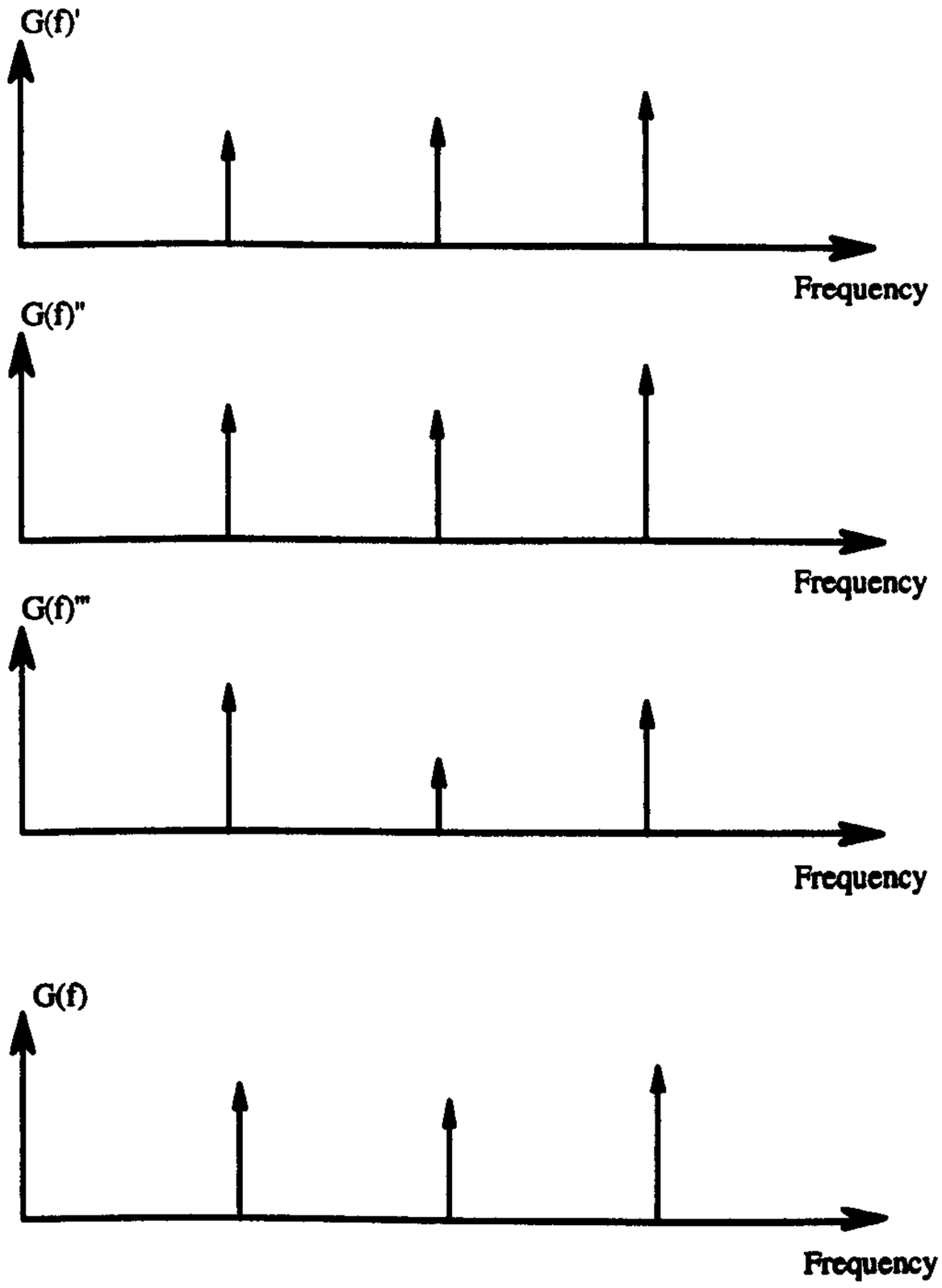

Figure 8.25a : Schematic Diagram of Ensemble Averaging, $G(f) = \frac{1}{n}\sum_{i=1}^{n} G^i(f)$

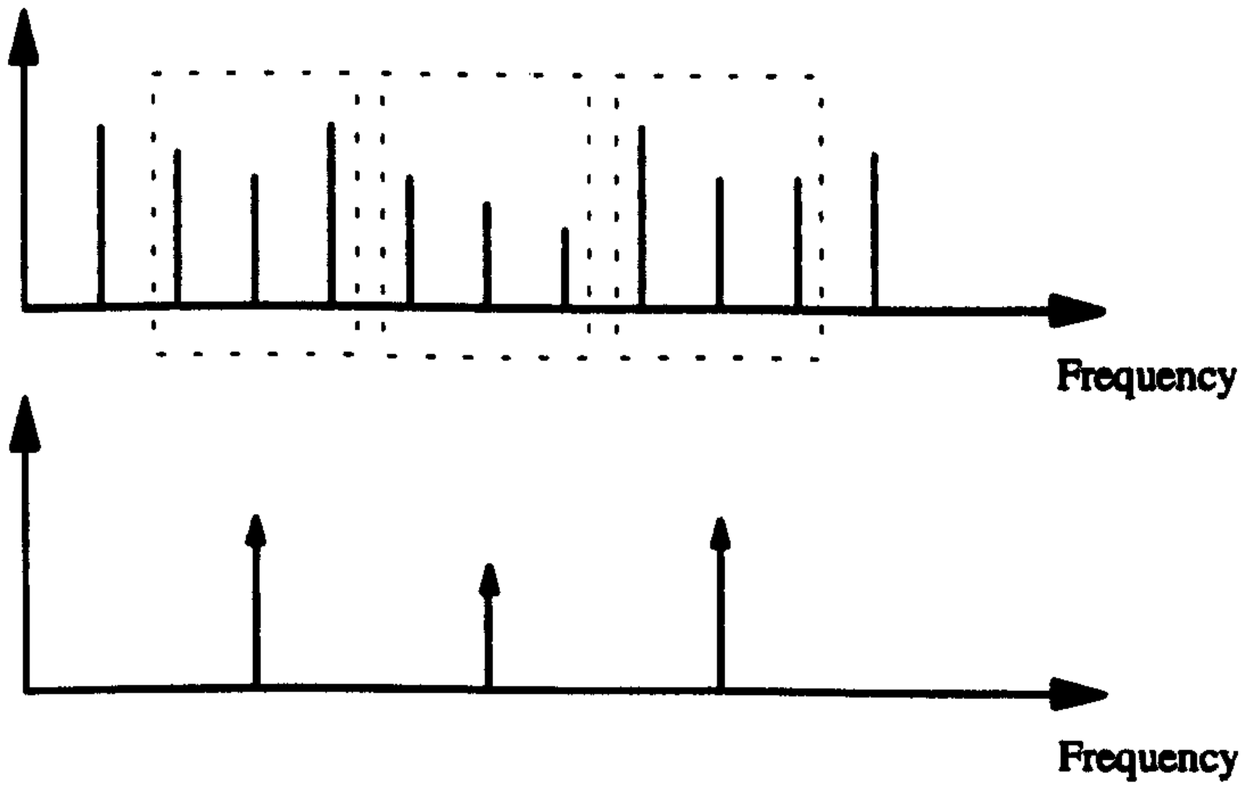

Figure 8.25b : Schematic Diagram of Block Averaging

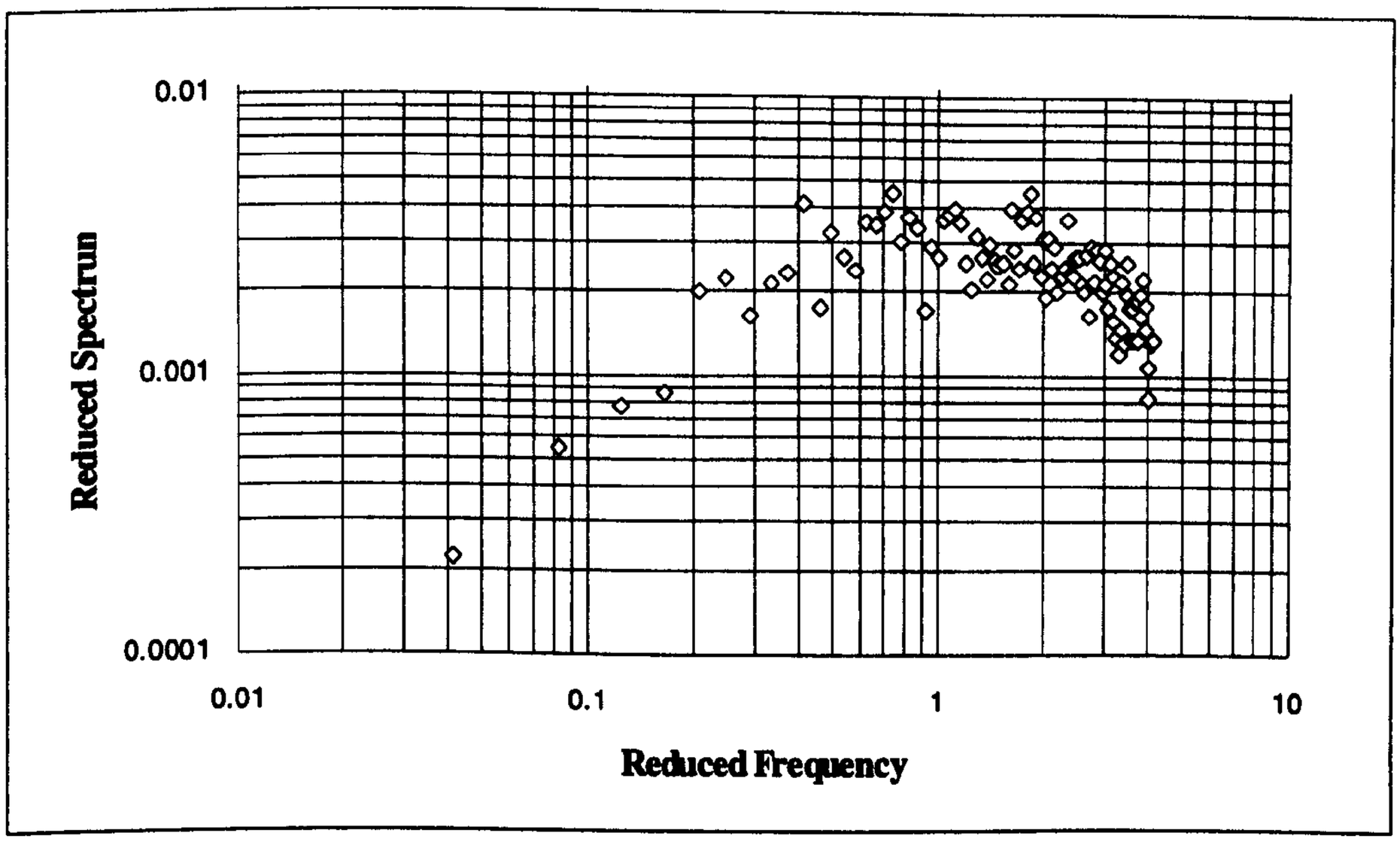

Figure 8.26 : Reduced Wind Spectrum, Westerly, Speed=10.86 m/s

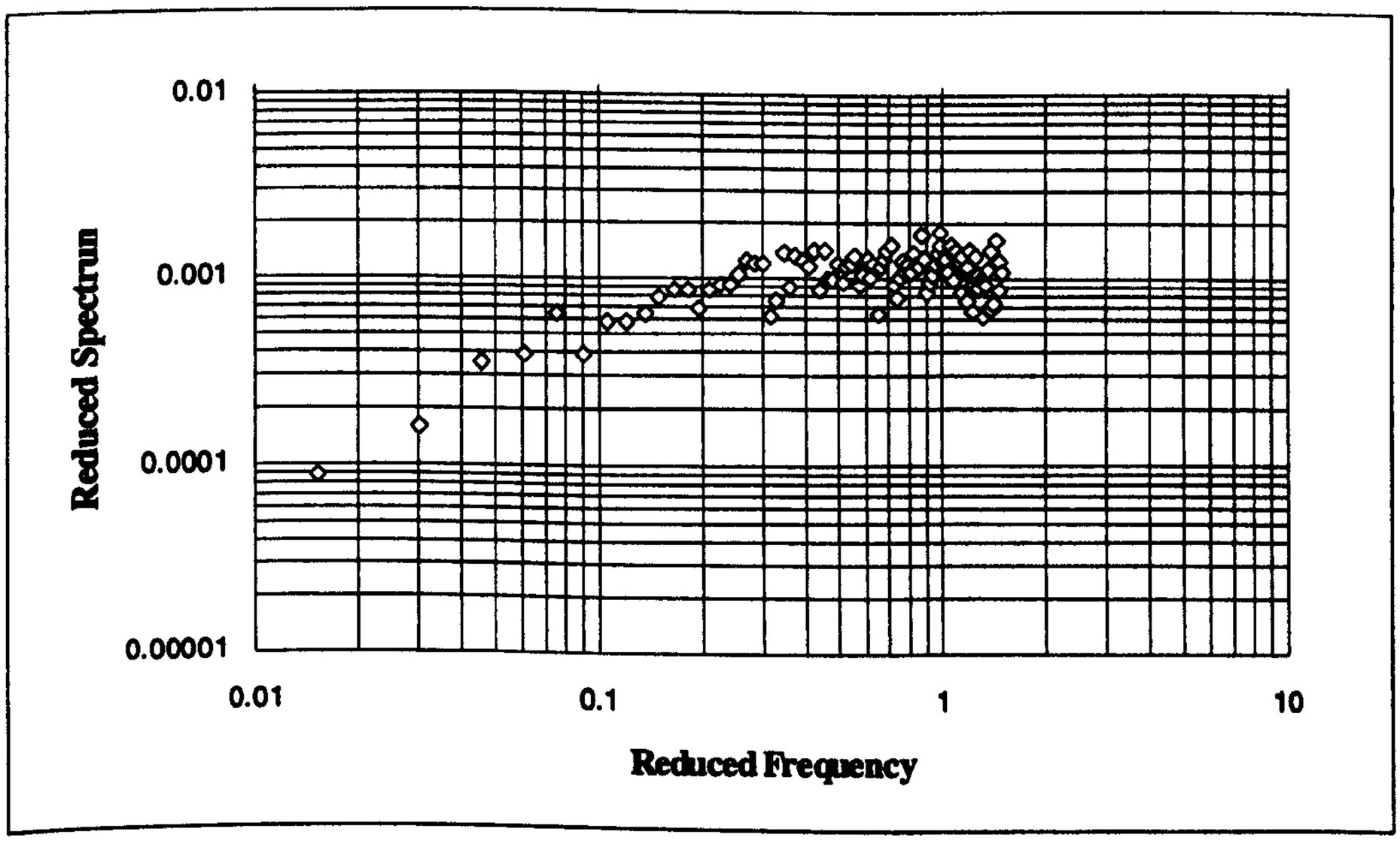

Figure 8.27 : Reduced Wind Spectrum, Westerly, Speed=27.49 m/s

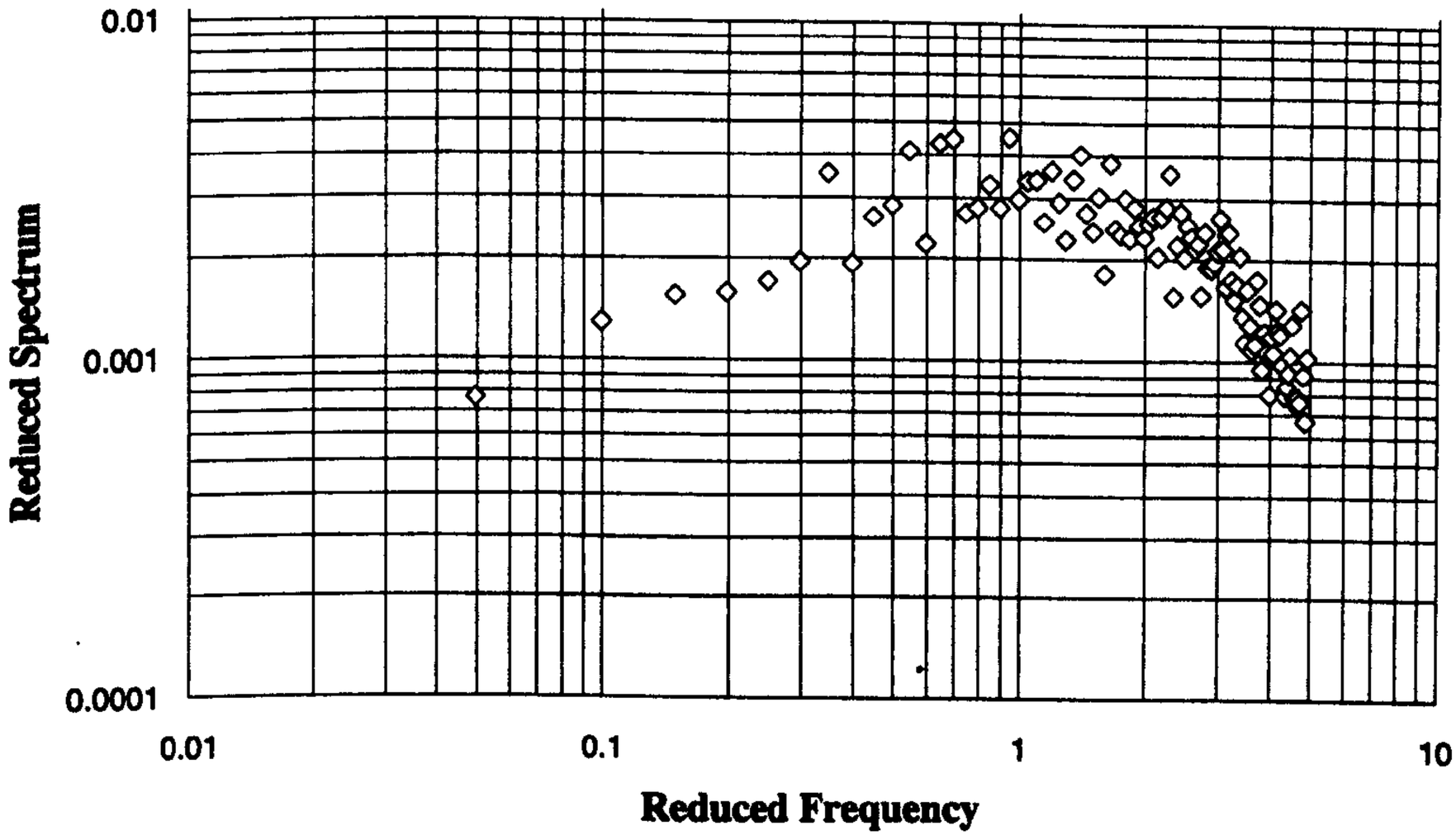

Figure 8.28a : Mean Wind Spectrum, Easterly, Speed=10.24 m/s

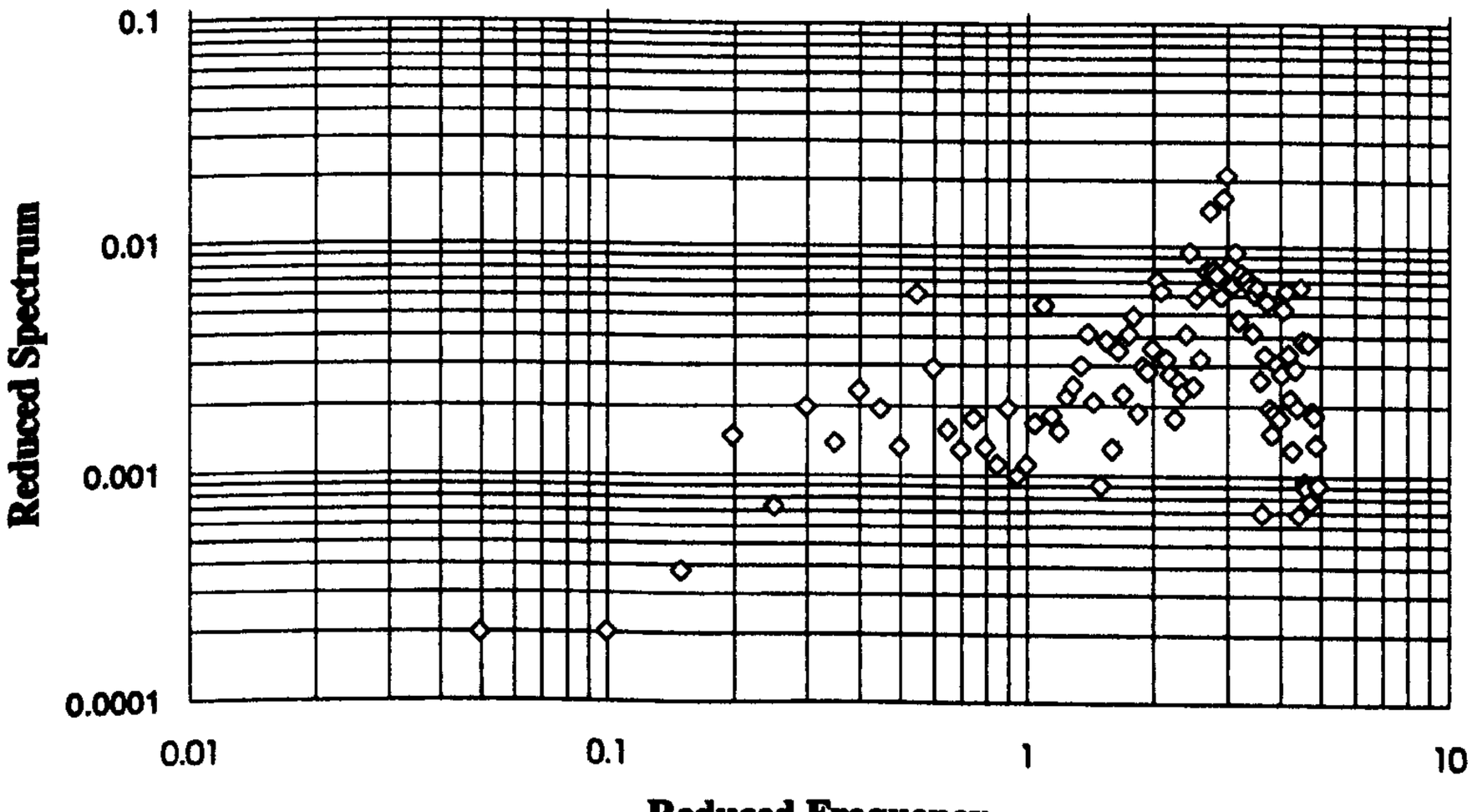

Figure 8.28a : Wind Spectrum for Anemometer 3, Easterly, Speed=10.24 m/s

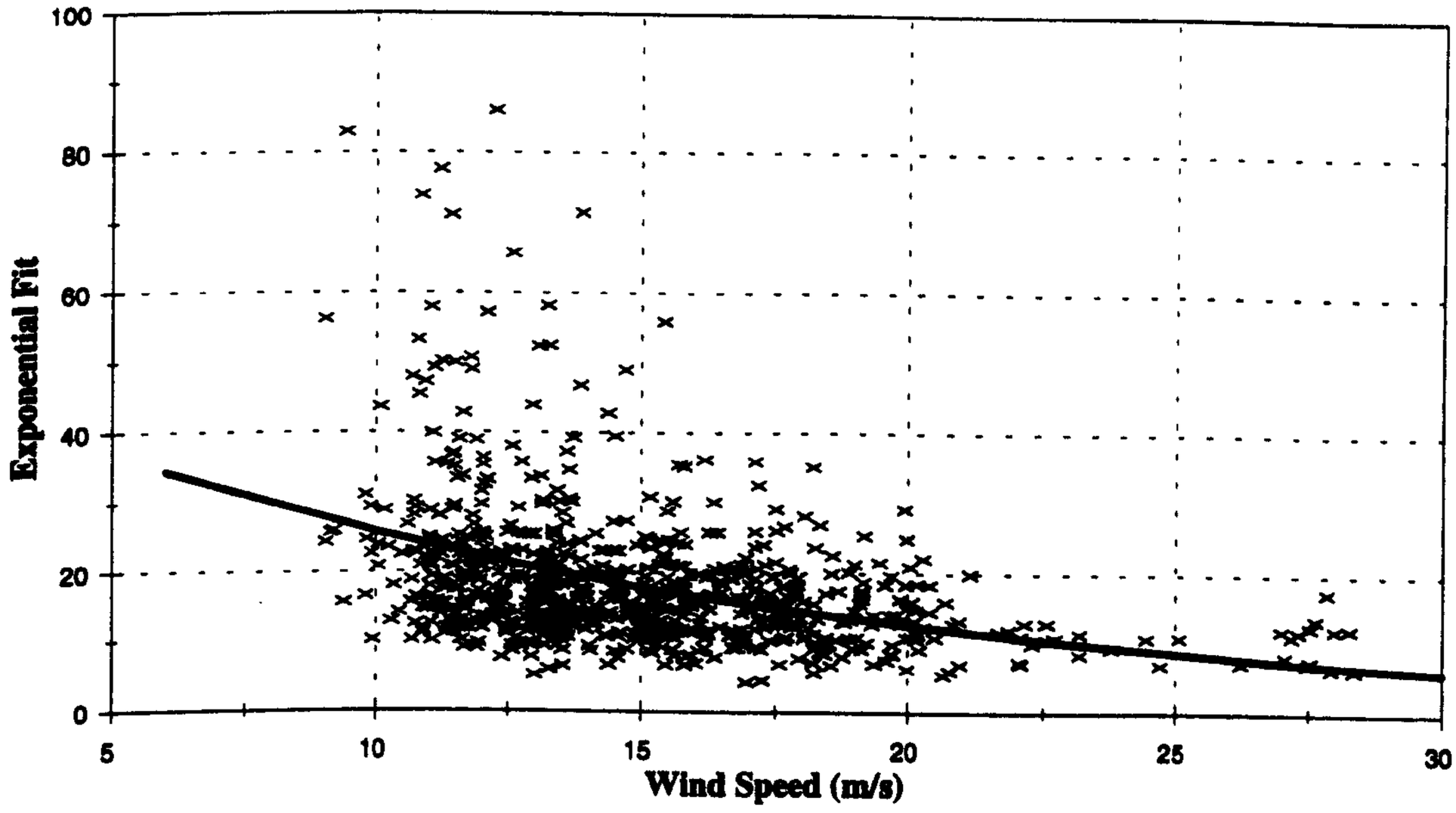

Figure 8.29 -:- Variation In Exponential Fit With Wind Speed, Anemometers 4 And 5

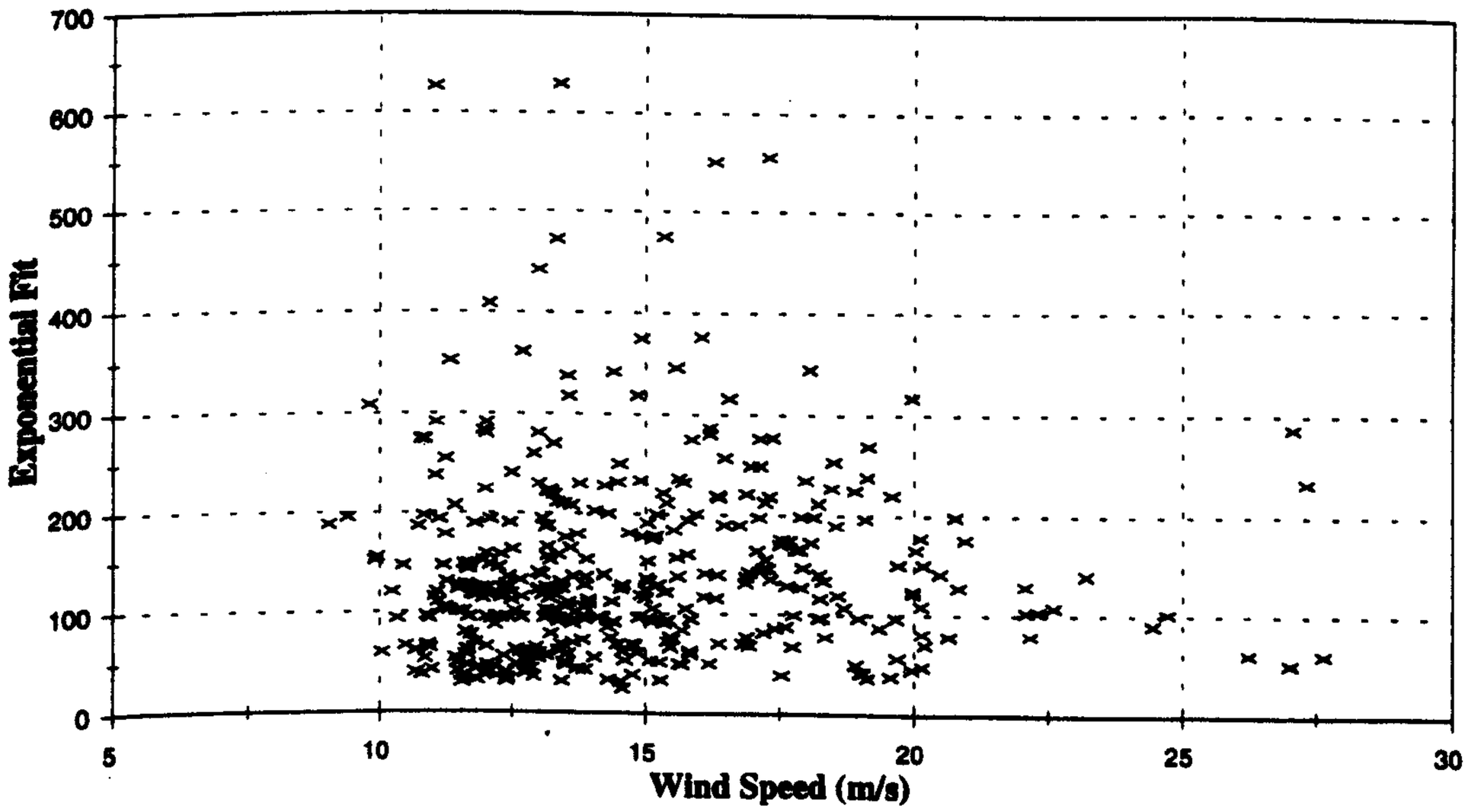

Figure 8.30 -:- Variation In Exponential Fit With Wind Speed, Anemometers 4 And 6

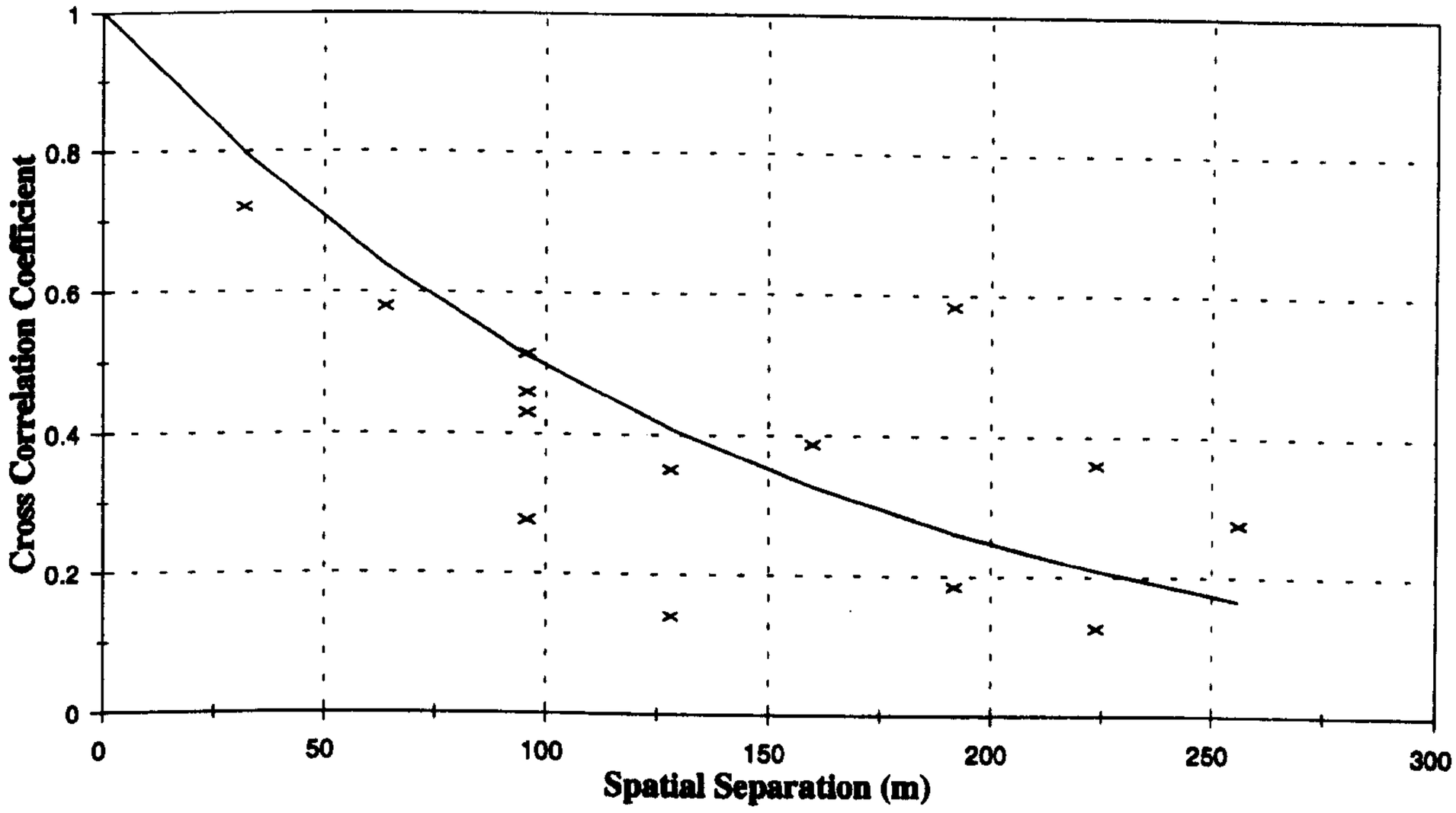

Figure 8.31 -:- Typical Variation Of Cross Correlation With Anemometer Separation

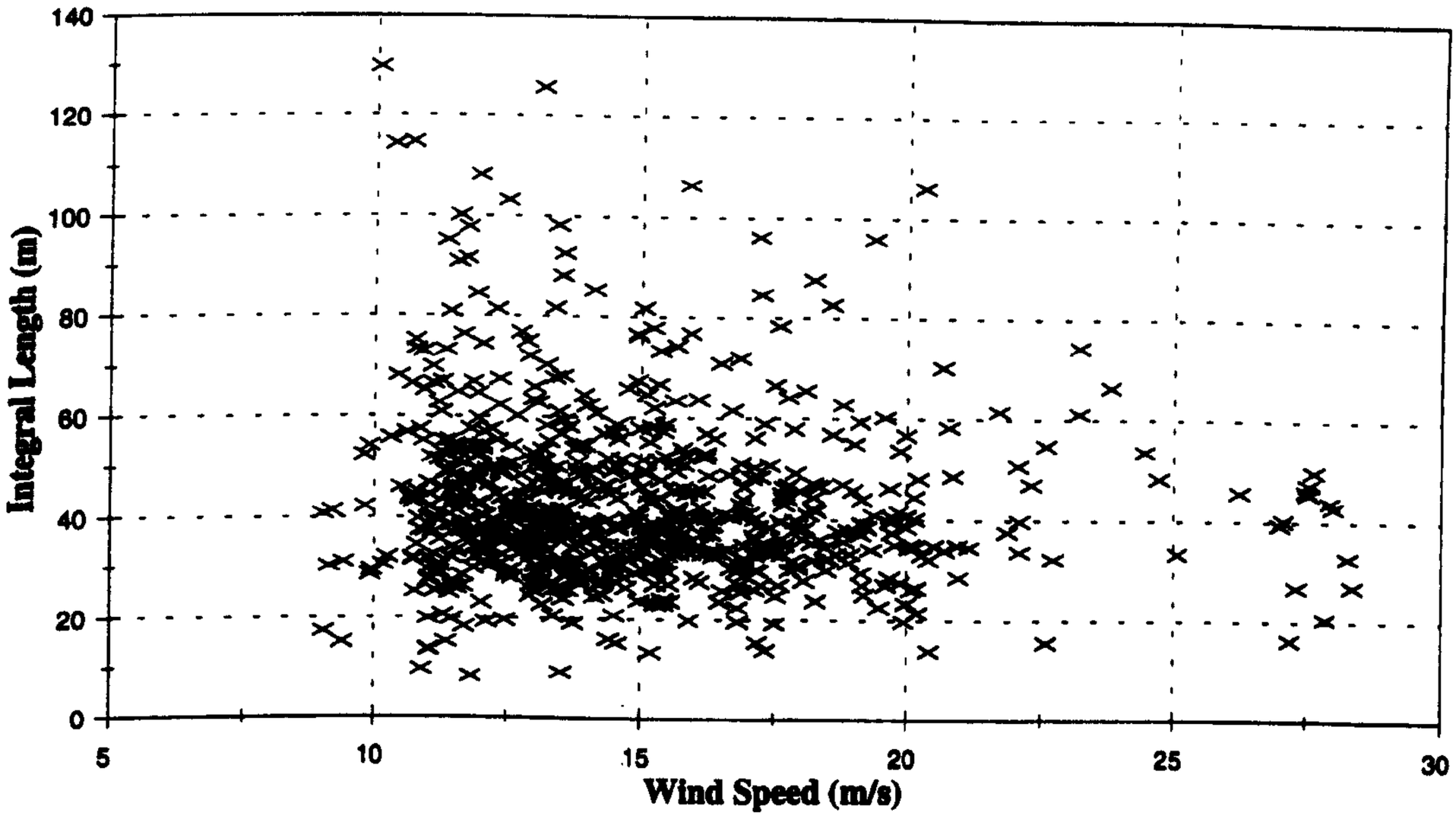

Figure 8.32 -:- Variations In Integral Length With Wind Speed, Westerly Winds

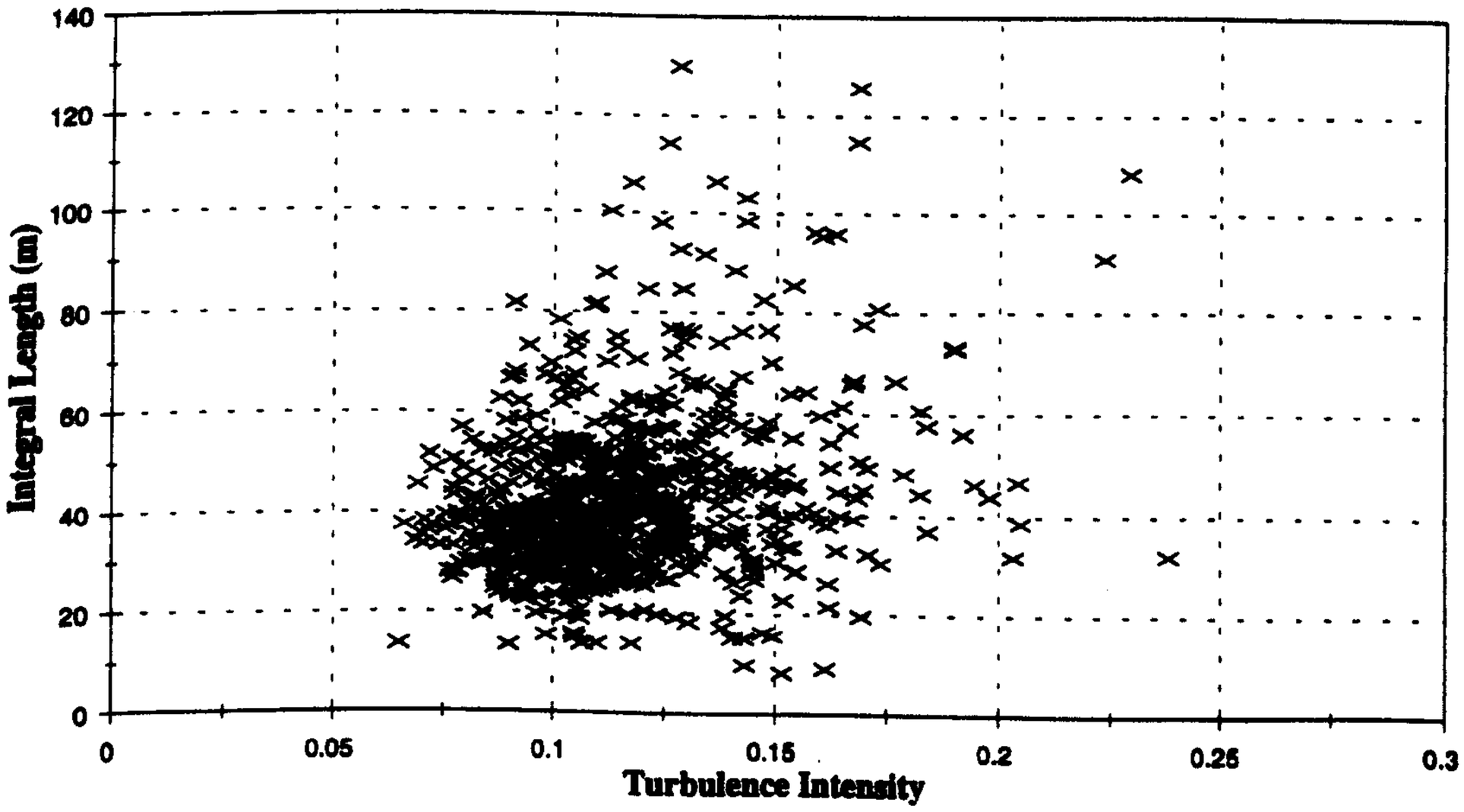

Figure 8.33 -:- Variations In Integral Length With Turbulence Intensity, Westerly Winds

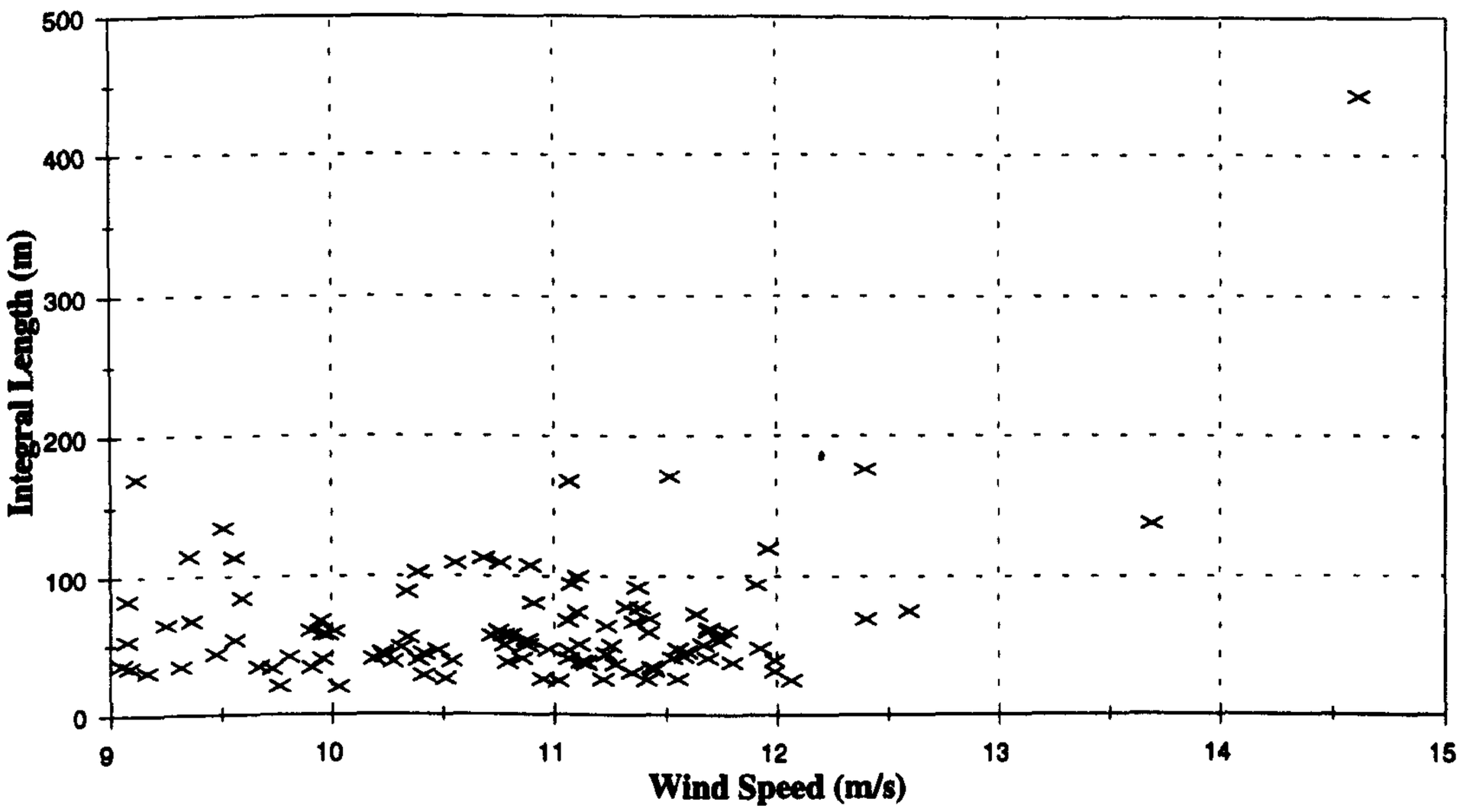

Figure 8.34 -:- Variations In Integral Length With Wind Speed, Easterly Winds

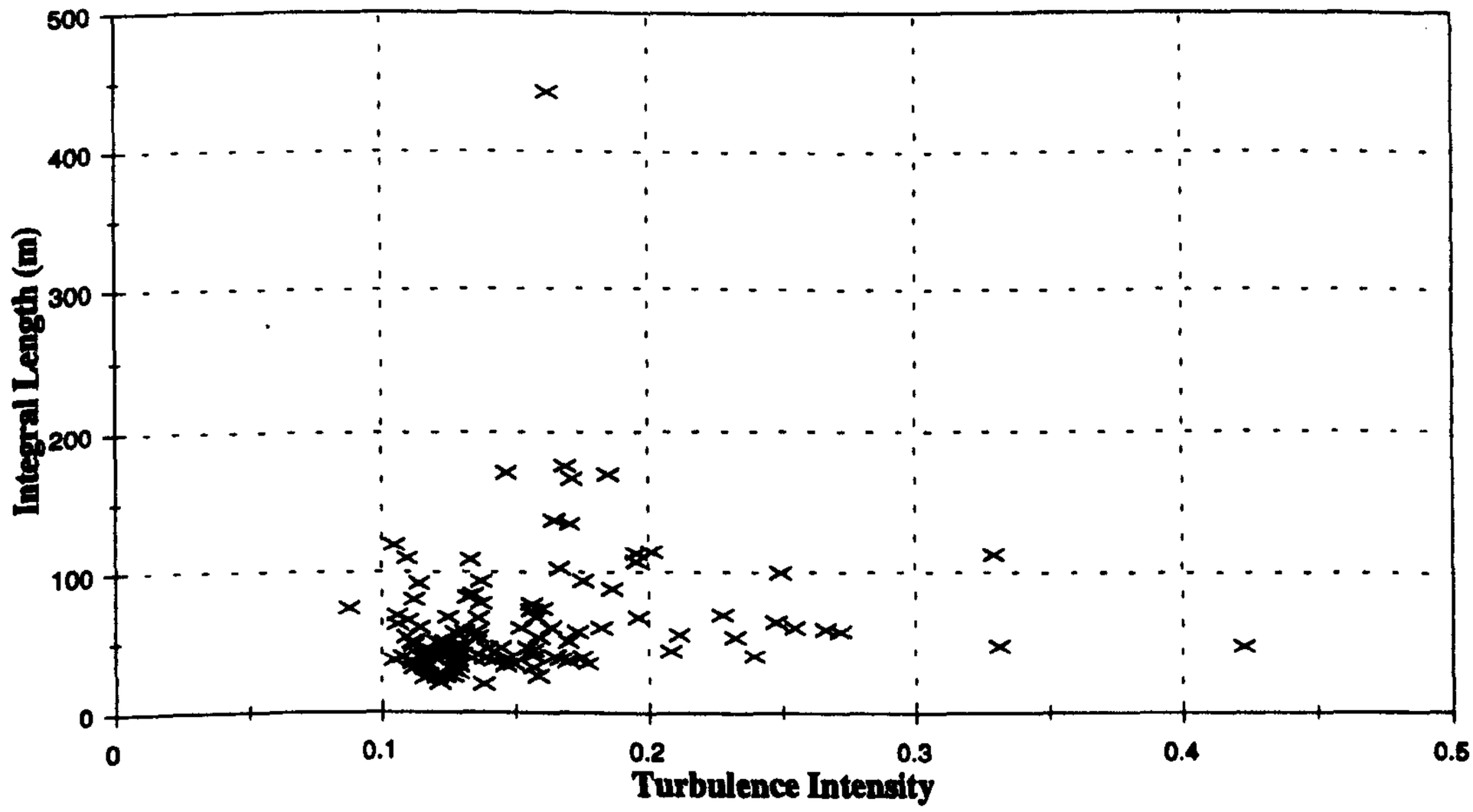

Figure 8.35 -:- Variations In Integral Length With Turbulence Intensity, Easterly Winds

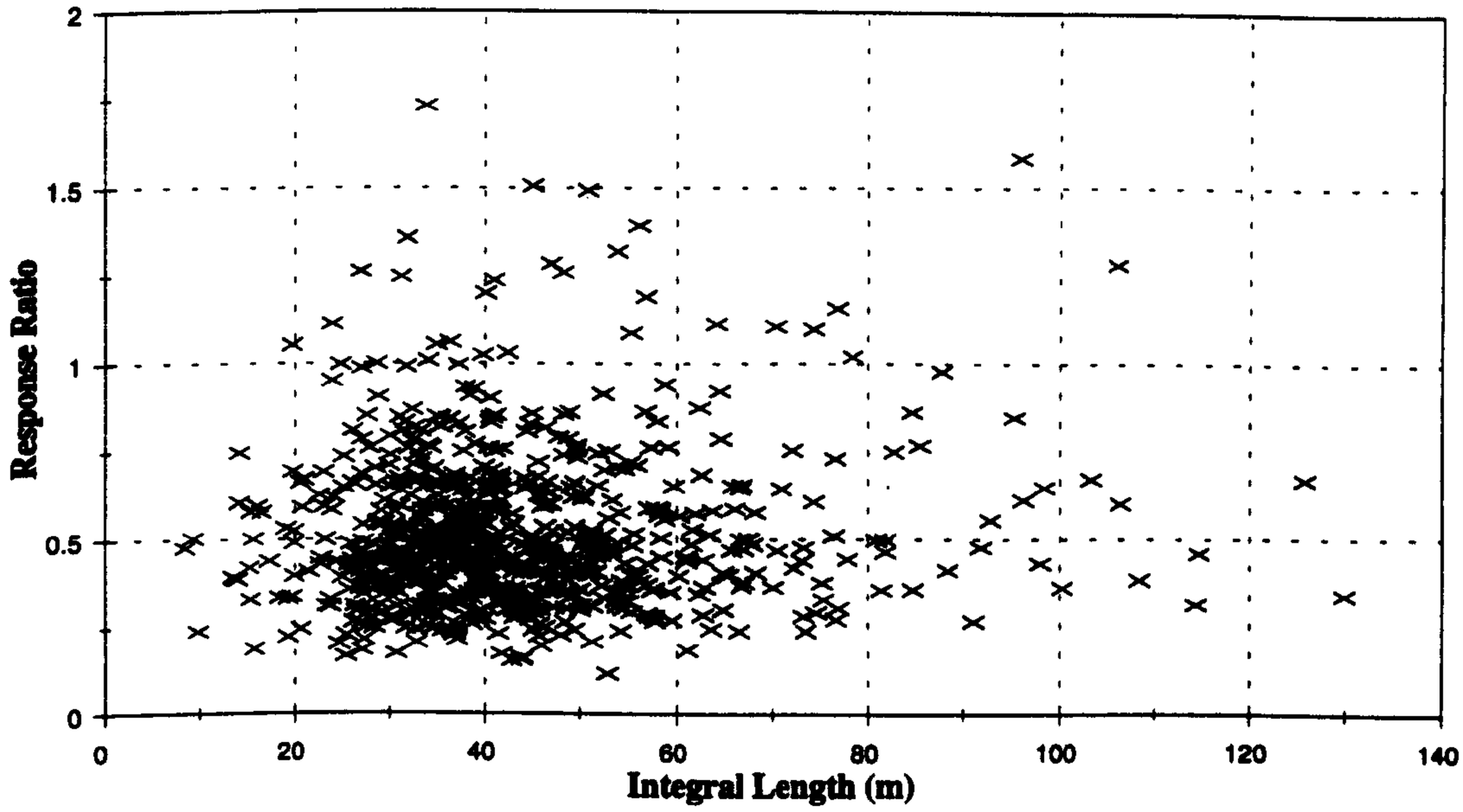

Figure 8.36 -:- Variation in Response Ratio With Integral Length, Modes 1 and 2, Westerly Wind

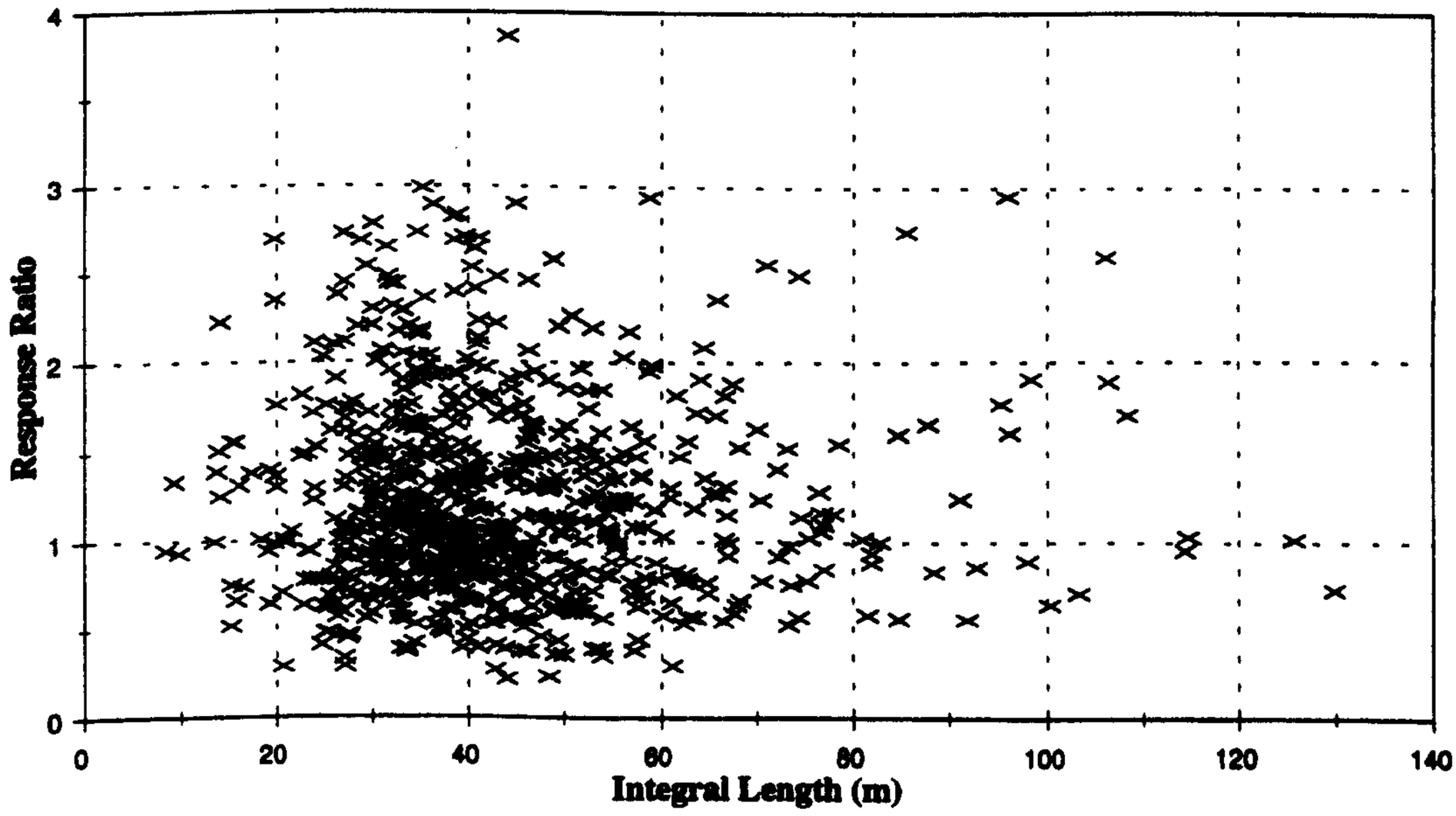

Figure 8.37 -:- Variation In Response Ratio With Integral Length, Modes 1 and 3, Westerly Wind

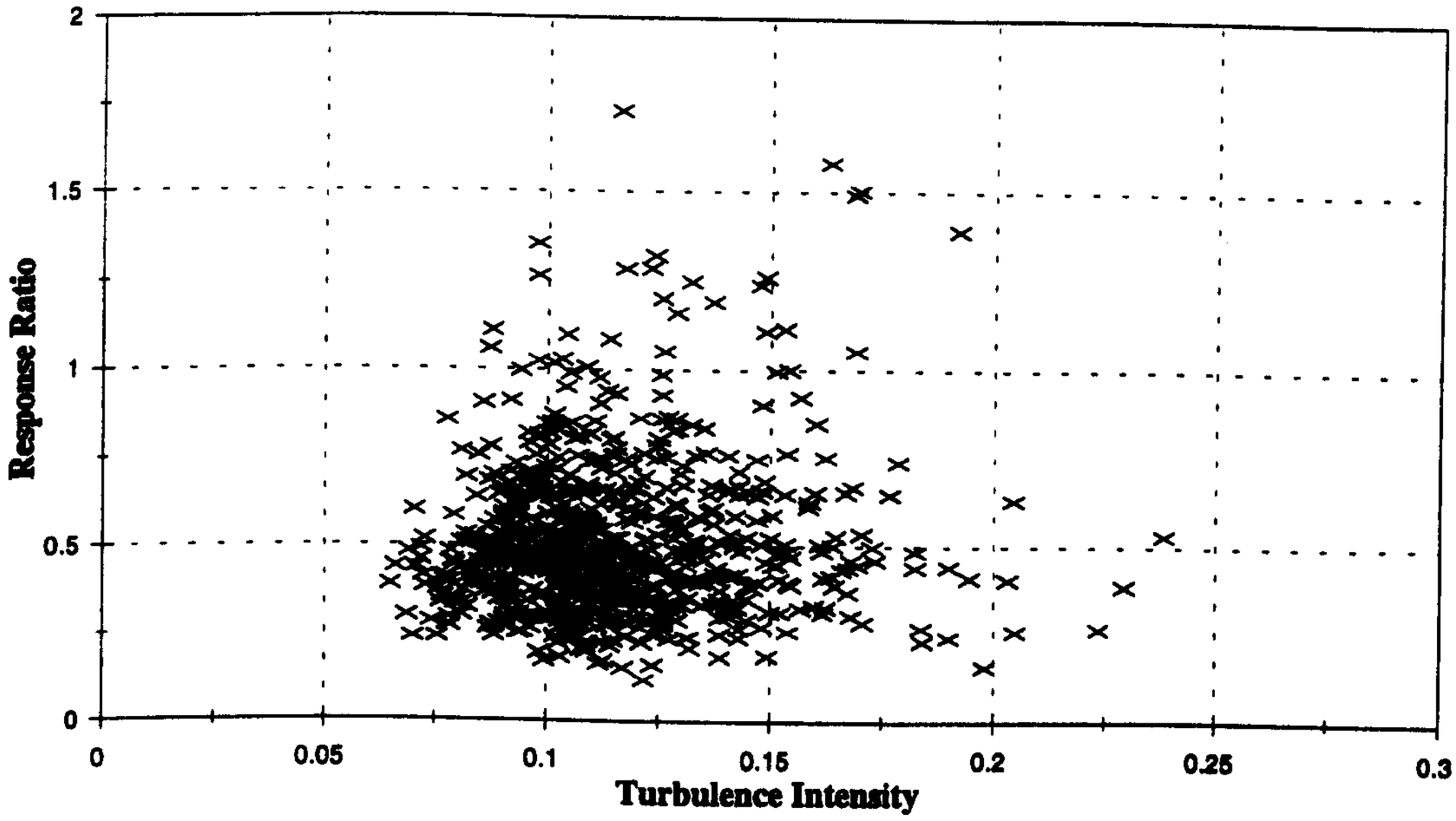

Figure 8.38 -:- Variation in Response Ratio With Turbulence Intensity, Modes 1 & 2, Westerly Wi

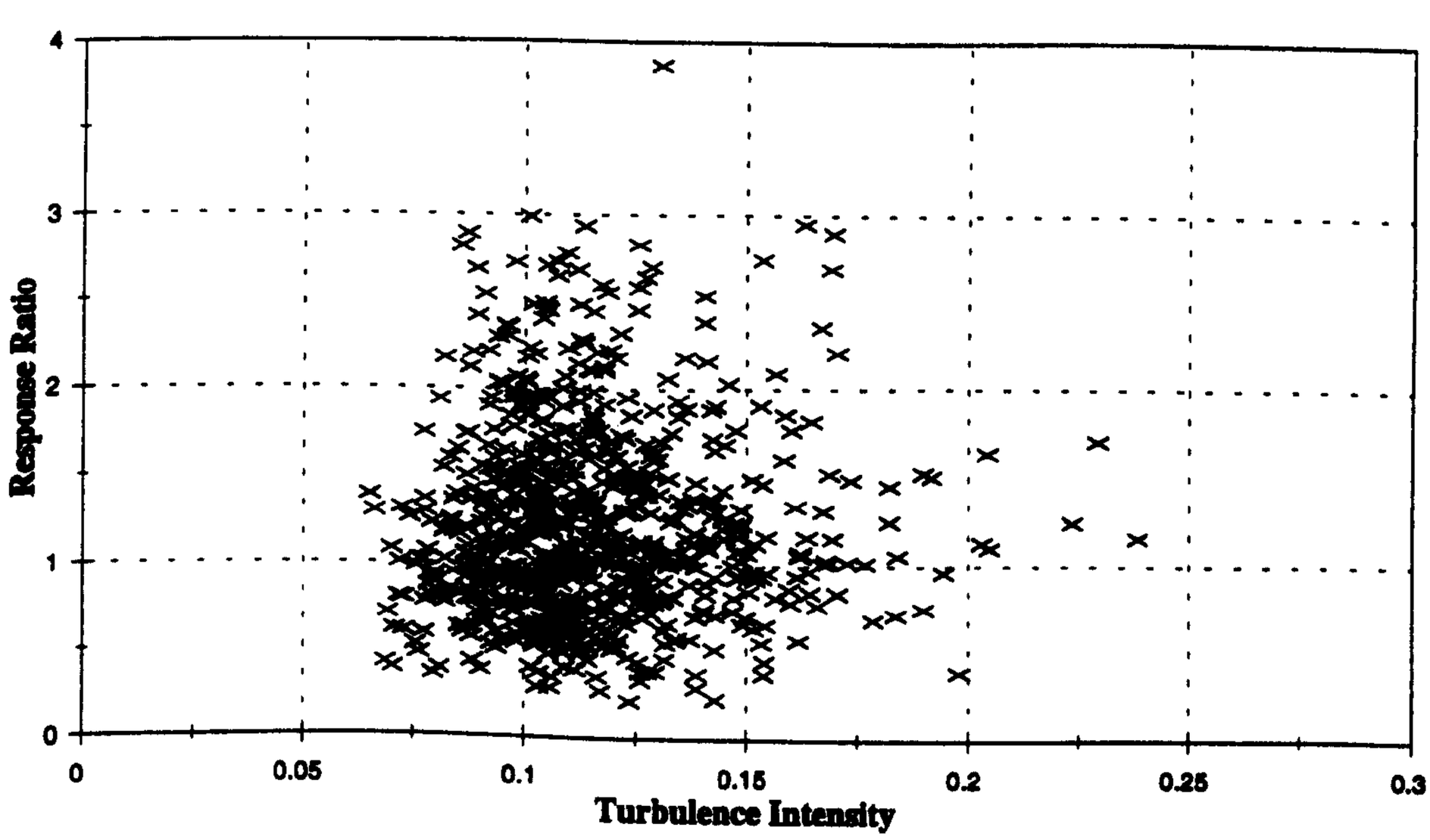

Figure 8.39 -:- Variation in Response Ratio With Turbulence Intensity, Modes 1 & 3, Westerly Wi

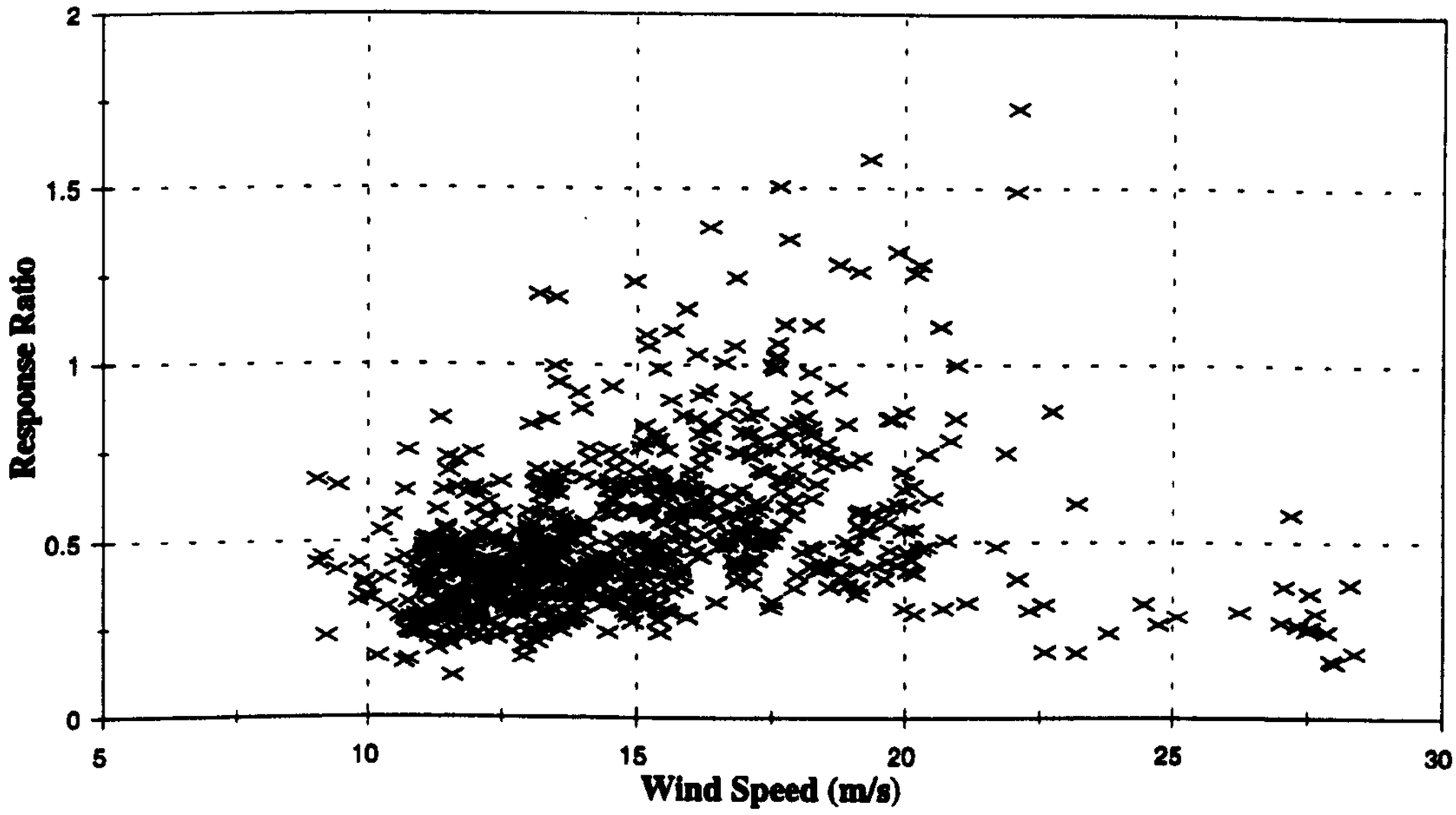

Figure 8.40 -:- Variation in Response Ratio With Wind Speed, Modes 1 & 2, Westerly Winds

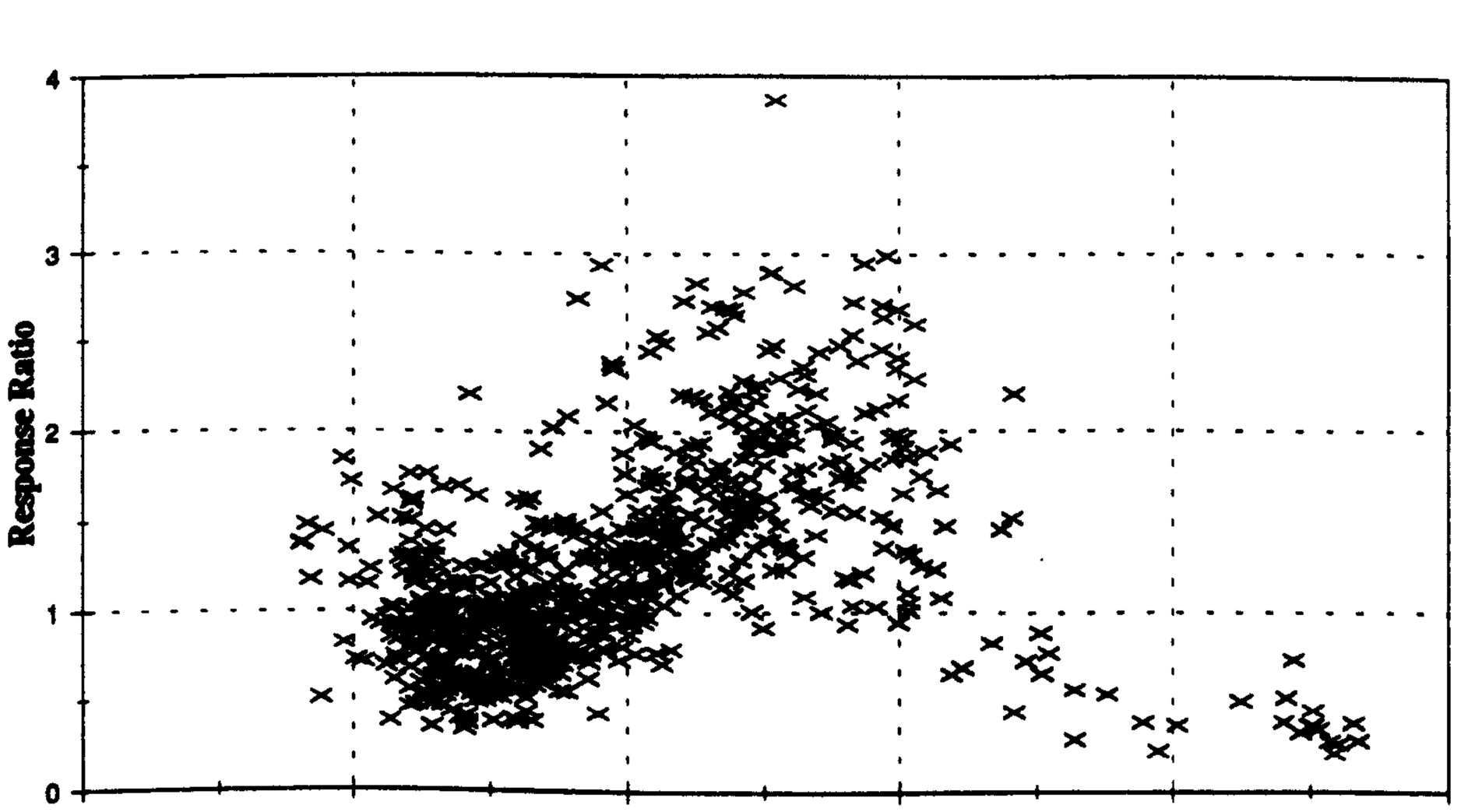

Figure 8.41 -:- Variation in Response Ratio With Wind Speed, Modes 1 & 3, Westerly Winds

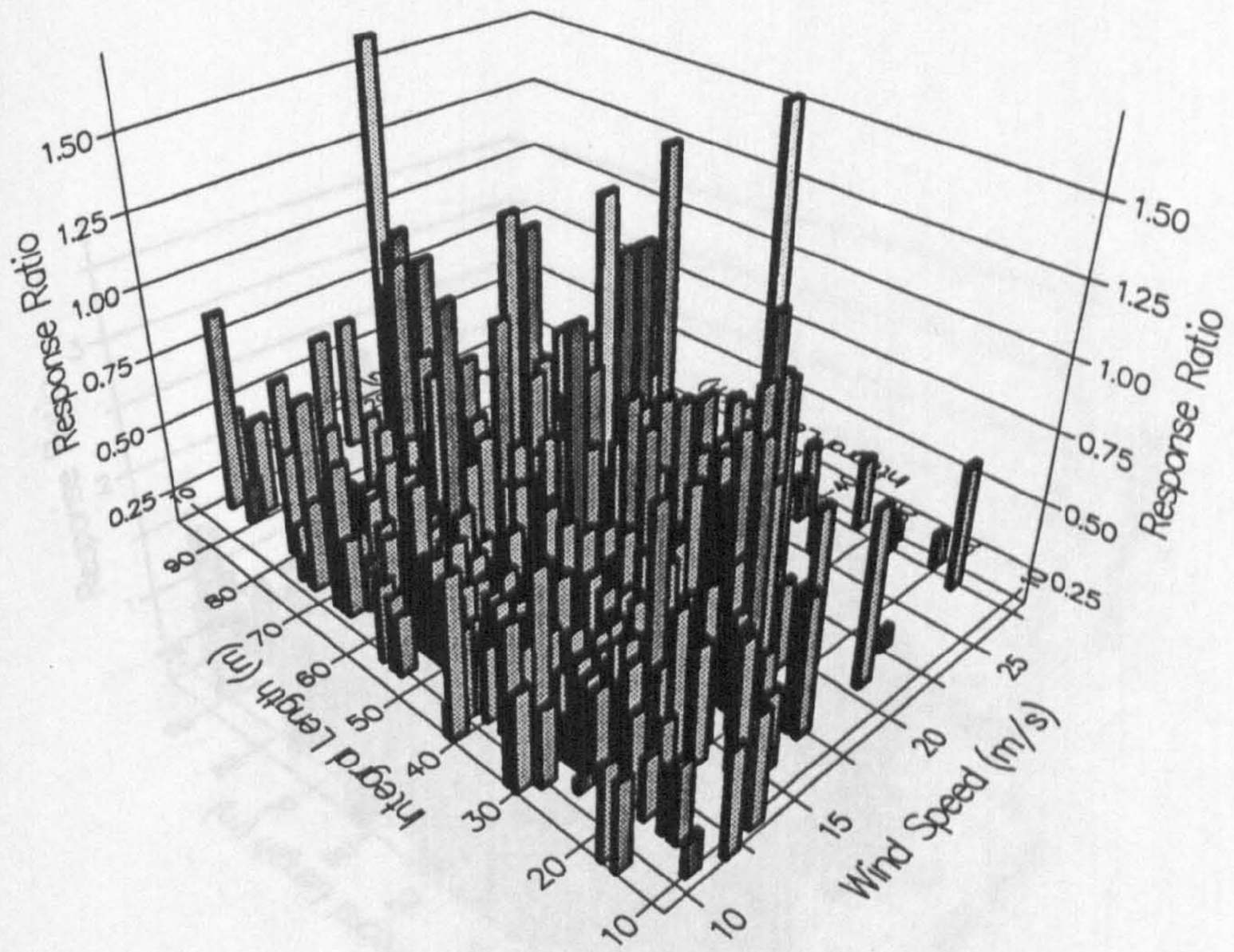

Figure 8.42 : Response Ratio Modes 1 & 2, Raw Data, Westerly Winds

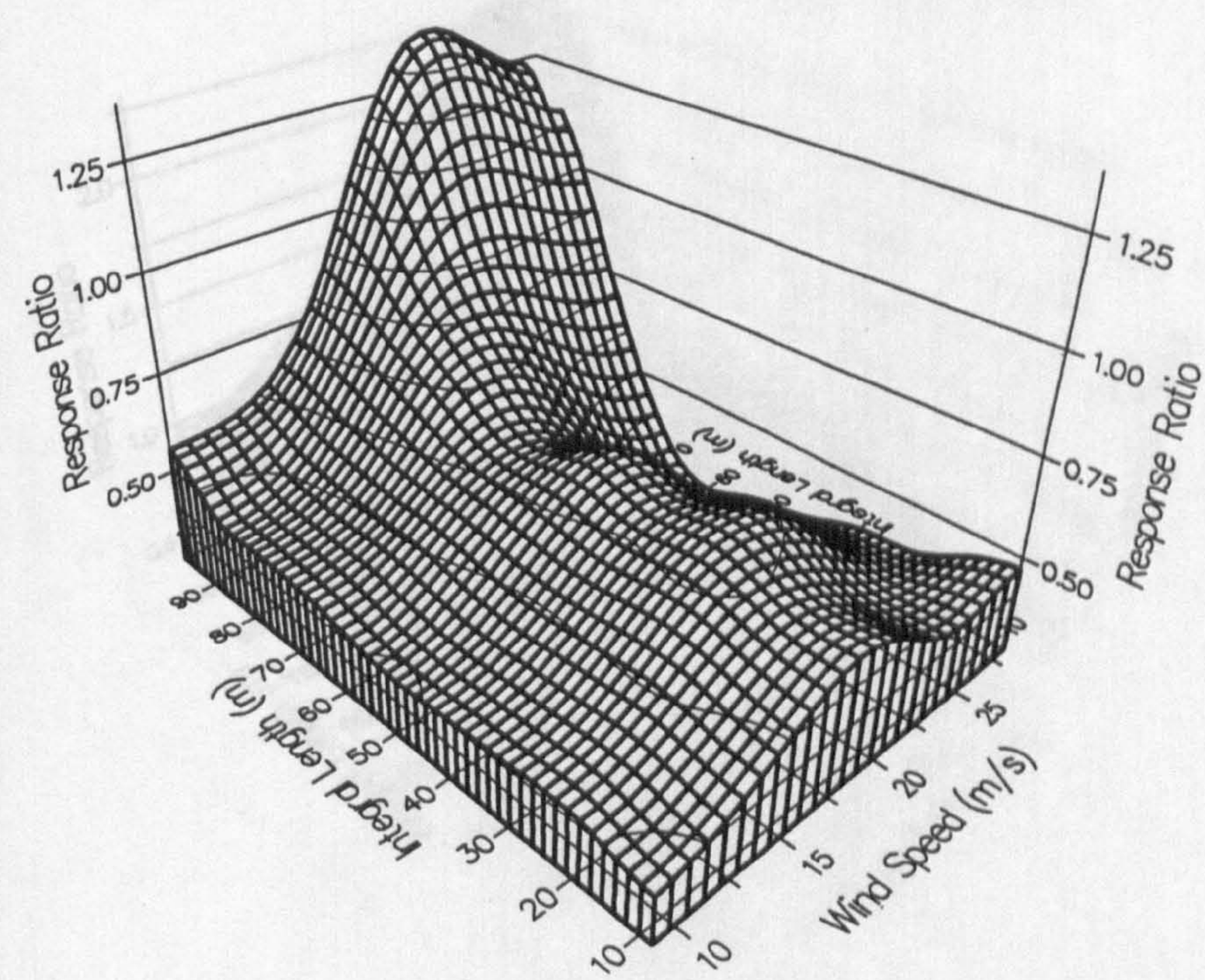

Figure 8.43 : Response Ratio Modes 1 & 2, Bilinear Fit, Westerly Winds

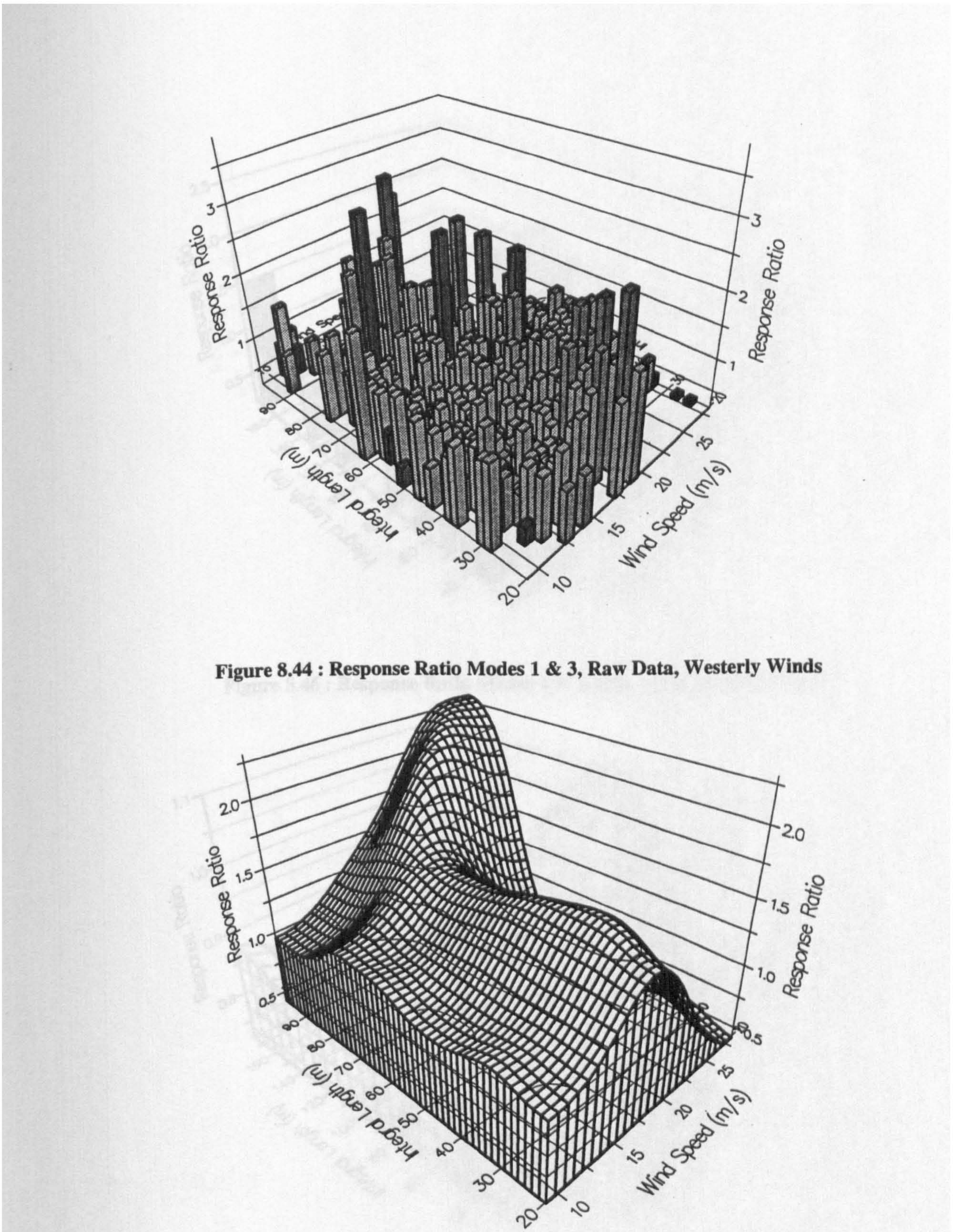

Figure 8.44 : Response Ratio Modes 1 & 3, Raw Data, Westerly Winds

Figure 8.45 : Response Ratio Modes 1 & 3, Bilinear Fit, Westerly Winds

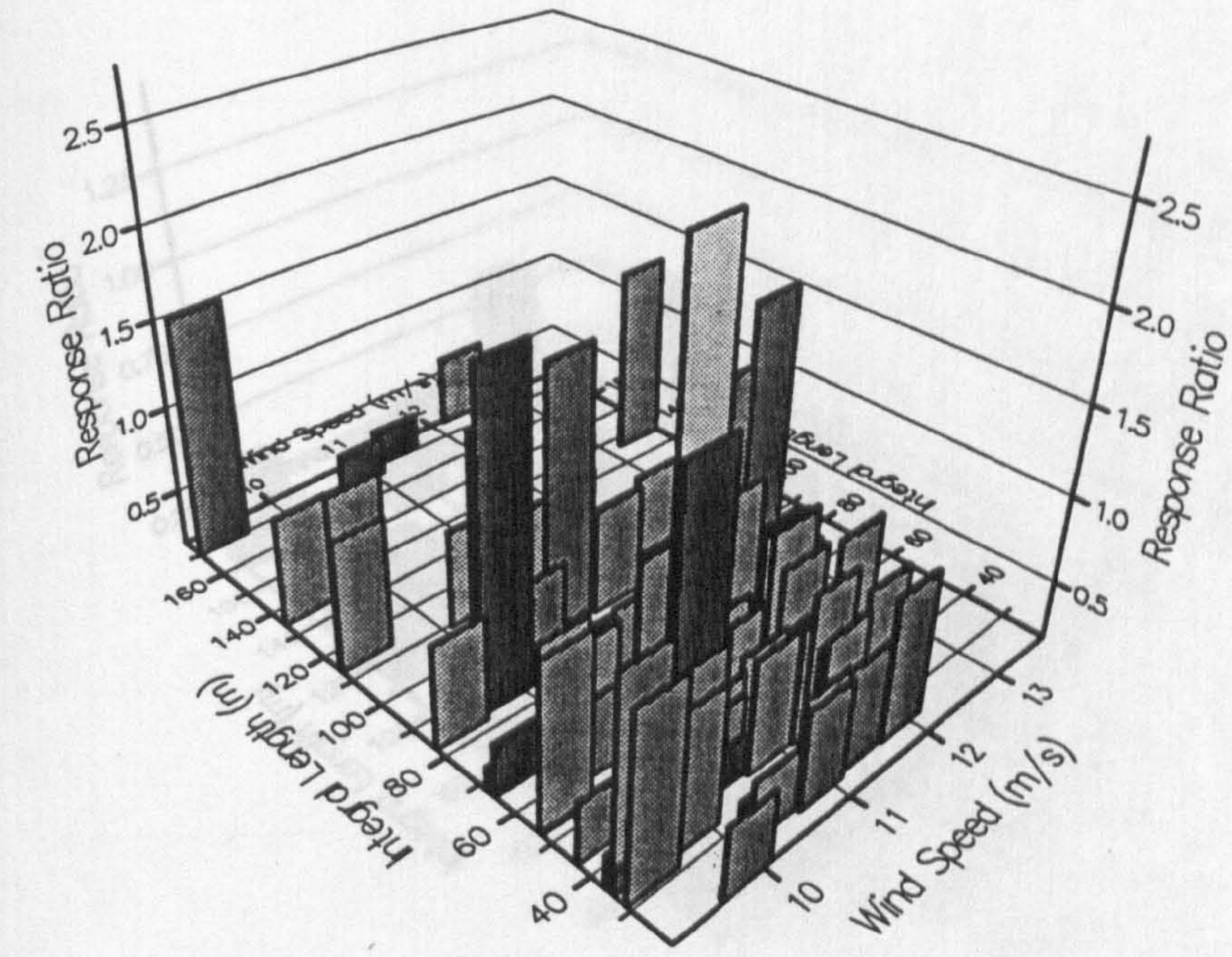

Figure 8.46 : Response Ratio Modes 1 & 2, Raw Data, Easterly Winds

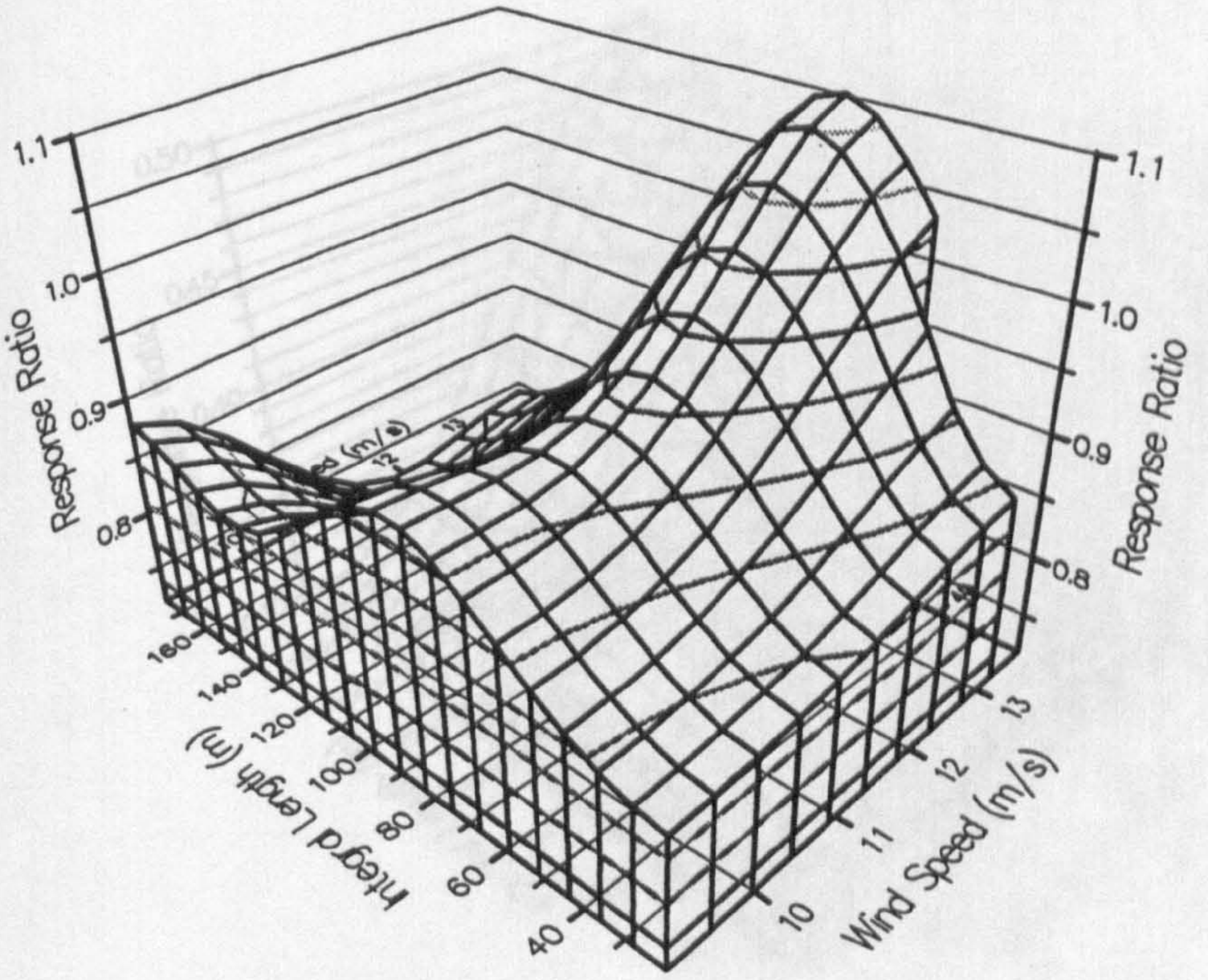

Figure 8.47 : Response Ratio Modes 1 & 2, Bilinear Fit, Easterly Winds

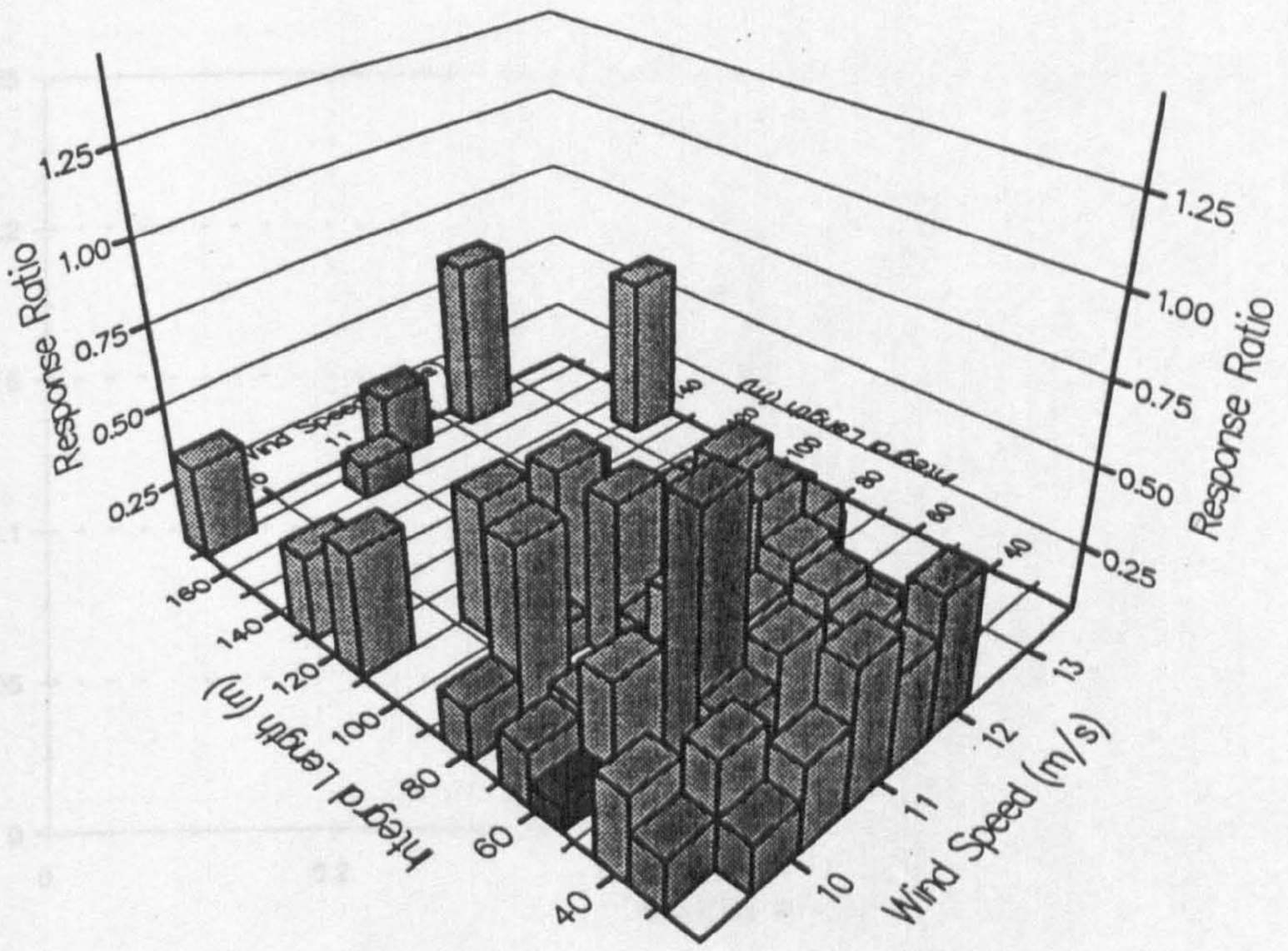

Figue 8.48 : Response Ratio Modes 1 & 3, Raw Data, Easterly Winds

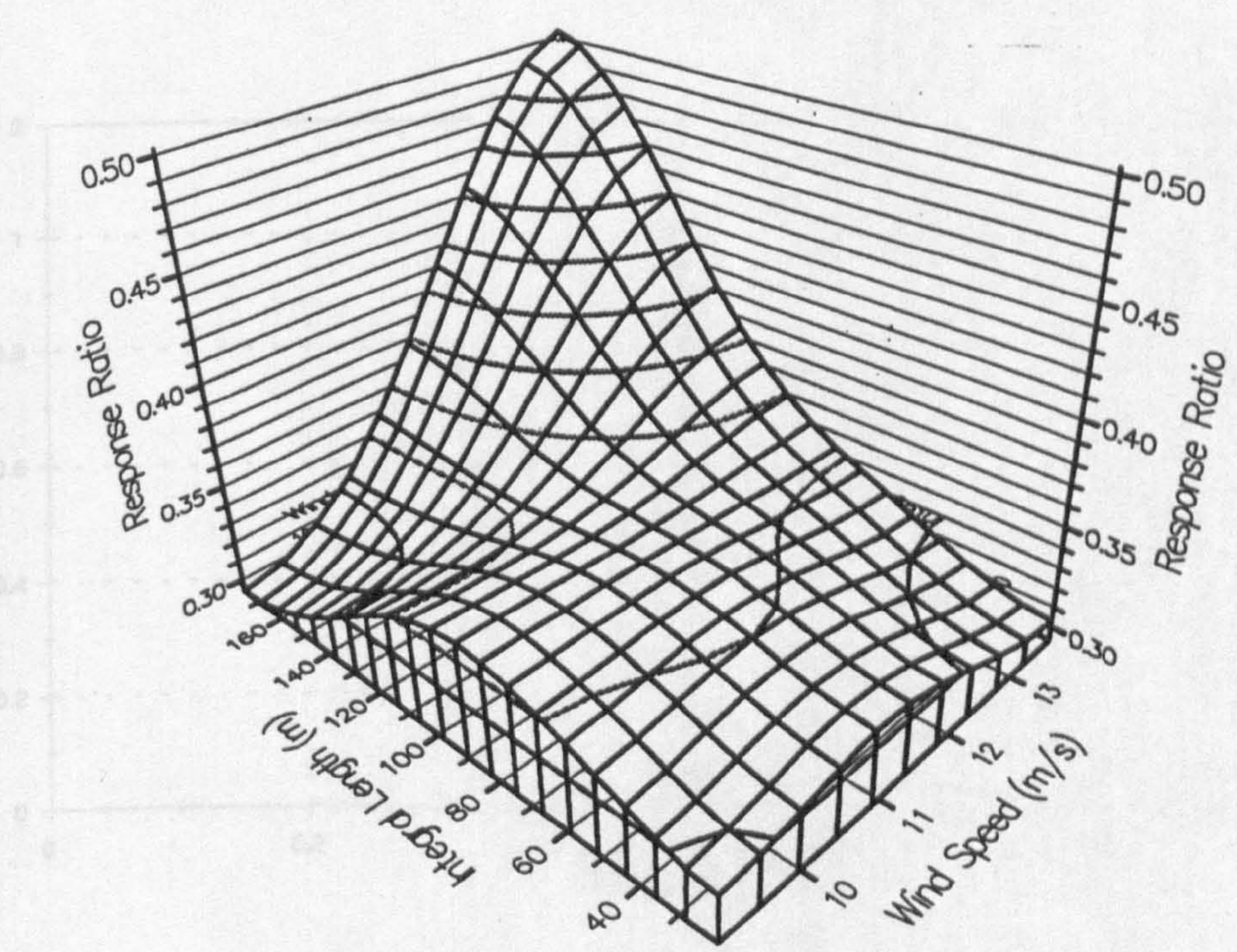

Figure 8.49 : Response Ratio Modes 1 & 3, Bilinear Fit, Easterly Winds

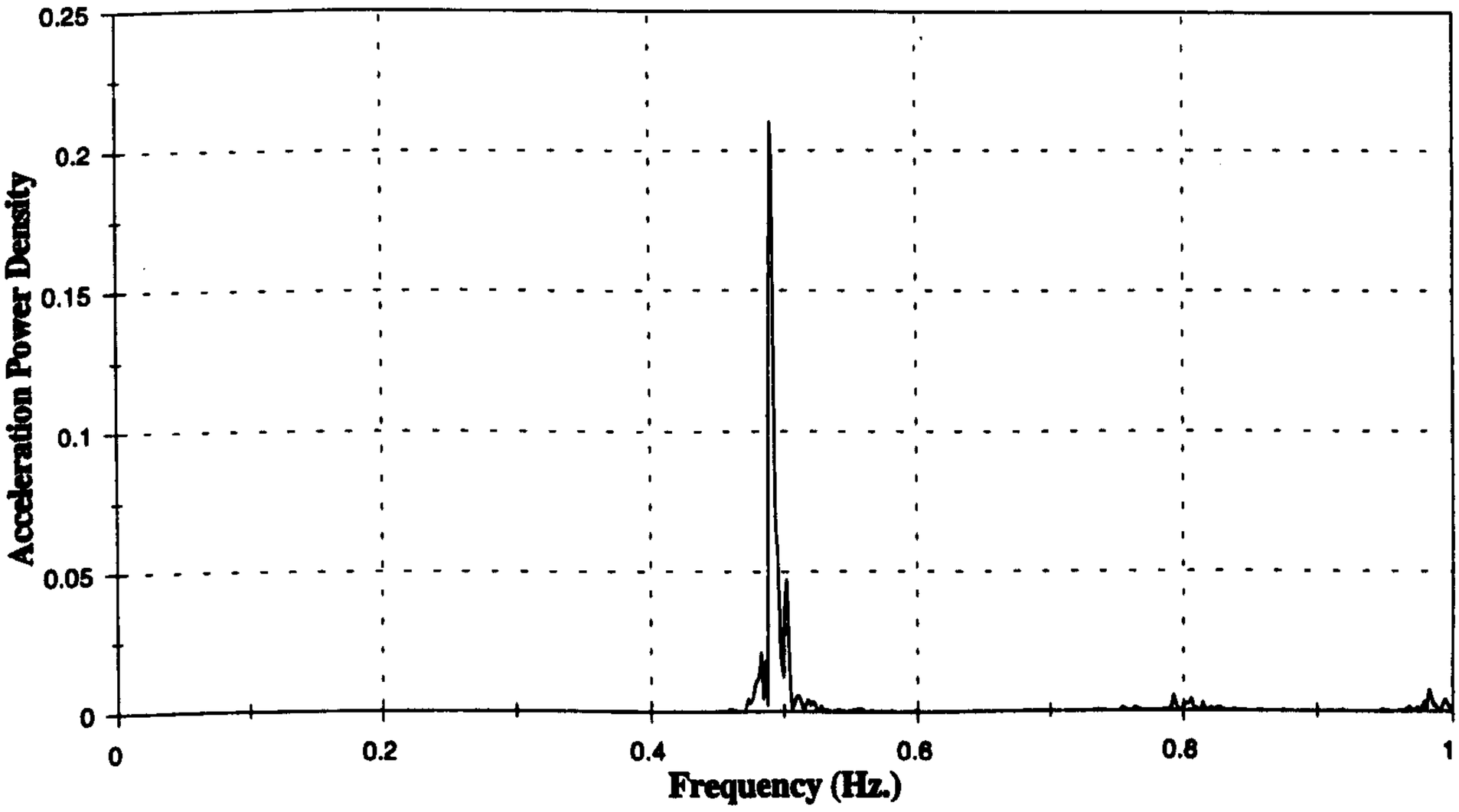

Figure 8.50a -:- Power Spectrum of Bridge Response At 50 m, 10:27 1 April

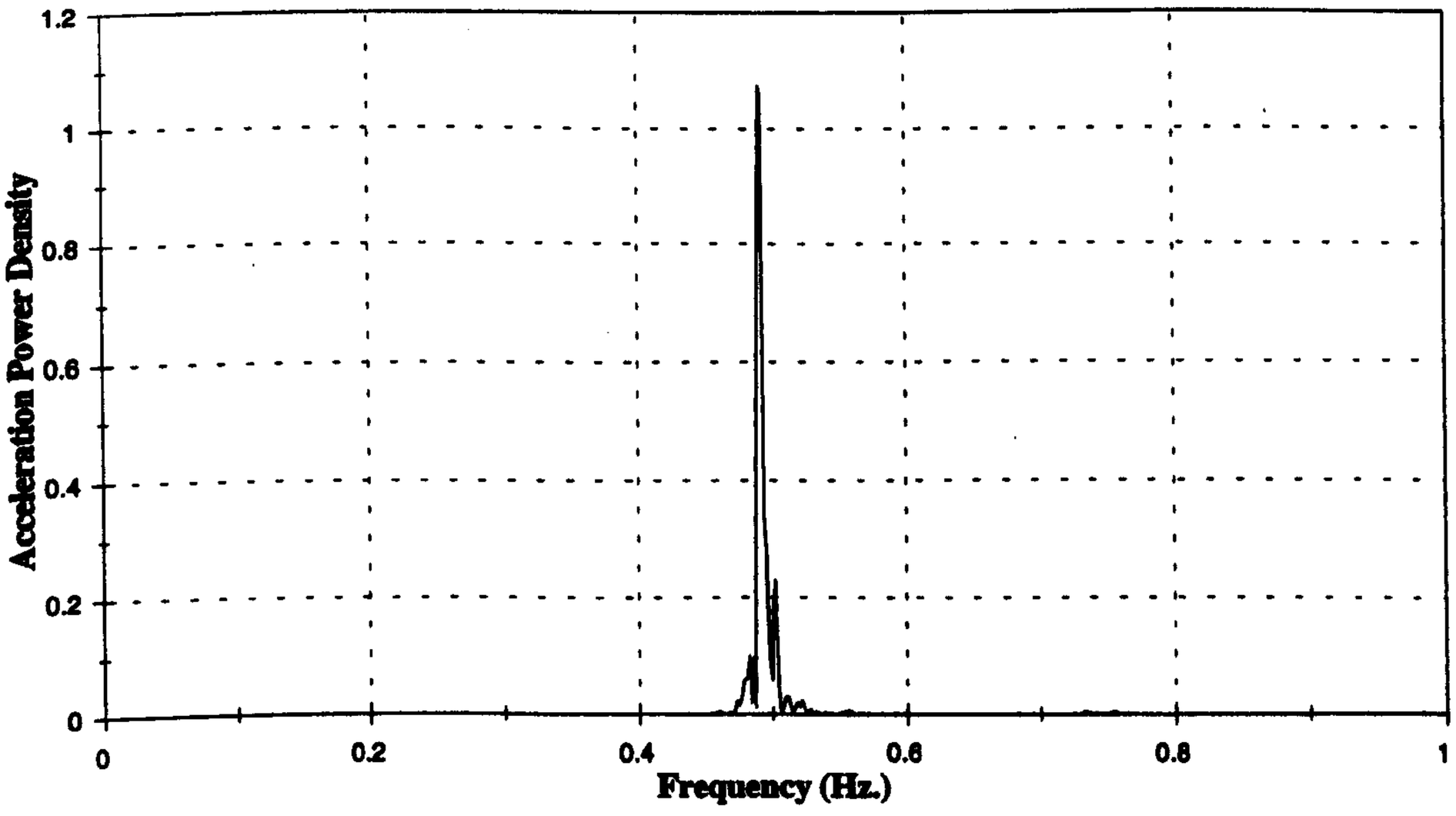

Figure 8.50b -:- Power Spectrum of Bridge Response At Mid Span, 10:27 1 April

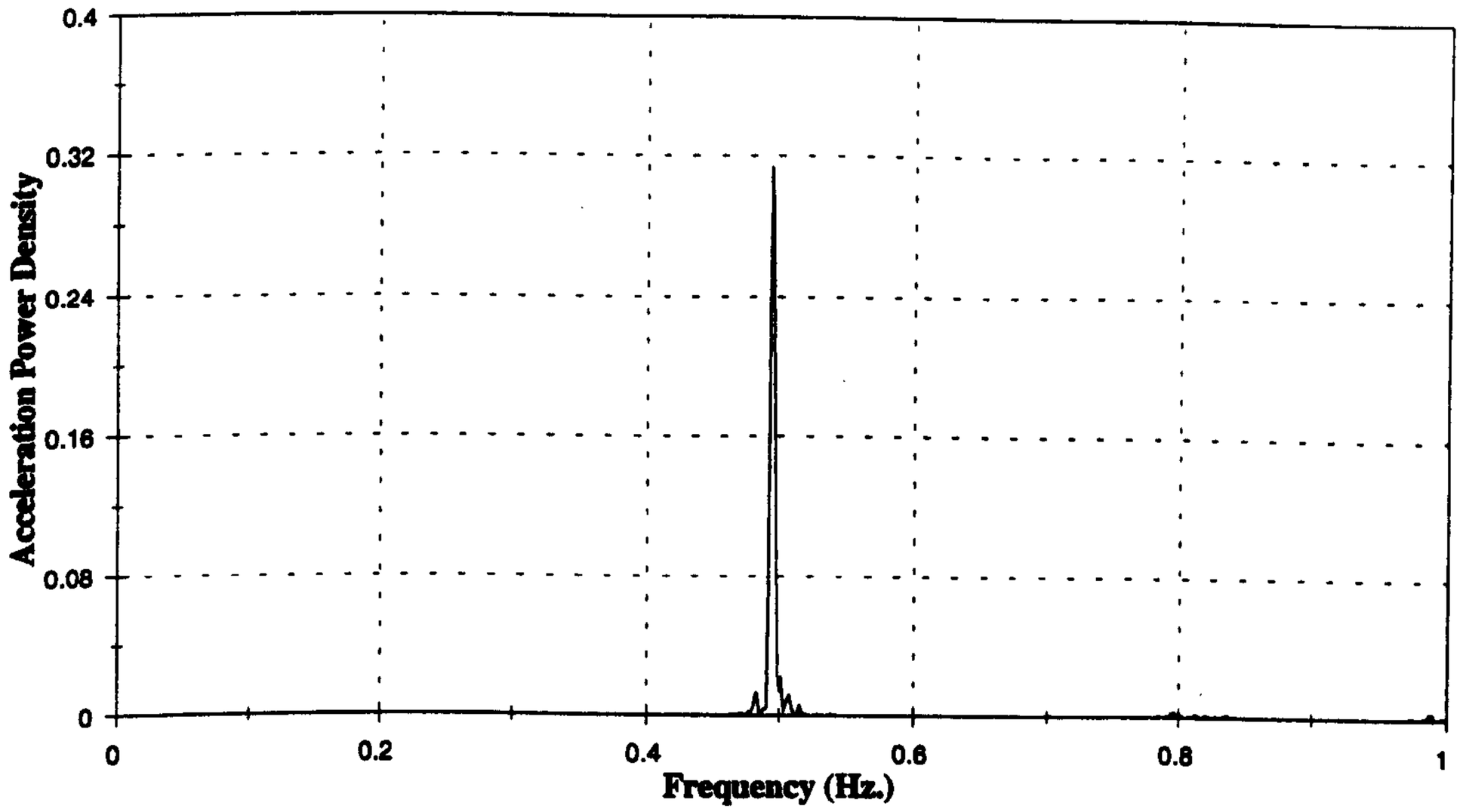

Figure 8.51a -:- Power Spectrum of Bridge Response At 50 m, 11:44 1 April

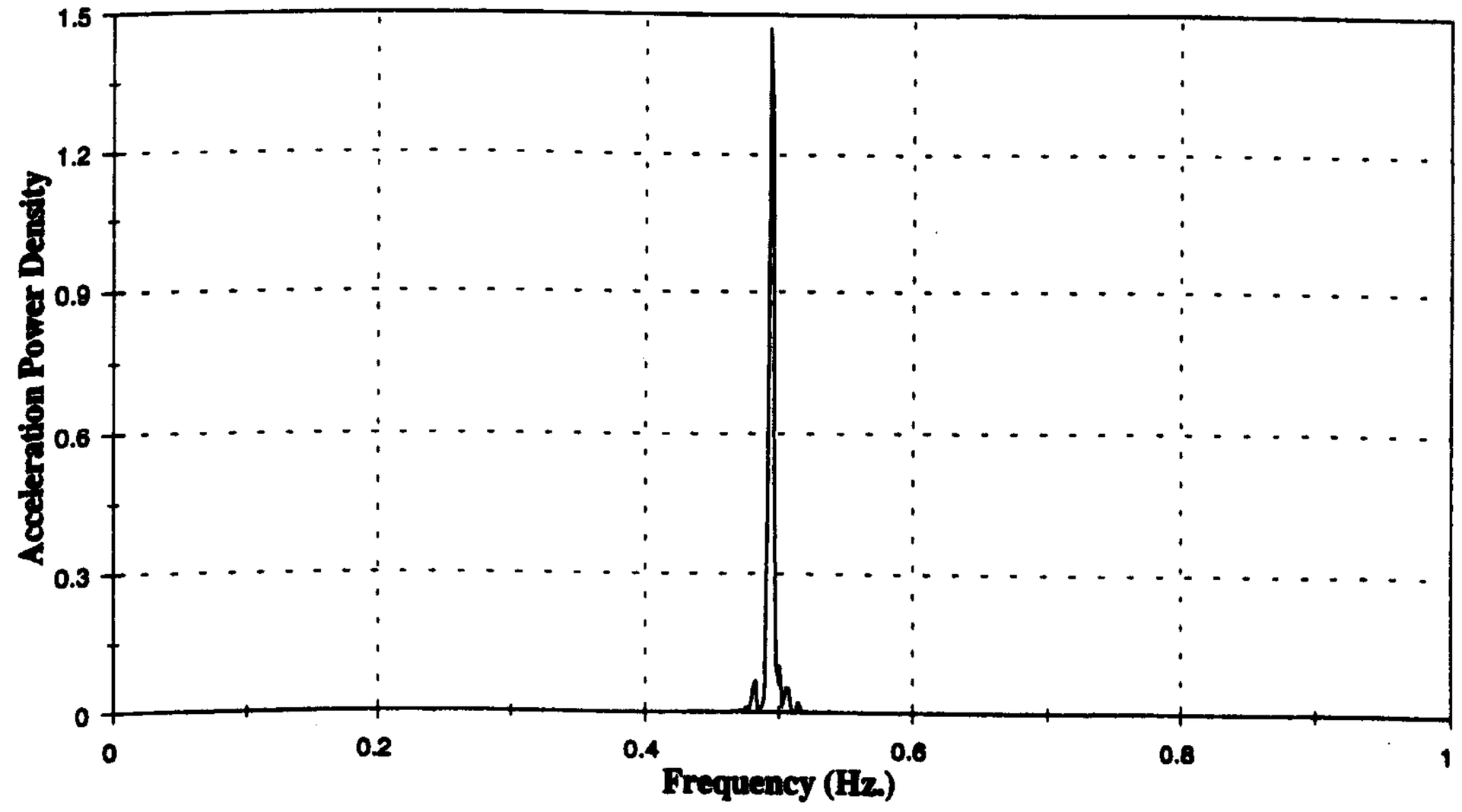

Figure 8.51b -:- Power Spectrum of Bridge Response At Mid Span, 11:44 1 April

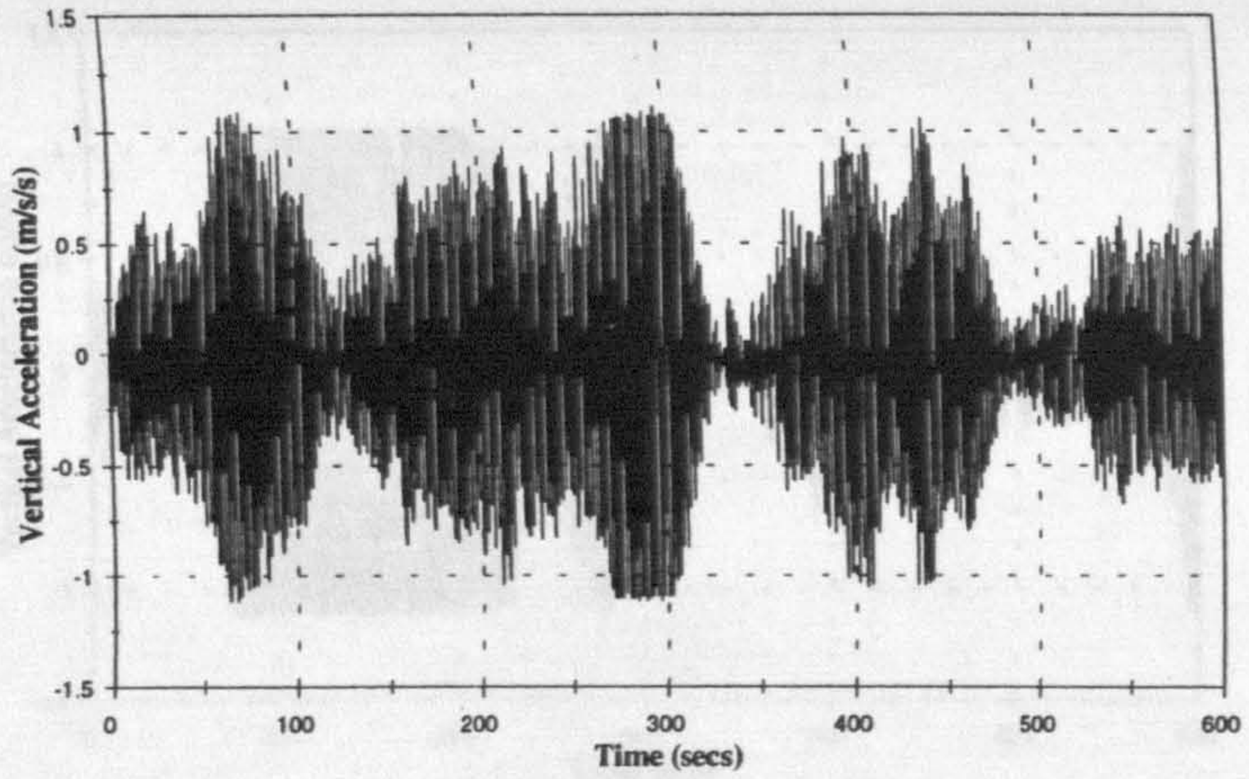

Figure 8.52a -:- Bridge Acceleration at Mid Span, 10:27 1 April

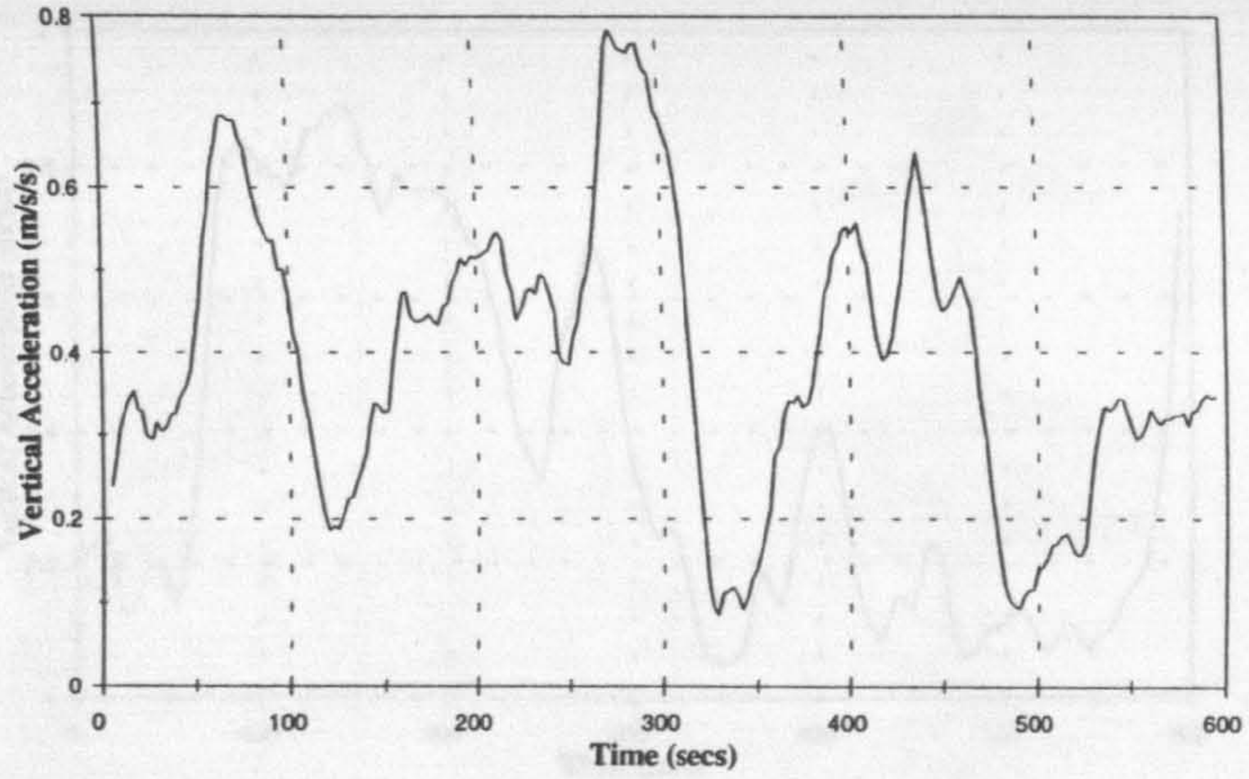

Figure 8.52b -:- 10 Second RMS Bridge Acceleration

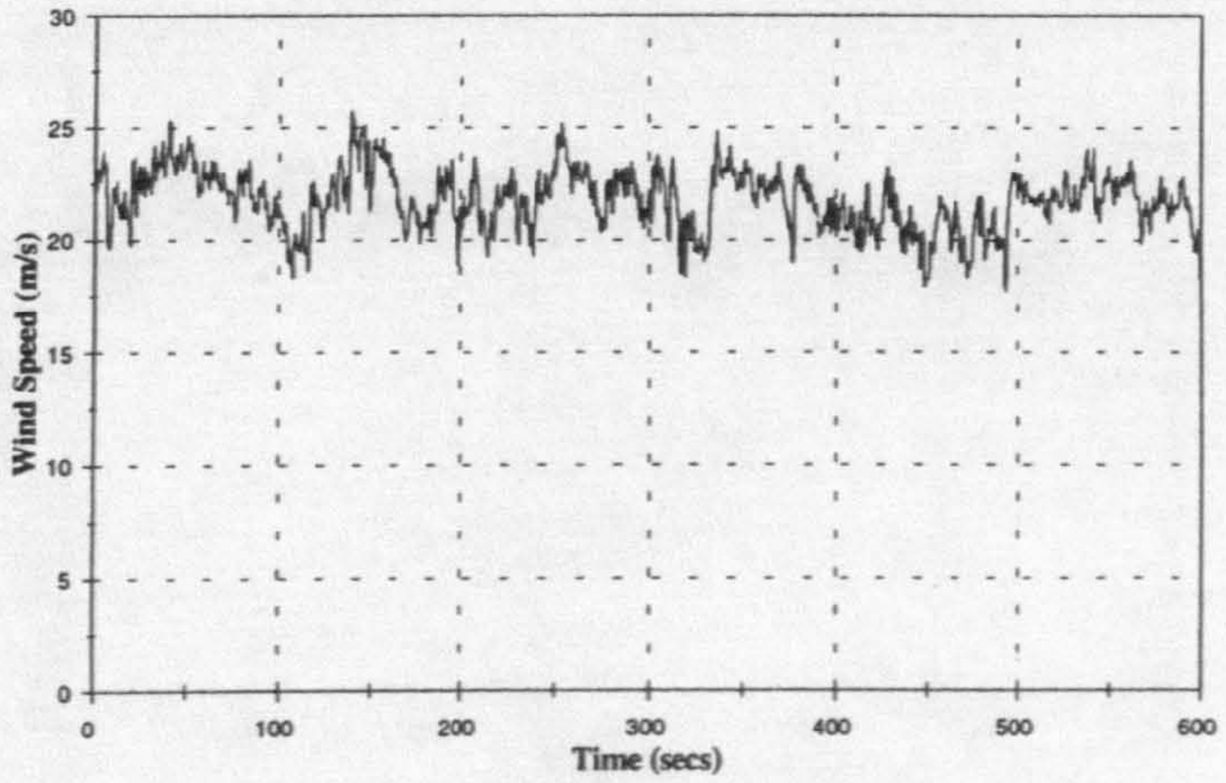

Figure 8.52c -:- Wind Speed at Mid Span, 10:27 1 April

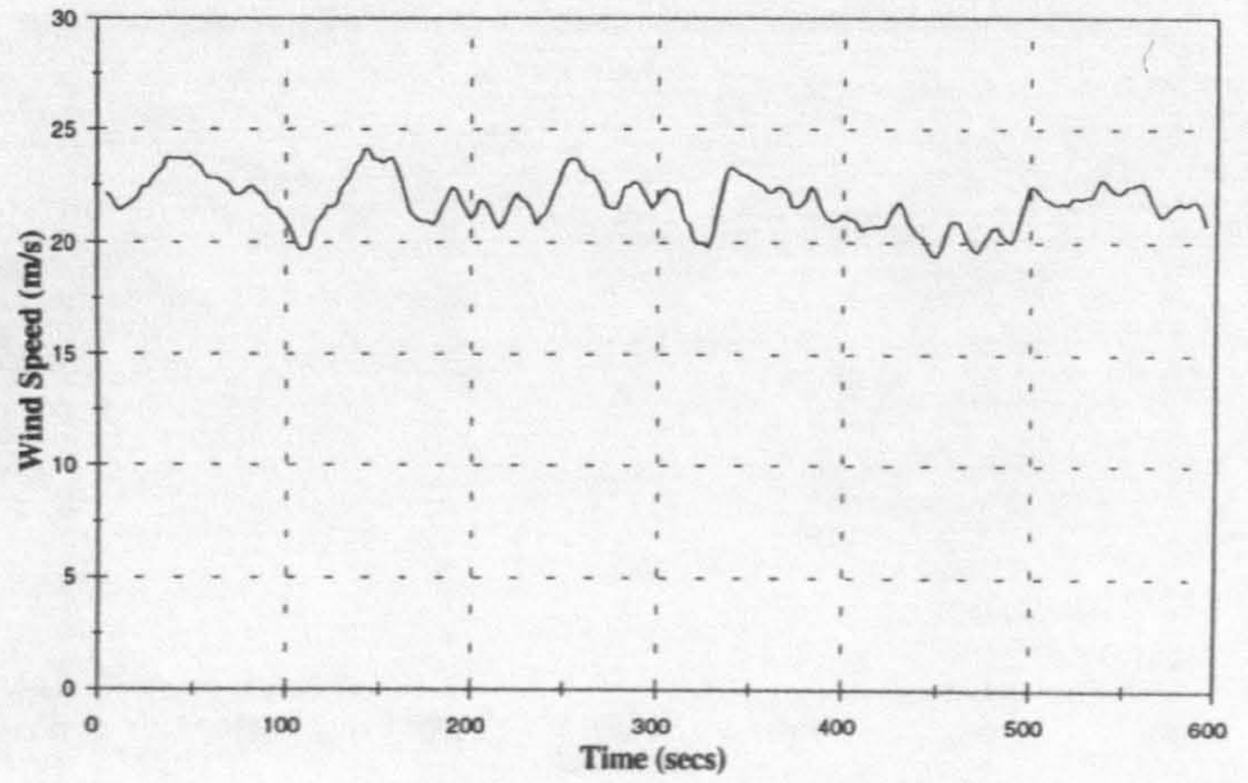

Figure 8.52d -:- 10 Second Average Wind Speed

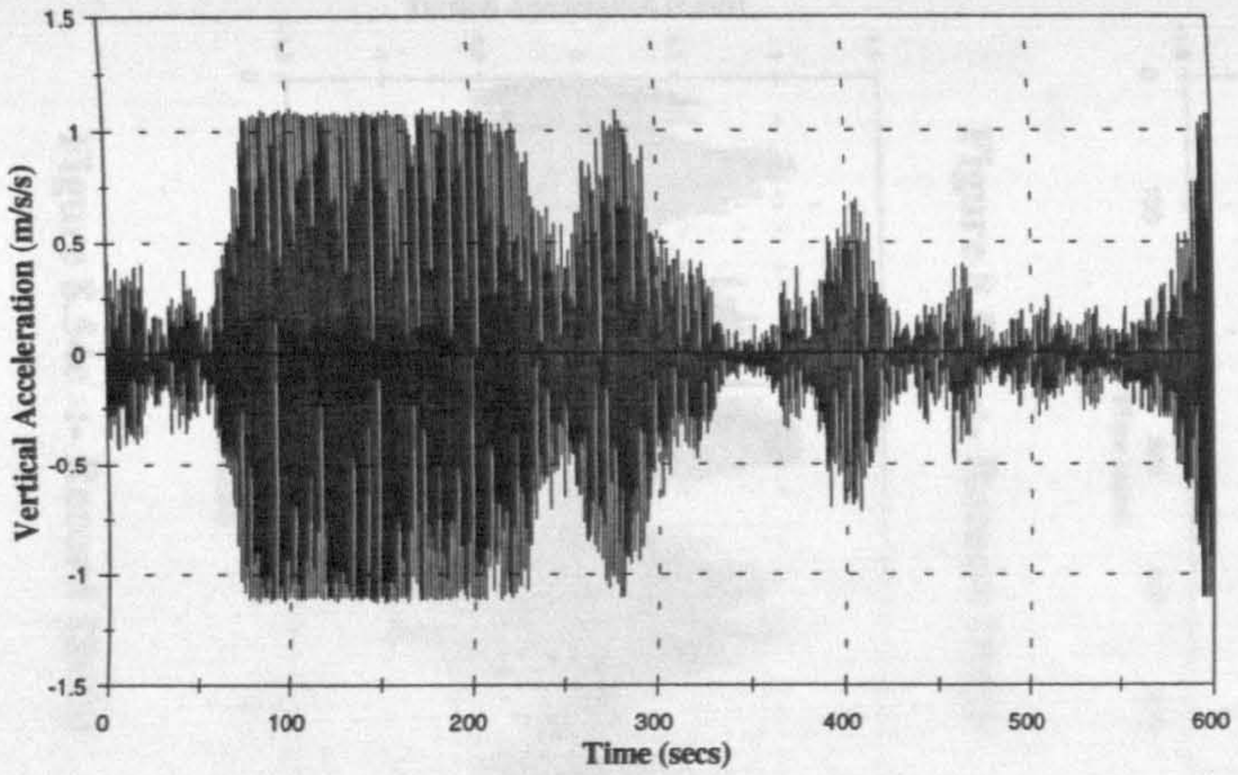

Figure 8.53a -:- Bridge Acceleration at Mid Span, 11:44 1 April

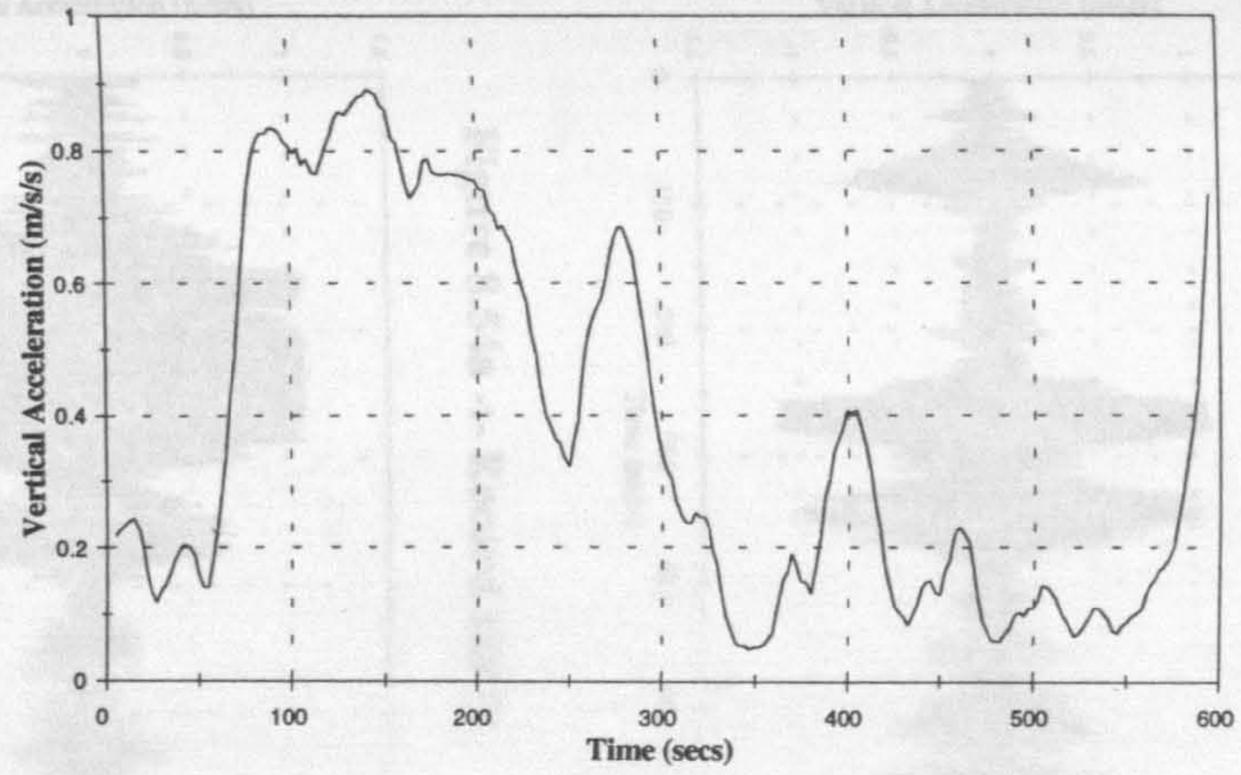

Figure 8.53b -:- 10 Second RMS Bridge Acceleration

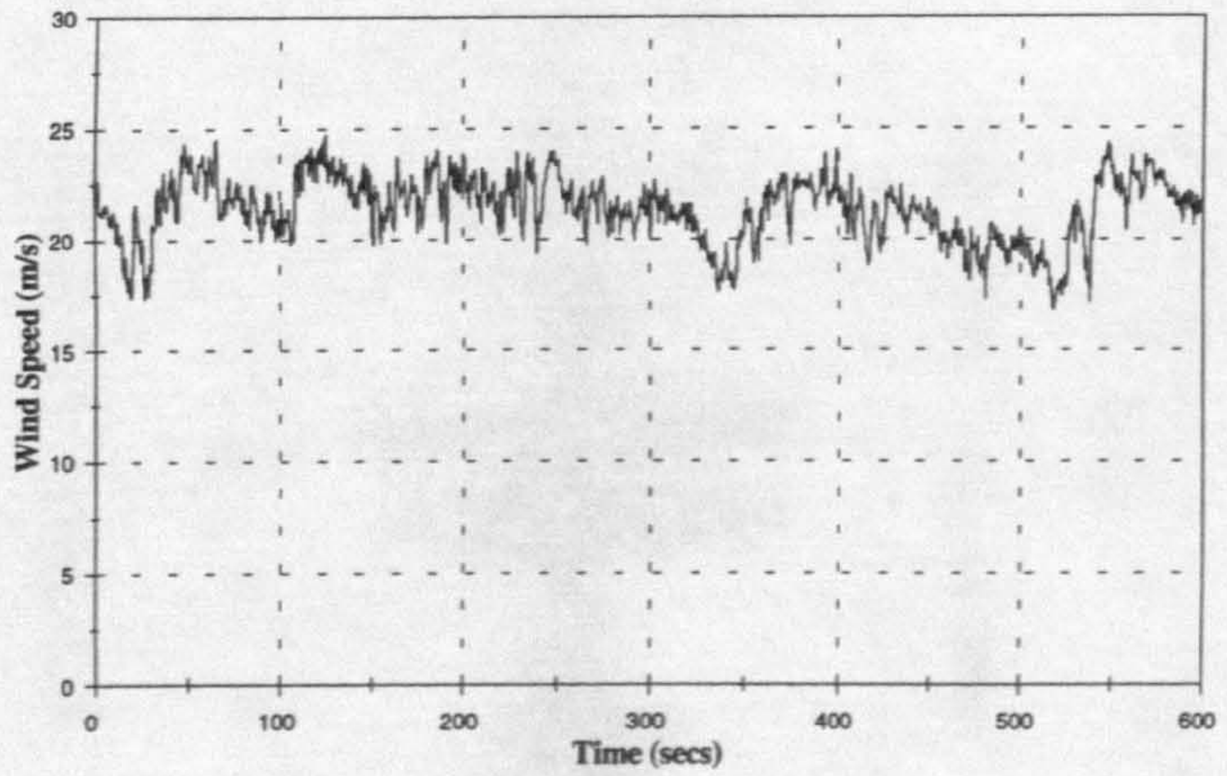

Figure 8.53c -:- Wind Speed at Mid Span, 11:44 1 April

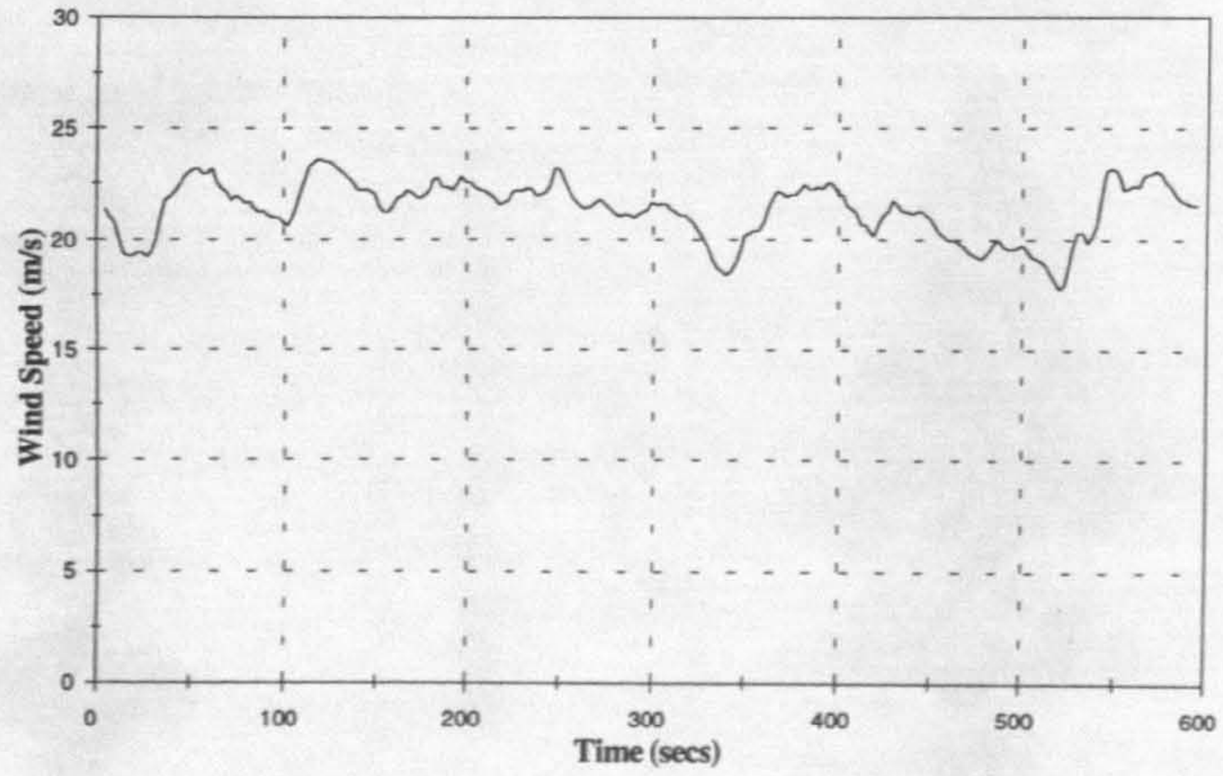

Figure 8.53d -:- 10 Second Average Wind Speed

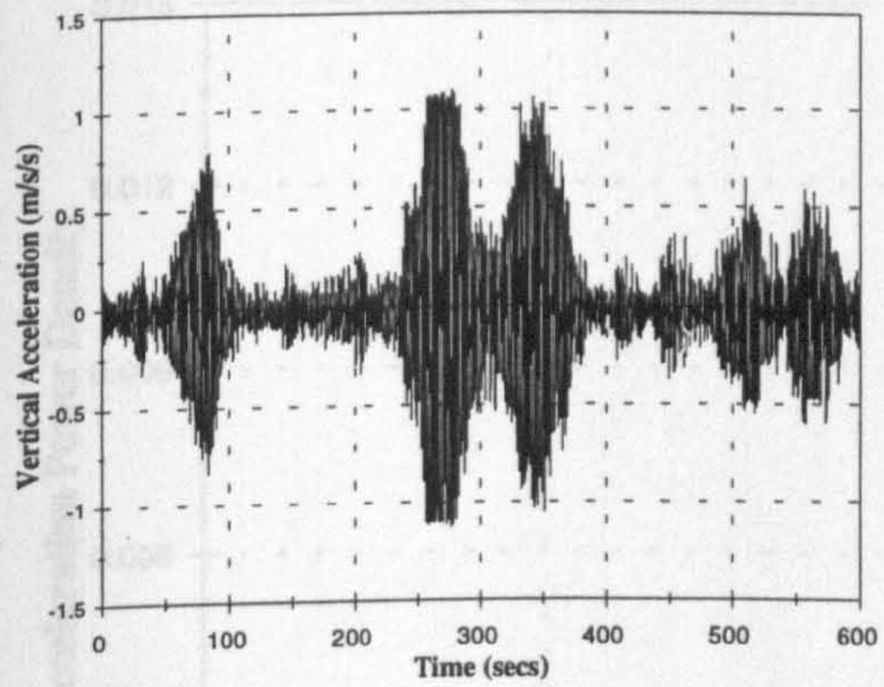

Figure 8.54a -:- Record 18077

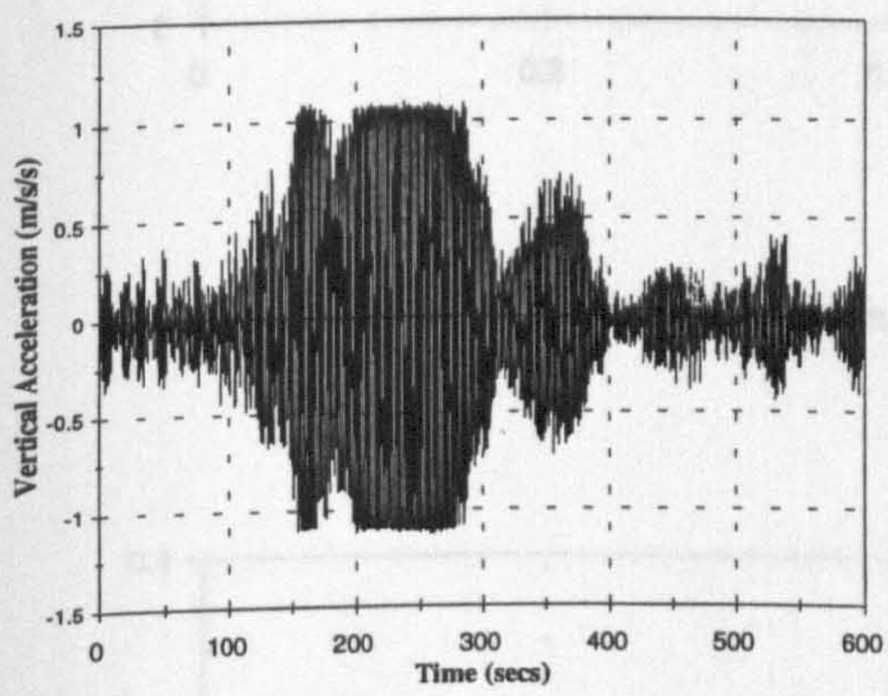

Figure 8.54b -:- Record 18078

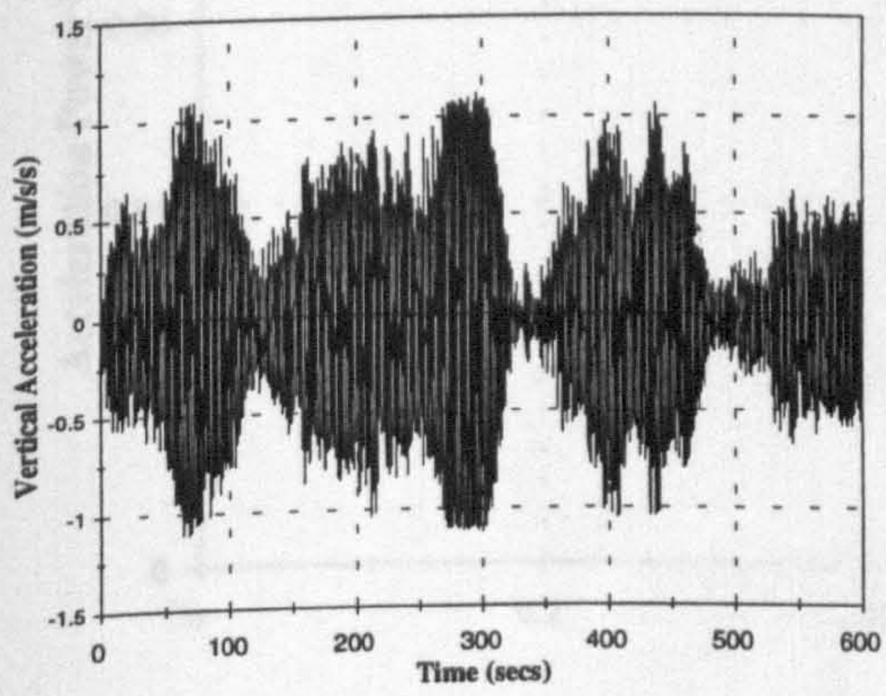

Figure 8.54c -:- Record 18079

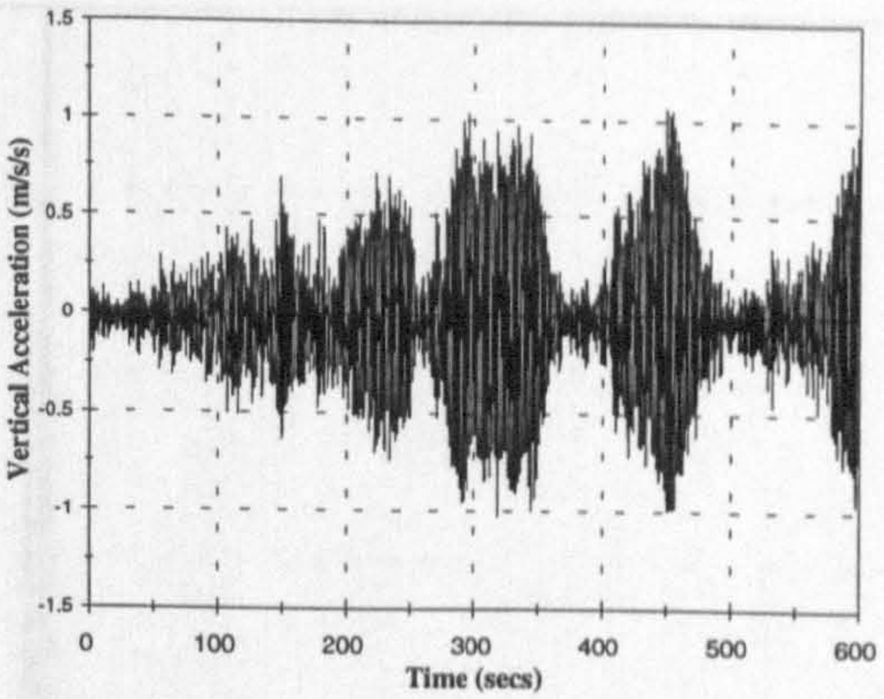

Figure 8.54d -:- Record 18082

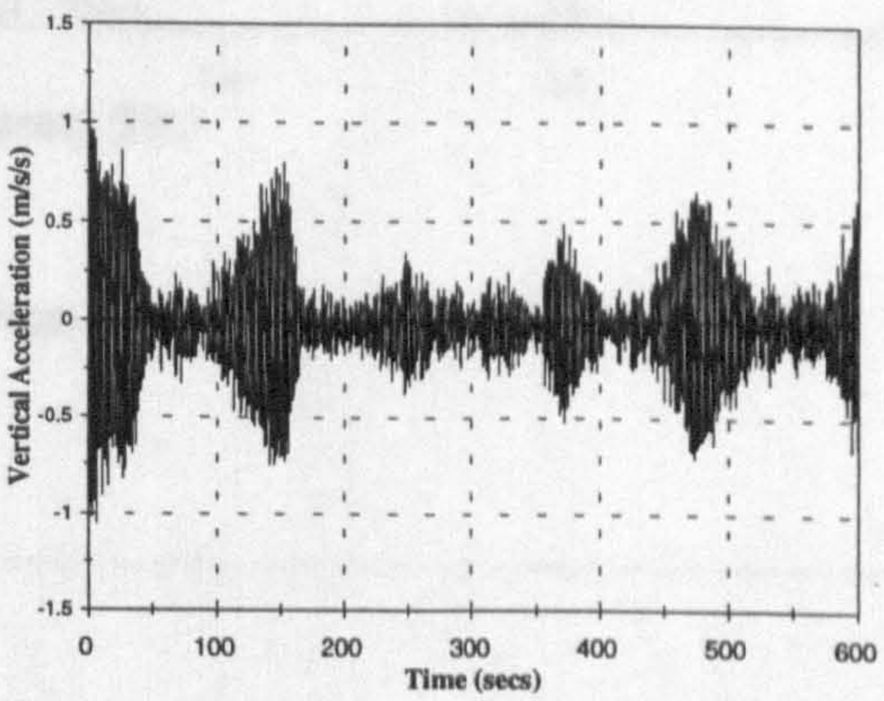

Figure 8.54e -:- Record 18083

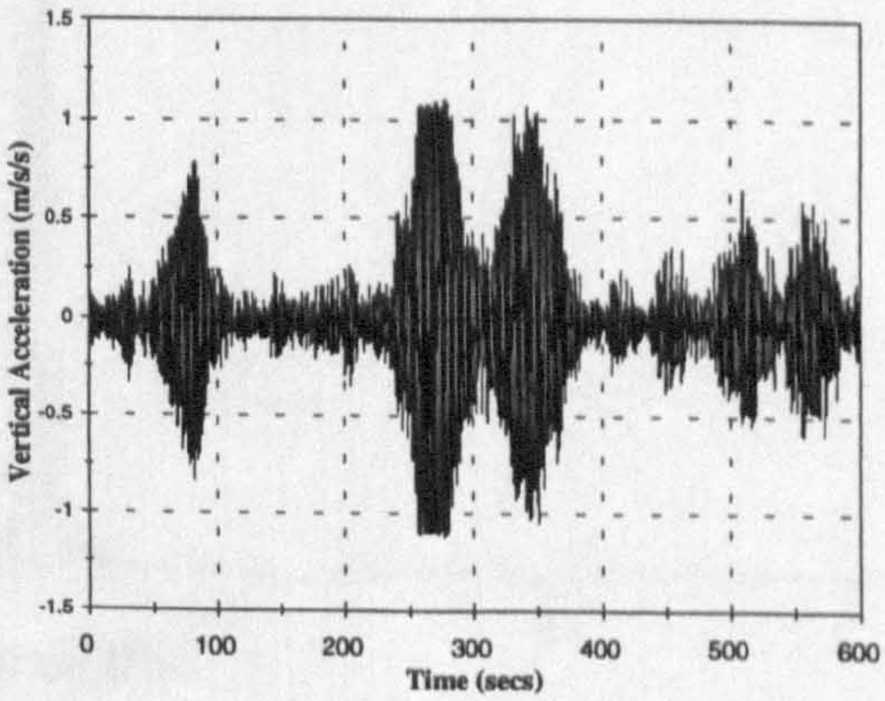

Figure 8.54f -:- Record 18086

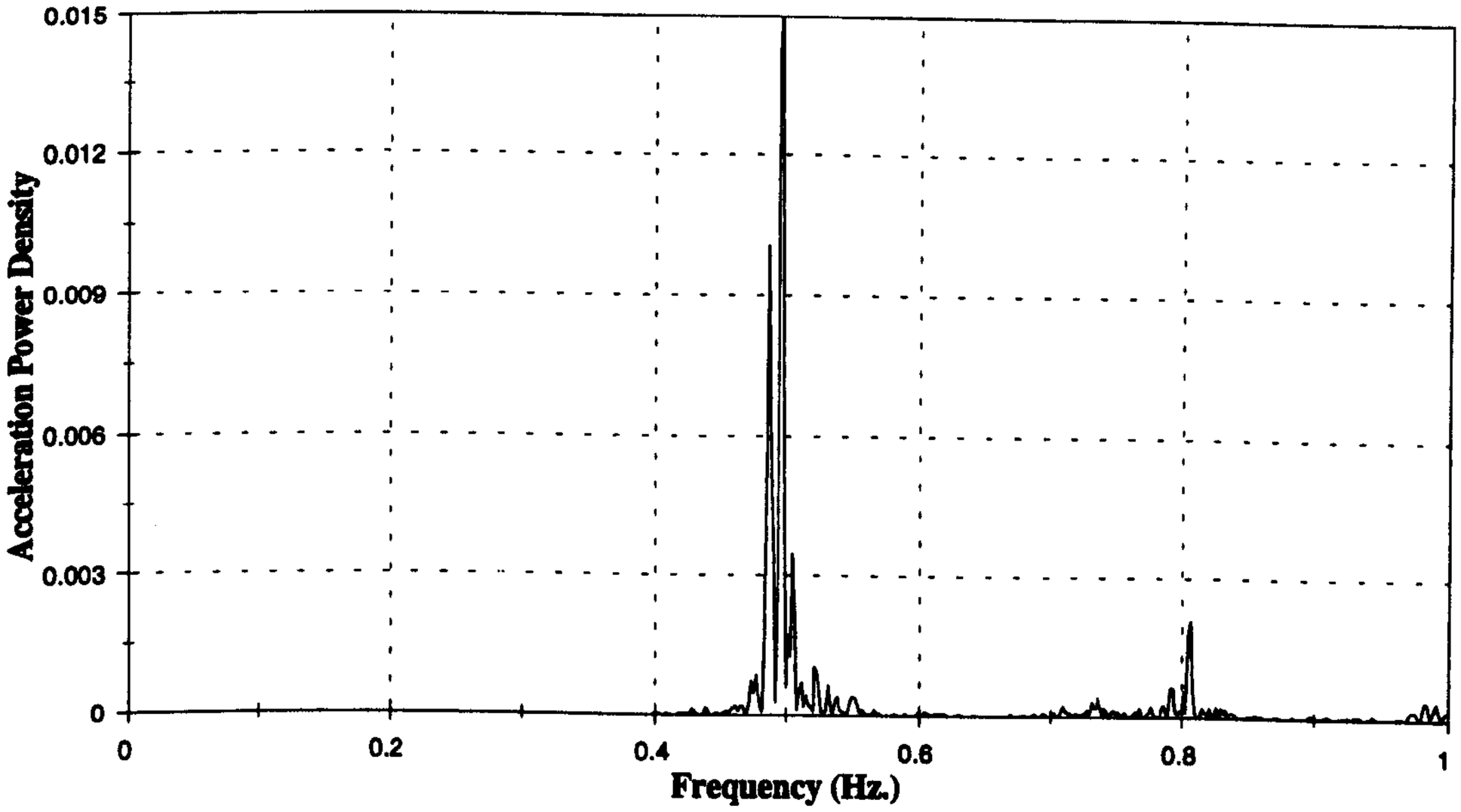

Figure 8.55a -:- Power Spectrum of Bridge Response At 50 m, 12:19 12 May

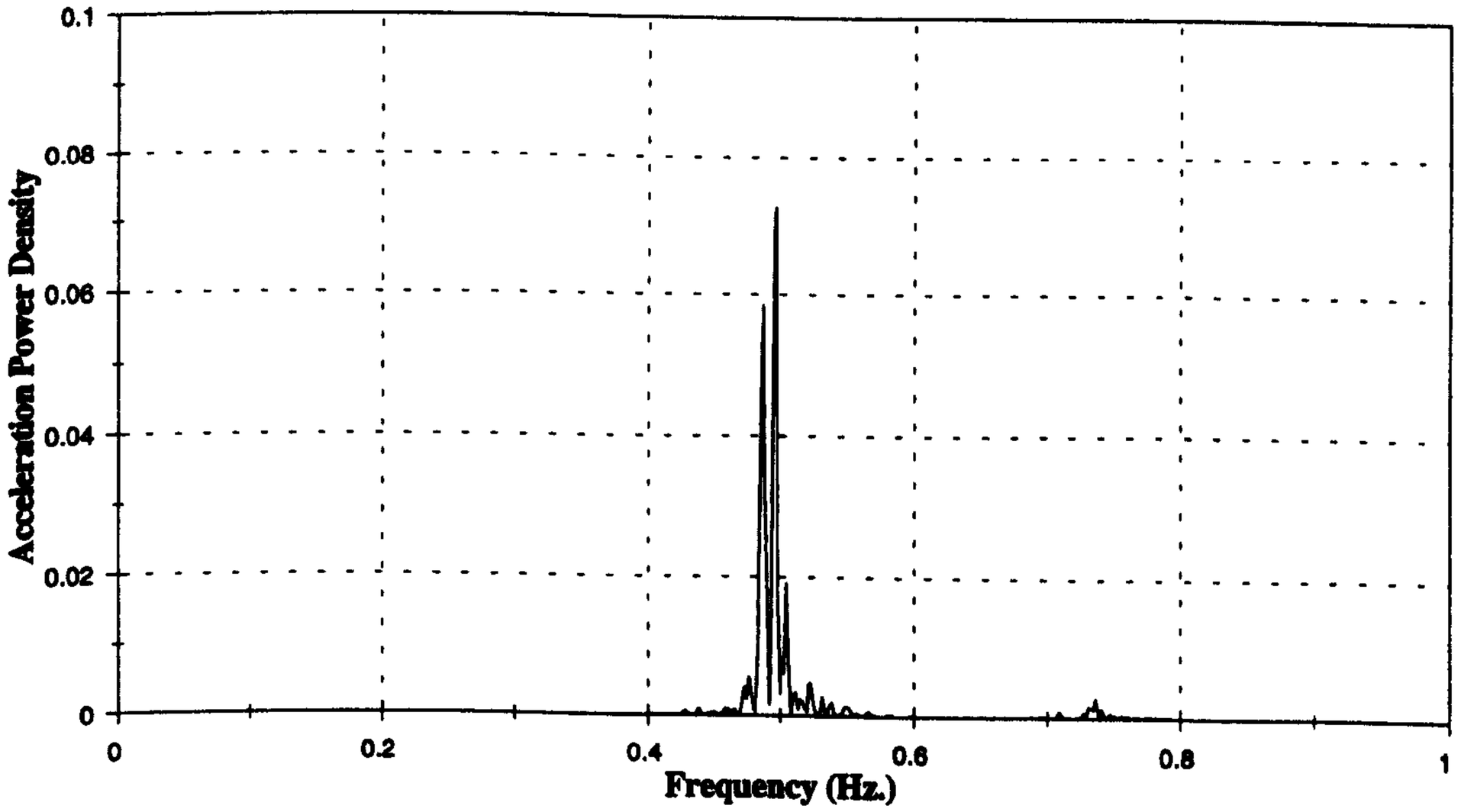

Figure 8.55b -:- Power Spectrum of Bridge Response At Mid Span, 12:19 12 May

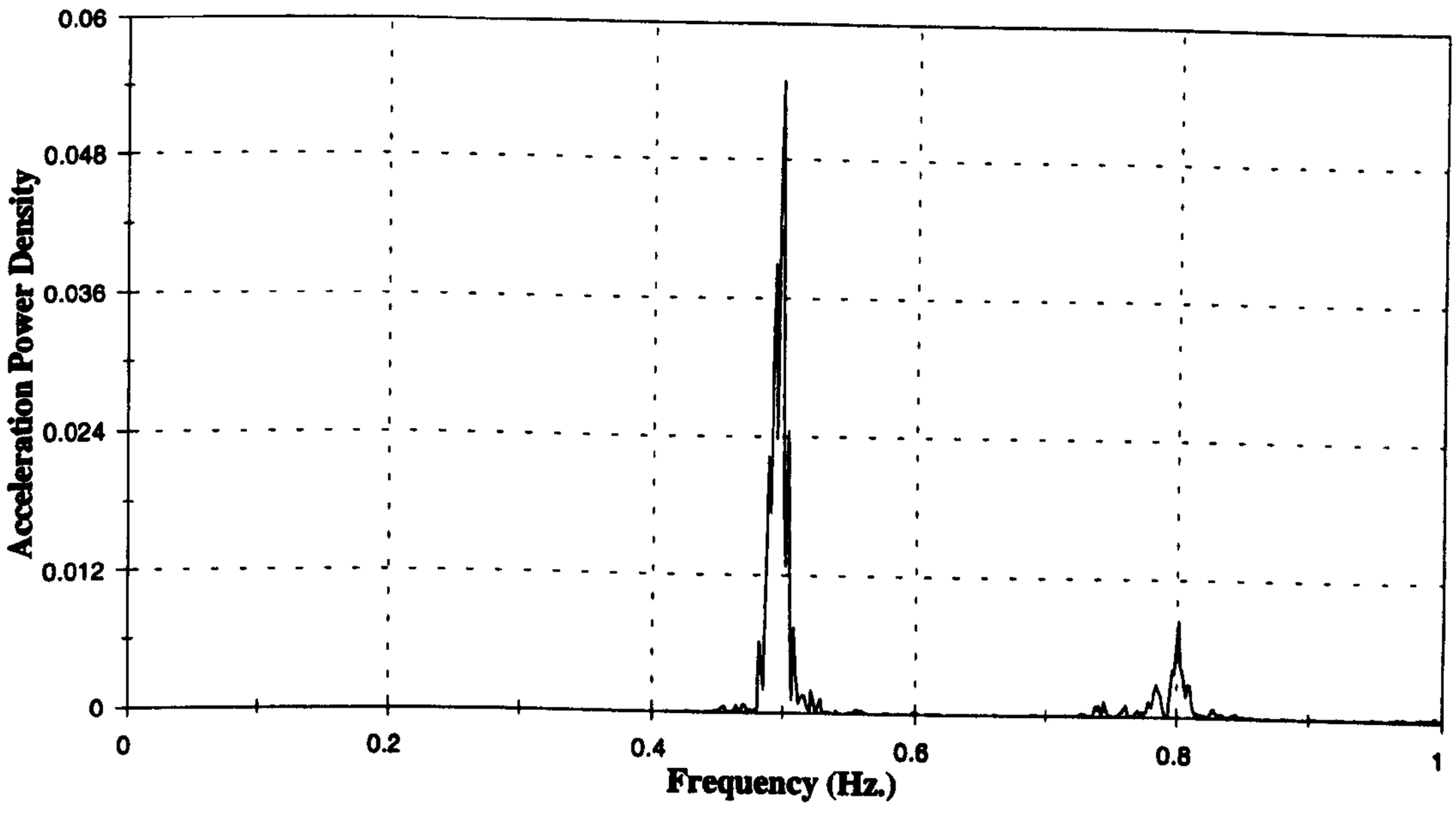

Figure 8.56a -:- Power Spectrum of Bridge Response At 50 m, 13:05 12 May

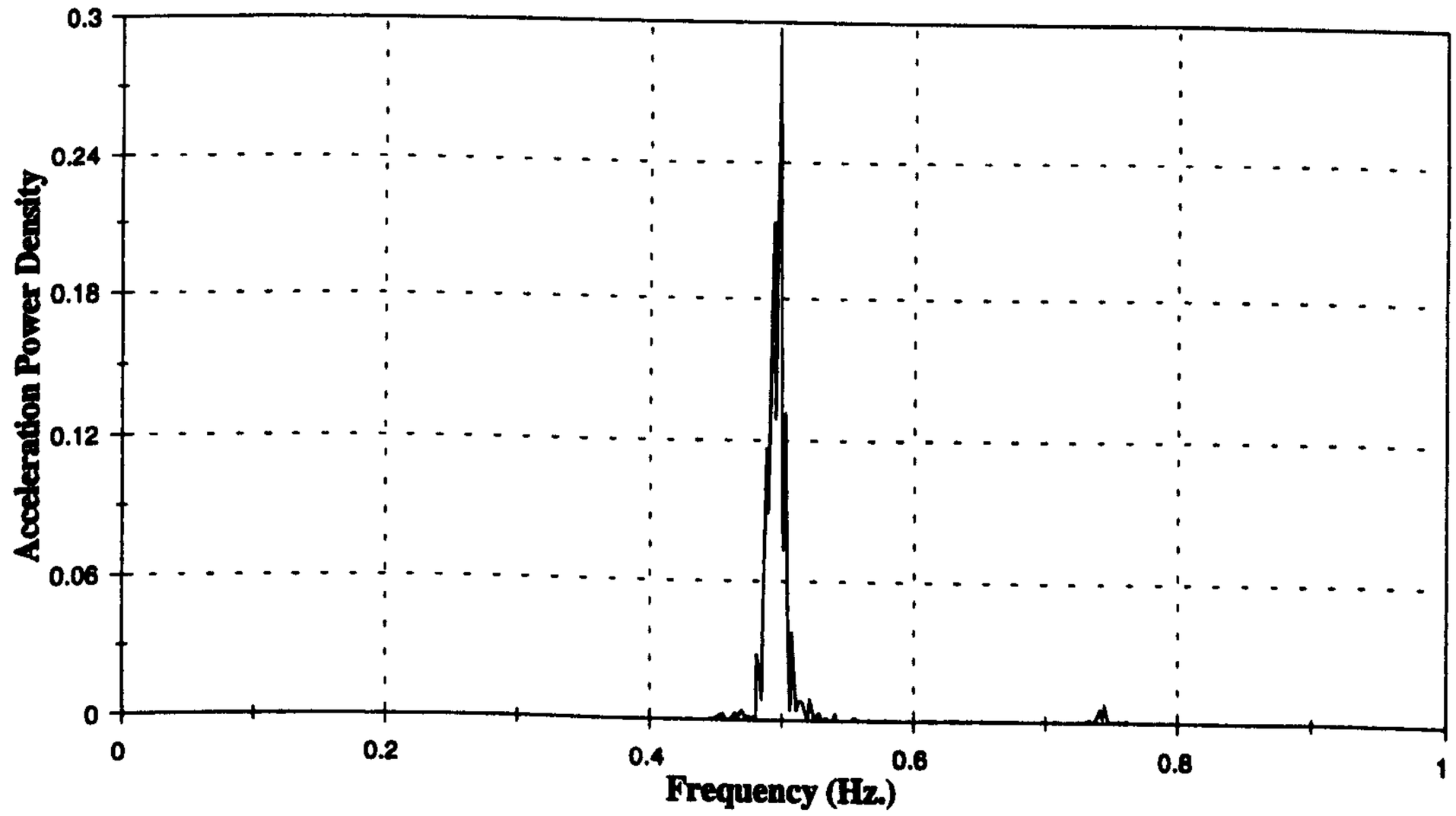

Figure 8.56b -:- Power Spectrum of Bridge Response At Mid Span, 13:05 12 May

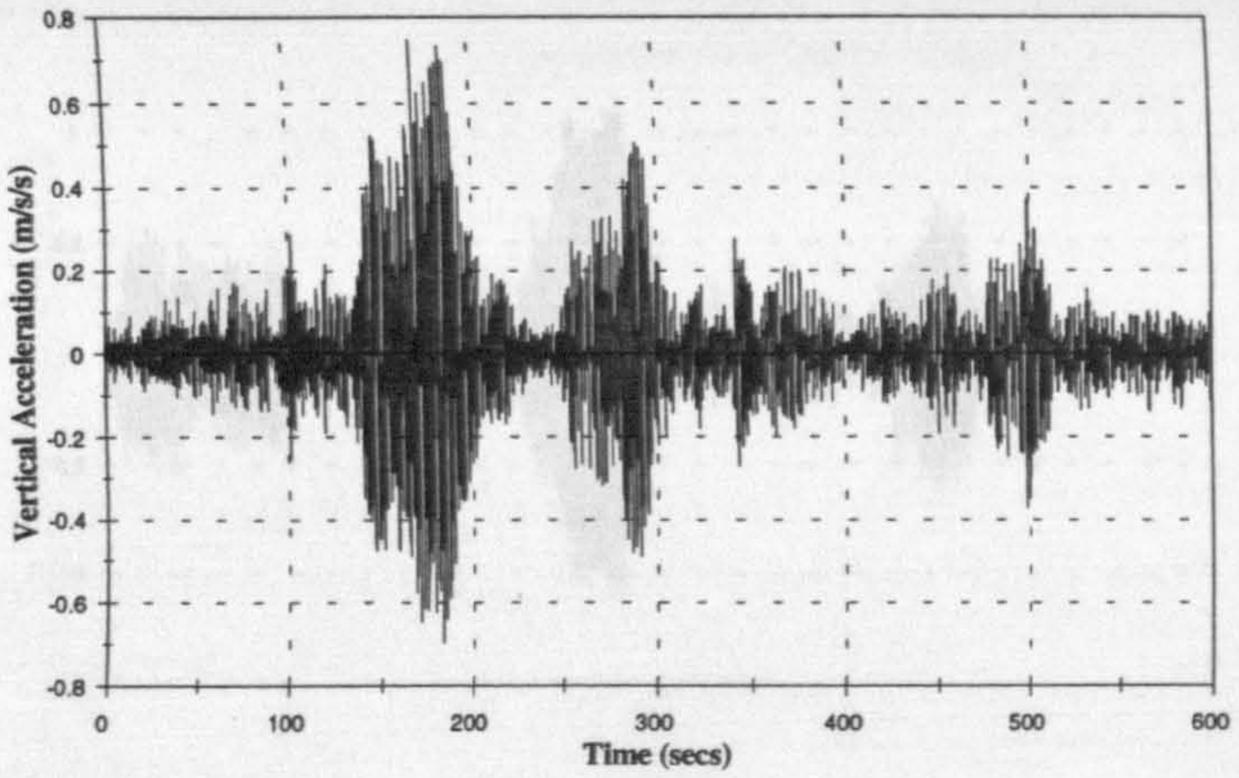

Figure 8.57a -:- Bridge Acceleration at Mid Span, 12:19 12 May

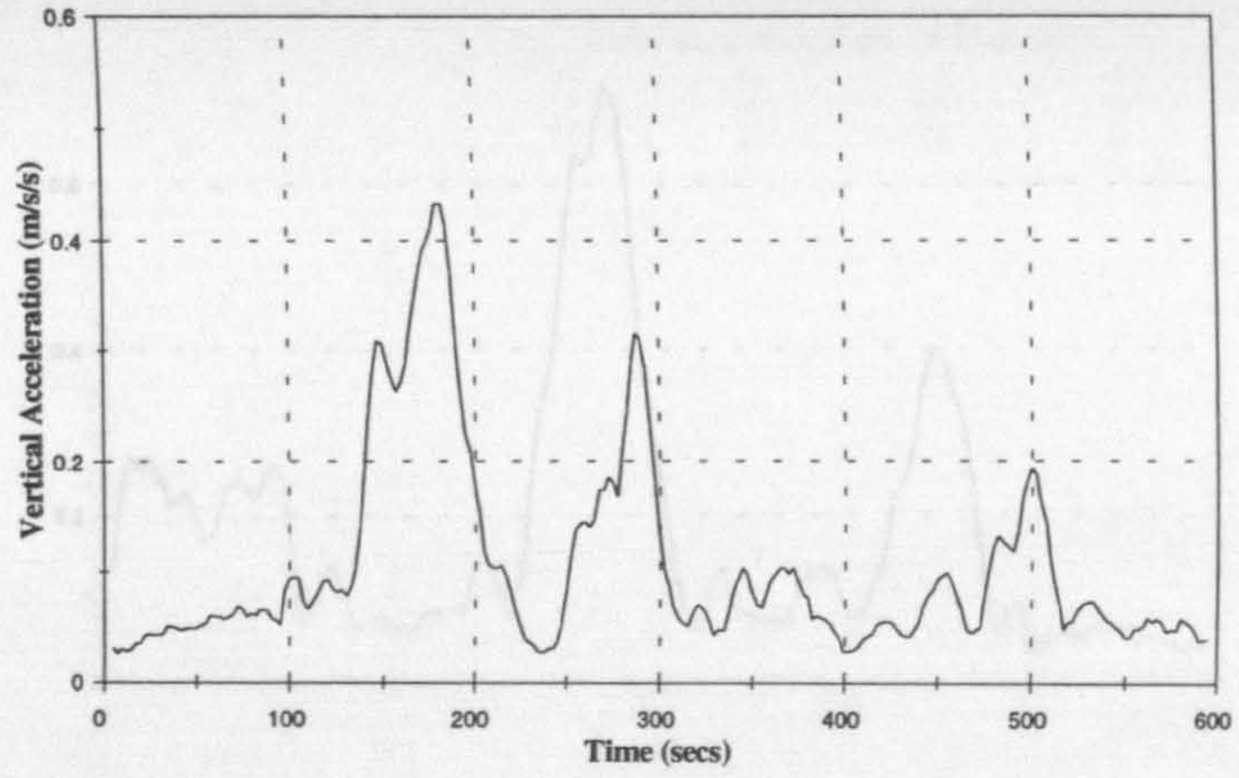

Figure 8.57b -:- 10 Second RMS Bridge Acceleration

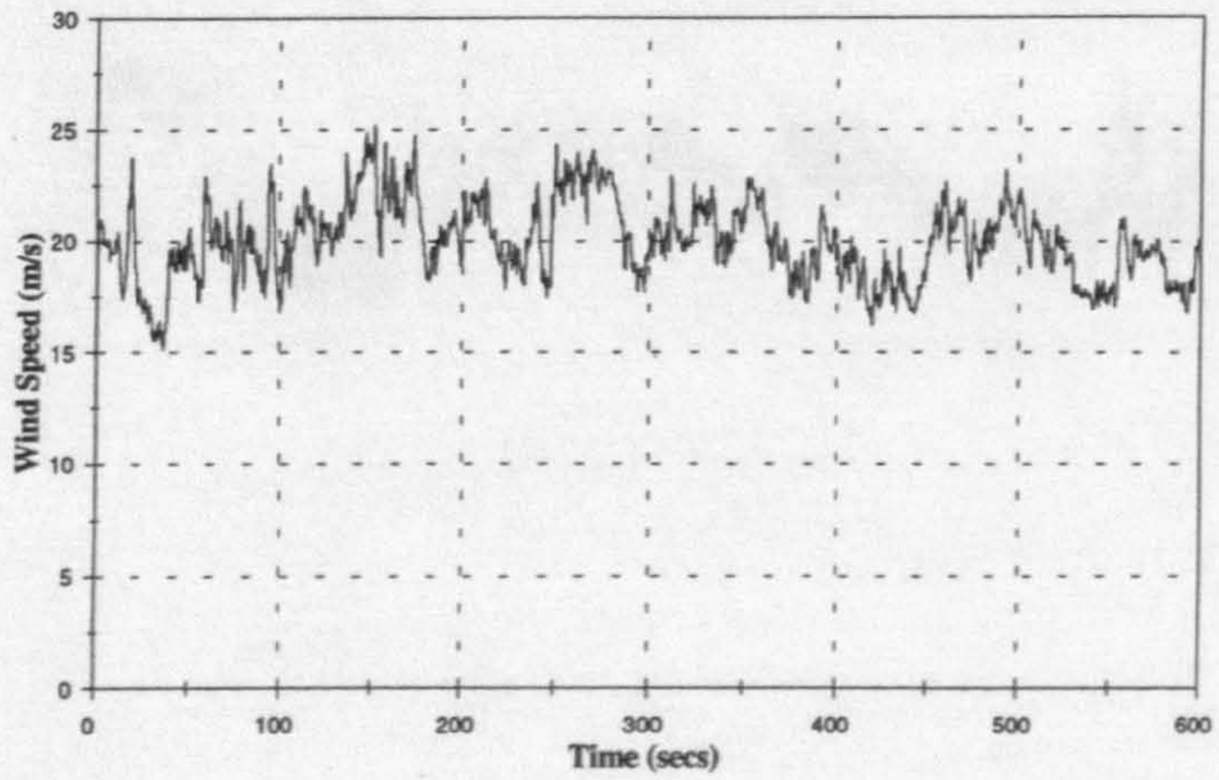

Figure 8.57c -:- Wind Speed at Mid Span, 12:19 12 May

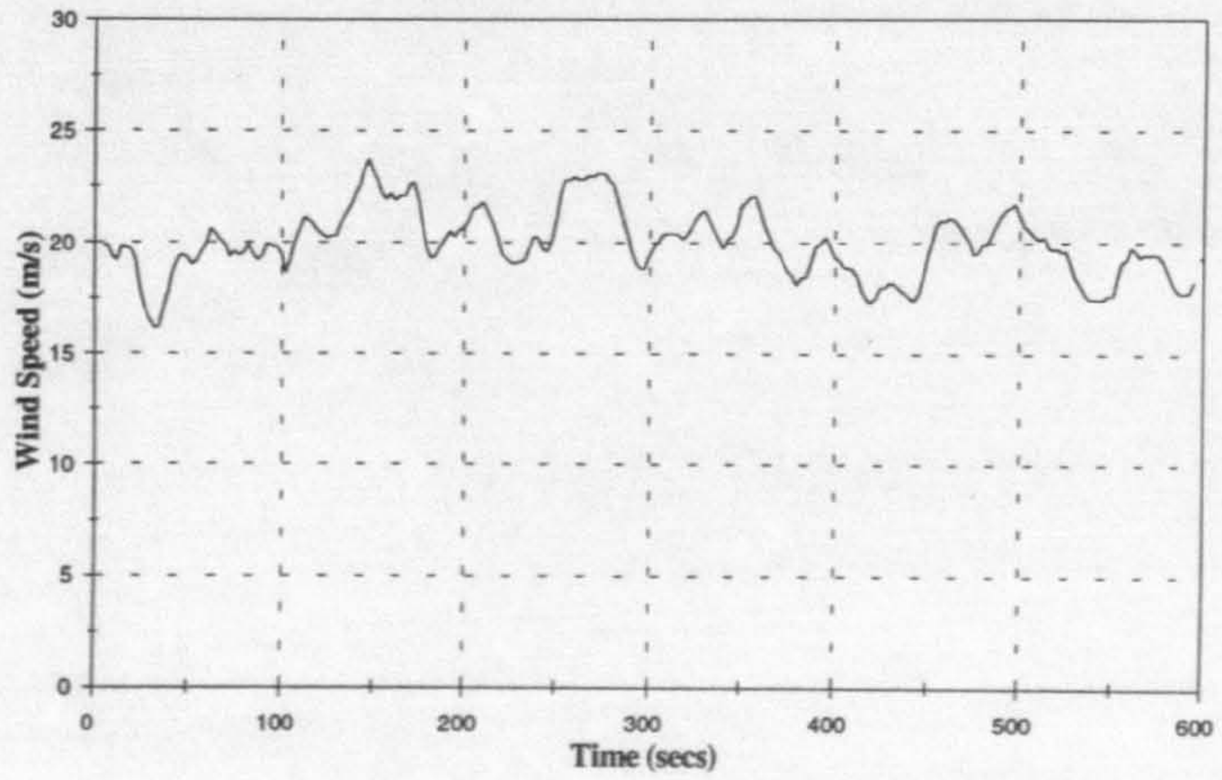

Figure 8.57d -:- 10 Second Average Wind Speed

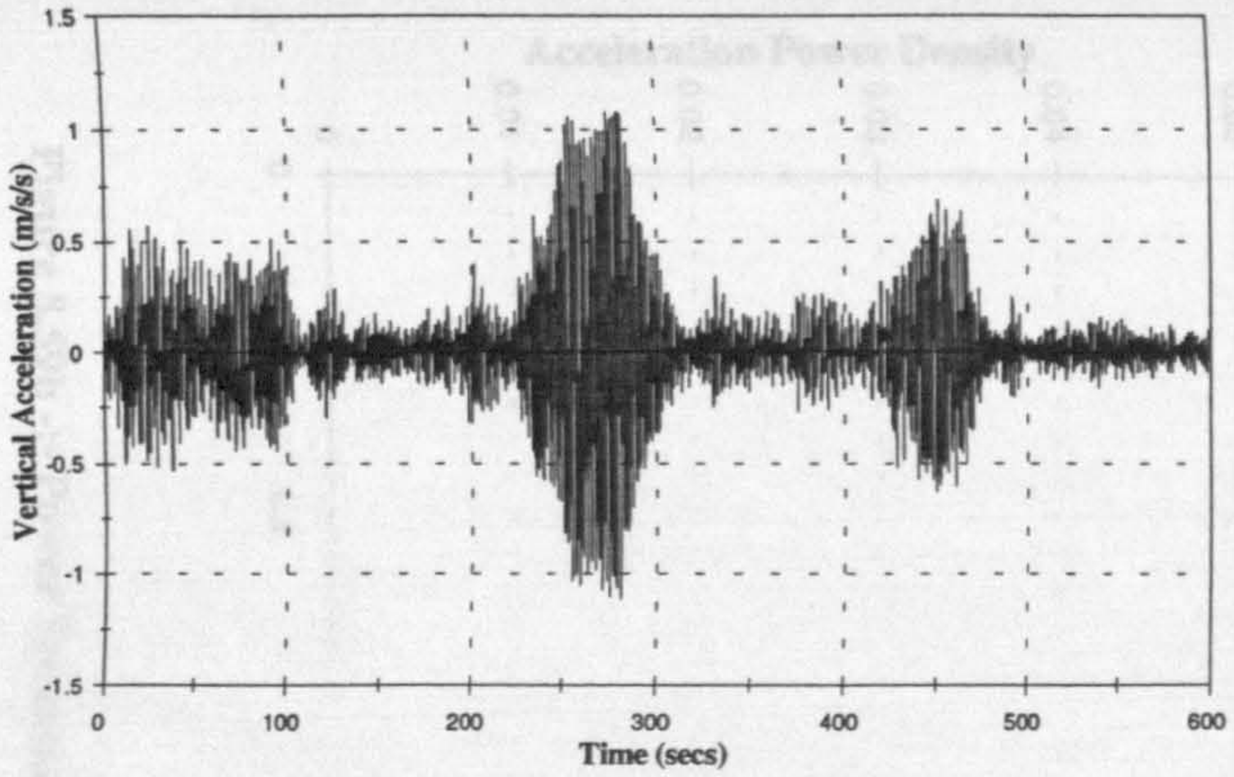

Figure 8.58a -:- Bridge Acceleration at Mid Span, 13:05 12 May

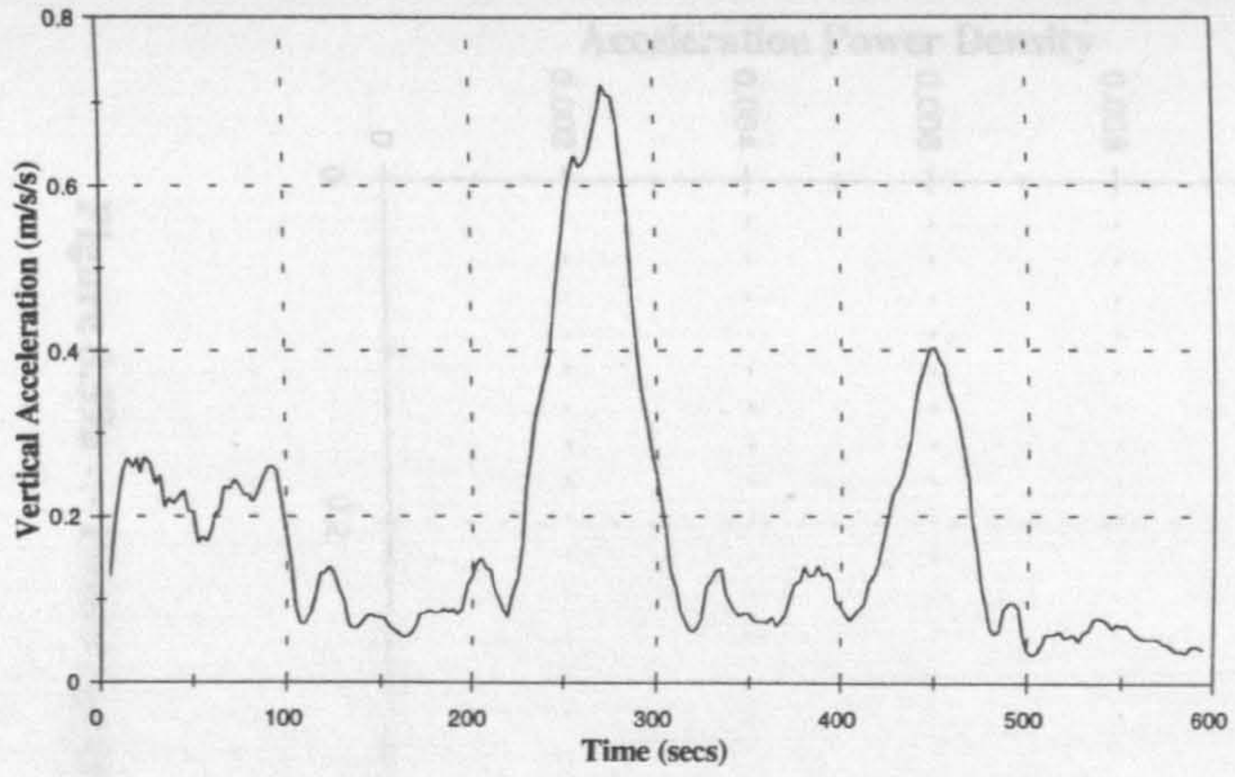

Figure 8.58b -:- 10 Second RMS Bridge Acceleration

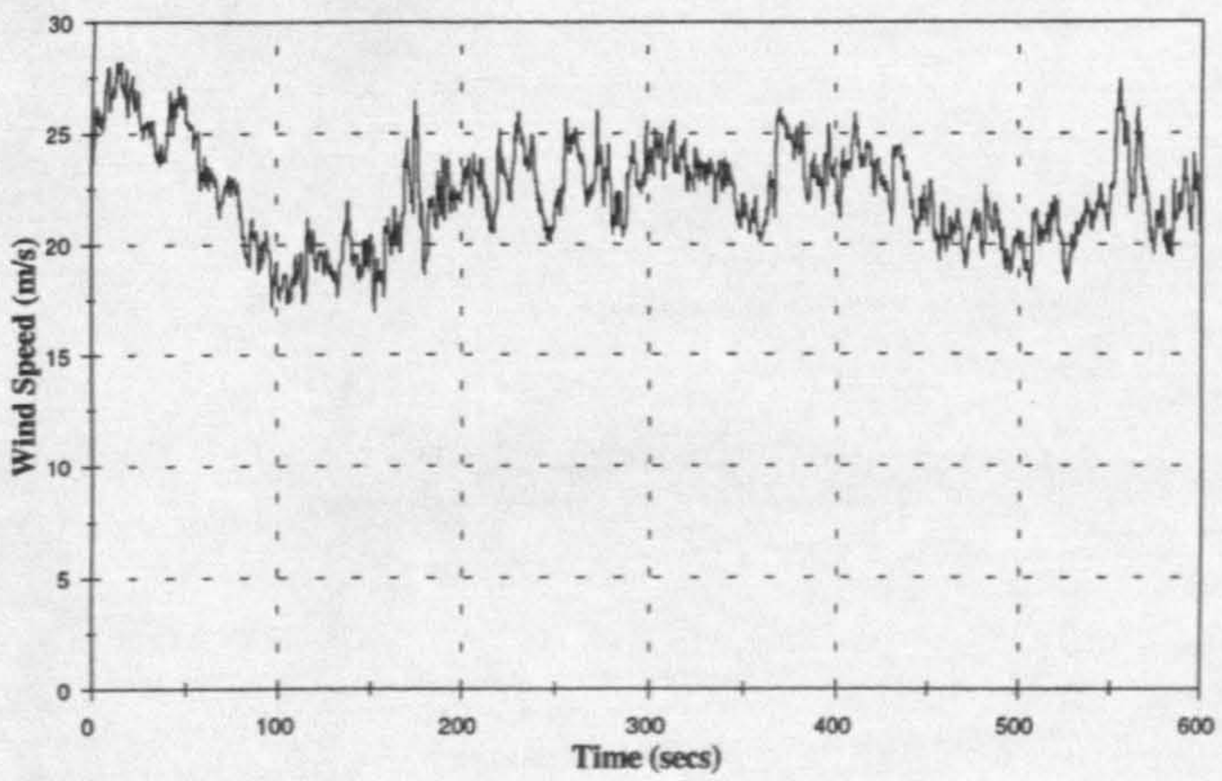

Figure 8.58c -:- Wind Speed at Mid Span, 13:05 12 May

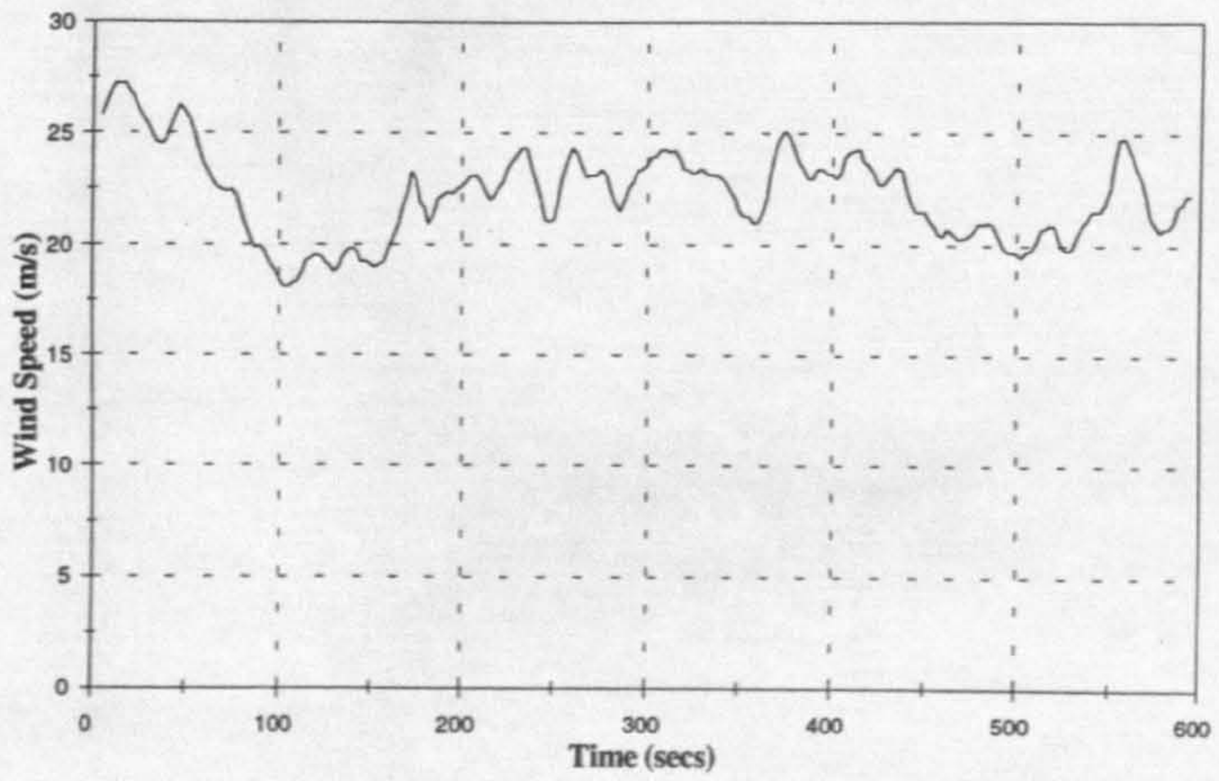

Figure 8.58d -:- 10 Second Average Wind Speed

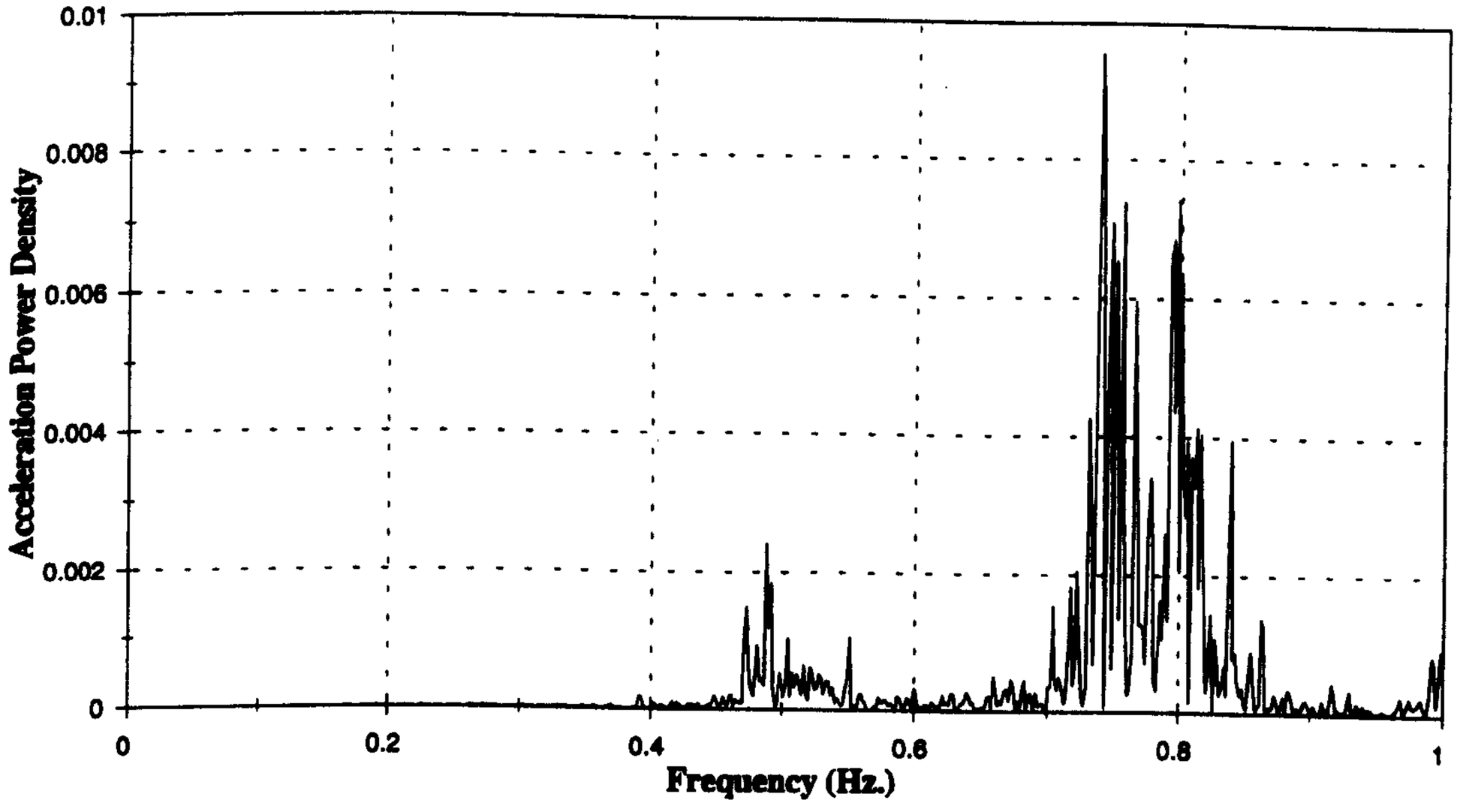

Figure 8.59a -:- Power Spectrum of Bridge Response At 50 m, 09:37 15 May

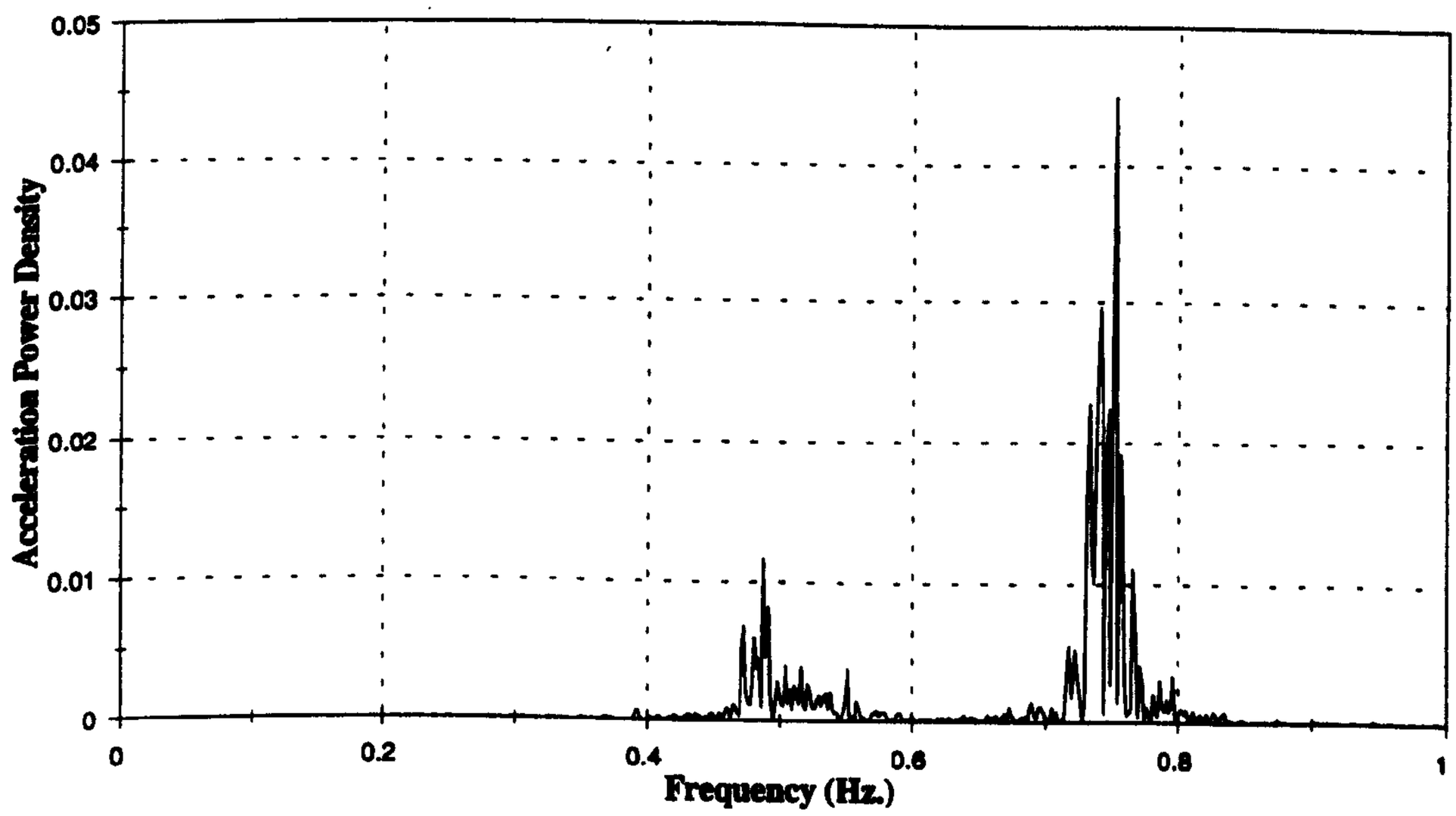

Figure 8.59b -:- Power Spectrum of Bridge Response At Mid Span, 09:37 15 May

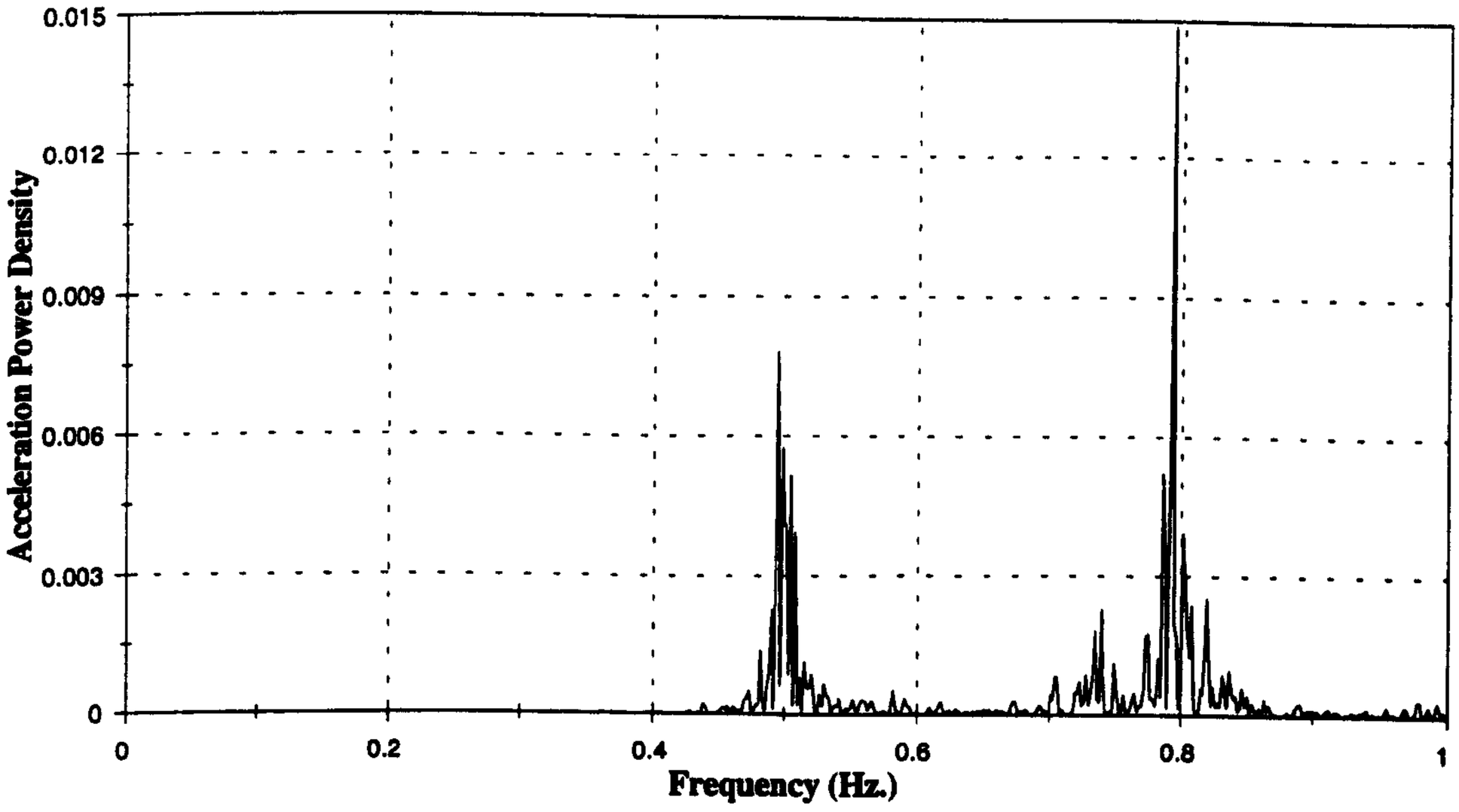

Figure 8.60a -:- Power Spectrum of Bridge Response At 50 m, 10:58 15 May

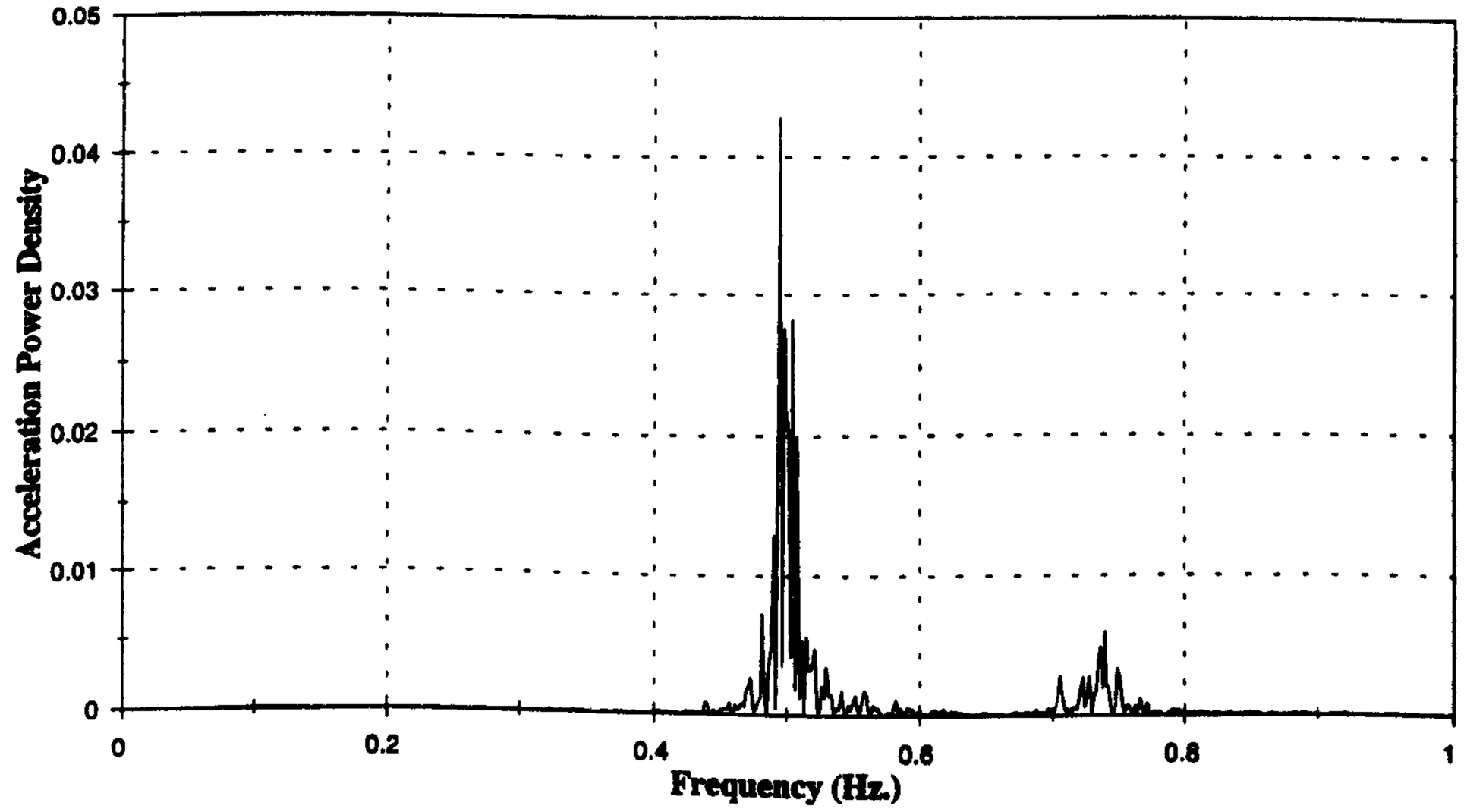

Figure 8.60b -:- Power Spectrum of Bridge Response At Mid Span, 10:58 15 May

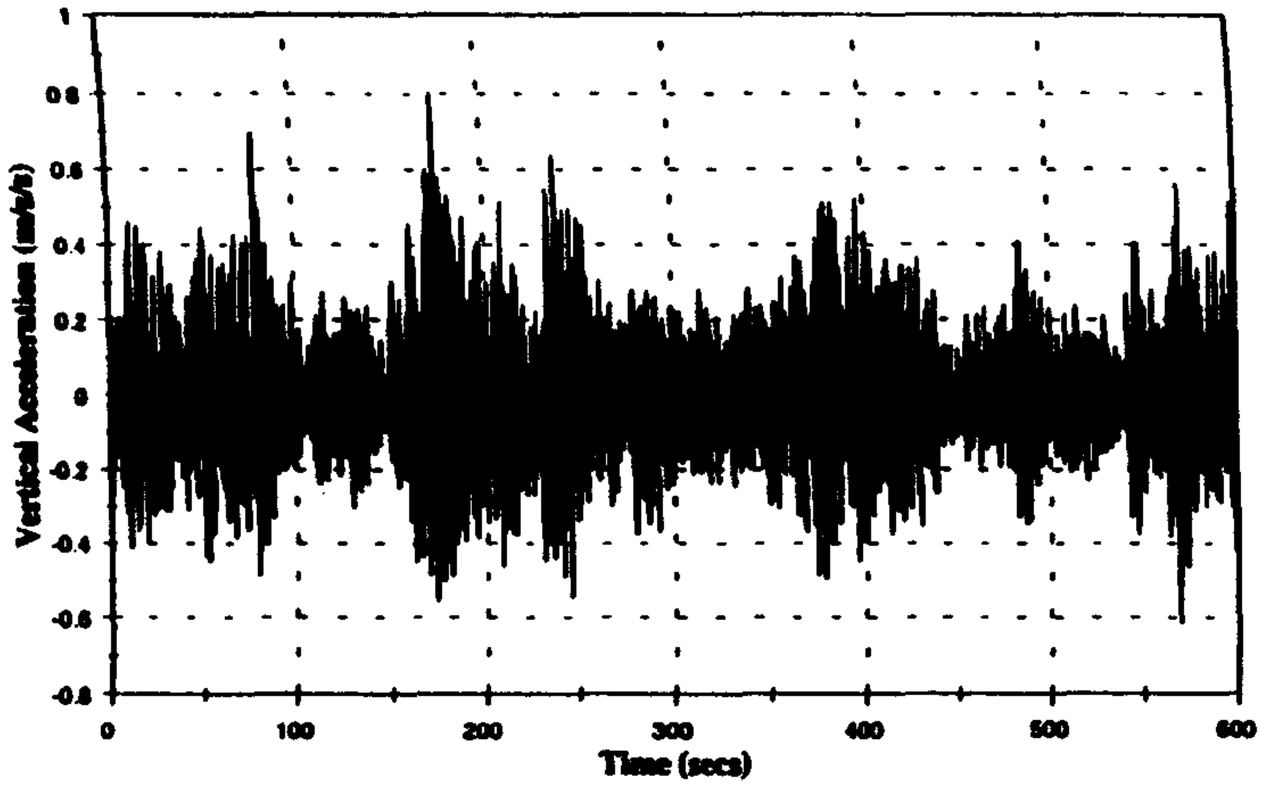

Figure 8.61a -:- Bridge Acceleration at Mid Span, 09:37 15 May

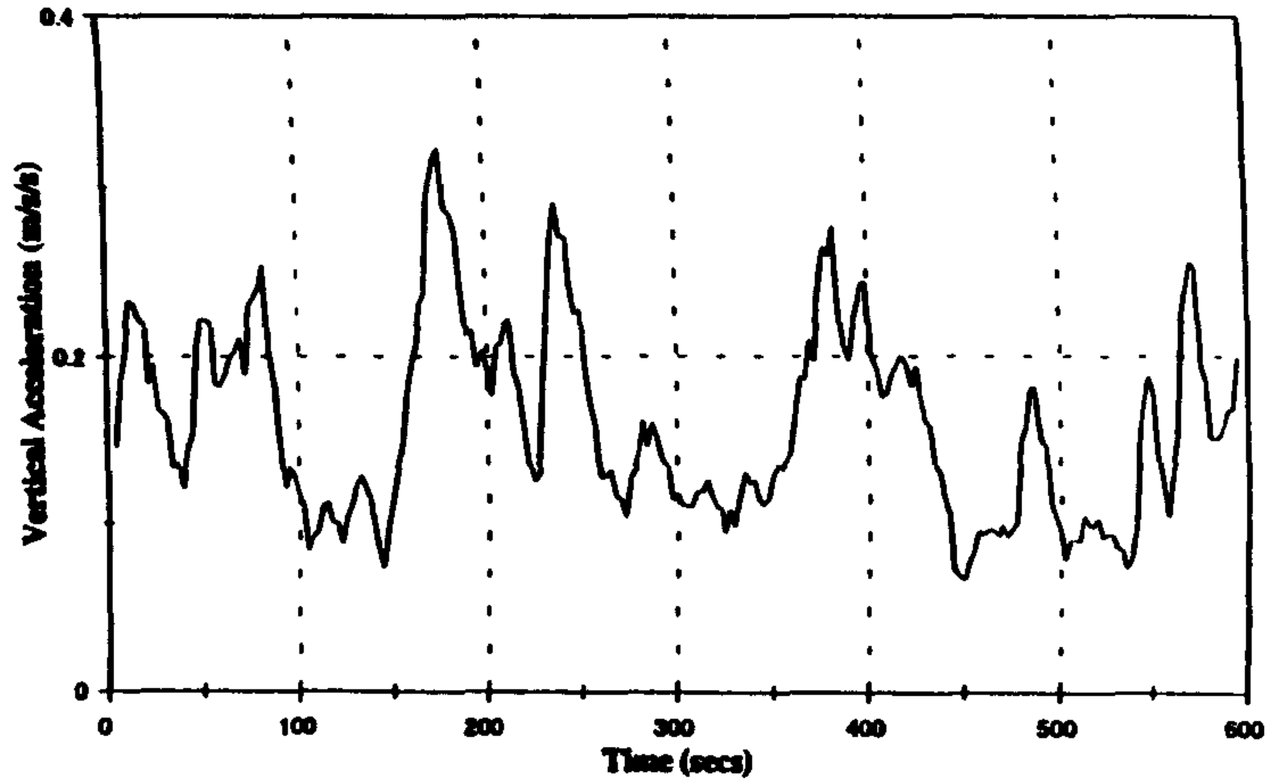

Figure 8.61b -:- 10 Second RMS Bridge Acceleration

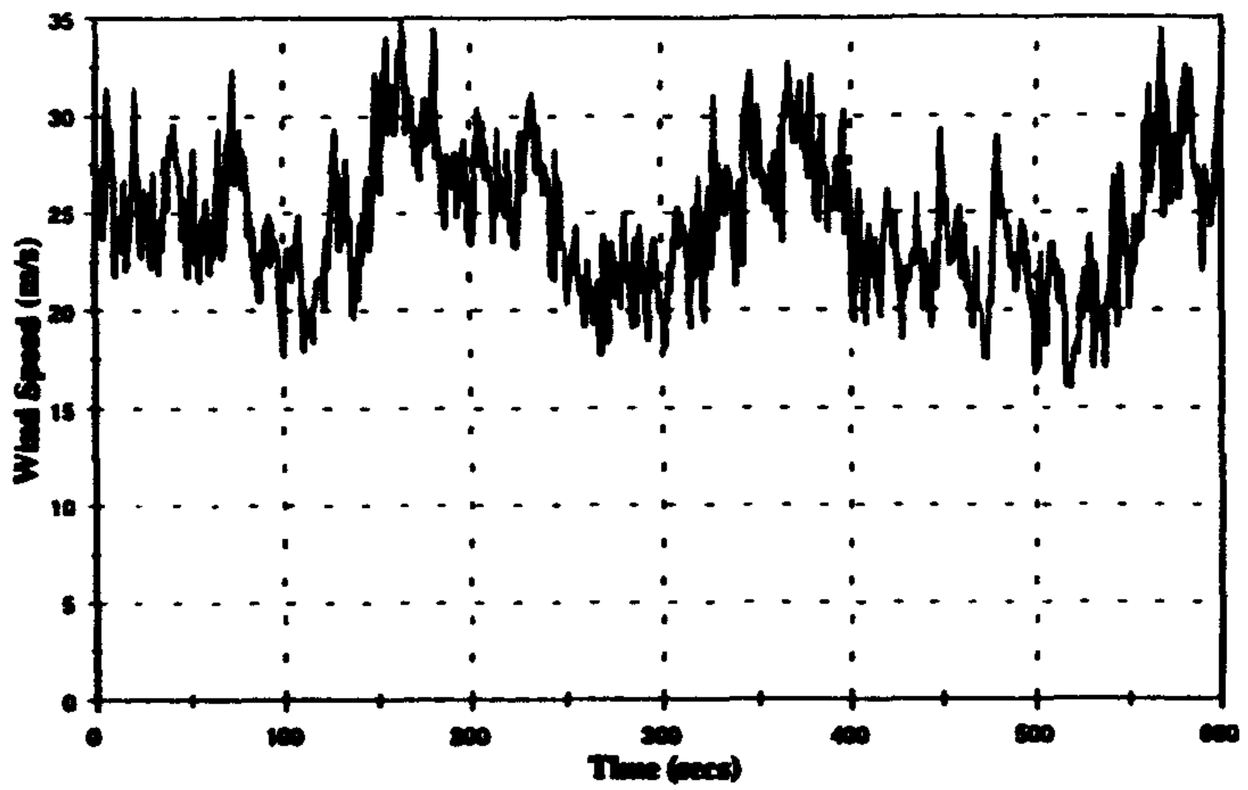

Figure 8.61c -:- Wind Speed at Mid Span, 09:37 15 May

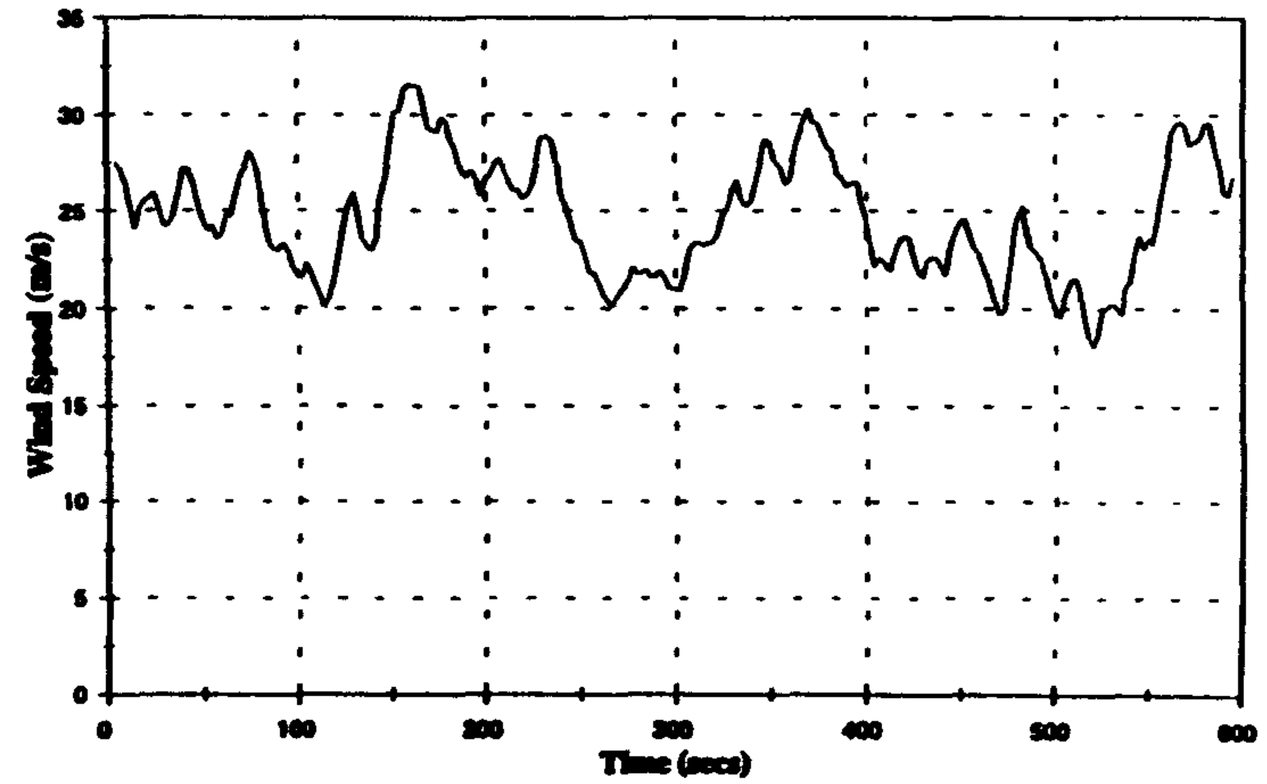

Figure 8.61d -:- 10 Second Average Wind Speed

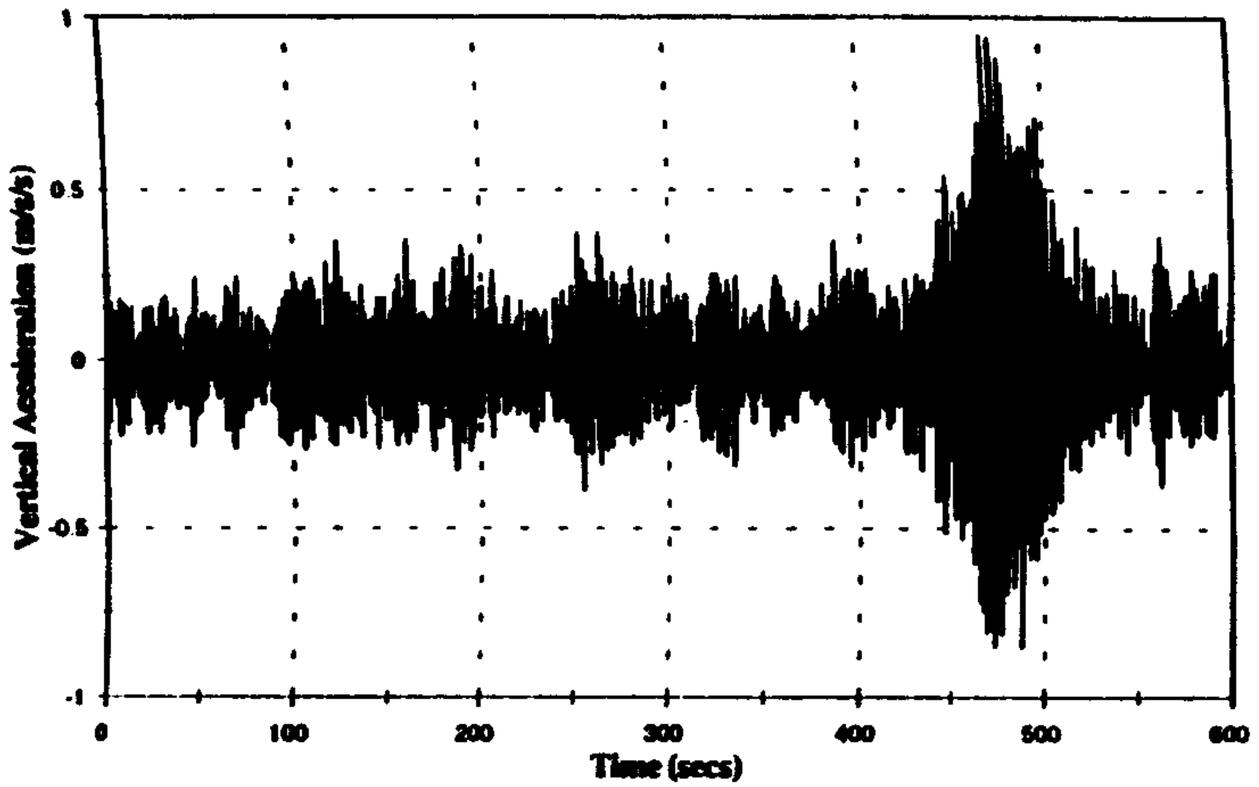

Figure 8.62a -:- Bridge Acceleration at Mid Span, 10:58 15 May

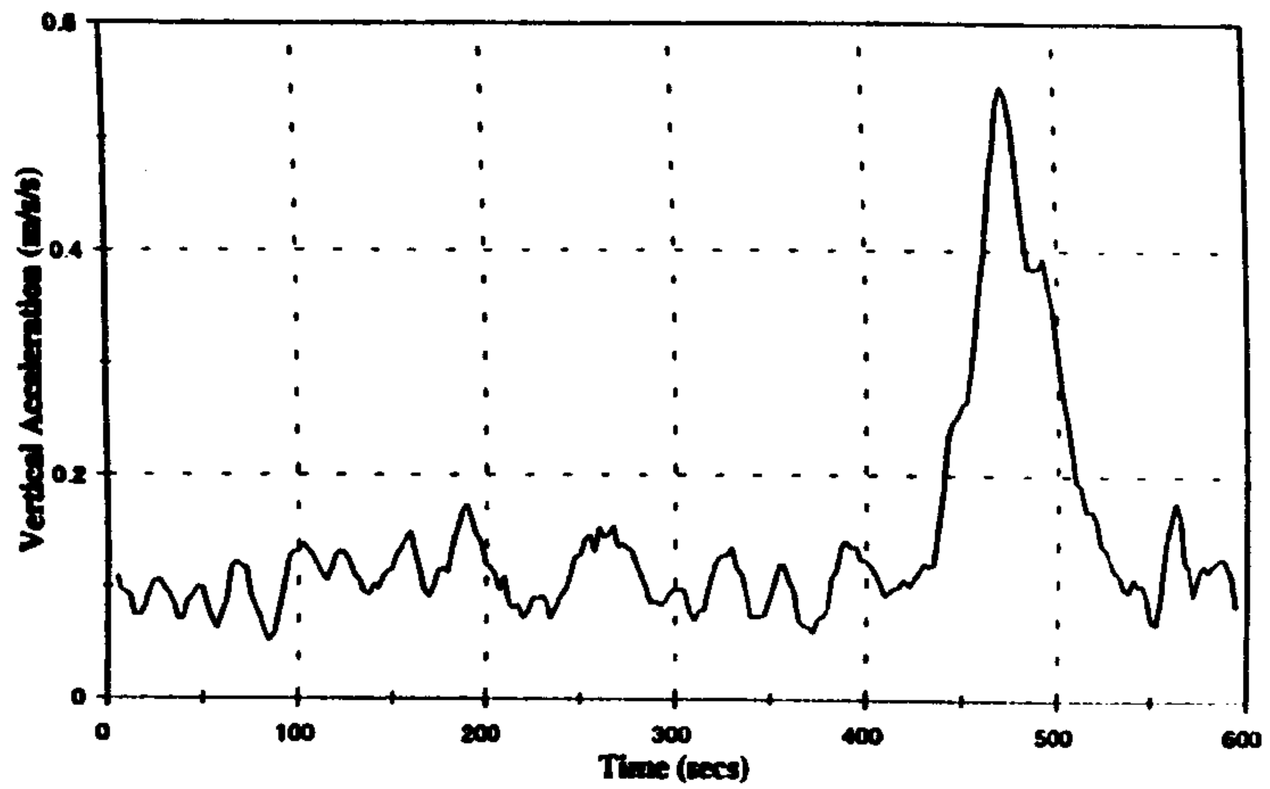

Figure 8.62b -:- 10 Second RMS Bridge Acceleration

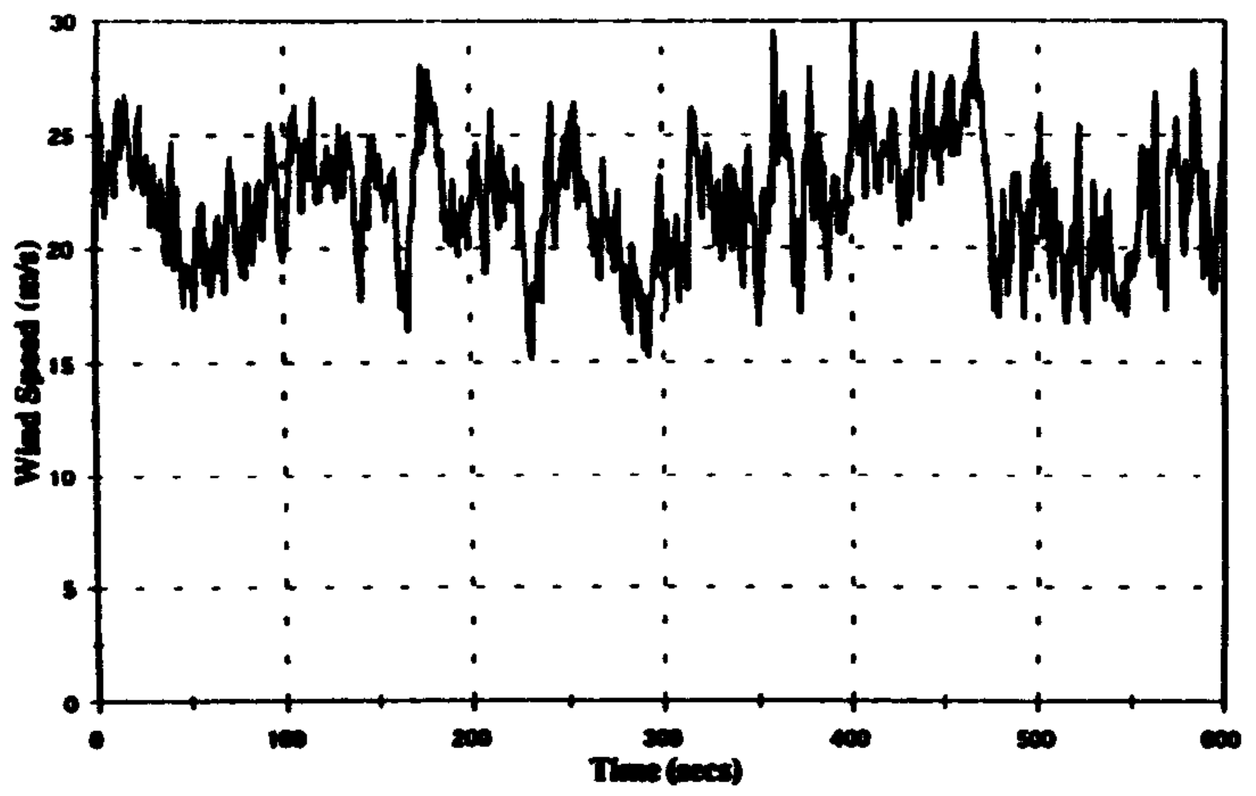

Figure 8.62c -:- Wind Speed at Mid Span, 10:58 15 May

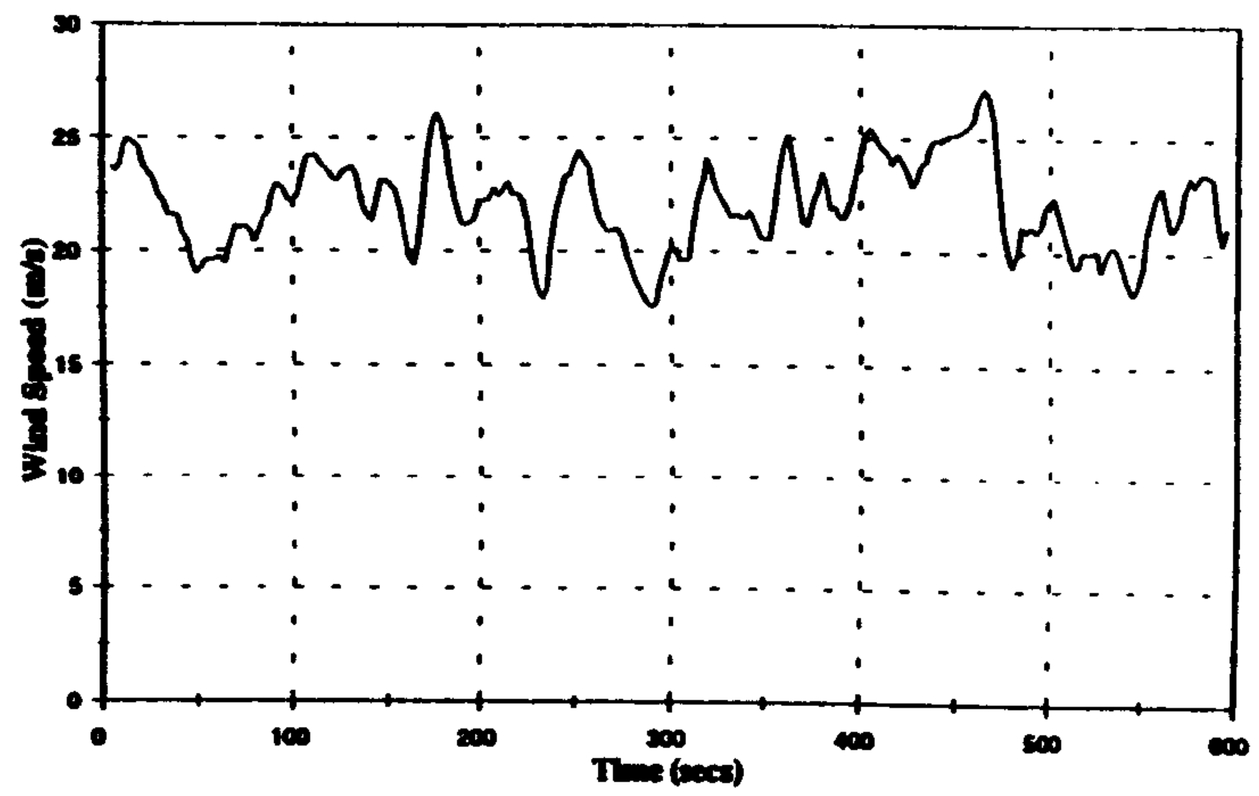

Figure 8.62d -:- 10 Second Average Wind Speed

Chapter Nine

Conclusions And Recommendations For Further Study

9.0 Introduction

In chapter one, the problems of spatially varying seismic and wind excitation which form the subject of this thesis were introduced, and two objectives were stated. Firstly, an analytical approach was to be developed that could be used to calculate the response of cable stayed bridges to spatially varying seismic excitation. This had to take account of the random nature of the excitation as well as the spatial variations, so that it could be used to investigate the response without being restricted to a specific event. Secondly, the response of a prototype bridge to spatially varying loads was to be measured to determine whether or not this phenomena is important and whether or not the analytical method developed is applicable.

The subsequent chapters of this thesis have outlined the work which has been done to meet these objectives, and have presented the results obtained from both analytical and practical phases of the project. To draw the thesis to a close, it is now useful to give an appraisal of the work which has been done, outlining both areas where the objectives have been achieved or surpassed, and those where mistakes were made or further work is needed. Having appraised the project, it will then be possible to be draw conclusions from the work which are either of relevance to the practising bridge engineer or can be used to outline areas for further study. Therefore the aim of this chapter is to present an appraisal of the work done, together with the conclusions, and then to propose areas for further research.

9.1 Appraisal Of The Research

As might be expected, the twin objectives of the research have lead to work which has covered two of the three principal sources of dynamic excitation of bridges, wind and seismic loading. This has therefore lead to a thesis which is very wide ranging and has looked at many aspects of the dynamic response of cable stayed bridges. However, the breadth of the work has necessarily been at the expense of depth in certain areas; indeed a major criticism of the thesis is that it does not explore in depth some important subject areas that are mentioned in passing. It is now best to consider the work in each of these two areas separately.

9.1.1 The Response To Spatially Varying Seismic Excitation.

The first point to make about the work on the response to spatially varying seismic excitation is that it has produced an analytical method which can be applied to this problem. The approach deals with both the random nature of the loading and the spatial variations, and therefore it can be concluded that the first objective has been met. However, it was also important to use the method once it had been developed to investigate the importance of spatially varying seismic excitation and this was done for two example structures. The results of these analyses, both of the portal frame and the cable stayed bridge, showed that asynchronous excitation can have a significant effect on the response of the structure. They also showed that these effects are determined by the interaction of the relative ground wave speed, the dynamic properties of the structure and the direction of the ground shaking. The comparison of the results in chapter four demonstrated the strength of the power spectral approach to the analysis, and how important it is to take account of the random or pseudo random nature of the loading. This point is reinforced by the range of results that were achieved using the time history approach.

However, there were three major omissions from the seismic part of the thesis:

a. No comparison was made with measured data

b. The method was not applied to general multi support excitation

c. No comparison was made with current design practice.

In answer to the first of these points it has to be noted that modelling multi support excitation in the laboratory presents various problems both in controlling the excitation and modelling the wave propagation. This is why it was decided to expand the range of the project to cover wind excitation as well, so that comparisons could be made with measured data from a prototype structure. However, as has become apparent, the length of time required both to collect and process an adequate amount of useful data was beyond the limits of the project funding, and only limited conclusions could be drawn. This aspect of the project will be discussed further below.

The failure to apply the approach to the more general case of multi support excitation is a direct result of the breadth of the project not allowing the time for the calculations to be performed. As was pointed out in chapter three the method developed is applicable to multi support excitation, and this is an obvious area for the work to be extended in the future.

The third criticism is, perhaps, the most important since ultimately the objective of engineering research is to develop better engineering solutions. However, there are several mitigating factors that made direct comparisons difficult and which need to be considered on this point. Firstly, most design codes use the response spectrum to define the earthquake excitation, although the new Eurocode does allow use of power spectra in certain cases. Therefore direct comparisons with these design codes is not possible. Secondly, whilst some codes acknowledge the need to consider the spatial variations in the seismic load for certain applications, they fail to provide detailed methods for doing this. The

work presented in this thesis has clearly shown the need to take the problem of asynchronous loading seriously in aseismic design, even for relatively short span structures. It also, in demonstrating the effectiveness of the power spectral approach, has added weight to the call for a more widespread use of stochastic methods in design which has been made by other researchers in the field of earthquake engineering. Clearly, therefore, whilst it is inappropriate to make comparisons with current design codes, the work presented here does have important implications that need to be considered when future design methodologies are developed.

9.1.2 - The Response To Wind Excitation

The prototype testing of Kessock bridge was an attempt to extend the approach developed for seismic excitation to wind loading so that comparisons could be made with measurements taken from a real structure. To this end the monitoring project was not a clear success since the quality and amount of data obtained was insufficient to form the two dimensional power spectral representation of the wind required. However, having made this point, it is also worth noting that a great deal of useful information and experience was gained from the project. Firstly, the data have shown that the eddy size can influence the response of the bridge suggesting that spatial variations in the loading are important. Secondly, the results have also provided an insight into the factors that influence the dynamic response of these bridges; the relative importance of wind and traffic loading, the effects of buffeting and the potentially damaging nature of aeroelastic behaviour. Finally, the experience of setting up the project and collecting and processing data will be very useful for future exercises. This is especially important since the lack of data, mentioned above, could be overcome by setting up a new and more extensive program of monitoring; the lessons learnt from the Kessock project will be of great benefit in this. Such an exercise should hopefully yield the necessary two dimensional wind spectrum and thus unite the two halves of this thesis.

Once again, as with the seismic excitation, it is essential to relate the work to the design of bridges, and this has not been possible within the time available. As mentioned above, the results of the long term monitoring did provide useful information on the factors that influence the response of the bridge to wind excitation and the relative importance of wind and traffic excitation. The results showed that the most significant response was caused by vortex shedding and for the period of time considered the response to buffeting was less severe. However, as pointed out in chapter eight, the short duration of the monitoring exercise meant that the extreme winds experienced were lighter than those which are likely to be used in design. Therefore, the response to buffeting during the life of the structure is likely to be more severe than experienced during this study. It is difficult to relate these observations to the design rules since these give very little guidance on how to approach these problems. For example the current British Standard for bridge design, BS 5400, says (Pt 2 1978 para. 5.3.9):

> ***Aerodynamic Effects.*** *Consideration shall be given to wind excited oscillations, and where necessary this behaviour shall be determined by tests.*

Since there are detailed recommendations available from other sources for both the aerodynamic response of deck sections, and the spatial and temporal distribution of wind loading, it is surprising that the code does not address these areas in more detail. This is clearly an area to which the work in this thesis could and should be applied at a later date.

9.2 Conclusions

1. The power spectral approach developed in this thesis to analyse the response to asynchronous and multi support excitation is a quick and reliable method for investigating the response of extended structures to spatially varying seismic excitation.

2. Asynchronous loading has a strong influence on the response of cable stayed bridges to seismic excitation and should be accounted for in aseismic design. It has two principal effects:

   a. It influences the magnitude of the response

   b. It influences the point in the deck where the peak response occurs

3. Because spatial variations in the loading preferentially excite different vibration modes, the direction of the excitation, mode shapes, natural frequencies and ground wave velocity are important factors in determining the bridge response.

4. The random nature of seismic excitation must be taken into account in aseismic design, a normal time history analysis is not sufficient to predict the results.

5. The integral length scale of turbulence influences the relative response of the bridge in different modes.

6. Aeroelastic effects represent the most serious design load for long span bridges.

9.3 Suggestions For Further Study

Having looked at an overview of the project, it is clear that there are several areas where further research and study are needed; the breadth of the project has revealed many areas that require further exploration. This research should concentrate on three areas:

   a. Unifying the two aspects of the work

   b. Developing the seismic analysis to overcome limits imposed by assumptions

   c. Deriving detailed design methodologies from the work.

9.3.1 Unification Of Wind and Seismic Approaches

As the thesis stands the two principal areas, wind and seismic excitation, are disparate and need to be brought together. It should be noted here that this is not an academic goal, but a real aim that can be achieved with benefits for both aspects of the work. Two avenues should be explored, further experimental work and development of the analysis technique so that it can be applied to wind loading.

9.3.1.1 Further Experimental Work

The experimental project on Kessock bridge was successful in identifying that there is a phenomenon to be investigated, however insufficient data were processed to draw any further conclusions. It is therefore necessary to process more of the data collected during this exercise which can be achieved both by adapting the non-stationary data and by considering other wind directions. A further monitoring program to collect more data could also prove useful. As identified in chapter eight, several mistakes were made during the monitoring of Kessock bridge and these lessons should now be incorporated in the new study. This project has also identified the main factors which need to be considered during the monitoring, and it is now possible to implement a more efficient monitoring strategy which will ensure that the optimum amount of useful data is stored.

9.3.1.2 Analysis Of Wind Excitation

The extension of the power spectral approach developed in chapter three to the problem of wind loading was briefly discussed in chapter six. However, the analytical method has not been rigorously developed nor the appropriate computer code produced. Therefore, an important aspect of the further study will be the development and validation of appropriate computer code. It should, however, be

noted that such code must rely on an appropriate two dimensional power spectral representation of the wind loading which must come from the results of further prototype testing.

9.3.2 Development Of The Seismic Analysis

The two areas which are most promising for expanding the earthquake engineering work presented in this thesis are the application of the method to multi support excitation and taking account of non linearities in structures. The response to multiple support excitation was briefly touched upon in chapter three, and it should be quite simple to extend the program used in chapters four and five to this problem. In contrast, applying spectral methods to non linear structures represents a more fundamental study although one which will be essential if power spectral techniques are to be fully utilised in design. This is especially so for steel structures, where plastic design is important, and aseismic design where ductile elements are often included to absorb energy. The problem is that spectral methods axiomatically apply only to linear systems. Two alternatives could be investigated, firstly the use of appropriate factors to take account of the non linearities and secondly the modification of the spectral analysis itself. This second alternative could prove fruitful, higher order transforms provide a means of considering non linear systems in a spectral manner and there is a body of experimental evidence that the variation of response with frequency of a non linear system shows a level of repeatability.

9.3.3 Application To Design

The comments earlier in this chapter indicate that current design codes allow little provision for considering the dynamic response to spatially varying excitation. The approach developed in this thesis provides a quick and reliable means of predicting this response and so a suitable step forward, both for the development of this approach and for its application, would be to produce a methodology which could be applied in design

References

Abdel Ghaffar A. M., "Free lateral vibrations of suspension bridges." J. Struct. Div. ASCE, Vol. 104 pp. 503-525 (**1978**a)

Abdel Ghaffar A. M., "Vibration studies and tests of a suspension bridge." Earthquake Engineering & Structural Dynamics, Vol. 6 pp. 473ff (**1978**b)

Abdel Ghaffar A. M., "Free torsional vibrations of suspension bridges." J. Struct. Div. ASCE, Vol. 105 pp. 767ff (**1979**)

Abdel Ghaffar A. M., "Vertical vibration analysis of suspension bridges." J. Struct. Div. ASCE, Vol. 106 pp. 2053ff (**1980**)

Abdel Ghaffar A. M., "Suspension Bridge Vibration: Continuum Formulation." J. Eng. Mech. Div. ASCE, Vol. 108, pp 1215-1231 (**1982**)

Abdel Ghaffar A. M. & Housner G. W., "Ambient vibration tests of suspension bridges." J. Eng. Mech. Div. ASCE, Vol. 104 pp. 983ff (**1978**)

Abdel Ghaffar A. M. & Khalifa M. A., "Importance of Cable Vibration In Dynamics of Cable Stayed Bridges." J. Eng. Mech. Div. ASCE, Vol. 117, pp 2571-2589 (**1991**)

Abdel-Ghaffar A. M. & Nazmy A. S., "3-D Nonlinear Seismic Behaviour Of Cable-Stayed Bridges.", J. Struct. Div. ASCE, Vol. 117, pp. 3456-3476, (**1991**)

Abdel Ghaffar A. M. & Rubin L. I., "Suspension bridge response to multi-support excitations." J. Eng. Mech. Div. ASCE, Vol. 108 pp. 419-435 (**1982**)

Abdel Ghaffar A. M. & Rubin L. I., "Non Linear Free Vibrations of Suspension Bridges: Theory." J. Eng. Mech. Div. ASCE, Vol. 109 pp. 313-329 (**1983a**)

Abdel Ghaffar A. M. & Rubin L. I., "Non linear free vibrations of suspension bridges: Application." J. Eng. Mech. Div. ASCE, Vol. 109pp. 330-345 (**1983b**)

Abdel Ghaffar A. M. & Rubin L. I., "Vertical seismic behaviour of suspension bridges." Earthquake Engineering & Structural Dynamics, Vol. 11 pp. 1-19 (**1983c**)

Abdel Ghaffar A. M. & Rubin L. I., "Lateral earthquake response of suspension bridges." J. Struct. Div. ASCE, Vol. 109, pp. 664-675 (**1983d**)

Abdel Ghaffar A. M. & Rubin L. I., "Lateral earthquake response of suspension bridges." J. Eng. mech. Div. ASCE, Vol. 110, pp. 1467-1484 (**1984**)

Abdel Ghaffar A. M. & Scanlan R. H., "Ambient vibration studies of the Golden Gate bridge : Pt. I Suspended structure." J. Eng. Mech. Div. ASCE, Vol. 111, pp. 463ff (**1985a**)

Abdel Ghaffar A. M. & Scanlan R. H., "Ambient vibration studies of the Golden Gate bridge : Pt. II Towers." J. Eng. Mech. Div. ASCE, Vol. 111, pp. 483ff (**1985b**)

Abdel Ghaffar A. M. & Stringfellow R. G., "Response of suspension bridges response to travelling earthquake excitation: part 1 vertical response." Soil Dynamics and Earthquake Engineering, Vol. 3 pp. 62-72 (**1984a**)

Abdel Ghaffar A. M. & Stringfellow R. G., "Response of suspension bridges response to travelling earthquake excitation: part 2 lateral response." Soil Dynamics and Earthquake Engineering, Vol. 3 pp. 73-81 (**1984b**)

Aboul-ella F., "Analysis of cable stayed bridges supported by flexible towers." J. Struct. Div. ASCE, Vol. 114, pp. 2741-2754 (**1988**)

Aki K., "State Of The Art Report: Seismological Synthesis Of Strong Ground Motion." Proc. 9th W.C.E.E., Vol. 8 pp. 9-17 (**1988**)

Altinisik D. & Severn R. T., "Multiple support and asynchronous base excitation of structures." Proc. Instn. Civ. Engrs., Part 2, Vol. 71 pp. 407-426 (**1981**)

Amin M. & Ang A. H., "Non-Stationary Stochastic Model Of Earthquake Motions." J. Eng. Mech. Div. ASCE, Vol. 94 pp. 559-583 (**1968**)

Bailey A. & Vincent N. D. G., "Wind pressure experiments at the Severn bridge." Journal of the I.C.E., Vol. 11 pp. 363ff (**1939**)

Bampton M. C. C., Ramsdell J. V., Graves R. E. & Sytrope L. A., "Deer Isle - Sedgwick suspension bridge, wind and motion analysis." U.S. Federal Highway Authority report number FHWA/RD-86/183 (**1986**)

Baron F. & Lien S-Y., "Analytical studies of a cable stayed girder bridge." Computers and Structures, Vol. 3, pp. 443ff, (**1973**)

Bendat J. S. & Piersol A. G., "Random Data: Analysis and measurement procedures." Wiley Interscience, New York (**1971**)

Benioff H., "The Physical Evaluation Of Seismic Destructiveness." Bull. Seism. Soc. Am. Vol. 24, pp. 398-403 (**1934**)

Benjamin J. R. & Cornell C. A., "Probability, statistics and decision for civil engineers." McGraw-Hill, New York (**1970**)

Berman S. & Stearns C. R., "Near Earth turbulence and coherence measurements at Aberdeeen proving ground, Md." Boundary Layer Meteorology, Vol. 11 pp. 485-506 (**1976**)

Berrah M. & Kausel E., "Response spectrum analysis of structures subjected to spatially varying motions." Earthquake Engineering & Structural Dynamics Vol. 21, pp. 461-470 (**1992**)

Billington D. P., "History and aesthetics in suspension bridges." J. Struct. Div. ASCE, Vol. 103, pp. 1655ff (**1977**)

Billington D. P. & Nazmy A., "History and aesthetics of cable-stayed bridges." J. Struct. Div. ASCE, Vol. 117, pp. 3103-3134 (**1990**)

Biot M. A., "A mechanical analyzer for the prediction of earthquake stresses." Bull. Seism. Soc. Am. Vol. 31 pp. 151-171 (**1941**)

Bocciolone M., Cheli F., Curami A. & Zasso A., "Wind measurements on the Humber Bridge and numerical simulations." Journal of Wind Engineering and Industrial Aerodynamics, Vol. 42, pp1393-1404 (**1991**)

Bolt B. A., Tsai Y. B., Yeh K. & Hsu M. K., "Earthquake strong motions recorded by a large near source array of digital seismographs." Earthquake Engineering & Structural Dynamics, Vol. 10, pp. 561-573 (**1982**)

Borino G., M. Di Paola & G. Muscolino, "Non-Stationary Spectral Moments Of Base Excited MDOF Systems." Earthquake Engineering & Structural Dynamics Vol. 16 pp. 745-756 (**1988**)

Borland International Ltd., "Object Vision Reference Guide." (**1991**)

Bosch H. R., "Section Model Studies Of The Deer Isle-Sedgwick Suspension Bridge." Journal of Wind Engineering and Industrial Aerodynamics, Vol. 36, pp. 601-610, (**1990**)

Brownjohn J. M. W., Dumanoglu A. A., Severn R. T. & Taylor C. A., "Ambient vibration measurements of the Humber suspension bridge and comparison with calculated characteristics." Proceedings I.C.E. Pt. 2 Vol. 83, pp. 561-600, (**1987**)

Brownjohn J. M. W., Dumanoglu A. A., Severn R. T. & Blakeborough A. B., "Ambient vibration survey of the Bosporus suspension bridge." Earthquake Engineering & Structural Dynamics, Vol. 18, pp. 263-283 (**1989**)

Brownjohn J. M. W., Dumanoglu A. A. & Severn R. T., "Ambient vibration survey of the Fatih Sultan Mehmet (Second Bosporus) suspension bridge." Earthquake Engineering & Structural Dynamics, Vol. 21, pp. 907-924 (**1992**)

Bryja D. & Šniady P., "Spatially coupled vibrations of a suspension bridge under random highway traffic." Earthquake Engineering & Structural Dynamics, Vol. 20, pp. 999-1010 (**1991**)

Buckland P. G., Hooley R., Morgenstern B. D., Rainer J. H. & Van Selet A. M., "Suspension bridge vibration : computed and measured." J. Struct. Div. ASCE, Vol. 105, pp. 859ff (**1979**)

Button M. R., Der Kiureghian A. & Wilson E. L., "STOCAL User information manual." Report Nº UCB/SESM-81/02, Department of Civil Engineering, University of California, Berkeley, California. (**1981**)

Bycroft G.N., "White noise representation of earthquakes." J. Eng. Mech. Div. ASCE, Vol. 86 pp. 1-16 (**1960**)

Christian J. T., "Relative motion of two points during an earthquake." J. Geotech. Eng. Div. ASCE, Vol. 102, pp. 1191ff (**1976**)

Christian J. T., "Generating seismic design power spectral density functions." Earthquake Spectra, Vol. 5, pp. 531-368 (**1989**)

Clough R. W. & Penzien J., "Dynamics of structures." McGraw-Hill, New York (**1975**)

Cook R. G., "Digital simulation of random vibration." PhD Thesis, Massachusetts Institute of Technology (**1964**)

Corotis R. B., Vanmarcke E. H. & Cornell C. A., "First passage of non-stationary random processes" J. Eng. Mech. Div. ASCE, Vol. 98, pp. 401-414 (**1972**)

Counihan J., "Adiabatic atmospheric boundary layers : a review and analysis of data from the period 1880 - 1970." Atmos. Environ., Vol. 9, pp. 871 - 905 (**1975**)

Crouch & Hogg, "Kessock Bridge Wind Influence." Engineer's Report, Crouch & Hogg (Now Crouch Hogg Waterman), Glasgow (**1988**)

Cullen-Wallace A. A., "Wind Influence On Kessock Bridge.", Engineering Structures, Vol. 7, pp. 18-22 (**1985**)

Danniell W. E., "Seismic behaviour of reservoir intake towers." PhD Thesis, University of Bristol, Department of Civil Engineering, (**1992**)

Danniell W. E. & Taylor C. A. "The dynamic testing and analysis of Wimbleball intake tower." International Conference, Structural Dynamics Modelling, Test, Analysis and Correlation, Cranfield, UK (**1993**)

Davenport A. G., "A statistical approach to the treatment of wind loading on tall masts and suspension bridges." PhD Thesis, University of Bristol, Department of Civil Engineering, (**1961a**)

Davenport A. G., "The application of statistical concepts to the wind loading of structures." Proc. I.C.E., Vol. 19, pp. 449-472 (**1961b**)

Davenport A. G., "The response of slender, line-like structures to a gusty wind." Proc. I.C.E., Vol. 23, pp. 389-407 (**1962**)

Davenport A. G. "Note on the distribution of the largest value of a random function with application to gust loading." Proc. I.C.E., Vol. 28, pp. 187-196 (**1964**)

Davenport A. G., "The relationship of wind structure to wind loading." Wind Effects On Buildings And Structures, National Physical Laboratory Symposium No. 16, Paper 2, pp. 54-102, (**1965a**)

Davenport A. G., "The buffeting of structures by gusts." Wind Effects On Buildings And Structures, National Physical Laboratory Symposium No. 16, Paper 9, pp. 357-391, (**1965b**)

Davenport A. G. & King J. P. C., "The influence of topography on the dynamic wind loading of long span bridges." Journal of Wind Engineering and Industrial Aerodynamics, Vol. 36, pp. 1373-1382, (**1990**)

Davis J. P. & Vann A. M. "Intelligent Monitoring of Civil Engineering Systems". Applications of Artificial Intelligence in Engineering VII - Proceedings of AIENG92. Southampton: Computational Mechanics Publications, (**1992**)

Davis J. P., Vann A. M., Cairns J. & Linfoot B. T., "Intelligent Logging for Fish Farm Monitoring", pp. 275-281 in Proceedings of the First International Conference on Fish Farming Technology, Reinerston, Dahle, Jorgensen, Tvinnereim (Eds.), Trondheim, Norway, (**1993**)

Der Kiureghian A., "Structural response to stationary excitation." J. Eng. Mech. Div. ASCE, Vol. 106, pp. 1195-1213 (**1980**)

Der Kiureghian A. & Neuenhofer A, "Response spectrum method for mult-support seismic excitations." Earthquake Engineering & Structural Dynamics, Vol. 6, pp. 715-740 (**1992**)

Diana G., Cheli F., Zasso A., Collina A. & Brownjohn J. M. W., "Suspension bridge parameter identification in full scale test." 8th International Conference on Wind Engineering, London, Ontario, Canada, (**1991**)

Duchêne-Marullaz P., "Effect of high roughness on the characteristics of turbulence in the case of strong winds." 5th International Conference on Wind Engineering, Vol. 1, (**1980**)

Dumanoglu A. A. & Severn R.T., "Dynamic response of dams and other structures to differential ground motions." Proc. I.C.E., Part 2, Vol. 77, pp. 333-352 (**1984**)

Dumanoglu A. A. & Severn R. T., "Seismic response of modern suspension bridges to asynchronous vertical ground motion." Proc. I.C.E., Part 2, Vol. 83, pp. 701-703 (**1987**)

Dumanoglu A. A. & Severn R. T., "Stochastic response of suspension bridges to earthquake forces." Earthquake Engineering & Structural Dynamics, Vol. 19, pp. 133-152 (**1990**)

Dumanoglu A. A., Brownjohn J. M. W. & Severn R. T., "Seismic analysis of the Fatih Sultan Mehmet (Second Bosporus) suspension bridge." Earthquake Engineering & Structural Dynamics, Vol. 21, pp. 881-906, (**1992**)

Ehsan F., Scanlan R. H. & Bosch H. R., "Modelling spanwise correlation effects in the vortex-induced response of flexible bridges." Journal of Wind Engineering and Industrial Aerodynamics, Vol. 36, pp. 1105-1114, (**1990**)

"Eurocode Nº 8 "(1988)

Farquharson F. B., "Aerodynamic stability of suspension bridges with special reference to the Tacoma Narrows, Part 1 Investigations prior to October 1941." University Of Washington Engineering Research Bulletin Number 116, (**1950**)

Fleming J. F., "Non linear static analysis of cable stayed bridge structures." Computers and Structures, Vol. 10, pp. 621ff (**1979**)

Fleming J. F. & Egesli E. A., "Dynamic behaviour of a cable-stayed bridge." Earthquake Engineering & Structural Dynamics, Vol. 8, pp. 1-16 (**1980**)

Garevski M. A.,"Dynamic analysis of cable-stayed bridges by means of analytical and physical modeling." PhD Thesis, University of Bristol, Department of Civil Engineering (**1990**)

Garevski M. A., Brownjohn J. M. W., Blakeborough A. & Severn R. T., "Resonance search tests on a small scale model of a cable stayed bridge." Engineering Structures, Vol. 13, pp. 59-66 (**1990**)

Garevski M. A., Dumanoglu A. A. & Severn R. T., "Dynamic characteristics and seismic behaviour of Jindo Bridge, South Korea." Structural Engineering Review, Vol. 1, pp. 141-149 (**1988**)

Gasparini D. A. & Vanmarcke E. H., "Simulated earthquake motions compatible with prescribed response spectra." Massachusetts Institute of Technology, Department of Civil Engineering, Report No. R76-4 (**1976**)

Greenway M. E.,"Performance tests on a prototype cup-anemometer and wind vane for 'Danjay Designs'." Oxford University Engineering Laboratory, Report No. 1224/77 (**1977**)

Grigoriu M., Ruiz E. & Rosenblueth E., "The Mexico earthquake of September 19 1985 - Nonstationary models of ground acceleration." Earthquake Spectra, Vol. 4, pp. 551-568 (**1988**)

Harrichandran R. S., "Random vibration under propagating excitation : Closed form solutions." J. Eng. Mech. Div. ASCE, Vol. 118, pp. 575-586 (**1992**)

Harrichandran R. S. & Vanmarcke E. H.,"Stochastic variation of earthquake ground motion in space and time." J. Eng. Mech. Div. ASCE, Vol. 112, pp. 154-174 (**1986**)

Harrichandran R. S. & Wang W., "Response of a simple beam to spatially varying earthquake excitation." J. Eng. Mech. Div. ASCE, Vol. 114, pp. 1526-1541 (**1988**)

Harrichandran R. S. & Wang W., "Response of indeterminate two-span beam to spatially varying seismic excitation." Earthquake Engineering & Structural Dynamics, Vol. 19, pp. 173-187 (**1990**)

Harris R. I., "Wind measurements on the Severn road bridge." ERA 72-16 (**1971**)

Hay J., "The wind induced response of the Kessock bridge" unpublished (**1986**)

Hay J., "Response of bridges to wind." Transport Research Laboratory, State of the art review / 5, HMSO, London (**1992**)

Hegab I. A., "Energy analysis of cable stayed bridges." J. Struct. Div. ASCE, Vol. 112, pp. 1182-1195 (**1986**)

Hou S., "Earthquake simulation models and their application." M.I.T. Dept. Civ. Eng. Rep. R68-17, (**1968**).

IMC Meßsysteme GmbH., "User's guide, Signal analysis program, FAMOS." (**1992**)

Intellicorp Inc., "KAPPA PC Reference manual." (**1991**)

Institution of Civil Engineers, "Bridge Aerodynamics" Proceedings of a conference held at the ICE, London, 25-26 March (**1981**)

Kaimal J. C., Wyngaard J. C., Izumi Y., & Coté O. R., "Spectral characteristics of surface layer turbulence." Quarterly Journal of the Royal Meteorological Society, Vol. 98, pp. 563-589 (**1972**)

Kanai K., "Semi-empirical formula for seismic characterisation of the ground." Bull. Earthquake Research Inst., Univ. Of Tokyo, Vol. 35, pp. 309-325 (**1957**)

Kanai K., "An empirical formula for the spectrum of strong earthquake motions." Bull. Earthquake Research Inst., Univ. of Tokyo, Vol. 39, pp. 85-85 (**1961**)

Kanok-Nukulchai W., Yiu P. K. A. & Brotton D. M., "Mathematical modelling of cable stayed bridges." Structural Engineering International, Vol. 2, pp. 108-113 (**1992**)

Kristensen L., Panofsky H. A. & Smith S. D., "Lateral coherence of longitudinal wind components in strong winds." Boundary Layer Meteorology, Vol. 21, pp. 199-205 (**1981**)

Kumarasena T., Scanlan R. H. & Morris G. R., "Deer Isle Bridge : Efficacy of stiffening systems." J. Struct. Div. ASCE, Vol. 115, pp. 2297-2312, (**1989a**)

Kumarasena T., Scanlan R. H. & Morris G. R., "Deer Isle Bridge : Field and computed vibrations." J. Struct. Div. ASCE, Vol. 115, pp. 2313-2328, (**1989b**)

Kumarasena T., Scanlan R. H. & Bosch H., "Wind response prediction of flexible bridges." Journal of Wind Engineering and Industrial Aerodynamics, Vol. 36, pp. 1365-1372, (**1990**)

Kumarasena T., Scanlan R. H. & Ehsan F., "Wind induced motions of Deer Island Bridge." J. Struct. Div. ASCE, Vol. 117, pp. 3357-3374, (**1991**)

Kumarasena T., Scanlan R. H. & Ehsan F., "Recent observations in bridge deck aeroelasticity." Journal of Wind Engineering and Industrial Aerodynamics, Vol. 40, pp. 225-247, (**1992**)

Langley R. S., "Structural response to non-stationary, non-white stochastic ground motions." Earthquake Engineering & Structural Dynamics, Vol. 14, pp. 909-924 (**1986**)

Lazar B. E., "Stiffness analysis of cable stayed bridges." J. Struct. Div. ASCE, Vol. 98, pp. 1605ff (**1972**)

Lazar B. E., Troitsky M. S. & McDouglas M., "Load balancing analysis of cable stayed bridges." J. Struct. Div. ASCE, Vol. 98, pp. 1725ff (**1972**)

Lin Y. K., "Probabilistic theory of structural dynamics." McGraw-Hill, New York (**1967**)

Lin Y. K. & Yong Y., "Evolutionary Kanai-Tajimi earthquake models." J. Eng. Mech. Div. ASCE, Vol. 113, pp. 1119-1137 (**1987**)

Loh C-H. & Yeh Y-T., "Spatial variation and stochastic modelling of seismic differential ground motion." Earthquake Engineering & Structural Dynamics, Vol. 16, pp. 583-596 (**1988**)

Loh C-H. Penzien J. & Ysai Y. B., "Engineering analysis of SMART1 array accelograms." Earthquake Engineering & Structural Dynamics, Vol. 10, pp. 525-591 (**1982**)

Luco J. E. & Wong H. L., "Response of a rigid foundation to a spatially random ground motion." Earthquake Engineering and Structural Dynamics, Vol. 14, pp. 891-908, (**1986**)

Morris N. F., "The use of modal superposition methods in non linear dynamics." Computers and Structures, Vol. 7, pp. 65ff (**1977**)

Muria-Vila D., Gomez R. & King C., "Dynamic properties of cable-stayed Tampico Bridge", ASCE J. Struct. Eng., Vol. 117, pp. 3396-3416, (**1991**)

Narayanan G., Krishnamoorthy C. S., & Rajagopolan N., "Bibliography on cable stayed bridges", International conference on cable stayed bridges, Bangkok, pp. 1497-1545, (**1987**)

Nazmy A. S. & Abdel-Ghaffar A. M., "Three dimensional non linear static analysis of cable-stayed bridges." Computers and Structures, Vol. 34, pp. 257-271 (**1990a**)

Nazmy A. S. & Abdel-Ghaffar A. M., "Non-linear earthquake response analysis of long-span cable-stayed bridges: theory." Earthquake Engineering & Structural Dynamics, Vol. 19, pp. 45-62 (**1990b**)

Nazmy A. S. & Abdel-Ghaffar A. M., "Non-linear earthquake response analysis of long-span cable-stayed bridges: Applications." Earthquake Engineering & Structural Dynamics, Vol. 19, pp. 63-76 (**1990c**)

Nazmy A. S. & Abdel-Ghaffar A. M., "Effects of ground motion spatial variability on the response of cable-stayed bridges." Earthquake Engineering & Structural Dynamics, Vol. 21, pp. 1-20 (**1992**)

O'Rourke M. J., Bloom M. C. & Dobry R., "Apparent propagation of body waves." Earthquake Engineering & Structural Dynamics, Vol. 10, pp. 283-294 (**1982**)

O'Rourke M. J. & El Hmadi K., "Analysis of continuous buried pipelines for seismic wave effects." Earthquake Engineering & Structural Dynamics, Vol. 16, pp. 917-929 (**1988**)

O'Rourke M. J. & Castro G., "Effects of seismic wave propagation upon buried pipelines." Earthquake Engineering & Structural Dynamics, Vol. 8, pp. 455-467 (**1980**)

Panofsky H. A., Thomson D. W., Sullivan D. A. & Moravek D. E., "Two point velocity statistics over Lake Ontario." Boundary Layer Meteorology, Vol. 7, pp. 309-321 (**1974**)

Panofsky H. A. & Mizuno T., "Horizontal coherence and Pasquill's beta." Boundary Layer Meteorology, Vol. 9, pp. 247-256 (**1975**)

Perrotti F., "Structural response to non-stationary multi-support random excitation." Earthquake Engineering & Structural Dynamics, Vol. 19, pp. 513-527 (**1990**)

Podolny W. & Scalzi J. B., "Construction and design of cable stayed bridges." John Wiley & Sons (**1976**)

Priestly M.B., "Evolutionary spectra and non-stationary processes." J. Royal Statistical Society, series B, Vol. 27, pp. 204-237 (**1965**)

Priestly M.B., "Power spectral analysis of non-stationary random processes." J. Sound And Vibration, Vol. 6, pp. 86-97 (**1967**)

Provis W. A., "Observations on the effects produced by wind on the suspension bridge over the Menai Straits, more especially as relates to the injuries sustained by the roadways during the storm of January 1839; together with brief notes of various suggestions for repairing the structure." [Included as an appendix to **Farquharson F. B. (1950)**], Transactions of the I.C.E., London, England, Vol. 3, p. 358, (**1839**)

Quek S-R., Teo Y-P. & Balendra T., "Non-stationary structural response with evolutionary spectra using seismological input model." Earthquake Engineering & Structural Dynamics, Vol. 19, pp. 275-288 (**1990**)

Rajaraman A., Loganathan K. & Raman N. V., "Non linear analysis of cable stayed bridges." IABSE Proceedings, Vol. P37/80, pp. 205 (**1980**)

Ropelewski C. F., Tennekes H. & Panofsky H. A., "Horizontal coherence of wind fluctuations." Boundary Layer Meteorology, Vol. 5, pp. 353-363 (**1973**)

Rosenblueth E. & Bustamente J., "Distribution of structural response to earthquakes." J. Eng. Mech. Div. ASCE, Vol. 88, pp. 75-106 (**1962**)

Ruiz P. & Penzien J., "Probabilistic study of structures during earthquakes." University of California, Berkeley, Earthquake Engineering Research Centre, Report 69-3 (**1969**)

Ruiz P. & Penzien J., "Stochastic seismic response of structures." J. Eng. Mech. Div., ASCE, Vol. 97, pp.12-41 (**1971**)

Rutenberg A. & Heidebrecht A. C., "Approximate spectral multi support seismic analysis : travelling wave approach." Proc. I.C.E. Part 2, Vol. 85, pp. 223-236 (**1988**)

Safak E. & Boore D. M., "On low frequency errors of uniformly modulated filtered white-noise models for earthquake ground motion." Earthquake Engineering & Structural Dynamics, Vol. 16, pp. 381-388 (**1988**)

Saragoni G. R. & Hart G. C., "Simulation of artificial earthquakes." Earthquake Engineering & Structural Dynamics, Vol. 6, pp. 249-267 (**1974**)

Scott-Russell J., "On the vibration of suspension bridges and other structures, and the means of preventing injury from this cause." [Included as an appendix to **Farquharson F. B. (1950)**], Transactions Royal Scottish Society Of Arts, Vol. 1, (**1841**)

Severn R. T., Taylor C. A., & Brownjohn J. M. W., "Full-scale dynamic testing and mathematical model validation of arch dams." Dam Engineering, Vol. 1, pp. **-** (**1990**)

Shinozuka M. & Y. Sato, "Simulation of non-stationary random processes" J. Eng. Mech. Div, ASCE, Vol. 93, pp. 11-40 (**1967**)

Shinozuka M., "Stochastic fields and their digital simulation." pp. 93-133 in Stochastic Methods in Structural Dynamics, Martinus Nijhoff Publishers, Boston (**1987**)

Shinozuka M., "State of the art report: engineering modeling of ground motion." Proc. 9th W.C.E.E., Vol. 8, pp. 51-62 (**1988**)

Simiu E. & Scanlan R. H., "Wind Effects On Structures, An introduction to wind engineering." John Wiley & Sons, New York (**1986**)

Smith B. S., "The single plane cable stayed girder bridge: a method of analysis suitable for computer use." Proc. I.C.E., Vol 37, pp. 183ff (**1968**)

Smith B. S., "A linear method of analysis for double plane cable stayed girder bridges." Proc. I.C.E., Vol 39, pp. 85ff (**1968**)

SOLVIA Engineering AB, Manuals for SOLVIA finite element analysis package (**1989**)

Soo H. S-W. & Scanlan R. H., "Calculation of the wind buffeting of the Lion's Gate bridge and comparison with model studies." Journal of Wind Engineering and Industrial Aerodynamics, Vol. 14, pp. 201-211, (**1983**)

Tajimi H., "A statistical method for determining the maximum response of building structure during an earthquake." Proc. 2nd W.C.E.E., Tokyo, pp. 781-797 (**1960**)

Tang M. C., "Analysis of cable stayed girder bridges." J. Struct. Div. ASCE, Vol. 97, pp.1481ff (**1971**)

Taylor C. A., "Eqsim, a program for generating spectrum compatible earthquake ground acceleration time histories. Referance Manual." Research Report, University of Bristol Department of Civil Engineering, (**1989**)

Teunissen H. W., "Structure of mean winds and turbulence in the planetary boundary layer" Boundary Layer Meteorology, Vol. 19, pp.187-221 (**1980**)

To C. W. S., "Non-stationary random responses of a multi-degree-of-freedom system by the theory of evolutionary spectra." J. Sound And Vib., Vol. 83, pp. 273-291 (**1982**)

To C. W. S.,"Time-dependent variance and covariance of responses of structures to non-stationary random excitations." J. Sound And Vib., Vol. 93, pp. 135-156 (**1984**)

Troitsky M. S., "Cable stayed bridges." 2nd Ed., Blackwell Scientific Publishing (**1988**)

Vanmarcke E. H.,"On the distribution of the first-passage time for normal stationary random processes." Journal of Applied Mechanics, Transactions of the ASME, Vol. 42, pp. 215-220 (**1975**)

Vanmarcke E. H., "Structural response to earthquakes." Seismic Risk And Engineering Decisions, Ch. 8, Elsevier Scientific Publishing, Eds. C. Lomnitz & E. Rosenblueth (**1976**)

Vanmarcke E. H., "Efficient modelling of random media." 3rd International Conference on Structural Safety and Reliability, Norwegian Institute of Technology, Trondheim (**1981**)

Vanmarcke E. H., "Random fields, new concepts and engineering applications." 4th ASCE speciality conference on probabilistic mechanics and structural reliability. (**1984**)

Vann A. M., "Intelligent monitoring of civil engineering systems." PhD Thesis, University of Bristol, Department of Civil Engineering, (**1994**)

Walther R., Houriet B., Isler W. & Moia P., "Cable stayed bridges." Thomas Telford (**1988**)

Werner S. D., Lee L. C., Wong H. L. & Trifunac M. D., "Structural response to travelling seismic waves." J. Struct. Div. ASCE, Vol. 105, pp. 2547-2564 (**1979**)

Wilson E. L., Der Kiureghian A. & Bayo E. P., "Replacement for the SRSS method in seismic analysis." Earthquake Engineering & Structural Dynamics, Vol. 9, pp. 187-194, (**1982**)

Wilson J. C. & Gravelle W., "Modelling of a cable-stayed bridge for dynamic analysis." Earthquake Engineering & Structural Dynamics, Vol. 20, pp. 707-721, (**1991**)

Wilson J. C. & Tao Liu, "Ambient vibration measurements on a cable-stayed bridge." Earthquake Engineering & Structural Dynamics, Vol. 20, pp. 723-747, (**1991**)

Wood C.J., "Calibration of a TW 8204 combined wind speed and direction sensor for Danjay Designs." Oxford University Engineering Laboratory, Report No. 1417/82 (**1982**)

Yang J-N., "Nonstationary envelope process and first excursion probability." J. Struct. Mech., Vol. 1, pp. 231-248 (**1972**)

Yeh C.H. & Wen Y.K., "Modeling of non-stationary ground motion and analysis of inelastic response." Structural Safety, Vol. 8, pp. 281-298 (**1989**)

Zembaty Z., "A note on non-stationary stochastic response and strong motion duration." Earthquake Engineering & Structural Dynamics, Vol. 16, pp. 1189-1200 (**1988**)

Zerva A., Ang A. H-S. & Wen Y. K., "Lifeline response to variable ground motions." Earthquake Engineering & Structural Dynamics, Vol. 19, pp. 819-832 Vol. 16 361-379 (**1988**)

Zerva A., "Response of multispan beams to spatially incoherent seismic ground motions." Earthquake Engineering & Structural Dynamics, Vol. 19, pp. 819-832 (**1990**)

Zerva A., "Seismic loads predicted by spatial variability models." Structural Safety, Vol. 11, pp. 227-243 (**1992a**)

Zerva A., "Seismic Ground Motion Simulations From A Class Of Spatial Variability Models." Earthquake Engineering & Structural Dynamics, Vol. 21, pp. 351-361 (**1992b**)